ACS SYMPOSIUM SERIES 998

Low-Energy Nuclear Reactions Sourcebook

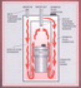

EDITED BY

Jan Marwan and Steven B. Krivit

Downloaded by 89.163.34.136 on July 1, 2012 | http://pubs.acs.org
Publication Date: August 1, 2008 | doi: 10.1021/bk-2008-0998.fw001

Low-Energy Nuclear Reactions Sourcebook

About the Cover

The design on the front cover is an SRI International flow calorimeter surrounding cold fusion cell. (Drawing courtesy of Craig Erlick, originally published in *The Rebirth of Cold Fusion* by Steven B. Krivit and Nadine Winocur. Used with permission of Pacific Oaks Press.)

Downloaded by 89.163.34.136 on July 1, 2012 | http://pubs.acs.org
Publication Date: August 1, 2008 | doi: 10.1021/bk-2008-0998.fw001

ACS SYMPOSIUM SERIES **998**

Low-Energy Nuclear Reactions Sourcebook

Jan Marwan, Editor
Dr. Marwan Chemie

Steven B. Krivit, Editor
New Energy Times, *Editor*

Downloaded by 89.163.34.136 on July 1, 2012 | http://pubs.acs.org
Publication Date: August 1, 2008 | doi: 10.1021/bk-2008-0998.fw001

Sponsored by the
ACS Division of Environmental Chemistry, Inc.

American Chemical Society, Washington, DC

Downloaded by 89.163.34.136 on July 1, 2012 | http://pubs.acs.org
Publication Date: August 1, 2008 | doi: 10.1021/bk-2008-0998.fw001

ISBN 978-0-8412-6966-8

The paper used in this publication meets the minimum requirements of American National Standard for Information Sciences—Permanence of Paper for Printed Library Materials, ANSI Z39.48-1984.

Copyright © 2008 American Chemical Society

Distributed by Oxford University Press

All Rights Reserved. Reprographic copying beyond that permitted by Sections 107 or 108 of the U.S. Copyright Act is allowed for internal use only, provided that a per-chapter fee of $40.25 plus $0.75 per page is paid to the Copyright Clearance Center, Inc., 222 Rosewood Drive, Danvers, MA 01923, USA. Republication or reproduction for sale of pages in this book is permitted only under license from ACS. Direct these and other permission requests to ACS Copyright Office, Publications Division, 1155 16th Street, N.W., Washington, DC 20036.

The citation of trade names and/or names of manufacturers in this publication is not to be construed as an endorsement or as approval by ACS of the commercial products or services referenced herein; nor should the mere reference herein to any drawing, specification, chemical process, or other data be regarded as a license or as a conveyance of any right or permission to the holder, reader, or any other person or corporation, to manufacture, reproduce, use, or sell any patented invention or copyrighted work that may in any way be related thereto. Registered names, trademarks, etc., used in this publication, even without specific indication thereof, are not to be considered unprotected by law.

PRINTED IN THE UNITED STATES OF AMERICA

Downloaded by 89.163.34.136 on July 1, 2012 | http://pubs.acs.org
Publication Date: August 1, 2008 | doi: 10.1021/bk-2008-0998.fw001

Foreword

The ACS Symposium Series was first published in 1974 to provide a mechanism for publishing symposia quickly in book form. The purpose of the series is to publish timely, comprehensive books developed from ACS sponsored symposia based on current scientific research. Occasionally, books are developed from symposia sponsored by other organizations when the topic is of keen interest to the chemistry audience.

Before agreeing to publish a book, the proposed table of contents is reviewed for appropriate and comprehensive coverage and for interest to the audience. Some papers may be excluded to better focus the book; others may be added to provide comprehensiveness. When appropriate, overview or introductory chapters are added. Drafts of chapters are peer-reviewed prior to final acceptance or rejection, and manuscripts are prepared in camera-ready format.

As a rule, only original research papers and original review papers are included in the volumes. Verbatim reproductions of previously published papers are not accepted.

ACS Books Department

Acknowledgments

The editors thank the American Chemical Society (ACS) Books Department and the ACS Division of Environmental Chemistry, Inc. for sponsoring this book. We also thank the authors who contributed chapters to this book and the volunteer reviewers who greatly improved the quality of this book. We also thank Sally Robertson for her help in the production of this book, and also thank the sponsors of New Energy Institute for their help.

Jan Marwan
Dr. Marwan Chemie
Rudower Chaussee 29
12489 Berlin
Germany
http://www.marwan-chemie.com/

Steven B. Krivit
Editor, *New Energy Times*
369–B Third Street
Suite 556
San Rafael, CA 94901
http://www.newenergytimes.com

Downloaded by 89.163.34.136 on July 1, 2012 | http://pubs.acs.org
Publication Date: August 1, 2008 | doi: 10.1021/bk-2008-0998.pr001

Downloaded by 89.163.34.136 on July 1, 2012 | http://pubs.acs.org
Publication Date: August 1, 2008 | doi: 10.1021/bk-2008-0998.pr001

Downloaded by 89.163.34.136 on July 1, 2012 | http://pubs.acs.org
Publication Date: August 1, 2008 | doi: 10.1021/bk-2008-0998.pr001

Low-Energy Nuclear Reactions Sourcebook

In Low-Energy Nuclear Reactions Sourcebook; Marwan, J., et al.;
ACS Symposium Series; American Chemical Society: Washington, DC, 2008.

Downloaded by 89.163.34.136 on July 1, 2012 | http://pubs.acs.org
Publication Date: August 1, 2008 | doi: 10.1021/bk-2008-0998.ch001

Chapter 1

Low Energy Nuclear Reactions: The Emergence of Condensed Matter Nuclear Science

Steven B. Krivit

**Editor, *New Energy Times*, 369-B Third Street, Suite 556,
San Rafael, CA 94901**

Introduction

It is helpful to begin with an introduction of relevant terminology. Low energy nuclear reactions (LENR) is the chosen term to describe the observations in the field of condensed matter nuclear science (CMNS).

Initially, the media labeled the field "cold fusion." However, that is a less-than-optimal name for this research. One of the primary reasons is that the term cold fusion implies that these reactions were just a "colder" form of conventional thermonuclear reactions, which they are not. This has resulted in significant confusion. As well, other nonfusion reactions have been clearly observed in addition to the possible fusion reaction.

The field is in its 19th year. It was introduced in 1989 by Martin Fleischmann and Stanley Pons at the University of Utah. The field evolved from their research, which used an electrolysis experiment with the elements palladium and deuterium.

Fleischmann and Pons' first significant experiment occurred in the spring of 1985, when they informally reported that, overnight, an experimental cell had exhibited significant anomalous behavior that included the melting and partial vaporization of the palladium cube used for their cathode. They also informally reported the partial destruction of their lab bench, a small hole in the concrete floor and damage to the fume hood.

The two electrochemists worked as quietly as possible for several years and, after using up their own research funds, applied to the Department of Energy for a grant. This led to the eventual public disclosure of their work at a press conference on March 23, 1989.

Fleischmann and Pons discovered an electrochemical method of generating nuclear energy, in the form of heat, in a way that was previously unrecognized by nuclear physicists. Much drama and unscientific reaction followed the

In Low-Energy Nuclear Reactions Sourcebook; Marwan, J., et al.;
ACS Symposium Series; American Chemical Society: Washington, DC, 2008.

announcement and the unexpectedness of their claim. The claim flew in the face of hot fusion research, which had yet to demonstrate a commercially viable product, and thus triggered no small amount of disbelief and hostility.

To the surprise of many people, the research in the field has shown consistently positive, coherent sets of results. Progress has been slow, but the research shows considerable promise.

Low energy nuclear reaction research composes a new field of science. It does not belong exclusively to chemistry, physics, or any other previous scientific discipline. Much is known about the science, but many significant facts remain unknown.

Two general groups of reactions exist in the field. In addition to the heat-producing reaction discovered by Fleischmann and Pons, the field encompasses a set of experiments that demonstrate transmutation with heavy elements that are not all fusion reactions. This is another reason for referring to the field as low energy nuclear reactions rather than cold fusion.

The LENR term does not imply that the potential energy output is low; rather, it distinguishes the research from high-energy nuclear physics, which involves either the use of high temperatures or energetic devices such as particle accelerators and magnetic confinement fusion machines.

Downloaded by 89.163.34.136 on July 1, 2012 | http://pubs.acs.org
Publication Date: August 1, 2008 | doi: 10.1021/bk-2008-0998.ch001

The First Department of Energy Cold Fusion Review

An early significant milestone in the history of LENR occurred in the first year of what was then called cold fusion. The president of the United States in 1989, George H.W. Bush, sought the guidance of Glenn T. Seaborg, a Nobel prize winner in chemistry and former chairman of the Atomic Energy Commission, to counsel the White House on the highly public matter of cold fusion.

Seaborg was convinced that the whole idea was entirely wrong. Nevertheless, he recommended that Bush form a committee to review the idea. He predicted that the committee would decide that the idea was not a valid form of science and not a worthwhile application of government funding.

Bush followed Seaborg's advice, and through the Energy Resources Advisory Board, an investigative panel was formed. John Huizenga, a professor of chemistry and physics at the University of Rochester, a major government-funded hot fusion research facility, was selected to lead the panel. Huizenga, later wrote in his book *Cold Fusion: The Scientific Fiasco of the Century* that cold fusion was entirely a mistake.

Not surprisingly, six months later, the panel concluded that cold fusion did not produce fusion products in the expected quantities and proportion. Therefore, the panel said, the experimental results reported by Fleischmann and Pons were entirely mistaken.

The members of the panel either failed to recognize or failed to communicate the possibility that some other novel nuclear process may have been at work.

Public Confusion

During the confusion about cold fusion in the following years, many people lost sight of the developing science.

The first significant milestone occurred in July 1990 with the publication of Fleischmann and Pons' seminal paper, "Calorimetry of the Palladium- Deuterium-Heavy Water System," in the *Journal of Electroanalytical Chemistry* (*1*).

They reported very strong results: Nineteen runs registered positive excess heat, with an average of 586 milliwatts. Fourteen control runs showed negative excess heat, averaging -1.3 milliwatts. Their detection limit was 1 milliwatt, and their signal over background ratio was 450-1. (Fleischmann and Pons provided an explanation for the slight negative readings in their paper.)

Later that year, University of Minnesota professor Richard Oriani published the first corroboration of Fleischmann and Pons' excess heat claim in the December 1990 issue of *Fusion Technology* (*2*).

A common public perception is that the Fleischmann-Pons claims were disproved because others failed to replicate their experiment. This is a gross misunderstanding that not only presents a lesson to historians and observers of this subject but provides insight to future explorers in other fields of science. As the example of the cold fusion episode shows, failure to replicate does not equal disproof of a claim.

The key question to consider is whether critics found an explicit error of protocol, procedure, or analysis in the Fleischmann-Pons work. With the exception of flawed gamma/neutron data, which was a minor component of their laboratory evidence, the Fleischmann-Pons 1990 paper and that of Oriani were never refuted successfully in the formal, scientific literature.

In July 1992, the Wilson group from General Electric did its best to find fault with the Fleischmann-Pons 1990 *Journal of Electroanalytical Chemistry* paper; however, the group failed to disprove it. In fact, the effort effectively, and likely unintentionally, provided a third-party confirmatory analysis. Wilson concluded that the Fleischmann and Pons cell generated 40 percent excess heat, amounting to 736 milliwatts, more than 10 times the error level associated with the data.

Downloaded by 89.163.34.136 on July 1, 2012 | http://pubs.acs.org
Publication Date: August 1, 2008 | doi: 10.1021/bk-2008-0998.ch001

Excess Heat

Excess heat is the fundamental observation and claim of Fleischmann and Pons. In electrochemistry, when a researcher applies a certain amount of electrical energy to an electrolytic cell, he or she expects a commensurate amount of heat to come out of the cell based on Joule heating.

Fleischmann and Pons found that, in their cold fusion cell, more heat was coming out of their experiment – on the order of 1,000 times more – than could be explained by normal chemistry.

Calorimetry

Part of the challenge of this field has always been the acceptance of the phenomenon of excess heat. Calorimetry was a relatively obscure art, and the levels of heat in these experiments were, and still are, typically registering in the milliwatt range, though occasional experiments have registered in the tens of watts. Experiments performed at such low power require the utmost care and precision with the instrumentation and data analysis. These issues gave rise to much skepticism and doubt in the early period of this history.

However, many researchers responded to the distrust that many critics had with Fleischmann and Pons' isoperibolic calorimetry and initiated experiments using far simpler methods. Isoperibolic calorimetry is not intrinsically complex, however, it becomes so when a mixture of radiative, conductive, and convective heat flows must be accounted for.

One alternative method which became popular in the early 1990s is the use of the Seebeck-type enclosure. This method uses a fully enclosed thermally insulated container in which an experiment is placed. Many thermocouples are embedded within the walls of the enclosure, and they measure temperature both within the container and outside it. These data are collected and used to determine the heat generated from the experiment.

Another method uses mass-flow calorimetry (Figure 1). These systems are practically more difficult but they have the advantage of being much easier to calibrate and errors are easier to recognize. In this method, the experiment is fully enclosed within a chamber, and a recirculating fluid surrounds this chamber or uses a closely contacting heat exchanger to extract heat. The temperature of the fluid is measured when it enters the chamber as well as when it exits the chamber. The difference in the temperatures along with the flow rate can be used to accurately calculate the heat coming from the reaction.

One disadvantage of the mass-flow calorimeter system is that it has the effect of cooling an experiment. Researchers have found that, when an experiment starts to generate heat, the heating effect, if allowed, provides positive feedback and amplifies heat generation from the reaction.

LENR Materials

Deuterium, in the form of heavy water, as well as palladium, as used by Fleischmann and Pons in 1989, still appear to be the essential materials used in most LENR research.

However, many experiments also have been performed with deuterium gas and palladium, as well as with normal water and nickel and, occasionally, other metals, too. An important question remains unresolved: To what extent is palladium consumed in the reactions, if at all?

Downloaded by 89.163.34.136 on July 1, 2012 | http://pubs.acs.org
Publication Date: August 1, 2008 | doi: 10.1021/bk-2008-0998.ch001

What is Known

Many facts are now understood about these reactions, and several other essential mysteries remain. Somewhere on the order of five hundred researchers from a dozen nations have been active in the field, most since it began. Three thousand papers exist on the subject, a third of them in peer-reviewed journals. Together, they represent many thousands of experiments.

The dominant byproducts of the palladium-deuterium experiments are excess energy, in the form of heat, and helium-4. LENR reactions contrast with conventional nuclear fusion, in which helium-4 is the least dominant byproduct, which, when observed in conventional nuclear fusion is always accompanied by gamma radiation. LENR reactions do not produce gamma radiation at anywhere near the levels seen in conventional nuclear fusion.

Half a dozen independent reports show a very close correlation between the excess heat and the evolution of helium-4 (*3-7*). This correlation matches the energy that would be expected as a release from the fusion of two deuterons. Remaining discrepancies between the expected amount of helium-4 and the observed amount are accounted for by the expected absorption of helium into the palladium in the experiments.

On very rare occasions and in low but statistically significant proportions, tritium and helium-3 (thought to be decay from tritium) have been observed in LENR experiments. Tritium has been measured both in the gas phase and in the electrode.

Required Threshold Parameters for Excess Heat

Michael McKubre of SRI International was one of the first to identify three essential parameters that, when obtained, produce excess heat reactions repeatedly. By far the most significant of these is the ratio between deuterium and palladium atoms within a cathode. This is also called the loading ratio.

In general, a minimum deuterium to palladium loading ratio of 0.90 is required to achieve the excess heat effect. Loading ratios lower than 0.90 sometimes produce the excess heat effect, but it becomes increasingly unlikely below this threshold. A 1-1 ratio, along with the other required parameters, appears to yield consistently excess heat.

In most, but not all cases, many days, if not weeks, were required before researchers could get bulk palladium loaded to these levels. This long wait was one of the crucial facts that appeared to be unknown to most of the people involved in early replication attempts, and a major culprit for most early failures to replicate. In most of these failed attempts, people did not even bother to measure the loading. In addition, they were doing their electrochemistry in such a way that they would never have obtained the required loading. More recently,

Downloaded by 89.163.34.136 on July 1, 2012 | http://pubs.acs.org
Publication Date: August 1, 2008 | doi: 10.1021/bk-2008-0998.ch001

Downloaded by 89.163.34.136 on July 1, 2012 | http://pubs.acs.org
Publication Date: August 1, 2008 | doi: 10.1021/bk-2008-0998.ch001

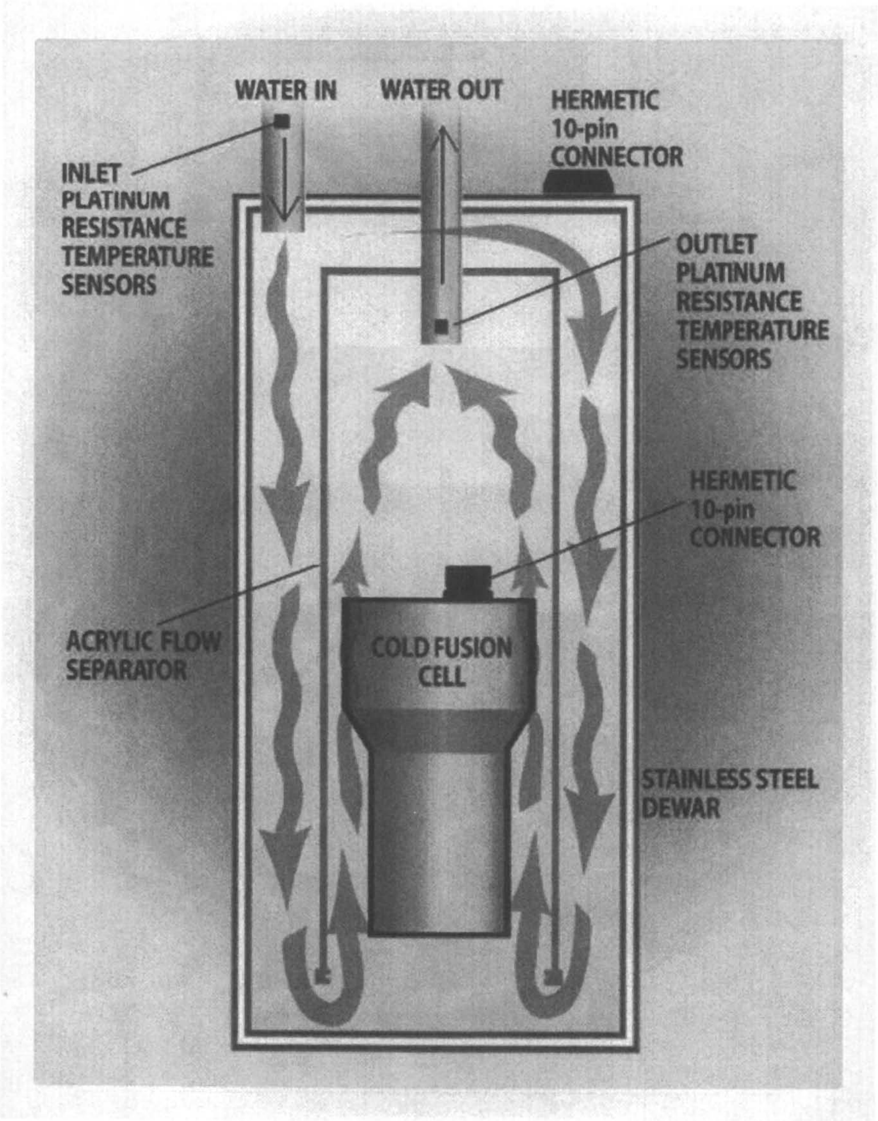
WATER IN
WATER OUT
HERMETIC 10-pin CONNECTOR
INLET PLATINUM RESISTANCE TEMPERATURE SENSORS
OUTLET PLATINUM RESISTANCE TEMPERATURE SENSORS
HERMETIC 10-pin CONNECTOR
ACRYLIC FLOW SEPARATOR
COLD FUSION CELL
STAINLESS STEEL DEWAR

Figure 1. SRI-International Type Mass-Flow Calorimeter

researchers have found ways to obtain the required loading quite early, without the long wait.

The second threshold requirement is a relatively high current density through the cathode surface, a minimum of 250 mA/cm2. However, this parameter varies somewhat based on cathode size and geometry.

The third requirement calls for some sort of a dynamic trigger, a stimulus which will cause the electrochemical cell to enter a state of disequilibrium. For example, Fleischmann and Pons' dramatic 1985 reaction occurred after the current was increased abruptly from 0.75 amperes to 1.5 amperes. Additional known triggers that others have used are the application of temperature changes, low-power (30 mW) laser excitation, external electrical fields, and external magnetic fields.

Downloaded by 89.163.34.136 on July 1, 2012 | http://pubs.acs.org
Publication Date: August 1, 2008 | doi: 10.1021/bk-2008-0998.ch001

Power and Energy Release

Numerous energy-releasing reactions have been reported, though reproducibility is inconsistent. Several of the recorded reactions have indicated relatively large capacities for power and energy release.

One of the earliest was in 1992, when Akito Takahashi of Osaka University observed 130 watts of excess heat. Edmund Storms attempted and successfully reproduced the experiment using some of the same palladium used by Takahashi.

The potential energy density of LENR experiments is difficult to predict because the mechanism is so far from being sufficiently understood. However, some attempts have been made to quantify the volumetric energy density relative to the volume of the palladium cathode. These estimates indicate that LENR might have a very high energy density, even higher than that of the uranium fuel rods used in fission reactors.

Fleischmann and Pons (*8*) and Giuliano Preparata (*9*) published papers showing volumetric power densities in the range of 10^4 and 10^5 watts/cm^3 based on single and nonreproduced experiments. More conservative estimates from McKubre suggest that the maximum rates presently being observed are in the range of 10^3 to 10^4 watts/cm^3. The estimate may even be conservative because the fuel consumed is believed to be deuterium, not palladium.

Excess Heat after Boil-Offs

Several rare excess heat reactions have been reported in which the reactions appear to reach some kind of critical point and run autonomously, long after the input current is turned off or disconnected.

Many of these reports are anecdotal, and none has been repeatable. Only a few have been precisely instrumented and observed because the reactions have come as a surprise.

In 1992, Fleischmann and Pons did not replenish the electrolyte in a cell and allowed it to run dry. When the electrolytic circuit was broken as a result of the absence of the electrolyte, the cell continued to give off excess heat for three hours. A Kel-F plastic support melted, indicating temperatures above 300°C (*8*). Fleischmann and Pons videotaped this experiment.

At an MIT symposium in the early 1990s, Lawrence Forsley of JWK Technologies Inc. reported on a cell in which the electrolytic current was turned off momentarily. The cell had been running at 80°C, at equilibrium, for one day. After the abrupt power interruption, the cell temperature shot up to 125°C, cracked a plastic insulator, and boiled off all the electrolyte – at a power input far below that required for Joule heating.

In the early 1990s, Tadahiko Mizuno of Hokkaido University reported the boil-off of a cell initially running 24 watts of input power that, in its last eight days with current turned off, boiled more than 15 liters of water. Mizuno had placed the cell in a bucket of water after disconnecting it from the power supply. According to Mizuno's calculations, during the time the cell was turned off, it evaporated enough water to account for 8.2 x 107 joules of energy (*10*).

Other researchers to report excess heat after boil-offs are Giuliano Mengoli of the Instituto di Polarografia and Melvin Miles of the U.S. Navy's China Lake Weapons Center.

A recent boil-off event occurred in a U.S. military laboratory in the spring of 2007. However, the researchers have decided not to report it publicly; instead, they are struggling to find how to make it repeatable.

Downloaded by 89.163.34.136 on July 1, 2012 | http://pubs.acs.org
Publication Date: August 1, 2008 | doi: 10.1021/bk-2008-0998.ch001

Low Energy Nuclear Transmutation Reactions

Transmutation of heavy elements has been observed in LENR experiments as early as 1990, largely through the work of John O'Mara Bockris at Texas A&M University.

A significant body of work in transmutations has been reported by George Miley, director of the Fusion Studies Laboratory at the University of Illinois, Urbana, and former editor of the American Nuclear Society's journal *Fusion Technology*.

In 2003, he performed a survey, "Review of Transmutation Reactions in Solids"(*11*). He reported LENR transmutation evidence obtained by 15 independent laboratories. Three general combinations of reactions have been described: fusion of various light elements, fusion of light elements with heavy elements, and fission of heavier elements. The resultant elements are often reported as anomalous isotopic ratios, adding support to the hypothesis that such elements are created by LENRs (*12*).

A rigorous set of LENR transmutation experiments has been performed by Yasuhiro Iwamura et al. at Mitsubishi Heavy Industries in Japan. These experiments cause deuterium gas to pass through a multilayered substrate containing palladium and calcium oxide. On the front side of the substrate, atoms from the new element are found in place of the elements initially deposited there.

Iwamura et al. have reported three groups of transmutation reactions: cesium into praseodymium, barium into samarium, and strontium into molybdenum (*13-16*).

Normal Water Reactions

The role of normal water, sometimes inaccurately called light water, is perplexing as it applies to LENR research. Many researchers within the field are skeptical of light-water excess heat claims. In typical heavy-water experiments, introduction of light water to a cell containing some heavy water will poison and halt the excess heat effect. However, some researchers have been investigating anomalous reactions with normal water and nickel and reporting excess heat.

One such group was that of physicist S. Focardi, which published an experiment in *Il Nuovo Cimento* (then the journal of the Italian Physical Society) that produced an average excess heat of 18 watts for 319 days with an integrated energy of 600 MJ (*17*). One author of that paper, Francesco Piantelli, reported later that the introduction of deuterium into their nickel-hydrogen experiment terminated the excess heat effect.

It is possible that the introduction of deuterium into hydrogen experiments as well as the introduction of hydrogen into deuterium experiments may poison the experiments.

Nuclear Evidence

LENR experiments produce various forms of nuclear radiation. Types of prompt radiations detected include x-ray (*18, 19*), gamma ray (*20*), and energetic particles (ions and electrons) (*21, 22*). All of these radiations are emitted at very low intensities so they are difficult to measure in LENR experiments. Furthermore, most x-rays and energetic particles rarely travel outside of a LENR experiment so, typically, a detector for them must be located inside the experimental vessel.

Some of the most significant in-situ particle detection has been observed in experiments and replications of work originating from the U.S. Navy's Space and Naval Warfare Systems Command Center in San Diego, California (*23*).

Pamela Mosier-Boss, Stanislaw Szpak, and Frank Gordon developed such a method using solid-state nuclear track detectors, also known as CR-39 plastic track detectors, and the co-deposition LENR method.

Other researchers have detected helium-4 and helium-3 (*3-7, 18*) and tritium in other experiments (*24-26*).

A variety of anomalous physical effects on the cathodes has been observed, such as the melting and vaporization of palladium in experiments. None of these

Downloaded by 89.163.34.136 on July 1, 2012 | http://pubs.acs.org
Publication Date: August 1, 2008 | doi: 10.1021/bk-2008-0998.ch001

effects can be the result of Joule heating, because the energy inputs are too low (*1, 4, 27*). Other changes to the cathodes include unusual morphological deformations (*28*), craters (*10, 28*), and "hot spots" (*29*).

Environmental Issues

As was known from very early in the history of LENR research, all of the observed reactions appear to lack significant high-energy neutron and gamma ray emissions. As a result, this new science shows promise as the possible basis for new types of nuclear power systems that do not need complex containment or disposal systems.

Low levels of radiation are found in at least some of these reactions, but this radiation is usually absorbed directly and promptly within the experiments. Consequently, they offer hope of practical applications that do not pose major health hazards or compromise the environment.

In addition to the lack of high-energy radiation, the experiments do not appear to produce any greenhouse gases or long-lived radioactive decay emissions.

Numerous LENR Methods

Fleischmann and Pons' original method used electrolysis of heavy water, a method which has been used worldwide many times to achieve excess heat.

However, a wide variety of methods has been reported to produce both excess heat and anomalous nuclear products. These include other variations of electrolysis, pressurized deuterium gas, gas-electric field discharge, gas diffusion, plasma electrolysis, ion bombardment, acoustic and mechanically induced cavitation, nanostructured or finely divided palladium, and even biological mechanisms.

No Lack of Theories

The proposed theories for the anomalous effects are numerous and therefore, unfortunately, pose great difficulty for someone trying to develop a coherent understanding of the underlying mechanisms.

Most of the LENR theories incorporate the idea that fusion and/or fission processes are primarily responsible for the observed experimental results. These theories invoke the strong interaction as the underlying physical mechanism.

An alternative approach proposed by Allan Widom and Lewis Larsen of Lattice Energy LLC, which is considered with great skepticism by many researchers within the field, tries to understand and predict LENR phenomena

Downloaded by 89.163.34.136 on July 1, 2012 | http://pubs.acs.org
Publication Date: August 1, 2008 | doi: 10.1021/bk-2008-0998.ch001

by postulating the creation of extremely cold neutrons that facilitate low energy nuclear reactions. This theory, unlike other LENR theories, uses the weak interaction and does not need to explain how to overcome the Coulomb barrier repulsion problem because neutrons have no charge.

Concluding Remarks

The challenge presented by Fleischmann and Pons was unexpected and surprising, to say the least, for most nuclear experts of the day. Most researchers who initially attempted this difficult work gave up within six weeks of its introduction. Only a few careful, persistent researchers had early success. Their firsthand experience gave them the confidence to trust what they saw in their own labs.

However, during the 1989 Department of Energy cold fusion review, only one member of the panel was willing to entertain the validity of the discovery. Dr. Norman Ramsey, Nobel laureate and professor of physics at Harvard University, was selected as co-chair of the panel, though the historical record (*30*) suggests that this title granted him little authority or influence. To see that his dissenting view was included, he had to threaten to resign from the panel unless the following preamble was included in the Department of Energy report: "Ordinarily, new scientific discoveries are claimed to be consistent and reproducible; as a result, if the experiments are not complicated, the discovery can usually be confirmed or disproved in a few months. The claims of cold fusion, however, are unusual in that even the strongest proponents of cold fusion assert that the experiments, for unknown reasons, are not consistent and reproducible at the present time. However, even a single short but valid cold fusion period would be revolutionary."

Thanks to the work of Fleischmann and Pons, and those who followed them, a complex and important chapter in scientific history is evolving for all the world to witness.

Downloaded by 89.163.34.136 on July 1, 2012 | http://pubs.acs.org
Publication Date: August 1, 2008 | doi: 10.1021/bk-2008-0998.ch001

References

1. Fleischmann, M.; Pons, S.; Anderson, M. W.; Li, L. J.; Hawkins, M. Calorimetry of the Palladium-Deuterium-Heavy Water System. *J. Electroanal. Chem.* **1990**, *287*, 293.
2. Oriani, R. A.; Nelson, J. C.; Lee, S. K.; Broadhurst, J. H. Calorimetric Measurements of Excess Power Output During the Cathodic Charging of Deuterium Into Palladium. *Fusion Technology* **1990**, *18*, 652.
3. Miles, M. Correlation of Excess Enthalpy and Helium-4 Production: A Review. In *Condensed Matter Nuclear Science: Proceedings of the 10th International Conference on Cold Fusion*, Cambridge, MA, Aug. 24-29, 2003; Hagelstein, P. L.; Chubb, S. R., Eds.; World Scientific Publishing Co.: Singapore, 2006.

4. Bush, B. F.; Lagowski, J. J.; Miles, M.; Ostrom, G. S. Helium Production during the Electrolysis of D2O in Cold Fusion Experiments. *J. Electroanal. Chem.* **1991**, *304*, 271.
5. Bush, B. F.; Lagowski, J. J. Methods of Generating Excess Heat with the Pons and Fleischmann Effect: Rigorous and Cost-Effective Calorimetry, Nuclear Products Analysis of the Cathode and Helium Analysis. In *Proceedings of the Seventh International Conference on Cold Fusion*, Vancouver, Canada, April 19-24, 1998; ENECO, Inc.: Salt Lake City, UT, 1988; 38.
6. McKubre, M.; Tanzella, F. L.; Tripodi, P.; Hagelstein, P. L. The Emergence of a Coherent Explanation for Anomalies Observed in D/Pd and H/Pd System: Evidence for 4He and 3He Production. In *ICCF8: Proceedings of the Eighth International Conference on Cold Fusion*, Lerici (La Spezia), Italy, May 21-26, 2000; Scaramuzzi, F., Ed.; Italian Physical Society: Bologna, Italy, 2001; 3.
7. De Ninno, A.; Frattolillo, A.; Rizzo, A.; Del Giudice, E.; Preparata, G. *Experimental Evidence of 4He Production in a Cold Fusion Experiment.* ENEA - Unita Tecnico Scientfica Fusione Centro Ricerche Frascati: Rome, 2002.
8. Fleischmann, M.; Pons, S. Calorimetry of the Pd-D2O System: From Simplicity via Complications to Simplicity. *Phys. Lett. A* **1993**, *176*, 118-139.
9. Preparata, G.; Scorletti, M.; Verpelli, M. Isoperibolic Calorimetry on Modified Fleischmann-Pons Cells. *J. Electroanal. Chem.* **1996**, *411*, 9-18.
10. Mizuno, T. *Nuclear Transmutation: The Reality of Cold Fusion.* Infinite Energy Press: Bow, NH, 1998.
11. Miley, G. H.; Shrestha, P. Review of Transmutation Reactions in Solids. In *Condensed Matter Nuclear Science: Proceedings of the 10th International Conference on Cold Fusion*, Cambridge, MA, Aug. 24-29, 2003; Hagelstein, P. L.; Chubb, S. R., Eds.; World Scientific Publishing Co.: Singapore, 2006; 361.
12. Violante, V.; Castagna, E.; Sibilia, C.; Paoloni, S. Analysis of Ni-Hydride Thin Film after Surface Plasmons Generation by Laser Technique. In *Condensed Matter Nuclear Science: Proceedings of the 10th International Conference on Cold Fusion*, Cambridge, MA, Aug. 24-29, 2003; Hagelstein, P. L.; Chubb, S. R., Eds.; World Scientific Publishing Co.: Singapore, 2006; 421.
13. Iwamura, Y.; Sakano, M.; Itoh, T. Elemental Analysis of Pd Complexes: Effects of D2 Gas Permeation. *Jpn. J. Appl. Phys.* **2002**, *41*, 4642.
14. Iwamura, Y. Observation of Nuclear Transmutation Reactions Induced by D2 Gas Permeation through Pd Complexes. In *Condensed Matter Nuclear Science: Proceedings of the 11th International Conference on Cold Fusion*, Marseilles, France, Oct. 31 -Nov. 5, 2004; Biberian, J.-P., Ed.; World Scientific Publishing Co.: Singapore, 2006; 339.

Downloaded by 89.163.34.136 on July 1, 2012 | http://pubs.acs.org
Publication Date: August 1, 2008 | doi: 10.1021/bk-2008-0998.ch001

15. Iwamura, Y.; Itoh, T.; Sakano, M.; Sakai, S.; Kuribayashi, S. Low Energy Nuclear Transmutation in Condensed Matter Induced by D2 Gas Permeation through Pd Complexes: Correlation Between Deuterium Flux and Nuclear Products. In *Condensed Matter Nuclear Science: Proceedings of the 10th International Conference on Cold Fusion*, Cambridge, MA, Aug. 24-29, 2003; Hagelstein, P. L.; Chubb, S. R., Eds.; World Scientific Publishing Co.: Singapore, 2006; 435.
16. Iwamura, Y.; Itoh, T.; Sakano, M.; Yamazaki, N.; Kuribayashi, S.; Terada, Y.; Ishikawa, T. Observation of Surface Distribution of Products by X-Ray Fluorescence Spectrometry During D2 Gas Permeation through Pd Complexes. In *Condensed Matter Nuclear Science: Proceedings of the 12th International Conference on Cold Fusion*, Yokohama, Japan, Nov. 27-Dec. 2, 2005; Takahashi, A.; Ota, K.-I.; Iwamura, Y., Eds.; World Scientific Publishing Co.: Singapore, 2006; 178.
17. Focardi, S.; Gabbani, V.; Montalbano, V.; Piantelli, F.; Veronesi, S. Large Excess Heat Production in Ni-H Systems. *Il Nuovo Cimento* **1998**, *111A* (112), 1233.
18. Gozzi, D.; Cellucci, F.; Cignini, P. L.; Gigli, G.; Tomellini, M.; Cisbani, E.; Frullani, S.; Urciuoli, G. M. X-Ray, Heat Excess and 4He in the D:Pd System. *J. Electroanal. Chem.* **1998**, *452*, 253.
19. Szpak, S.; Mosier-Boss, P. A.; Smith, J. J. On the Behavior of Pd Deposited in the Presence of Evolving Deuterium. *J. Electroanal. Chem.* **1991**, *302*, 255.
20. Narita, S.; Yamada, H.; Arapi, A.; Sato, N.; Kato, D.; Yamamura, M.; Itagaki, M. Gamma Ray Detection and Surface Analysis on Palladium Electrode in DC Glow-Like Discharge Experiment. In *Condensed Matter Nuclear Science: Proceedings of the 10th International Conference on Cold Fusion*, Cambridge, MA, Aug. 24-29, 2003; Hagelstein, P. L.; Chubb, S. R., Eds.; World Scientific Publishing Co.: Singapore, 2006; 603.
21. Lipson, A.G.; Lyakhov, B.F.; Roussetski, A.S.; Akimoto, T.; Mizuno, T.; Asami, N.; Shimada, R.; Miyashita, S.; Takahashi, A. Evidence for Low-Intensity D-D Reaction as a Result of Exothermic Deuterium Desorption From Au/Pd/PdO:D Heterostructure. *Fusion Technology* **2000**, *38*, 238-252.
22. Lipson, A.G.; Roussetski, A. S.; Miley, G. H.; Saunin, E. I. Phenomenon of an Energetic Charged Particle Emission from Hydrogen/Deuterium Loaded Metals. In *Condensed Matter Nuclear Science: Proceedings of the 10th International Conference on Cold Fusion*, Cambridge, MA, Aug. 24-29, 2003; Hagelstein, P. L.; Chubb, S. R., Eds.; World Scientific Publishing Co.: Singapore, 2006; 539-558.
23. Szpak, S.; Mosier-Boss, P. A.; Gordon, F. E. Further Evidence of Nuclear Reactions in the Pd/D Lattice: Emission of Charged Particles. *Naturwissenschaften* **2007**, *94*, 511-514.
24. Wolf, K. L.; Wass, J. C.; Kainthla, R. C.; Bockris, J. Production of Tritium from D2O Electrolysis at a Palladium Cathode. *J. Electroanal. Chem.* **1989**, *289*, 451.

Downloaded by 89.163.34.136 on July 1, 2012 | http://pubs.acs.org
Publication Date: August 1, 2008 | doi: 10.1021/bk-2008-0998.ch001

25. Storms, E.; Talcott, C. L. Electrolytic Tritium Production. *Fusion Technology* **1990**, *17*, 680.
26. Claytor, T. N.; Seeger, P.; Rohwer, R. K.; Tuggle, D G.; Doty, W. R. Tritium and Neutron Measurements of a Solid State Cell. *Proceedings of the EPRI-NSF Workshop on Anomalous Effects in Deuterated Metals*, Washington, DC, October 16-18, 1989; EPRI: Palo Alto, CA, 1993.
27. Stringham, R. Cavitation Foil Damage. Presented at APS March Meeting, Baltimore, MD, March 13-17, 2006; Paper W41.00008.
28. Szpak, S.; Mosier-Boss, P. A.; Young, C.; Gordon, F. The Effect of an External Electric Field on Surface Morphology of Co-Deposited Pd/D Films. *J. Electroanal. Chem.* **2005**, *580*, 284-290.
29. Mosier-Boss, P. A.; Szpak, S. The Pd/(N)H System: Transport Processes and Development of Thermal Instabilities. *Nuovo Cimento, Soc. Ital. Fis. A* **1999**, *112*, 577.
30. Huizenga, J. *Cold Fusion: The Scientific Fiasco of the Century*, 2nd edition; Oxford University Press: New York, 1993; pp 41-43.

Downloaded by 89.163.34.136 on July 1, 2012 | http://pubs.acs.org
Publication Date: August 1, 2008 | doi: 10.1021/bk-2008-0998.ch001

Downloaded by PENNSYLVANIA STATE UNIV on July 1, 2012 | http://pubs.acs.org
Publication Date: August 1, 2008 | doi: 10.1021/bk-2008-0998.ch002

Chapter 2

Background to Cold Fusion: The Genesis of a Concept[1]

Martin Fleischmann

Bury Lodge, Duck Street, Tisbury, Salisbury, Wilts. SP3 6LJ, United Kingdom

The scheme of research which led to the start-up of the project now known as "Cold Fusion" is illustrated by Figure 1. We note that it is commonly believed that there is absolutely no way of influencing Nuclear Processes by Chemical means: therefore, any results that demonstrate that this might be possible must be due to faulty experimentation, delusion, fraud, etc. However, any enquiry as to the experimental foundation of the first statement in Figure 1 is normally met by the response: "Because quantum mechanics, Q.M., shows that this is so"[2] (see further below). We are driven to the conclusion that this first statement is just part of the belief system of Natural Scientists and we naturally also have to ask the question: "What conclusion would we draw if we subject the statement to the dictates of Field Theory?"[3,4]

---

[1] Reprinted with permission from *Condensed Matter Nuclear Science: Proceedings of the 10th International Conference on Cold Fusion*, Cambridge, MA, Aug. 24-29, 2003; Hagelstein, P. L.; Chubb, S. R., Eds.; World Scientific Publishing Co.: Singapore, 2006.

[2] Which coincidentally explains why I did not start this project at any time during the period 1947-1983.

[3] It is well known that the Quantum Mechanical Paradigm is incomplete and that the inconsistencies produced by this paradigm are removed by Quantum Field Theory, Q.F.T., (or Quantum Electrodynamics, Q.E.D., for applications to ordinary matter).

[4] Critiques based on the application Q.M. to dilute plasmas are usually extended to cover fusion in condensed matter. The statement "no neutrons, no fusion" is a typical example of this reasoning. We note that an excellent textbook covering the application of Q.E.D. to condensed matter is available (*1*).

Downloaded by PENNSYLVANIA STATE UNIV on July 1, 2012 | http://pubs.acs.org
Publication Date: August 1, 2008 | doi: 10.1021/bk-2008-0998.ch002

In the 1960s we started a series of research projects aimed at answering the question; "can we find illustrations in Chemistry (especially Electrochemistry) of the need to invoke the Q.E.D. paradigm to explain the results obtained?" The opposition we encountered in applying this line of reasoning to the first of these projects, the kinetics of fast reactions in solution at short space-times (2×10^{-22} cm s to 3×10^{-12} cm s), see Figure 1, convinced us that such research had to be carried out using "hidden agendas," see Figure 2.

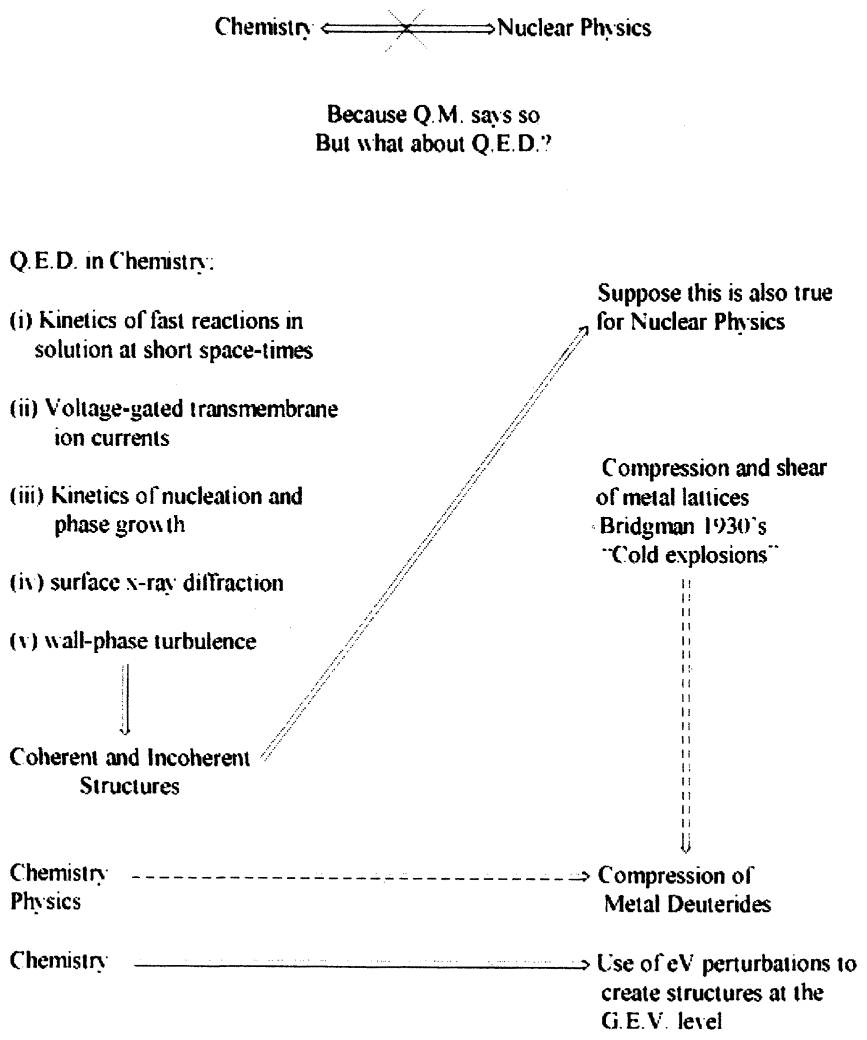
Chemistry
Nuclear Physics
Because Q.M. says so
But what about Q.E.D.?
Q.E.D. in Chemistry:
(i) Kinetics of fast reactions in solution at short space-times
(ii) Voltage-gated transmembrane ion currents
(iii) Kinetics of nucleation and phase growth
(iv) surface x-ray diffraction
(v) wall-phase turbulence
Coherent and Incoherent Structures
Suppose this is also true for Nuclear Physics
Compression and shear of metal lattices
Bridgman 1930's
"Cold explosions"
Chemistry
Physics
Compression of Metal Deuterides
Chemistry
Use of eV perturbations to create structures at the G.E.V. level

Figure 1. The scheme of research which led to the start-up of the "Cold Fusion" project.

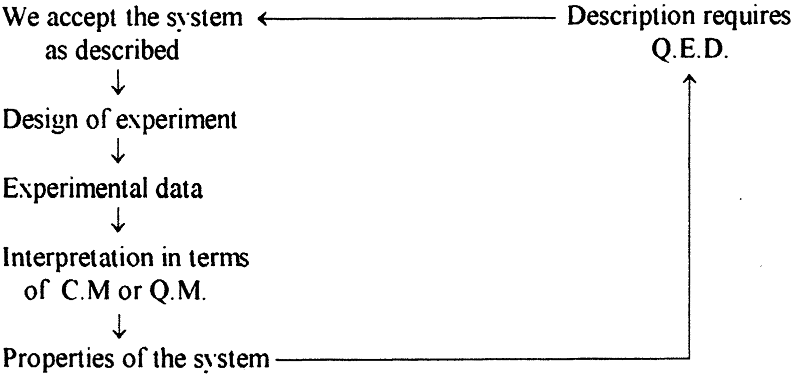
We accept the system as described
Design of experiment
Experimental data
Interpretation in terms of C.M or Q.M.
Properties of the system
Description requires Q.E.D.

Figure 2. The "hidden agendas" of the research projects.

Downloaded by PENNSYLVANIA STATE UNIV on July 1, 2012 | http://pubs.acs.org
Publication Date: August 1, 2008 | doi: 10.1021/bk-2008-0998.ch002

Thus, using such agendas, the systems are investigated within the accepted models of C.M. or Q.M.: the influence of many-body effects and of Q.E.D. had to emerge from the interpretation of the results. It will be evident that this particular strategy had the advantage of avoiding the presupposition of the importance of Q.E.D.; for example, it might well have turned out that such effects were unimportant and/or not measurable. The strategy also had the advantage of avoiding the premature criticisms of the multitude of scientists opposed to the application of Q.E.D. to condensed phase systems! The overall aim was the illustration of the developments of inconsistencies arising from the purely atomistic view of Quantum Physics: we need to answer the question whether the description of Nature requires collective dynamics (*field* dynamics in the physical jargon) for the analysis of the seemingly individual phenomena.

One conclusion which followed from these investigations of (i)-(iv) (Figure 1) was that condensed phase systems developed structures having dimensions lying between ~100-1000 Å, structures that played a crucial rôle in the behaviour of the systems.[5]

At a later date, we adopted the terminology of Q.E.D. Coherence (*1*) by describing the separation of the bulk material into Coherent and Incoherent Domains. We will confine attention here to just one of these topics (i)-(v) (Figure 1) namely, surface X-ray diffraction, (iv), as this methodology gives direct information about the structure of electrolyte solutions (topics (i) and (ii) were described briefly in the *Proceedings of the 9th International Conference on Cold Fusion* (*2*)). Two factors made such a seemingly impossible project feasible (*3*). The first was the advent of position sensitive single photon counting, Figures 3A and B; the second was the use of modulation techniques to enhance the selectivity towards surface diffraction, Figures 4A and B. Figure 3A illustrates the details of the methodology originally proposed, the use of a multiwire proportional counter in combination with a bright rotating anode source. However, in view of restrictions in the funding, the project was eventually carried out with a linear position sensitive detector in combination with a fixed anode source. We estimated that this caused a degradation in the performance by a factor in the range 100 to 1000. Figure 4A illustrates the diffractogram obtained when using a thin layer cell containing an electrode consisting of a thin film of silver. We observe the (111) and (200) diffractions of silver superimposed on a broad background due to diffraction from the aqueous solution in the cell. Clearly, such diffractograms do not give any useful information. However, modulation of the potential between the values for the observation of the silver surface alone and that for underpotential deposition of a single layer of lead (*4*) coupled to long data acquisition and the use of a 15-point triangular smoothing window, gave the difference diffractogram illustrated in Figure 4B.[6] The main features seen in Figure 4B are a loss of order around $2\theta = 17°$ and 44°, a differential shaped feature centered around $2\theta = 26°$ and, associated with this a differentiation of the peak at $2\theta = 38°$ due to the Ag (111) reflection. The loss of structure at 44° is particularly interesting as this corresponds to the Ag (200) peak which is reduced in magnitude as the lead monolayer is formed. From optical and voltametric studies it has been concluded (*4*) that deposition of lead on Ag (100) surfaces corresponds to a higher order phase transformation which would lead to a marked change in the structure factor but no clearly defined diffraction peak. By contrast deposition on Ag (111) surfaces has been assigned to a first order phase transformation. It is logical therefore to assign the differential peak to the formation of an incommensurate monolayer on the (111) facets of the polycrystalline silver film electrode. However, the most surprising results of the investigation were the observation of the differential peak centered around $2\theta = 26°$ and the loss of structure around $2\theta = 17°$. The first is most logically attributed to a lengthening of the O-O distance in the water near the electrode surface as the lead monolayer is formed (the large peak centered around $2\theta = 26°$ is generally attributed to hydrogen bonded water). We can judge this change in structure to involve the equivalent of 20-50 monolayers of water. The second, corresponding to a nearest neighbour distance of 6-8 Å is most likely due to a change in the ion distribution; we can see that the distribution of ions is much more highly ordered than that predicted by present day models of electrolyte solutions.

---

[5] It follows, therefore, that the effects of these structures are most readily investigated by carrying out experiments on systems having such small dimensions.

---

[6] We note that it is possible to observe such difference diffractograms notwithstanding the degradation of the performance implied by using the instrumentation illustrated in Figure 3B rather than that originally envisaged, Figure 3A.

Downloaded by PENNSYLVANIA STATE UNIV on July 1, 2012 | http://pubs.acs.org
Publication Date: August 1, 2008 | doi: 10.1021/bk-2008-0998.ch002

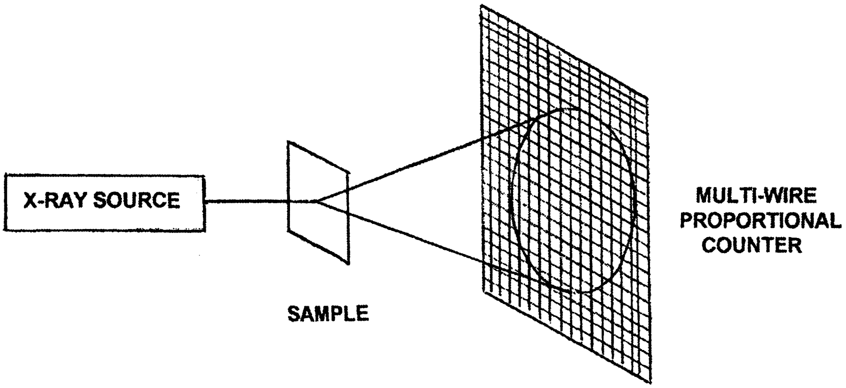

Figure 3A. Proposed experiment for measuring x-ray diffraction.

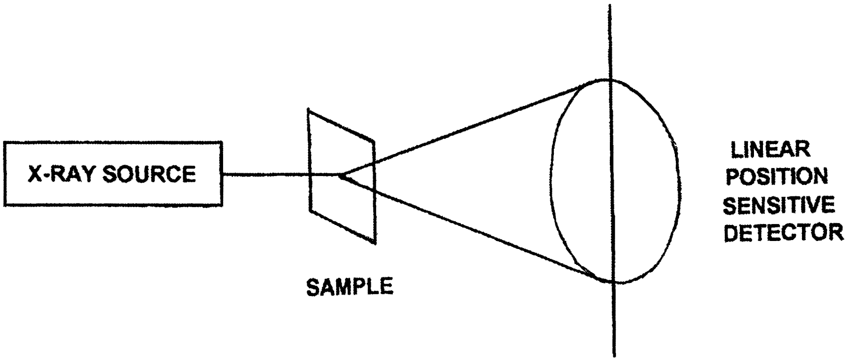

Figure 3B. Execution of the experiment on surface x-ray diffraction.

The main conclusion which follows from the investigation is that we cannot achieve a complete description of the system in terms of the left-hand-side of the "hidden agendas" of Figure 2. Such a description must clearly involve strong interactions between all the species in the interfacial regions, i.e., we have to consider the many-body problem within the context of field theory. We note that the application of Q.E.D. to the solvent and electrolyte solutions shows that the solvent (water) must be divided into two domains, one in which the solvent is highly structured (the coherent regions) and the second (the incoherent regions) in which the solvent is disordered; electrolyte is expelled from the coherent into the incoherent regions where it in turn forms ordered

Downloaded by PENNSYLVANIA STATE UNIV on July 1, 2012 | http://pubs.acs.org
Publication Date: August 1, 2008 | doi: 10.1021/bk-2008-0998.ch002

Downloaded by PENNSYLVANIA STATE UNIV on July 1, 2012 | http://pubs.acs.org
Publication Date: August 1, 2008 | doi: 10.1021/bk-2008-0998.ch002

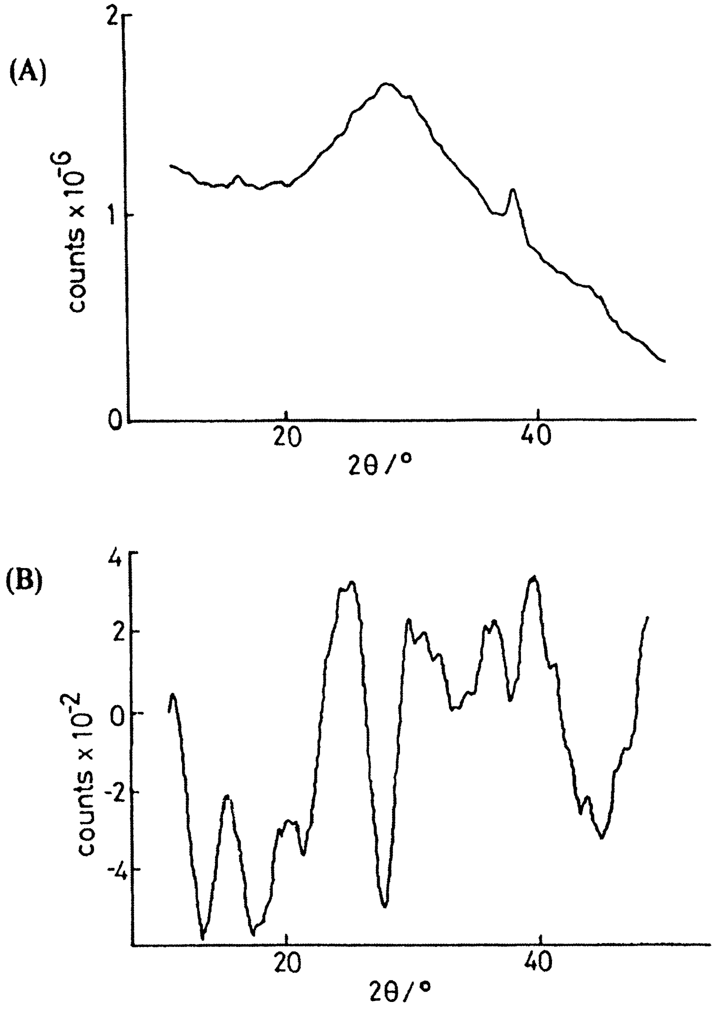

Figure 4. In situ x-ray diffractograms for a thin silver electrode in 100 mM $Pb(ClO_4)_2$ + 0.5M $NaClO_4$ + 1mM $HClO_4$. (A) Diffractogram obtained after 50 h at –400 mV. (B) Difference diffractogram (diffractogram at –400 mV minus that at –100 mV) after 100 h modulation at 10^{-2} Hz.

domains (*1, 2, 5, 6*). This line of reasoning prompts us to attribute the changes in the diffractogram, Figure 4B, at $2\theta < 26°$ to the selection of coherent domains by the underpotential monolayer of lead on the silver substrate coupled to an enhancement of the scattering from the incoherent regions.

By 1983 we had reached a position where it seemed logical to ask the next question posed in Figure 1: suppose the division of solid phases into coherent and incoherent structures was also true for Nuclear Physics. If that was so, then would we be able to use the perturbations at the 1 eV level (characteristic of chemical changes) to create coherent structures at the GEV level? Furthermore, would we be able to observe nuclear processes in such structures? Of course, in posing these questions we were also influenced by other relevant work such as the interpretation of Mossbauer spectra, see (*1*), and, especially, the observations of "Cold Explosions" by Bridgman in the 1930s (*7*).[7] Furthermore, we knew that the absorption of hydrogen isotopes can lead to a similar fragmentation. This then was the background which led to the specification of the first system for our investigations; the highly forced electrolytic charging of palladium cathodes with deuterons.[8] It is appropriate here to comment also on the chosen methodology, the measurement of the thermal balances using calorimetry (*8, 9*). It was clear at that time that the favoured methods of Nuclear Physics could only be applied to the systems we had in mind following many modifications and with numerous restrictions. Furthermore, there were ambiguities in the interpretation of some of the results which had been obtained.[9] On the other hand, the measurement of thermal balances would be straightforward and inexpensive (an important factor as we were carrying out the initial investigation at our own expense) and such methods could achieve a high sensitivity and be reasonably free from ambiguities (however, see further below).

We therefore embarked on this project but without any expectation that we would obtain definitive results. The Pd/D system was investigated (coupled to the use of the Pt/D system as a suitable "blank"). However, the outcome was

Downloaded by PENNSYLVANIA STATE UNIV on July 1, 2012 | http://pubs.acs.org
Publication Date: August 1, 2008 | doi: 10.1021/bk-2008-0998.ch002

---

[7] Intense compression and shear of lattices can lead to their fragmentation into small particles in which the high energy of the initial system is converted into kinetic energy of the fragments. We believed (and still believe) that this is a process which can only be explained by Q.E.D.

[8] Although we could see that the results obtained opened the way for very wide-ranging investigations, our own work never progressed beyond this initial concept. We described the resources required for the much wider investigations as equivalent to a Manhattan II project; this was true even for the much more limited scope of a project which remained restricted to the charging with deuterium of palladium based host lattices.

[9] See, for example, the interpretation of the tracks due to $^{3}T^{+}$ and $^{1}H^{+}$ in a Wilson Cloud Chamber (*10, 11*), an experiment carried out following the discovery of the first hot fusion reaction (*12*).

radically different to our expectations: the generation of excess enthalpy without any significant formation of the fusion products produced in dilute high temperature plasmas.[10] When the project reached the public domain (*8, 9*), it became clear that our expectations with regard to the use of calorimetric methods could not be realised and it is important at this stage to ask why this might have been so?

One of the causes is undoubtedly the inherent irreproducibility of the phenomenon. We believe that the process which we have observed takes place in the bulk of the electrode (*8, 9*), as mediated by the surface reactions. We can see that this immediately builds in inherent irreproducibilities into the system. Moreover, it has not generally been appreciated that although it is relatively straightforward to produce palladium electrodes, the metallurgy of palladium is difficult leading to the use of unsatisfactory (and inadequately specified) electrode materials.

However, the major reason is undoubtedly the fact that the calorimetry of electrode reactions has not emerged as a viable methodology (it remains confined to a number of sub fields such as the measurement of self-discharge in batteries). Papers dealing with the precision and accuracy of calorimetric methods and comparisons of various studies[11] are rejected outright by Journal Editors and referees[12,13] so that the study of calorimetry does not advance. The rather wild statements which have been made in the literature about the precision and accuracy of calorimetry as applied to the Pd-D system have undoubtedly also been due to the complexities of excess enthalpy generation in this system. Thus, it does not appear to have been realised that it is impossible to calibrate any calorimetric system if this is subject to fluctuating sources of enthalpy generation. Such calibrations require at the very least a constancy of the rate of excess enthalpy generation but, better, a zero value of this rate. It follows, therefore, that such calibrations must be carried out when using suitable "blank" systems. The intervention of "positive feedback" in the Pd-D system is especially troublesome in this regard (*14*). We illustrate this point by two calibrations carried out by the New Hydrogen Energy Group in Japan, Figures 5A and B. The onset of "positive feedback" leads to a delayed approach to the steady state following the application of the calibration pulse and a delayed decay to the base-line following the termination of this pulse, Figure 5B. Not

Downloaded by PENNSYLVANIA STATE UNIV on July 1, 2012 | http://pubs.acs.org
Publication Date: August 1, 2008 | doi: 10.1021/bk-2008-0998.ch002

---

[10] The formation of ^3T could be shown to be far above that which could be attributed to isotopic separation with any reasonable choice of separation factors; the formation of neutrons appeared to be confined to the non-steady state of operation of the cells; the formation of ^4He could be detected but could not be related to the magnitude of the excess enthalpy generation.

[11] Admittedly with regard to studies in "Cold Fusion."

[12] However, the usual outcome is that such papers are simply returned to the authors without comment.

[13] For one such study see Ref. (13).

Downloaded by PENNSYLVANIA STATE UNIV on July 1, 2012 | http://pubs.acs.org
Publication Date: August 1, 2008 | doi: 10.1021/bk-2008-0998.ch002

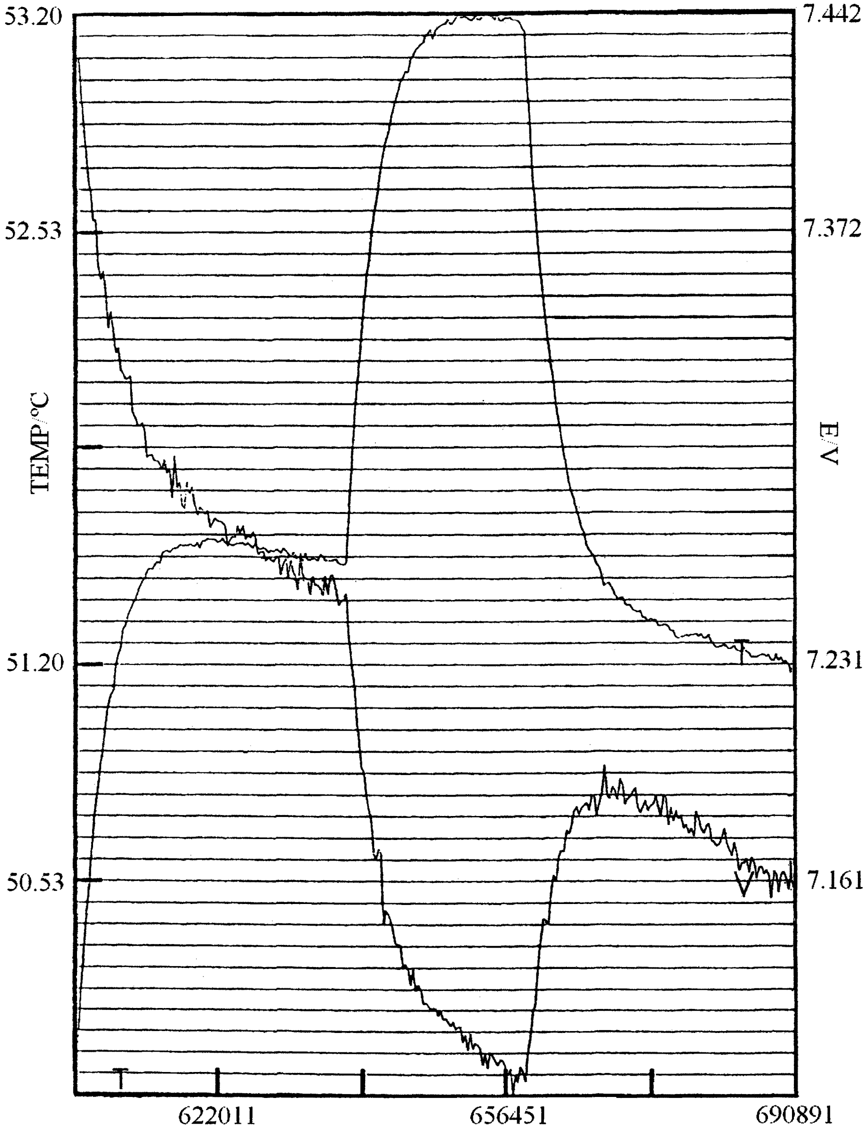

Figure 5A. calibration of an Icarus cell during the early stages of experiment 4661 conducted by N.H.E. Cathode: 0.4 cm diameter by 1.25 cm length polarised in 0.1 M LiOD/D_2O; cell current 0.5A; calibration pulse $\Delta Q = 0.2504$ W

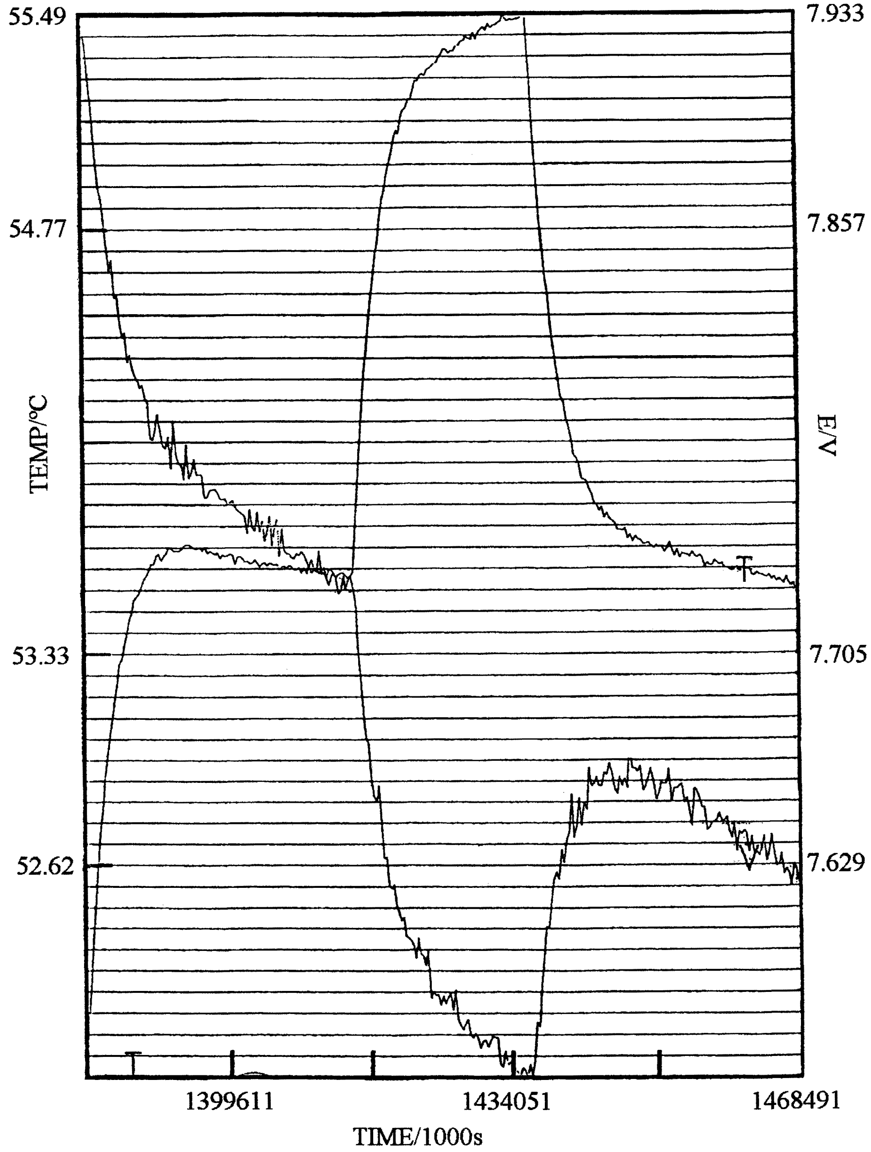

Figure 5B. A calibration during the later stages of experiment 4661.

Downloaded by PENNSYLVANIA STATE UNIV on July 1, 2012 | http://pubs.acs.org
Publication Date: August 1, 2008 | doi: 10.1021/bk-2008-0998.ch002

surprisingly, attempts to derive the true heat transfer coefficient from calibrations subject to such effects lead to the impossible result that the true heat transfer coefficient is smaller than the lower-bound value, e.g. see Ref. (*15*). As we have already noted, exact evaluations of the precision and accuracy of the instrumentation require experiments using "blank systems," e.g., see Ref. (*13*).

We must also acknowledge the fact that in the presence of excess enthalpy generation a part of this excess enthalpy may be generated outside certain designs of calorimetric cells (e.g. by the intervention of soft x-rays). This is a further factor which could lead to invalid estimates of the accuracy and precision of calorimeters investigated solely by using the Pd-based systems in D_2O-based electrolytes.

Our Conference Chairman has suggested that it would be useful if I were to give an indication of the papers on the general area of "Cold Fusion" which I have found especially interesting. I have found this to be an invidious task because, having Catholic tastes in science, I have found all the papers interesting even when I have approached these with some scepticism. Moreover, the field of publications is now very wide. However, Table I gives some indication of those which have aroused my special interest.

I note in the first place, the papers which attempt to find a theoretical basis for the subject, Chapter 8 in Refs. (*1, 16-19*). Clearly, it will prove to be impossible to advance the research in the absence of such a theoretical foundation (or, at any rate, progress would be greatly impeded). As my interest in the subject area was part of a general investigation of the role of Q.E.D. in the Natural Sciences, I have naturally been strongly drawn to the approach of Giuliano Preparata.

It will be seen that I have separated from this section (dealing with theoretical aspects) the paper by Del Giudice, De Ninno, and Frattolillo covering a possible consequence of Q.E.D. Coherence namely, the question of whether we can explain transmutations at low energies (*20*). This subject area (*21*) (and see also Ref. (*22*)) originally seemed quite unreasonable. It also remains to be established how the generation of ^{4}He (*23, 24*) is related to the wider area of low energy transmutations. The contributions of Miles and McKubre are noteworthy in that they establish a correlation between excess heat production and the formation of ^{4}He; that of Bockris and his co-workers in that they establish the formation of ^{4}He in the lattice of Pd. I note also that Miles has reported the first measurements using fluidized beds of Pd particles (*26*). The work of McKubre et al. using flow calorimetry has established that excess heat production is not an artefact of isoperibolic calorimetry!

The listing in Table I has also singled out a number of other contributions including that on charged particle emissions (*27*) and laser stimulation of excess heat production (*28*). Measurements at much lower incident energies of the deuteron beam than those used hitherto in the investigation of "Hot Fusion" have shown that more complicated collision processes come into play at such lower energies such as the channel (D) (*29*) than the channels (A) - (C) which have been observed in "Hot Fusion":

Downloaded by PENNSYLVANIA STATE UNIV on July 1, 2012 | http://pubs.acs.org
Publication Date: August 1, 2008 | doi: 10.1021/bk-2008-0998.ch002

Downloaded by PENNSYLVANIA STATE UNIV on July 1, 2012 | http://pubs.acs.org
Publication Date: August 1, 2008 | doi: 10.1021/bk-2008-0998.ch002

Table I. Some Milestones in Cold Fusion Research

G. Preparata et al.	Theory of the subject, Chapter 8 in (*1*), (*16*)
P. Hagelstein	Theories of the subject (*17*)
Scott R. Chubb	Theories of the subject (*18*)
Y. Kim	Theories of the subject (*19*)
E. Del Giudice, De Ninno, et al.	Theory of transmutations at lower energies (*20*)
Y. Iwamura	Low energy transmutations (*21*)
G. H. Miley	Low energy transmutations (*22*)
M. H. Miles	Correlation of excess heat with production of ^{4}He (*23*); fluidized beds (*26*)
M. McKubre	Correlation of excess heat with production of ^{4}He; flow calorimetry (*24*)
J. O'M. Bockris	Generation of ^{4}He in the lattice; transmutations (*25*)
E. Del Giudice; De Ninno, et al.	The importance of the vector potential; generation of ^{4}He; melting of electrodes (*30, 31*)
F. E. Cecil et al.; and others	Charged particle emissions (*27*)
D. Letts	Laser stimulation (*28*)
E. Takahashi	"Hot fusion" processes at low incident deuteron beam energies
Y. Arata	Generation of heat in small particles (*36*); see also comments in main text (*37*)
S. Szpak	Hot spots and mini explosions (*38*); codeposition of Pd and D (*39, 40*)
G. Mengoli	Heat after Death (after effect) (*41*)
Dispersed authorship	Isotopic abundances; evidence for photofission; transmutations

$D^{+} + D^{+} \rightarrow H^{+}$ (3 MeV) + T^{+} (1 MeV) ~ 50% (A)

$D^{+} + D^{+} \rightarrow$ n (2.5 MeV) + $^{3}He^{+4}$ (0.81 MeV) ~ 50% (B)

$D^{+} + D^{+} \rightarrow {}^{4}He + \gamma$ (24 MeV) ~ 50% (C)

$D^{+} + D^{+} + D^{+} \rightarrow T^{+}$ (4.75 MeV) + $3He^{2+}$ (4.75 MeV) ~ 10^{-2}% (D)

One can therefore speculate whether channel (C) which has a very low cross-section for fusion at low pressures, may not have a much higher cross-section for fusion in a lattice where the production of ^{4}He is evidently not accompanied by the generation of a γ-ray (*1*).

The development of the theoretical studies (*1, 16*) has led to a recognition that one can use the electric potential developed along a thin strip (a component of the vector potential) to enhance the generation of excess enthalpy (*30, 31*). This is in fact the Quantum Mechanical consequence of coherence in the electrodiffusion of deuterium in palladium.[14] The formation of ^{4}He commensurate with excess enthalpy generation has been observed. Under extreme conditions the thin strips melt (boil?) in the most negatively polarised region.[15] In this context, I also note the work of Arata (*36*) on the generation of excess enthalpy in nanoparticles of palladium. A plausible interpretation of these experiments is that these particles are destroyed by a single step (or, at any rate, by a small number of steps).[16] Our own consideration of such limiting patterns of behaviour (*37*) led us to the consideration of the compound Na_2ReD_9. At the time of our discussions, this compound did not exist whereas Na_2ReH_9 was known. Moreover, two research groups expert in the Chemistry of relevant syntheses, failed to make the deuterated species. Although it is possible to devise numerous arguments to explain the non-existence of Na_2ReD_9, the simplest of these is that this compound disintegrates on the typical time-scales of chemical syntheses. It is evident that we need to develop "calorimetric syntheses" to study the production of such potentially high energy materials.

In this context, we should also note the direct thermal imaging of "hot spots" on the surfaces of electrodes using infra-red imaging (*38*). Developments of this methodology (e.g. by using scanning laser-thermometry) should allow the direct determination of the space-time distributions of the fusion steps as well as

---

[14] The electrodiffusion of hydrogen in palladium was first observed by A. Coehn in 1929 (*32*). The propagation of the γ-phase of Pd-H along a wire is discussed in (*33*).

[15] The importance of this observation is that we can estimate the specific rate of excess enthalpy generation required to achieve this condition. These estimates lie in the range 0.5-50$MWcm^{-3}$ depending on the nature of the assumptions. Such high rates must be contrasted with the prolonged generation of excess enthalpy at the boiling points of the electrolyte in a "conventional" electrochemical system where the specific excess rate remained restricted to ~ 2$KWcm^{-3}$ (*34, 35*).

[16] Which will explain our choice of "massive" electrodes for our investigations.

Downloaded by PENNSYLVANIA STATE UNIV on July 1, 2012 | http://pubs.acs.org
Publication Date: August 1, 2008 | doi: 10.1021/bk-2008-0998.ch002

of the Q-values of these steps. Two of the authors have also introduced a new variant of the electrochemical method of generating excess enthalpy: the electrolytic codeposition of palladium and deuterium (*39*). It has been shown that this method leads to enhanced rates of excess enthalpy generation as compared to the standard method of electrolytic charging of massive electrodes with deuterium (*40*).

I note finally an extreme example of enthalpy generation but at zero enthalpy input at temperatures close to the boiling point of the electrolyte, a phenomenon which has been variously called "After-Effect" (*41*), "Heat-after-Death," and "Heat-after-Life." Such enthalpy production has been maintained for durations of up to 8 days.

I believe that the work carried out thus far amply illustrates that there is a new and richly varied field of research waiting to be explored. Moreover, it seems likely that it will be possible to develop new sources of energy which will be able to operate over a wide range of conditions. Most of the work to date has been carried out at temperatures below the boiling point of the electrolyte but we note that more than 50% of the world's energy is consumed at temperatures below 70°C. We also note that it would be relatively straightforward to raise the Quality of the heat by using well-established methods.

Downloaded by PENNSYLVANIA STATE UNIV on July 1, 2012 | http://pubs.acs.org
Publication Date: August 1, 2008 | doi: 10.1021/bk-2008-0998.ch002

References

1. Preparata, G. *QED Coherence in Matter.* World Scientific: Singapore, 1995.
2. Fleischmann, M. Searching for the Consequences of Many-Body Effects in Condensed Phase Systems. In *Condensed Matter Nuclear Science: Proceedings of the 9th International Conference on Cold Fusion*, Beijing, China, May 19-24, 2002; Li, X. Z., Ed.; Tsinghua Univ. Press: Beijing, 2002; III.
3. Fleischmann, M.; Oliver A.; Robinson, J. In Situ X-ray Diffraction Studies of Electrode Solution Interfaces. *Electrochimica Acta* **1986**, *31*, 899-906.
4. Bewick, A.; Thomas, B. Effects of Substrate Orientation on Underpotential Monolayers of Pb and Tl Deposited on Single Crystals. *J. Electroanal. Chem.* **1976**, *70* (2), 239-244. See also Bewick, A.; Thomas, B. Optical and Electrochemical Studies of the Underpotential Deposition of Metals. Part III: Lead Deposition on Silver Single Crystals. *J. Electroanal. Chem.* **1977**, *84*, 127-140, and Bewick, A.; Thomas, B. Optical and Electrochemical Studies of the Underpotential Deposition of Metals. Part II: Phase Transitions and Two-Dimensional Nucleation. *J. Electroanal. Chem.* **1977**, *85*, 329-337.
5. Arani, A.; Bono, I.; Del Giudice, E.; Preparata, G. QED Coherence and the Thermodynamics of Water. *Int. J. Mod. Phys. B* **1995**, *B9* (15), 1813-1841.
6. Del Giudice, E.; Preparata, G.; Fleischmann, M. QED Coherence and Electrolyte Solutions. *J. Electroanal. Chem.* **2000**, *482* (2), 110-116.
7. Bridgman, P.W. *The Physics of High Pressure*, International Textbooks of Exact Science: London, UK, 1947.

8. Fleischmann, M.; Pons, S.; Hawkins, M. Electrochemically Induced Nuclear Fusion of Deuterium. *J. Electroanal Chem.* **1989**, *261*, 301; Errata, **1989**, *263*, 187.
9. Fleischmann, M.; Pons, S.; Anderson, M. W.; Li, L. J.; Hawkins, M. Calorimetry of the Palladium-Deuterium-Heavy Water System. *J. Electroanal. Chem.* **1990**, *287*, 293.
10. Dee, P.I. *Nature* **1934**, *113*, 564.
11. Dee, P. I. Some Experiment upon Artificial Transmutations Using the Cloud-Track Method. *Proc. Roy. Soc.* **1935**, *148A*, 623.
12. Oliphant, M. C.; Harteck, P.; Lord Rutherford. Transmutation Effect Observed With Heavy Hydrogen. *Nature* **1934**, *113*, 413.
13. Fleischmann, M.; Miles, M. H. The Instrument Function of Isoperibolic Calorimeters: Excess Enthalpy Generation due to the Parasitic Reduction of Oxygen. In *Condensed Matter Nuclear Science: Proceedings of the 10th International Conference on Cold Fusion*, Cambridge, MA, Aug. 24-29, 2003; Hagelstein, P. L.; Chubb, S. R., Eds.; World Scientific Publishing Co.: Singapore, **2006**; 247-268.
14. Fleischmann, M.; Pons, S.; Le Roux, M.; Roulette, J. Calorimetry of the Pd-D2O System: The Search for Simplicity and Accuracy. *Trans. Fusion Technol.* **1994**, *261*, 323-343.
15. Fleischmann, M.; More About Positive Feedback; More About Boiling. In *Proceedings of the Fifth International Conference on Cold Fusion*, Monte Carlo, Monaco, April 9-13, 1995; Pons, S., Ed.; IMRA Europe: Sophia Antipolis Cedex, France, **1995**; 140.
16. Bressani, T.; Del Giudice, E.; Preparata, G. First Steps toward an Understanding of "Cold" Nuclear Fusion. *Nuovo Cimento* **1989**, *105A*, 845. See also Preparata, G. Setting Cold Fusion in Context: A Reply. In *Proceedings of the Fifth International Conference on Cold Fusion*, Monte Carlo, Monaco, April 9-13, 1995; Pons, S., Ed.; IMRA Europe: Sophia Antipolis Cedex, France, **1995**; 265-284.
17. Hagelstein, P. Unified Phonon-Coupled SU(N) Models for Anomalies in Metal Deuterides. In *Condensed Matter Nuclear Science: Proceedings of the 10th International Conference on Cold Fusion*, Cambridge, MA, Aug. 24-29, 2003; Hagelstein, P. L.; Chubb, S. R., Eds.; World Scientific Publishing Co.: Singapore, **2006**; 837-869.
18. Chubb, S. R. Nuts and Bolts of the Ion Band State Theory. In *Condensed Matter Nuclear Science: Proceedings of the 10th International Conference on Cold Fusion*, Cambridge, MA, Aug. 24-29, 2003; Hagelstein, P. L.; Chubb, S. R., Eds.; World Scientific Publishing Co.: Singapore, **2006**; 735-751.
19. Kim, Y. Quantum Many-Body Theory of Low Energy Nuclear Reaction Induced by Acoustic Cavitation in Deuterated Liquid. In *Condensed Matter Nuclear Science: Proceedings of the 10th International Conference on Cold Fusion*, Cambridge, MA, Aug. 24-29, 2003; Hagelstein, P. L.; Chubb, S. R., Eds.; World Scientific Publishing Co.: Singapore, **2006**; 779-787.

Downloaded by PENNSYLVANIA STATE UNIV on July 1, 2012 | http://pubs.acs.org
Publication Date: August 1, 2008 | doi: 10.1021/bk-2008-0998.ch002

20. Del Giudice, E.; De Ninno, A.; Frattolillo, A. Are Nuclear Transmutations Observed at Low Energies Consequences of Qed Coherence? In *Condensed Matter Nuclear Science: Proceedings of the 10th International Conference on Cold Fusion*, Cambridge, MA, Aug. 24-29, 2003; Hagelstein, P. L.; Chubb, S. R., Eds.; World Scientific Publishing Co.: Singapore, **2006**; 831-835.
21. Iwamura, Y.; Itoh, T.; Sakano, M. Nuclear Products and Their Time Dependence Induced by Continuous Diffusion of Deuterium through Multi-Layer Palladium Containing Low Work Function Material. In *ICCF8: Proceedings of the Eighth International Conference on Cold Fusion*, Lerici (La Spezia), Italy, May 21-26, 2000; Scaramuzzi, F., Ed.; Italian Physical Society: Bologna, Italy, 2001; 141-146. See also Iwamura, Y.; Itoh, T.; Sakano, M.; Sakai, S. Observation of Low Energy Nuclear Reactions Induced By D2 Gas Permeation Through Pd Complexes. In *Condensed Matter Nuclear Science: Proceedings of the 9th International Conference on Cold Fusion*, Beijing, China, May 19-24, 2002; Li, X. Z., Ed.; Tsinghua Univ. Press: Beijing, 2002; 141-146.
22. Miley, G. H.; Shrestha, P. Review of Transmutation Reactions in Solids. In *Condensed Matter Nuclear Science: Proceedings of the 10th International Conference on Cold Fusion*, Cambridge, MA, Aug. 24-29, 2003; Hagelstein, P. L.; Chubb, S. R., Eds.; World Scientific Publishing Co.: Singapore, 2006; 361.
23. Bush, Benjamin F.; Lagowski, J. J.; Miles, M.; Ostrom, G. S. Helium Production during the Electrolysis of D2O in Cold Fusion Experiments. *J. Electroanal. Chem.* **1991,** *304,* 271.
24. McKubre, M.; Tanzella, F. L.; Tripodi, P.; Hagelstein, P. L. The Emergence of a Coherent Explanation for Anomalies Observed in D/Pd and H/Pd System: Evidence for 4He and 3He Production. *Proceedings of the Eighth International Conference on Cold Fusion*, Lerici (La Spezia), Italy, May 21-26, 2000; Scaramuzzi, F., Ed.; Italian Physical Society: Bologna, Italy, 2000; 3.
25. Chien, C. C.; Hodko, D.; Minevski, Z.; Bockris, J. O'M. On an Electrode Producing Massive Quantities of Tritium and Helium. *J. Electroanal. Chem.* **1992,** *338,* 189.
26. Miles, M. H. Fluidized Bed Experiments Using Platinum and Palladium Particles in Heavy Water. In *Condensed Matter Nuclear Science: Proceedings of the 10th International Conference on Cold Fusion*, Cambridge, MA, Aug. 24-29, 2003; Hagelstein, P. L.; Chubb, S. R., Eds.; World Scientific Publishing Co.: Singapore, 2006; 23-28.
27. Cecil, F. E.; Lin, H.; Galovich, C. S. Energetic Charged Particles from Deuterium Metal Systems. In *Condensed Matter Nuclear Science: Proceedings of the 10th International Conference on Cold Fusion*, Cambridge, MA, Aug. 24-29, 2003; Hagelstein, P. L.; Chubb, S. R., Eds.; World Scientific Publishing Co.: Singapore, 2006; 535-538.

Downloaded by PENNSYLVANIA STATE UNIV on July 1, 2012 | http://pubs.acs.org
Publication Date: August 1, 2008 | doi: 10.1021/bk-2008-0998.ch002

28. Letts, D.; Cravens, D. Laser Stimulation of Deuterated Palladium: Past and Present. In *Condensed Matter Nuclear Science: Proceedings of the 10th International Conference on Cold Fusion*, Cambridge, MA, Aug. 24-29, 2003; Hagelstein, P. L.; Chubb, S. R., Eds.; World Scientific Publishing Co.: Singapore, 2006; 159.
29. Isobe, Y., Uneme, S.; Yabuta, K.; Mori, H.; Omote, T.; Ueda, S.; Ochiai, K.; Miyamaru, H.; Takahashi, A. Search for Coherent Deuteron Fusion by Beam and Electrolysis Experiments. In *ICCF8: Proceedings of the Eighth International Conference on Cold Fusion*, Lerici (La Spezia), Italy, May 21-26, 2000; Scaramuzzi, F., Ed.; Italian Physical Society: Bologna, Italy, 2001; 17.
30. Del Giudice, E.; De Ninno, A.; Frattolillo, A.; Preparata G.; Scaramuzzi F.; Bulfone A.; Cola M.; Giannetti C. The Fleischmann-Pons Effect in a Novel Electrolytic Configuration. In *ICCF8: Proceedings of the Eighth International Conference on Cold Fusion*, Lerici (La Spezia), Italy, May 21-26, 2000; Scaramuzzi, F., Ed.; Italian Physical Society: Bologna, Italy, 2001; 47-54.
31. De Ninno, A.; Fratolillo, A.; Rizzo; A.; Del Giudice, E. 4He Detection in a Cold Fusion Experiment. In *Condensed Matter Nuclear Science: Proceedings of the 10th International Conference on Cold Fusion*, Cambridge, MA, Aug. 24-29, 2003; Hagelstein, P. L.; Chubb, S. R., Eds.; World Scientific Publishing Co.: Singapore, 2006; 133-138.
32. Cöhn, A. Protonen in Metallen. Z. *Elektrochem.* **1929**, *35*, 676.
33. Bartolomeo, C.; Fleischmann, M.; Laramona, G.; Pons, S.; Roulette, J.; Sugiura, H.; Preparata, G. Alfred Cöhn and After: The Alpha, Beta and Gamma of the Palladium-Hydrogen System. *Fusion Technol.* **1994**, *26*, 23.
34. Roulette, J.; Roulette, J.; Pons, S. Results of ICARUS 9 Experiments Run at IMRA Europe. In *Proceedings of the Sixth International Conference on Cold Fusion: Progress in New Hydrogen Energy*, Hokkaido, Japan, Oct. 13-18, 1996; Okamoto, M., Ed.; New Energy and Industrial Technology Development Organization: Tokyo, 1996; 85.
35. Fleischmann, M. Cold Fusion: Past, Present and Future. In *Proceedings of the Seventh International Conference on Cold Fusion*, Vancouver, Canada, April 19-24, 1998; ENECO, Inc.: Salt Lake City, UT, 1988; 119.
36. Arata, Y.; Zhang, Y. C. Picnonuclear Fusion Generated in "Lattice-Reactor" of Metallic Deuterium Lattice within Metal Atom-Clusters. In *Condensed Matter Nuclear Science: Proceedings of the 9th International Conference on Cold Fusion*, Beijing, China, May 19-24, 2002; Li, X. Z., Ed.; Tsinghua Univ. Press: Beijing, 2002; 5.
37. Pons, S.; Fleischmann, M. Unpublished work.
38. Szpak, S.; Mosier-Boss, P.A.; Dea, J.; Gordon, F. Polarized D+/Pd-D2O System: Hot Spots and "Mini-Explosions." In *Condensed Matter Nuclear Science: Proceedings of the 10th International Conference on Cold Fusion*, Cambridge, MA, Aug. 24-29, 2003; Hagelstein, P. L.; Chubb, S. R., Eds.; World Scientific Publishing Co.: Singapore, 2006; 13-22.

Downloaded by PENNSYLVANIA STATE UNIV on July 1, 2012 | http://pubs.acs.org
Publication Date: August 1, 2008 | doi: 10.1021/bk-2008-0998.ch002

39. Mosier-Boss, P. A.; Szpak, S. The Pd/(N)H System: Transport Processes and Development of Thermal Instabilities," *Nuovo Cimento, Soc. Ital. Fis. A* **1999**, *112*, 577.
40. Szpak, S.; Mosier-Boss, P. A.; Miles, M. H.; Fleischmann, M. Thermal Behavior of Polarized Pd/D Electrodes Prepared by Co-Deposition. *Thermochimica Acta* **2004**, *410*, 101-107.
41. Mengoli, G.; Bernadini, M.; Manduchi, C.; Zannoni, G. Calorimetry Close to the Boiling Temperature of the D2O/Pd Electrolytic System. *J. Electroanal. Chem.* **1998**, *444*, 155-167.

Downloaded by PENNSYLVANIA STATE UNIV on July 1, 2012 | http://pubs.acs.org
Publication Date: August 1, 2008 | doi: 10.1021/bk-2008-0998.ch002

Downloaded by YORK UNIV on July 1, 2012 | http://pubs.acs.org
Publication Date: August 1, 2008 | doi: 10.1021/bk-2008-0998.ch003

Chapter 3

An Approach to Nuclear Energy without Strong Nuclear Radiation

X. Z. Li, Q. M. Wei, and B. Liu

Department of Physics, Tsinghua University, Beijing 100084, China

Collaboration between chemists and physicists has been essential in the history of scientific discovery. In order to make the discovery more convincing to mainstream science, we have to have the theoretical prediction verified by the various independent experimental results. The splendid goal of nuclear energy without strong nuclear radiation has been the motivation of this untiring worldwide effort. The next steps are a self-sustaining reactor and the detection of the neutrino emission from the metal-hydrides (deuterides).

Introduction

Chemists have been the pioneers of scientific discovery because they are confident about their experimental tools such as calorimeters, chemical analysis, etc. However, they have always faced strong rejection from those physicists who were believers in their own theory without considering the limitations of their theory. The history of nuclear energy is a good example. Early in 1933, the famous physicist, Ernst Rutherford, alleged that any energy source based on nuclear transmutation was just "moonshine" (*1*). Six years later, in 1939, when Otto Hahn discovered barium after the bombardment of uranium by neutrons, he was so afraid of the physicists that he was always trying to figure out what was wrong with his experiment because barium was incredible (*2*). Unfortunately, Martin Fleischmann and Stanly Pons faced the same strong objections from physicists again in 1989, because physicists could not find the "commensurable neutron" emission. The physicists alleged that it was impossible to have "thunder without lightning." If they did not see the lightning they would not believe any thunder. Thus the physicists denied the experimental results in terms of their own theory, even if the amount of "excess heat" is greater than that from

In Low-Energy Nuclear Reactions Sourcebook; Marwan, J., et al.;
ACS Symposium Series; American Chemical Society: Washington, DC, 2008.

any conceivable chemical reactions. To their minds, the neutron was the "lightning" and the thunder was the "nuclear reaction."

Indeed the neutron is not a necessary product of any nuclear reaction. After a nuclear reaction between two positively charged nuclei only the charged particle is the necessary product, but not the neutron. Solar energy is an example (*3*). However, why did so many nuclear physicists try to detect the neutron emission from the electrolytic cell using a palladium cathode in heavy water? They were looking for deuteron-deuteron fusion, of which they had knowledge based on beam-target experiments only. Using accelerators, the physicists established two reactions:

$$d + d \rightarrow \begin{cases} n + {}^{3}He \\ p + T \end{cases}.$$

The physicists further inferred from these equations that whenever two deuterons enter in the nuclear force region they will emit neutrons. The physicists unconsciously assumed that the choice of the reaction channel would be independent of the penetration of the Coulomb barrier. They forgot the important effect of the resonance on tunneling, and the selectivity of the resonant tunneling.

Downloaded by YORK UNIV on July 1, 2012 | http://pubs.acs.org
Publication Date: August 1, 2008 | doi: 10.1021/bk-2008-0998.ch003

Importance of the Resonance on Tunneling

Early in the 1990s, a professor at Princeton University wrote a textbook on quantum mechanics (*4*). There was a special section to discuss "cold fusion." He intended to make some estimate favorable to cold fusion. Eventually he mistakenly proved that there was no way to have any detectable penetration of Coulomb barrier at low energy.

He made a great mistake when he assumed that the entire wave of penetrating deuterons would be absorbed by nuclear potential well immediately after its penetration. It looked like an assumption favorable to cold fusion, because there would be no reflected wave inside the nuclear potential well, and the entire deuteron wave entering the nuclear potential well would disappear instantly. Indeed this was the worst assumption for cold fusion because it killed the resonance. Consequently, there would be no resonant tunneling, which was essential to cold fusion.

Why is the reflection so important for resonance? Since resonance is essentially the constructive interference phenomenon, there must be two waves—incident wave and the reflected wave—in order to have this constructive interference. When the absorption kills the reflection totally, it kills the resonance too.

Without the constructive interference, the amplitude of the deuteron wave function would not be built up inside the nuclear potential well; hence, the tunneling current through the Coulomb barrier becomes negligible (exponentially small). This was just the result of Peebles' calculation (*4*).

In fact, Peebles' calculation just shows how important the resonance is by assuming an infinite absorption. Without resonance, there is no way to penetrate the Coulomb barrier at low energy.

Neutron Emission Should not be Taken as an Indication of Resonance at Low Energy

Downloaded by YORK UNIV on July 1, 2012 | http://pubs.acs.org
Publication Date: August 1, 2008 | doi: 10.1021/bk-2008-0998.ch003

Physicists might argue that all the negative results in neutron detection from the electrolytic cell just showed no resonance for a pair of deuterons at low energy. This was a mistake again because the neutron emission was no longer a good indication of the resonance at low energy due to the selectivity of the resonant tunneling.

The selectivity of the resonant tunneling means that the choice of the reaction channel depends on the thickness and the height of the Coulomb barrier. When the Coulomb barrier is very thick and high, the tunneling wave becomes very weak (exponentially small). It requires a lot of bouncing back and forth to build up the amplitude of the wave function in terms of the constructive interference inside the nuclear potential well in order to have a detectable effect of tunneling. This simply requires a long life-time of the probability wave of deuterons inside the nuclear potential well. Thus the resonant tunneling will select the long life-time channel only in the case of a thick and high barrier. The neutron emission channels are short life-time channels because they are induced by the strongest nuclear interaction. Hence, for the neutron emission channel there will be no chance to have any resonant tunneling at low energy.

Some physicists believed that the tunneling happens in two independent steps: penetration first, then decay independently. Hence they always asked why two deuterons could not emit neutrons when they stayed together. They forgot that penetration and decay were dependent processes. For the rapid decay channel there was no way to have any detectable tunneling at low energy.

This selectivity of resonant tunneling should be true for both cold fusion and "hot fusion"; hence, we may justify this concept first in terms of hot fusion data.

"Hot Fusion" Data Justify Selectivity of Resonant Tunneling

Having started from basic quantum mechanics, we may write the general expression of fusion cross-section of S-wave as (*5,6*):

$$\sigma_r = \frac{\pi}{k^2}\frac{(-4W_i)}{W_r^2 + (W_i - 1)^2}. \tag{1}$$

Here, k is the wave number of the incoming wave function; $W \equiv Cot\delta$, and δ is the phase shift when the incoming wave is scattered by a nuclear potential well. When nuclear fusion happens, there is absorption of the deuteron wave in the nuclear potential well. Hence, the nuclear potential is a complex potential; and this phase shift, δ, is a complex number as well. Thus $W = Cot\delta$ becomes a complex number, as does $W = W_r + iW_i$. This W just shows the resonance effect and the selectivity of resonance clearly. When its real part, W_r, approaches zero, there is a peak of cross-section. However, the height of peak depends on the imaginary part, W_i. If $W_i = 0$, it corresponds to the case of elastic scattering, and fusion cross-section $\sigma_r = 0$. If $W_i = -\infty$, it corresponds to the case of strong damping (Peebles' assumption (*4*)). The strong damping might kill the resonance totally, and the peak height of the fusion cross-section vanishes also. Indeed the peak height of the fusion cross-section reaches its maximum when $W_i = -1$. This is the selectivity of resonance which selects the matching damping.

We successfully applied this concept to the hot fusion data for deuteron-triton, for deuteron-helium3, and for deuteron-deuteron. Figure 1 shows the results of calculations based on the selective resonant tunneling model and comparison with the experimental data. The crosses are the experimental data points from the National Nuclear Data Center (NNDC) and the open circles are the results of calculation (*6*). Their agreements are better than those of the empirical five-parameter formula which has been listed in the Handbook of Plasma Physics for more than 25 years (*7*). This calculation even corrected an error in old NNDC data in 2002 (*8*). It further verifies the dependence of the reaction on the penetration using the data of astrophysics factor in 2004 (*6*).

Thus, hot fusion data have justified the selectivity of resonanttunneling. Thisselectivity of the resonant tunneling would be much sharper in the case of confined deuterons in the lattice potential well because the Coulomb barrier would be much higher and thicker there.

Downloaded by YORK UNIV on July 1, 2012 | http://pubs.acs.org
Publication Date: August 1, 2008 | doi: 10.1021/bk-2008-0998.ch003

Selectivity of Resonant Tunneling for a Pair of Confined Deuterons

The boundary condition plays the key role in wave mechanics. When an inward spherical wave was assumed at the boundary of the nuclear potential well (*4*), there was no chance for any resonance (Figure 2a) When a matching damping was assumed inside the nuclear potential well (i.e., $W_i = -1$), the resonance appeared and there was incoming spherical wave only at the distant edge of the Coulomb potential without any outgoing spherical wave (Figure 2b). The boundary condition for a pair of confined deuterons is very different from that in the beam-target case. An exponentially decaying wave has to be assumed

Downloaded by YORK UNIV on July 1, 2012 | http://pubs.acs.org
Publication Date: August 1, 2008 | doi: 10.1021/bk-2008-0998.ch003

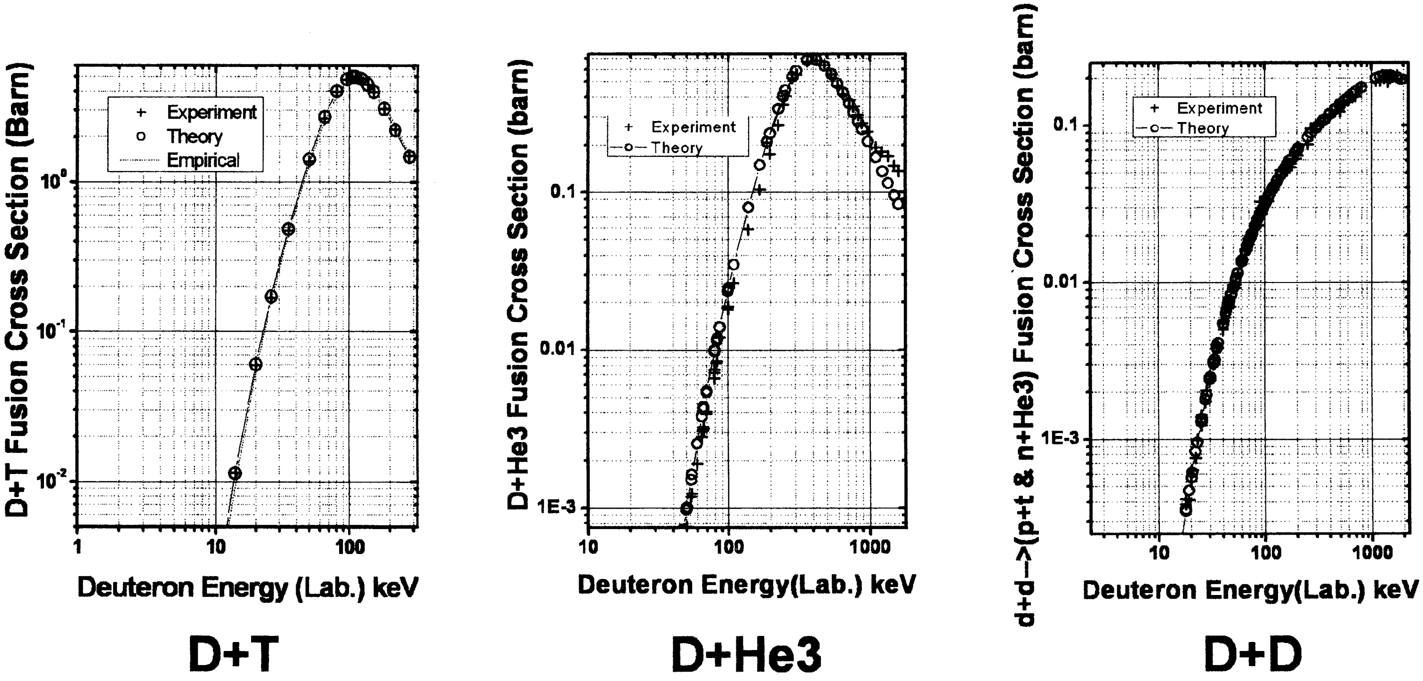

Figure 1. Comparison between theory and experiment.

In Low-Energy Nuclear Reactions Sourcebook; Marwan, J., et al.;
ACS Symposium Series; American Chemical Society: Washington, DC, 2008.

at the boundary of the lattice potential well (Figure 3). There is no deuteron beam to supply the incoming wave; hence, the conceptof fusion cross-section is no longer applicable here. Instead we have to introduce the concept of "tunneling current" of the confined particles. In order to keep a steadystate, we have to introduce another imaginary part of potential, U_{2i}, outside the nuclear potential well in order to balance the imaginary part, U_{1i} in the nuclear potential well. The tunneling current, J, is a function of U_{1i} and U_{2i}. As a result of conservation of the probability, the normalized tunneling current is

$$J = -\frac{1}{\hbar}\frac{U_{1i}U_{2i}}{(U_{1i}-U_{2i})}. \tag{2}$$

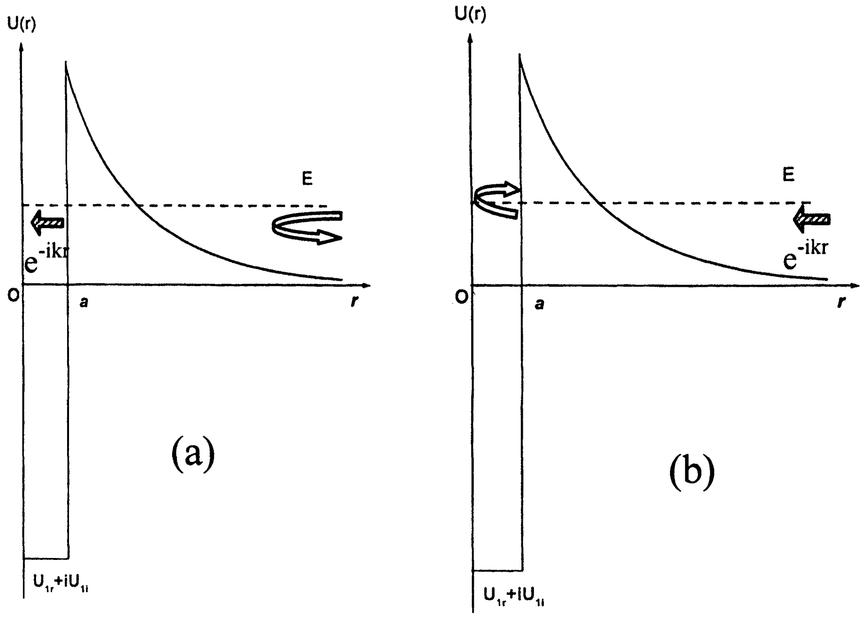

Figure 2. The boundary conditions for beam-target configuration: (2a) no reflection inside the nuclear potential well(W_i=-∞); and (2b) no reflection outside the nuclear potential well(W_i=-1).

Here, $U_{1i}< 0$ for the absorption in the nuclear potential well; and $U_{2i}> 0$ for the deuterium loading outside the nuclear potential well. $J< 0$ means a tunneling

Downloaded by YORK UNIV on July 1, 2012 | http://pubs.acs.org
Publication Date: August 1, 2008 | doi: 10.1021/bk-2008-0998.ch003

Downloaded by YORK UNIV on July 1, 2012 | http://pubs.acs.org
Publication Date: August 1, 2008 | doi: 10.1021/bk-2008-0998.ch003

current inward to the nuclear potential well. The maximized tunneling current, J_{max}, would appear when $|U_{1i}| = U_{2i}$. $J_{max} = -|U_{1i}|/2\hbar$.

On the other hand, U_{1i} and U_{2i} are related by the eigenequation for a pair of confined deuterons. In the case of resonance, the eigenequation gives (*9*)

$$U_{1i}U_{2i} = -\frac{C}{\theta^2}. \tag{3}$$

Here $(1/\theta)^2$ is the Gamow penetration factor, an exponentially small number.

$$J = -\frac{C}{\theta^2\hbar\left(|U_i| + \frac{C}{|U_i|\theta^2}\right)}. \tag{4}$$

θ is extremely large in the case of confined deuterons in lattice potential well; hence, the peak of the tunneling current becomes very sharp (Figure 4). In the case of resonance, there is a matching number of

$$[U_{1i}]_{peak} \sim -\frac{\sqrt{C}}{\theta}, \tag{5}$$

which makes the tunneling current peaked. The peak value of the tunneling current is $J_{peak} = -\sqrt{C}/(2\hbar\theta)$.

In general cases, $U_{2i} \neq |U_{1i}|$ and the tunneling current is on the order of $(1/\theta)^2$: $J \approx -O\left(\frac{1}{\theta^2}\right)$. Hence, the tunneling current would be enhanced by a factor of θ due to resonant tunneling. This is a very large enhancement. The width of this peak is on the order of $(1/\theta)$; hence, it is a very sharp peak. In other words, the resonant tunneling for a pair of deuterons selects a specific absorption rate, $|U_{1i}|_{\text{peak}}$, inside the nuclear potential well because of the exponentially large number, θ, at the very low incident energy. For any other absorption rate deviated from $|U_{1i}|_{\text{peak}}$, the tunneling current is suppressed by a factor of θ (see Eq. (4)) hence, the tunneling effect is not observable for any other absorption rate deviated from $|U_{1i}|_{\text{peak}}$.

U_{1i} is related to the life-time of the deuteron wave inside the nuclear potential well: $\tau_{life} \approx \hbar/|U_{1i}|$. The constant in eigenequation (*9*) may be written as $C = C_1\hbar^2 / \tau_N\tau_L$. Here, τ_N is the flight-time of the deuteron inside the nuclear potential well (see Figure 3), τ_L is the flight-time of the deuteron outside the nuclear potential well, and C_1 is a dimensionless constant on the order of 1.

Downloaded by YORK UNIV on July 1, 2012 | http://pubs.acs.org
Publication Date: August 1, 2008 | doi: 10.1021/bk-2008-0998.ch003

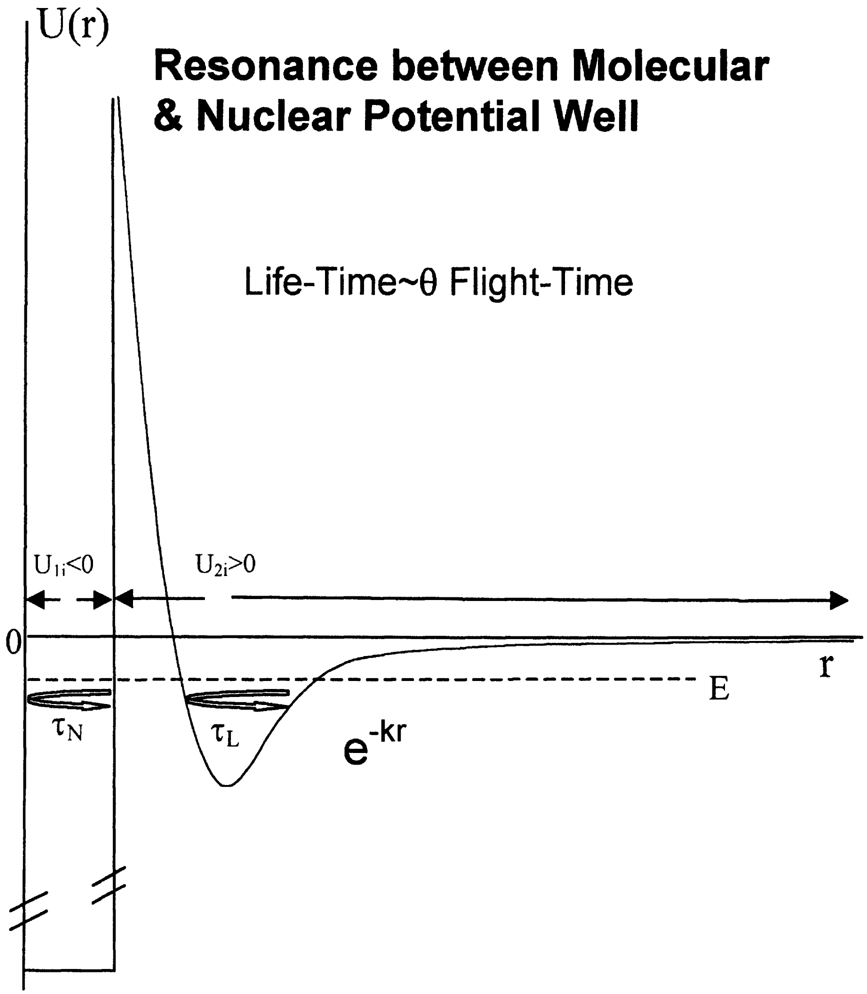
U(r)
Resonance between Molecular & Nuclear Potential Well
Life-Time~θ Flight-Time
$U_{1i}<0$
$U_{2i}>0$
0
τ_N
τ_L
E
r
e^{-kr}

Figure 3. The boundary condition for a pair of confined deuterons in lattice potential well.

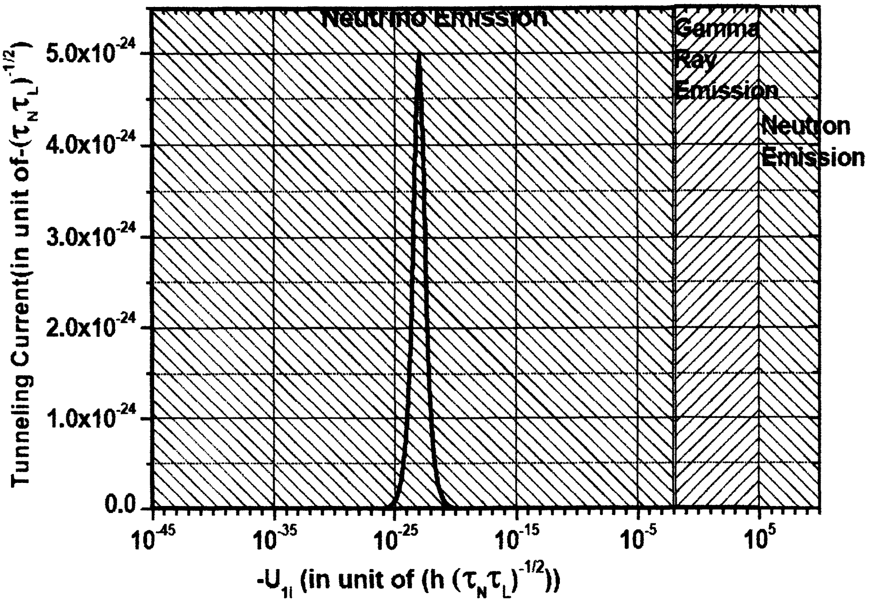

Figure 4. The peak shows the sharp selectivity of resonant tunneling ($\theta=10^{23}$).

Hence, the life-time of the deuteron inside the nuclear potential well has to satisfy

$$\tau_{life} \approx \theta\sqrt{\tau_N \tau_L} \qquad (6)$$

in order to have a detectable tunneling current. Since $\tau_{life} >> \tau_N$, the resonant tunneling selects only very slow reaction channels. For the neutron emission channel, the reaction time is on the order of τ_N. The matching condition, Eq. (5) or Eq. (6), is not satisfied; hence, there is no way to have any neutron emission as a result of selective resonant tunneling at low energy. This explains why the neutron emission cannot be taken as an indication of resonance between the nuclear potential well and the lattice potential well. The same argument might be applied to the gamma radiation. The electromagnetic interaction is still too strong to have any resonant tunneling for the reaction channel which emits the gamma ray or hard X-ray. Only the weak interaction (beta decay or K-capture) is slow enough to have an opportunity for resonant tunneling at low energy (see Figure 4). Consequently, the selective resonant tunneling solved the three puzzles proposed by a nuclear physicist in the 1990s (*10*).

Downloaded by YORK UNIV on July 1, 2012 | http://pubs.acs.org
Publication Date: August 1, 2008 | doi: 10.1021/bk-2008-0998.ch003

3-Deuteron Fusion Reaction – the Evidence of Resonant Tunneling

Is there really a long life-time state of two deuterons as a result of selective resonant tunneling? This should be a critical test of this resonant tunneling model. Fortunately, the anomalous yield of 3-deuteron fusion reaction provided the positive answer to this necessary test.

If there is a long life-time state of two deuterons as a result of selective resonant tunneling (the wave function of two deuterons changes from D_2-molecule-like to the linear combination of $^4He^*$-like and D_2-molecule-like), then these two deuterons would have a chance to see the third deuteron. Hence, we are supposed to see the 3-deuteron fusion reactions if there is any resonant state of two deuterons with a long life-time in the target. In the traditional beam-target experiment, the target is made of titanium or palladium loaded with deuterium. When the deuterons in the beam from the accelerator impinge on the target, usually there would be chances for 2-deuteron fusion reactions; however, it is almost impossible to detect any 3-deuteron fusion because the probability of seeing three deuterons together is less than 10^{-31}. Professor Kasagi, a nuclear physicist at Tohoku University, made a highly loaded target (TiD_x, x>1.4) and used a cold finger to cool the titanium target during the beam bombardment (5~15°C) (*11*) (Figure 5). He found the products of a 3-deuteron fusion reaction, i.e.,

$$d + d + d \rightarrow p + n + \alpha + 21.62 MeV$$

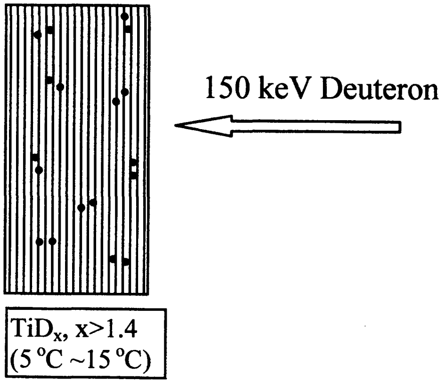

Figure 5. Beam-target experiment to find the 3-deuteron fusion reactions.

The products of 3-deuteron fusion are distinct from that of 2-deuteron fusion because 3-deuteron fusion gives more energetic products and they have a

Downloaded by YORK UNIV on July 1, 2012 | http://pubs.acs.org
Publication Date: August 1, 2008 | doi: 10.1021/bk-2008-0998.ch003

Downloaded by YORK UNIV on July 1, 2012 | http://pubs.acs.org
Publication Date: August 1, 2008 | doi: 10.1021/bk-2008-0998.ch003

continuous energy distribution among three nuclear products. The maximum energy of alpha-particles is 6.5 MeV, and the maximum energy of protons is 17 MeV. There is no way to explain these maximum values of energy in terms of any 2-deuteron reactions.

Professor Takahashi of Osaka University confirmed this 3-deuteron reaction in terms of another 3-deuteron reaction channel (*12*):

$$d + d + d \rightarrow \mathrm{T}(4.75\mathrm{MeV}) + {}^{3}\mathrm{He}(4.75\mathrm{MeV}).$$

Triton and helium-3 from this 3-deuteron reaction channel have equal energy and equal yields; hence, they provided another strong piece of evidence for 3-deuteron fusion reactions in crystal lattice. The ratio of 3-deuteron to 2-deuteron fusion reactions was on the order of 10^{-5} in both Kasagi's and Takahashi's experiments. Indeed this ratio provided an estimate of the life-time of this 2-deuteron resonance state. Fortunately, this estimate is on same order as that of the selective resonant tunneling model(~10^{4} seconds).

This 3-deuteron fusion reaction has been further confirmed by Naval Research Laboratory in the United States as well (*13*).

Correlation between "Excess Heat" and Abnormal Deuterium Flux

Are there any other phenomena which may be induced by this resonant tunneling? The deuterium flux permeating the palladium film is one of them. This collisional diffusion process would be enhanced if there is any enhancement in collision. In quantum mechanics, any resonance in the inelastic scattering would cause an enhancement in elastic scattering (*14*). While the resonant tunneling causes an enhancement in the deuteron-deuteron fusion reaction, it causes an enhancement in deuteron-deuteron elastic scattering as well. As a result, we might expect to observe the correlation between the "excess heat" and the deuterium flux.

Figure 6 shows the experimental results of this expected correlation. A SETARAM high-precision calorimeter was used to detect the heat flow from the reaction vessel (*15*). A palladium tube was stuck into the reaction vessel, and deuterium gas was fed into this thin-wall palladium tube of which one end is blocked. When the whole vessel was heated by the electrical heater in the calorimeter, the deuterium gas diffused through the thin wall, and was pumped out through a coaxial tube on the top. The pressure in the vessel was monitored to calculate this deuterium flux through the palladium thin wall. When the electrical heater was turned off, the vessel was cooled down slowly through the thermal insulation surrounding the calorimeter. When the temperature of the vessel was cooling down in the interval of 150°C-140°C, there were two peaks in heat flow (dash-dot-dash line in the lower plot). At the same time there were two peaks in deuterium flux as well (thin solid line). It shows clearly the correlation between the deuterium flux and the heat flow. This high-precision calorimeter is able to detect one microwatt of heat flow (e.g., the metabolic heat of a singing cricket), and the peak of heat flow is on the order of a milliwatt. The normal diffusion declines with the temperature monotonically. It is subtracted and the figure shows only the abnormal deuterium flux which has peaks when the temperature drops. The slow dip in the heat flow after 138°C is caused by the degassing.

The most important discovery in that correlation experiment was the temperature range, 150°C-140°C, where the resonant tunneling appears. This could not be observed in any previous electrolytic cell. This temperature range was confirmed later in 2005 (*16*).

Downloaded by YORK UNIV on July 1, 2012 | http://pubs.acs.org
Publication Date: August 1, 2008 | doi: 10.1021/bk-2008-0998.ch003

Self-Sustaining Reactor and the Neutrino Emission

If we had been able to improve the thermal insulation of the calorimeter and increase the surface area of palladium tube, there might have been a possibility of keeping the temperature of the palladium tube in the desired range; then, a self-sustaining reactor would have appeared. The palladium tube would have maintained its temperature around 145°C by the excess heat itself as long as the deuterium flux continued. This self-sustaining system would have been the best evidence for the excess heat effect (*17*).

Early in 1942, just three years after nuclear fission was discovered by Otto Hahn, Enrico Fermi built the first self-sustaining fission reactor. Although its thermal power was less than 1 watt, it persuaded all the skeptics. The G-M counter clearly showed the process of start-up, control of the power level using control rod, shut-down of the reactor, and the nuclear nature of the power.

The neutrino emission would be the possible evidence to show the nuclear nature of this excess heat. Because the selective resonant tunneling selects the weak interaction process only, we may use the neutrino emission as the necessary product even though we are not clear about what these weak interaction processes are. If this neutrino emission from palladium with deuterium flux is confirmed in experiment there would be no skeptics regarding this nuclear energy without strong nuclear radiation.

The weak interaction does not mean a weak power source. Even if the lifetime is as long as 10^4 seconds (~3 hours), a cubic centimeter of palladium might produce megawatts of thermal power. Its power density is higher than that of the fuel rod in a fast fission reactor.

Further Studies on Nuclear Energy without Strong Nuclear Radiation

Up to now, the highest continuous excess-heat power was 144.5 watts (3.7kW per cm^3 palladium) in a heat-after-death experiment (*18*). The earliest

Downloaded by YORK UNIV on July 1, 2012 | http://pubs.acs.org
Publication Date: August 1, 2008 | doi: 10.1021/bk-2008-0998.ch003

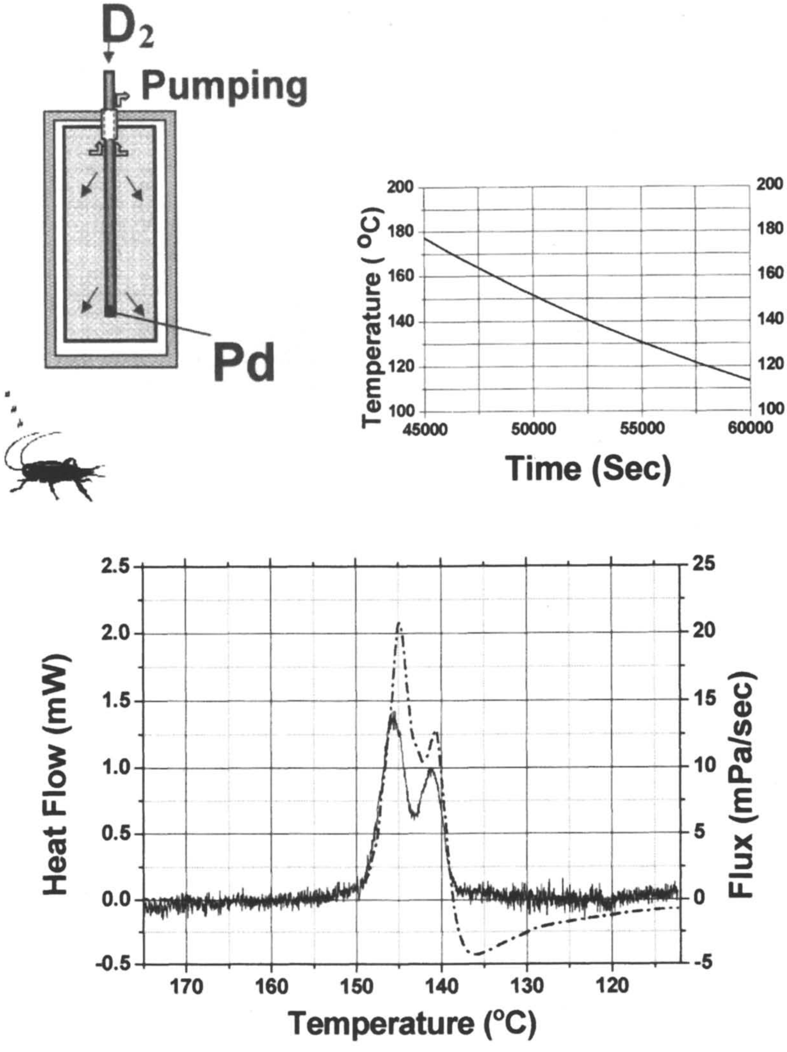

Figure 6. Correlation data (right and lower plots) and SETARAM calorimeter (left plot)

"helium-excess heat" correlation experiment was done in an electrolytic cell (*19*). Both have been confirmed since by more than one experiment. They did not violate any basic law of physics. Just based on conventional quantum mechanics, we have been able to answer the three puzzles of condensed matter nuclear science (*10*); calculate the three major hot fusion cross-sections (*6*); explain the anomalous yield of 3-deuteron fusion reactions (*11,12*); find the correlation between deuterium flux and heat flow (*15*); and make the conjecture about neutrino emission (*20*). In order to build a self-sustaining reactor, we have to further solve a series of physics problems:

- We have to study the mechanism which explains the function of the super-wave (*21*), or the function of the ultrasonic wave (*22*), or the laser triggering (*23*). They have promoted the resonant tunneling in experiments.
- We have to study the mechanism which transfers the energy from nuclei to lattice without any hard X-ray. Phonon laser mechanism has been proposed as a candidate (*24*).
- We have to study the mechanism which provides the negative feedback to keep the D/Pd system in the right temperature range. Deuteron Ion Band theory has been proposed (*25*).
- We have to study the mechanism which works also for adding 4 deuterons into high-Z nuclei such as Cs or Sr. Poly-neutron has been proposed to neutralize the deuterons (*26*). Another even more boldhearted assumption was made with braveness by another researcher (*27*).
- We have to study the mechanism which may explain the abnormally long memory of metal deuterides (*28*).
- We have to study the mechanism which may explain the loading (*29*) and the extraordinary absorption of deuterium into the nanometer-size grain of palladium (*30, 31*).
- We have to study mechanisms which may work at much higher temperatures in order to raise the heat efficiency of future power reactors (*32*).
- We have to study the mechanism which explains the screening effect and its dependence on temperature (*33, 34*).
- We have to study the mechanism which makes the hydrogen work as deuterium (*35-37*).
- We might anticipate that the combination of gas-loading and the electrolytic cell would lead to a glow discharge tube as the future element of the condensed matter nuclear science reactor (*38-42*).

Downloaded by YORK UNIV on July 1, 2012 | http://pubs.acs.org
Publication Date: August 1, 2008 | doi: 10.1021/bk-2008-0998.ch003

Acknowledgements

This work is supported by the Natural Science Foundation of China (#10475045).

References

1. Rutherford, E. Quoted in the London *Times*, September 12, 1933.
2. Hahn, O.; Strassman, F. Concerning the Existence of Alkaline Earth Metals Resulting from Neutron Irradiation of Uranium. *Naturwissenschaften* **1939**, *27*, 11; summary, translated in Graetzer, H. *The Discovery of Nuclear Fission*; Van Nostrand Reinhold: New York, 1971, pp 44-47.
3. Bethe, H. A.; Critchfield, C. L. The Formation of Deuterons by Proton Combination. *Phys. Rev.* **1938**, *54*, 248.
4. Peebles, P. I. E. *Quantum Mechanics*; Princeton University Press: Princeton, NJ, 1992, pp 52-60.
5. Li, X. Z.; Tian, J.; Mei, M. Y.; Li, C. X. Sub-Barrier Fusion and Selective Resonant Tunneling. *Phys. Rev.* C **2000**, *61*, 024610.
6. Li, X. Z.; Liu, B.; Chen, S.; Wei, Q. M.; Hora, H. Fusion Cross-Sections for Inertial Fusion Energy. *Laser and Particle Beam* **2004**, *22*, 469-477.
7. Huba, J. D. *NRL Plasma Formulary*; Naval Research Laboratory, 2007, p 44.
8. Li, X. Z. Nuclear Physics for Nuclear Fusion. *Fusion Sci. and Tech.* **2002**, *41*, 63.
9. Li, X. Z. A New Approach Towards Fusion Energy with No Strong Nuclear Radiation. *Journal of New Energy* **1996**, *1* (4), 44-54.
10. Huizenga, J. R. *Cold Fusion: The Scientific Fiasco of the Century*; University of Rochester Press: Rochester, NY, 1992, pp 111-114.
11. Kasagi, J.; Ohtsuki, T.; Ishii K.; Hiraga, M. Energetic Protons and α Particles Emitted in 150-keV Deuteron Bombardment on Deuterated Ti. *J. Phys. Soc. Japan* **1995**, *64* (3), 778.
12. Takahashi, A.; Maruta, K.; Ochiai, K.; Miyamaru H.; Iida, T. Anomalous Enhancement of Three-Body Deuteron Fusion in Titanium-Deuteride with Low-Energy D^+ Beam Implantation. *Fusion Technol.* **1998**, *34*, 256.
13. Grabowski, K. S.; Hubler, G. K.; Knies, D. L.; Walker, R. A.; Qadri, S. B.; Wang, T. S.; Nagel, D. J. Particle Emission from Low Energy Proton Bombardment of TiH_2 and TiD_2. *J. Phys. Soc. Japan* **2002**, *71*, 757.
14. Landau, L. D.; Lifshitz, E. M. *Quantum Mechanics: Non-Relativistic Theory*; Pergamon Press: Oxford, 1977, pp 591-592.
15. Li, X. Z.; Liu, B.; Tian, J.; Wei, Q. M.; Zhou, R.; Yu, Z. W. Correlation Between Abnormal Deuterium Flux and Heat Flow in a D/Pd System. *J. Phys. D: Appl. Phys.* **2003**, *36*, 3095-3097.
16. Arata, Y.; Zhang, Y. C. Development of "DS-Reactor" as a Practical Reactor of "Cold Fusion" Based on the "DS-Cell" with "DS-Cathode." In *Condensed Matter Nuclear Science: Proceedings of the 12th International Conference on Cold Fusion*, Yokohama, Japan, Nov. 27-Dec. 2, 2005; Takahashi, A.; Ota, K.-I.; Iwamura, Y., Eds.; World Scientific Publishing Co.: Singapore, 2006; 44-54.

Downloaded by YORK UNIV on July 1, 2012 | http://pubs.acs.org
Publication Date: August 1, 2008 | doi: 10.1021/bk-2008-0998.ch003

17. Li, X. Z.; Liu, B.; Wei, Q. M. A Self-Sustaining Excess Heat Device Using Deuterium Flux. Chinese Patent 032646682, August 4, 2004.
18. Fleischmann, M.; Pons, S. Calorimetry of the Pd-D_2O System: From Simplicity via Complications to Simplicity. *Phys. Lett. A* **1993**, *176*, 119-129.
19. Miles, M. H. M.; Bush, B. F. Search for Anomalous Effects Involving Excess Power and Helium during D_2O Electrolysis Using Palladium Cathodes. In *Frontiers of Cold Fusion: Proceedings of the Third International Conference on Cold Fusion*, Nagoya, Japan, October 21-25, 1992; Ikegami, H., Ed.; Universal Academic Press: Tokyo, 1993; 189-200.
20. Li, X. Z.; Wei, Q. M.; Liu, B.; Ren, S. L. The Conjecture of the Neutrino Emission from the Metal Hydrides. *J. of Condensed Matter Nuclear Science*, 1, 2007; 11-15.
21. Dardik, I.; Zilov, T.; Branover, H.; El-Boher, A.; Greenspan, E.; Khachaturov, B.; Krakov, V.; Lesin, S.; Tsirlin, M. Excess Heat in Electrolysis Experiments at Energetics Technologies. In *Condensed Matter Nuclear Science: Proceedings of the 11th International Conference on Cold Fusion*, Marseilles, France, Oct. 31 - Nov. 5, 2004; Biberian, J.-P., Ed.; World Scientific Publishing Co.: Singapore, 2006; 84-101.
22. Stringham, R. Low Mass 1.6MHz Sonofusion Reactor. In *Condensed Matter Nuclear Science: Proceedings of the 11th International Conference on Cold Fusion*, Marseilles, France, Oct. 31 - Nov. 5, 2004; Biberian, J.-P., Ed.; World Scientific Publishing Co.: Singapore, 2006; 238-252.
23. Violante,V.; Moretti, S.; Bertolotti, M.; Castagna, E.; Sibilia, C.; Sarto, F.; Mckubre M.; Tanzella, F.; Dadik, I.; Lesin, S.; Zilov, T. Progress in Excess of Power Experiments with Electrochemical Loading of Deuterium in Palladium. In *Condensed Matter Nuclear Science: Proceedings of the 12th International Conference on Cold Fusion*, Yokohama, Japan, Nov. 27-Dec. 2, 2005; Takahashi, A.; Ota, K.-I.; Iwamura, Y., Eds.; World Scientific Publishing Co.: Singapore, 2006; 55-64
24. Hagelstein, P. L. Models for Anomalies in Condensed Matter Deuterides. In *Condensed Matter Nuclear Science: Proceedings of the 12th International Conference on Cold Fusion*, Yokohama, Japan, Nov. 27-Dec. 2, 2005; Takahashi, A.; Ota, K.-I.; Iwamura, Y., Eds.; World Scientific Publishing Co.: Singapore, 2006; 441-453.
25. Chubb, S. R.; Chubb, T. A. Ion Band State Fusion: Reactions, Power Density, and the Quantum Reality Question. *Fusion Technol.* **1993**, *24*, 403.
26. Fisher, J. C. Polyneutron Theory of Transmutation. In *Condensed Matter Nuclear Science: Proceedings of the 12th International Conference on Cold Fusion*, Yokohama, Japan, Nov. 27-Dec. 2, 2005; Takahashi, A.; Ota, K.-I.; Iwamura, Y., Eds.; World Scientific Publishing Co.: Singapore, 2006; 516-520.
27. Takahashi, A. Time-Dependent Eqpet Analysis of TSC. In *Condensed Matter Nuclear Science: Proceedings of the 12th International Conference*

Downloaded by YORK UNIV on July 1, 2012 | http://pubs.acs.org
Publication Date: August 1, 2008 | doi: 10.1021/bk-2008-0998.ch003

on Cold Fusion, Yokohama, Japan, Nov. 27-Dec. 2, 2005; Takahashi, A.; Ota, K.-I.; Iwamura, Y., Eds.; World Scientific Publishing Co.: Singapore, 2006; 454-461.

28. Wang, D. L.; Qin, J. G.; Lai, C. F.; Li, Y. J.; Li, B.; Liu, R. Experimental Measurement of New Spectral Series of Hydrogen Gas Discharge Source Bombarding Target. *High Power Laser and Particle Beams* (in Chinese) **2006**, *18* (11), 1913-1916.
29. Mckubre, M. C. H.; Tanzella, F. L. Using Resistivity to Measure H/Pd and D/Pd Loading: Method and Significance. In *Condensed Matter Nuclear Science: Proceedings of the 12th International Conference on Cold Fusion*, Yokohama, Japan, Nov. 27-Dec. 2, 2005; Takahashi, A.; Ota, K.-I.; Iwamura, Y., Eds.; World Scientific Publishing Co.: Singapore, 2006; 392-403.
30. Yamaura, S. I.; Sasamori, K.; Kimura, H.; Inoue, A.; Zhang, Y. C.; Arata Y. Hydrogen Absorption of Nanoscale Pd Particles Embedded in ZrO_2 Matrix Prepared from Zr-Pd Amorphous Alloys. *J. Mater. Res.* **2002**, *17* (6), 1329-1334.
31. Celani, F.; Spallone, A.; Righi, E.; Trenta, G.; Andreassi, V.; Marmigi, A.; Quercia, P.; Cappuccio, G.; Hampai, D. Studies About Palladium Nano-Particles Synthesis for Deuterium Absorption at High Temperatures. Presented at the 13th International Conference on Condensed Matter Nuclear Science, Sochi, Russia, June 25 - July 1, 2007; Paper HP3.
32. Ramodanov, V. A. Tritium Generation from the Interaction of a Glow Discharge Plasma with Metals and with a Magnetic Field. In *Condensed Matter Nuclear Science: Proceedings of the 10th International Conference on Cold Fusion*, Cambridge, MA, Aug. 24-29, 2003; Hagelstein, P. L.; Chubb, S. R., Eds.; World Scientific Publishing Co.: Singapore, 2006; 325-352.
33. Hora, H.; Kelly, J. C.; Patel, J. U.; Prelas, M. A.; Miley, G. H.; Tompkins, J. W. Screening in Cold Fusion Derived from D-D Reactions. *Phys. Lett.* **1993**, *175*, 138.
34. Raiola, F.; Migliardi, P.; Gang, L.; Bonomo, C.; Gyürky, G.; Bonetti, R.; Broggini, C.; Christensenl, N. E.; Corvisierof, P.; Cruzg, J.; D'Onofrio, A.; Fülöp, Z.; Gervino, G.; Gialanella, L.; Jesus, A. P.; Junker, M.; Langanke, K. ; Prati , P.; Roca, V.; Rolfs , C.; Romano, M.; Somorjai, E.; Strieder, F.; Svanel, A.; Terrasi, F.; Winter, J. Electron Screening in d(d, p)t for Deuterated Metals and the Periodic Table. *Phys. Lett. B* **2002**, *547*, 193-199.
35. Miley, G. H.; Shresha, P. J. Overview of Light Water/Hydrogen-Based Low Energy Nuclear Reactions. In *Condensed Matter Nuclear Science: Proceedings of the 12th International Conference on Cold Fusion*, Yokohama, Japan, Nov. 27-Dec. 2, 2005; Takahashi, A.; Ota, K.-I.; Iwamura, Y., Eds.; World Scientific Publishing Co.: Singapore, 2006; 34-43.
36. Focardi, S.; Gabbani, V.; Montalbano, V.; Piantelli, F.; Veronesi, S. Large Excess Heat Production in Ni-H Systems. *Nuovo Cimento A* **1999**, *112*, 921.

Downloaded by YORK UNIV on July 1, 2012 | http://pubs.acs.org
Publication Date: August 1, 2008 | doi: 10.1021/bk-2008-0998.ch003

37. Dash, J. Evidence of Nuclear Transmutation After Loading Metals with Hydrogen and/or Deuterium. Presented at the 13th International Conference on Condensed Matter Nuclear Science, Sochi, Russia, June 25 -July 1, 2007; Paper NT1.
38. Mills, R. J.; Ray, P. C.; Dhandapani, B.; Mayo, R. M.; He, J. Comparison of Excessive Balmer αline Broadening of Glow Discharge and Microwave Hydrogen Plasmas with Certain Catalysts. *J. of Applied Physics* **2002**, *92* (12), 7008-7022.
39. Benson, T. B.; Passel, T. O. Calorimetry of Energy-Efficient Glow Discharge Apparatus Design and Calibration. In *Condensed Matter Nuclear Science: Proceedings of the 11th International Conference on Cold Fusion*, Marseilles, France, Oct. 31 - Nov. 5, 2004; Biberian, J.-P., Ed.; World Scientific Publishing Co.: Singapore, 2006; 147-160.
40. Karabut, A.B. Presented at the 13th International Conference on Condensed Matter Nuclear Science, Sochi, Russia, June 25 - July 1, 2007; Paper GP1.
41. Storms, E. Anomalous Radiation Produced by Glow Discharge in Low-Pressure Deuterium Gas. Presented at the 8th International Workshop on Anomalies in Hydrogen/Deuterium Loaded Metals, Catania, Sicily, Oct. 13-18, 2007.
42. Cantwell, R. F.; Booth, S. S.; McConnell, M. L. A Flow Calorimeter for Glow Discharge Experiments. Presented at the 13th International Conference on Condensed Matter Nuclear Science, Sochi, Russia, June 25 - July 1, 2007; Paper IP1.

Downloaded by YORK UNIV on July 1, 2012 | http://pubs.acs.org
Publication Date: August 1, 2008 | doi: 10.1021/bk-2008-0998.ch003

Downloaded by STANFORD UNIV GREEN LIBR on July 1, 2012 | http://pubs.acs.org
Publication Date: August 1, 2008 | doi: 10.1021/bk-2008-0998.ch004

Chapter 4

Study on 4D/Tetrahedral Symmetric Condensate Condensation Motion by Non-Linear Langevin Equation

Akito Takahashi and Norio Yabuuchi

High Scientific Research Laboratory, Marunouchi 24–16, Tsu, Mie, 514–0033, Japan

Tetrahedral symmetric condensate (TSC) with 4 deuterons and 4 electrons has been proposed as a seed of clean 4D fusion with ^{4}He product in condensed matter in our previous works. To solve molecular dynamics motion of 4D/TSC condensation, a nonlinear Langevin equation was formulated with a Coulombic main condensation force term under Platonic symmetry, 6 balancing forces of dde*(2,2) EQPET molecules on 6 faces of TSC cube, and a random quantum mechanical fluctuation term f(t) for deuteron-to-deuteron distance R_{dd}. The form of ensemble average <f(t)> becomes C/R_{dd}^2 type deceleration force as positive bias to main condensation force, to be about 15% bias. Molecular dynamics calculation with TSC Langevin equation by the Verlet time-step method was then done. Barrier factors for fusion reactions as a function of $R_{dd}(t)$ and 4D fusion rate per TSC generation were calculated using modeled potentials and Fermi's golden rule. We found that 4D/TSC got to the TSC-minimum state with 10 fm-20 fm radius in 1.4007 fs and 4D fusion rate was about 100% per 4D/TSC generation-condensation. Thus we concluded that ^{4}He production rate by 4D/TSC was equal to two times the 4D/TSC generation rate in condensed matter (e.g., PdDx).

Introduction

In our previous work to be reported in the proceedings of ICCF13 (*1*), we introduced a non-linear Langevin equation to study molecular dynamics motion of 4D/TSC condensation and gave the first-step results. This paper describes the extended detail of the study on 4D/TSC condensation motion and resulting fusion rates producing almost purely ^{4}He with 23.8 MeV per ^{4}He. We will show in this paper that 4D fusion takes place about 100% per TSC generation.

The concept of Tetrahedral Symmetric Condensate (TSC) and theoretical EQPET models with numerical analyses from our past studies are reviewed in references (*2-13*).

In our past studies on 4D/TSC or 4H/TSC models (*2-13*), Coulomb barrier shielding is conceived to be achieved automatically by strong condensation motion to the central focal point keeping averaged charge neutrality of the system (focal point is T-site in one of our models for PdDx lattice dynamics; see Figure 1). Barrier penetration probability calculation for 2d pair or 4d cluster can be approximated by the EQPET formalism in average.

An empirical treatment was applied for multi-body strong interaction between many deuterons under the Platonic symmetry. After the molecular dynamics calculation of 4D/TSC condensation motion, we have extended the EQPET model to the HMEQPET model (described in this paper) to treat time-dependent (equivalently R_{dd}- d-d distance-dependent) d-d pair trapping potential of squeezing TSC. The HMEQPET model utilizes the concept of heavy mass Cooper pair e*(m,2) to approximate the time-dependent d-d trapping potential continuously – hence we use non-integer values for m (mass number of electronic quasi-particle) according to the change of R_{dd} with time. Using approximate trapping potentials by HMEQPET, we can systematically calculate barrier factors (quantum mechanical tunneling probability of d-d pair and 4d cluster through HMEQPET potentials). Using time-integrated barrier factors and Fermi's golden rule for nuclear fusion rate (*8*), time-integrated 4D fusion yield per 4D/TSC condensation was calculated to be about 100% 4D fusion per a TSC generation. Using the same formalisms, we calculated 2D fusion rates for D_2 molecule, muonic-dd-molecule and dde*(2,2) Cooper pair dd molecule to result in quite reasonable values.

To initiate TSC formation, three models are speculated (modeled with assumptions) in our previous papers (*2, 5, 6, 8, 10*). One is the TSC formation in regular PdD lattice in D-flow from O-site to T-site by D-lattice-phonon excitation (see Figure 1). The second model is the TSC formation by the collision-combination process between trapped D_2 molecule, being lost freedom of rotation, and incoming D_2 molecule on surface of metal-D systems. The third idea is the random formation of TSC by combination of two "bosonized" molecules of dde*(2,2) in the near surface of Fermi-level gap of PdDx and CaO (or other insulator layer with low work function); generation of Cooper pair near on Fermi surface may play a key role in this case (*10*). In every model, we have required the "bosonization" of electron-pair to make dde*(m,Z) molecular size

Downloaded by STANFORD UNIV GREEN LIBR on July 1, 2012 | http://pubs.acs.org
Publication Date: August 1, 2008 | doi: 10.1021/bk-2008-0998.ch004

diminished. Diminished TSC cluster or dde*(m,Z) molecule can move to a focal point (T-site, for instance in PdDx lattice) in the gap of tight lattice structure for further condensation motion. We need further detailed modeling for these TSC generation process in/on condensed matter. In this work, we start from the assumption that 4D/TSC at t=0 state exists and we try to solve the TSC condensation motion by molecular dynamics calculation with non-linear Langevin equation.

We used the following acronyms in the paper:

- TSC: tetrahedral symmetric condensate
- EQPET: electronic quasi-particle expansion theory
- HMEQPET: heavy mass electronic quasi-particle expansion theory
- DPS: double Platonic symmetry
- GWF: Gaussian wave function
- QM: quantum mechanics
- PEF: pion exchange force

Downloaded by STANFORD UNIV GREEN LIBR on July 1, 2012 | http://pubs.acs.org
Publication Date: August 1, 2008 | doi: 10.1021/bk-2008-0998.ch004

Non-Linear Langevin Equation For TSC Motion

We treat the TSC squeezing motion from TSC (t=0; just formed) to TSCmin (minimum size), as illustrated in Figure 2. The electron wave function at t=0 is set to a vector wave function of 6 wings, each of which is an electron wave function of D_2 molecule as given in reference (*11*), on 6 faces of TSC cube (see Figure 3). On each face of TSC cube, we have a “dede molecular like” arrangement. Therefore, TSC(t=0) system can be regarded as a combination of two orthogonally coupled D_2-type molecules having 6 “d-e-de”-molecular-like faces which are confined by main Coulombic condensation force $-8.38/R_{de}^2$ as derived in our reference (*11*). In Figure 3, the feature of quantum mechanical electron cloud of 4D/TSC(t=0) is copied from our previous works (*7, 11*). Four “electron balls” of “bosonized electron pair” sit at vertexes of cube, alternatively with four deuterons, to form an orthogonally coupled two regular tetrahedrons of deuterons and electron-balls (Double Platonic Symmetry). A d-e-d-e- molecular-like system has an electron torus of “bosonized” electron bond. By condensation of 4D/TSC, every d-e-d-e system on 6 faces diminishes and its d-d pair trapping potential is, in our final stage of this work, given by approximate HMEQPET potential as a function of time (or function of d-d distance $R_{dd}(t)$). Electron kinetic energy of torus bond in a d-e-de system at t=0 is the same with that for D_2 molecule (18 eV), and increases with time-elapse to reach 57.6 keV at R_{dd}=20.5 fm of TSC-min state, as we show in this work. However, double Platonic symmetry (DPS) was kept until when 4D/TSC got to the TSC-min state, according to the results by the present molecular dynamics calculation with non-linear Langevin equation.

In our previous work (*1*), we introduced the following non-linear Langevin equation for TSC motion, with distance in pm unit and energy in keV unit.

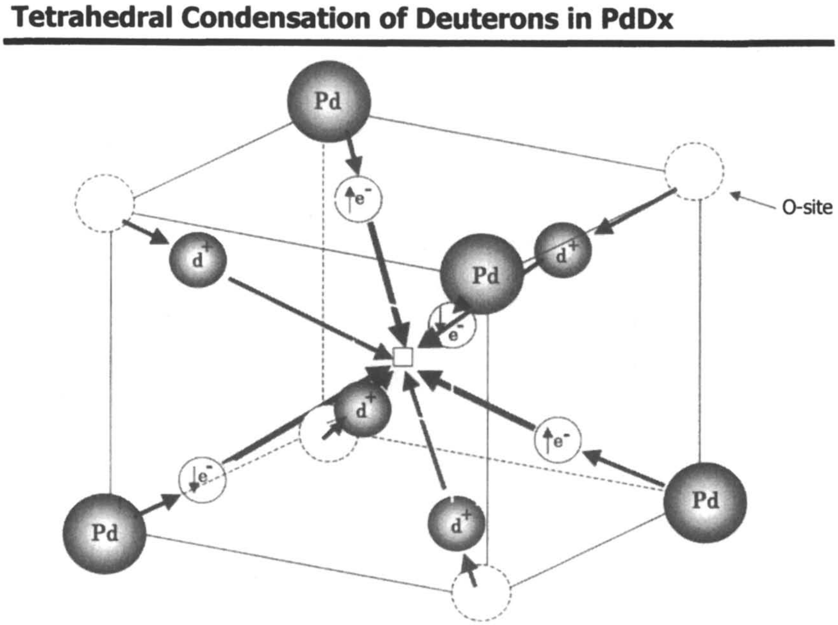

Figure 1. A model of 4D/TSC (t=0) formation in PdDx lattice, by phonon excitation of Deuterons motion at O–sites. 4Ds (4 deuterons+ 4 electrons) may form transiently a TSC cube around the central T-site.

$$6m_d \frac{d^2R_{dd}(t)}{dt^2} = -BA\times\frac{11.85}{[R_{dd}(t)]^2} - 6\frac{\partial V_s(R_{dd}(t);m,Z)}{\partial R_{dd}(t)} + f(t) \qquad (1)$$

The first term on the right side is the acceleration force to diminish d-d distance, by the main condensation force of TSC as we derived in our previous work (*11*) for a DPS condition of TSC. The factor BA is usually 1.0. We later use adjusted BA factor (smaller than 1.0) for averaged treating of random fluctuation term f(t). The second term on the right side of Eq. (1) is the friction term by quantum mechanical electron clouds of 6 d-e-d-e systems on 6 faces of TSC cube. This is the balancing force (acceleration force for $R_{dd}>R_{min}$, but mostly deceleration force to d-d distance diminishment for $R_{dd}<R_{min}$) forcing d-e-d-e system to get back to the original d-e-d-e state. This frictional force is given by the following derivative of EQPET potential,

$$\frac{\partial V_s(R_{dd};m,Z)}{\partial R_{dd}} = -\frac{1.44}{{R_{dd}}^2} + \frac{(J'+K')(1+\Delta)+(J+K)\Delta'}{(1+\Delta)^2} \qquad (2)$$

detail function of which is given in the appendix.

Downloaded by STANFORD UNIV GREEN LIBR on July 1, 2012 | http://pubs.acs.org
Publication Date: August 1, 2008 | doi: 10.1021/bk-2008-0998.ch004

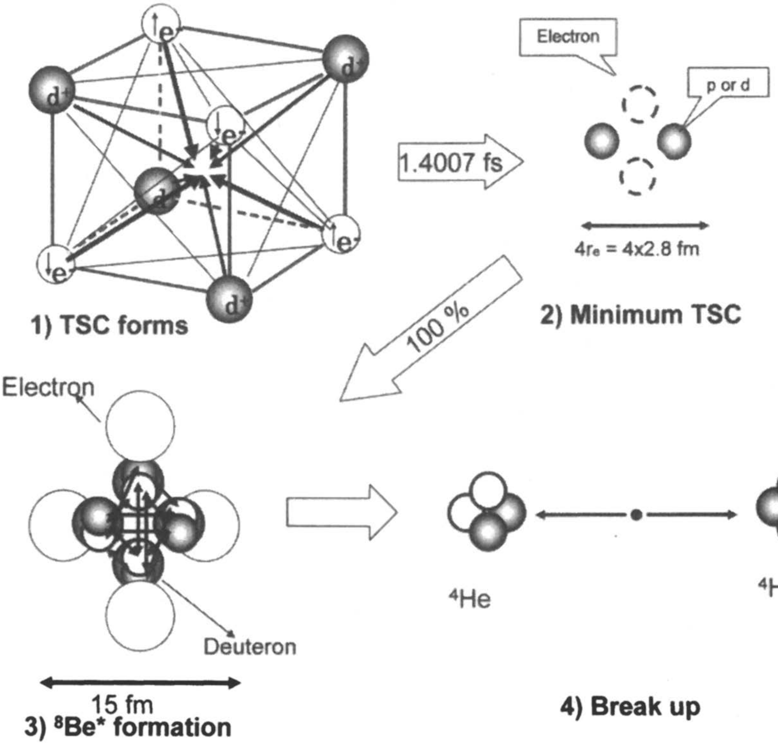
e
d
d
e
d
e
e
d
1) TSC forms
1.4007 fs
Electron
p or d
4re = 4x2.8 fm
2) Minimum TSC
100 %
Electron
Deuteron
15 fm
3) 8Be* formation
4He
4He
4) Break up

Figure 2. Illustration of 4D/TSC condensation motion to TSC-min state, 4D fusion to form $^8Be^*$ intermediate compound nucleus and break-up to two ^4He particles.

The third term on the right side of Eq. (1) is due to random fluctuation force. We model that this fluctuation source is generated by the quantum mechanical uncertainly of deuteron positions of TSC. We treat the formulation of f(t) and its ensemble average <f(t)> in the next section.

Quantum Mechanical Fluctuation of Deuteron Positions

Gaussian Wave Functions

To treat easily the wave function of d-d pair trapped by the shielded Coulomb potential $V_s(R_{dd}; m,Z)$, we adopt here squared wave function of Gaussian form, as illustrated in Figure 4.

Downloaded by STANFORD UNIV GREEN LIBR on July 1, 2012 | http://pubs.acs.org
Publication Date: August 1, 2008 | doi: 10.1021/bk-2008-0998.ch004

Downloaded by STANFORD UNIV GREEN LIBR on July 1, 2012 | http://pubs.acs.org
Publication Date: August 1, 2008 | doi: 10.1021/bk-2008-0998.ch004

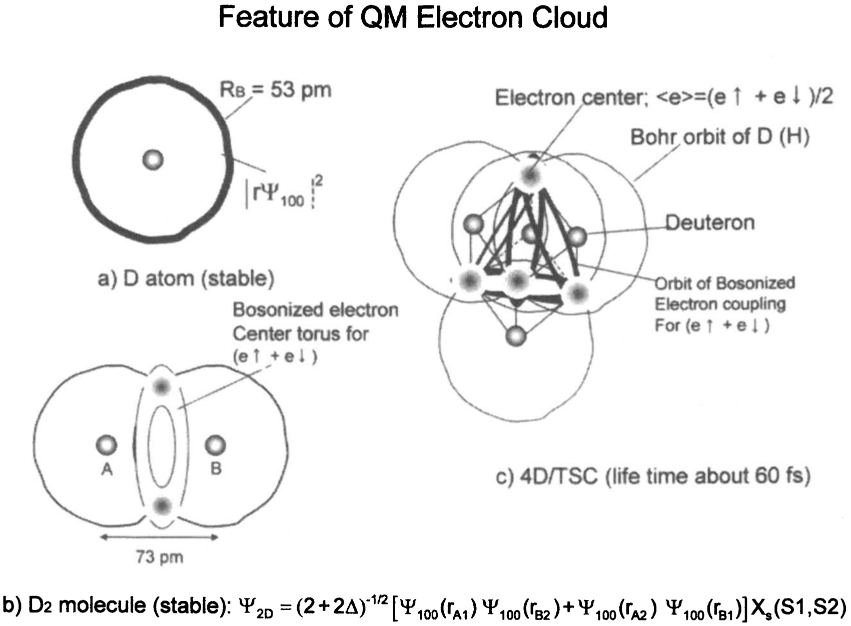
Feature of QM Electron Cloud
RB = 53 pm
$|r\Psi_{100}|^2$
a) D atom (stable)
Bosonized electron
Center torus for
(e↑ + e↓)
A
B
73 pm
Electron center; <e>=(e↑ + e↓)/2
Bohr orbit of D (H)
Deuteron
Orbit of Bosonized
Electron coupling
For (e↑ + e↓)
c) 4D/TSC (life time about 60 fs)

b) D2 molecule (stable): $\Psi_{2D} = (2+2\Delta)^{-1/2}[\Psi_{100}(r_{A1})\,\Psi_{100}(r_{B2}) + \Psi_{100}(r_{A2})\,\Psi_{100}(r_{B1})]X_s(S1,S2)$

Figure 3. Feature of quantum mechanical electron cloud for 4D/TSC (t=0) c), compared with weight distribution of electron clouds a) and b) for D-atom and D_2 molecule, respectively.

The squared wave function of Gaussian form for time dependent calculation is:

$$X^2(R'_{dd};R_{dd}(t)) = \frac{1}{\sqrt{2\pi\sigma^2}}\exp[-(R'_{dd} - R_{dd}(t))^2/(2\sigma^2)] \qquad (3)$$

Unknown parameter σ was determined as explained below, based on the variational principle.

$$X(R_{dd}) = \frac{1}{(2\pi)^{1/4}\sqrt{\sigma}}\exp[-(R_{dd} - R_{gs}(m,Z))^2/(4\sigma^2)] \qquad (4)$$

First, we need to make survey study on appropriate Gaussian wave functions (Eq. (4)) for known D_2 molecule and ddμ (muonic dd) molecule, so as to find appropriate σ-formula, associating proper R_{gs} and E_{gs} values. We survey system total energy to find energy-minimum condition by the following variational method.

Downloaded by STANFORD UNIV GREEN LIBR on July 1, 2012 | http://pubs.acs.org
Publication Date: August 1, 2008 | doi: 10.1021/bk-2008-0998.ch004

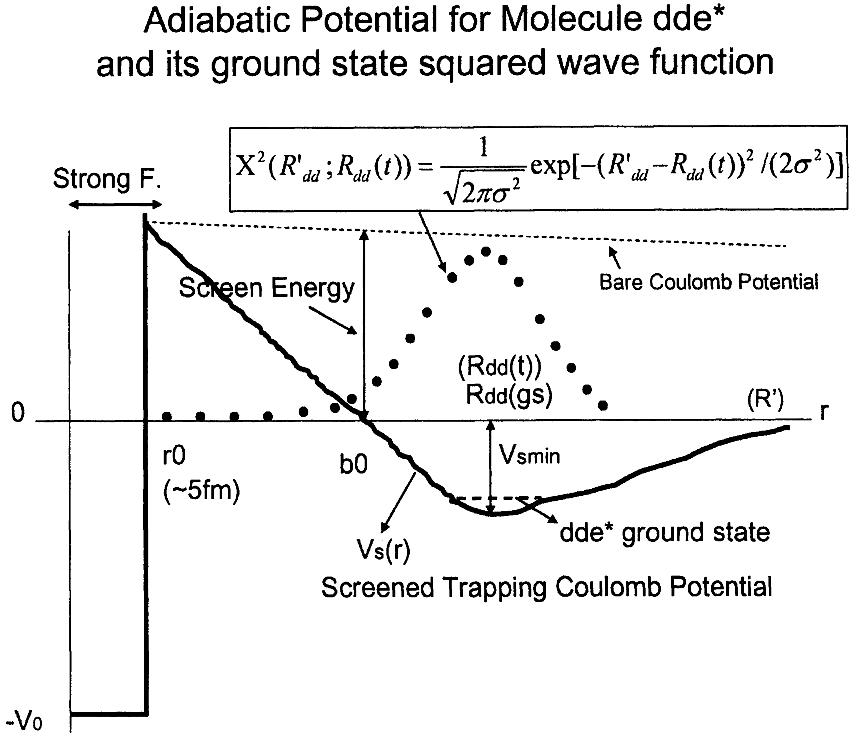
Adiabatic Potential for Molecule dde* and its ground state squared wave function
$X^2(R'_{dd};R_{dd}(t))=\frac{1}{\sqrt{2\pi\sigma^2}}\exp[-(R'_{dd}-R_{dd}(t))^2/(2\sigma^2)]$
Strong F.
Screen Energy
Bare Coulomb Potential
(Rdd(t))
Rdd(gs)
(R')
r
0
r0
(~5fm)
b0
Vsmin
dde* ground state
Vs(r)
Screened Trapping Coulomb Potential
-Vo

Figure 4. Screened tapping Coulomb potential of EQPET dde molecule and Gaussian squared wave function for d-d pair. R_{min} value is at V_{smin}. $R_{gs}=R_{dd}(gs)$, ground state d-d distance, and ground state energy E_{gs} are calculated by GWF2 code, as explained later, based on variational principle. Strong interaction for nuclear fusion works only for $R_{dd}\leqq r_0$ (5 fm), so that we need to estimate barrier factor from R_{min} to r_0 and <W> value for fusion rate formula by Fermi's golden rule (8).*

$$\delta\langle X(R_{dd})|H|X(R_{dd})\rangle=\frac{\partial\langle X(R_{dd})|H|X(R_{dd})\rangle}{\partial\sigma}\delta\sigma+\frac{\partial\langle X(R_{dd})|H|X(R_{dd})\rangle}{\partial R_{gs}}\delta R_{gs}=0 \tag{5}$$

where H is the system Hamiltonian with reduced mass μ (1 for d-d and 1.2 for d-d),

$$H=-\frac{\hbar^2}{2\mu}\nabla^2+V_s(R_{dd};m,Z) \tag{6}$$

We look for the conditions as,

$$\frac{\partial}{\partial\sigma}\langle X(R_{dd})|H|X(R_{dd})\rangle = 0 \tag{7}$$

$$\frac{\partial}{\partial R_{gs}}\langle X(R_{dd})|H|X(R_{dd})\rangle = 0 \tag{8}$$

Downloaded by STANFORD UNIV GREEN LIBR on July 1, 2012 | http://pubs.acs.org
Publication Date: August 1, 2008 | doi: 10.1021/bk-2008-0998.ch004

We made a simple computer code GWF2 for this variational calculation to find R_{gs}, E_{gs} and σ-formula.

First we show the results for ddμ (muonic dd) molecule, for which we have good reference data (*14*). Figure 5 shows the survey for σ-formula.

In Figure 6, we show the results of a search for R_{gs} and E_{gs} for muonic dd molecule. Obtained Gaussian wave function was shown in Figure 7, compared with Hale-Talley results (*14*) in Figure 8. We can say that we have realized a practically useful Gaussian wave function for muonic-dd molecule. Here, we note that the difference between dd and dt molecules is the difference in reduced masses; 1 for dd and 1.2 for dt. This difference does not make significant difference in calculated wave functions and potentials.

Then we extended the variational search for D_2 molecule and dde*(2,2) EQPET molecule. We obtained the same value, **σ/R_{gs} = 0.3** for every case, which we decided to use for time-dependent molecular dynamics calculations for TSC condensation motion. Gaussian wave functions and trapping potentials are shown in Figure 9 and Figure 10, for D_2 and dde*(2,2) molecules.

We also note that the Gaussian wave function is an approximate one, and is useful for analyses around mean values (expectation values). However, the accuracy of probability in tails of Gaussian wave function is so poor that we cannot use it for estimating barrier factor of fusion reaction. We need to introduce the other method for barrier factor calculation. We will introduce the HMEQPET method for this purpose below.

Distortion of System Coulomb Energy by d-d Distance Fluctuation

Following the uncertainty weighted by Gaussian wave function, d-d distance of 4D/TSC will fluctuate and distortion of Platonic arrangement (DPS) takes place. We have estimated approximately the changes of total system Coulomb energy and main TSC condensation force by considering the simple balance of geometrical Coulombic forces between deuterons and electrons, as illustrated in Figure 11. Distortion of system Coulombic force is obtained by elementary geometry practice (we omit explanation) as,

Downloaded by STANFORD UNIV GREEN LIBR on July 1, 2012 | http://pubs.acs.org
Publication Date: August 1, 2008 | doi: 10.1021/bk-2008-0998.ch004

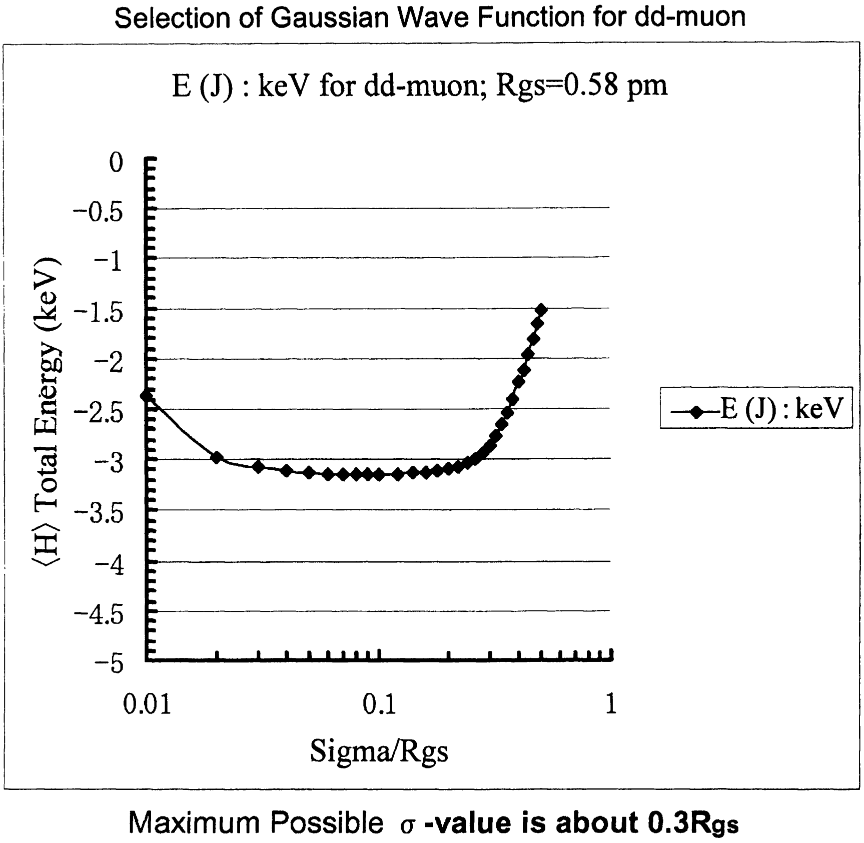
Selection of Gaussian Wave Function for dd-muon

Maximum Possible σ -value is about 0.3Rgs

Figure 5. Search for appropriate σ-formula, in the case of ddμ (muonic dd) molecule. We have chosen σ /R_{gs} = 0.3 as appropriate value, in comparison with known wave function by Hale-Talley (14).

$$-\frac{\partial \Delta E_c(R'_{dd})}{\partial R_{dd}} = 6.60\frac{[\Delta R_{dd}]^2}{[R_{dd}(t)]^4} \tag{9}$$

where energy is given in units of keV and R_{dd} in units of pm.

Now the random fluctuation source term of Langevin equation (Eq. (1)) is given as,

$$f(t) = \left[-\frac{\partial \Delta E_c(R'_{dd}}{\partial R_{dd}} \right] \mathrm{mod}\left[X^2(R'_{dd}; R_{dd}(t)) \right] \tag{10}$$

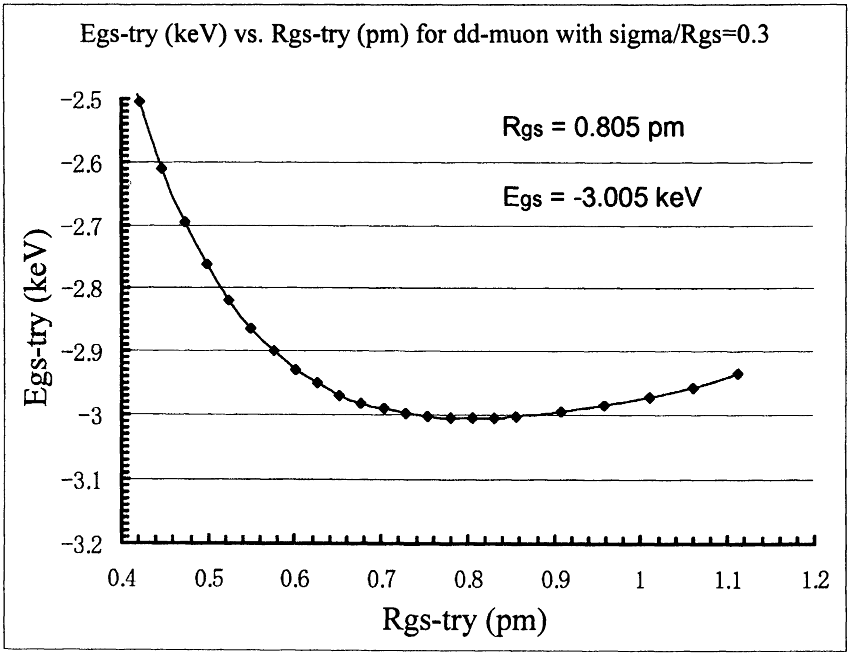

Figure 6. Search for R_{gs} (ground stated-d distance) and E_{gs} (ground state d-d pair energy) values with Gaussian wave function of ddμ molecule.

with

$$\Delta R_{dd} = R'_{dd} - R_{dd}(t) \tag{11}$$

Here we use generation of random Gaussian probability with mod-function for Monte-Carlo calculation.

Since we have two d-e-d-e molecular systems, namely up- and down-D_2-type quasi-molecules in TSC, total fluctuation becomes

$$f(t) \Rightarrow f_{up}(t) + f_{down}(t) \tag{12}$$

Using the squared wave function of Eq. (3), we obtain a formula for ensemble-averaged fluctuation force <f(t)> as follows:

$$\langle f(t) \rangle = 2 \times 6.6 \int_0^\infty \frac{[R' - R_{dd}(t)]^2}{[R_{dd}(t)]^4} \mathrm{X}^2(R') dR' \tag{13}$$

$$\langle f(t) \rangle = \frac{13.2\sigma^2}{\sqrt{\pi}[R_{dd}(t)]^4} \int_0^\infty \sqrt{x}\exp(-x)dx = 13.2\frac{\sigma^2}{[R_{dd}(t)]^4} \tag{14}$$

Downloaded by STANFORD UNIV GREEN LIBR on July 1, 2012 | http://pubs.acs.org
Publication Date: August 1, 2008 | doi: 10.1021/bk-2008-0998.ch004

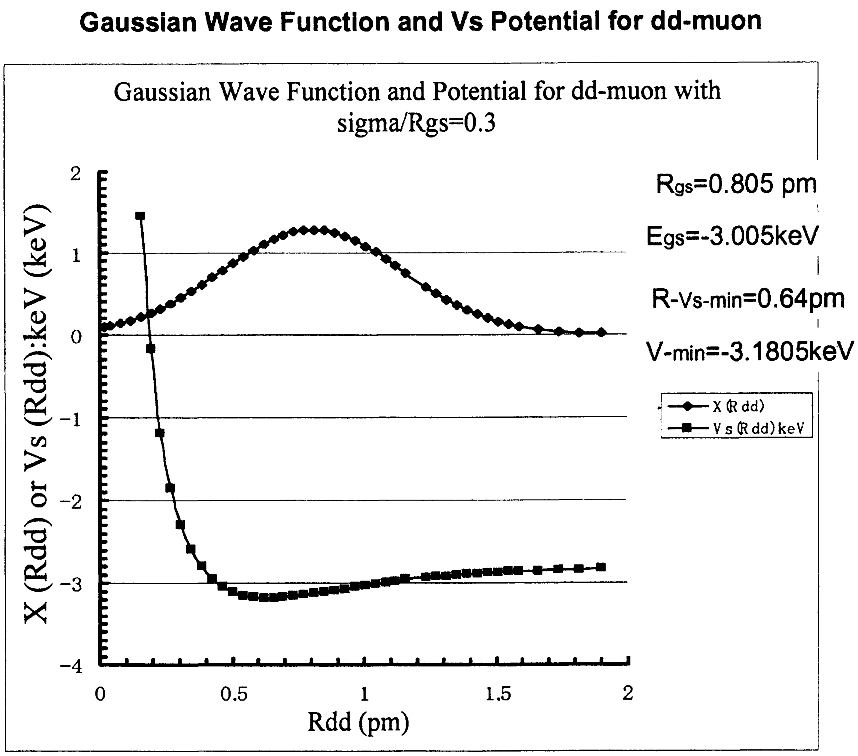

Figure 7. Gaussian wave function and shielded trapping Coulomb potential for ddμ molecule, calculated by GWF2 Code.

with

$$\sigma = 0.372R_{dd}(t) \tag{15}$$

Here we have decided to adopt a little larger σ-value (0.373R_{dd}(t) was used) than 0.3R_{dd}(t) to do conservative estimation of fluctuation effect. Substituting Eq. (15) into Eq. (14), we obtain

$$\langle f(t) \rangle \approx \frac{1.83}{[R_{dd}(t)]^2} \tag{16}$$

Now the Langevin equation for expected values (simply setting $\langle R_{dd}(t) \rangle = R_{dd}(t)$) becomes

Downloaded by STANFORD UNIV GREEN LIBR on July 1, 2012 | http://pubs.acs.org
Publication Date: August 1, 2008 | doi: 10.1021/bk-2008-0998.ch004

After Hale-Tally, Proc. ICCF4, Trans. Fusion Technology, 26,4T (1994)448

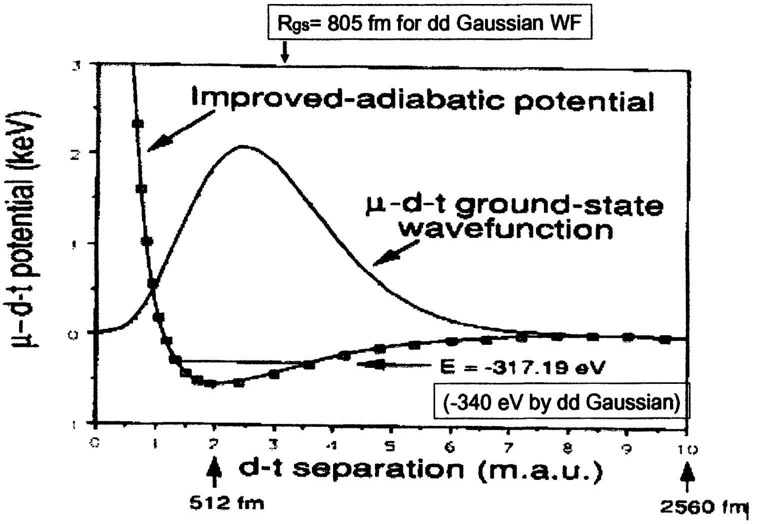

Figure 8. Wave function and trapping Coulomb potential for muonic-dt molecule (14), compared with parameters for muonic-dd molecule by GWF2 Code; Hale and Talley adopted "improved potential" by biasing about + 2.8 keV for original shielded trapping Coulomb potential.

$$6m_d \frac{d^2 R_{dd}(t)}{dt^2} = -\frac{11.85}{[R_{dd}(t)]^2} - 6\frac{\partial V_s(R_{dd}(t);m,Z)}{\partial R_{dd}(t)} + \frac{1.83}{[R_{dd}(t)]^2} \qquad (17)$$

As a result, <f(t)> makes about 15% positive bias (deceleration force) to main condensation force term (first term of right side of Eq. (17)), and we can merge this bias into the first term using BA factor (BA=0.873 in this case) in Eq. (1).

Numerical Solution By Verlet Method

Equation (17) is highly non-linear, but we can solve numerically by the Verlet's time-step method (15) using the following formulas:

$$G(r,t) = \frac{1.975}{m_d[R(0)-r(t)]^2} + \frac{1}{m_d}\frac{\partial V_s(R_{dd};m,Z)}{\partial R_{dd}} \qquad (18)$$

$$R_{dd}(t) = R(0) - t(t) \qquad (19)$$

Downloaded by STANFORD UNIV GREEN LIBR on July 1, 2012 | http://pubs.acs.org
Publication Date: August 1, 2008 | doi: 10.1021/bk-2008-0998.ch004

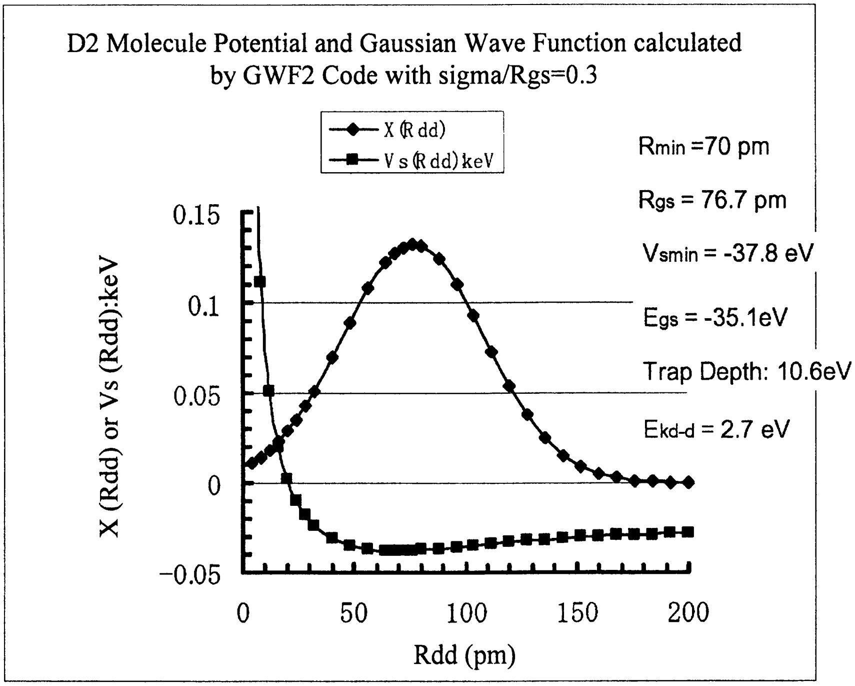

Figure 9. Gaussian wave function and shielded trapping Coulomb potential for D_2 molecule, calculated by GWF2 Code; Ground state d-d distance R_{gs} = 76.7 pm, which is slightly larger than exact value 74.1 pm. Approximate Gaussian wave function gives in general a slightly larger R_{gs} value.

$$\frac{d^2r(t)}{dt^2} = G(r,t) \tag{20}$$

$$r(t+\Delta t) = r(t) + v(t)\Delta(t) + \frac{1}{2}G(r,t)(\Delta t)^2 \tag{21}$$

$$v(t+\Delta t) = v(t) + \frac{\Delta t}{2}[G(r,t+\Delta t) + G(r,t)] \tag{22}$$

by using

$$m_d = E/c^2 = 2.096x10^{-5}[(keV)/(fs)^2/(pm)^2] \tag{23}$$

Downloaded by STANFORD UNIV GREEN LIBR on July 1, 2012 | http://pubs.acs.org
Publication Date: August 1, 2008 | doi: 10.1021/bk-2008-0998.ch004

Downloaded by STANFORD UNIV GREEN LIBR on July 1, 2012 | http://pubs.acs.org
Publication Date: August 1, 2008 | doi: 10.1021/bk-2008-0998.ch004

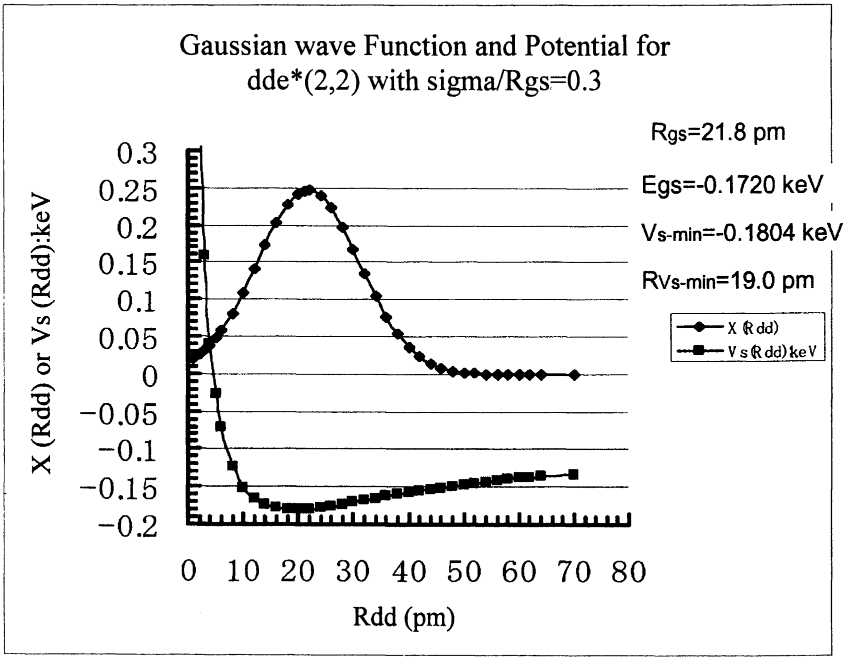

Figure 10. Gaussian wave function and shielded trapping Coulomb potential for Cooper-pair did molecule, dde(2,2); we will use these data for estimating 2D (d-d) fusion rate in condensed matter.*

$$G(r,t)=\frac{0.94\times10^5}{[R(0)-t(t)]^2}+4.77\times10^4\,\frac{\partial V_s(R_{dd};m,Z)}{\partial R_{dd}} \qquad (24)$$

for BA=1.0.

A simple computer code TSC Langevin was made to carry out numerical computation for 4D/TSC condensation motion. Since equation (17) is highly non-linear, we need to be careful about the adiabatic choice of time mesh Δt. Time mesh may start with 0.01 fs, and we need to make stepwise smaller setting, e.g., 0.001 fs for intermediate range and finally very small time-mesh of 0.00001 fs (10^{-20} s). An example of results for BA=0.873 is shown in Figure 12, which is the standard result for 4D/TSC condensation motion. The last stage of condensation took place in a very short time interval of about 2×10^{-20} s.

As an another trial, we used $V_s(R_{dd};1,1)$ potential for balancing force term and got the results shown in Figure 13. TSC finished condensation in 3.02095 fs in this case. Trend of acceleration in the intermediate stage is steeper than the case of $V_s(R_{dd};2,2)$ potential, but the situation to get to TSC-min state with similar size is the same.

Downloaded by STANFORD UNIV GREEN LIBR on July 1, 2012 | http://pubs.acs.org
Publication Date: August 1, 2008 | doi: 10.1021/bk-2008-0998.ch004

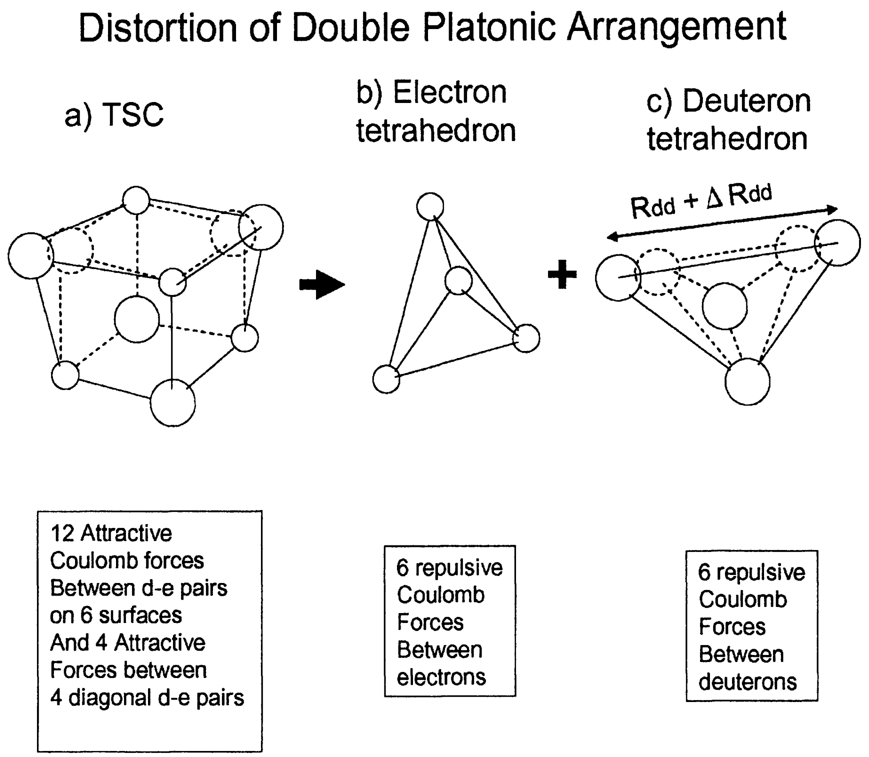
Distortion of Double Platonic Arrangement
a) TSC
b) Electron tetrahedron
c) Deuteron tetrahedron
Rdd + ΔRdd
12 Attractive Coulomb forces Between d-e pairs on 6 surfaces And 4 Attractive Forces between 4 diagonal d-e pairs
6 repulsive Coulomb Forces Between electrons
6 repulsive Coulomb Forces Between deuterons

Figure 11. Distortion of Platonic Symmetry of 4D/TSC by the QM fluctuation of d-d distance.

When the friction term of the Langevin equation becomes large, we may have a constant velocity motion, as is the case with raindrops in the sky. A trial calculation using BA=0.73 is shown in Figure 14. In this virtual case, condensation motion moves with almost constant velocity (kinetic energy) for $R_{dd} < 10$ pm until the TSC-min state comes.

HMEQPET Method

Now we move to formulate time-dependent d-d trapping potential of TSC condensation motion. The ensemble-averaged Langevin equation is rewritten as

$$6m_d \frac{d^2\langle R_{dd}\rangle}{dt^2} = -\frac{11.85}{\langle R_{dd}\rangle^2} - 6\frac{\partial V_s(\langle R_{dd}\rangle; m, Z)}{\partial\langle R_{dd}\rangle} + 6.6\left\langle \frac{(R' - R_{dd})^2}{R_{dd}{}^4} \right\rangle \quad (25)$$

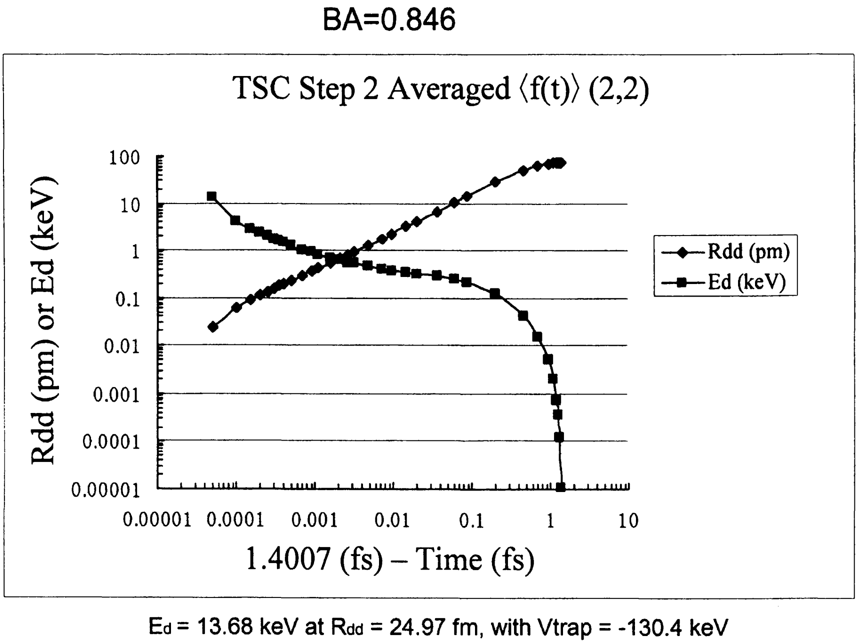

Figure 12. Results of TSC Langevin calculation for 4D/TSC condensation motion. TSC finishes condensation in 1.4007 fs (and 100% breaks up by 4D fusion as explained later). At TSC-min state around R_{dd}=25 fm, relative kinetic energy of d-d pair becomes 13.68 keV and d-d pair is trapped within deep trapping potential with -130.4 keV depth (as explained below). For balancing force, $V_s(R_{dd};2,2)$ potential is used in this case.

We speculate the total d-d trapping potential form, assuming that $<R_{dd}>$ can be simply replaced with $R_{dd}(t)$ for the first and second term of right side and the last term can be integrated with respect to R', to get

$$V_{tsc}(R':R_{dd}(t)) = -\frac{11.85}{R_{dd}(t)} + 6V_s(R_{dd}(t);m,Z) + 2.2\frac{|R' - R_{dd}(t)|^3}{[R_{dd}(t)]^4} \qquad (26)$$

The potential curve as calculated by Eq. (26) is shown in Figure 15, for the final stage of TSC condensation. Potential depth (Vtsc-min)= -130.4 keV and mean kinetic energy of d-d pair 13.68 keV are obtained. This is very fast transient state with about 10^{-20} s of adiabatic time interval. However we can regard this state as an adiabatic state with 13.68 keV ground state energy with V_{tsc} (R_{dd};R') potential, for that short time interval.

We can calculate the corresponding kinetic energy of electron in "d-e-d-e" system of TSC-min state using the semi-classical geometry of Figure 16.

Downloaded by STANFORD UNIV GREEN LIBR on July 1, 2012 | http://pubs.acs.org
Publication Date: August 1, 2008 | doi: 10.1021/bk-2008-0998.ch004

Downloaded by STANFORD UNIV GREEN LIBR on July 1, 2012 | http://pubs.acs.org
Publication Date: August 1, 2008 | doi: 10.1021/bk-2008-0998.ch004

We obtained mean electron kinetic energy E_{ke} = 57.6 keV of "bosonized" electron torus (see Figure 3c)) for d-e-d-e system at R_{dd} = 25 fm. At t =0 state, electron kinetic energy is 18 eV (16.2 eV in our previous study (*11*) is underestimation). Despite such high kinetic energy at TSC-min state, electrons are trapped tightly with deep potential (-130.4 – 57.6 keV = -187.6 keV) in "d-e-d-e" system of a face of 4D/TSC system. We can draw similar "adiabatic" state for d-d distances of R_{dd} > 25 fm.

Unfortunately, thus-obtained trapping potentials and corresponding Gaussian wave functions cannot be used to calculate barrier factors (tunneling probabilities for fusion reaction) calculation, because the accuracies in small and large R_{dd} values are poor. Gaussian wave function is useful to estimate deviation from mean (expectation) values, $<R_{dd}>$, R_{gs} and E_{gs}, but is not useful to interpolation to r_0 position where nuclear strong interaction works.

To obtain more useful approximate potential for continuously varying $R_{dd}(t)$ value, we have introduced the concept of Heavy Mass Cooper Pair e*(m,2) to form virtual dde*(m,2) molecule. If we can establish one-to-one relation between m and $R_{dd}(t)$, we can replace all V_{tsc} ($R_{dd}(t)$) potentials with $V_s(R_{dd}(t)$; m,2) potentials. First, we have made survey calculations for V_s(R; m,2) as a function of mass number (relative to electron mass) m, as results are shown in Table I. In this table, we have eventually found tight empirical relations as

$$b_0(m,2) = 0.206 R_{gs}(m,2) \tag{27}$$

$$m = 9000 / b_0(m,2) \tag{28}$$

Here b_0 and R_{gs} are in units of fm. Using R_{gs} = 805 fm for muonic-dd molecule, we obtain m = 54 for mononic dd molecule. So, $V_s(R_{dd}$; 54,2) potential can be used instead of $V_s(R_{dd}$;207,1) potential of dd-muonic molecule. Similarly, m= 200-500 range can correspond to V_{tsc} potentials in the final stage of TSC condensation.

Using these HMEQPET potentials, we can approximately calculate barrier factors for time-dependent R_{dd} values, continuously. We can use there, real number (non integer) for m value, virtually. In our previous study of time-dependent EQPET analysis, we assumed three steps of adiabatic potentials (*7*), which was difficult in the method, but we can make a smooth calculation of barrier factors continuously changing HMEQPET potentials, in this work.

4D Fusion Rates and Discussion

Using HMEQPET potentials as a function of $R_{dd}(t)$ with the results of TSC Langevin calculation, we can easily calculate barrier factors for d-d pair and 4d cluster.

First we calculate Gamow integral,

Downloaded by STANFORD UNIV GREEN LIBR on July 1, 2012 | http://pubs.acs.org
Publication Date: August 1, 2008 | doi: 10.1021/bk-2008-0998.ch004

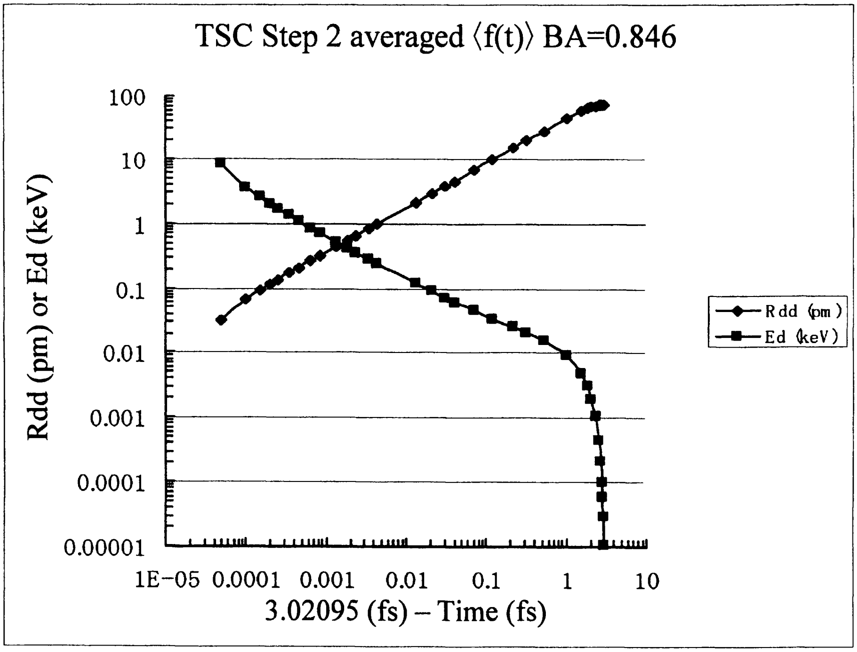

Figure 13. Results of TSC Langevin calculation using $V_s(R_{dd}; 1,1)$ potential for balancing term.

Table I. Main Parameters of HMEQPET Potentials Calculated by GWF2 Code

Molecule	*b0 (pm)*	*Rmin (pm)*	*Vs-min (keV)*	*Vs-min – V(∞) (keV)*	*Rgs (pm)*	*Egs (keV)*
D_2	22	70	-0.03782	-0.0106	76.69	-0.0351
dde*(2,2)	4.5	19.3	-0.1804	-0.0716	21.82	-0.1702
dde*(5,2)	1.9	7.6	-0.4509	-0.1789	8.72	-0.4300
dde*(10,2)	0.90	3.8	-0.9019	-0.3579	4.36	-0.8601
dde*(20,2)	0.45	1.9	-1.8039	-0.7159	2.18	-1.7202
dde*(50,2)	0.18	0.76	-4.5097	-1.7894	0.873	-4.3003
dde*(100,2)	0.09	0.38	-9.0194	-3.5790	0.436	-8.5998
dde*(200,2)	0.045	0.19	-18.039	-7.1590	0.218	-17.196
dde*(500,2)	0.018	0.076	-45.097	-17.89	0.0873	-42.968
dde*(1000,2)	0.009	0.038	-90.194	-35.79	0.0436	-85.858
dde*(2000,2)	.0045	0.019	-180.39	-71.59	0.0218	-171.40

By Choosing BA<1.0, we roughly estimate averaged effect of <f(t)>

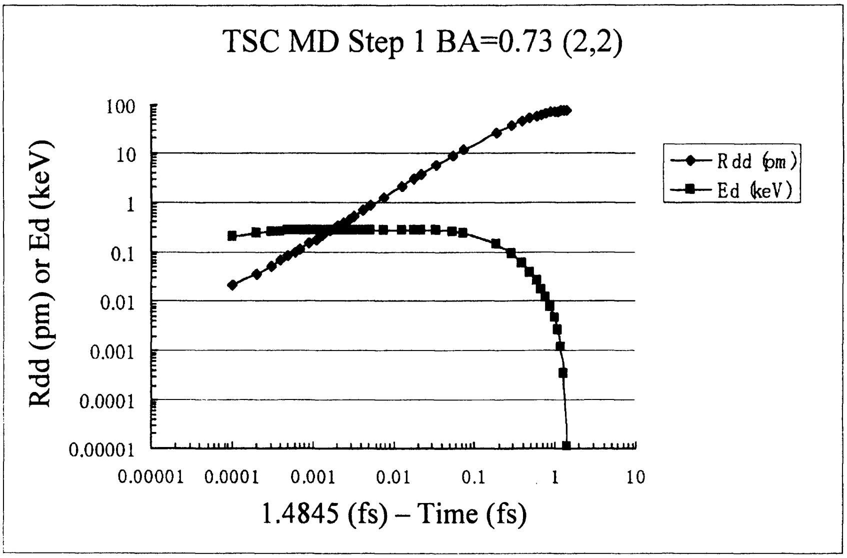

In this case; **acceleration for Rdd>1pm, and deceleration for Rdd<1pm**

Figure 14. A trial calculation for large friction term (BA=0.73) by random fluctuation. This is virtual case.

$$\Gamma_{dd}(m,Z) = 0.218\sqrt{\mu}\int_0^{b_0(m,z)} \sqrt{V_s(R;m,Z) - E_d}\,dR \qquad (29)$$

with R_{dd} in units of fm and

$$m = 4.37 \times 10^4 / R_{dd}(t) \qquad (30)$$

For the calculation of Gamow integral of steady dde* molecule, $b_0(m,Z)$ should be redefined as the lower crossing distance of potential on the level of E_{gs}. Since E_{gs} is negative value, we need to bias V_s potential in Eq. (29) with $-E_{gs}$ to have positive value in root operator. Approximate calculation can be done, however, by regarding $b_0(m,Z) = R_{gs}$, instead of using the biased V_s. We applied this approximation in the present calculation of Gamow integrals.

Barrier factor is calculated by

$$P_{nd}(m,Z) = \exp(-n\Gamma_{dd}(m,Z)) \qquad (31)$$

Downloaded by STANFORD UNIV GREEN LIBR on July 1, 2012 | http://pubs.acs.org
Publication Date: August 1, 2008 | doi: 10.1021/bk-2008-0998.ch004

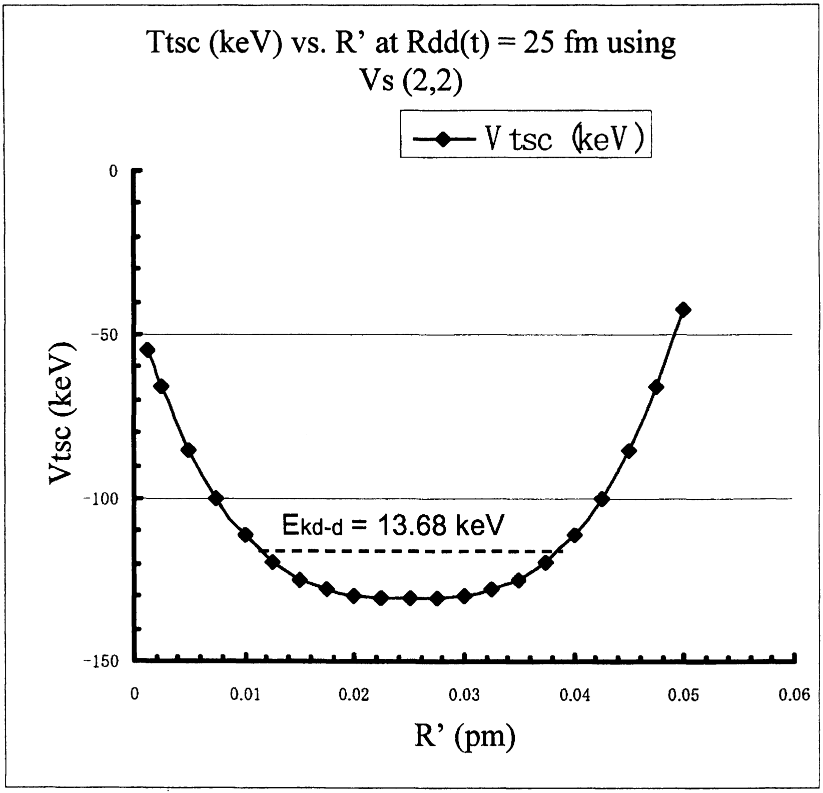

Figure 15. Estimated approximate d-d trapping potential of 4D/TSC at $R_{dd}(t)=25$ fm.

Using Fermi's golden rule (*8*), fusion rate is obtained by

$$\lambda_{nd} = \frac{2}{\hbar}\langle W\rangle P_{nd}(r_0) = 3.04\times10^{21} P_{nd}(r_0)\langle W\rangle \qquad (32)$$

Here the <W> value is in units of MeV.

Calculated barrier factors for typical R_{dd} values are shown in Table II.

In Table II, approximate barrier factors are given according to known D_2-molecule and muonic dd molecule, and also for EQPET dde*(2,2) molecule, respectively.

The imaginary part of optical potential <W> for effective interaction, namely fusion, is estimated by the empirical rule for PEF (pion exchange force number) values (*8*), and given in Table III. Fusion rates are shown in Table IV. Here we used the following relations between astrophysical S-value S_{nd}, T-matrix for the effective interaction Hamiltonian of nuclear fusion T_n, and pion exchange number PEF, in <W> estimation (*8*).

Downloaded by STANFORD UNIV GREEN LIBR on July 1, 2012 | http://pubs.acs.org
Publication Date: August 1, 2008 | doi: 10.1021/bk-2008-0998.ch004

Downloaded by STANFORD UNIV GREEN LIBR on July 1, 2012 | http://pubs.acs.org
Publication Date: August 1, 2008 | doi: 10.1021/bk-2008-0998.ch004

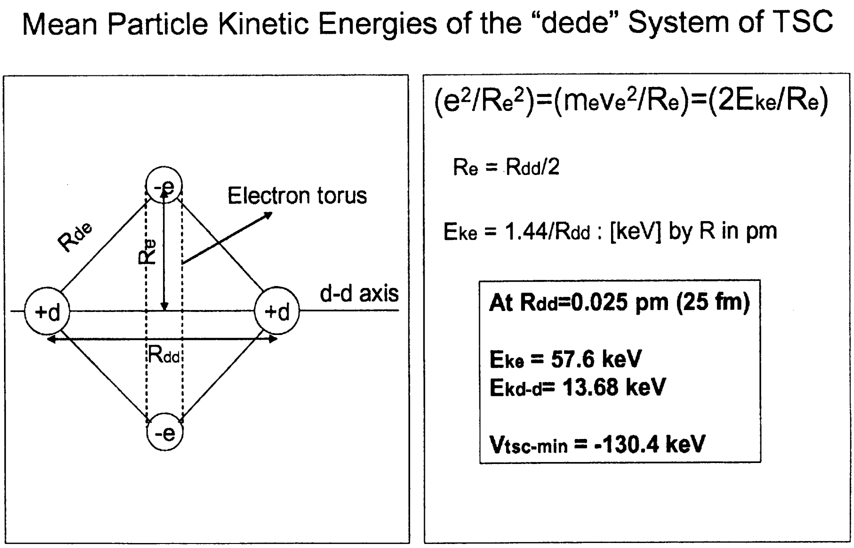

Mean Particle Kinetic Energies of the "dede" System of TSC

$(e^2/R_e^2)=(m_e v_e^2/R_e)=(2E_{ke}/R_e)$

$R_e = R_{dd}/2$

$E_{ke} = 1.44/R_{dd}$: [keV] by R in pm

At R_{dd}=0.025 pm (25 fm)

E_{ke} = 57.6 keV
$E_{kd\text{-}d}$= 13.68 keV

$V_{tsc\text{-}min}$ = -130.4 keV

Figure 16. Estimation of mean kinetic energy of "d-e-d-e" system of diminished 4D/TSC.

$$S_{nd} \propto T_n^2 \propto (PEF)^{10} \tag{33}$$

$$T_n = \langle W \rangle \propto (PEF)^5 \tag{34}$$

And we used known S-values at E_d=0 and <W> values for DD (*16*) and DT reactions, as reference values.

Calculated fusion rate for dd-muon molecule, 2.4×10^{10} f/s/pair corresponds well to fusion rate of dt-muon by Hale-Talley (*14*), $(1.08\text{-}1.29)\times10^{12}$ f/s/pair, considering the dt fusion cross section is 200 times of dd fusion in low energy region. Value for D_2 molecule also looks appropriate.

Calculated 4D fusion rate 3.7×10^{20} f/s/cluster is very large, however this is the value for virtual steady molecule state of 4D/TSC-min. In reality, 4D/TSC-min state can exist only for about 2×10^{-20} s in the final stage of condensation. Now we need to derive formulas for fusion yield for transient 4D/TSC condensation.

Microscopic fusion yield η_{4d} per 4D/TSC is defined, using condensation time t_c (1.4007 fs), as

Downloaded by STANFORD UNIV GREEN LIBR on July 1, 2012 | http://pubs.acs.org
Publication Date: August 1, 2008 | doi: 10.1021/bk-2008-0998.ch004

$$\eta_{4d} = 1 - \exp(-\int_0^{t_c} \lambda_{4d}(t)dt) \tag{35}$$

$$\lambda_{4d}(t) = 3.04\times10^{21}\langle W\rangle P_{4d}(r_0;R_{dd}(t)) = 1.88\times10^{23} P_{4d})r_0;R_{dd}(t)) \tag{36}$$

$$\int_0^{t_c} \lambda_{4d}(t)dt = 1.88\times10^{23}\int_0^{t_c} P_{4d}(r_0;R_{dd}(t))dt \tag{37}$$

$$\int_0^{t_c} P_{4d}(r_0 : R_{dd}(t)dt = 2.31\times10^{-22} \tag{38}$$

We obtain that η_{4d} is very close to 1.0. As a consequence, we get the simplest result:

$$\eta_{4d} \cong 1.0 \tag{39}$$

Therefore macroscopic 4D fusion yield becomes equal to 4D/TSC generation rate in condensed matter (e.g., in PdDx under excitation). Defining the TSC generation rate by Q_{tsc}, we define 4D fusion yield Y_{4d} as

$$Y_{4d} = Q_{tsc}\eta_{4d} \tag{40}$$

Table II. Calculated Barrier Factors for 2d-Pair and 4d-Cluster under TSC Condensation

R_{dd}=R_{gs} (pm)	*P_{2d}; 2D Barrier Factor*	*P_{4d}; 4D Barrier Factor*
0.0206 (TSC-min)	4.44E-2	1.98E-3
0.0412	1.06E-2	1.12E-4
0.103	1.43E-3	2.05E-6
0.206	3.35E-5	1.12E-9
0.412	9.40E-7	2.16E-13
0.805 (μdd): muonic dd	1.00E-9	1.00E-18
1.03	9.69E-11	9.40E-21
2.06	6.89E-15	4.75E-29
4.12	9.38E-21	8.79E-41
10.3	2.16E-32	4.67E-64
21.8 (dde*(2,2)	1.30E-46	1.69E-92
74.1 (D_2 molecule)	1.00E-85	1.00E-170

Table III. Estimation of <W> Values

Cluster	*<W> (MeV)*
DD	0.008
DT	0.115
3D	1.93
4D	62.0

Table IV. Fusion Rates Calculated by Fermi's Golden Rule (Eq. (32))

Molecule	$R_{dd}=R_{gs}$ *(pm)*	P_{nd} *; B-Factor*	*<W> (MeV)*	λ_{2d} *(f/s)*	λ_{4d} *(f/s)*
D_2	74.1	1.0E-85	0.008	2.4E-66	
dde*(2,2)	21.8	1.3E-46	0.008	3.16E-27	
μdd	0.805	1.0E-9	0.008	2.4E+10	
4D/TSC min	0.021	1.98E-3	62		3.7E+20

Practically,

$$Y_{4d} \approx Q_{tsc} \tag{41}$$

4D fusion and its product are:

$$D+D+D+D \rightarrow {}^{8}B^{*} \rightarrow {}^{4}He + {}^{4}He + 47.6MeV \tag{42}$$

Finally, we have reached the simplest conclusion that 4D fusion yield Y_{4d} (f/s/cc) is equal to 4D/TSC generation rate Q_{tsc} (tsc/s/cc) in condensed matter, and the formulation and estimation of Q_{tsc} becomes essentially important for further theoretical elaboration and guiding experiments.

In the case of muonic-dd fusion rate of $2.4x10^{10}$ (f/s) with $2x10^{-6}$ s muon lifetime, almost 100% dd fusion takes place in 200 ps ($2x10^{-10}$ s). So that, muon goes out after one dd-fusion, will be trapped in another muonic-dd molecule and will make plural chain reactions within muon lifetime, as well known.

Since 4d fusion yield is 100% for 4D/TSC-min state, we have no 2d fusion rate in the final stage. In the present model calculation, 2D fusion may take place by dde*(2,2) state just after Cooper pair formation. Fusion yield by dde*(2,2) is estimated in analogous way.

$$\eta_{2d} = 1 - \exp(-\lambda_{2d(2,2)}\tau_{(2,2)}) \tag{43}$$

$$\eta_{2d} \approx \lambda_{2d(2,2)}\tau_{(2,2)} \tag{44}$$

Downloaded by STANFORD UNIV GREEN LIBR on July 1, 2012 | http://pubs.acs.org
Publication Date: August 1, 2008 | doi: 10.1021/bk-2008-0998.ch004

Here τ (2,2) is the lifetime of dde*(2,2). If we may assume very long lifetime as 10^4 s (as asserted by X. Z. Li (*16*)), we obtain $\eta_{2d} = 3.1 \times 10^{-23}$ (f/pair). Even if assuming maximum level of dde*(2,2), or Cooper pair, generation rate of 10^{22} (dde*/s/cc), we get 2D fusion yield of $Y_{2d} = 0.3$ (f/s/cc), so-called Jones' level.

However, we may have small probability that 4D/TSC under condensation may deviate far from expectation position $<R_{dd}(t)>$ and Platonic symmetry would be broken to split into two diminished dde*(m,2) molecules which may cause higher 2D fusion rates. To obtain a quantitative answer to this question, we need to further develop a Monte-Carlo Langevin code to treat random f(t) source for TSC condensation motion. This is one of our future works. Another minor neutron production may come from break-up of ^{8}Be* with 47.6 MeV excited state by 4D fusion going out to minor branch of n + ^{7}Be (Q = - 18.9 MeV).

Downloaded by STANFORD UNIV GREEN LIBR on July 1, 2012 | http://pubs.acs.org
Publication Date: August 1, 2008 | doi: 10.1021/bk-2008-0998.ch004

Conclusions

1. We have introduced a non-linear Langevin equation for the study of molecular dynamics motion of TSC condensation. Developed calculations were very successful in estimating condensation time, barrier factors, and fusion rates.
2. Molecular dynamics of 4D/TSC condensation was numerically solved by the Verlet's time step method.
3. Condensation time of 4D/TSC was very short as 1.4 fs, compared with our primitive analysis (*11*).
4. 4D fusion happens in about 2×10^{-20} s in the last stage of condensation with 100% probability.
5. 4D fusion yield and ^{4}He production yield becomes equal to 4D/TSC generation rate in condensed matter.
6. 2D fusion rate is negligibly small.
7. The concept of heavy mass Cooper pair and HMEQPET potentials is a useful tool to quantify time-dependent d-d trapping potential under condensation of TSC.
8. We need elaboration for developing Monte-Carlo Langevin code, quantitative models for 4D/TSC or 4H/TSC formation in circumstances in/on condensed matter, TSC + host metal interaction for transmutation reactions, etc.

Acknowledgements

We are grateful to Prof. Akira Kitamura, Kobe University, for his valuable discussions on this work.

References

1. Takahashi, A.; Yabuuchi, N. Condensed Matter Nuclear Effects under Platonic Symmetry. Presented at the 13th International Conference on Condensed Matter Nuclear Science, Sochi, Russia, June 25 - July 1, 2007; Paper TM2.
2. Takahashi, A. Mechanism of Deuteron Cluster Fusion by EQPET Model. In *Condensed Matter Nuclear Science: Proceedings of the 10th International Conference on Cold Fusion*, Cambridge, MA, Aug. 24-29, 2003; Hagelstein, P. L.; Chubb, S. R., Eds.; World Scientific Publishing Co.: Singapore, 2006; 809-818.
3. Takahashi A. ^{3}He/^{4}He Production Ratios by Tetrahedral Symmetric Condensation. In *Condensed Matter Nuclear Science: Proceedings of the 11th International Conference on Cold Fusion*, Marseilles, France, Oct. 31 - Nov. 5, 2004; Biberian, J.-P., Ed.; World Scientific Publishing Co.: Singapore, 2006; 730-742.
4. Takahashi, A. Deuteron Cluster Fusion and Related Nuclear Reactions in Metal-Deuterium/Hydrogen Systems. *Recent Res. Devel. Physics* **2005**, *6*, 1-28.
5. Takahashi, A. Deuteron Cluster Fusion and Ash. *J. Condensed Matter Nuclear Science* **2007**, *1*, in press.
6. Takahashi, A. A Theoretical Summary of Condensed Matter Nuclear Effects, Proc. Siena2005 Workshop, *J. Condensed Matter Nuclear Science*, **2007**, *1*, in press; see also Takahashi, A. Brief Theoretical Summary of Condensed Matter Nuclear Effects. *Acta Physica et Chemica* **2005**, *38-39*, 341-356.
7. Takahashi, A. Time-Dependent EQPET Analysis of TSC. In *Condensed Matter Nuclear Science: Proceedings of the 12th International Conference on Cold Fusion*, Yokohama, Japan, Nov. 27-Dec. 2, 2005; Takahashi, A.; Ota, K.-I.; Iwamura, Y., Eds.; World Scientific Publishing Co.: Singapore, 2006; 454-461.
8. Takahashi, A.; Yabuuchi, N. Fusion Rates for Bosonized Condensates. *J. Condensed Matter Nuclear Science* **2007**, *1*, in press.
9. Yabuuchi, N.; Takahashi, A. Comments on Role of CaO-Layer in Iwamura Cold Transmutation. *Proceedings of the JCF7*, Kagoshima, Japan, April 2006; to be published at http://dragon.elc.iwate-u.ac.jp/jcf/index.html.
10. Takahashi, A.; Yabuuchi, N. Comments on Role of CaO Layer in Iwamura Transmutation. *Proceedings of the JCF7*, Kagoshima, Japan, April 2006; to be published at http://dragon.elc.iwate-u.ac.jp/jcf/index.html.
11. Takahashi, A.; Yabuuchi, N. On Condensation Force of TSC. *J. Condensed Matter Nuclear Science*, **2007**, *1*, in press.
12. Takahashi, A.; Yabuuchi, N. Deuterons-to-He-4 Channels. Presented at the 13th International Conference on Condensed Matter Nuclear Science, Sochi, Russia, June 25 - July 1, 2007; Paper TM3.

Downloaded by STANFORD UNIV GREEN LIBR on July 1, 2012 | http://pubs.acs.org
Publication Date: August 1, 2008 | doi: 10.1021/bk-2008-0998.ch004

13. Yabuuchi, N.; Takahashi, A. Form of Nuclear Fusion in Solid Crystals. Presented at the 13th International Conference on Condensed Matter Nuclear Science, Sochi, Russia, June 25 - July 1, 2007; Paper TM34.
14. Hale, G. M.; Talley, T. L. Deuteron-Induced Fusion in Various Environments. *Fusion Technol.* **1994**, *26*, 442-450.
15. Verlet, L., Computer Experiments on Classical Fluids. I. Thermodynamical Properties of Lennard-Jones Molecules. *Phys. Rev.* **1967**, *159*, 98. See also Ueda, A. *Computer Simulation, Atomic Motion in Macroscopic Systems,* Chapter 2; Asakura Publ.: Tokyo, 1996.
16. Li, X. Z., et al., Sub-Barrier Fusion and Selective Resonant Tunneling. *Phys. Rev. C* **2000**, *61*, 24610.

Downloaded by STANFORD UNIV GREEN LIBR on July 1, 2012 | http://pubs.acs.org
Publication Date: August 1, 2008 | doi: 10.1021/bk-2008-0998.ch004

Appendix

Shielded Coulomb potential, equivalently d-d trapping potential, for dde*(m,Z) EQPET molecule is given in our previous works (*4, 8*) as

$$V_s(R_{dd};m,Z) = V_h + \frac{1.44}{R_{dd}} + \frac{J+K}{1+\Delta} \qquad \text{(A-1)}$$

with

$$V_h = -0.013mZ^2[keV] \qquad \text{(A-2)}$$

$$J = 0.0272Z^2m\left(-\frac{1}{y} + \left(1+\frac{1}{y}\right)\exp(-2y)\right) \qquad \text{(A-3)}$$

$$K = 0.0272Z^2m(1+y)\exp(-y)) \qquad \text{(A-4)}$$

$$\Delta = \left(1+y+\frac{y^2}{3}\right)\exp(-y) \qquad \text{(A-5)}$$

$$y = \frac{Zm}{52.9}R_{dd} \qquad \text{(A-6)}$$

The derivative of the potential becomes, with R_{dd} in units of pm and energy in units of keV,

$$\frac{\partial V_s(R_{dd};m,Z)}{\partial R_{dd}} = -\frac{1.44}{R_{dd}{}^2} + \frac{(J'+K')(1+\Delta)+(J+K)\Delta'}{(1+\Delta)^2} \qquad \text{(A-7)}$$

with

$$J' = 5.14\times10^{-4} Z^3 m^2 \left(\frac{1-\exp(-2)}{y^2} - 2\left(1+\frac{1}{y}\right)\exp\left(-2y\right) \right) \quad \text{(A-8)}$$

$$K' = -5.14\times10^{-4} Z^3 m^2 y \exp(-y) \quad \text{(A-9)}$$

$$\Delta' = -6.30\times10^{-3} (y + y^3) \exp(-y) \quad \text{(A-10)}$$

Here R and r are given in units of [pm], energy in units of [keV], and time in units of [fs].

Downloaded by STANFORD UNIV GREEN LIBR on July 1, 2012 | http://pubs.acs.org
Publication Date: August 1, 2008 | doi: 10.1021/bk-2008-0998.ch004

Downloaded by COLUMBIA UNIV on July 1, 2012 | http://pubs.acs.org
Publication Date: August 1, 2008 | doi: 10.1021/bk-2008-0998.ch005

Chapter 5

How to Explain Cold Fusion?

Edmund Storms

Energy K. Systems, 2140 Paseo Ponderosa, Santa Fe, NM 87501

Cold fusion has been a challenge to explain. Hundreds of attempts have been made, most of which are inconsistent with either observation or well-established conventional theories. This paper evaluates some of the attempts and suggests approaches and observations that need to be considered.

Introduction

The phenomenon conventionally called "cold fusion" (*1-3*) and now more accurately termed "low energy nuclear reaction" (LENR) has been generally rejected because it is difficult to replicate and to explain. The problem of replication has been examined previously in detail (*4*). This examination concluded that the nuclear effects have been duplicated many times when the correct conditions within the so-called nuclear-active-environment (NAE) were created. These special conditions are only now, 18 years after the original discovery by Profs. Fleischmann and Pons (*5-12*), well enough understood to make frequent replication possible. Nevertheless, considerable skill is still required.

Even though evidence for nuclear reactions has been obtained in many experiments using a variety of methods, the magnitude of the nuclear reactions has a very wide range, being between the detection limit near 1 event/sec to over 10^{14} events/sec. Reactions near the low end of the range can be explained by making minor modifications to conventional theory. On the other hand, reaction rates near the high end defy conventional explanation. This discussion concerns attempts to explain the high end of the range.

Unlike heat energy, detection of radiation is generally unambiguous and clearly indicative of a nuclear process. Only the source is unknown. People should take notice when unexpected nuclear activity is produced by "normal" chemical reactions, as has been reported. Even if no excess energy is detected at the same time, these observations demand an explanation. Naturally, unexpected

In Low-Energy Nuclear Reactions Sourcebook; Marwan, J., et al.;
ACS Symposium Series; American Chemical Society: Washington, DC, 2008.

Downloaded by COLUMBIA UNIV on July 1, 2012 | http://pubs.acs.org
Publication Date: August 1, 2008 | doi: 10.1021/bk-2008-0998.ch005

energy will be found when the nuclear rate becomes large enough, as has happened on many occasions.

The nuclear reactions have been initiated under a variety of conditions using several methods. If a model appropriate to only one of these conditions is proposed, we are then forced to believe that different unique mechanisms operate to produce similar results when the other conditions are present. In other words, we must accept many "miracles" to explain all of the observations. Just how many mechanisms are operating in the LENR process is an important question. The correct theory is the one that explains the effects regardless which method is used.

This discussion focuses on proposed explanations without addressing the mathematical arguments. Mathematical logic is only as good as the assumptions on which it is based. If the assumptions are wrong or if the mathematical logic leads to a conclusion at odds with observation, the mathematical equations are not relevant, no matter how correct, complex, or clever they might be. Consequently, this paper will focus on the assumptions needed to explain the novel observations. Evaluation of proposed models is frequently made difficult when authors build one assumption upon another, any one of which could invalidate the effort. As a result, hundreds of theoretical variations have been suggested containing a variety of assumptions. Hopefully, this general discussion will help guide thinking away from some of the less productive ideas without an evaluation of each theory being necessary.

LENR describes nuclear processes that operate in a special solid under relatively low-energy conditions. These reactions include fusion-like reactions involving deuterium that result mostly in ^{4}He production. Occasionally, tritium, transmutation products, and elements that appear to result from fission of elements in the solid are found even when light hydrogen is used instead of deuterium. Energetic radiation consisting of alpha, beta, gamma, and/or X-ray is produced on occasion. Neutron production is observed infrequently and at very low levels. On occasion some of the nuclear reactions occur at rates sufficient to make measurable heat. The nuclear products and types of energetic radiation reported depend on the conditions and, as expected, on the detection methods used by the experimenter. As the detection methods improve, an increasing amount of anomalous nuclear behavior is being seen. Details about the observations can be found in a recent book (*4*).

These reactions are very sensitive to the solid environment in which they occur, which makes duplication of the critical conditions very difficult. As a result, replication is achieved only after many attempts. The effects do not occur in "normal" material. All theories need to take this important fact into account by identifying the unique and rarely created conditions, i.e., the NAE. In addition, applied voltage and electric current are not required to make the nuclear process occur and should not be part of the proposed mechanism. In other words, the proposed mechanism can occur in difficult-to-create structures containing rare conditions without external stimulation. Nevertheless, the rate of reaction, once the unique conditions are created, is increased by applied energy such as provided by lasers (*13-15*), increased temperature (*9, 16, 17*), or ion bombardment (*18-22*).

No matter how the proposed process is structured, the Coulomb barrier must be addressed. Conventional thinking recognizes its penetration by neutrons, its neutralization by electrons (screening), or penetration using the brute force of energetic charged particles (hot fusion). Once sufficient energy has been applied, resonance or tunneling processes can enhance the effect. Nevertheless, these processes require the localization of considerable energy before they can operate. If the neutrons are not initially present in the environment, they must be created. This requires that 0.78 MeV be added to an electron to permit it to react with a proton. If electrons are accumulated and forced to concentrate near the nucleus, in order to produce sufficient screening, their energy must be increased. This energy has to come from the surrounding atoms. How can energy required to form a neutron or cause sufficient screening be localized? Energy of this magnitude simply does not concentrate in single atoms or electrons and would be a violation of the Second Law of Thermodynamics if it did occur. Even quantum mechanics, which is invoked by several models, requires energy to surmount the barrier between atoms. Therefore, the first test of a proposed mechanism asks the question, "Is a plausible source of energy available?" Of course, if energy sufficient to initiate a nuclear reaction could be spontaneously concentrated in a few atoms or electrons, chemistry as we know it could not exist. A sudden and random concentration of energy would initiate chemical reactions, with easily observed consequences, long before sufficient energy had been accumulated to cause a nuclear reaction. As a result, such models have to make an unstated and unsupported assumption, i.e., that the energy used to overcome the Coulomb barrier or to make a neutron does not interact with the chemical environment even though this is the source of the energy.

This discussion focuses on recent suggested models because early attempts were severely handicapped by lack of reliable observation on which to base a theory. Only a few of the suggested models are cited here, so as to provide examples without belaboring the point. By now, sufficient information is available to eliminate many imagined mechanisms.

How to Test a Theory

A model is useless unless it can be tested. Normally, proposed models are tested by comparing the logical consequence of their action to what has been observed. In addition, a theory must also be consistent with what is not observed, while remaining consistent with well-established and accepted behavior, in this case nuclear behavior. For example, if neutrons are proposed to be involved in the process, the normally observed decay energy and half-life of neutron decay should be detected. In addition, when the neutrons react with other nuclei, gamma emission and radioactive isotopes will be produced. Other energetic particles can also produce secondary nuclear reactions and emissions under

Downloaded by COLUMBIA UNIV on July 1, 2012 | http://pubs.acs.org
Publication Date: August 1, 2008 | doi: 10.1021/bk-2008-0998.ch005

certain conditions. For example, beta emission will result in energetic X-rays (Bremsstrahlung), and energetic alpha emission can produce neutrons. These secondary products must be detected or their absence explained if the proposed primary process is to be accepted.

Neutron Emission

Initially, the claims of Fleischmann and Pons were explained as being caused by a "normal" fusion reaction, similar to the one known to occur at high energy. This reaction generates neutrons and tritium as the most easily detected products. The presence of no more than a few neutrons and hardly any tritium led to a search for helium as the main nuclear product, as will be discussed in the next section. In spite of very few neutrons being detected, a model based on the involvement of neutrons as a cause rather than a result is attractive because the absence of a charge on the neutron eliminates the need to overcome the Coulomb barrier when fusion or transmutation occurs. However, a source of neutrons has to be available, which several people have attempted to identify.

Kozima (*23, 24*) proposes that neutrons occupy all materials in a stable assembly called the Trapped Neutron Catalyzed Fusion model. The cold fusion environment can break up these assemblies, allowing the free neutrons to initiate nuclear reactions. Fisher (*25, 26*) proposes that extra neutrons are lightly stuck to normal nuclei. These polyneutrons are released under certain conditions and enter into nuclear reactions. If extra neutrons are present, as these two models propose, the measured density of material should reflect the extra mass, which has not been observed. However, Oriani (*27*) found what appears to be extra-heavy CO_2 in a mass spectrum after a cold fusion experiment. Once the proposed stabilizing condition has been destroyed, evidence of neutron emission and decay should be detected. For example, vaporization of the stabilizing structure in the case of neutron clusters, or bombardment of a nuclei with energetic ions in the case of polyneutrons, should cause neutron release and detection. These expectations have not been satisfied.

Some researchers (*28-35*) have proposed that isolated protons or deuterons can take up normal electrons to create neutrons or dineutrons, respectively. Because this is an endothermic process, it is not expected to occur spontaneously. No experimental evidence has been provided to show that spontaneous formation of neutrons from protons and electrons actually occurs in nature under ambient conditions. However, this conversion can take place within a nucleus by a natural process called k-capture. K-capture occasionally occurs when an unstable nucleus can gain more energy by converting a proton into a neutron than it expends by making this conversion. In the process, the electron is sucked into the nucleus from the k-shell of the surrounding electrons. Zhang and Zhang (*36*) examine the half-life of isotopes that experience k-capture and relate this to the number of neutrons present in the nucleus. Based on this analysis, they estimate the half-life for deuteron k-capture to be 10^{11} years. This rate is too

Downloaded by COLUMBIA UNIV on July 1, 2012 | http://pubs.acs.org
Publication Date: August 1, 2008 | doi: 10.1021/bk-2008-0998.ch005

small to have any importance to the LENR process even if the process actually occurs in nature. In addition, the naturally occurring, stable elements, as are present in a cold fusion cell, are not known to experience this process. Even if the process should occur, characteristic X-rays are produced and would reveal which element is involved in the conversion. At reaction rates above the middle of the observed range, these X-rays should be easy to detect and dangerous at higher rates. X-rays have been detected, but they have not been shown to result from k-capture.

A mechanism has been suggested recently by Widom and Larsen (*37-40*) based on a series of especially extraordinary assumptions, as follows:

1. Energy provided by the voltage gradient on an electrolyzing surface can add incrementally to an electron, causing its mass to increase. This implies the existence of energy levels within the electron able to hold added energy long enough for the total to be increased to 0.78 MeV mass equivalent by incremental addition. This idea, by itself, is extraordinary and inconsistent with accepted understanding of the electron.
2. Once sufficient energy has accumulated, the massive electron will combine with a proton to create a neutron having very little thermal energy. This implies that the massive electron reacts only with a proton rather than with the more abundant metal atoms making up the sample and does not shed energy by detectable X-ray emission before it can be absorbed.
3. This "cold" neutron will add to the nucleus of palladium and/or nickel to change their isotopic composition. This implies that the combination of half-lives created by beta emission of these created isotopes will quickly result in the observed stable products without this beta emission being detected.
4. The atomic number distribution of transmutation products created by this process matches the one reported by Miley (*41*) after he electrolyzed Pd+Ni as the cathode and Li_2SO_4+H_2O as the electrolyte. This implies that the periodic function calculated by the authors actually has a relationship to the periodic behavior observed by Miley in spite of the match being rather poor. In addition, residual beta decay has not been detected.
5. Gamma radiation produced by the neutron reaction is absorbed by the super-heavy electrons. This implies that the gamma radiation can add to the mass and/or to the velocity of the super-heavy electron without producing additional radiation. In addition, to be consistent with observation, total absorption of gamma radiation must continue even after the cell is turned off. If this assumption were correct, super-heavy electrons would provide the ideal protection from gamma radiation.

These assumptions are not consistent with the general behavior of the LENR phenomenon nor with experience obtained from studies of electron behavior. Indeed, these assumptions, if correct, would have extraordinary importance independent of cold fusion.

Downloaded by COLUMBIA UNIV on July 1, 2012 | http://pubs.acs.org
Publication Date: August 1, 2008 | doi: 10.1021/bk-2008-0998.ch005

Neutron production has been observed when energy much greater than ambient but less than 0.78 MeV is present (*42-45*), suggesting either that energy can be added incrementally or that neutron behavior can occur without complete formation of a neutron. This and other observations cause several authors (*46-49*) to conclude that a virtual neutron could form for a brief time if an electron could shield a proton long enough for it to overcome the Coulomb barrier without actually forming a neutron. This shielding mechanism is also proposed to take place when hydrinos form by the process suggested by Mills (*50, 51*). If the shielding electron remains outside of the resulting nucleus after the nuclear interaction, this process would be equivalent to a proton or deuteron entering the target nucleus rather than a neutron or dineutron. The Mills variation on this mechanism has several attractive features. Formation of the "virtual" neutron, i.e., hydrino or deutrino, is an exothermic process, thereby eliminating the need to concentrate energy at a few particles; the hydrino or deutrino can form clusters, as have been found to be involved in the transmutation process (*52, 53*); and transmutation can take place without delayed beta emission, as has been generally observed. Prompt emission of the Mills electrons might explain how the energy leaves the nuclear reaction site without being detected by present efforts. This process would also explain the apparent lack of the required second reaction product when transmutation occurs (*52, 54, 55*).

Regardless of the manner by which a neutron, either virtual or real, is made, the unique conditions that cause the neutron to form must be identified. Only Mills (*51, 56*) has clearly identified this unique condition. In this case, a special catalyst is required to reduce the electron to a level near the nucleus. If this claim were correct, past reproducibility would be related in part to the chance presence or absence of this catalyst.

Downloaded by COLUMBIA UNIV on July 1, 2012 | http://pubs.acs.org
Publication Date: August 1, 2008 | doi: 10.1021/bk-2008-0998.ch005

Alpha Emission

Generation of energy has been clearly correlated with helium production (*57-63*), with 25±5 MeV/helium being the weighted average of the various measurements (*4*). This suggests alpha particles are emitted with considerable energy. In the absence of detected gamma emission, this energy must be shared between at least two particles. The more particles involved in this process, the less energy each has to carry. Chubb and Chubb (*64-67*) propose that this energy is coupled directly to the surrounding atoms within the lattice structure by a process that involves particle-wave conversion. By immediately sharing the energy with many atoms, emission of detectable energetic emission is avoided. Hagelstein (*68, 69*) also proposes that energy is coupled to the lattice, but in this case by phonons. Except for the Mössbauer process, such direct coupling of nuclear energy has not been observed before. Takahashi (*70*) proposes that several deuterons condense into a cluster such that two alphas can form simultaneously, thereby sharing the energy and momentum. Formation of such a cluster by the proposed method requires localized energy, hence is unlikely to occur spontaneously at the required rate. Each of these models is addressing one narrow aspect of the phenomenon by making several unsupported assumptions.

Because these particles have a very limited range even in air, their detection has been difficult. Nevertheless, efforts need to be made to demonstrate experimentally whether energetic particles are emitted or not. Arguments based on mathematical models are not sufficient. Toward this end, a number of efforts have succeeded in detecting energetic particle emission, including alpha (*71-76*). These observations raise the following questions:

1. Does the detected alpha emission originate from the heat-helium producing reaction?
2. Does the detected alpha emission instead originate from a low-rate reaction having no relationship to the heat-helium reaction?

Downloaded by COLUMBIA UNIV on July 1, 2012 | http://pubs.acs.org
Publication Date: August 1, 2008 | doi: 10.1021/bk-2008-0998.ch005

If the answer to Question #1 is yes, direct coupling of energy to the lattice is no longer required, and additional issues are raised. If the answer to Question #2 is yes, we need to discover just how many unexpected nuclear processes are operating in these benign environments.

Any model proposing that energetic alpha emission results from a nuclear reaction has to also take into account the expected (α, n) reaction. Energetic alphas will react with various nuclei to produce neutrons. For example, ^{11}B bombarded by energetic alpha will produce ^{14}N along with neutrons at energies up to 6 MeV (*77*). Some boron is expected to deposit on an active cathode during Fleischmann-Pons electrolysis because slow dissolution of the Pyrex container by the LiOD electrolyte will provide boron to the electrolyte. Such energetic neutrons have been reported (*78*), but at a very low level. Energetic alphas can also produce neutrons by reacting with isotopes of carbon, oxygen, and nitrogen. Beryllium is particularly susceptible to this reaction, but its presence in a Fleischmann-Pons cell is unlikely. In the case of nitrogen, radioactive isotopes of fluorine having detectable half-lives are produced. Consequently, generation of energetic alpha emission at rates able to produce detectable heat is expected to produce detectable neutron emission and perhaps radioactivity. Efforts to correlate heat production with neutron emission or the presence of radioactive products have been largely unsuccessful. This failure suggests the helium is not produced with significant energy. Proposed theories need to address the question, "Why does the nuclear energy resulting from a fusion-like reaction not cause the consequences expected of energetic alpha emission?"

Beta Emission

Energetic electrons (beta emission) result from neutron decay and from many radioactive isotopes. Beta emission is stopped easily by the wall of a typical cold fusion cell. As a result, it will not be detected outside of the apparatus unless special provisions are made. However, beta emitters have a half-life that frequently is long enough to allow detection by examining an energy-producing cathode after an experiment. On occasion, beta emitters other than tritium are detected after heat production, but this is rare. Even when transmutation products are made, they are very seldom radioactive. Nevertheless, radioactive isotopes having a very short or a very long half-life could be easily overlooked.

Most of the detected transmutation products, if they originate from neutron absorption, will produce a decay chain involving beta emitters with a wide range of half-lives. Unless evidence for this decay chain is obtained, the initiating model cannot be accepted. In addition, beta emission will produce X-rays (Bremsstrahlung), which, if it is intense enough, can be detected outside of a typical cell. Failure to detect these X-rays is a reason to reject an intense beta source being present. Too few active cells have been examined by the necessary detectors to know if this X-radiation is always present or not.

Downloaded by COLUMBIA UNIV on July 1, 2012 | http://pubs.acs.org
Publication Date: August 1, 2008 | doi: 10.1021/bk-2008-0998.ch005

Gamma Emission

Gamma emission is expected to result when two deuterons fuse to make helium, when a neutron enters a nucleus, and frequently when beta emission occurs. Unlike alpha and beta radiation, each of which has a definite range in materials, a gamma flux degrades by an amount that depends on the half-thickness associated with the energy and the type of material. In other words, if the gamma flux is sufficiently intense, some fraction can be detected outside of the apparatus. The energy of the photon will not be changed; only the number of photons will be reduced. Consequently, the energy of each remaining photon can be used to identify the source. As a result, gamma and X-ray emission are easy to detect and, when found, demonstrate the occurrence of anomalous nuclear reactions in LENR environments.

Conclusion

Nuclear processes always result in a variety of associated behaviors. These associations need to be acknowledged by all theories applied to the LENR process. The usefulness and correctness of a theory can be judged by how well these interacting behaviors are described. Enough information is now available that theory no longer has to make as many unsupported assumptions as were required in the past. In fact, the process is looking increasingly "normal" except for the conditions required for its initiation.

References

1. Mallove, E. *Fire from Ice*; John Wiley: New York, 1991.
2. Beaudette, C. G. *Excess Heat: Why Cold Fusion Research Prevailed*; Oak Grove Press (Infinite Energy, Distributor): Concord, NH, 2000.
3. Krivit, S. B.; Winocur, N. *The Rebirth of Cold Fusion: Real Science, Real Hope, Real Energy*; Pacific Oaks Press: Los Angeles, CA, 2004.
4. Storms, E. *The Science of Low Energy Nuclear Reaction*; World Scientific: Singapore, 2007.
5. Fleischmann, M.; Pons, S.; Hawkins, M. Electrochemically Induced Nuclear Fusion of Deuterium. *J. Electroanal. Chem.* **1989**, *261*, 301 (and errata in *263*).
6. Fleischmann, M.; Pons, S.; Anderson, M. W.; Li, L. J.; Hawkins, M. Calorimetry of the Palladium-Deuterium-Heavy Water System. *J. Electroanal. Chem.* **1990**, *287*, 293.
7. Pons, S.; Fleischmann, M. Calorimetric Measurements of the Palladium/Deuterium System: Fact and Fiction. *Fusion Technol.* **1990**, 17, 669.
8. Fleischmann, M.; Pons, S. Some Comments on the Paper "Analysis of Experiments on the Calorimetry of LiOD-D_2O Electrochemical Cells," R.H. Wilson et al., J. Electroanal. Chem. 332 [1992] 1. *J. Electroanal. Chem.* **1992**, *332*, 33.
9. Fleischmann, M.; Pons, S. Calorimetry of the Pd-D_2O System: From Simplicity via Complications to Simplicity. *Phys. Lett. A* **1993**, *176*, 118.
10. Pons, S.; Fleischmann, M. Heat after Death. *Trans. Fusion Technol.* **1994**, *26*, 97.
11. Pons, S.; Fleischmann, M. Etalonnage du systeme Pd-D_2O: Effets de protocole et feed-back positif ["Calibration of the Pd-D_2O System: Protocol and Positive Feedback Effects"]. *J. Chim. Phys.* **1996**, *93*, 711.
12. Fleischmann, M. Reflections on the Sociology of Science and Social Responsibility in Science, in Relationship to Cold Fusion. *Accountability Res.* **2000**, *8*, 19.
13. Letts, D.; Cravens, D. Laser Stimulation of Deuterated Palladium: Past and Present. In *Condensed Matter Nuclear Science: Proceedings Of The 10th International Conference On Cold Fusion*, Cambridge, MA, Aug. 24-29, 2003; Hagelstein, P. L.; Chubb, S. R., Eds.; World Scientific Publishing Co.: Singapore, 2006; 159.
14. Nassisi, V. Transmutation of Elements in Saturated Palladium Hydrides by an XeCl Excimer Laser. *Fusion Technol.* **1998**, *33*, 468.
15. Di Giulio, M.; Filippo, E.; Manno, D.; Nassisi, V. Analysis of Nuclear Transmutations Observed in D- and H-Loaded Films. *J. Hydrogen Eng.* **2002**, *27*, 527.
16. Mengoli, G.; Bernardini, M.; Manduchi, C.; Zannoni,, G. Calorimetry Close to the Boiling Temperature of the D_2O/Pd Electrolytic System. *J. Electroanal. Chem.* **1998**, *444*, 155.
17. Lonchampt, G.; Biberian, J.-P.; Bonnetain, L.; Delepine, J. Electrolysis of LaAlO3 Single Crystals and Ceramics in a Deuteriated Atmosphere. In

Downloaded by COLUMBIA UNIV on July 1, 2012 | http://pubs.acs.org
Publication Date: August 1, 2008 | doi: 10.1021/bk-2008-0998.ch005

Proceedings of The Seventh International Conference on Cold Fusion, Vancouver, Canada, April 19-24, 1998; ENECO, Inc.: Salt Lake City, UT, 1988; 202.

18. Czerski, K.; Heide, P.; Huke, A. Electron Screening Constraints for the Cold Fusion. In *Condensed Matter Nuclear Science: Proceedings Of The 11th International Conference On Cold Fusion*, Marseilles, France, Oct. 31 - Nov. 5, 2004; Biberian, J.-P., Ed.; World Scientific Publishing Co.: Singapore, 2006; 228.
19. Takahashi, A.; Miyadera, H.; Ochiai, K.; Katayama, Y.; Hayashi, T.; Dairaku, T. Studies on 3D Fusion Reactions in TiDx under Ion Beam Implantation. In *Condensed Matter Nuclear Science: Proceedings of the 10th International Conference on Cold Fusion*, Cambridge, MA, Aug. 24-29, 2003; Hagelstein, P. L.; Chubb, S. R., Eds.; World Scientific Publishing Co.: Singapore, 2006; 657.
20. Kasagi, J.; Yuki, H.; Itoh, T.; Kasajima, N.; Ohtsuki, T.; Lipson, A. G. Anomalously Enhanced D(d,p)T Reaction in Pd and PdO Observed at Very Low Bombarding Energies. In *Proceedings of the Seventh International Conference on Cold Fusion*, Vancouver, Canada, April 19-24, 1998; ENECO, Inc.: Salt Lake City, UT, 1988; 180.
21. Karabut, A. Research into Low-Energy Nuclear Reactions in Cathode Sample Solid with Production of Excess Heat, Stable and Radioactive Impurity Nuclides. In *Condensed Matter Nuclear Science: Proceedings of the 12th International Conference on Cold Fusion*, Yokohama, Japan, Nov. 27-Dec. 2, 2005; Takahashi, A.; Ota, K.-I.; Iwamura, Y., Eds.; World Scientific Publishing Co.: Singapore, 2006; 214.
22. Savvatimova, I.; Gavritenkov, D. V. Influence of Parameters of Glow Discharge on Change of Structure and the Isotope Composition of the Cathode Materials. In *Condensed Matter Nuclear Science: Proceedings of the 12th International Conference on Cold Fusion*, Yokohama, Japan, Nov. 27Dec. 2, 2005; Takahashi, A.; Ota, K.-I.; Iwamura, Y., Eds.; World Scientific Publishing Co.: Singapore, 2006; 231.
23. Kozima, H. The TNCF model - A Phenomenological Model for the Cold Fusion Phenomenon. *J. New Energy* **1997**, *2*, 43.
24. Kozima, H. *The Science of the Cold Fusion Phenomenon*; Elsevier Science: London, UK, 2006.
25. Fisher, J. C. Liquid-Drop Model for Extremely Neutron Rich Nuclei. *Fusion Technol.* **1998**, *34*, 66.
26. Fisher, J. C. Outline of Polyneutron Physics (Basics). Presented at the Sixth International Workshop on Hydrogen/Deuterium Loaded Metals, Siena, Italy, May 13-15, 2005.
27. Oriani, R. A. Anomalous Heavy Atomic Masses Produced by Electrolysis. *Fusion Technol.* **1998**, *34*, 76.
28. Pokropivnii, V. V. Bineutron Theory of Cold Nuclear Fusion. *Dokl. Akad. Nauk. Ukr.* **1993**, 86.
29. Chen, X.; Yang, J., Studies on Dineutron Model of Cold Fusion (I). *Hunan Shifan Daxue Ziran Kexue Xuebao* **1993**, *16*, 42.
30. Yang, J. (2)(1)H-e Touched Capturing and (2)(1)H-(2)(0)N Fusion. *Acta Sci. Nat. Univ. Norm. Hunanensis* **1992**, *15*, 18.

Downloaded by COLUMBIA UNIV on July 1, 2012 | http://pubs.acs.org
Publication Date: August 1, 2008 | doi: 10.1021/bk-2008-0998.ch005

31. Timashev, S. F. Possible Mechanisms for Nuclear-Chemical Trans-formations in a Palladium Matrix during Heavy Water Electrolysis. *Zh. Fiz. Khim.* **1989,** *63*, 2283.
32. Russell, J. L., Jr. On the Nature of the Cold Fusion Process. *Ann. Nucl. Energy* **1993,** *20*, 227.
33. Yang, J.; Tang, L.; Chen, X. Possible Nuclear Process in Deuterium-Metal System. *J. Changsa Univ. Elec. Power (Nat. Sci.)* **1996,** *11*, 289.
34. Moon, D. Mechanisms of a Disobedient Science: A Cold Fusion Theory, *Infinite Energy* **1995,** *1*, 34.
35. Chatterjee, L. Electrolysis in Thin-Film Nickel Coatings: Mimicking Supernova Physics? *Fusion Technol.* **1998,** *34*, 147.
36. Zhang, Z.-L.; Zhang, W.-S. Possibility of Electron Capture by Deuteron. In *Condensed Matter Nuclear Science: Proceedings of the 9th International Conference on Cold Fusion*, Beijing, China, May 19-24, 2002; Li, X. Z., Ed.; Tsinghua Univ. Press: Beijing, 2002; 439.
37. Widom, A.; Larsen, L. Nuclear Abundances in Metallic Hydride Electrodes of Electrolytic Chemical Cells. 2006. arXiv:cond-mat/0602472. arXiv.org e-Print archive. http://arxiv.org/abs/cond-mat/0602472.
38. Widom, A.; Larsen, L. Theoretical Standard Model Rates of Proton to Neutron Conversions near Metallic Hydride Surfaces. 2006. arXiv:nuclth/0608059. arXiv.org e-Print archive. http://arxiv.org/abs/nucl-th/0608059.
39. Widom, A.; Larsen, L. Ultra Low Momentum Neutron Catalyzed Nuclear Reactions on Metallic Hydride Surfaces. *Eur. Phys. J.* **2006,** *C46*, 107.
40. Widom, A.; Larsen, L. Absorption of Nuclear Gamma Radiation by Heavy Electrons on Metallic Hydride Surfaces. 2005. arXiv:cond-mat/0509269. arXiv.org e-Print archive. http://arxiv.org/abs/cond-mat/0509269.
41. Miley, G., On the Reaction Product and Heat Correlation for LENRs. In *ICCF8: Proceedings of the Eighth International Conference on Cold Fusion*, Lerici (La Spezia), Italy, May 21-26, 2000; Scaramuzzi, F., Ed.; Italian Physical Society: Bologna, Italy, 2001; 419.
42. Conte, E.; Pieralice, M. Experimental Evidence on the Cold Fusion of Protons and Electrons into Neutrons. *Infinite Energy* **1999,** *24*, 55.
43. Kamada, K.; Kinoshita, H.; Takahashi, H. Anomalous Heat Evolution of Deuterium-Implanted Al upon Electron Bombardment. *Jpn. J. Appl. Phys. A* **1996,** *35*, 738.
44. Borghi, C.; Giori, C.; Dall'Olio, A. Experimental Evidence on the Emission of Neutrons from Cold Hydrogen Plasma. *Phys. At. Nucl.* **1993,** *56*, 939.
45. Conte, E.; Pieralice, M. An Experiment Indicates the Nuclear Fusion of a Proton and Electron into a Neutron. *Infinite Energy* **1999**, *4*, 67.
46. Daddi, L. Proton-Electron Reactions as Precursors of Anomalous Nuclear Events. *Fusion Technol.* **2001,** *39*, 249.
47. Das, D.; Ray, M. K. S. Fusion in Condensed Matter -A Likely Scenario. *Fusion Technol.* **1993,** *24*, 115.
48. Dufour, J. Cold Fusion by Sparking in Hydrogen Isotopes. *Fusion Technol.* **1993,** *24*, 205.
49. Miley, G. H.; Shrestha, P. J. Review of Transmutation Reactions in Solids. In *Condensed Matter Nuclear Science: Proceedings of the 10th International*

Downloaded by COLUMBIA UNIV on July 1, 2012 | http://pubs.acs.org
Publication Date: August 1, 2008 | doi: 10.1021/bk-2008-0998.ch005

Conference on Cold Fusion, Cambridge, MA, Aug. 24-29, 2003; Hagelstein, P. L.; Chubb, S. R., Eds.; World Scientific Publishing Co.: Singapore, 2006; 361.

50. Mills, R. L.; Good, W. R.; Shaubach, R. M., Dihydrino Molecule Identification. *Fusion Technol.* **1994**, *25*, 103.
51. Mills, R. *The Grand Unified Theory of Classical Quantum Mechanics*; Cadmus Professional Communications: Ephrata, PA, 2006.
52. Iwamura, Y.; Itoh, T.; Sakano, M.; Yamazaki, N.; Kuribayashi, S.; Terada, Y.; Ishikawa, T. Observation of Surface Distribution of Products by X-Ray Fluorescence Spectrometry during D_2 Gas Permeation through Pd Complexes. In Condensed Matter Nuclear Science: P*roceedings of the 12th International Conference on Cold Fusion*, Yokohama, Japan, Nov. 27-Dec. 2, 2005; Takahashi, A.; Ota, K.-I.; Iwamura, Y., Eds.; World Scientific Publishing Co.: Singapore, 2006; 178.
53. Iwamura, Y.; Sakano, M.; Itoh, T. Elemental Analysis of Pd Complexes: Effects of D_2 Gas Permeation. *Jpn. J. Appl. Phys. A* **2002**, *41*, 4642.
54. Iwamura, Y.; Itoh, T.; Sakano, M.; Yamazaki, N.; Kuribayashi, S.; Terada, Y.; Ishikawa, T.; Kasagi, J. Observation of Nuclear Transmutation Reactions Induced by D_2 Gas Permeation through Pd Complexes. In *Condensed Matter Nuclear Science: Proceedings of the 11th International Conference on Cold Fusion*, Marseilles, France, Oct. 31 - Nov. 5, 2004; Biberian, J.-P., Ed.; World Scientific Publishing Co.: Singapore, 2006; 339.
55. Iwamura, Y.; Itoh, T.; Sakano, M.; Sakai, S.; Kuribayashi, S. Low Energy Nuclear Transmutation in Condensed Matter Induced by D_2 Gas Permeation through Pd Complexes: Correlation between Deuterium Flux and Nuclear Products. In *Condensed Matter Nuclear Science: Proceedings of the 10th International Conference on Cold Fusion*, Cambridge, MA, Aug. 24-29, 2003; Hagelstein, P. L.; Chubb, S. R., Eds.; World Scientific Publishing Co.: Singapore, 2006; 435.
56. Mills, R. L.; Ray, P. The Grand Unified Theory of Classical Quantum Mechanics. *J. Hydrogen Eng.* **2002**, *27*, 565.
57. Bush, B. F.; Lagowski, J. J.; Miles, M. H.; Ostrom, G. S. Helium Production during the Electrolysis of D_2O in Cold Fusion Experiments. *J. Electroanal. Chem.* **1991**, *304*, 271.
58. Bush, B. F.; Lagowski, J. J. Methods of Generating Excess Heat with the Pons and Fleischmann Effect: Rigorous and Cost-Effective Calorimetry, Nuclear Products Analysis of the Cathode and Helium Analysis. In *Proceedings of the Seventh International Conference on Cold Fusion*, Vancouver, Canada, April 19-24, 1998; ENECO, Inc.: Salt Lake City, UT, 1988; 38.
59. Apicella, M.; Castagna, E.; Capobianco, L.; D'Aulerio, L.; Mazzitelli, G.; Sarto, F.; Rosada, A.; Santoro, E.; Violante, V.; McKubre, M. C.; Tanzella, F.; Sibilia, C. Some Recent Results at ENEA. In *Condensed Matter Nuclear Science: Proceedings of the 12th International Conference on Cold Fusion*, Yokohama, Japan, Nov. 27-Dec. 2, 2005; Takahashi, A.; Ota, K.-I.; Iwamura, Y., Eds.; World Scientific Publishing Co.: Singapore, 2006; 117.
60. McKubre, M. C. H.; Tanzella, F. L.; Tripodi, P.; Hagelstein, P. L. The Emergence of a Coherent Explanation for Anomalies Observed in D/Pd and

Downloaded by COLUMBIA UNIV on July 1, 2012 | http://pubs.acs.org
Publication Date: August 1, 2008 | doi: 10.1021/bk-2008-0998.ch005

H/Pd System: Evidence for 4He and 3He Production. In ICCF8: *Proceedings of the Eighth International Conference on Cold Fusion*, Lerici (La Spezia), Italy, May 21-26, 2000; Scaramuzzi, F., Ed.; Italian Physical Society: Bologna, Italy, 2001; 3.

61. Gozzi, D.; Caputo, R.; Cignini, P. L.; Tomellini, M.; Gigli, G.; Balducci, G.; Cisbani, E.; Frullani, S.; Garibaldi, F.; Jodice, M.; Urciuoli, G. M. Helium-4 Quantitative Measurements in the Gas Phase of Cold Fusion Electrochemical Cells. In *Proceedings of the Fourth International Conference on Cold Fusion*, Lahaina, Maui, Dec. 6-9, 1993; Passell, T. O., Ed.; Electric Power Research Institute: Palo Alto, CA, 1994; 6.
62. Arata, Y.; Zhang, Y. C. Anomalous Production of Gaseous ^{4}He at the Inside of 'DS cathode' during D_2O-Electrolysis. *Proc. Jpn. Acad., Ser. B* **1999**, *75*, 281.
63. Arata, Y.; Zhang, C. Presence of Helium($^2He_4$, $^2He_3$) Confirmed in Deuterated Pd-black by the "Vi-effect" in a Closed QMS" Environment. *Proc. Japan. Acad. B* **1997**, *73*, 62.
64. Chubb, T. A. Is a Quantum-of-Mass Always a Particle? *Infinite Energy* **2006**, *12*, 24.
65. Chubb, T. A. Bloch Ions. In *Condensed Matter Nuclear Science: Proceedings of the 11th International Conference on Cold Fusion*, Marseilles, France, Oct. 31 - Nov. 5, 2004; Biberian, J.-P., Ed.; World Scientific Publishing Co.: Singapore, 2006; 665.
66. Chubb, T. A., Inhibited Diffusion Driven Surface Transmutations. In *Condensed Matter Nuclear Science: Proceedings of the 11th International Conference on Cold Fusion*, Marseilles, France, Oct. 31 - Nov. 5, 2004; Biberian, J.-P., Ed.; World Scientific Publishing Co.: Singapore, 2006; 678.
67. Chubb, T. A. Bloch Nuclides, Iwamura Transmutations, and Oriani Showers. In *Condensed Matter Nuclear Science: Proceedings of the 11th International Conference on Cold Fusion*, Marseilles, France, Oct. 31 - Nov. 5, 2004; Biberian, J.-P., Ed.; World Scientific Publishing Co.: Singapore, 2006; 685.
68. Hagelstein, P. L. Models for Anomalies in Condensed Matter Deuterides. In *Condensed Matter Nuclear Science: Proceedings of the 12th International Conference on Cold Fusion*, Yokohama, Japan, Nov. 27-Dec. 2, 2005; Takahashi, A.; Ota, K.-I.; Iwamura, Y., Eds.; World Scientific Publishing Co.: Singapore, 2006; 441.
69. Hagelstein, P. L. Phonon-Exchange Models: Some New Results. In *Condensed Matter Nuclear Science: Proceedings of the 11th International Conference on Cold Fusion*, Marseilles, France, Oct. 31 - Nov. 5, 2004; Biberian, J.-P., Ed.; World Scientific Publishing Co.: Singapore, 2006; 743.
70. Takahashi, A. ^{3}He/^{4}He Production Ratios by Tetrahedral Symmetric Condensation. In *Condensed Matter Nuclear Science: Proceedings of the 11th International Conference on Cold Fusion*, Marseilles, France, Oct. 31 - Nov. 5, 2004; Biberian, J.-P., Ed.; World Scientific Publishing Co.: Singapore, 2006; 730.
71. Lipson, A. G.; Miley, G.; Lyakhov, B. F.; Roussetski, A. S. Energetic Charged Particles Emission from Hydrogen-Loaded Pd and Ti Cathodes and its Enhancement by He-4 Implantation. In *Condensed Matter Nuclear Science:*

Downloaded by COLUMBIA UNIV on July 1, 2012 | http://pubs.acs.org
Publication Date: August 1, 2008 | doi: 10.1021/bk-2008-0998.ch005

Proceedings of the 11th International Conference on Cold Fusion, Marseilles, France, Oct. 31 - Nov. 5, 2004; Biberian, J.-P., Ed.; World Scientific Publishing Co.: Singapore, 2006; 324.

72. Lipson, A. G.; Lyakhov, B. F.; Rousstesky, A. S.; Asami, N. Evidence for DD-reaction and a Long-Range Alpha Emission in Au/Pd/PdO:D Heterostructure as a Result of Exothermic Deuterium Deposition. In *ICCF8: Proceedings of the Eighth International Conference on Cold Fusion*, Lerici (La Spezia), Italy, May 21-26, 2000; Scaramuzzi, F., Ed.; Italian Physical Society: Bologna, Italy, 2001; 231.
73. Lipson, A. G.; Karabut, A. B.; Roussetsky, A. S. Anomalous Enhancement of DD-reaction, Alpha Emission and X-ray Generation in the High Current Pulsing Deuterium Glow-Discharge with Ti-Cathode at the Voltages Ranging from 0.8-2.5 kv. In *Condensed Matter Nuclear Science: Proceedings of the 9th International Conference on Cold Fusion*, Beijing, China, May 19-24, 2002; Li, X. Z., Ed.; Tsinghua Univ. Press: Beijing, 2002; 208.
74. Kowalski, L.; Jones, S.; Letts, D.; Cravens, D. Charged Particles from Ti and Pd Foils. In *Condensed Matter Nuclear Science: Proceedings of the 11th International Conference on Cold Fusion*, Marseilles, France, Oct. 31 - Nov. 5, 2004; Biberian, J.-P., Ed.; World Scientific Publishing Co.: Singapore, 2006; 269.
75. Roussetski, A. S. Investigation of Nuclear Emissions in the Process of D(H) Escaping from Deuterized (Hydrogenized) PdO-Pd-PdO and PdO-Ag Samples. In *Proceedings of the Sixth International Conference on Cold Fusion: Progress in New Hydrogen Energy*, Hokkaido, Japan, Oct. 13-18, 1996; Okamoto, M., Ed.; New Energy and Industrial Technology Development Organization: Tokyo, 1996; 345.
76. Campari, E. G.; Fasano, G.; Focardi, S.; Lorusso, G.; Gabbani, V.; Montalbano, V.; Piantelli, F.; Stanghini, C.; Veronesi, S. Photon and Particle Emission, Heat Production and Surface Transformation in Ni-H System. In *Condensed Matter Nuclear Science: Proceedings of the 11th International Conference on Cold Fusion*, Marseilles, France, Oct. 31 - Nov. 5, 2004; Biberian, J.-P., Ed.; World Scientific Publishing Co.: Singapore, 2006; 405.
77. Friedlander, G.; Kennedy, J. W.; Miller, J. M. *Nuclear and Radiochemistry*; John Wiley & Sons, Inc.: New York, 1955.
78. Takahashi, A.; Takeuchi, T.; Iida, T.; Watanabe, M. Short Note: Emission of 2.45 MeV and Higher Energy Neutrons from D_2O-Pd Cell under Biased-Pulse Electrolysis. *J. Nucl. Sci. Technol.* **1990**, *27*, 663.

Downloaded by COLUMBIA UNIV on July 1, 2012 | http://pubs.acs.org
Publication Date: August 1, 2008 | doi: 10.1021/bk-2008-0998.ch005

Chapter 6

Resonant Electromagnetic Interaction in Low-Energy Nuclear Reactions

Scott R. Chubb

Research Systems Inc., 9822 Pebble Weigh Court, Burke, VA 22015

Downloaded by YORK UNIV on July 1, 2012 | http://pubs.acs.org
Publication Date: August 1, 2008 | doi: 10.1021/bk-2008-0998.ch006

Basic ideas about how resonant electromagnetic interaction (EMI) can take place in finite solids are reviewed. These ideas not only provide a basis for conventional, electron energy band theory (which explains charge and heat transport in solids), but they also explain how through finite size effects, it is possible to create many of the kinds of effects envisioned by Giuliano Preparata. The underlying formalism predicts that the orientation of the external fields in the SPAWAR protocol (*1, 2*) has direct bearing on the emission of high-energy particles. Resonant EMI also implies that nano-scale solids, of a particular size, provide an optimal environment for initiating Low Energy Nuclear Reactions (LENR) in the PdD system.

Introduction

In cold fusion (CF), a variant of the helium-4 (α particle) producing fusion reaction (which rarely occurs in conventional fusion) appears to be dominant. Most nuclear physicists assume the conventional form of this reaction occurs infrequently because it creates considerably more energy than the other fusion reactions and that the most frequent reactions minimize the amount of energy that is released. This assumption is wrong. It does not include subtleties involving EMI. It does apply when deuterons (d's) have high velocity, initially, and collide at a point, provided they are not "prepared" (through EMI), in a particular way. Far from the reaction, for the $d+d \rightarrow \alpha + \gamma$ reaction to take place, particular selection rules apply, involving total d-d spin and angular momentum. In a solid, richer forms of time-dependent EMI can take place

In Low-Energy Nuclear Reactions Sourcebook; Marwan, J., et al.;
ACS Symposium Series; American Chemical Society: Washington, DC, 2008.

through non-linear coupling between photons, electrons, their spins, and other charged particles. Further complicating the problem is the fact that the γ ray that one would expect to be present in the normal helium-4 (α-particle) producing reaction can appear and disappear through adsorption and emission by electrons in the associated environment, that can (and must, in most situations) result in "parametric down-conversion" (PDC) processes (*3*), even in relatively small crystals.

In particular, PDC processes occur through non-linear forms of coupling between a single photon and matter that result in the photon being split into two or more (and possibly many, many more) entangled (lower frequency—potentially considerably lower frequency) photons. These kinds of effects are known to occur when photons propagate through insulators. In these situations, because the scattering processes occur only at a small number of points, the possibility of massive PDC processes that can create many photons from a single photon has not been observed. Also, the theoretical basis of the process, though well understood, has been limited to two photons, primarily because the fields that are involved do not include significant coupling to the kinds of cooperative forms of electronic excitation that are possible in metals.

In larger metal crystals, typically, the associated forms of coupling rapidly attenuate any electromagnetic wave propagation, and because approximate boundary conditions can be used in these kinds of situations, the possibility of observing and understanding PDC processes, involving one or more (optical) photons, has not been investigated. As discussed in the present paper, when more precise boundary conditions are invoked, in finite lattices, elastic forms of resonant coupling become possible. Because it is never possible to define the boundary of a solid, precisely, in principle, it is never possible to determine if a portion of the solid moves rigidly (or actually accelerates) through a process in which the available momentum from an applied field (static or dynamic) rigidly couples to the center of mass of a collection of atomic centers and electrons. This means a potentially huge degeneracy can result, provided the applied field is sufficiently weak and the crystal has finite extent (but has a characteristic nano-scale dimension). As discussed in the final section of the paper, this, in principle, can result in the possibility of a large number of different photons, with varying, but well-defined frequencies, being produced, from an applied, AC or DC electric or magnetic field.

In metallic-hydride or metallic-deuteride compounds, like PdH or PdD, one should investigate both the possibility that such an effect might occur and the possibility that it might not occur. In particular, the analysis presented in this paper suggests that experiments should be conducted, associated with what has taken place with the SPAWAR protocols (*1, 2*), involving a detailed analysis of how these protocols work and the orientations of externally applied electric/magnetic fields that seem to be responsible for initiating emissions of radioactivity.

This possibility implies that through these PDC processes, the γ ray associated with the conventional d+d→α + γ reaction can be converted into

Downloaded by YORK UNIV on July 1, 2012 | http://pubs.acs.org
Publication Date: August 1, 2008 | doi: 10.1021/bk-2008-0998.ch006

many different optical, Infra-Red, microwave, or lower-frequency forms of radiation, coherently or incoherently, and that the "α" particle (henceforth referred to as helium-4 when it occurs in lower-energy environments < 1000 eV but as an "α" particle when its energy is greater than this) can be "emitted" with negligibly small energy.

This paper provides a starting point for understanding how this might take place in smaller, approximately ordered crystals. The associated PDC effects possibly can explain how a static magnetic or electric field could lead to localized phenomena associated with the emission of higher-energy α particles that apparently have been observed in experiments (*1*) associated with replicating the SPAWAR protocol (*2*). This possibility is addressed in the final section of this paper, based on a form of Bragg Resonant scattering, in which the "photons" are effectively "trapped" as a result of the kinds of effects suggested by Giuliano Preparato. The simplest way of explaining how this can take place involves forms of scattering that are allowed to take place in one particular region of space, but not in other regions of space.

Nothing, classically, in the relevant physics of EMI forbids this kind of thing. It happens all the time when forms of "impedance mismatch" are allowed to take place. This possibility has not been considered in previous theoretical pictures and reviews that have led to the predominat view that LENR are not possible.

Good reasons exist for associating these kinds of effects with an entirely counterintuitive limit in which the lowest forms of momentum and energy conservation are required to obey a form of symmetry, Bloch symmetry, that is related to periodic order, that, as a consequence, can lead to forms of resonant coupling, similar to Bragg scattering in solids that can create an imbalance in momentum that can create the kinds of effects that Giuliano Preparata intuitively identified.

Here, in general terms, resonant scattering can take place, along the lines that Giuliano Preparata recognized, involving matching conditions, associated with situations in which many particles and photons approximately share a common phase, resulting from conservation of momentum and energy. This can occur through the requirement that many of the potentially radiation-emitting particles receive and transmit their signals in a way that can constructively interfere and cause a positive form of feedback, very similar to the resonant laser-like effect that he suggested was involved. In the most basic form of radiation-emitting situation that appears to be relevant in PdD, how this occurs is closely related to how the deuterons can become coupled coherently. In the simplest situation, this involves forms of charge and current conservation that are non-local. This can occur as the stoichiometry of PdD_x effectively varies between $x=1+\delta$ and $x=1-\delta$ (provided δ is sufficiently small), as a result of the strongly anti-bonding nature of the electronic states near the Fermi energy of PdD, when an applied DC field (or pressure), which is required to confine the D within the lattice, is maintained for a sufficiently long period of time, and collisions are effectively stifled. The associated coupling occurs through a

Downloaded by YORK UNIV on July 1, 2012 | http://pubs.acs.org
Publication Date: August 1, 2008 | doi: 10.1021/bk-2008-0998.ch006

highly polarized bond that, in larger crystals, involves the lowest-energy acoustic phonons, which, as envisioned by Giuliano Preparata, can be viewed as a form of semi-classical oscillation of the electromagnetic zero (or trapped photons) of the solid.

An important point is that in a finite crystal of PdD, discretely defined forms of momentum (P_{cm}) can be transferred rigidly to the center-of-mass of all or a portion of the solid, through resonant processes that, in larger crystals, mimic the kind of oscillation envisioned by Preparata. An illustrative example of how this can occur involves a 1-dimensional lattice, with real boundaries, defined by a set of unit cells, each separated from the others by an integer (**n**) multiple of the lattice constant **a**. Constructive interference can occur whenever an integer multiple (**m**) of the deBroglie wavelength (λ_d) equals **a**, or **na**. The allowable coupling (which is defined by $P_{cm} = \hbar / \lambda_d$) as a consequence, associated with the lowest-energy fluctuations, from rigid translations, involves size-dependent forms of momentum transfer. Effectively, the associated EMI can be viewed as involving a form of antenna, defined by **na/m**. In the reference frame that is stationary with respect to the lattice, as illustrated in this paper, when there are **2N** unit cells in the lattice, the kinds of rigid translations that are consistent with these lowest-energy fluctuations occur when, for $\mathbf{j} = \mathbf{m}$ or $\mathbf{j} = \mathbf{n}$, $-\mathbf{N} + \mathbf{1} \leq \mathbf{j} \leq \mathbf{N}$ or $-\mathbf{N} \leq \mathbf{j} \leq \mathbf{N-1}$.

The associated coupling involves a form of degeneracy, associated with potential motion of a lattice, in which, in the periodically ordered regions, the electromagnetic fields resonantly scatter between many possible wavelengths without altering the energy within the reference frame that is stationary with respect to the lattice. Outside the lattice (which is defined by the requirement that each unit cell is not electromagnetically neutral), however, in the reference frame that is stationary with respect to any externally applied (static) fields, the lattice is allowed to move. Each possible velocity or acceleration that can take place without causing a collision defines a possible energy state that is degenerate with respect to the others.

The presence of any form of collision has the potential of removing these degeneracies. When interaction with the external region, outside the lattice, is sufficiently weak but persists for a sufficiently long time, the differences in energy that result from collisions can be quite small. This means that a continuum or quasi-continuum of states exists that can potentially couple either to an external electromagnetic field or one associated with potential nuclear reactions (which technically occur in regions external to the lattice since locally reactions occur in regions where net charge is allowed to accumulate). In the analogy of viewing the solid as a kind of antenna, the associated coupling can be viewed as a form of tuning in which it can become possible for fields to induce changes in momentum (and wavelength) and frequency that cooperatively can vary over many orders of magnitude.

When x varies between $1+\delta$ and $1-\delta$, in PdD_x, ionic charge enters and leaves the solid, and instantaneously, charge need not be conserved locally within the solid since it is impossible to measure either the charge or current.

Downloaded by YORK UNIV on July 1, 2012 | http://pubs.acs.org
Publication Date: August 1, 2008 | doi: 10.1021/bk-2008-0998.ch006

Also when this occurs, a form of broken gauge symmetry can take place (resulting from finite size effects), in which portions of the "lattice" can appear to not conserve charge, as a consequence of many charged particles moving in lock-step in a way that is contrary to the conventional situation in which charge is conserved locally, and the associated response, referred to as gauge symmetry, cannot be violated locally (*4*). As a consequence, in the interior regions of a solid, charge conservation can occur non-locally, but at the boundaries and outside this region, this is not possible. The possibility that such a region can exist and be important in potential fusion reactions has been ignored in the theoretical pictures that have formed the basis for rejecting CF-related phenomena.

At the boundaries of solids, these kinds of effects can occur in situations in which the associated momentum and energy can grow with increasing time. In particular, as x varies between 1+δ and 1–δ, fluctuations in charge (of deuterons and electrons into and away from the lattice for values of x immediately above and below the value x=1) can cause this kind of effect to occur because the net electron-deuteron charge that is allowed to enter the lattice can increase (when x is above the value x=1) and decrease (when x is below the value x=1). As a result, in a finite metallic PdD lattice, a form of "preparation" can take place (involving, effectively, a form of dissociation between the nucleus of each D from its electron). This can occur (through the kind of antenna-resonant form of coupling outlined above), provided the fluctuations in charge into and away from the lattice are sufficiently small and occur over a sufficiently long period of time, and this can result in possible nuclear effects.

This kind of effect can alter possible forms of nuclear fusion in PdD because:

1. Since deuterium atoms (D's) do not have core electrons, their nuclei (d's) intrinsically have the potential to interact through EMIs involving each other and the host electrons without being required to move rapidly in order for the separation between deuterons to be reduced (which is not the case in situations involving atoms that have more than one electron).
2. It is known that EMI effects are required in the one form of nuclear fusion reaction, associated with the d+d→α + γ, that seems to be important in CF-related phenomena.
3. d + d →helium-4 + 23.8 MeV reactions (in a host material) are allowed to occur, provided momentum is allowed to change sufficiently rapidly (even in a quasi-discontinuous manner, for example, through wave function cusps (*5*)).

An important point is that even classically, when a particle has mass m, velocity $\vec{v}$, charge q, and momentum $\vec{p}$, the relationship between these variables is

$$m\vec{v} = \vec{p} - \frac{e}{c}\vec{A},$$

Downloaded by YORK UNIV on July 1, 2012 | http://pubs.acs.org
Publication Date: August 1, 2008 | doi: 10.1021/bk-2008-0998.ch006

as opposed to the situation associated with a static, time-independent Coulomb potential situation, where $m\vec{v}=\vec{p}$. (Here, $\vec{A}$, which is a non-local function, is the vector potential (*4*); as an operator, in 2nd quantized form, it is defined to create or destroy a photon.) In particular, in the more general situation associated with the last two reactions, non-local effects are required.

More generally, it follows from basic electrodynamical considerations that simply by stressing a metal with sufficient force in particular ways, as the metal approaches nano-scale dimension, potentially new effects can occur through resonant EMI that can induce a spectrum of x-rays, lower-frequency forms of light, microwaves, and/or phonons. Thus, in any nano-scale PdD "crystal," instead of a static, electrostatic, "Coulomb" barrier being involved in d+d→helium-4 (or α-particle) reactions, for example, a more sophisticated, time-dependent, quantum electro-dynamic, "QED" barrier is probably involved. Giuliano Preparata (*6, 7*) recognized this possibility and that the barrier that prevents fusion in free space should be very different in solids, but superficially it appeared that he relied on an over-simplified model, in which interactions with charged matter were treated semi-classically, through a modified form of free particle interaction.

In fact, in a more realistic theory (*8-10*), based on a generalization of the conventional semi-classical model of (electron (*11*), and ion (*5, 12*)) energy band theory (which, in the case of electrons, is known to accurately describe heat and charge transport), the simplest approximation of the most relevant picture shares many of the intuitive features of the plasma picture suggested by Giuliano Preparata. Important differences exist. Giuliano Preparata assumed well-defined boundaries exist in a solid, so that the lattice could be treated as being stationary with respect to its external environment. In a real solid, it is never possible to determine precisely where the lattice begins and ends, where its boundaries are located, and whether or not it is in motion. The generalized energy band picture that applies to finite lattices is considerably richer because it includes quantum mechanical effects that are implied by these facts. Starting from these assumptions in the paper, the more general theory is used to predict a number of effects, including the possibility that in the SPAWAR co-deposition experiments, the emission of high-energy particles might be related to the orientation of the applied fields.

This paper is organized in the following way. The next section discusses details about known results associated with the importance of electromagnetic interactions (EMIs) that are not widely appreciated and have been neglected, by physicists, in the (conventional) d+d→α+γ and (possible) d+d→helium-4 + 23.8 MeV reactions. As opposed to the sudden impact situation (in which details about the EMI are important only at the location where two d's collide, at a point), as in the Coulomb barrier approximation, a different situation can occur in resonant EMI, involving an adiabatic process in which, for example, momentum can be imparted repetitively in such a way that constructive interference occurs between incoming and outgoing matter (deuteron-d) waves. As a consequence of symmetry-related effects, in these resonant EMIs, these

Downloaded by YORK UNIV on July 1, 2012 | http://pubs.acs.org
Publication Date: August 1, 2008 | doi: 10.1021/bk-2008-0998.ch006

kinds of changes in momentum can occur at many locations and in ways that can significantly reinforce the associated effects. As a consequence, an important resonant effect can take place in which small amounts of momentum are imparted, repetitively, to an ordered lattice, rigidly. This can, over time, lead to large, non-local changes in momentum. (A useful analogy for how momentum can increase through these kinds of processes is how the momentum of a tether ball can increase, with time, when a child repetitively hits the tether ball just as its momentum is approaching a minimum.)

In the third and fourth sections, a new, important result is identified, associated with this form of coupling: A particular limit in which Bragg scattering and the resonant coupling of a many-d/many-electron energy band system can systematically take place, based on a common theorem known from solid state physics but not widely recognized in situations involving EMI – that single photons and particles, in the limit of perfect resonance (which occurs when energy and momentum are conserved relative to the center of mass of the solid) can obey a form of Bloch Symmetry, defined by Bloch's theorem, as it applies in the single particle Schroedinger equation that is used to describe electrons in periodically ordered solids.

This theorem can also apply in situations involving "many-body" configurations of charged particles (*8*) and (as identified here, for the first time) photons, in the approximate limit associated with the single particle situation, i.e., when the collisions within the configuration are minimized, within bounds defined by the relevant time-scales associated with potential collisions. In particular, X-ray Bragg scattering occurs when single photons obey Bloch's theorem. The generalization of Bloch's theorem, as it applies to many electrons and deuterons (*8-10*), also applies to situations involving many photons. This limit, in fact, has, as its starting point, phenomena that have some of the same physics (involving "trapped photons"/"fluctuations in energy zero") that Giuliano Preparata identified (*6, 14*).

In the fourth (final) section, the semi-classical equations are used to describe the limit in which these resonant effects can lead to d+d LENR reactions in solids, in triggering x-ray emission in smaller crystals, and the emission of high-energy particles. The analysis suggests that the orientation of static, external, magnetic and/or electric fields used in experiments involving the SPAWAR protocol (*1, 2*) can cause the emission of high-energy particles.

Importance of the QED (as Opposed to the Coulomb) Barrier in d+d→α+γ and d+d→Helium-4+23.8 MeV

In the conventional picture of nuclear fusion, a static Coulomb barrier is used to explain how same-charged d's can have appreciable overlap. This limit makes good sense when the initial and final particles have high velocity, and the relevant quantum mechanics does not require that details about the time-dependence of the EMI be included when the d's are far apart. In this

Downloaded by YORK UNIV on July 1, 2012 | http://pubs.acs.org
Publication Date: August 1, 2008 | doi: 10.1021/bk-2008-0998.ch006

conventional picture, d's at nuclear distances interact entirely through the strong force, the distinction between protons (p's) and neutrons (n's), at the point of nuclear contact is effectively inconsequential (except through differences in kinetic energy associated with changes in mass that do not relate to time-dependent EMI effects) and nuclear physicists' normal, intuitive picture applies: The most frequent reactions occur when the amount of nuclear energy that is released is minimized. For this reason, the common intuition is that the least common reaction (d+d→α+γ) occurs infrequently because the energy release (23.8 MeV) is considerably (7 to 8 times) larger than it is in the remaining reactions. In fact, this picture is not right. Important details about time-dependent EMI effects have been ignored and are responsible for the fact that the d+d→α+γ reaction occurs rarely (a fact that was not appreciated even by Schwinger (*13*) or Preparata (*6*)).

In particular, although d+d→α+γ rarely occurs, the reverse reaction (the photo-dissociation process: γ+α→d+d) has been studied in detail. As a consequence, it is known implicitly that, as opposed to a static Coulomb barrier being required (which is widely believed to inhibit nuclear fusion), and the common, intuitive idea that the large energy release that is involved is responsible for the reaction occurring infrequently, an alternative model applies: Selection rules exist and a well-defined, time-dependent EMI transition is involved in the photo-dissociation process. From a detailed comparison between measurements of d-d photo-dissociation cross-section and theoretical studies (based on the Resonant Group Method (*15*)), the analysis shows quite conclusively that the reaction can be explained, in terms of a well-characterized (quadrupolar) transition, in which the total spin of the final state d's vanishes. The analysis also shows that it is necessary to include the effects of EMI (including implicit rules associated with the fact that the d's must obey Bose-Einstein statistics with respect to EMI) on length and time-scales that are far from the location of the photo-dissociation process. Because, in QED, the rate of any transition is proportional to the absolute square of the associated transition matrix element, by construction, the theory requires that a transition rate forward in time be equal to the comparable rate for a transition backward in time. This means that the selection rules that apply in the photo-dissociation process, γ+α→d+d, also apply in the d+d→α+γ reaction. As a consequence, the common intuition, that this reaction does not occur frequently because of the large energy release, is wrong.

Unfortunately, because of nuances in language and limited communication by Giuliano Preparata and other theorists initially, a key, common point of agreement was not appreciated in early theoretical work associated with cold fusion: that EMI (and QED by implication) could (and probably does) provide a rational framework for understanding the most important aspects of any theory that could (or would) be acceptable and/or be useful for explaining why relevant effects occur that should be dominant in the most well-understood and potentially important processes (*13*). Reasons for believing this include:

Downloaded by YORK UNIV on July 1, 2012 | http://pubs.acs.org
Publication Date: August 1, 2008 | doi: 10.1021/bk-2008-0998.ch006

1. The nuclear effects appear to take place in a number of different environments where specific, alternative mechanisms (weak interaction, Coulomb barrier with screening, etc.), based on particular forms of triggering, at best, because of the variability of the environments, probably are secondary.
2. In the most important reaction in which helium-4 is produced, the observed energy balance (23.8 MeV), in the most carefully performed experiments (*13*), between incident deuteron mass and helium-4 is consistent with a quasi-conventional, $d+d \rightarrow \alpha+\gamma$ reaction, in which the energy of the 23.8 MeV γ ray is re-distributed between many photons (and/or phonons).
3. It is known (from the photo-dissociation reaction, $\alpha+\gamma \rightarrow d+d$ reaction) that this reaction is caused by an electromagnetic transition between different, stable, static nuclear states.

Downloaded by YORK UNIV on July 1, 2012 | http://pubs.acs.org
Publication Date: August 1, 2008 | doi: 10.1021/bk-2008-0998.ch006

An important point has been and continues to be the role of time-dependent effects in QED phenomena. The potential relationship of these EMI reactions to potential nuclear reactions is not widely appreciated because it is widely believed that charge-neutral, strong force physics is dominant. Also, most physicists either ignore or do not believe that, through non-linear forms of EMI coupling involving many charged particles or partially charged quasi-particles, a massively entangled state can be created through PDC processes and that this kind of effect can create many low-frequency photons from a single photon, through processes that appear to involve "a single γ ray." An important reason for this is that the common (Coulomb-barrier) picture involves a semi-classical limit that does not include the possibility that, as outlined in the Introduction, many channels for de-excitation can effectively become possible through resonant phenomena in which an approximately ordered lattice is involved and allowed to move and accelerate rigidly. In this situation, all of the charged particles in the solid can couple through resonant EMI in such a way that many forms of partial excitation are allowed to take place. In free space, these forms of excitation are not available. As we will see, in a finite solid, not only through these kinds of effects can the "single γ ray" be converted into many (lower-frequency) photons, but the phenomenon can occur through a time-dependent process involving a form of coherent tunneling in which the necessary momentum for triggering the reaction builds up with time.

This can be illustrated through a generalization of conventional solid-state and atomic physics. The analysis shows that the effects can occur at lower energies and/or in smaller (nano-scale) PdD crystals. In the modified form of the $d+d \rightarrow \alpha+\gamma$ reaction, the coherent, resonant coupling occurs between a macroscopically small number of d's throughout the solid, the γ ray effectively either is converted into one (or more) many-photon, entangled state(s) (in finite solids) and/or phonons (in larger solids), and small concentrations of each d and small concentrations of each helium-4 nucleus are involved (effectively, in each case, by the d or helium-4 occupying an ion band state (5)).

The associated phenomena can be viewed as a series of massive PDC processes. The origin of these processes involves fluctuations of charge into and away from the lattice (or a portion of it). In fact, as alluded to in the resonant-antenna analogy discussed above, because it is never possible to tell if the lattice (or sub-lattice of a lattice) is in motion or at rest without disturbing it, the ground state (GS) and the lowest lying excited states are required to obey certain rules associated with the implicit degeneracy that results from uncertainties associated with this fact: Because it is never possible to determine precisely where the volume enclosed by the lattice (or sub-lattice) is located, with respect to these fluctuations, new effects associated with how the "lattice" potentially "moves" or does not "move" can alter EMI effects that can induce non-linear forms of interaction and PDC processes. (These forms of fluctuation are associated with the longest-wavelength ion band states. The conditions for creating these forms of fluctuation are consistent with the fluctuations that are induced when electrons immediately above and below the Fermi energy in PdD_x become occupied (*9, 10*).)

As a consequence, a form of Galilean relativity can come into play that can alter the relevant dynamics, provided the electromagnetic fields that are introduced do not induce collisions between charged particles, within the volume associated with the region that can be arbitrarily in motion or at rest. When this occurs in the reference frame that is stationary with respect to the center of mass of the lattice, because these fluctuations can appear to accelerate, time-dependent magnetic and electric fields can be induced.

When the associated fluctuations are sufficiently weak but persist for a sufficiently long time, the associated coupling and interaction can induce resonant Bragg scattering effects that can effectively result in a build-up of momentum (associated with the relative motion between the center of mass and the fluctuations) that can lead to many-photon scattering phenomena and massive entanglement, which can be viewed as being very similar to the kinds of trapped photon phenomena suggested by Preparata. The resulting picture is strikingly similar to the intuitive picture that he suggested. Two key points are involved:

1. the relationship between the importance of EMI and the insignificance of dynamical changes in the strong force in the $d+d \rightarrow \alpha+\gamma$ reaction, and
2. the manner in which, through many-particle physics (in the language of solid-state/condensed matter physics), an effective form of PDC process (in the language of atomic physics) can take place in which the highly-energetic γ ray is converted into many lower-frequency, entangled photons.

Single-Particle Resonant Processes in Solids

Bloch pointed out (*16*) that, for an infinitely-repeating periodic lattice, each energy band eigenvalue ε is also a periodic function with respect to dis-

Downloaded by YORK UNIV on July 1, 2012 | http://pubs.acs.org
Publication Date: August 1, 2008 | doi: 10.1021/bk-2008-0998.ch006

placements by reciprocal lattice vectors $\vec{G}$ (*17*),

$$\varepsilon(\vec{k}) = \varepsilon(\vec{k}+\vec{G}). \tag{3}$$

Eq. (3) implies forms of degeneracy that have physical consequences known to be important at low temperature. However, this degeneracy has been treated in an approximate fashion. Intuitively, one would think that finite size effects must affect this relationship. In fact, this is true. In order to quantify potential deficiencies associated with this, it is both useful and necessary to examine how conventional textbooks deal with the "apparent" ambiguities and redundancies associated with Eq. (3). In particular, the language and "rigor" (or language and lack of "rigor") are associated with the idea that each electron is a "quasi-particle." In the initial picture, each electron is assumed to behave as a wave that is represented using a quasi-particle wave function $\psi_{\varepsilon(\vec{k})}(\vec{r})$, which is assumed to be an eigenstate of a single-particle Hamiltonian, has an energy eigenvalue, $\varepsilon(\vec{k})$, and both $\psi_{\varepsilon(\vec{k})}(\vec{r})$ and $\varepsilon(\vec{k})$ are derived from a single-particle Schroedinger equation of the form

$$\frac{-\hbar^2}{2m}\nabla^2\psi_{\varepsilon(\vec{k})}(\vec{r}) + V(\vec{r})\psi_{\varepsilon(\vec{k})}(\vec{r}) = \varepsilon(\vec{k})\psi_{\varepsilon(\vec{k})}(\vec{r}). \tag{4}$$

Here, $V(\vec{r}) = V(\vec{r}+\vec{R}_n)$ is a periodic function with respect to spatial displacements defined by discrete Bravais lattice vectors, $\vec{R}_n$. Each of these vectors is constructed from a linear combination of integer (n_α) multiples of primitive vectors $\vec{b}_\alpha$,

$$\vec{R}_n = \sum_{\alpha=1,3} n_\alpha \vec{b}_\alpha \; ; -N_\alpha \leq n_\alpha \leq N_\alpha - 1, \tag{5}$$

and N_α is (traditionally) assumed to be a large number. In particular, when Born-von Karman boundary conditions (*18*) are imposed, $\psi_{\varepsilon(\vec{k})}(\vec{r})$ is required to be a periodic function with respect to translations $\vec{L}_\alpha = 2N_\alpha\vec{b}_\alpha$

$$\psi_{\varepsilon(\vec{k})}(\vec{r}) = \psi_{\varepsilon(\vec{k})}(\vec{r}+\vec{L}). \tag{6}$$

Also, since it is assumed that V is periodic with respect to translations, defined by $\vec{R}_n$, $\psi_{\varepsilon(\vec{k})}(\vec{r})$ can be required to be an eigenstate of the translation operator $T(\vec{R}_n)$ associated with the same form of translation; i.e.,

Downloaded by YORK UNIV on July 1, 2012 | http://pubs.acs.org
Publication Date: August 1, 2008 | doi: 10.1021/bk-2008-0998.ch006

$$T(\vec{R}_n)\psi_{\varepsilon(\vec{k})}(\vec{r}) = \psi_{\varepsilon(\vec{k})}(\vec{r}+\vec{R}_n) = \lambda(\vec{R}_n)\psi_{\varepsilon(\vec{k})}(\vec{r}), \tag{7}$$

where $\lambda(\vec{R}_n)$ is the eigenvalue associated with the translation. Because repetitively translating the coordinate $\vec{r}$ by $\vec{b}_\alpha$ involves applying the translation operator $T(\vec{b}_\alpha)$ repetitively to, $\psi_{\varepsilon(\vec{k})}(\vec{r})$ repetitive multiplications of $\psi_{\varepsilon(\vec{k})}(\vec{r})$ by $T(\vec{b}_\alpha)$ result in repetitive additions of $\vec{b}_\alpha$ to $\vec{r}$. This implies that Eq. (7) can be re-written in terms of the eigenvalues $\lambda(\vec{R}_n)$ (with R_n defined by Eq. (5)), using

$$T(\vec{R}_n)\psi_{\varepsilon(\vec{k})}(\vec{r}) = \psi_{\varepsilon(\vec{k})}(\vec{r}+\vec{R}_n) = \lambda(\vec{b}_1)^{n_1}\lambda(\vec{b}_2)^{n_2}\lambda(\vec{b}_3)^{n_3}\psi_{\varepsilon(\vec{k})}(\vec{r}). \tag{8}$$

To determine $\lambda(\vec{b}_\alpha)$, the right-hand side of Eq. (8) is evaluated in the limit that $\vec{R}_n \Rightarrow \vec{L}_\alpha = 2N_\alpha \vec{b}_\alpha$ and the result is substituted into Eq. (6). Then, it follows that $\lambda(\vec{b}_\alpha)^{2N_\alpha} = 1$. This last expression, in principle, has an infinite number of solutions, defined by the requirement that $2N_\alpha \ln(\lambda(\vec{b}_\alpha)) = 2\pi i m_\alpha$, where, in principle, m_α could be any arbitrary integer, and

$$\lambda(\vec{b}_\alpha) = e^{\frac{\pi i m_\alpha}{N_\alpha}}. \tag{9}$$

In fact, in a real situation, involving a finite crystal lattice, possible values for m_α only occur that are consistent with the system being in its ground state (GS) or its lowest-lying excited states (which in the absence of outside interactions are degenerate with the GS), provided $-N_\alpha \leq m_\alpha \leq N_\alpha - 1$ or $-N_\alpha + 1 \leq m_\alpha \leq N_\alpha$.

Eqs. (8) and (9) are the basis of the single-particle form of Bloch's theorem. In particular, after Eq. (9) is substituted into Eq. (8), it follows that

$$\psi_{\varepsilon(\vec{k})}(\vec{r}+\vec{R}_n) = e^{i\pi \sum_{\alpha=1,3} \frac{(n_\alpha m_\alpha)}{N_\alpha}} \psi_{\varepsilon(\vec{k})}(\vec{r}) = e^{i\vec{k}_m \cdot R_n}\psi_{\varepsilon(\vec{k})}(\vec{r}), \tag{10}$$

where

$$\vec{k}_m = \sum_{\alpha=1,3} \frac{m_\alpha \vec{g}_\alpha}{2N_\alpha}, \tag{11}$$

and the three reciprocal lattice primitive vectors $\vec{g}_\alpha$ are constructed using,

Downloaded by YORK UNIV on July 1, 2012 | http://pubs.acs.org
Publication Date: August 1, 2008 | doi: 10.1021/bk-2008-0998.ch006

$$\vec{g}_\alpha \bullet \vec{b}_{\alpha'} = 2\pi\delta_\alpha^{\alpha'}.$$

(Here, $\delta_\alpha^{\alpha'}$ is the Kroneker delta symbol, which is defined to equal unity when $\alpha=\alpha'$ and to vanish when $\alpha \neq \alpha'$.)

As alluded to above, although technically the value of m_α can be any arbitrary integer, in the true many-body system, in order for the GS of the system to have minimal overlap with external perturbations, the analysis outlined here (*8-10*) requires that $-N_\alpha \leq m_\alpha \leq N_\alpha - 1$ (or $-N_\alpha + 1 \leq m_\alpha \leq N_\alpha$) when the Bravais Lattice vector space indices are also restricted to the values $-N_\alpha \leq n_\alpha \leq N_\alpha - 1$ (or $-N_\alpha + 1 \leq n_\alpha \leq N_\alpha$). This result is required in order for the forward and inverse transformations of the discrete Fourier transformation to be defined.

To minimize overlap with the GS, it also is necessary to de-numerate possible states near to, and including, the GS in finite lattices, provided the lowest energy states of the system preserve a restricted form of translational symmetry (*9, 10, 19, 20*). The symmetry occurs as a result of Galilean invariance with respect to rigid translations that can take place during any scattering process that can be viewed as coherently displacing the lattice, by transferring all of the momentum that is imparted during the process directly to the center of mass of the lattice, while preserving periodic order within the lattice. This can take place when rigid displacements occur in which the center of mass of any sub-lattice within the lattice is translated by a Bravais Lattice vector, while the separation between each pair of potentially interacting particles is held fixed. As a result of this kind of symmetry, it is possible to identify potential states that are mutually orthogonal to each other but are degenerate in the limit in which the lattice does not interact with the external environment. Each of these states is defined by one of the values of m_α in Eq. (11).

This symmetry is also responsible for the (implicit) degeneracy that exists associated with the propagation either of photons (Eq. (2)) or quasi-particles (Eq. (3)) in the single-particle situation. In particular, the frequency (energy) of the associated photon (particle) does not change in Eq. (2) (Eq. (3)) within the context of Bragg scattering (energy band theory) when a reciprocal lattice vector $\vec{G}$ is added to the wave-vector $\vec{k}$. In an infinitely-repeating, stationary lattice, the associated degeneracy is unrestricted and not unique. It occurs when $N_\alpha \leq |m_\alpha|$; in particular, this condition holds when $m_\alpha = j_\alpha 2N_\alpha + m'_\alpha$ and $-N_\alpha \leq m'_\alpha \leq N_\alpha - 1$ in Eq. (11). In this situation,

$$\vec{k}_m = \sum_{\alpha=1,3} \frac{m_\alpha \vec{g}_\alpha}{2N_\alpha} = \sum_{\alpha=1,3} j_\alpha \vec{g}_\alpha + \vec{k}_{m'} = \vec{G}_j + \vec{k}_{m'}, \qquad (12)$$

Downloaded by YORK UNIV on July 1, 2012 | http://pubs.acs.org
Publication Date: August 1, 2008 | doi: 10.1021/bk-2008-0998.ch006

where the reciprocal lattice vector $\vec{G}_j$ is defined as a linear combination of integer (j_α) multiples of the reciprocal lattice primitive vectors, g_α,

$$\vec{G}_j = \sum_{\alpha=1,3} j_\alpha \vec{g}_\alpha, \tag{13}$$

and

$$\vec{k}_{\alpha'} = \sum_{\alpha=1,3} \frac{m'_\alpha \vec{g}_\alpha}{2N_\alpha} \tag{14}$$

is a wave-vector that is consistent with the constraint (which has been conventionally stated as the requirement that the wave-vector $\vec{k}_{m'}$ have a restricted magnitude and direction) that requires it to be in the First Brillouin Zone – which is equivalent to requiring that $-N_\alpha \le m'_\alpha \le N_\alpha - 1$.

In most modern textbooks, Eq. (2) is derived by demonstrating that it is equivalent to Eq. (1), based on wave-vectors and Reciprocal Lattice Vectors, defined by the boundary conditions associated with Eqs. (5-11). The possibility that Eqs. (5-11) also might apply to photons is new. When this possibility applies, intuitive ideas suggested by Giuliano Preparata about "trapped photons" can provide a basis for understanding how forms of oscillation and resonance can take place that can induce the kind of plasma picture that he suggested.

Bloch actually identified Eq. (3) in the context of Eqs. (4-11) using a more general formalism (involving multiple scattering theory (*21, 22*), which actually is related to Eq. (2)) that is very different from how his theory is presented in most modern textbooks. Bloch identified that Eqs. (3-5) could be related to the more general problem, associated with a "well-defined" form of scattering, in which, as opposed to solving an imprecise eigenvalue problem involving approximate boundary conditions, the associated solutions can be derived from an asymptotic limit involving single particles scattering off an array of scattering centers, in which the lifetime of the resulting state becomes infinitely long (*8-10, 22*).

Such a state involves a situation in which energy and momentum are rigorously conserved in a particular region of space, as a result of a "perfect" form of matching condition, in which the net flux of particles into the region vanishes. This form of matching provides a useful way to define perfect resonance. The associated state can be viewed as arising from a situation in which, effectively, "no scattering" occurs within the region. Modern textbooks suggest the associated problem can be expressed through forms of a related eigenvalue problem involving "quasi-particles" and energy minimization. Although this is a convenient way to present the material, the manner in which it is presented is imprecise.

Downloaded by YORK UNIV on July 1, 2012 | http://pubs.acs.org
Publication Date: August 1, 2008 | doi: 10.1021/bk-2008-0998.ch006

Downloaded by YORK UNIV on July 1, 2012 | http://pubs.acs.org
Publication Date: August 1, 2008 | doi: 10.1021/bk-2008-0998.ch006

In the (multiple-scattering) situation considered by Bloch, charge is not required to be conserved locally in the dynamic form that most high-energy physicists assume to be true, in which the time evolution of the density ρ and flux of charged particles, $\rho\vec{v}$, are related through the equality, $\frac{\partial\rho}{\partial t} = -\nabla \bullet (\rho\vec{v})$. In the context of multiple scattering, charge is conserved, but not locally. At the boundaries of the lattice, relative to the zero of energy (V_o) of the solid, for each value of $\vec{k}$, oscillatory solutions, $\varepsilon(\vec{k}) - V_o > 0$, and static or exponentially decaying solutions, $\varepsilon(\vec{k}) - V_o \leq 0$, are required to match wave functions that do require that charge be conserved locally.

This can occur (in an operative sense) by using the kinds of semi-classical pictures, suggested by Bloch, that are consistent with multiple-scattering theory, involving single-particle forms of scattering in which "discontinuous" changes in logarithmic derivative of the single-particle wave function are allowed to take place at the boundaries. Within the context of the semi-classical physics that formed the basis of Bloch's theory, these forms of discontinuities are allowed to occur by allowing for forms of negative kinetic energy through imaginary forms of wave-vector $\vec{k}$ and momentum (defined by $\vec{p} = \hbar\vec{k}$). A potentially important point, in this context, is that when these negative forms of kinetic energy are allowed, a generalization of "tunneling" associated with the conventional (Gamow-Teller) picture can occur in which, as opposed to a situation in which the tunneling is assumed to involve two particles at a specific location, a more general form of "tunneling" can take place involving quasi-particles (in Bloch's and, later, Zener's pictures) at a microscopically large but macroscopically small number of locations, involving a large number of particles.

In a more precise argument, the complete many-body, physical picture actually does reduce to this limit when it is required that, as opposed to the approximate picture involving "quasi-particles," an alternative picture applies involving an extreme limit in which vanishingly small levels of interaction are allowed to take place. In particular, in the limit of vanishingly small interaction, at any particular location (associated with rigidly moving the lattice), implicit forms of degeneracy associated with forms of EMI that are not included in the conventional pictures suggested by Bloch can come into play. Within this context, Bloch's ideas about using these kinds of semi-classical arguments can be replaced by more refined, microscopically defined forms of interaction (*8-10*) that do not alter the limiting boundary effects and equations suggested by Bloch.

These forms of interaction involve the simplest forms of degeneracy associated with Eqs. (2) and (3). In particular, these forms of degeneracy can involve changes in the spins of the charged particles that are involved. Both forms of degeneracy are associated with non-local forms of coupling that involve the vector potential $\vec{A}$ and the implicitly important point that, for situations involving non-neutral regions of space, the momentum of a particle or a collection of particles is not simply related to the product of the mass of the particle or collection of particles with the associated velocity of the particle or collection of particles. An important point is that, in the limit in which nearly perfectly elastic forms of resonance are allowed to take place, the semi-classical picture and the more precise picture based on a more specific, microscopic theory of the relevant EMI both apply.

Bloch suggested that a semi-classical picture, involving wave-packet propagation, could be useful for understanding how the "quasi-particle" eigenstates he postulated, heuristically, could be used to describe charge transport. Within this context, he used a semi-classical wave packet picture to develop an approximate form of EMI based on the Lorentz force law. Here, he replaced the physical velocity of each charge with a form of "group velocity," $\vec{v}_G(\vec{k})$, defined by

$$\vec{v}_G(\vec{k})=\frac{1}{\hbar}\nabla_{\vec{k}}\varepsilon(\vec{k}). \tag{15}$$

He also suggested that, beginning from this approximate picture, the propagation of charge (through quasi-particle wave-packets) could be explained by replacing the physical charge with the quasi-particle charge and the physical velocity with the "quasi-particle group velocity," $\vec{v}_G(\vec{k})$, and by allowing the momentum $\vec{p}=\hbar\vec{k}$ to evolve using a form of Lorentz force law in which $\vec{p}$ propagates in time as if it is replaced by $\hbar\vec{k}$, based on the assumption that the physical velocity $\vec{v}$, is replaced with $\vec{v}_G(\vec{k})$. As a consequence, he identified an effective electromagnetic force F_{em}, which he related to time rate of change of an effective momentum p(t):

$$\frac{dp(t)}{dt}=\frac{\hbar dk(t)}{dt}=F_{em}-q\vec{E}+\frac{qv_G(k(t))}{c}\times\vec{B}, \tag{16}$$

where $\vec{E}$ and $\vec{B}$, respectively, are the applied electric and magnetic fields, and $v_G(k(t))$ satisfies Eq. (15).

Bloch pointed out that, when the same kind of wave-packet propagation picture is used in the limit involving a constant, time-independent electric field $\vec{E}$ (which means $\vec{B}$ vanishes), a form of resonance could take place in which in the presence of $\vec{E}$, the momentum distribution of the wave packet, would oscillate when a resonant condition takes place, which he reasoned would occur when the product of the applied, constant electrical force $q\vec{E}$, with an interval of time t_n, equals $\hbar\vec{G}_n$. The associated form of resonance is referred to as a Bloch oscillation.

In the limit in which perfect or nearly perfect forms of resonance occur, approximate forms of Bloch oscillations can occur in which momentum associated with scattering events can take place, and the lattice, as a whole,

Downloaded by YORK UNIV on July 1, 2012 | http://pubs.acs.org
Publication Date: August 1, 2008 | doi: 10.1021/bk-2008-0998.ch006

moves coherently. Quantum mechanics actually requires that this kind of effect take place, provided the imparted momentum is sufficient and occurs for a sufficiently long time. In principle, eigenstates can be identified through asymptotically vanishing forms of scattering from multiple-scattering theory. This idea applies universally in situations involving elastic processes (i.e., when energy is conserved) in finite solids through a generalization associated with situations involving many particles (*8, 10, 19, 20*).

Resonant EMIs Involving Many Photons and Many Charged Particles in Low Energy Nuclear Reactions (LENR) in PdD

Downloaded by YORK UNIV on July 1, 2012 | http://pubs.acs.org
Publication Date: August 1, 2008 | doi: 10.1021/bk-2008-0998.ch006

In the generalization of the multiple-scattering formalism (*8-10*), many particles are included and solutions to the wave equation are replaced with a general form of interaction, involving arbitrarily perturbing a configuration that is close to being in its GS. Within this context, Bloch's theorem can also be generalized. As opposed to requiring that Born-von Karman boundary conditions apply, the only restriction associated with the theory is that no net flux of particles into a particular volume of space take place, either for describing the GS or the lowest-lying excited states.

Because it is never possible to determine, in the absence of any form of interaction, if a "lattice" is in motion or at rest, its zero of velocity (or momentum) is not known. As a consequence, the effect of its relative motion and possible acceleration, or "its gauge" (i.e., the gradient of the phase of the many-body wave function, in situations in which many particles can share a common phase, through preferred forms of coherent motion) is not known, in general. Although, in most situations, the associated many-body physics is extremely complicated, how the GS and lowest-lying excited states evolve, in a number of the heuristically derived results related to applying the semi-classical theory of transport, based on Eqs. (2-16), also is applicable to the complete many-body situation, where the same equations are used to determine the zeroes of energy and momentum. In this more general situation, all of the relevant QED effects are also included (*8-10*).

Within the context of the generalization of multiple-scattering theory, photons (as a consequence of Eqs. (1) and (2)) can be required to obey Bloch's theorem, as they would in situations involving non-interaction, in a particular region of space (where a fixed gauge can be assumed) provided at the boundaries of the region appropriate wave function matching conditions, involving solutions to the Helmholtz equation, that are consistent with Maxwell's equations, and the requirement that photons behave as they do asymptotically far from the solid, are imposed. These "conditions" require that the wave propagation of emitting "photons," in conventional situations, would not appear to be exponentially growing or decreasing, as a function of time, and that the transmissions preserve gauge symmetry.

By assumption, when an appropriate solution for the GS and lowest-lying excited states occurs, no interactions are assumed to take place, no net flux of particles occurs, associated with any solution involving the particles, into regions where the wave equations apply, either for the photons or the charged particles. Because the region associated with where this form of "noninteraction" can take place can be infinitesimally small, the single-particle problem, involving either photons or electrons, can be related to more general problems. Where and how electrons or photons propagate in this region can:

1. be treated as being entirely elastic (a situation associated with identifying the eigenstates of the GS) or involve partially elastic solutions (which introduce forms of dissipation at the boundaries of the region);
2. occur with different forms of scattering, when periodic order either is present or approximately present;
3. involve approximate forms of boundary conditions (previously assumed to require large dimension—for example, the boundary conditions that apply when the Born-von Karman boundary conditions are used) that may be assumed but need not be required; and
4. involve resonant forms of reaction, in which small amounts of momentum can be imparted to the center of mass of all of the charged particles associated with possible interactions, from an external force, periodically, that can be stored and amplified, with time, resulting in LENR.

A novel result is that Bragg scattering of light also potentially can couple to electrons and deuterons in unexpected but similar ways (through Bloch's theorem), but because of our inability to distinguish dissipation effects involving poorly defined resonance from potentially more dominant forms of resonance, a number of important, unifying ideas associated with the resonance problem (considered by Bloch) and how it has been presented, have been ignored. Very important points are:

1. In the true many-body physics situation, the origin of the approximate single-particle picture that has been quoted in textbooks, being related to what Bloch proposed, has not been appropriately expressed.
2. The possible consequences of this relate to a very foreign limit, in the context of conventional thinking associated with nuclear physics—the limit associated with an effective form of coupling in which momentum can be stored as a result of elastic forms of scattering in which the "lattice" effectively can acquire higher velocity, quantum mechanically, in response to an externally applied, static field, with low velocity, and *without any tangible forms of collision.*
3. It can be possible, through resonant effects coupled to a limit involving negligible perturbation over sufficiently long periods of time, to induce coherent forms of momentum transfer involving many particles being released preferentially in particular ways.

Downloaded by YORK UNIV on July 1, 2012 | http://pubs.acs.org
Publication Date: August 1, 2008 | doi: 10.1021/bk-2008-0998.ch006

Downloaded by YORK UNIV on July 1, 2012 | http://pubs.acs.org
Publication Date: August 1, 2008 | doi: 10.1021/bk-2008-0998.ch006

In this context, particular forms of resonant phenomena (*8-10, 22*) can be described at a basic level through approximate forms of attenuation (losses) when possible quasi-elastic reflections can occur gradually over a sufficient period of time. The underlying, asymptotic boundary conditions, which are quite foreign to situations involving thermonuclear fusion, are quite attainable in nano-crystalline structures.

The generalized form of Bloch's theorem (*9, 10*) applies for each kind of charged particle, asymptotically, for arbitrary many-body interactions, provided overlap between the GS and lowest-lying excited states is minimized. A new and novel result is that a many-photon wave function also obeys the same generalized form of Bloch's theorem (*10*) in interior (bulk) regions (where rigid translations are allowed to take place). This requires that the photons share a specific, common gauge, which we may define by the requirement that, as the lattice moves rigidly, each charged particle coordinate remains fixed relative to its center of mass and to the center of mass (R_{cm}) of all of the charged particles in the lattice. The generalization of Bloch's theorem to situations involving many particles has a complicated mathematical relationship (*9, 10*). In the most coherent situation (which is associated with the Zener tunneling limit (*19, 20*)) discussed below, all of the d's that can occupy an ion band state can occupy the same state, since d's are bosons and they obey Bose-Einstein statistics. For this reason, in its lowest-energy configuration, the many-body wave function Φ_d of the ion band state d's can be written in a considerably simpler form than is presented elsewhere (*10, 19, 20*):

$$\Phi_d = \exp(iN_d \bullet \vec{k}_m \bullet \vec{R}^{d}_{cm})\Psi_d, \qquad (17)$$

where $\vec{R}^{d}_{cm}$ is the center of mass of all of the deuterons in the lattice, Ψ_d is the complete many-body deuteron wave function, relative to a reference frame that is stationary with respect to the center of mass of the lattice,

$$\vec{k}_m = \sum_{\alpha=1,3} \frac{m_\alpha \vec{g}_\alpha}{2N_\alpha}, \qquad -N_\alpha \le m_\alpha \le N_\alpha - 1$$

is one of the wave-vectors in the first Brillouin zone, and N_d, is the number of deuterons that occupy ion band states within the lattice.

In finite crystalline structures, in the limit involving the lowest-energy excitations of the GS and lowest-lying excited states, the only allowable perturbations occur through rigid translations in which the integers n_α and m_α, which are used, respectively, to define the Bravais Lattice Vectors and Reciprocal Lattice Vectors, are required to have the same range of possible values (between $-N_\alpha$ and $N_\alpha-1$ or $-N_\alpha+1$ and N_α, relative to a reference frame that is stationary with respect to the center of mass of the lattice). This requirement insures that both the discrete Fourier transformation of quantities related to the Bravais Lattice and the inverse transformation are unique. It also minimizes the overlap between any of the lowest-lying states.

The lowest-energy configurations permit this when the motion is perfectly rigid, provided the lattice is sufficiently large but also sufficiently small. Within this context, when this can take place, in a situation involving either minimizing the available energy or through a carefully configured environment involving a dynamical form of interaction (for example, in appropriately engineered nanoscale crystals), EMI resonant effects that can create higher-energy nuclear particles can occur when externally applied, static electromagnetic fields (electrical or magnetic, or both) are applied. Richer forms of coupling are also possible, associated with applying alternating electrical and magnetic fields. The associated forms of coupling involve, in the simplest approximation, a generalization of the ideas suggested by Giuliano Preparata.

As opposed to the picture involving "plasmas" in solids that Giuliano Preparata suggested, there is a picture first identified by Bloch and further developed by Zener associated with a situation in which collisions by charged particles are stifled (in a situation involving electrons). In this picture, oscillations of the lowest-energy "quasi-particles" are envisioned to take place in a lattice possessing a fixed orientation. The associated oscillations, as mentioned in the previous section, are referred to as "Bloch oscillations." Zener suggested that if these oscillations are real, at a certain point, tunneling, based on an approximate picture associated with single-particle quantum mechanics, would have to take place. This phenomenon (which was observed, indirectly, fifteen years ago (*23*)) can explain a new effect (*19, 20*) not envisioned by Preparata in which (in the PdD situations) momentum can be stored through rigid displacements of the charge of the electrons and ions that occupy or potentially can occupy energy band states.

The picture associated with Bloch oscillations in a finite lattice can be generalized, and the idea that the tunneling concept might apply (which Zener (*24*) suggested, by assumption) can also be generalized (*9, 10, 19, 20*). For Bloch oscillations to lead to Zener tunneling, a natural form of resonance has to take place in which, as a function of time t, when the applied force $q\vec{E}$ is sufficiently weak (so that collisions within the solid actually are stifled) an equality $q\vec{E}t = \hbar\vec{G}$ ($\vec{G}$ = reciprocal lattice vector) can occur any number of times in which momentum is transferred elastically to the center of mass of the lattice. In most situations involving electrons, this form of interaction is stifled by collisions. But for understanding the lowest energy and momentum situation involving ions (d's), the effect can be quite real in PdD. The reason is that, asymptotically, fluctuations involving small changes in the loading parameter x in PdD_{1+x} can induce the kinds of small perturbations in the external forcing that can lead to the kinds of resonant effects associated with Zener tunneling, involving ions, d's, as opposed to electrons.

Zener suggested, in the context of Bloch's imprecise model, a unifying theme that can provide a way to overcome doubts that most nuclear physicists have about how "tunneling might occur" in a way that they possibly would agree with through an alternative effect in which a lattice conceivably could

Downloaded by YORK UNIV on July 1, 2012 | http://pubs.acs.org
Publication Date: August 1, 2008 | doi: 10.1021/bk-2008-0998.ch006

allow tunneling to take place coherently. Unfortunately, because of subtleties involved in how this might take place, most nuclear physicists would not appreciate what Zener suggested. He suggested that each time $q\vec{E}t = \hbar\vec{G}$, a "beating phenomenon," could take place, in which momentum (not energy) could be transferred to all of the charged energy band state "quasi-particles" (electrons, in the case he considered) and that this momentum could "be stored" and "amplified" appropriately.

In earlier papers, I pointed out that the insulator model that Zener was referring to could apply to fully-loaded $PdD_{1\pm\delta}$, as δ becomes vanishingly small, and that, as opposed to a situation potentially involving electrons, it could involve d's. Within this context, because d's are bosons, forms of coherence can take place in which the d's effectively behave as a Bose-Einstein condensate, similar to the kind of Bose-Einstein condensates that can form when neutral alkali atoms are optically cooled and interact with an optical lattice (*9, 25*). When this takes place, the resonant effects can involve a macroscopically small but microscopically large number of nuclei that are effectively tuned to a form of resonant condition that, with time, can induce non-local forms of coupling that can result in d+d→helium-4 forms of reaction. An important point involves the role of EMI and resonant EMI in making this possible. The failure of conventional physicists to recognize this has undermined meaningful dialogue about this subject.

Downloaded by YORK UNIV on July 1, 2012 | http://pubs.acs.org
Publication Date: August 1, 2008 | doi: 10.1021/bk-2008-0998.ch006

By requiring that the associated dynamics occur in the reference frame that is stationary with respect to the relative motion of the center of mass, it follows that when the semi-classical equations associated with Eq. (16) are valid, as a function of time, in order for the most coherent forms of reaction to take place, the center of mass of the lattice accelerates in such a way that its acceleration does not occur too rapidly or too slowly. Bounds for not accelerating too rapidly or too slowly are responsible for the limits that were estimated previously (*19, 20*). These bounds imply that crystal size is important and plays a role in how "tunneling" can take place as rapidly as possible in order for nuclear reaction to take place. Other effects can be important. Whether or not avoiding collisions that could disrupt the associated process is potentially valuable is an open question. These earlier estimates of relevant forms of transport have suggested that optimal sizes for potentially reactive crystals should have characteristic dimensions of ~ 30-50 nm.

In the rest frame of the laboratory, when the solid is exposed to an outside, external electric field (as in conventional LENR), in the alternative rest frame, in which the center of mass is stationary but accelerates relative to the laboratory rest frame, the external electric field that is applied in the laboratory rest frame will be different than the electric field in the center-of-mass rest frame, and a magnetic field will also be created. The presence of these different fields can result in new forms of interaction that can lead to new effects.

A concrete example that illustrates the origin of the resulting effects involves estimating the power P that is transferred to a charge in the rest frame of the ordered solid, and how P changes as a function of time. In particular, in the rest frame of the location that is stationary with respect to the center of mass, P is defined by the dot product of the local force F_{em} and velocity v; i.e., when $P = \vec{F}_{em} \bullet \vec{v}$, and, to insure that, as a function of time, minimal coupling to outside processes take place, instantaneously, P is required to be constant. Then coupling can take place between the electric and magnetic fields that can result in forms of dissipation that can impede electromagnetic propagation from taking place. In particular, in the limit in which P from possible reactions is constant, for each state, possessing wave-vector $\vec{k}$, involving mass M, the associated power is $\frac{\hbar\vec{k} \bullet F_{em}}{M}$. In the "rest frame" that is stationary with respect to the center of mass, $\hbar\frac{d\vec{k}}{dt} = 0$. This means that,

$$\frac{dP}{dt} = \frac{q\hbar}{M}\frac{d\vec{k} \bullet F_{em}}{dt} = \frac{q\hbar}{M}\frac{\vec{k} \bullet \partial(\vec{E} + \nabla_k \varepsilon(k)/c \times \vec{B})}{\partial t} = 0 \tag{17}$$

where q is the charge and M is the mass of the particle that interacts with the electromagnetic field. Eq. (17) implies

$$-q\frac{\partial\vec{k} \bullet \vec{E}}{\partial t} = q \bullet \vec{k} \bullet \left(\frac{\nabla_{\vec{k}} \varepsilon(\vec{k})}{c} \times \frac{\partial\vec{B}}{\partial t} \right) = -q \bullet \vec{k} \bullet (\nabla_{\vec{k}} \varepsilon(\vec{k}) \times (\nabla \times \vec{E})). \tag{18}$$

In the co-deposition experiments, we may assume that the dominant applied field is vertically oriented, approximately, relative to the samples, and approximately constant. If $\vec{A}$ is real at the boundary of the lattice, its imaginary component vanishes. This condition can be imposed by assigning a particular gauge condition and/or by requiring that the "boundary" of the lattice be defined as occurring at a location $\vec{r}_{boundary}$ where $\vec{k} \bullet \vec{r}_{boundary} = \pi n$, where n is an integer. When the electric field in Eq. (18) is uniformly constant, both sides of Eq. (18) vanish identically, but if the lattice is allowed to move, in principle, the lowest-energy (Bloch state) photon fields will emit radiation whenever $\vec{k} \bullet \vec{r}_{boundary} = \pi n$. If an applied field $\vec{E}'$ perpendicular to the initial field is introduced, the requirement that $\vec{A}$ be real at the boundary of the lattice leads to a different situation. In particular, in the idealized limit that $\vec{E}'$ varies in the vertical direction and is pointed in the x direction, Eq. (18) implies

$$\frac{\partial\vec{k} \bullet \vec{E}'}{\partial t} = \frac{\partial k_x E_x'}{\partial t} = \nabla_{k_x} \varepsilon(\vec{k}) \frac{\partial k_x E_x'}{\partial z}. \tag{19}$$

Eq. (19) is a wave equation. Its solution is an arbitrary, differentiable function P(t):

Downloaded by YORK UNIV on July 1, 2012 | http://pubs.acs.org
Publication Date: August 1, 2008 | doi: 10.1021/bk-2008-0998.ch006

$$P = k_x E_x' = P\left(t + \frac{z}{\nabla_{k_z}\varepsilon}\right). \qquad (20)$$

When $\nabla_{k_x}\varepsilon(\vec{k})$ becomes vanishingly small or large, the solution to Eq. (20) either becomes time-independent or spatially uniform. In either case, the fields can be expected to become localized. This form of localization of the electromagnetic fields is strikingly similar to the kind of effect that Giuliano Preparata referred to as "trapped photons." When this kind of effect can take place, provided sufficient momentum is available, as opposed to the forms of X-ray emission that would be expected when $\vec{k} \bullet \vec{r}_{\text{boundary}} = \pi n$, because the momentum is required to be localized at the boundaries of the lattice, it is plausible that high-energy particles would be released. This argument suggests that details about the orientation of the applied fields in the SPAWAR protocol experiments might be important.

Downloaded by YORK UNIV on July 1, 2012 | http://pubs.acs.org
Publication Date: August 1, 2008 | doi: 10.1021/bk-2008-0998.ch006

References

1. Krivit, S. B. Extraordinary Courage: Report on some LENR Presentations at the 2007 American Physical Society Meeting. *New Energy Times* [Online] **2007**, *21*, 10. http://newenergytimes.com/news/2007/NET21.htm.
2. Szpak, S.; Mosier-Boss, P. A.; Gordon, F. E. Further Evidence of Nuclear Reactions in the Pd Lattice: Emission of Charged Particles. *Naturwissenschaften* **2007**, *94*, 511-514.
3. Klyshko, D. N. *Photons and Nonlinear Optics.* Gordon and Breach Science Publishers: New York, 1988.
4. Chubb, S. R.; Chubb, T. A. Relationship Between Microscopic and Macroscopic Interactions in Low Energy Nuclear Reactions: Lessons Learned from d + d → ^{4}He. In *Condensed Matter Nuclear Science: Proceedings of the 9th International Conference on Cold Fusion*, Beijing, China, May 19-24, 2002; Li, X. Z., Ed.; Tsinghua Univ. Press: Beijing, 2002; 57.
5. Chubb, S. R.; Chubb, T. A. Ion Band State Fusion: Reactions, Power Density, and the Quantum Reality Question. *Fusion Technol.* **1993**, *24*, 403.
6. Preparata, G. Theoretical Ideas on Cold Fusion. In *Proceedings of the First International Conference on Cold Fusion*, Salt Lake City, UT, Mar. 28-31, 1990; National Cold Fusion Institute: Salt Lake City, 1990; 91.
7. Preparata, G. *QED Coherence in Matter*. World Scientific: Hackensack, New Jersey, 1995; pp. 25-40, 153-178. Also Preparata, G. Private communication, in which Preparata referred to fluctuations in the zero of energy within a solid as fluctuations in the vacuum, and the possibility of tapping into these as trapped photons that occupy a super-radiant state.

8. Chubb, S. R.; Chubb, T. A. Theoretical Framework for Anomalous Heat and 4He in Transition Metal Systems. In *ICCF8: Proceedings of the Eighth International Conference on Cold Fusion*, Lerici (La Spezia), Italy, May 21-26, 2000; Scaramuzzi, F., Ed.; Italian Physical Society: Bologna, Italy, 2001; 385.
9. Chubb, S. R. Role of Broken Gauge Symmetry in Transport Phenomena Involving Neutral and Charged Particles in Finite Lattices. 2005, arXiv:cond-mat/0512363v1. arXiv.org e-Print archive. http://arxiv.org/abs/cond-mat/0512363v1.
10. Chubb, S. R. Nuts and Bolts of the Ion Band State Theory. In *Condensed Matter Nuclear Science: Proceedings of the 10th International Conference on Cold Fusion*, Cambridge, MA, Aug. 24-29, 2003; Hagelstein, P. L.; Chubb, S. R., Eds.; World Scientific Publishing Co.: Singapore, 2006; 735.
11. Ashcroft, N. W.; Mermin, N. D. *Solid State Physics.* Saunders College Publishing: Fort Worth, TX, 1976; pp 213-242.
12. Chubb, T. A.; Chubb, S. R. Cold Fusion as an Interaction Between Ion Band States. *Fusion Technol.* **1991**, *20*, 93.
13. Hagelstein, P. L.; McKubre, M. C. H.; Nagel, D. J.; Chubb, T. A.; Hekman, R. J. New Physical Effects in Metal Deuterides. In *Condensed Matter Nuclear Science: Proceedings of the 11th International Conference on Cold Fusion*, Marseilles, France, Oct. 31 - Nov. 5, 2004; Biberian, J.-P., Ed.; World Scientific Publishing Co.: Singapore, 2006; 23.
14. Preparata, G. *QED Coherence in Matter.* World Scientific: Hackensack, New Jersey, 1995; pp 1-40.
15. Thompson, D. R. Effect of d+d Final State Interactions on He-4 (Gamma, d) H-2 Cross Section. *Nucl Phys A* **1970**, *A154*, 442.
16. Ashcroft, N. W.; Mermin, N. D. *Solid State Physics.* Saunders College Publishing: Fort Worth, TX, 1976; p 141.
17. Ashcroft, N. W.; Mermin, N. D. *Solid State Physics.* Saunders College Publishing: Fort Worth, TX, 1976; pp 86-94.
18. Ashcroft, N. W.; Mermin, N. D. *Solid State Physics.* Saunders College Publishing: Fort Worth, TX, 1976; p 135.
19. Chubb, S. R. Framework for Understanding LENR Processes, Using Conventional Condensed Matter Physics. In *Condensed Matter Nuclear Science: Proceedings of the 11th International Conference on Cold Fusion*, Marseilles, France, Oct. 31 -Nov. 5, 2004; Biberian, J.-P., Ed.; World Scientific Publishing Co.: Singapore, 2006; 646.
20. Chubb, S.R. Context for Understanding why Particular Nano-Scale Crystals Turn-On Faster and Other LENR Effects. In *Condensed Matter Nuclear Science: Proceedings of the 12th International Conference on Cold Fusion*, Yokohama, Japan, Nov. 27-Dec. 2, 2005; Takahashi, A.; Ota, K.-I.; Iwamura, Y., Eds.; World Scientific Publishing Co.: Singapore, 2006; 430.
21. Melich, M. Private communication.

Downloaded by YORK UNIV on July 1, 2012 | http://pubs.acs.org
Publication Date: August 1, 2008 | doi: 10.1021/bk-2008-0998.ch006

22. Gonis, A.; Butler, W. H. *Multiple Scattering in Solids.* Springer-Verlag: New York, 2000.
23. Feldmann, J.; Leo, K.; Shah, J.; Miller, D. A. B.; Cunningham, J. E.; Meier, T.; von Plessen, G.; Schulze, A.; Thomas, P.; Schmitt-Rink, S. Optical Investigation of Bloch Oscillations in a Semiconductor Superlattice. *Phys. Rev. B* **1992**, *46*, 7252.
24. Zener, C. A Theory of the Electrical Breakdown of Solid Dielectrics. *Proc. R. Soc. A*, **1934**, *145*, 523-529.
25. Morsch, O.; Muller, J. H.; Cristiani, M.; Ciampini, D.; Arimondo, E. Bloch Oscillations and Mean-Field Effects of Bose-Einstein Condensates in 1D Optical Lattices. *Phys. Rev. Lett.* **2001**, *87*, 1040402/1-4.

Downloaded by YORK UNIV on July 1, 2012 | http://pubs.acs.org
Publication Date: August 1, 2008 | doi: 10.1021/bk-2008-0998.ch006

Downloaded by STANFORD UNIV GREEN LIBR on July 2, 2012 | http://pubs.acs.org
Publication Date: August 1, 2008 | doi: 10.1021/bk-2008-0998.ch007

Chapter 7

Excess Heat and Calorimetric Calculation: Evidence of Coherent Nuclear Reactions in Condensed Matter at Room Temperature

A. De Ninno[1], E. Del Giudice[2], and A. Frattolillo[1]

[1]ENEA, Centro Ricerche Frascati, C.P. 65-00044 Frascati, Roma, Italy
[2]INFN Milano, Via Celoria 16, 20133 Milano, Italy

The aim of this paper is to show that the existence of "cold" nuclear fusion in the palladium lattice cannot be just an irrelevant oddity since it derives from the peculiar interplay of electromagnetic and matter fields. Hence its understanding requires the conceptual frame established by Quantum Electrodynamics (QED). Here we sketch a conceptual path starting from the knowledge of unexplained facts known for decades. Along this path we come to the proposal of a new field of research initiated by the experiments performed by Martin Fleischmann and Stanley Pons (*1*) from 1984 to 1989. We conclude our review with the description of the experiments we did in 2002 where we observed simultaneously both excess heat and ^{4}He production in an electrolytic cell with heavy water and a Pd cathode.

In Low-Energy Nuclear Reactions Sourcebook; Marwan, J., et al.;
ACS Symposium Series; American Chemical Society: Washington, DC, 2008.

Background

The debate on cold fusion has been sometimes represented to the public as a quarrel between "true believers" (supporting the cause of this peculiar kind of nuclear phenomenon out of an attitude of rebellion against the prevailing paradigm) and the "true unbelievers" (acting as "defensores fidei", struggling against the people who try to subvert the scientific rationality). This misrepresentation has obscured the real scientific roots of the research approach that has brought some scientists to conceive the point of view that nuclear reactions could occur inside condensed matter, in particular within metal lattices at room temperature.

The usual objections against cold fusion are based on the tenet that physics of nuclei embedded in a lattice should not differ from physics of nuclei in vacuo, in the empty space. This statement is known as Asymptotic Freedom (AF). As a matter of fact, the space-time scale of nuclear phenomena is smaller by six orders of magnitude than the space-time scale of the lattice. Let us assume that nuclear reactions among deuterium nuclei *d* could occur within the lattice as physical events localized at definite sites. Consider in particular the reaction

$$d + d \rightarrow \text{compound\_excited\_nucleus\_}{}^{4}\text{He} \rightarrow \text{final\_products}$$

The energy release from the compound nucleus in order to relax to a stationary state should follow the Heisenberg uncertainty principle $\Delta E \times \Delta T \approx \hbar$. Since $\Delta E \approx 24$ MeV then $\Delta T \approx 10^{-22}$s.

Actually the lattice could play a role in the decay of the compound nucleus only if the energy released by the nuclear reaction should involve several lattice components within the decay time ΔT. However, this is impossible since the velocity of the energy transfer required to overcome the distance between first neighbors in a metal lattice, about 3 Å, would exceed the speed of light *c* by a factor of 10^4. This consideration would rule out any possibility of a nuclear reaction occurring in a lattice according to a dynamics different than in vacuo.

However, there is a phenomenon, well known in nuclear physics as the Mössbauer effect (*2*), that seems to defy the above argument. According to the Mössbauer effect, a crystal made up of nuclei able to exhibit γ-decay recoils as a whole when this decay occurs. It behaves as an infinitely stiff lattice where independent movements of the components during the decay are forbidden (*3*). According to the data available (*4*), as many as 2×10^9 nuclei would recoil together. The existence of such a collective dynamics in lattices could support the possibility of an interplay between nuclear reactions and lattice dynamics; however, as in the Mössbauer effect, nuclear reactions could be no longer conceived as localized events, but should occur in a delocalized way.

The possibility of such delocalization arises from Quantum Field Theory, where it is shown (*3, 5*) that the interplay between the quantum fluctuation of

Downloaded by STANFORD UNIV GREEN LIBR on July 2, 2012 | http://pubs.acs.org
Publication Date: August 1, 2008 | doi: 10.1021/bk-2008-0998.ch007

the microscopic components (atoms, molecules, nuclei, electrons) and the gauge field (in our case, the electromagnetic field), prescribed by the requirement of the local phase invariance of the Lagrangian, produces, under suitable conditions, the formation of extended domains (coherence domains), where the components are correlated in a collective coherent configuration. Within such domains, the correlation among components is kept by the gauge field and travels at the phase velocity of the field, that, as well known, may exceed *c*. This explains the Mössbauer paradox and opens the way to the possibility of nuclear reactions occurring in condensed matter in a way different than in vacuo.

Quantum Electrodynamics (QED) implies that nuclear transformations of deuterons compressed into a palladium lattice would substantially differ from the reactions observed in diluted plasmas. This intuition was largely shared by Julian Schwinger (*6*).

The existence of a collective dynamics in condensed matter able to produce relevant energy outcomes not accountable in terms of localized events is supported by a number of phenomena. A topic relevant to this research is the work carried out by Bridgman in the 1930s (*7*). He found that the energy stored in a lattice, when intense shear and compression are applied, gets released in "cold explosions," where the energy stored in the lattice is converted into kinetic energy of fragments. An amplification of the energy through the collective dynamics of the lattice is thus obtained.

A second phenomenon has emerged from the work of Cöhn on electro-diffusion of hydrogen in the Pd lattice (*8*). Hydrogen was found to be present in the lattice (at that time deuterium had not yet been discovered) in the form of protons. This posed an energy puzzle to solid-state physicists, since the formation of ionic hydrogen in the lattice demands a very high energy. A possible Born-Haber cycle (*9*) based on the dissolution of H^+ requires an energy as large as 31.7 eV ($H_2 \rightarrow 2H$ requires 4.48 eV, whereas $2H \rightarrow 2H^+ + 2e$ requires 27.2 eV).

A third point emerges from the very early literature on the subject of fusion (*10*, *11*). By investigating the fusion process $d+d \rightarrow t$ (tritium)$+H^+$ in a Wilson cloud chamber, a significant number of tracks angled at 180° was observed; under the experimental conditions the tracks should have exhibited an angle of 160°! This result would suggest the occurrence of fusion between species which had already lost most energy in the target!

The above topics suggest that collective phenomena could play a relevant role in our story. Recently Widom and Larsen (*12*) have suggested a possible role for weak interactions in cold fusion. They invoke collective proton layer oscillations on the surface of palladium able to produce a field capable of "dressing" electrons with an enhanced mass. Such a renormalization via electromagnetic fluctuations enhances the capture probability and the consequent low momentum neutron production that can induce a chain of reactions in the neighboring condensed matter. However, according to the universally accepted principles of physics, it is impossible to dissipate energies of MeVs simply by "heating" the lattice without any emission of very energetic

Downloaded by STANFORD UNIV GREEN LIBR on July 2, 2012 | http://pubs.acs.org
Publication Date: August 1, 2008 | doi: 10.1021/bk-2008-0998.ch007

fragments that have not been observed in these phenomena. So cold fusion cannot be a localized event but implies the revision of some of our implicitly assumed facts about condensed matter.

In 1989, one of us (Del Giudice), together with the late Giuliano Preparata and Tullio Bressani (*13*), investigated the system in the context of QED. This approach is based on a critical analysis of the ground state of QED (*3*). The ground state in condensed matter involves the atoms/molecules of a macroscopic piece of matter in an intricate dynamical interplay mediated by a large (classical) electromagnetic field. In such a scenario the AF is not a general property of such coherent ground state because the e.m field fills the vacuum among the particles inside the matter and interacts strongly with the charges. Let us briefly summarize the main points of this dynamics.

Downloaded by STANFORD UNIV GREEN LIBR on July 2, 2012 | http://pubs.acs.org
Publication Date: August 1, 2008 | doi: 10.1021/bk-2008-0998.ch007

Coherent Dynamics in Cold Fusion

Experimental reports on cold fusion show the following facts, that appear to be "strange" in the conventional framework of nuclear physics:

- At room temperature and pressure, under suitable electrochemical conditions, a rate of nuclear fusions d-d is reported that exceeds by 60 orders of magnitude the rate η of tunneling below the Coulomb barrier in a D_2 molecule ($\eta \sim 10^{-90}$ fusions per pair of deuterons).
- The fusions predominantly give rise to ^4He, with a low fraction of events belonging to the channel tritium+proton and a very few events neutron+He^3.

These experimental reports could be addressed in the QED framework on the basis of the following concepts (*3, 8, 10*):

1. There is a first element which is able to increase the rate η of fusion by about 40 orders of magnitude. In a Pd crystal at room temperature the d-electron shells are in a coherent regime within "coherence domains" (CD) as large as a few hundred Angstroms. Electron shells oscillate in tune with a coherent electromagnetic field trapped in the CD, whose frequency is in the range of soft X-rays. The coherent plasma of the d-shells is so inflexible, that, at selected points in the lattice, it produces permanent lumps of negative charge able to catalyze nuclear fusion in a way akin to the muon catalyzed fusion. This catalysis amounts to an increase in the barrier penetration factor among deuterons by about 40 orders of magnitude. However, this enhancement is not enough to justify the fusion yields observed by the experimentalists.
2. As discussed in Ref. (*3*), hydrogen filling the metal enters into a coherent state when $x=H(D)/Pd>0.7$. The corresponding CDs have a size between 1 and 10 μm and oscillations are tuned with a self trapped electromagnetic field, whose frequency is in the IR interval.

3. As discussed in Ref. (*3*), in the case of deuterium, when the loading ratio $x>1$, the above coherent state induces a further magnification of the probability of tunneling of deuterons across the Coulomb barrier, thus allowing the large number of fusions needed to produce the observed large amounts of excess heat. The excess energy is also released in a time shorter than that required to split the "boiling" ^{4}He nucleus by the nuclear dynamics (about 10^{-21} s), thus preventing a massive emission of neutrons and tritium (*13, 14*). Therefore, the main nuclear ash of the process is a ^{4}He atom. This acceleration of the rate of energy release from a coherent system is the consequence of the fact that the coherence (see Refs. (*3*) and (*5*)) increases the value of the coupling constant e (the electric charge) to $e\sqrt{N}$, where N is the number of the components of the coherent system, so that the time scales are shortened by a factor $\sqrt{N}$. Since at x=1 the density of deuterons N/V is 7×10^{22} cm^{-3} and the volume of the coherence domain has been estimated to be 10^{-10} cm^3 (see Ref. (*3*)), the number of deuterons per coherence domain can be estimated as 7×10^{12}, thus giving rise to a reduction of the timescale of the energy release by a factor $\sqrt{N}\sim\sqrt{7\times10^{12}}\sim2.6\times10^6$. Since the average time scale τ for electromagnetic decay is in the range of $10^{-15}\div10^{-16}$ sec, it can be concluded that a coherence domain containing 7×10^{12} deuterons is able to release energy in a time smaller than 10^{-21} sec. On the other hand, on the boundaries of the coherent region, where the fraction of the coherent deuterons decreases, this "coherent" timescale increases, becoming longer than the "nuclear" timescale of 10^{-21} sec that is necessary for the spitting of the compound ^{4}He nucleus. Thus, the nuclear decay of the compound nucleus may occur and more conventional decay products, such as tritium, may appear. This point has been discussed in Ref. (*14*).

Energy Output of Cold Fusion

It is straightforward to see that such a peculiar release of energy into the lattice poses an acute question: How can the heat produced into the lattice be extracted (and measured) avoiding the destruction of the lattice itself ? In other words, could cold fusion be developed into a practicable source of energy? During the experiments performed at the ENEA laboratories in Frascati, it has been seen (see Figure 1) that the thin strip of palladium used as a cathode in an electrolytic experiment melts after loading with deuterium and crossing of the threshold foreseen by the theory. The scale-up of the experiments must take into account the geometry required to induce the phenomenon, while such a geometry must be robust enough to dissipate the expected energy density (for civilian applications, this will lie in the range of 1-10 kW/cm^3).

Downloaded by STANFORD UNIV GREEN LIBR on July 2, 2012 | http://pubs.acs.org
Publication Date: August 1, 2008 | doi: 10.1021/bk-2008-0998.ch007

Downloaded by STANFORD UNIV GREEN LIBR on July 2, 2012 | http://pubs.acs.org
Publication Date: August 1, 2008 | doi: 10.1021/bk-2008-0998.ch007

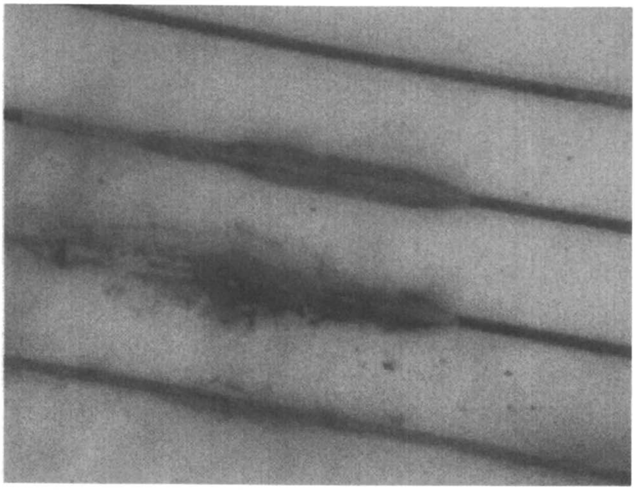

Figure 1. Thin-film palladium cathode after a cold fusion experiment. The peculiar geometry of the melted area (several melted spots unrelated and not contiguous) led us to exclude that the Joule effect is responsible for the damage of the film.

The Nature of the Nuclear Reaction Responsible for the Generation of Excess Enthalpy

Let us analyze in more detail the process of energy release in cold fusion. The production of ^{4}He, unaccompanied by γ-rays, demands a very fast (t<10^{-21} s) energy transfer to the lattice electrons. The time T_0 needed for releasing the energy of 3.4 MeV, necessary to put the "boiling" nucleus below the threshold of splitting, is

$$T_0 \sim 1/2\ 10^{-21}\ \text{s} < 10^{-21}\ \text{s}$$

10^{-21} s is the time required by nuclear dynamics to split the nucleus (*14*).

In conclusion the output energy of each fusion is quickly transferred to the Pd electron plasma, where it gives rise to an excitation at much lower frequency i.e., X rays, IR radiation.

In this very short time interval, a short-lived electromagnetic field, which has the frequency of γ-rays, exists in the Coherence Domain. At the rate of 10 kW/cc, estimated both from theory and experiments (*14, 15*), one can calculate that in each Coherence Domain the average fusion rate is 2.5×10^3 s^{-1} and the energy released by each fusion is transferred to the lattice in a time of 10^{-14} s, so that there is no superposition between the two events. Each fusion produces a γ-ray electromagnetic classic field lasting about 10^{-21} s which fills the whole volume of the Coherence Domain.

A Cold Fusion Experiment

The objections raised by a part of the scientific community against the experimental evidence of excess heat production in heavy water electrolysis on a Pd cathode are mainly based on the opinion that such a phenomenon is inconceivable on the basis of the commonly accepted condensed matter physics. This is something we have already disproved in the former section. More objections address the lack of reproducibility. To overcome these kinds of opinions and prejudices the scientists involved in cold fusion research are required to be exceptionally rigorous and careful. Actually, the legitimate requirement of reproducibility has been quite difficult to fulfill since the theory has not focused on the parameters which are particularly relevant for the experiment control. It is worth noticing that the literature that has appeared over the past 18 years in reputed journals has reported only negative experiments (*16*). The crucial factor of the loading ratio is still to be published in a respected journal. The theoretical prediction of QED suggests that crossing of the threshold x=1 of the loading ratio remains a necessary condition for cold fusion. As a matter of fact, we know that the complex $Pd\text{-}D_{(x=1)}$ is not a state in chemical equilibrium. As shown by Fleischmann and many others, it is necessary to exert "pressure" from outside to keep the concentration of deuterium at such a high level. This consideration explains why a flow of external deuterons is necessary. Moreover, the ratio x=1 could not be reached homogeneously in the whole cathode volume, so that one could expect an observed "effective" critical ratio slightly lower than 1, just taking into account that some fraction of the cathode volume has not been loaded and therefore has not produced any fusion reaction.

A critical point for the reproducibility is actually the difficulty of overcoming the above loading threshold. Solving such a problem required extensive studies of the palladium metallurgy since, as widely reported in the literature, palladium spontaneously (exothermic reaction) forms hydrides (or deuterides) in concentrations as high as x=0.7 but a higher concentration can be obtained only by forcing hydrogen inside powdered palladium at very high pressure (on the order of MPa). Of course, this technique, as widely known, is completely useless for cold fusion purposes because it destroys the lattice. Cold fusion scientists have been forced to investigate this highly interdisciplinary area of science between electrochemistry and material science. These studies produced interesting data (*17, 18*) in the literature even though the words "cold fusion" have been carefully avoided in the texts.

Even on such issues, QED provides an interesting and powerful insight.

The QED Description of the Pd-H System

Palladium hydrides exhibit very interesting features. Let us list some of them:

Downloaded by STANFORD UNIV GREEN LIBR on July 2, 2012 | http://pubs.acs.org
Publication Date: August 1, 2008 | doi: 10.1021/bk-2008-0998.ch007

a) The dissolved hydrogens get ionized when entering into the lattice and settle in their equilibrium position in ionic form. Ionization may actually occur just at the surface of the crystal and ions reach their equilibrium positions later on (*23*).

b) The Pd-H system exhibits a complex phase diagram. At room temperature and pressure, hydrogen is in a gas-like situation within the Pd lattice when $x<=$ 0.05 (α phase). For higher values of x, an α-β phase emerges which coexists with the α phase; in the β phase, hydrogen is confined in the octahedral sites of the Pd lattice. We get a pure β phase at $x\sim0.6$; for higher values of x, new phases appear (*19*): γ that coexist with the β phase, which gets increasingly depleted as far as x increases.

c) Evidence for the β→γ transition is also provided by the interesting experiment of Wisniewski and Rostocki published in 1971 (*20*). The authors show that a sharp discontinuity appears in the number of the carriers of the electric current, as measured by the Hall effect in a Pd-H system. They found that below a threshold, at about x=0.85, each hydrogen entering the Pd lattice (in the β phase) contributes about 0.75 electrons to the conduction band, whereas, for x exceeding that threshold, each entering hydrogen contributes more than 4 electrons to the conduction band; since hydrogen only has one electron on its own it must persuade more than three Pd electrons to jump into the higher energy band, so that the entering of one hydrogen implies a local reshuffling of the Pd structures. The above sharp discontinuity suggests the existence of a phase transition.

d) The electrical resistivity $\rho(x)$ of the Pd-H system as a function of x exhibits a peculiar behaviour (*21*). In the α-β phase, ρ increases almost linearly with x up to the x_0 value where the β-γ transition occurs. For higher values of x, ρ decreases quite sharply reaching the value ρ_0 of the empty metal at $x\sim1.1$. This feature may be considered a consequence of c): the sharp increase in the number of the carriers implies an increased electrical conductivity.

e) In the γ phase, the mobility D of the hydrogen isotopes within the Pd lattice exhibits an odd pattern; actually, the heavier deuterium is more mobile than the lighter hydrogen, whereas the still heavier tritium is, as reasonably expected, the slowest one, namely $D(d^+)>D(h^+)>D(t^+)$ (*22*). Since d^+ is a boson whereas h^+ and t^+ are fermions, the above result hints at the existence of some sort of collective behavior of d^+ as compared to the other hydrogen isotopes. Actually, the collective dynamics, as is well known, privileges bosons to fermions (^{4}He, a boson, gets superfluid at 2.16 K, whereas ^{3}He gets superfluid at $\sim10^{-3}$ K).

f) There is electrochemical evidence (*23*) that, at high values of x, the hydrogen species perform wide oscillations in an almost unbounded state in the Pd lattice.

The last two items point to the existence of a collective oscillation of hydrogens within the lattice. However the existence of a strong cooperation among hydrogens is hardly understandable in the framework of the usual lattice

Downloaded by STANFORD UNIV GREEN LIBR on July 2, 2012 | http://pubs.acs.org
Publication Date: August 1, 2008 | doi: 10.1021/bk-2008-0998.ch007

dynamics (*24*). One should consider the possibility that a macroscopic ensemble of oscillating hydrogen could no longer be described by a density matrix, where the phases of the different oscillations are not correlated. On the contrary the collective dynamics of the hydrogens give rise to a common phase of the oscillators, that can thus be described by a single quantum state created by the collective dynamics. This point of view has been suggested in the last decade by G. Preparata (*3*) in the framework of coherent quantum electrodynamics. Should it be correct, a testable consequence would emerge. A quantum system, which has a well-defined phase, is able to "see" an externally applied potential as a chemical potential. This effect is the well-known Böhm-Aharonov effect (*25*); the dynamics of a quantum system is affected by a change of the electromagnetic potential through a modification of the wave function phase. Should the ensemble of hydrogen atoms be in a single quantum state, the chemical potential μ of $h^+(d^+)$ in Pd depicted in Figure 2 would be shifted by the applied electric potential $V(\vec{r})$, multiplied by the screened charge Z^*e of the $h^+(d^+)$ in Pd

$$\mu[V(\vec{r})] = \mu[\vec{0}] + Z * \mathrm{eV}(\vec{r})$$

In the above equation, $\mu[\vec{0}]$ could be taken as the chemical potential of the point $\vec{0}$ of the Pd-H specimen where the electric potential is the highest, so that V is the (negative) relative potential of the point $\vec{r}$ with respect to $\vec{0}$. The profile of the chemical potential μ is changed in such a way that the chemical potential in some regions of the system may fall below the chemical potential μ_{ext} of the ions outside (see Figure 2b). Consequently an ion inflow would occur in those regions (*26*).

This effect might be increased if one could apply large electric potential differences across the system without inducing sizeable Joule heating which could inhibit the precondition for the effect, i.e., the $h^+(d^+)$ coherence. The optimal effect is expected in a one-dimensional specimen, whose resistance

$$R = \rho \frac{l}{S}$$

is increased as much as possible by taking a large length l and a very small cross-section S. Since the expected height of the chemical potential barrier is a fraction of one eV and Z^* has been estimated as about 0.1, a voltage of about 10 V applied along the wire should be sufficient to induce a massive inflow of ions, thus increasing the loading by a factor 1.3-1.4 with respect to a two- or three-dimensional specimen (plate or rod) under identical conditions. Figures 3a and 3b compare the electrochemical loading, expressed by the normalized resistance of a Pd sheet and a Pd strip deposited onto a substrate. On the right scale the electrolytic current density in mA/cm^2 (*27*) is shown.

Downloaded by STANFORD UNIV GREEN LIBR on July 2, 2012 | http://pubs.acs.org
Publication Date: August 1, 2008 | doi: 10.1021/bk-2008-0998.ch007

Downloaded by STANFORD UNIV GREEN LIBR on July 2, 2012 | http://pubs.acs.org
Publication Date: August 1, 2008 | doi: 10.1021/bk-2008-0998.ch007

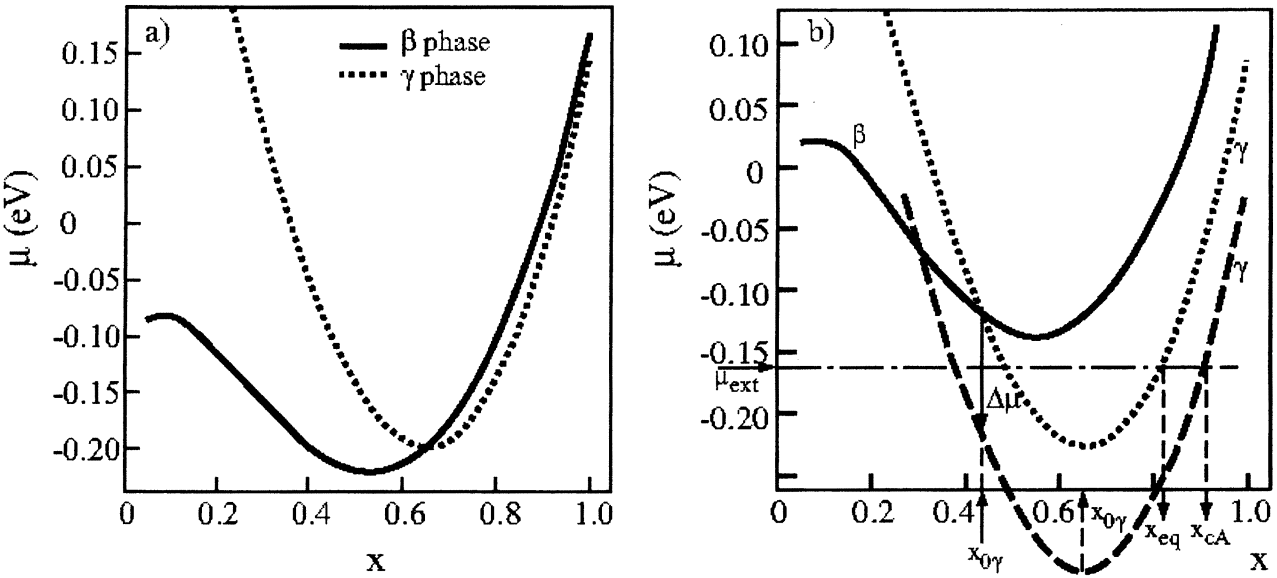

Figure 2. a) Chemical potential μ of d in Pd. The continuous curve describes μ for the β–phase, the dashed curve corresponds to γ phase. b) Influence of the negative electric potential V on the chemical potential μ. (Reproduced from reference 26. Copyright 2000 SIF.)

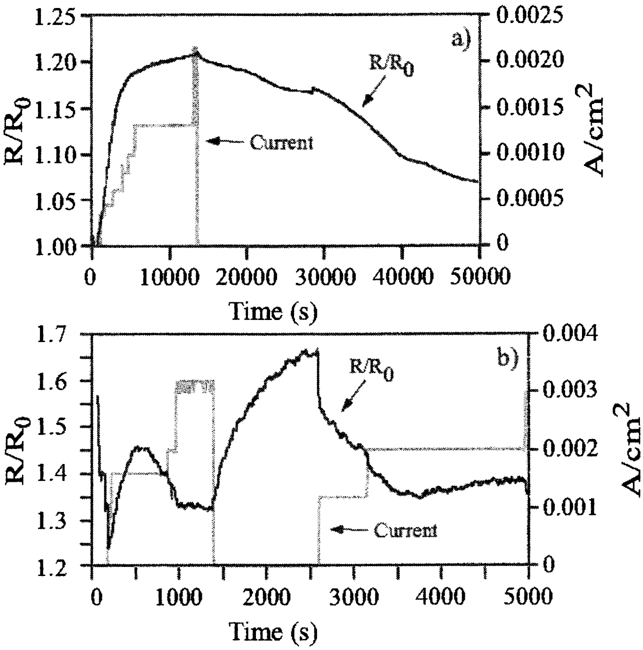

Figure 3. a) Electrolytic loading of an extended deposition. b) Electrolytic loading of a strip. (Reproduced from reference 26. Copyright 2000 SIF.)

Experiment Design

By the end of the 1990s, about 10 years of experience in cold fusion experiments were available, performed all over the world by many unrelated groups of scientists. It was clear to us at that time that the phenomenon, even though weak and unsystematic, was real and well understandable within a defined theoretical framework. It must be said, however, that most of the experiments met a widespread skepticism in the scientific community because of the erratic reproducibility of the results reported. This situation has two possible explanations: either the phenomenon does not exist, or there was insufficient control over the relevant experimental parameters. Today, we know that such poor control is the consequence of the difficulties one faces when trying to reach and keep the right concentration of deuterium in palladium, as already pointed out by many experimenters.

One common feature of earlier experiments is the unpredictability of the start and stop time of the excess heat generation. Sometimes, several weeks were required to start the phenomenon without any apparent change in the system, because no care was taken in measuring the concentration, while at other times the excess heat appeared soon after the start-up of electrolysis. Such an apparent lack of reproducible correlation between the action of the

Downloaded by STANFORD UNIV GREEN LIBR on July 2, 2012 | http://pubs.acs.org
Publication Date: August 1, 2008 | doi: 10.1021/bk-2008-0998.ch007

experimenters and the response of the system left room for spurious interpretations which could affect the observations and pollute the results.

It was bearing in mind the theoretical framework (*3*, *13*) that we started an experimental program aimed at detecting the contemporary evidence of: a) the existence of a threshold in the loading ratio; b) excess heat production; and c) ^{4}He production. According to the QED suggestion, we should have been able to control the loading, thus removing the oddities of long waiting times. The above-described Böhm-Aharonov effect applied to a palladium cathode during electrolysis in heavy water provides a powerful tool capable of forcing the reaching of the threshold. In fact, the decrease in the chemical potential of the Pd-D system, as described above, attracts more deuterons to enter into the lattice because deuterons "see" a chemical potential inside the lattice lower than the chemical potential in the solution, exactly as happens in the α and β phase of Pd-D (it is well known that up to x=0.6 the H(D) absorbtion into Pd is a spontaneous process). The "triple coincidence" technique should rule out the spurious events. The main difficulties arise from the cathode geometry and the helium detection. As shown in the previous subsection, the best candidate to minimize the Joule effect is a "quasi" one-dimensional structure, such as a thin film deposition shaped as a very long and narrow strip. Unfortunately, palladium deuteride becomes very brittle with increasing loading, and thin films detach from the substrate. The solution was found after several attempts of deposition in different physical conditions, leading to the geometry shown in Figure 4.

An innovative technique has been developed, able to produce thin films that are able to resist several loading and de-loading cycles (*28*). The films have been produced by ion-assisted sputtering in Ar atmosphere. In order to face the well-known problem of the detachment of Pd from the substrate during loading, we used several buffer layers of different thickness and metals with an overall thickness less than 200 Å. The final pattern was obtained by using a photolithographic process followed by a physical etching.

However, the very tiny cathode mass used (1.2×10^{-5} moles) reduces the expected amount of released helium. Actually, for a given excess power $\Delta P(W)$, the expected yield is given by:

$$\frac{\delta n_{He}}{\delta t} = \frac{\Delta P(W)}{24\text{MeV}\times N_A} = 4.32\times10^{-13}\times\Delta P(W)\text{mole}\times\text{s}^{-1}$$

For a typical excess power in the range of a few tens of mW

$$\frac{\delta n_{He}}{\delta t} \approx 10^{-15} \div 10^{-14}\,\text{mole}\cdot\text{s}^{-1}$$

Downloaded by STANFORD UNIV GREEN LIBR on July 2, 2012 | http://pubs.acs.org
Publication Date: August 1, 2008 | doi: 10.1021/bk-2008-0998.ch007

Moreover the typical composition of the gas mixture in an electrolytic experiment is: a) atmospheric air which contains about 5.2 ppm of ^4He; b) D_2O vapor in equilibrium with the liquid electrolyte; c) D_2 and O_2 dissociated at the electrodes. The atmospheric air can be removed by purging the experimental environment, for instance with ultra-pure (99.99999%) N70 nitrogen gas, and the D_2 and O_2 moles can be accurately evaluated using Faraday's law. Thus it can be expected that the concentration of ^4He produced in the gas mixture will be in the range of a few ppb as to N_2, and a few ppm as to D_2.

Downloaded by STANFORD UNIV GREEN LIBR on July 2, 2012 | http://pubs.acs.org
Publication Date: August 1, 2008 | doi: 10.1021/bk-2008-0998.ch007

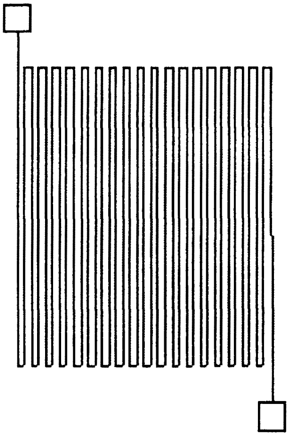

Figure 4. The palladium cathode geometry used for cold fusion experiment: 2μ thick × 54 μ wide × 100 cm long; Pd mass m=1.29 mg (=1.2×10^{-5} moles)

Conventional mass spectroscopy techniques seem inadequate to detect such a small quantity of ^4He in an environment mainly full of N_2 and D_2. A high-resolution quadrupolar mass analyzer is required to resolve the difference between the masses of ^4He and D_2 molecules. However, the huge background of D_2 is likely to hide the smaller ^4He signal in the tail of the D_2 signal. In order to solve the problem, a sample purification system was introduced at the QMA (Quadrupole Mass Analyzer) entrance, consisting, as a first approach, of an activated charcoal trap at liquid nitrogen temperature and a non-evaporable Getter (NEG) pump operating at room temperature. Dry N_2 from boil-off from a liquid nitrogen tank was used as purging gas.

An experimental campaign lasting about two years has been conducted. In these preliminary experiments with heavy water, heat and ^4He production have been observed in 3 out of 5 trials. In the remaining experiments neither excess heat nor helium were measured. Figure 5 shows the results of one of these experiments. The trend of ^{40}Ar signal, shown for comparison in Figure 5, is not correlated to that of ^{4}He, thus pointing to the absence of any environmental pollution.

The results of the following 11 experiments (5 of them were control experiments) showed an average content of ^{4}He atoms in heavy-water experiments 10 times higher than in light-water experiments.

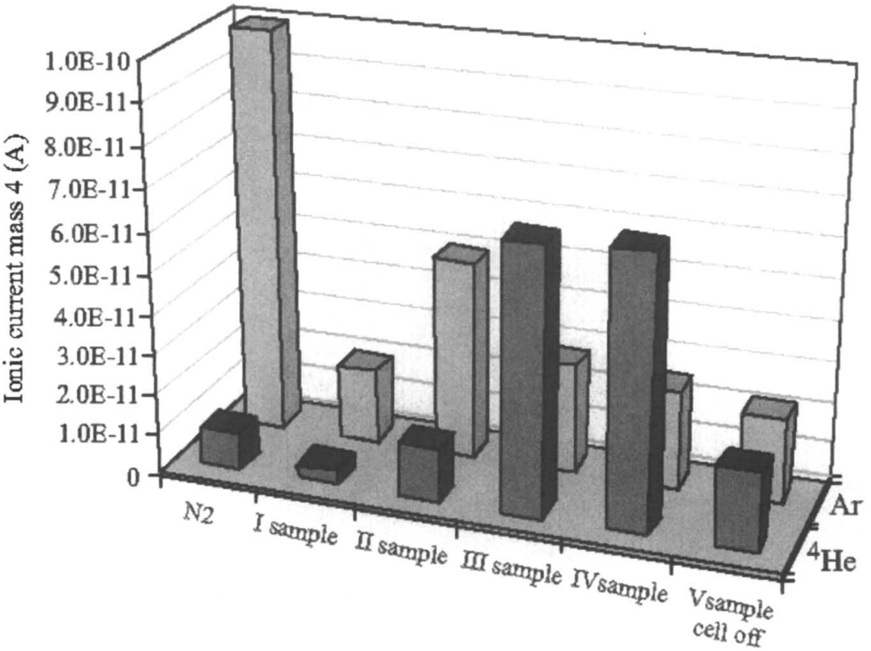

Figure 5. Values of the ionic current as read by mass quadrupole analyzer (QMA) in a typical experiment of electrolysis of LiOD on Pd cathode.

In these early experiments, the gas sampling was operated manually, roughly every two hours. However, we wanted to have a real-time monitoring of the ^{4}He production rate during the electrolysis in order to quantitatively compare the results with the data of loading and excess heat. We were then forced to solve a number of technical problems such as: a) the sampling of gases evolving from the cell at regular intervals of time without perturbing the electrolysis, and b) the accurate measurement of very small and complicated volumes in order to give an exact evaluation of the number of atoms detected. The detailed description of the techniques used is given in Refs. (*29, 30*).

Moreover, a suitable filtering process was realized based on the use of two NEG pumps (*31*) to remove all the chemically active gases present in the atmosphere to be analyzed. The overall experimental layout of the experiment is depicted in Figure 6.

Downloaded by STANFORD UNIV GREEN LIBR on July 2, 2012 | http://pubs.acs.org
Publication Date: August 1, 2008 | doi: 10.1021/bk-2008-0998.ch007

Downloaded by STANFORD UNIV GREEN LIBR on July 2, 2012 | http://pubs.acs.org
Publication Date: August 1, 2008 | doi: 10.1021/bk-2008-0998.ch007

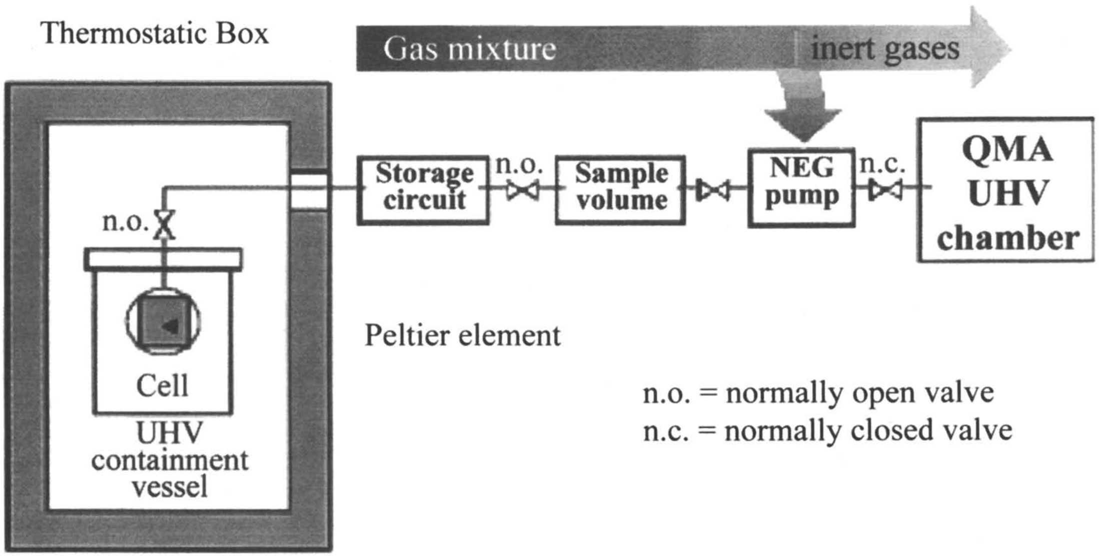
Thermostatic Box
Gas mixture
inert gases
n.o.
Cell
UHV
containment
vessel
Storage
circuit
n.o.
Sample
volume
NEG
pump
n.c.
QMA
UHV
chamber
Peltier element
n.o. = normally open valve
n.c. = normally closed valve

Figure 6. Black diagram of the cell and of the helium sampling circuit.

The cell is enclosed in an ultra-high-vacuum (UHV) containment vessel, filled with N70 nitrogen gas to prevent contamination from outside, and kept in thermal contact with a Peltier element. The cell is located inside a box thermoregulated within ±0.01 °C. Gases from the cell are collected inside a storage volume. A fraction of the gas mixture (sample volume) is periodically sent to the non-evaporable Getter (NEG) pumps and then to the quadrupole mass analizer (QMA). The NEG pumps remove to a high degree all non-inert components of the gas mixture (especially hydrogen isotopes).

The triple coincidence experiment described hereinafter is the result of a steady improvement of the experimental technique and the refinement of the experimental set-up. The detailed sequence of the steps of the typical experimental run is depicted in Figure 7:

- *Preloading phase.* A feeble electrolytic current, about 5 ma, is flowing across the cell; in a time of about one hour, R/R_0 smoothly reaches the peak value of 2 corresponding, according to (*21*), to the value x=0.7 (β-phase). This state is at its chemical equilibrium where the system could remain indefinitely.
- *Loading phase.* At this point, we apply a voltage V_c along the cathode. This voltage is applied by proportionally increasing the cell current to a value ranging from 10 to 40 ma (corresponding to a current density ranging from 20 to 80 ma/cm^2). When the cathode is a narrow and thin strip, as in our case, R/R_0 drops from 2 to about 1.4 in a very short time (some minutes). In order to verify that indeed we are above the maximum of the R/R_0 vs. x curve, we switch off the current for a short time, thus producing a small, temporary deuterium unloading of the cathode, with an observed increase of R/R_0 (rather than a decrease).
- *Supercritical phase.* The value R/R_0=1.4 corresponds to $x\approx 1$(see Ref. (*21*)).
- *Control phase.* After some hours of cell operation, the cathode potential V_c is switched off.

Results

The overall outcome of the experiments so far has been as follows (cf. Figure 8):

a) a suitable electrical potential was applied across the cathode at the end of the preloading phase and excess heat appears as soon as R/R_0 decreases below 1.4, (namely when $x \geq 1$);

b) ^{4}He appears simultaneously with the excess heat within its sampling time (about 20 minutes; for a detailed explanation of this time, see Refs. (*29-31*));

c) at the end of each experiment and for several hours after the switch-off of the cell current, excess heat and ^{4}He compatible with the baseline were measured;

d) there is a discrepancy between the excess power P_{He} estimated by counting ^{4}He atoms and the excess power P_c given by the calorimeter.

Downloaded by STANFORD UNIV GREEN LIBR on July 2, 2012 | http://pubs.acs.org
Publication Date: August 1, 2008 | doi: 10.1021/bk-2008-0998.ch007

Downloaded by STANFORD UNIV GREEN LIBR on July 2, 2012 | http://pubs.acs.org
Publication Date: August 1, 2008 | doi: 10.1021/bk-2008-0998.ch007

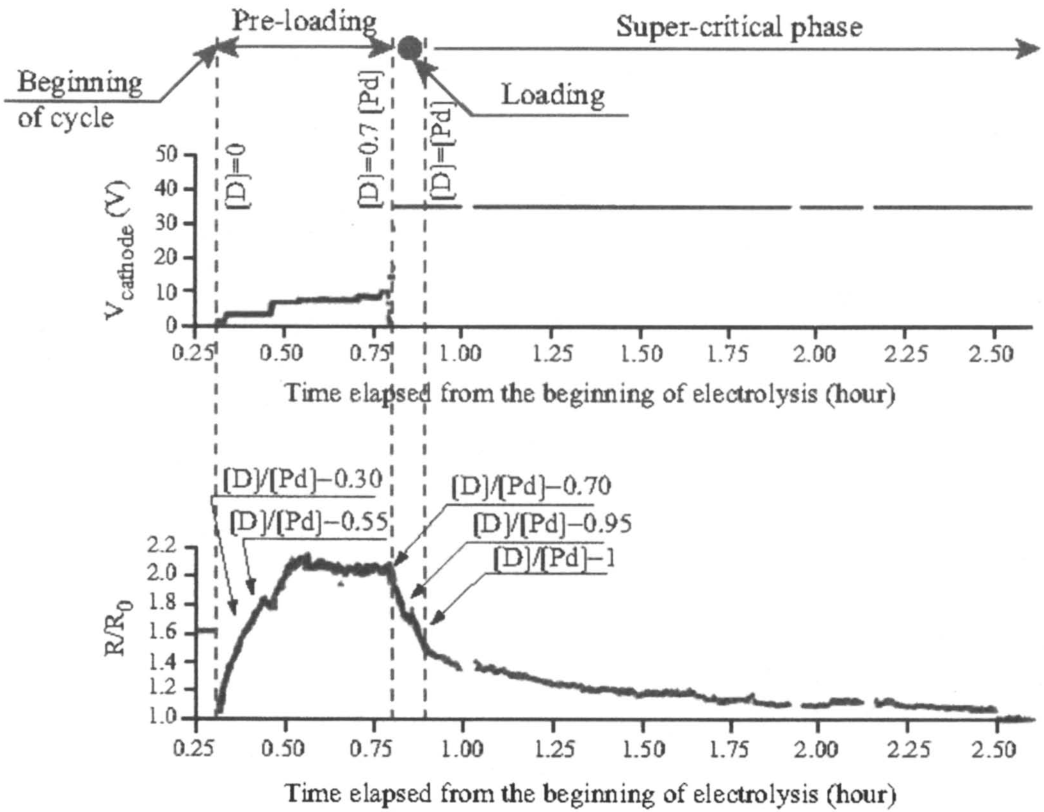

Figure 7. Influence of $V_{cathode}$ on the Pd loading

The last item can be understood as a consequence of the peculiarities of this reaction: nuclear "microfurnaces" may appear in the sections of the one-dimensional cathode where the electric potential is most negative and consequently the loading is the largest (x>1).

Since, most likely, the critical threshold has been crossed by only a narrow margin, the erratic appearance of "hot spots" (having the size of a crystal grain, namely a few microns), where the temperature T may become very high, has been observed. In this case, a significant fraction of the energy output is released in the form of X-rays, which thermalize far from the cathode. The consequences of these high T spots are the predominance of the radiative Stefan-Boltzmann channel in the heat release and the possible appearance of film boiling on the cathode surface which might open convective channels to heat dissipation. Furthermore ^{4}He produced in the "hot spots" will not be confined in the Pd lattice and should therefore be found almost exclusively in the gas evolving from the cell. Therefore the mismatch between the excess heat measured thermally and the heat evaluated by the ^{4}He rate increases with the power produced.

The measurements were completed by comparing three experimental situations: a) electrolysis in heavy water 10^{-4}M with a critically loaded (x>1) cathode; b) electrolysis in heavy water 10^{-4}M with an under-critically loaded cathode (x<1); and c) electrolysis in light water (H_2O) 10^{-4}M with a critically loaded (x>1) cathode. The electrolytic conditions are the same shown in Figure 7.

In experiment (a), an anomalous production of ^{4}He was detected (about 25 times the estimated initial content), which cannot be accounted for on any conventional basis, such as contamination. Furthermore, the start of the helium production coincides with the achievement of the super-critical loading and the appearance of thermal anomalies, as shown by Figure 8. Experiment (b) demonstrates that, in a sub-critical system, no excess helium production occurs, nor is desorbtion from electrolyte observed. A small content of He exceeding the initial content estimated is recorded in experiment (c). However, a factor of 1.82 may be compatible with the hypothesis of desorbtion if we account for the roughness of initial content estimation. The detailed discussion of this point is outside the scope of this paper. The simultaneous absence of any increase in the Ar content (omitted here for the sake of brevity) indicates that no contamination from the environment had occurred.

The ability of our experimental set-up to carry out a real-time analysis of the content of inert gases during the electrolysis allows us:

a) to check the coincidence of three independent parameters, i.e., cathode loading, excess heat, and helium production;
b) to establish whether the helium production may be due to a contamination source, by comparing the yields of helium and argon.

Downloaded by STANFORD UNIV GREEN LIBR on July 2, 2012 | http://pubs.acs.org
Publication Date: August 1, 2008 | doi: 10.1021/bk-2008-0998.ch007

Table I. Comparative Results of ^{4}He Production from an Electrolytic Cell

		Loading	*Average ^{4}He Yield (Atoms/s)*	*Total Number of ^{4}He Atoms Measured in Gas Phase*	*^{4}He Atoms Produced/ Initial*
Exp. (a)	LiOD	x>1	$6.1 \pm 0.8 \times 10^{10}$	$8.1 \pm 0.2 \times 10^{14}$	25.5 ± 0.8
Exp. (b)	LiOD	*x*<1	$-2 \pm 3 \times 10^{8}$	$-2 \pm 3 \times 10^{11}$	-0.2 ± 0.1
Exp. (c)	LiOH	*x*>1	$4 \pm 3 \times 10^{9}$	$1.37 \pm 0.04 \times 10^{14}$	1.82 ± 0.03

Downloaded by STANFORD UNIV GREEN LIBR on July 2, 2012 | http://pubs.acs.org
Publication Date: August 1, 2008 | doi: 10.1021/bk-2008-0998.ch007

Are Nuclear Transmutations, Observed at Low Energies, Consequences of QED Coherence?

Many reports (*33*) point to the existence of nuclear transmutations occurring in solid metal lattices when they are loaded with hydrogen isotopes beyond a threshold. Elements absent before the loading were found thereafter, and the natural relative abundances of the isotopes of the host metal were modified. The high energies required cannot be produced in any conceptual frame where phonon excitations only are present. A major conceptual difficulty arises from the large Coulomb barrier between the nuclei, whose overcoming would require large amounts of energy. Actually, only the fusion of nuclei having $Z=1$ can be made possible by the enhancement mechanisms due to coherence, whereas, for $Z>1$, since the dependence upon Z of the Gamov penetration factor is exponential, the probability of the barrier crossing is negligible. The only possible agents for nuclear transmutations should be in our case the uncharged ones: neutrons or electromagnetic fields. Leaving aside for now the possibility of having thermal neutrons in the lattice as suggested by Widom and Larsen (*12*) let us direct our attention to the field of 24 MeV lasting in the lattice 10^{-21}s, as explained above.

Almost sixty years ago the phenomenon of Giant Dipole Resonance, GDR, was discovered (*34-36*) and interpreted in the framework of the Nuclear Shell Model. The cross-section for γ photons scattering off nuclei exhibits a wide maximum between 14 and 16 MeV and is connected with the excitation of quantum collective modes in nuclei. Goldhaber & Teller (*36*) have thoroughly analyzed the phenomenon of GDR, showing that the peak energy actually coincides with the binding energy of two closed shells in a nucleus. In a certain sense, under the γ field, the nucleus enters a vibrational state capable of breaking the binding, thus releasing a single nucleus or full shells. This is standard textbook nuclear physics. Now we consider a related proposal, daring but not unreasonable. The event of fusion, as discussed in Ref. (*14*), releases its energy as an electromagnetic excitation of the coherence domain of deuterons, lasting for a time shorter than 10^{-21} sec. The full amount of the energy produced by the fusion (24 MeV) is then released to the coherence domains of the Pd

Downloaded by STANFORD UNIV GREEN LIBR on July 2, 2012 | http://pubs.acs.org
Publication Date: August 1, 2008 | doi: 10.1021/bk-2008-0998.ch007

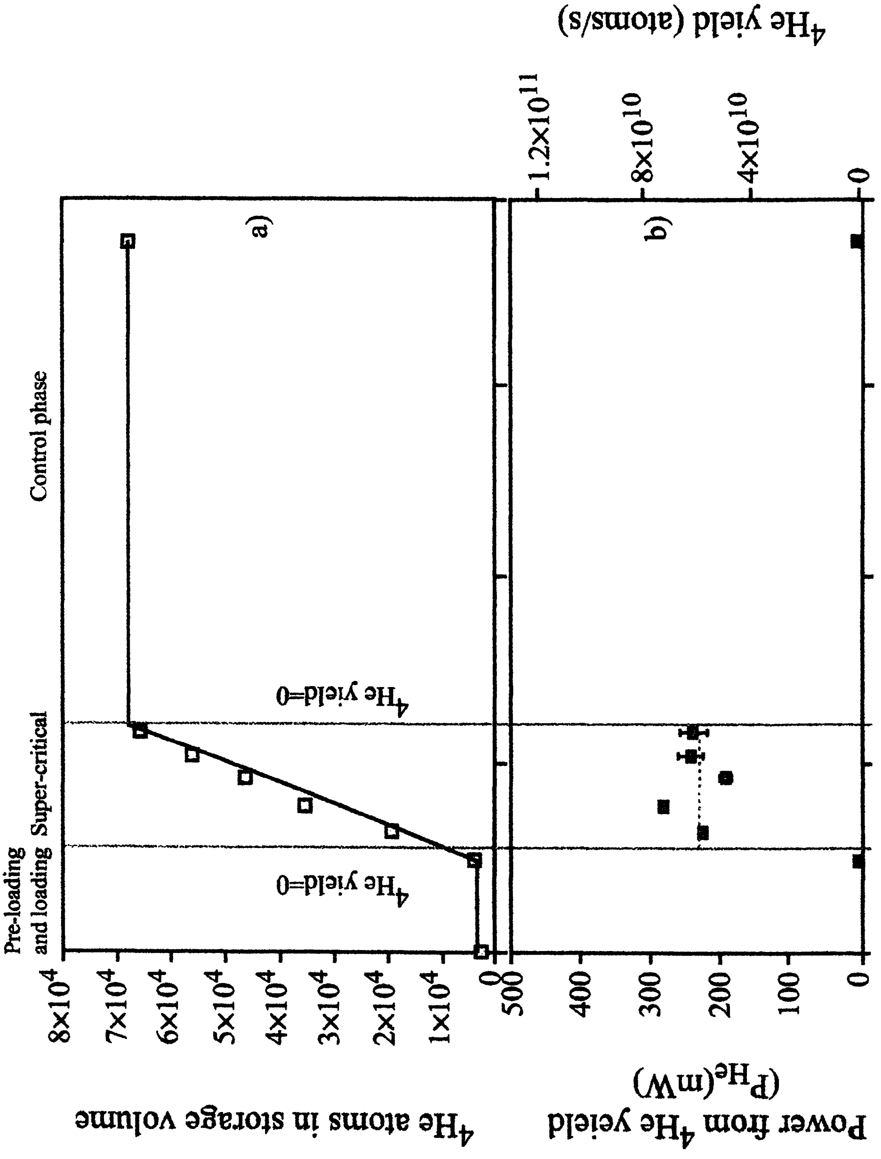

Downloaded by STANFORD UNIV GREEN LIBR on July 2, 2012 | http://pubs.acs.org
Publication Date: August 1, 2008 | doi: 10.1021/bk-2008-0998.ch007

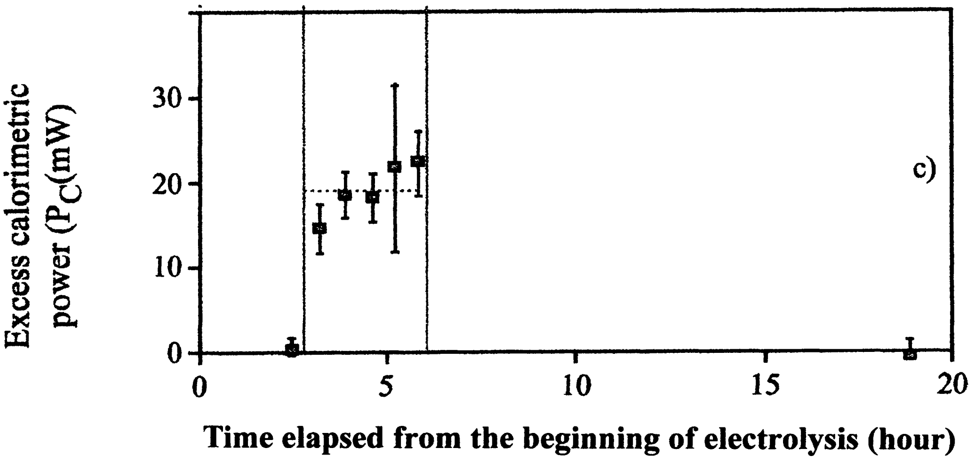

Figure 8. a) ^{4}He content of the gas mixture inside the storage volume, b) excess power P_{He} derived from helium yield and c) average excess calorimetric power P_{Cr}. The data are shown as a function of time, allowing us to check for coincidence. (Reproduced from reference 32. Copyright 2003 ANS.)

electrons, giving rise to oscillations at lower frequency. The energy, and thus the frequency of the electromagnetic excitation of the coherence domain of deuterons, could match for a short time, whose order of magnitude is less than 10^{-21} sec, the interval of GDR, thus giving rise to collective excitations of nuclei present within the volume of the coherence domain, namely the nucleus of Pd. These excitations could produce a number of nuclear reactions, including the "unscrewing" of the two closed shells that are the components of the Pd nucleus and correspond to Ni and Ar nuclei. In order to check this daring hypothesis, we propose the following experiment (*37*).

There is a preliminary indication (*38*) that Ni nuclei may be present in cathodes subsequent to cold fusion. We propose to look for nuclear transmutations of Pd according to a probable scheme of a split of the nucleus into closed shells, i.e., the anomalous production of argon isotopes as partner nuclei of Ni in a possible Pd fission process.

The closed shells that could appear in a Pd nucleus (Z=46) have the following magic numbers: 28 protons (Ni) and 20 neutrons (^{38}Ar) which correspond to the reactions:

$$^{104}\mathrm{Pd}+\gamma\ \mathrm{field}\rightarrow{}^{66}\mathrm{Ni}+{}^{38}\mathrm{Ar}$$

$$^{102}\mathrm{Pd}+\gamma\ \mathrm{field}\rightarrow{}^{64}\mathrm{Ni}+{}^{38}\mathrm{Ar}$$

A detailed calculation is needed of the interaction parameters of the coupling of the extended γ-ray field (which is not a single photon!) with nuclei.

However the existence of such extended γ-ray fields is a necessary consequence of the coherent theory of cold fusion. Such fields appear, in the framework of accepted principles of quantum physics, as the likeliest engine to give rise to nuclear transmutations in the metal lattice at room temperature.

Conclusions

The existence of an anomalous excess heat produced in Pd cathodes during the electrolysis of heavy water has been proved by several experimenters around the world with different (sometimes very different) experimental procedures, and it has been approached by many theoreticians starting from different (sometimes very different) descriptions of condensed matter. However, in the last fifteen years, some fundamental points have been agreed upon by the physicists involved in cold fusion research: a) the existence of a threshold in the deuterium loading in palladium (generally assumed to be necessary even though some scientists consider it not to be sufficient); b) the absence of the yield of neutrons and tritium, correlated to the heat measured, as foreseen by the theory of nuclear fusion in vacuum; c) the presence of ^{4}He as nuclear ash of the process; d) the existence of other nuclear reactions, such as transmutations of heavy elements, in condensed matter at room temperature; e) the need for

Downloaded by STANFORD UNIV GREEN LIBR on July 2, 2012 | http://pubs.acs.org
Publication Date: August 1, 2008 | doi: 10.1021/bk-2008-0998.ch007

collaboration in the field of condensed matter in order to cope with this new phenomenology.

The next question is: "May such a phenomenon be envisaged, in the near future, as a new source of energy?" The main efforts of the "cold fusion community" have been devoted to clarifying the physical or chemical-physical environment in which the phenomenon takes place and convincing the scientific community of its reality. However, it could be wise to start considering this question.

In order to create a device able to produce significant amounts of energy for civilian uses, it is mandatory to know: a) the highest temperature reached by the palladium during the ignition (the extremely high-density power – 1-10 kW/cm^3 – evaluated by the experiments poses severe limits to the design of the device); b) "out equilibrium" calorimetry in order to evaluate and correctly catch all the heat produced, since the heat emitted at very high temperature is mainly emitted in the form of radiation; c) the duration of a possible device for energy production which would be subjected not only to the possible "burning" of the cathode but also to its possible contamination due to several cycles of loading-deloading when the device is switched on and off.

It is clear that, from an engineering point of view, we are just launching the challenge, but the peculiarity of this possible source of energy is meaningful. Cold fusion is, actually, a very high-density source of energy, very different from fossil fuels and also from the other known nuclear energy (fission, thermonuclear fusion) devices, which require large-scale power plants. This means that its best use will be for non-centralized production of energy right at the site where it will be consumed, thus reducing the cost of energy losses in distribution and thermal waste, i.e., the fact that a significant part of energy produced in a conventional plant is subsequently released as waste heat into the environment. Moreover, the easy management of fuel (water), materials (it is reasonable to think that palladium metal could be replaced by special Pd based material or, better, by another more abundant and cheap element such as nickel or Ni compounds), and waste (^{4}He) makes cold fusion a promising energy source for the future, for people willing to take the challenge.

Downloaded by STANFORD UNIV GREEN LIBR on July 2, 2012 | http://pubs.acs.org
Publication Date: August 1, 2008 | doi: 10.1021/bk-2008-0998.ch007

References

1. Fleischmann, M.; Pons, S. Electrochemically Induced Nuclear Fusion of Deuterium. *J. Electroanal. Chem.* **1989**, *261*, 301-308.
2. Mössbauer, R. L. Kernresonanzfluoreszenz von Gammastrahlung in Ir191. *Z. Phys.* **1958**, *151*, 124.
3. *QED in Condensed Matter*; Preparata G., Ed.; World Scientific: Singapore, 1995.
4. Pound, R. V.; Rebka, G. A. Attempt to Detect Resonance Scattering in Zn^{67}: The Effect of Zero-Point Vibrations. *Phys. Rev. Lett.* **1960**, *4*, 337-341.

5. Del Giudice, E.; Vitiello, G. The Role of the Electromagnetic Field in the Formation of Domains in the Process of Symmetry Breaking Phase Transitions. *Phys. Rev.* **2006,** *A74*, 022105-0221014.
6. Schwinger, J. Nuclear Energy in an Atomic Lattice. In *Proceedings of the First International Conference on Cold Fusion*, Salt Lake City, UT, Mar. 28-31, 1990; National Cold Fusion Institute: Salt Lake City, 1990; 130.
7. Bridgman, P. W. *The Physics of High Pressure*; International Textbooks of Exact Science: London, 1947.
8. Cöhn, A. Protonen in Metallen. *Z. Elektrochem.* **1929,** *35*, 676.
9. Fleischmann, M.; Pons, S.; Preparata, G. Possible Theories on Cold Fusion. *Nuovo Cimento* **1994,** *107A* (1), 143-156.
10. Oliphant, M. C.; Harteck, P.; Lord Rutherford. Transmutation Effect Observed With Heavy Hydrogen. *Nature* **1934,** *113*, 413.
11. Dee, P. I. Some Experiment upon Artificial Transmutations Using the Cloud-Track Method. *Proc. Roy. Soc.* **1935,** *148A*, 623.
12. Widom, A.; Larsen, L. Ultra Low Momentum Neutron Catalyzed Nuclear Reactions on Metallic Hydride Surfaces. 2005, arXiv:cond-mat/0505026v1. arXiv.org e-Print archive. http://arxiv.org/abs/cond-mat/0505026v1.
13. Bressani, T.; Del Giudice, E.; Preparata, G. First Steps Toward an Understanding of "Cold" Nuclear Fusion. *Nuovo Cimento* **1989,** *101A*, 845.
14. Preparata, G. Theoretical Ideas on Cold Fusion. In *Proceedings of the First International Conference on Cold Fusion*, Salt Lake City, UT, Mar. 28-31, 1990; National Cold Fusion Institute: Salt Lake City, 1990; 91-97.
15. Preparata, G. Setting Cold Fusion in Context: A Reply. In *Proceedings of the Fifth International Conference on Cold Fusion*, Monte Carlo, Monaco, April 9-13, 1995; Pons, S., Ed.; IMRA Europe: Sophia Antipolis Cedex, France, 1995; 265-284.
16. Farewell (not fond) to Cold Fusion (editorial) *Nature* **1990,** *344*, 365.
17. De Ninno, A.; La Barbera, A.; Violante, V. Consequences of Lattice Expansive Strain Gradients on Hydrogen Loading in Palladium. *Phys. Rev.* **1997,** *B26*, 2417-2420.
18. Felici, R.; Bertalot, L.; De Ninno, A.; La Barbera, A.; Violante, V. In Situ Measurement of the Deuterium (Hydrogen) Charging of a Palladium Electrode During Electrolysis by Energy Dispersive X-Ray Diffraction. *Rev. Sci. Instrum.* **1995,** *66* (5), 3344-3348.
19. Alefeld, G.; Völkl, J. *Hydrogen in Metals*; Springer Verlag: Berlin, 1978; Vol. II, pp 73-151.
20. Wisniewski, R.; Rostocki, J. Hall Effect in the Pd-H System. *Phys. Rev.* **1971,** *B3* (2), 251-252.
21. Bambakidis, G.; Smith, R. J.; Otterson, D. A. Electrical Resistivity Versus Deuterium Concentration in Palladium. *Phys. Rev.* **1969,** *177*, 1044-1048.
22. Alefeld, G.; Völkl, J. *Hydrogen in Metals*. Springer Verlag: Berlin, 1978; Vol. I, pp 337-341.
23. Dandapani, B.; Fleischmann, M. Electrolytic Separation Factors on Palladium. *J. Electroanal. Chem.* **1972,** *39*, 323.

Downloaded by STANFORD UNIV GREEN LIBR on July 2, 2012 | http://pubs.acs.org
Publication Date: August 1, 2008 | doi: 10.1021/bk-2008-0998.ch007

24. Preparata, G.; Scorletti, M.; Verpelli, M. Isoperibolic Calorimetry on Modified Fleischmann-Pons Cells. *J. Electroanal. Chem.* **1996**, *411*, 9-18.
25. Aharonov, Y.; Böhm, D. Significance of Electromagnetic Potentials in the Quantum Theory. *Phys. Rev.* **1959**, *115*, 485-491.
26. Cola, M.; Del Giudice, E.; De Ninno, A.; Preparata, G. A Simple Model of the "Cöhn-Aharonov" Effect in a Peculiar Electrolytic Configuration. In *ICCF8: Proceedings of the Eighth International Conference on Cold Fusion*, Lerici (La Spezia), Italy, May 21-26, 2000; Scaramuzzi, F., Ed.; Italian Physical Society: Bologna, Italy, 2001; 349-356.
27. Del Giudice, E.; De Ninno, A.; Frattolillo, A.; Preparata, G.; Scaramuzzi, F.; Bulfone, A.; Cola, M.; Giannetti, C. The Fleischmann-Pons Effect in a Novel Electrolytic Configuration. In *ICCF8: Proceedings of the Eighth International Conference on Cold Fusion*, Lerici (La Spezia), Italy, May 21-26, 2000; Scaramuzzi, F., Ed.; Italian Physical Society: Bologna, Italy, 2001; 47-54.
28. De Ninno, A.; Del Giudice, E.; Frattolillo, A.; Preparata, G.; Rizzo, A. *Experimental Evidence of ^{4}He Production in a Cold Fusion Experiment.* ENEA: Rome, 2002, ENEA Report RT/2002/41/FUS. http://www.lenr-canr.org/acrobat/DeNinnoAexperiment.pdf.
29. Frattolillo, A. New Simple Method for Fast and Accurate Measurement of Volumes. *Rev. Sci. Instrum.* **2006**, *77*, 045107.
30. Frattolillo, A. Simple Automatic Device for Real Time Sampling of Gas Production by a Reactor. *Rev. Sci. Instrum.* **2006**, *77*, 065108.
31. Frattolillo, A.; De Ninno, A.; Rizzo, A. Quantitative Detection of Tiny Amounts of Helium Isotopes in a Hydrogen Isotope Atmosphere Using a Standard-Resolution Quadrupole Mass Spectrometer. *J. Vac. Sci. Technol.* **2007**, *A25* (1), 75-89.
32. De Ninno, A.; Frattolillo, A.; Rizzo, A. 4He Detection in a Cold Fusion Experiment. *Trans. Am. Nucl. Soc.* **2003**, *88*, 633-635.
33. Iwamura, Y.; Itoh, T.; Sakano, M.; Sakai, S. Observation of Low Energy Nuclear Reactions Induced By D_2 Gas Permeation Through Pd Complexes. In *Condensed Matter Nuclear Science: Proceedings of the 9th International Conference on Cold Fusion*, Beijing, China, May 19-24, 2002; Li, X. Z., Ed.; Tsinghua Univ. Press: Beijing, 2002; 141-146.
34. Migdal, A. B. Quadrupole and Dipole γ Emission from Nuclei. *Eksp. Teor. Fiz.* **1943**, *15*, B1.
35. Baldwin, G. C.; Klaiber, G. S. Photo-Fission in Heavy Elements. *Phys.Rev.* **1947**, *71*, 3.
36. Goldhaber, M.; Teller, E. On Nuclear Dipole Vibrations. *Phys. Rev.* **1948**, *74*, 1046.
37. Del Giudice, E.; De Ninno, A.; Frattolillo, A. Are Nuclear Transmutations Observed at Low Energies Consequences of Qed Coherence? In *Condensed Matter Nuclear Science: Proceedings of the 10th International Conference on Cold Fusion*, Cambridge, MA, Aug. 24-29, 2003; Hagelstein, P. L.; Chubb, S. R., Eds.; World Scientific Publishing Co.: Singapore, 2006.

Downloaded by STANFORD UNIV GREEN LIBR on July 2, 2012 | http://pubs.acs.org
Publication Date: August 1, 2008 | doi: 10.1021/bk-2008-0998.ch007

38. Li, X.Z.; Yan, Y.J.; Tian, J.; Mei, M. Y.; Deng, Y.; Yu, W. Z.; Tang, G. Y.; Cao, D. X.; De Ninno, A. Nuclear Transmutation In Pd Deuteride. In *ICCF8: Proceedings of the Eighth International Conference on Cold Fusion*, Lerici (La Spezia), Italy, May 21-26, 2000; Scaramuzzi, F., Ed.; Italian Physical Society: Bologna, Italy, 2001; 123-128.

Downloaded by STANFORD UNIV GREEN LIBR on July 2, 2012 | http://pubs.acs.org
Publication Date: August 1, 2008 | doi: 10.1021/bk-2008-0998.ch007

Chapter 8

Accuracy of Isoperibolic Calorimetry Used in a Cold Fusion Control Experiment

Melvin H. Miles[1] and Martin Fleischmann[2]

[1]Department of Chemistry, University of LaVerne, LaVerne, CA 91750
[2]Bury Lodge, Duck Street, Tisbury, Salisbury, Wilts SP3 6LJ, United Kingdom

Downloaded by COLUMBIA UNIV on July 1, 2012 | http://pubs.acs.org
Publication Date: August 1, 2008 | doi: 10.1021/bk-2008-0998.ch008

This control or "blank" experiment proves that anomalous excess power is measurable to within ±0.1 mW using this electrochemical calorimetry. The precision and accuracy is better than 99.99%. The most accurate results were obtained using backward integration of the experimental data sets. The rate of enthalpy production due to the reduction of electrogenerated oxygen (recombination) was measurable at ± 0.1 mW in these experiments where the cell input power was generally about 800 to 1000 mW. The logical conclusion from this control study is that excess enthalpy measurements in cold fusion experiments using this calorimetric system cannot be scientifically dismissed simply as calorimetric errors.

Introduction

The cold fusion controversy centers on the precision and accuracy of the calorimetric systems used to measure excess enthalpy generation (*1-3*). For this open, isoperibolic calorimetric system there is no true steady state during D_2O+LiOD electrolysis. Exact calorimetric measurements, therefore, require modeling by a differential equation that accounts for all heat flow pathways into and out of the calorimetric system *(1-8)*. The lack of use or the improper use as well as the misunderstanding of this differential equation is a major source of confusion concerning cold fusion calorimetric measurements (*1, 9-13*).

The precision and accuracy of isoperibolic cold fusion calorimetry can best be assessed by means of experiments on "blank" or control systems where no excess enthalpy generation due to cold fusion is expected. Therefore, a clean

In Low-Energy Nuclear Reactions Sourcebook; Marwan, J., et al.;
ACS Symposium Series; American Chemical Society: Washington, DC, 2008.

platinum (not palladium) cathode was polarized in D_2O+0.1M LiOD using platinum also as the anode. The only excess enthalpy generation expected would be from the recombination of the evolved D_2 and O_2 gases. Although the amount of recombination in cold fusion experiments has been a major source of controversy (*2, 3*), various experimental studies have shown that the recombination effect is small at the large current densities used in cold fusion experiments (*2, 3, 9, 14*).

Experiments

Long and narrow calorimetric cell designs promote rapid radial mixing of the electrolyte by the electrolysis gas evolution and minimize heat transfer through the top of the cell relative to the desired pathway through the cell wall to the water bath (*1, 9-13*). The use of Dewar cells makes the heat transfer pathway predominantly due to infrared radiation across the vacuum gap of the Dewar cell. Therefore, the heat transfer coefficient can be calculated theoretically by the product of the Stefan-Boltzmann coefficient and the radiant surface area of the cell (109.7 cm^2 in these experiments). Multiplying by the Stefan-Boltzmann coefficient, 5.6704 x 10^{-12} $Wcm^{-2}K^{-4}$, yields a theoretical radiative heat transfer coefficient of 0.6220 x 10^{-9} WK^{-4} for this particular calorimetric cell. The Dewar cell used was approximately 2.5 cm in diameter (I.D.) and 22.0 cm in height with the upper 8.0 cm silvered to minimize the effect of the electrolyte level (*1, 9*). Figure 1 illustrates the various components of this isoperibolic calorimetric cell. Key features and advantages of this calorimetric cell design have been previously discussed in detail (*11*).

The platinum cathode used in these experiments was 0.1 cm in diameter and 2.0 cm in length (A=0.63 cm^2). The temperature of the thermostated water bath (approximately 21°C) was precisely controlled to within ±0.01°C. Each experimental cycle lasted exactly two days over a total of 16 days. For each cycle, the internal cell heater was off for 12 hours, then turned on at $t=t_1$ for 12 hours and then off at $t=t_2$ for the final 24 hours. Addition of D_2O occurred at the beginning of each cycle (t=0). The cell current was constant at 0.2000 A.

Figure 2 gives a plot of the "raw data" (the cell temperature and rate of input enthalpy) for days 9 and 10 of the measurement cycles. Note the effect of the internal cell heater applied at $t=t_1$, and then turned off at $t=t_2$, as well as the effect of the D_2O addition at t=0 for this cycle. The small progressive decrease with time for the cell temperature is due to the progressive increase of the electrolyte concentration due to electrolysis. This, in turn, causes an increase of the conductance and hence a fall in the input power and a corresponding decrease of the cell temperature with time.

Calorimetric Equations

The complete misunderstanding of the correct equations used to model isoperibolic cold fusion calorimetry continues to be a major problem for this

Downloaded by COLUMBIA UNIV on July 1, 2012 | http://pubs.acs.org
Publication Date: August 1, 2008 | doi: 10.1021/bk-2008-0998.ch008

Downloaded by COLUMBIA UNIV on July 1, 2012 | http://pubs.acs.org
Publication Date: August 1, 2008 | doi: 10.1021/bk-2008-0998.ch008

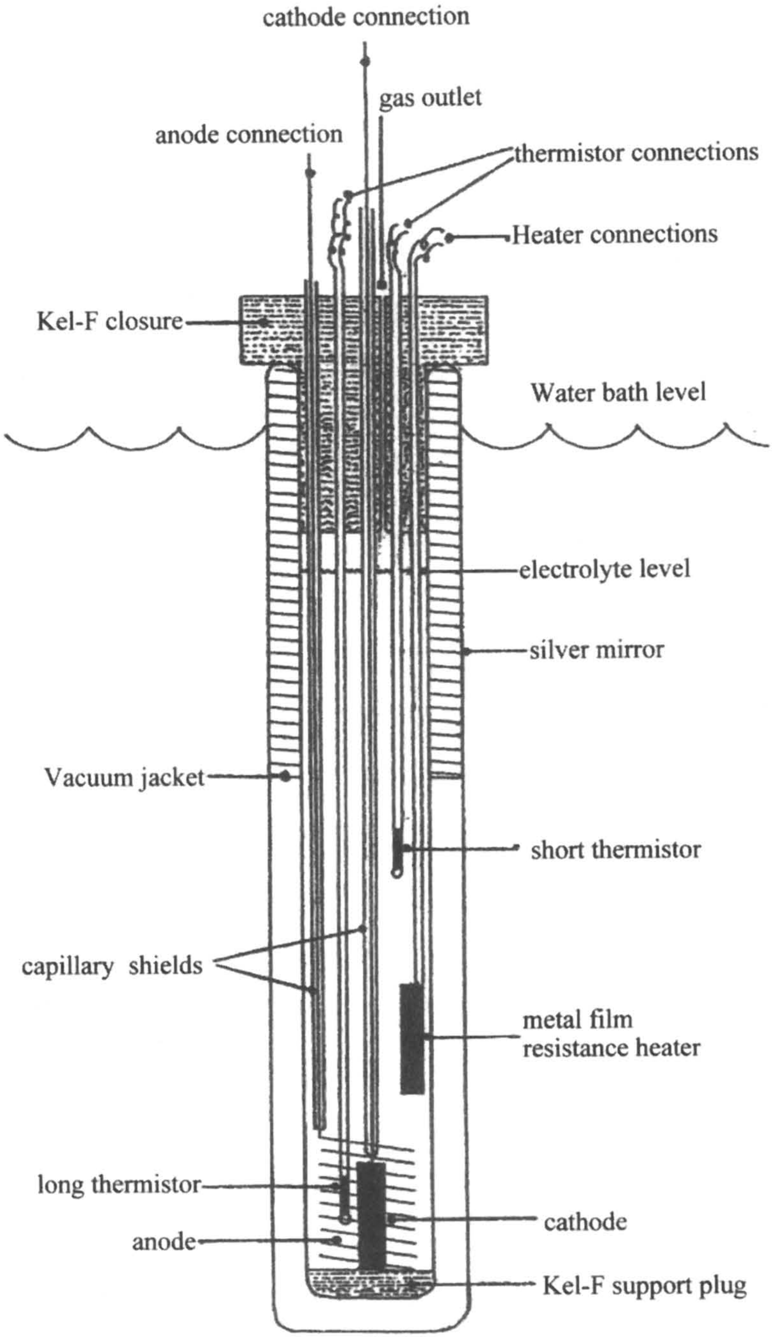
cathode connection
gas outlet
anode connection
thermistor connections
Heater connections
Kel-F closure
Water bath level
electrolyte level
silver mirror
Vacuum jacket
short thermistor
capillary shields
metal film
resistance heater
long thermistor
cathode
anode
Kel-F support plug

Figure 1. The isoperibolic calorimetric cell.

Downloaded by COLUMBIA UNIV on July 1, 2012 | http://pubs.acs.org
Publication Date: August 1, 2008 | doi: 10.1021/bk-2008-0998.ch008

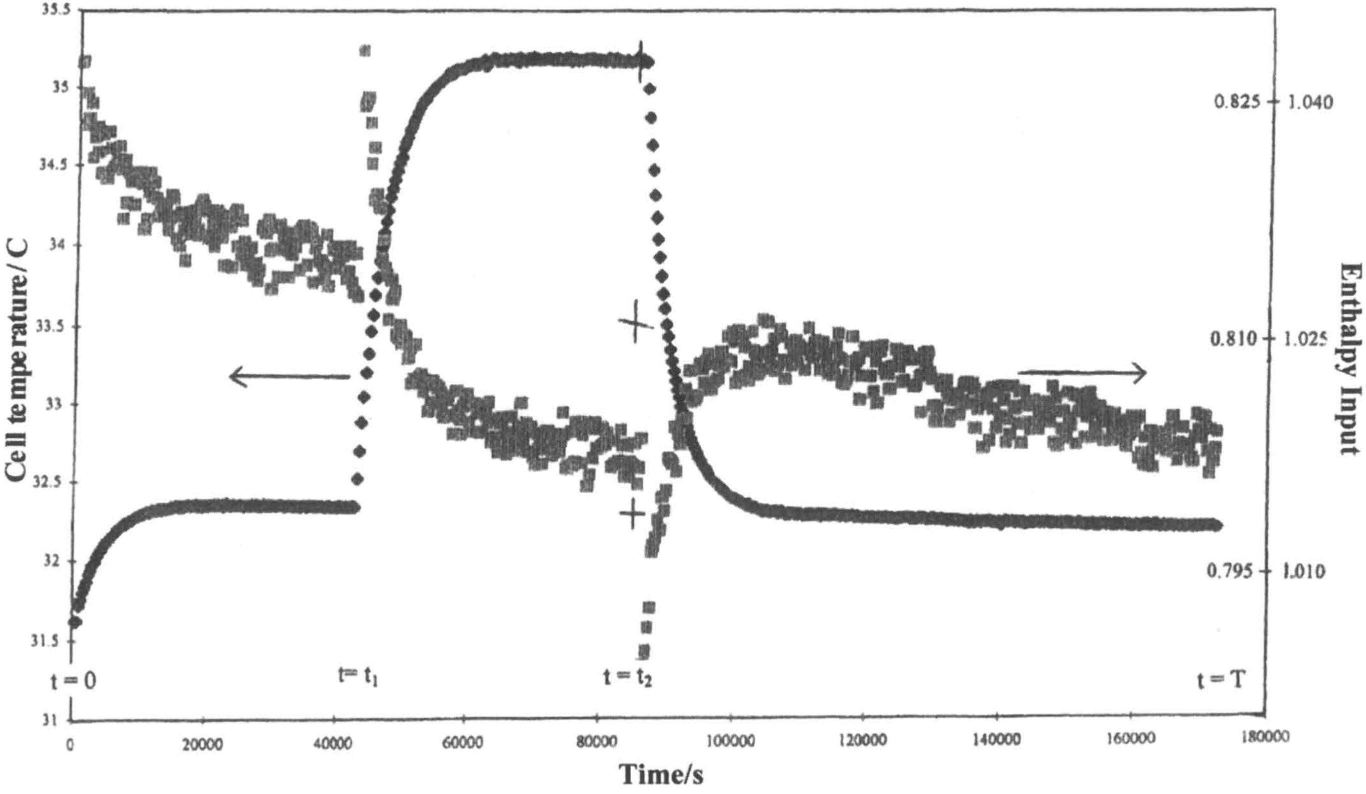

Figure 2. Plot of the "raw data" for days 9 and 10. The rate of enthalpy input (P_{EI}) is proportional to the cell voltage (Eq. (3)). The two different scales on the right axis are for times when the internal heater is off (inner scale) and when this heater is on (outer scale).

field (*12, 13*). Therefore, these calorimetric equations will be simplified and presented here in detail. It should be noted that a previous publication has pointed out major errors in the cold fusion calorimetric studies reported by Caltech, MIT, and Harwell (*1*).

From basic thermodynamic principles (*15*), the calorimetric cell is the system of interest, and the First Law of Thermodynamics expressed as power (J/s or W) becomes

$$P_{calor} = P_{EI} + P_H + P_X + P_{gas} + P_R + P_C + P_W \qquad (1)$$

Equation 1 represents the differential equation used to model this open, isoperibolic calorimetric system. Because both the cell temperature and cell voltage change with time (Figure 2), most of the terms in Eq. (1) also vary with the time, *t*. By definition, P_{calor} is the power for the calorimetric cell (system), P_{EI} is the electrochemical power, P_H is the internal heater power, P_X is any anomalous excess power, P_{gas} is the power resulting from the gas stream exiting the cell (D_2, O_2, D_2O vapor), P_R is the net power transferred by radiation between the cell and water bath, P_C is the power transferred by conduction, and P_W represents the rate of any pressure–volume work by the generated electrolysis gases. As usual in thermodynamics, positive quantities represent power added to the system (calorimetric cell) and negative quantities represent power given off by the system to the surroundings.

The mathematical expressions for the terms in Eq. (1) are as follows:

$$P_{calor} = C_pM(dT_{cell}/dt) \qquad (2)$$

$$P_{EI} = (E(t)-E_H)I \qquad (3)$$

$$P_{gas} = -(I/F)\{[0.5C_{P,D_2} + 0.25C_{P,O_2} + 0.75(\mathbf{P}/(\mathbf{P^*}-\mathbf{P}))C_{P,D_2O(g)}]\Delta T$$

$$+\ 0.75\ (\mathbf{P}\ /\ (\mathbf{P^*}-\mathbf{P}))\ L\}\ \text{ where } \Delta T = T_{cell} - T_b \qquad (4)$$

$$P_R = -k_R f(T) \text{ where } f(T) = T_{cell}^4 - T_b^4 \qquad (5)$$

$$P_C = -k_C\ (T_{cell} - T_b) \qquad (6)$$

$$P_W = -RT_{cell}\ (dn_g/dt) = -RT_{cell}(0.75I/F) \qquad (7)$$

Note that pressure terms in Eq. (4) are bolded to minimize confusion with power terms.

The change of the cell temperature with time as given by P_{calor} in Eq. (2) makes Eq. (1) a nonlinear, inhomogeneous differential equation (*1*). Definitions for the symbols are given in Appendix I and elsewhere (*1, 9*). For this study, P_H = 0.2000 W for $t_1 \leq t \leq t_2$ (see Figure 2) and zero elsewhere. The heat capacity of the system (C_pM) consists mainly of the heavy water content of the cell plus small contributions from glass and metal components of the cell (*9, 10*).

Downloaded by COLUMBIA UNIV on July 1, 2012 | http://pubs.acs.org
Publication Date: August 1, 2008 | doi: 10.1021/bk-2008-0998.ch008

Rate of Enthalpy Removal by the Gas Stream

The most complicated term, *Pgas*, in Eq. (4) requires additional analysis. In addition to heat transfer by radiation (Eq. (5)) and conduction (Eq. (6)), heat is transferred from the cell to the surroundings by the gas stream exiting the open calorimetric cell. The electrolysis reaction per Faraday (*1F* = 96485.3415 *C mol⁻¹*) involving one mole of electrons and the consumption of 0.5 mol of D_2O is given by

$$0.5\ D_2O_{(l)} \rightarrow 0.5\ D_{2(g)} + 0.25\ O_{2(g)} \tag{8}$$

This reaction produces 0.5 mol of D_2 gas and 0.25 mol of O_2 gas per Faraday that are used as coefficients in Eq. (4). The 0.75 moles total of electrolysis gases generated per Faraday obviously do not emerge dry from the liquid phase, thus they also carry away D_2O vapor present in the cell due to the equilibrium vapor pressure of D_2O, $\boldsymbol{P}=\boldsymbol{P}_{D_2O}$. Using Dalton's Law of Partial Pressures (*15*), the *2*moles of $D_2O_{(g)}$ carried away per Faraday are given by

$$moles\ D_2O_{(g)} = 0.75\ (\boldsymbol{P}/(\boldsymbol{P}_{D_2} + \boldsymbol{P}_{O_2})) = 0.75\ (\boldsymbol{P}/\boldsymbol{P}^* - \boldsymbol{P})) \tag{9}$$

where the gas pressure within the cell, $\boldsymbol{P}^*$, is given by

$$\boldsymbol{P}^* = \boldsymbol{P}_{D_{2(g)}} + \boldsymbol{P}_{O_{2(g)}} + \boldsymbol{P}_{D_2O(g)} \tag{10}$$

and is close to the atmospheric pressure for this open system. It should be noted that $\boldsymbol{P}^*$ may be slightly larger (perhaps by 1-2%) than the atmospheric pressure depending on the applied cell current and the degree of restriction for the gases exiting the cell. Nevertheless, Eq. (4) for P_{gas} dictates the monitoring of the atmospheric pressure for highly accurate calorimetric measurements (*9*).

The largest term for P_{gas} (Eq. (4)) stems from the enthalpy of vaporization of D_2O, L. The value for L is 41678.9 J/mol at the boiling temperature for D_2O (101.42°C). Values for L in J/mol at different temperatures (T) are given by

$$L=85263.9\ \ 173.429T+0.2586T^2-1.91913\times10^{-4}T^3-1805569/T \tag{11}$$

where T is in Kelvin (*16*). Another method for calculating L at other temperatures involves Kirchhoff's law (*15*). Assuming the heat capacities are constant over the temperature range considered, Kirchhoff's law yields

$$L(T) = L(T_o) + (C_p, D_2O_{(g)} - C_p, D_2O_{(l)})\ (T-T_o) \tag{12}$$

At T_o = 298.15 K, $L\ (T_o)$ = 45401 J/mol. Values for L and heat capacities needed for Eqs. (4) and (12) are given for several temperatures in Table I. Also included in Table I is the thermoneutral potential, E_H, required in Eq. (3). This E_H term compensates exactly for the enthalpy (ΔH) that would be obtained from the complete recombination of the D_2 and O_2 electrolysis gases that exit the cell.

Downloaded by COLUMBIA UNIV on July 1, 2012 | http://pubs.acs.org
Publication Date: August 1, 2008 | doi: 10.1021/bk-2008-0998.ch008

Table II presents calculated values for P_{gas} at 40°C and 80°C when I = 0.2000 A. The separate contributions from the gas stream (P_g) and from evaporation (P_L) are also presented where $P_{gas} = P_g + P_L$.

Table I. Values for L, EH and Heat Capacities at Several Temperatures

T *(K)*	*L kJ/mol*	$C_p, D_{2(g)}$ *J/mol K*	$C_p, O_{2(g)}$ *J/mol K*	$C_p, D_2O_{(g)}$ *J/mol K*	$C_p, D_2O_{(l)}$ *J/mol K*	E_H[a] *(V)*
298.15	45.401[b]	29.196[b]	29.355[b]	34.27[b]	84.35[b]	1.52667
313.15	4.6545	29.188	29.451	34.422	83.940	1.52357
333.15	3.6719	29.180	29.587	34.660	83.420	1.51943
353.15	42.7035	29.181	29.741	34.921	83.034	1.51530
373.15	41.7465	29.189	29.909	35.200	82.839	1.51116

[a] $E_H = 1.5318346 - 0.0002067\ (T - 273.15\ K)$, V

[b] From *J. Physical and Chemical Reference Data* **1982**, *11*, Supplement No. 2.

Table II. Calculated Value For P_{gas} at 40°C and 80°C when I = 0.2000 A and T_{bath} = 22.00°C (295.15 K).

T_{cell} *(K)*	P_g*(mW)*	P_L *(mW)*	P_{gas} *(mW)*[a]
313.15	-0.7386	-4.9103	-5.6489
353.15	-4.8396	-52.9857	-57.8253

[a] $P_{gas} = P_g + P_L$

Table II illustrates that the P_{gas} term becomes much more important at higher cell temperatures and that the L term makes a much larger contribution than the actual gas stream term (P_g). The values for P_{gas} are directly proportional to the current (Eq. (4)) and will be larger than the values in Table II at higher cell currents. It should be obvious that the P_{gas} term cannot be neglected in this calorimetry.

Pseudoradiative Heat Transfer Coefficients

Returning to the fundamental calorimetric equation (Eq. (1)), the use of a Dewar cell with a hard vacuum makes P_C much smaller than P_R. Furthermore,

Downloaded by COLUMBIA UNIV on July 1, 2012 | http://pubs.acs.org
Publication Date: August 1, 2008 | doi: 10.1021/bk-2008-0998.ch008

P_W is always less than 0.004 W for the conditions of these experiments. Assuming P_C and P_W are relatively small compared to P_R ($P_R \approx 0.8$ W as shown in Figure 2), then

$$P_R' = P_R + P_C + P_W = -\, k_R' f(T) \tag{13}$$

where k_R' is the pseudoradiative heat transfer coefficient. The validity of this assumption can be checked by comparing k_R' with the theoretical value calculated from the Stefan-Boltzmann coefficient. The electrolyte level decreases slowly with time during electrolysis, thus there is a weak time-dependency for k_R' given by

$$k_R' = (k_R')^0 (1 - \gamma t) \tag{14}$$

where $t=0$ is the beginning of the two-day cycle with the refilling of the cell. The magnitude of this time dependency is expressed by γ and depends on the cell size and geometry as well as the actual constant current selected.

The substitution of Eq. (13) into Eq. (1) yields

$$P_{calor} = P_{EI} + P_H + P_X + P_{gas} - k_R' f(T) \tag{15}$$

By assuming $P_X = 0$ a lower bound heat transfer coefficient, $(k_R')_1$, can be evaluated, i.e.

$$(k_R')_1 = (P_{EI} + P_H + P_{gas} - P_{calor}) / f(T) \tag{16}$$

The actual presence of any excess power would increase $f(T)$, thus yielding a lower value for $(k_R')_1$. The use of Eq. (16) is generally the simplest starting point for the analysis of the calorimetric data. For this blank or control experiment, P_X will be small, thus $(k_R')_1$, will be close to the true heat transfer coefficient, $(k_R')_2$, given by

$$(k_R')_2 = (P_{EI} + P_H + P_X + P_{gas} - P_{calor}) / f(T) \tag{17}$$

Estimates of $(k_R')_1$ and $(k_R')_2$ can be made near the end of the calibration period at $t=t_2$ (see Figure 2 and Appendix II).

For this blank or control experiment, any difference in $(k_R')_1$ and $(k_R')_2$ at any stated time will be due to excess power from the controversial recombination of the D_2 and O_2 electrolysis gases (*2, 3, 9, 14*). The actual rate of excess enthalpy production can be estimated from the equation obtained by simply subtracting Eq. (16) from Eq. (17), thus

$$P_X = [(k_R')_2 - (k_R')_1] f(T) \tag{18}$$

It is convenient to cast Eq. (17) into a straight-line form, $y=mx+c$, to yield

Downloaded by COLUMBIA UNIV on July 1, 2012 | http://pubs.acs.org
Publication Date: August 1, 2008 | doi: 10.1021/bk-2008-0998.ch008

$$(P_{EI}+P_H+P_X+P_{gas})/f((T)=(C_pM\,dT_{cell}/dt)/f(T)+(k_R')_2 \qquad (19)$$

where Eq. (2) is used for P_{calor}. The left-hand-side (L.H.S.) of Eq. (19) represents the variable y, the slope $m = C_pM$, $x = (dT_{cell}/dt)/f(T)$ and the constant $c=(k_R')_2$.

Analogous to the differential equations of chemical kinetics, mathematical integration yields more accurate results then the direct use of the differential equation. The numerical integration of Eq. (19), however, requires the selection of time periods where the excess power, P_X, is constant with time. It is also important to select time periods where there are significant changes in the cell temperature with time such as the time period where the internal cell heater power, P_H, is applied $(t^1 \leq t \leq t_2)$ as seen in Figure 2. Previous experiments have shown that backward integration from t_2 (cessation of heater power) produces the most accurate results (*9-13*). This backward integration of Eq. (19) from t_2 back to time, t, yields

$$\frac{\int_{t_2}^{t} P_{net}(t)dt + P_x(t-t_2)}{\int_{t_2}^{t} f(T)dt} = \frac{C_pM[T_{cell}(t)-T_{cell}(t_2)]}{\int_{t_2}^{t} f(T)dt} + (k_R')_{262} \qquad (20)$$

where $P_{net}(t) = P_{EI}(t) + P_H(t) + P_{gas}(t)$.

Various types of heat transfer coefficients such as $(k_R')_{262}$ in Eq. (20) are designated by $(k_R')_{i,j,k}$ where $i = 1$ designates differential, $i = 2$ signifies backward integration, $i = 3$ signifies forward integration, $k = 1$ denotes "lower bound" (assumes $P_X = 0$) and $k = 2$ signifies "true." If used, j designates the particular time period of the two-day cycle used for the integration. For example, $j = 6$ used in Eq. (20) is especially useful because this time period between t_1 and t_2 involves the application of the cell heater power and large changes in the cell temperature (see Figure 2). Note that Eq. (20) is in the straight-line-form where y = L.H.S., $m = C_pM$ and $c = (k_R')_{262}$. It should also be noted that the extrapolation of Eq. (20) to $x = 0$ $(t = t_2)$ automatically removes the effect of C_pM on the values of the derived heat transfer coefficient. This is a desirable feature because the heat capacity of the system, C_pM, has the highest error. Furthermore, $(k_R')_{262}$ is the value of the integral heat transfer coefficient at $t=t_2$, the mid-point of the two-day cycle (see Eq. (14)). Forward integration of this same experimental data simply involves the substitution of t_1 for t_2 in Eq. (20) to yield $(k_R')_{362}$. Similarly, assuming $P_X=0$ in Eq. (20) would yield $(k_R')_{261}$.

The use of Eq. (20) requires an evaluation of P_X for the time period of interest. The obvious advantage of blank or control experiments, such as this study, is that P_X will be close to zero. For other experiments, the calculation of $(k_R')_1$ using Eq. (16) can reveal time periods where P_X is small. The combination of Eq. (20) with thermal inputs made at one or a series of points

Downloaded by COLUMBIA UNIV on July 1, 2012 | http://pubs.acs.org
Publication Date: August 1, 2008 | doi: 10.1021/bk-2008-0998.ch008

can also be used (*11-13*). For example, a thermal balance can be made just before application of the heater pulse $(t=t_1)$, or near the end of the heater pulse $(t=t_2)$, then if the system has relaxed adequately, $dT_{cell}/dt\approx 0$ (see Figure 2).

Once the accurate determination of $(k_R')_{262}$ and C_pM is completed for a particular calorimetric cell, then Eq. (20) can be used directly in evaluating the excess power, P_X, during all time periods and even for future experiments using this same calorimetric system. However, the Dewar vacuum may soften with the passage of several years (due mainly to the slow diffusion of atmospheric helium through the glass walls of the Dewar cell) leading to a small increase in the radiative heat transfer coefficient (*9, 10*).

The application of Eq. (20) to obtain integral heat transfer coefficients requires that the excess power, P_X, be constant over the time period considered. In turn, this requires experiments using suitable "blank" or control systems. If the excess power generation varies with time, one will inevitably conclude that the instrumentation has enhanced errors. Moreover, such a conclusion will apply to any calorimetric system that is used. The lack of execution of appropriate "blank experiments" is undoubtedly a contributory factor to confusion concerning cold fusion calorimetry.

Downloaded by COLUMBIA UNIV on July 1, 2012 | http://pubs.acs.org
Publication Date: August 1, 2008 | doi: 10.1021/bk-2008-0998.ch008

Results

The first focus for a given time period is to determine if the excess power is constant with time. This can be done simply from the raw data shown in Figure 2. If the cell temperature relaxes back to the same baseline following the application of the internal cell heater from $t = t_1$ to $t= t_2$, then any excess power has remained constant. If there is a significant change in the excess power, then a shift in the baseline will be detected (*9, 10*). In addition, if the excess power increases then the cell temperature may continue to increase during the heater pulse rather than relaxing to give $dT_{cell}/dt\approx 0$ (*8-10*). Due to positive feedback, active cold fusion experiments will often yield larger excess power effects at higher cell temperatures, thus the baseline will shift to a higher cell temperature following the heater pulse (*8, 9*). For this control study, Figure 2 shows that the cell temperature relaxes back to the same baseline following the end of the heater pulse.

Figure 3 illustrates the determination of $(k_R')_{262}$ using backward integration for days 9 and 10 of the measurement cycle. From Eq. (20), x=0 at $t=t_2$, and extrapolation of the straight-line yields $(k_R')_{262} = 0.62085\times 10^{-9} WK^{-4}$. From the slope of the line, $C_pM=341.1\ JK^{-1}$. Figure 4 presents results for forward integration of this same time period, but now the origin (x=0) is set at $t=t_1$. Note the larger range in values for the y-axis leading to less accuracy. This analysis yields $(k_R')_{362}=0.62131\times 10^{-9}WK^{-4}$ and $C_pM=339.4\ JK^{-1}$. The detailed analyses of this experiment are presented elsewhere (*11-13*).

The excess power (or rate of excess enthalpy generation) in watts for this control experiment is shown in Figure 5 based on both the use of the differential

Downloaded by COLUMBIA UNIV on July 1, 2012 | http://pubs.acs.org
Publication Date: August 1, 2008 | doi: 10.1021/bk-2008-0998.ch008

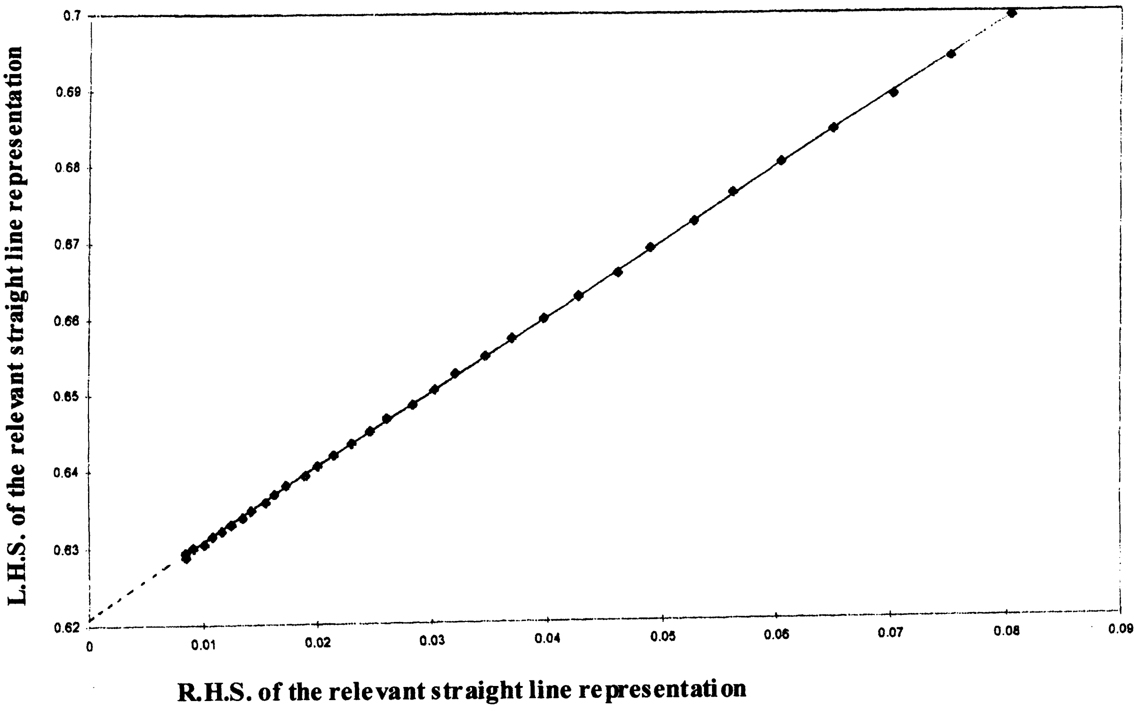

Figure 3. Evaluation of $(k_R')_{262}$ and C_pM for days 9 and 10 of the measurement cycles. The origin for this backward integration is set at $t=t_2$. L.H.S. and R.H.S. refer to the "y" and "x" components of Eq. (20) expressed in straight-line form where y has units of WK^{-4} and x has units of $K^{-3}s^{-1}$. The slope of the straight line (C_pM) therefore has units of JK^{-1}. The x-values were divided by a constant factor to give a slope near unity.

Downloaded by COLUMBIA UNIV on July 1, 2012 | http://pubs.acs.org
Publication Date: August 1, 2008 | doi: 10.1021/bk-2008-0998.ch008

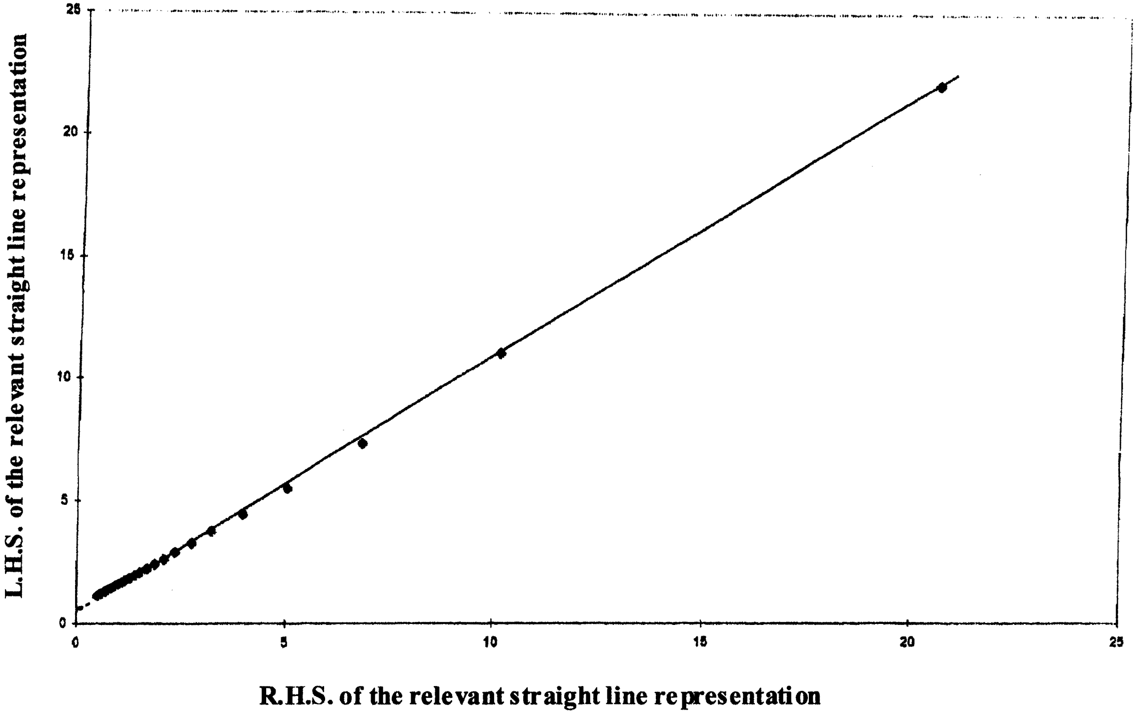

Figure 4. Evaluation of $(k_R')_{362}$ and C_pM for days 9 and 10 of the measurement cycles. The origin for this forward integration is set at $t=t_1$. L.H.S. and R.H.S. refer to the "y" and "x" components of Eq. (20) expressed in straight-line form where y has units of WK^{-4} and x has units of $K^{-3}s^{-1}$. The slope of the straight line (C_pM) therefore has units of JK^{-1}. The x-values were divided by a constant factor to give a slope near unity.

Downloaded by COLUMBIA UNIV on July 1, 2012 | http://pubs.acs.org
Publication Date: August 1, 2008 | doi: 10.1021/bk-2008-0998.ch008

equation directly (Eq. (1)) and the integration shown in Eq. (20). The differential values for P_X show the expected time variation as well as random variations that are gradually suppressed with increasing time. The integral values for P_X in Figure 5 yield nearly constant excess power values of 1.1 mW. The source of this small excess power is the controversial recombination of the evolved D_2 and O_2 gases. The only logical anomalous excess power source that would yield a steady 1.1 mW, as shown by the shaded squares in Figure 5, is recombination during this electrolysis experiment at 200 mA.

Table III presents experimental mean values for k_R' and C_pM for this calorimetric system as well as the theoretical values calculated. Individual values for each two-day cycle over 16 days are available (*11-13*). The derivation of a useful equation giving $(k_R')_2$ at $t=t_2$ by use of the heater pulse is given in Appendix II.

All experimental values obtained for k_R' are close to the theoretical result of 0.6220×10^{-9} WK^{-4} calculated from the Stefan-Boltzmann coefficient, and this result validates the assumption made in Eq. (13). Theoretical calculations based on the mass of heavy water used in the cell and the glass and metal components in contact with the electrolyte give C_pM values in approximate agreement with the experimental values. Various integration methods (*11-13*) yield an overall mean value of $C_pM=340.1\pm0.8$ JK^{-1}. This is the least accurate calorimetric parameter, but its effect can be minimized by evaluations made at the end of the 12-hour heating pulse at $t=t_2$ where $C_pM(dT_{cell}/dt)\approx 0$.

Table III. Mean Values for k_R' and C_pM

Description	$10^9(k_R')$, WK^{-4}	C_pM, JK^{-1}
Theoretical	0.6220[a]	340
Lower Bound	0.62013	
$(k_R')_1$	±0.00058	
True[b]	0.62059	
$(k_R')_2$	±0.00240	
Backward Integration	0.62083	339.2
$(k_R')_{262}$	±0.00059	±.1.7
Forward Integration	0.62031	339.8
$(k_R')_{362}$	±0.00156	± 18.3

[a] Calculated from Stefan-Boltzmann coefficient

[b] See Appendix II.

Downloaded by COLUMBIA UNIV on July 1, 2012 | http://pubs.acs.org
Publication Date: August 1, 2008 | doi: 10.1021/bk-2008-0998.ch008

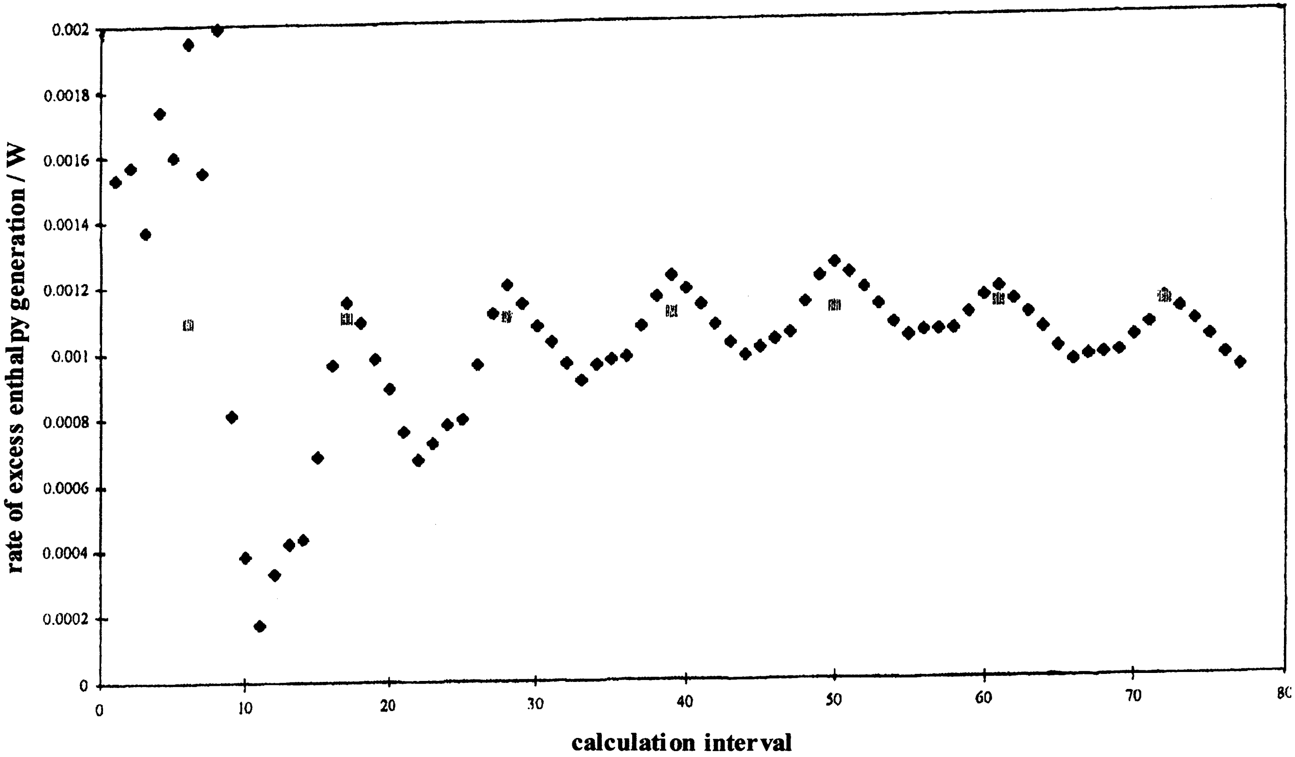

Figure 5. Rates of excess enthalpy generation (P_X) using the integral values of the heat transfer coefficient (shaded squares). This figure also shows the differential rates of excess enthalpy generation (P_X) using a single value of the true heat transfer coefficient at t=86,400 s or 24 hours (black diamonds).

Discussion

The differential rate of excess enthalpy production due to recombination in this blank system can be estimated using Eq. (18) to give $P_X = 0.6\ mW$. The more accurate calorimetric results using integration methods (see Figure 5) yields $P_X=1.1\pm0.1\ mW$ for recombination in these experiments. Theoretical calculations using Henry's Law and Fick's Law of Diffusion for rapidly stirred solutions yield approximately 1 mW due to the reduction of oxygen at the cathode in this electrolysis system (*17*). The electrochemical oxidation of deuterium or hydrogen does not occur at the platinum oxide surface of the anode. The recombination effect measured in this experiment is about 0.1% of the cell input power of about 800 to 1000 mW at 320 mA cm^{-2} (see Figure 2). A smaller recombination effect of 0.03% of the cell input energy at 400 mA cm^{-2} has been previously reported (*3, 14*).

The ability of this calorimetry to measure excess power to within ±0.1 mW with an enthalpy input to the cell of approximately 800 mW demonstrates a precision of 99.99%. Additional evaluations show that the accuracy of this calorimetry is also close to 99.99% (*11-13*). The small errors can in fact be estimated from the errors in the temperature measurements coupled to the averaging procedures that are described elsewhere (*9-13*). If the error range of this instrumentation were ± 1% instead of 0.01%, it would be impossible to measure the excess power due to recombination. Equally, it would be impossible to accurately measure excess power effects less than about 100 mW. The calorimetry used by Caltech, MIT, and Harwell in 1989 contained large errors in both and experimental design and methods of analysis (*1*). It is unfortunate that cold fusion has been dismissed by the mainstream scientific community because of the inferior calorimetry of these three institutions.

Results in Table III shows that the calibration of calorimetric cells could be based equally well on the determination of the lower bound heat transfer coefficient, $(k_R')_1$, for suitable control or "blank" experiments. The use of such coefficients in the data analysis for Pd-based cathodes in D_2O-based electrolytes would then automatically discriminate against the contribution of the reduction of electrogenerated oxygen to the total excess power production.

Palladium-boron alloy materials prepared at the Naval Research Laboratory (NRL) have shown a remarkable ability to produce the excess power effect (*9, 10, 17-20*). A Dewar calorimetric system almost identical except for size to the system used in this blank study yielded excess power effects that ranged up to 400 mW over a 65-day period (*9, 10, 17-19*). The average excess power was about 175 mW for this experiment using a Pd-B cathode (*9, 10*). The measured excess power increased to over 9 W (9000 mW) during the final boil-off phase (*9, 17, 19*). Excess power continued for several hours after this Pd-B cell boiled dry (*9, 10, 19*). The total excess enthalpy over the 65-day period was about 10^6 Joules.

Although the radiative and conductive heat transfer coefficients, k_R and k_C in Eqs. (5) and (6), are independent of the cell temperature, the use of the

Downloaded by COLUMBIA UNIV on July 1, 2012 | http://pubs.acs.org
Publication Date: August 1, 2008 | doi: 10.1021/bk-2008-0998.ch008

pseudoradiative heat transfer coefficient (Eq. (13)) introduces a slight temperature dependence. From Eq. (13),

$$P_R' = - [k_R (T_{cell}^4 - T_b^4) + k_C(T_{cell} - T_b) + RT_{cell} (0.75 I/F)] = - k_R'(T_{cell}^4 - T_b^4) \quad (21)$$

Solving Eq. (21) for k_R' yields

$$k_R' = k_R + [k_C(T_{cell} - T_b) + RT_{cell}(0.75I / F)] / (T_{cell}^4 - T_b^4) \quad (22)$$

As the cell temperature increases, k_R' decreases and approaches more closely the value of k_R. For the conditions of this study, calculations show that k_R' will be close to k_R.

It has been falsely asserted that conductive heat transfer pathways such as through the cell top or via the wire leads can cause large errors in this Dewar calorimetric cell (*12, 13*). However, calculations using known thermal conductivities yield less than 1 mW for the rate of heat transfer by the wire leads in this cell (*13*). From Eq. (21), it can be readily shown that the actual radiative power, P_R, is given by

$$P_R = -k_R (T_{cell}^4 - T_4^b) = P_R' (k_R / k_R') \quad (23)$$

Therefore, if only 50% of the heat transfer was by radiation ($P_R = 0.5 P_R'$), then $k_R' = 2 k_R$. Experimentally, $k_R' \approx k_R$ as calculated by Stefan – Boltzmann coefficient (see Table II), thus the rate of heat transfer by conduction is much smaller than the rate of heat transfer by radiation in this calorimetric system.

Summary

The high precision and accuracy of isoperibolic cold fusion calorimetry allows the measurement of excess power to within ±0.1 mW. The excess power due to the reduction of oxygen electrogenerated in the cell is measured as 1.1 ±0.1 mW in this blank or control system. The logical conclusion from this control study is that excess enthalpy measurements using this cold fusion calorimetry cannot be scientifically dismissed as calorimetric errors, although that is exactly what has happened within the mainstream scientific community.

Acknowledgments

One of us (M.H.M.) received financial help from an anonymous fund at the Denver Foundation. Dixie State College and the Dixie Foundation, especially Kalynn Larson, assisted in the administration of this fund.

Downloaded by COLUMBIA UNIV on July 1, 2012 | http://pubs.acs.org
Publication Date: August 1, 2008 | doi: 10.1021/bk-2008-0998.ch008

References

1. Miles, M. H.; Bush, B. F.; Stilwell, D. E. Calorimetric Principles and Problems in Measurements of Excess Power During Pd-D_2O Electrolysis. *J. Phys. Chem.* **1994**, *98*, 1948.
2. Miles, M. H. Reply to Examination of Claims of Miles et.al. in Pons-Fleischmann-Type Cold Fusion Experiments *J. Phys. Chem. B,* **1998**, *102*, 3642.
3. Miles, M. H. Calorimetric Studies of Pd/D_2O + LiOD Electrolysis Cells. *J. Electroanal. Chem.* **2000**, *482*, 56.
4. Fleischmann, M.; Pons, S.; Hawkins, M. Electrochemically Induced Nuclear Fusion of Deuterium. *J. Electroanal Chem.* **1989**, *261*, 301; Errata, **1989**, *263*, 187.
5. Fleischmann, M.; Pons, S.; Anderson, M. W.; Li, L. J.; Hawkins, M. Calorimetry of the Palladium-Deuterium-Heavy Water System. *J. Electroanal. Chem.* **1990**, *287*, 293.
6. Fleischmann, M.; Pons, S. Some Comments on the Proper Analysis of Experiments on Calorimetry of LiOD/D_2O Electrochemical Cells. *J. Electroanal. Chem.* **1992**, *332*, 33.
7. Szpak, S.; Mosier-Boss, P. A.; Miles, M. H. Calorimetry of the Pd+D Codeposition. *Fusion Technol.* **1999**, *36*, 234.
8. Szpak, S.; Mosier-Boss, P. A.; Miles, M. H.; Fleischmann, M. Thermal Behavior of Polarized Pd/D Electrodes Prepared by Codeposition. *Thermochimica Acta* **2004**, *410*, 101.
9. Miles, M. H.; Fleischmann, M.; Imam, M. A. *Calorimetric Analysis of a Heavy Water Electrolysis Experiment Using a Pd-B Alloy Cathode.* Report Number NRL/MR/6320-01-8526; Naval Research Laboratory: Washington, DC, March 26, 2001.
10. Fleischmann, M. Simulation of the Electrochemical Cell (ICARUS) Calorimetry. In *Thermal and Nuclear Aspects of the Pd/D_2O System,* Vol. 2, SPAWAR Systems Center Technical Report Number 1862; S. Szpak, S.; Mosier-Boss, P. A., Eds.; SPAWAR Systems Center: San Diego, CA, Feb. 2002.
11. Fleischmann, M.; Miles, M. H. The Instrument Function of Isoperibolic Calorimeters: Excess Enthalpy Generation Due to the Parasitic Reduction of Oxygen. In *Condensed Matter Nuclear Science: Proceedings of the 10th International Conference on Cold Fusion*, Cambridge, MA, Aug. 24-29, 2003; Hagelstein, P. L.; Chubb, S. R., Eds.; World Scientific Publishing Co.: Singapore, 2006; 247-268.
12. Fleischmann, M.; Miles M. H. The Precision and Accuracy of Isoperibolic Calorimetry as Applied to the Pt/D_2O Systems. Manuscript No. JP058292J submitted to *J. Phys. Chem.* **2006**. Note: Editor George C. Schatz rejected this manuscript and ruled that the two reviewers did not need to respond to the detailed rebuttal by the authors to the reviewer's comments.

Downloaded by COLUMBIA UNIV on July 1, 2012 | http://pubs.acs.org
Publication Date: August 1, 2008 | doi: 10.1021/bk-2008-0998.ch008

Downloaded by COLUMBIA UNIV on July 1, 2012 | http://pubs.acs.org
Publication Date: August 1, 2008 | doi: 10.1021/bk-2008-0998.ch008

13. Fleischmann. M.; Miles, M.H. The Precision and Accuracy of Isoperibolic Calorimetry as Applied to the Pt/D_2O Systems. In SPAWAR Systems Center Technical Report; S. Szpak, S.; Mosier-Boss, P. A., Eds.; SPAWAR Systems Center: San Diego, CA, (in press). Note: Contains complete *J. Phys. Chem.* manuscript (Ref. 12) as well as comments of the two reviewers and the unanswered rebuttal of these comments by the authors.
14. Will, F. G. Hydrogen + Oxygen Recombination and Related Heat Generation in Undivided Electrolysis Cells. *J. Electroanal. Chem.* **1997**, *426*, 177.
15. Atkins, P.; dePaula, J. *Physical Chemistry, 7th ed.*; W.H. Freeman: New York, 2002; pp 13-14, 30-65.
16. Miles, M. H.; Bush, B. F.; Johnson, K. B. *Anomalous Effects in Deuterated Systems*; Technical Report NAWCWPNS TP 8302; Naval Air Warfare Center: China Lake, CA, Sept. 1996.
17. Miles, M. H.; Fleischmann, M. Precision and Accuracy of Cold Fusion Calorimetry. Presented at the ACS Spring Meeting, Chicago, March 25-29, 2007; ENVR 0220. http://lenr-canr.org/acrobat/MilesMprecisiona.pdf.
18. Miles, M. H. Calorimetric Studies of Palladium Alloy Cathodes Using Fleischmann-Pons Dewar Type Cells. In *ICCF8: Proceedings of the Eighth International Conference on Cold Fusion*, Lerici (La Spezia), Italy, May 21-26, 2000; Scaramuzzi, F., Ed.; Italian Physical Society: Bologna, Italy, 2001; 97-104.
19. Miles, M. H.; Imam, M. A.; Fleischmann, M. Case Studies of Two Experiments Carried Out With the Icarus Systems. In *ICCF8: Proceedings of the Eighth International Conference on Cold Fusion*, Lerici (La Spezia), Italy, May 21-26, 2000; Scaramuzzi, F., Ed.; Italian Physical Society: Bologna, Italy, 2001; 105-119.
20. Miles, M. H.; Imam, M. A. Palladium-Boron Alloys and Methods for Making and Using Such Alloys. U.S. Patent 6,764,561, June 20, 2004.

Appendix I. List of Symbols

C_p = heat capacity at constant pressure, JK^{-1} mol^{-1}
E_H = thermoneutral potential, V
F = Faraday constant, 96485.3415 C mol^{-1}
I = cell current, A
k_C = conductive heat transfer coefficient, WK^{-1}
k_R = radiative heat transfer coefficient, WK^{-4}
k_R' = pseudoradiative heat transfer coefficient, WK^{-4}
L = enthalpy of evaporation for D_2O, J mol^{-1}
n_g = moles of electrolysis gases, mol
M = heavy water equivalent of the calorimetric cell, mol
$\boldsymbol{P}$ = partial pressure of D_2O, Pa
$\boldsymbol{P^*}$ = atmospheric pressure, Pa

P_C = power transferred by conduction, W
P_{calor} = rate of enthalpy change within the calorimeter, W
P_{EI} = power input due to electrolysis, W
P_{gas} = rate of enthalpy transport by the gas stream, W
P_g = rate of enthalpy transport by the gas stream (Eq. (4)) neglecting the evaporation of D_2O, W
P_H = power input due to the calibration heater, W
P_L = rate of enthalpy transport due to the L-term (evaporation) in Eq. (4), W
P_R = power transferred by radiation, W
P_W = rate of pressure-volume work by the generated gases, W
P_X = excess power generated, W
R = gas constant, 8.314472 $JK^{-1}\ mol^{-1}$
T_b = temperature of water bath, K
T_{cell} = temperature of cell, K
ΔT = $T_{cell} - T_b$, K
$f(T)$ = T_{cell}^4 - T_b^4 , K^4

Downloaded by COLUMBIA UNIV on July 1, 2012 | http://pubs.acs.org
Publication Date: August 1, 2008 | doi: 10.1021/bk-2008-0998.ch008

Appendix II. Derivation of Equation for Evaluating $(k_R')_2$

Heat balance for the cell is made at $t=t_2$ and at $t=t_2$' where t_2' gives extrapolated raw date for T_{cell} (t_2') and $E(t_2')$ if the heater power was not used (see Figure 2). Note extrapolated marks for E and $T_{cel}l$ at $t=t_2$). From Eq. (17).

$$(k_R')_2 f(T)_{t2} = (P_{EI}+P_H+P_X+P_{gas})_{t2} - C_pM(dT_{cell}/dt)_{t2} \tag{A.1}$$

$$(k_R')_2 f(T)_{t2} = (P_{EI}+0+P_X+P_{gas})_{t2} - C_pM(dT_{cell}/dt)_{t2} \tag{A.2}$$

Assuming P_X is constant and subtracting Eq. (A.2) from Eq. (A.1) yields

$$(k_R')_2[f(T)_{t2} - f(T)_{t2}] = P_H+[(P_{EI})_{t2} - (P_{EI})_{t2}] \\ +[(P_{gas})_{t2} - (P_{gas})_{t2}] - C_pM\,[(dT_{cell}/dt)_{t2} - (dT_{cell}/dt)_{t2}] \tag{A.3}$$

Because T_b is constant

$$f(T)_{t2} - f(T)_{t2} = (T_{cell}^4)_{t2} - (T_{cell}^4)_{t2} = f_2(T) \tag{A.4}$$

Therefore

$$(k_R')_2 = \{P_H + [(P_{EI})_{t2} - P_{EI})_{t2}] + [(P_{gas})_{t2} - P_{gas})_{t2}] \\ -C_pM[(dT_{cell}/dt)_{t2} - (dT_{cell}/dt)_{t2}]\}/f_2(T) \tag{A.5}$$

Downloaded by UNIV OF GUELPH LIBRARY on July 2, 2012 | http://pubs.acs.org
Publication Date: August 1, 2008 | doi: 10.1021/bk-2008-0998.ch009

Chapter 9

Transmutation Reactions and Associated Low-Energy Nuclear Reactions Effects in Solids

George H. Miley and Prajakti J. Shrestha

Department of Nuclear, Plasma, and Radiological Engineering, University of Illinois, 104 South Wright Street, Urbana, IL 61801

It has been found that cold fusion-type experiments can be designed to create nuclear reactions between the H or D in the electrolyte and the electrode lattice material. This field of research has been termed "Low Energy Nuclear Reactions (LENRs)". Studies of reaction (transmutation) products from LENRs are reviewed here, with emphasis on studies at UIUC using special thin-film electrodes designed to enhance such reactions. Evidence is presented for simultaneous production of excess heat (due to the exothermic nature of the reactions) and also low levels of very energetic (multi MeV) proton and alpha particles. Several theories have been proposed to address how the large coulombic field between reactants can be overcome in the highly loaded lattices. While these theories have attained some success in reproducing reaction product distributions, a number of theoretical issues remain open. Continued experimental/theoretical progress is bringing this basic research field closer to practical application as a power source or to drive transmutations for specific products.

In Low-Energy Nuclear Reactions Sourcebook; Marwan, J., et al.;
ACS Symposium Series; American Chemical Society: Washington, DC, 2008.

Introduction

Research at the University of Illinois (UIUC) has helped pioneer the new field of cold fusion termed “Low Energy Nuclear Reactions” (LENR) where proton or deuteron reactions with the hydrated solid lattice (e.g. Pd) result in a variety of nuclear transmutation products. In this article the UIUC LENR research is reviewed. This includes identification of reaction products and supporting evidence of simultaneous excess energy productions and energetic particle (e.g. MeV proton and alpha particle) production. The observation of LENR products represents a startling new aspect of cold fusion reactions in solids, something not anticipated by original workers in the field. Observations of such reactions, although varying in type, have been reported by a number of researchers worldwide. A brief review of the field is included here to illustrate how persuasive the evidence is that this startling effect occurs. Some comments are also included about LENR theory. While a variety of mechanisms have been proposed, a general consensus on the theory has not yet been reached.

This article is divided into three main parts: UIUC transmutation product studies are reviewed first. A brief survey of work by others is also provided. Evidence for simultaneous excess heat production and energetic charged particle emission observed at UIUC is also presented.

Downloaded by UNIV OF GUELPH LIBRARY on July 2, 2012 | http://pubs.acs.org
Publication Date: August 1, 2008 | doi: 10.1021/bk-2008-0998.ch009

UIUC Transmutation Product Studies

Studies of Reactions and Products

UIUC transmutation research is briefly reviewed here along with an update of a review of research on transmutation in solids worldwide, originally presented in ICCF 10 *(1)*.

There are a variety of “cold fusion”-type nuclear reactions. As illustrated in Figure 1, the original Pons-Fleishmann (P-F) reaction involved DD fusion, but instead of the normal hot fusion reaction channel, the P-F reaction passes through deactivation of the He-4 by energy transfer to the lattice. The energy transferred ultimately appears as heat. Alternately, a number of researchers have reported transmutation reactions that involve multiple-body (three or more) interactions between the deuterium (or hydrogen) with itself and/or atoms in the host lattice, typically heavy metals. Recently there has been a move to also include DD reactions as LENRs. In this review we concentrate on H/D reactions with host atoms. A key question remains regarding how it is possible to design an experiment in advance that would emphasize one of these channels over the others. Various experiments have “naturally” done this, but the key factors driving the channel selection are not entirely clear.

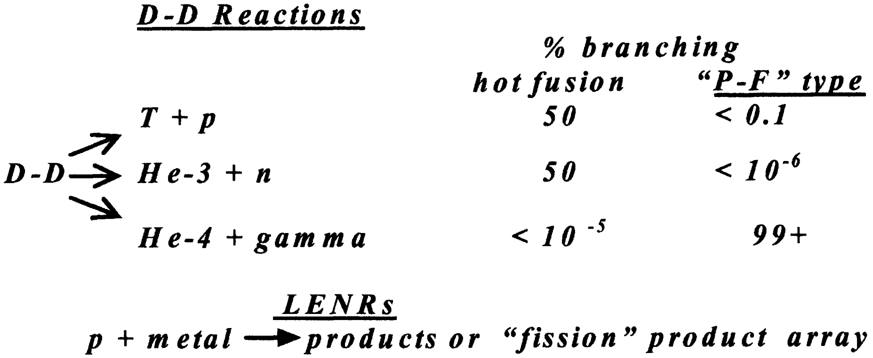

Figure 1. Comparison of P-F cold fusion, LENR, and hot fusion reactions.

Types of Transmutation Reactions

Transmutation reactions can be broadly classified according to their products. Some experiments have resulted in a large array of reaction products with mass numbers ranging across the periodic table. These reactions are traced to multi-body events leading to a heavy compound nucleus, which can both decay and fission into an array of elements (*2*). The second set of experiments leads to one or more distinct isolated products (*3*, *4*). These reactions may or may not involve multi-bodies but the net result is direct formation of the reaction products as opposed to the disintegration of a compound nucleus. In this discussion we will first briefly review reactions leading to an array of products, then discuss the "direct" product-type reactions.

Spectrum of Products – UIUC LENR Research

An array of reaction products was first observed by Karabut et al. (*5*) in experiments using a glow discharge to bombard and load various targets such as palladium. Later experiments leading to product arrays include those by Bockris et al. (*6*), Mizuno et al. (*7-9*), and Miley and Patterson (*10*). These experiments all used electrolytic methods to load a cathode. Here we briefly review the Miley-Patterson work (*10*), which is illustrative of this class of experiments. They employed multi-layer thin-film Ni/Pd coated on small (mm diameter) plastic spheres loaded to a high ratio of hydrogen/film metal using a packed bed-type electrolytic technique. One distinguishing feature of their work was the use of combined Secondary Ion Mass Spectroscopy-Neutron Activation Analysis (SIMS-NAA) diagnostics to obtain quantitative measurements of selected product yields. SIMS provides a rapid scan of localized surface areas, whereas

Downloaded by UNIV OF GUELPH LIBRARY on July 2, 2012 | http://pubs.acs.org
Publication Date: August 1, 2008 | doi: 10.1021/bk-2008-0998.ch009

NAA analysis allows an examination of the total sample volume. The NAA analysis was calibrated against the NIST standards to give absolute quantities of key reaction products which had detectable neutron interaction cross-sections. A typical gamma spectrum from NAA analysis is shown in Figure 2. Well-isolated lines for key elements like Cu and Ni are seen. All studies used a comparison of electrode compositions before and after runs. NAA was used to also identify impurity levels of the other system components, providing limits on minimum detectable quantities of elements, as shown in Figure 3.

Non-natural isotopic abundances were found for select products. Figure 3 shows that a distinctive characteristic for this experiment is a product yield curve vs. mass with four high yield peaks. As seen in Figure 3, higher-yield elements occurred in quantities well above maximum impurity limits, which include possible accumulation of isotopes on the cathode due to electrolytic field effects.

Non-natural isotopic distributions were studied for key elements and confirmed, consistent with a non-natural source such as a nuclear reaction. In addition, the observations of excess heat and MeV proton/alpha particle emission, described later, strongly support the hypothesis that nuclear reactions occurred.

The UIUC studies described here used thin films created on a substrate for electrodes, illustrated in Figure 4. The motivation for this came from the original swimming electron layer (SEL) theory (*11*). This theory suggests that the use of thin films with multi-layers, each having a large difference in Fermi energy level, results in a high electron density at the film interfaces, which can promote reactions. It is now recognized that the situation is more complex, involving, e.g., electron, ion flow, and ion cluster formation. However, this insight still provides a key parameter used in UIUC electrode design.

The electrode design of Figure 4, with thin films coated on a flat alumina substrate, is the outgrowth of initial studies that used a pebble bed-type electrolysis unit with thin films coated on plastic microspheres. In this design the electrical current flow is parallel to the thin-film surface so that a high current density and high proton flow rate are obtained. Results from this work are summarized in the paper by Miley et al. from ICCF 9 (*12*) and are also the basis for the excess heat and charged particle emission results reported in later sections.

Survey of Transmutation Experiments Elsewhere

LENR Studies Worldwide

Other laboratories have also reported transmutation reactions in solids under various H/D loading/flow conditions. These experiments have employed a variety of electrode materials ranging from carbon to palladium to uranium.

Downloaded by UNIV OF GUELPH LIBRARY on July 2, 2012 | http://pubs.acs.org
Publication Date: August 1, 2008 | doi: 10.1021/bk-2008-0998.ch009

Downloaded by UNIV OF GUELPH LIBRARY on July 2, 2012 | http://pubs.acs.org
Publication Date: August 1, 2008 | doi: 10.1021/bk-2008-0998.ch009

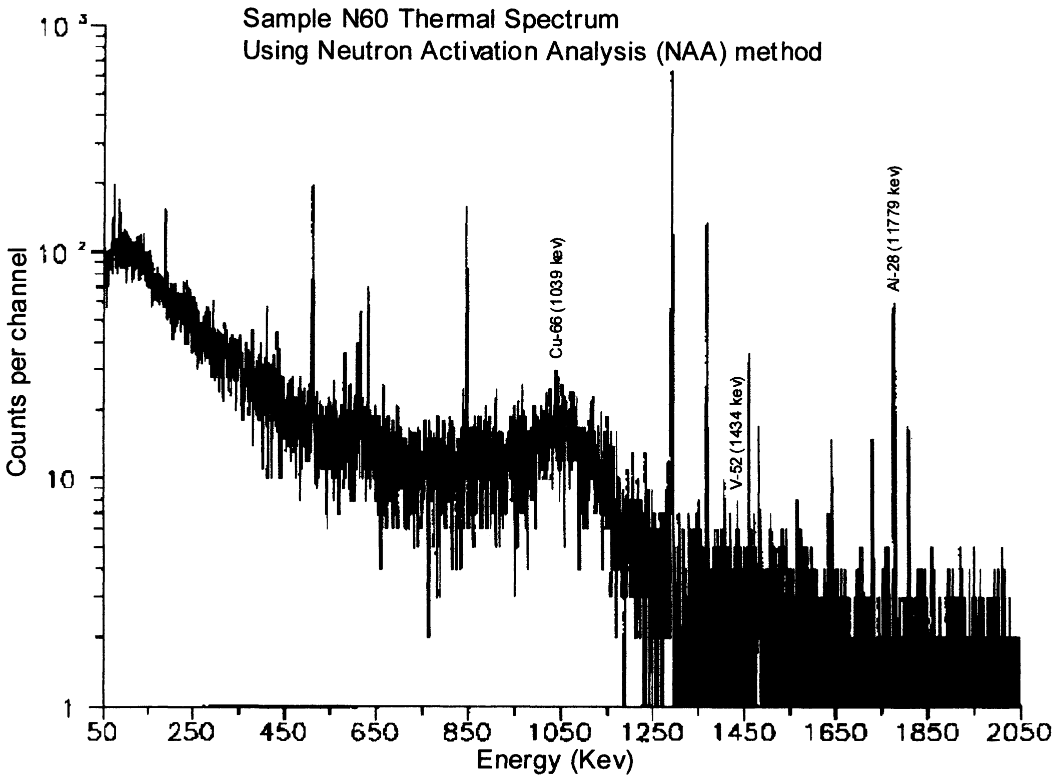

Figure 2. Gamma spectrum with sample chart of concentrations. The spectrum of gamma rays is used to identify and quantify the emitting element. A NIST standard was used for calibration.

Downloaded by UNIV OF GUELPH LIBRARY on July 2, 2012 | http://pubs.acs.org
Publication Date: August 1, 2008 | doi: 10.1021/bk-2008-0998.ch009

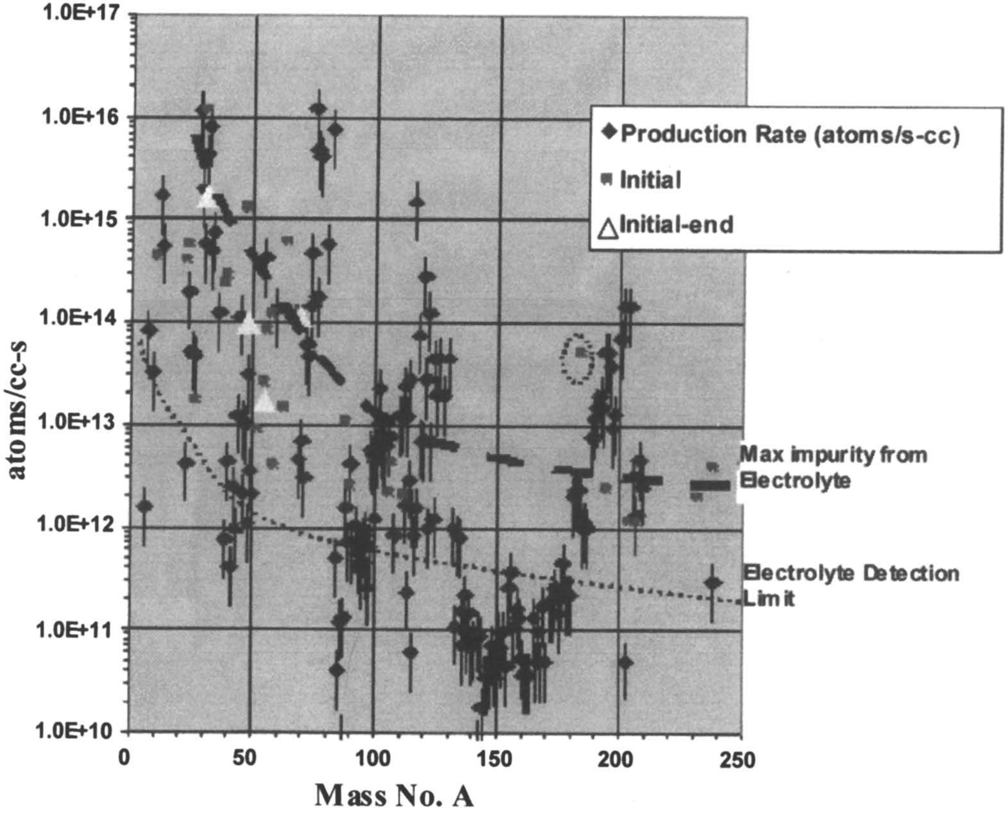

Figure 3. Reaction rate for product production vs. mass number showing upper limit curves for possible impurities.

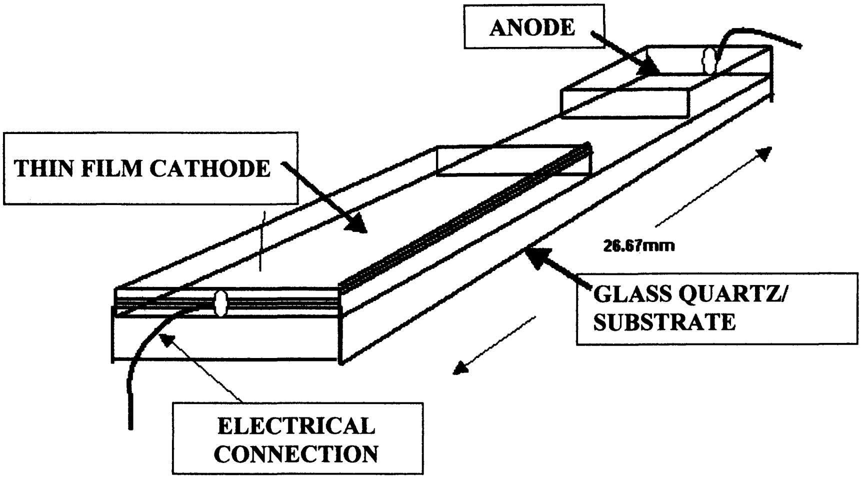

Figure 4. Unique integrated thin-film plate-type electrode used at UIUC.

They have used various loading methods, e.g., electrolytic, gas pressure, plasma discharge, ion implantation, bubble collapse loading, and laser initiation. Some insight can be obtained from Figure 5, which summarizes the frequency of observation reported for various elements in the various experiments surveyed. While elements with mass lighter than the electrode material are most frequently found, heavier elements have also been reported.

The most commonly reported elements for transmutation studies reporting multiple products are calcium, copper, zinc, and iron. They were reported in more than 20 different experiments. Forty percent of the least frequently observed elements were from the lanthanide group, hence are rare earth elements. The elements reported include lutetium, terbium, praseodymium, europium, samarium, gadolinium, dysprosium, holmium, neodymium, and ytterbium. It is widely accepted that these rare earth elements are less likely to occur as impurities, so this result is very striking.

A large number of studies also reported elements with a significant deviation from the natural abundance, although detailed data were not provided in all cases. Some of the best documented reports are tabulated in Figure 6.

Key experimental parameters that control the reactions observed are not clear from these various studies. Some work suggests that heavy-water electrolysis gives a larger amount of transmutation products than does light water (*13*). The number of transmutation products observed has been found to increase as a function of the thickness of the electrode metal in some cases (*14*). However, in the multiple thin-film studies at UIUC, higher product densities occurred at interfaces (*2*).

Downloaded by UNIV OF GUELPH LIBRARY on July 2, 2012 | http://pubs.acs.org
Publication Date: August 1, 2008 | doi: 10.1021/bk-2008-0998.ch009

Frequency	*Transmutation Elements*
1	13 (Ho, Rb, Se, Pr, Tb, Lu, Nd, W, La, Ce, Be, Th, Tc)
2	15 (Yb, Pd, B, Ba, Nb, Sc, Zr, Eu, Sm, Gd, Dy, Kr, N, Ne, P)
3	5 (Y, Ge, In, Cs, F)
4	6 (O, Li, Os, Xe, I, V)
5	8 (Hg, Mo, Au, Te, Sb, Sr, Re, Hf)
6	2 (Au, Pt)
7	4 (Br, Ir, Sn, Cl)
8	3 (As, Cd, Mn)
9	3 (C, Ga, Na)
10	1 (S)
11	2 (Ag, Pb)
12	3 (K, Co, Ni)
15	1 (Mg)
17	1 (Al)
18	1 (Si, Ti)
19	1 (Cr)
22	1 (Cu)
23	1 (Ca)
26	1 (Zn)
30	1 (Fe)

Figure 5. The frequency of observation of various transmutation elements as reported in 25 different experimental studies that used a wide range of experimental set-ups and electrode materials.

Downloaded by UNIV OF GUELPH LIBRARY on July 2, 2012 | http://pubs.acs.org
Publication Date: August 1, 2008 | doi: 10.1021/bk-2008-0998.ch009

The transmutation experiments were reported by over 15 separate laboratories worldwide. The laboratories actively involved in this type of study are shown in Table I.

There were other associated effects observed along with transmutation products. These include energetic charged-particle and photon emission. Emissions of a variety of particles such as proton, alpha, beta, neutron, gamma, and low-level soft X-ray have been reported by various labs. Such emissions have led many investigators to postulate their origins to be associated with transmutation-type reactions (*8, 20, 21*). Excess heat production has not been studied in many of the transmutation experiments but this will be discussed later relative to UIUC results.

Downloaded by UNIV OF GUELPH LIBRARY on July 2, 2012 | http://pubs.acs.org
Publication Date: August 1, 2008 | doi: 10.1021/bk-2008-0998.ch009

Isotopes	***Mizuno et al. (8)***	***Miley et al. (2)***	***Ohmori & Mizuno (15)***	***Ohmori et al. (16)***	***Chernov et al. (17)***	***Iwamura et al. (4)***	***Ohmori et al. (18)***	***Ohmori et al. (19)***
	1996	***1997***	***1998***	***1998***	***1998***	***2003***	***2000***	***2002***
K-41								**27.65%**
Cu-63	**30.83%**	**3.6%±1.6**			**44%**			
Cu-65	**-30.83%**	**8.1%±3.6**			**-44%**			
Fe-54			**-0.85%**	**-0.81%**			**0%**	
Fe-56	**-21.75%**		**-29.75%**	**-16.79%**			**-0.75%**	
Fe-57	**18.88%**		**30.88%**	**16.58%**			**0.78%**	
Fe-58				**1.01%**				
Re-185	**14.60%**						**11%**	
Re-187	**-14.60%**						**-11%**	
Ag-107		**3.9%±1.2**						
Ag-109		**4.3%±1.3**						
Mo-96						**26.26%**		
Ti-48					**-33.30%**			
Ti-49					**8.60%**			
Ti-50					**17.80%**			

Figure 6. Isotopic distribution of the transmutation elements reported by various labs.

Table I. Worldwide Research Laboratories Involved in Transmutation Studies with Data Included in the Present Review

	Research Laboratories Included
1	Hokkaido University, Japan – Mizuno et al.; Notoya et al.
2	Mitshubishi Corporation, Japan – Iwamura et al.
3	Osaka University, Japan – Takahashi et al., Arata et al.
4	University of Lecce, Italy – Vincenzo et al.
5	Frascati Laboratory, Italy – De Ninno et al.
6	SIA "LUTCH", Russia – Karabut et al.; Savvatimova et al.
7	Tomsk Polytechnical University, Russia – Chernov et al.
8	Lab des Sciences Nucleaires, France – Dufour et al.
9	Beijing University, China – Jiang et al.
10	Tsinghua University, China – Li et al.
11	Los Alamos National Laboratory, USA – Claytor et al.
12	University of Illinois, USA – Miley et al.
13	Portland State University, USA – Dash et al.
14	Texas A & M University, USA – Bockris et al.
15	Schizuoka University, Japan – Kozima et al.
16	Laboratori Nazionali di Frascati, Italy - Celani et al.
17	US Navy SPAWAR Systems Center, USA - Gordon et al.

Downloaded by UNIV OF GUELPH LIBRARY on July 2, 2012 | http://pubs.acs.org
Publication Date: August 1, 2008 | doi: 10.1021/bk-2008-0998.ch009

Single-Product "Direct"-Type Transmutation

Other experiments have focused on "single-element" transmutations vs. arrays shown earlier in Figure 3. Early studies of this type including those by Mitsubishi Corporation researchers recently reported a real-time measurement using built-in XPS diagnostics where a surface layer of Sr-88 was transmuted into Mo-96 over 200 hours, using diffusion of deuterium through a multi-layer thin-film Pd/CaO substrate (*4*). Cs-133 was also transmuted into Pr-141. Some results from these studies are shown in Figure 7.

These products exhibit a large deviation from natural isotopic abundance, and mass and charge changes of 8 and 4, respectively. In other words the reactions involved are as follows suggesting a 4 body D involvement with the reacting species in order to provide mass balance:

$$^{88}_{38}Sr \rightarrow {}^{96}_{42}Mo$$

$$^{133}_{55}Cs \rightarrow {}^{141}_{59}\mathrm{Pr}$$

Downloaded by UNIV OF GUELPH LIBRARY on July 2, 2012 | http://pubs.acs.org
Publication Date: August 1, 2008 | doi: 10.1021/bk-2008-0998.ch009

Celani et al. carried out a similar experiment (*22*). The results correlated with Iwamura (for instance they, too, found Sr to Mo). In addition, they also reported finding Th to Hg and almost always detected Cu and Zn. They found that, compared to light-water electroyte solution, heavy-water solution produced a larger amount of new elements.

Comments about LENR Theory

Various theories have been proposed to explain how the high-Z reactants in transmutations can overcome the coulombic barrier and why direct product reactions occur in some cases and arrays of "fission-like" products in others. Here we mention two theories that attempt to address these issues and that reasonably well reproduce the product spectrum shown in Figure 3. Additional theories have been advanced and are summarized in recent books on cold fusion by Kozima (*23*) and by Storm (*24*).

Earlier the authors developed a model (Riflex) that considers orbital mixing associated with charge accumulation and proton/deuteron flow at highly loaded interfaces. The subsequent formation of a cluster state overcomes the coulombic repulsion barrier restriction. Depending on the lattice structure and the species (the flowing H or implanted heavy elements) that restrict the hopping passages during diffusion of the H (D), either an array of products or single-element products are predicted. The product array is associated with fission of a compound nucleus as opposed to single-step nuclear reactions that produce the direct "isolated" products.

Hora and Miley (*25*) recently updated this theory by explaining the LENR reaction through cluster formation within the degenerate rigid electron background, especially within the swimming electron layer at the metal surface or at interfaces. This explanation builds on the original Maruhn-Greiner theory for fission processes. Miley et al. (*26*) further extended this approach to treat cluster formation in defects and disclocation loops in the heavily loaded electrodes. As a result they propose a new class of electrode, termed the Massive Cluster Electrode (MCE), where a nickel fiber cloth sandwiched between palladium films creates a high density of micro pore sites for cluster formation. The cluster formation theory is an extension of pioneering work on QED coherence in solids applied to cold fusion by Giuliano Preparata (*27*). In his treatment, however, coherence between the tetrahedral and octahedral site deuterium plasmas is assumed. In the Miley et al. cluster theory, the coherence forms between the high-density deuterium state in the micro pore and the zero point energy radiation field. The effective temperature of the cluster is significantly enhanced by momentum transfer to the cluster from the diffusing deuterium flux. Thus in this theory the two key parameters that initiate coherence and resulting reactions in the cluster are the amount by which the deuterium lattice density exceeds a certain threshold density and the degree to

Downloaded by UNIV OF GUELPH LIBRARY on July 2, 2012 | http://pubs.acs.org
Publication Date: August 1, 2008 | doi: 10.1021/bk-2008-0998.ch009

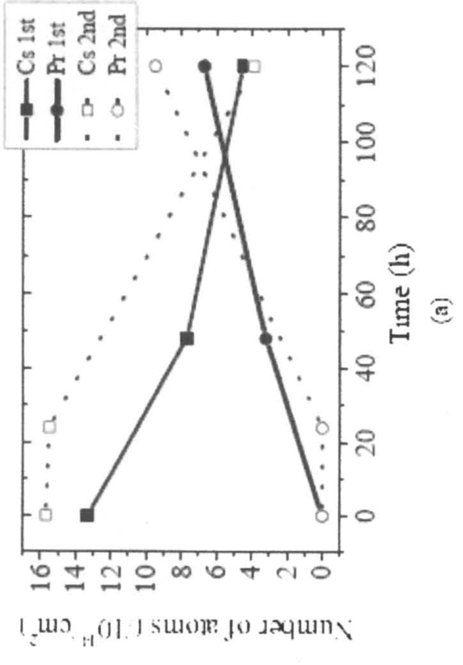

(a)

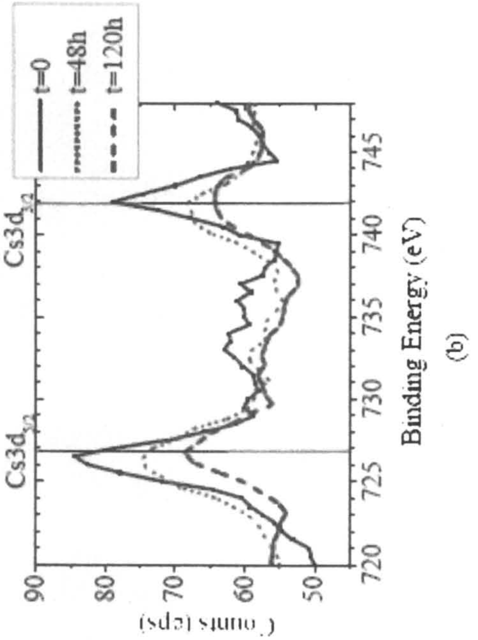

(b)

Downloaded by UNIV OF GUELPH LIBRARY on July 2, 2012 | http://pubs.acs.org
Publication Date: August 1, 2008 | doi: 10.1021/bk-2008-0998.ch009

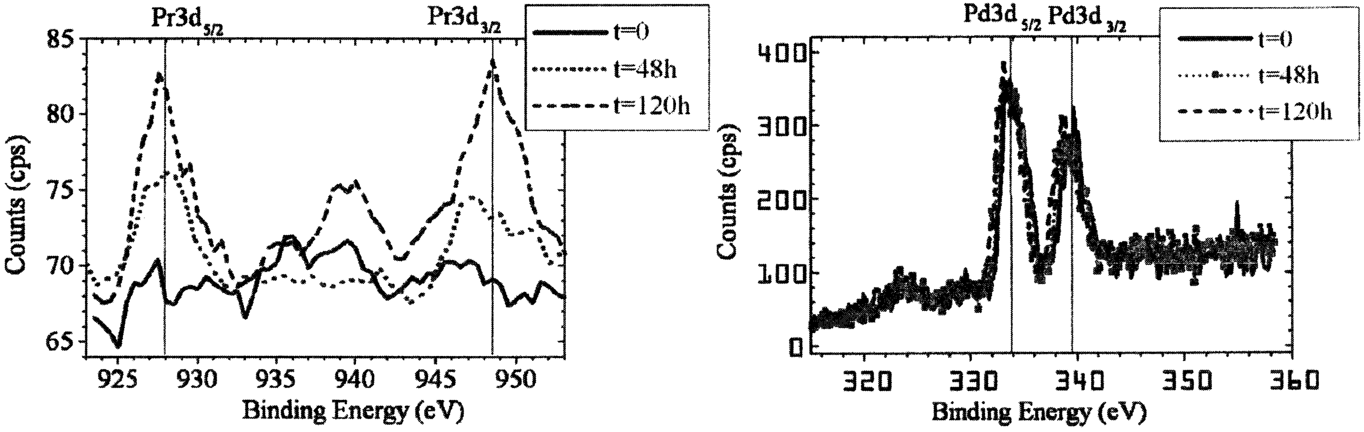

(c)

(d)

Figure 7. Experimental results obtained by D_2 gas permeation through Pd complex (Pd/CaO/Pd) deposited with Cs: (a) Time variation in number of Cs and Pr atoms, (b) XPS spectrum of Cs, (c) XPS spectrum for Pr, (d) XPS spectrum for Pd.

which the deuterium flux exceeds a threshold value. The resulting coherent multi-body reactions can lead to internal deuterium reactions in the cluster as well as to multi-body reactions with the boundary palladium atoms. This, then, explains the different reaction channels observed under varying experimental conditions of D loading density and flux.

In another approach proposed by Widom and Larsen (*28*), electromagnetic surface plasma oscillation energies in hydrogen-loaded metal cathodes may be combined with the normal electron-proton rest mass energies to allow for neutron-producing low energy nuclear reactions. The process of neutron production near metallic hydride surfaces is described in terms of the standard model for electroweak interactions. The neutrons produced have ultra-low momentum since the wavelength is that of a low mode isotopic spin wave spanning a surface patch. The radiation energy required for such ultra-low-momentum neutron production may be supplied by an applied voltage which pushes a strong charged current across the metallic hydride cathode surface. Alternatively, these conditions might, in principle, be achieved by laser radiation energy applied to a cathode surface. Widom and Larsen report that their theoretical transmutation calculations match the Miley, Patterson, et al. result in Figure 3 reasonably well (*29*).

Downloaded by UNIV OF GUELPH LIBRARY on July 2, 2012 | http://pubs.acs.org
Publication Date: August 1, 2008 | doi: 10.1021/bk-2008-0998.ch009

Excess Heat and Charged Particle Emission

Excess Heat Produced During Thin-Film Electrolysis with Transmutations

Over the last decade there were numerous reports concerning "excess" heat generation in the electrochemical cells with Pd or Ni cathodes. It was claimed that the bulk Pd cathode may generate some excess heat in heavy-water-based alkaline electrolyte (*30, 31*), both in open cells and in closed-type cells with a recombiner. At UIUC we have successfully demonstrated that excess heat production can occur with the same electrolytic cells where transmutations were measured as described earlier. Thus, the excess heat is assumed to be related to the exothermic character of the transmutation reaction.

In order to generate excess heat with a Pd cathode, a certain parameter regime is required to achieve high current densities and over-potentials, high loading ratio (x = D/Pd), and high deuterium diffusivity. Special treatment of the cathode samples (annealing, etching) is also important (*32*). Excess heat generation was found for electrolysis of massive Ni-cathodes in the H_2O-based electrolytes (*33, 34*). Heat production in the Ni-H system has been studied much less than in Pd-D. In the latter case possible heat generation has been attributed to formation of Ni-hydride β-phase under special loading conditions. At the same time it is well known that high loading for Ni samples is more difficult to obtain than that for Pd (*35*). Thus, the reproducibility of heat production in the Ni-H system with massive cathodes is generally regarded to be poor. Indeed this irreproducibility and the relatively low level of heat production when observed in Pd or Ni-cathodes during electrochemical loading has prompted some to propose alternative “trivial” explanations, e.g. gas H_2+O_2 recombination and/or changes in the faradic efficiency of open-cell electrolysis due to the cathodic polarization of Pd (*36*).

In view of this history, we decided to study heat generation in metal-hydrogen electrochemical systems using thin-metal film cathodes on dielectric substrates to increase the experimental repoducibilty (*37*). The advantages of the thin-film cathodes include: (i) a very short time is required to achieve as high hydrogen loading due to small metal thickness; (ii) an effective hydrogen flux reflection occurs at the Pd-dielectric interface from the dielectric side, increasing the effective concentration of hydrogen around the interface; (iii) the H-diffusion flux is increased concurrently with the very large input power density W_{in} possible with tin films (*32*) (e.g., with thickness of 2000 A, typically $W_{in} \sim 10^3$-10^4 W/cm^3 occurs).

In the work described here, a sensitive open-type calorimeter was used with Pd-Ni thin-film cathodes sputtered on an alumina dielectric substrate. During electrolysis in 1-M Li_2SO_4/H_2O with a Pt-wire anode, reproducibly generated heat was at ~20-25% of the input power during long time runs (*38*). The electrode configuration is essentially the same as that shown in Figure 4. The magnitude of excess heat observed over such a long run time cannot be explained by conventional chemical mechanisms, including H_2+O_2 recombination.

Experimental Technique – Excess Heat

In order to detect heat evolution during electrolysis runs, a high sensitivity open-type calorimeter is employed. This calorimeter consists of a large constant temperature water bath (30 liters of water) in which four double-wall glass cells are immersed. During the experiments the bath temperature was strictly stabilized with a circulating bath water device and precisely fixed at the point of 28.0 ± 0.05°C. Each cell was covered by a rubber cap and provided with two thermistors, magnetic stirrers (to exclude thermal gradients which can essentially distort the actual temperature in the cell due to convection), and a plastic cathode-holder to maintain the cathode inside the electrolyte. All thermistors were calibrated with a sensitive mercury thermometer. The uncertainty of this calibration was <0.1 °C. The temperature difference $\Delta T = T_x - T_0$ between the thermistors inside the cells (T_x) and the bath temperature (T_0) was monitored and recorded every five minutes.

Calibration of cells in the range of 0.05-5.0 W input power was carried out using a standard R = 70 ohm resistor. The calorimeter’s time constant (time for stabilization of the temperature after a change in input power) was ~4 hrs. The average resistor-calibration error was <25 mW. Measurements show a high sensitivity of 200 ± 25 mW/°C or 5.0°C per 1 W of input electric energy.

Downloaded by UNIV OF GUELPH LIBRARY on July 2, 2012 | http://pubs.acs.org
Publication Date: August 1, 2008 | doi: 10.1021/bk-2008-0998.ch009

To account for the actual ohmic heating of the electrolyte due to electrolysis (potential drop due to electrical resistance of electrolyte, cathode, anode, and electric circuit), the water dissociation potential (WDP) is subtracted from the electrolysis voltage. The minimal WDP value for oxygen acid salts electrolyte (*38*) can be estimated as:

$$U_0 = U_{th} + \eta_0 \qquad (1)$$

Here $U_{th} = 1.48$ V is the thermal neutral dissociation potential and η_0 is the sum of cathode and anode over-potentials (for a Ni(cathode)-Pt(anode) pair: $\eta_0 = 0.58$ V; for a Pt-Pt pair: $\eta_0 = 0.53$ V and so on). Direct experimental measurements of WDP (using volt-ampere characteristics in the cell measured between cathode and anode) performed for these electrode pairs show a good agreement (within the 5% of the theoretical value of U_0 values from equation (1)).

A double-layer Pd/Ni thin film sputtered on ceramic Al_2O_3 substrate was used as a cathode (*40*). The flat substrate had an area S = 12.5 cm^2 as cut from a ceramic plate of 1 mm thickness and roughness of 8-10 kÅ. After chemical and ultrasonic cleaning of substrate plates, magnetron sputtering of ~8000 Å Pd was performed at a rate ~ 0.41 Å/s. A 1000 Å thick Ni film was then sputtered on the top of the Pd film. Next the samples were annealed in high vacuum ($p = 10^{-7}$ tor) at t = 800 °C for 4 min using low heating and cooling rates.

Results – Excess Heat

To check actual performance, reference electrolysis runs (with alumina/Pd-Ni samples) were done including heat convection, bubbling, electrode's geometry, and positioning, as well as H_2+O_2 recombination. Smooth Pt sheets were used as cathodes in these runs, since Pt is known not to produce excess heat in the light-water electrolysis (*32*). The cathode Pt sheets were attached to the surface of a standard alumina substrate in order to simulate the heat-producing electrode geometry. Three different Pt-wire anode types were fixed at different distances from cathode Pt-sheets: (I) long-straight wire parallel in front of the center of the cathode surface (cathode-anode distance 10 mm); (II) loop-like wire coil parallel in front of the cathode surface and separated by 25 mm distance from the cathode; (III) hook-like coil 25 mm above the cathode surface. Reference runs were performed in 3 cells containing the same cathodes and anodes (I-III) with input power ranging from 0.1-3.0 W. The performance of these runs at various current (50-600 mA) is defined by the calorimeter "heat recovery" value R as follows:

$$R = P_{th}/I(U-U_0) \qquad (2)$$

Downloaded by UNIV OF GUELPH LIBRARY on July 2, 2012 | http://pubs.acs.org
Publication Date: August 1, 2008 | doi: 10.1021/bk-2008-0998.ch009

Here, P_{th} is the thermal power measured in calorimeter by thermistors; I and tsignificant excess heat, so R≈100%. That is, the thermal power generated is solely due to ohmic/Joule heating of the electrolyte by applied current and voltage. If R>100% for Pt/Pt electrodes it indicates that there is H_2+O_2 recombination. If R<100%, an incorrect calibration or increase of WDP (U_0) due to an anomalous increase in the cell inner resistance is suggested.

The results of experiments in cells I-III with the same Pt-cathodes and different Pt-anode configurations described above are presented in Table II (averaged by 50-600 mA current heat recovery values R). As seen, the R value closest to 100% was in cell II with a loop-like anode. Heat recovery R in cells I and III is larger than 100%, suggesting that H_2+O_2 recombination is not negligible. For anode I in cell I the recombination contribution would be about 16%, while for anode III in cell III it is about 10%. In contrast to these "bad anode geometries" (cells I and III), cell II shows that recombination contribution is ≤ 3.0%. Increasing the cathode-anode distance by 25 mm in cell I leads to a decrease in R from 116 to 108%. Thus, the "best" arrangement of the anode is taken to be II.

Downloaded by UNIV OF GUELPH LIBRARY on July 2, 2012 | http://pubs.acs.org
Publication Date: August 1, 2008 | doi: 10.1021/bk-2008-0998.ch009

Table II. Parameters of Electrolysis and "Heat Recovery" R for Pt-Pt Reference Runs in Cells I-III

Cell # / parameter	*M (Li_2SO_4/H_2O)*	*x, mm*	*R, %*
I	1.0	10.0	116.0 ± 6.2
I	1.0	25.0	108.0 ± 7.1
II	1.0	25.0	102.5 ± 5.0
II	0.8	25.0	101.5 ± 6.0
III	1.0	25.0	110 ± 5.5
III	1.2	25.0	110 ± 6.5

NOTE: Here, M is a molarity of electrolyte; x is the distance between the cathode and anode; R is the heat recovery of the cell, averaged by applied current (ranging from 50-600 mA) as defined by Eq. (2).

In the other reference experiments with the Pt-Pt electrodes, possible changes in electrolyte concentration were evaluated. Electrolysis runs carried out in electrolytes with different molarities show a quite constant R at Li_2SO_4/H_2O concentrations within 0.8-1.2 M (Table II). Such large changes could only be associated with evaporation of 20% volume of the cell. Therefore, changes in the electrolyte concentration during the cell operation do not significantly affect the heat recovery R.

Note that substitution of thermal-neutral dissociation potential U = 1.48 V (without accounting for electrode over-voltages) in Eq. (2) for cells I-III leads to a drastic decrease in R below 80%. This fact indicates that the electrode over-potentials cannot be neglected, at least for calorimetry measurements at current densities $j \geq 10$ mA/cm^2.

Heat generation experiments for alumina/Pd-Ni cathodes (foreground runs) were carried out at constant electrolysis current ranging from I =100-600 mA (j = 8.5-50.0 mA/cm^2) corresponding to a cell voltage U = 3.5-5.5 V. To calculate Joule heating of the electrolyte P* the effective WDP value U_0 = 2.06 V is used in Eq. (2). This U_0 corresponds to a Ni(cathode)/Pt(anode) electrode pair WDP (1000 Å Ni film used on the top of the Pd layer).

Typical kinetics of the heat measurement (P_{th} vs. elapsed time t) are presented in Figure 8. As seen after t > 2 hrs, the thermal yield P_{th} exceeds Joule heating P*. The maximal heat recovery R of 135% occurs at electrolysis current I = 100 mA (j = 8.0 mA/cm^2), while the corresponding absolute value of excess heat production is W_{ex} = 60 ± 28 mW. Increasing the current density to 48 mA/cm^2 leads to a decrease in heat recovery R from 135 to 115%. In typical cases the excess heat evolution from the cathode at I = 200 mA continues for ~15 days. The decrease in R during a long run is accompanied by an increase in cell voltage. This suggests an increase in the cell inner resistance due to defects and micro-crack generation in Pd/Ni cathode. Still the cathodes survive, i.e., the films did not detach from the alumina substrate during these long runs. Thermistor calibration runs repeated immediately after this run show that calorimeter parameters (including ΔT vs. W_{in}) did not change during the time of operation (15 days). This gives proof of the stability of the calorimetry system and supports the occurrence of the excess heat measurements.

Downloaded by UNIV OF GUELPH LIBRARY on July 2, 2012 | http://pubs.acs.org
Publication Date: August 1, 2008 | doi: 10.1021/bk-2008-0998.ch009

Error Analysis – Excess Heat

The main errors of open-type calorimetry are associated with calorimeter accuracy as well as with gas recombination. As noted earlier the recombination limit for the cell II-type configuration is estimated to be <3.0% of the input power. Other possible sources of errors are associated with parametric variations, e.g., thermistor accuracy, oscillation of bath and ambient temperatures, appearance of thermal gradients, and change in electrolyte volume due to evaporation. Results for the calorimetric accuracy with respect to the precision of excess heat measurement are summarized in Table III. The total average error of heat measurement, in accordance with error propagation, does not exceed $< \sigma_t > = \pm 30$ mW. In an actual experimental performance at low input power ($W_{in} < 1.0$ W) this error is $<\sigma_l> = \pm 20$ mW, while at high input power range ($W_{in} > 1.0$ W) it is twice as large: $<\sigma_h> = \pm 40$ mW.

In summary, comparison of calorimetry errors with excess power obtained in runs with the alumina/Pd-Ni cathode (as well as the theoretical analysis of oxygen reduction in the electrolytic cell) confirms that the excess heat measured is well above the error limits set by both the calorimetry accuracy and possible gas recombination. This result confirms that experiments producing a "fission

Downloaded by UNIV OF GUELPH LIBRARY on July 2, 2012 | http://pubs.acs.org
Publication Date: August 1, 2008 | doi: 10.1021/bk-2008-0998.ch009

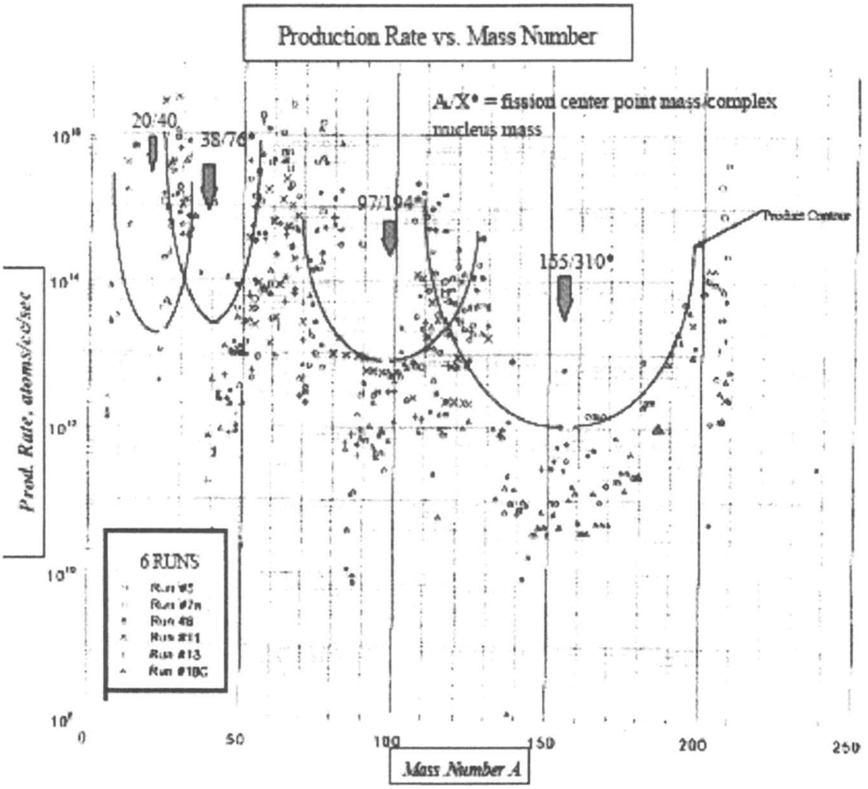

Figure 8. Reaction product yield vs. mass curve [10].

Table III. Sources of Errors with Respect to Accuracy of Calorimetry Measurements

Error source	*Accuracy/Precision*	*Error value, mW*
Thermistors	0.1°C /0.02 °C	± 5.0
Bath Temperature	0.05 °C	±13.0
Thermal Gradients	0.02 ° C	±5.0
Ambient temperature	0.02 °C/°C	± 20.0
Electrolyte evaporation	< 5.0 ml	< 3.0 %
Total Error $\langle\sigma_t\rangle$		± 30.0

Table III. Sources of Errors with Respect to Accuracy of Calorimetry Measurements

Error source	*Accuracy/Precision*	*Error value, mW*
Thermistors	0.1°C /0.02 °C	± 5.0
Bath Temperature	0.05 °C	±13.0
Thermal Gradients	0.02 ° C	±5.0
Ambient temperature	0.02 °C/°C	± 20.0
Electrolyte evaporation	< 5.0 ml	< 3.0 %
Total Error $<\sigma_t>$	-	± 30.0

Downloaded by UNIV OF GUELPH LIBRARY on July 2, 2012 | http://pubs.acs.org
Publication Date: August 1, 2008 | doi: 10.1021/bk-2008-0998.ch009

like" transmutation product array have an excess heat associated with the reactions. Further, as discussed in the next section, as might be anticipated, the excess heat appears to be correlated with the mass defect between reaction and product atoms.

Correlation between Transmutation Products and Excess Heat

Considerable research effort has been devoted to the establishment of a correlation between He-4 and excess heat from D-D reactions postulated to occur in Pons-Fleischmann-type cold fusion cells. Good progress has been made and recent measurements of the reaction product He-4 have achieved levels where background helium is a less significant factor in interpretation of the results (*41*). These results indicate, with a reasonable confidence level, that a direct correlation exists between He-4 production and excess heat, supporting the D-D reaction hypothesis.

In contrast, in the case of LENRs, a variety of reaction products (isotopes) with masses both higher and lower than that of host electrode material imply that proton-metal initiated reactions occur (*10, 42*). Miley et al. (*38, 42, 43*) considered the possible correlation of these reaction products with the excess heat observed in these experiments. These results are briefly reviewed here.

Reaction Pathways and Reaction Product-Heat Relationship

Due to the rich variety of reaction pathways in these LENR experiments, the reaction product-heat relationship is less useful for specifying a dominant reaction than He production in D_2O-Pd cells. Still, the data provide important circumstantial evidence about the reacting species, hypothesized here to be protons-metal atoms for LENRs.

The LENR reaction products measurements at UIUC were described earlier and summarized in Figure 3. The products are replotted in Figure 8 to emphasize that a variety of reaction products occur with masses lying well below and above that of the base electrode metal (Ni and Pd in this figure) and the pattern appears to evolve from fisson of four main compound nuclei.

A striking pattern consistently observed in these measurements is that the high-yield reaction products occur in four mass ranges, roughly A = 20-30, 50-80, 110-130, and 190-210 (*43*). Statistically significant shifts in isotope ratios from natural abundance are also observed for many of the products (*10, 42)*. As stressed earlier, numerous precautions were taken to guard against impurities in these measurements (*10, 42*). This includes use of special "clean" systems, blank runs, and precision diagnostics prior to and following runs. Consequently, the high-yield products (> 10^{13} atoms/cc-sec in Figures 3 and 8) are well above background impurity limits. For example, the yields of the high-yield products such as Ag and Cu in thin-film Ni cathodes typically exceeded the total amount (in weight) of impurity Ag and Cu found in the total system (including both the electrodes and the electrolyte) by one or two orders of magnitude. Some uncertainties due to possible impurities still plague measurements of the lower-yield products (<10 atoms/cc-sec in Figures 3 and 8). However, the present analysis is mainly dependent on the mass changes of high-yield products. Thus, the uncertainties for low-yield species are not a concern here.

As noted earlier, the general trends from these results are reasonably consistent with reaction product measurements by other workers (see discussion and references in *43, 44*). However, others have often viewed their work as pure "transmutation studies." For that reason, these workers have not generally focused on quantitative product yields or on correlations with heat.

Downloaded by UNIV OF GUELPH LIBRARY on July 2, 2012 | http://pubs.acs.org
Publication Date: August 1, 2008 | doi: 10.1021/bk-2008-0998.ch009

Energy/Nucleon Balances

The measurements of reaction products used analytic techniques that were benchmarked via neutron activation analysis techniques to allow a determination of absolute values of the yields as well as trends. The "production rates" shown represent a time average over the experiment run-time since, with the present experimental arrangement, it was only possible to take samples at the beginning and end of a run. Likewise, the excess heat reported represented an average over the run, so that a comparison of these two results is consistent.

To examine a possible correlation, the measured product yields are used along with their respective binding energies to compute a theoretical "excess power," W_{excess}, as shown in Figure 9.

The computation is straightforward but tedious due to the large number of reaction products produced. Basically, $W_{energies}$ is computed by taking the product of all the isotope yields times their binding energies and subtracting the corresponding product for the "fuel." A key point is the determination of the amount of original material that is consumed or "burned up." Since the decrease in the number of original metal atoms in the cathode is a small fraction of the original atoms, a direct measurement becomes imprecise (vs. the measurement of new isotopes that differ from the base electrode material itself). However, the

$$\left[\sum_{RPs}\left(RP * BE/n\right) - \sum_{\substack{metal\,atom,\\ p\,burned}} \left(fuel * BE/n\right)\right] / run\ time = \mathrm{P}_{out}$$

$$\Xi\ W_{excess}$$

Figure 9. Computation of excess power from measured reaction products and binding energies where: RP = reaction product yield or atoms of product formed nuclei; BE/n = binding energy per nucleon for RP or fuel; fuel = metal nuclei + protons reacted (from nucleon balance); and p = proton.

Downloaded by UNIV OF GUELPH LIBRARY on July 2, 2012 | http://pubs.acs.org
Publication Date: August 1, 2008 | doi: 10.1021/bk-2008-0998.ch009

number "consumed" can be obtained from the measured products by invoking the basic requirement that nucleons are conserved in the reaction. A nucleon balance is performed by first computing the total number of nucleons in each of the measured reaction products. The basic assumption is that these nucleons come from the base electrode metal (e.g., Ni) plus the reacting protons. This calculation is done by first allotting the maximum number of reaction product nucleons to the metal nucleons. Then, any remaining nucleons are attributed to the protons, allowing for a variable proton/metal atom ratio to retain generality (*45, 46*). This balance rests on the assumption that the protons plus the electrode metal (e.g., Ni in this case) are the reactants in LENR cells. This follows since protons in the light-water electrolyte cannot react with themselves (as D-D reactions in heavy-water electrolyte). Otherwise, this result does not rely on a knowledge of the reaction mechanism itself.

A counterview might assume the "salt" employed in the electrolyte, e.g., Li_2SO_4, was involved in the reaction. However, there is no evidence for this in LENR reactions, and the fact that various workers have used different salts while still obtaining similar reaction products seems to rule out this possibility.

Product yield results from three runs (run numbers refer to experiments described in Ref. (*10*)) where adequate information was available for this type of evaluation are summarized in Figure 10.

As seen from this figure, reasonably good agreement is obtained between the excess power measurement and the calculated values using the binding energy calculations described here. Two of the results show quite close agreement, but one has a mean measured value that is a factor of two larger than the calculated value. While these results are not definitive, still, in view of the many uncertainties in both of the calculated values (due to uncertainties in the yield measurements) and in the experimental calorimetry, the agreement obtained strongly suggests a relation between products and excess heat.

More studies of this type are clearly needed to fully confirm the validity of this correlation. Still, this result, combined with the reaction product data itself,

Run Number (Ref. 10, 41)	***Excess Power (W)***	
	Calculated	Measured
#7	1.9 ±0.6	4.0 ±0.8
#8	0.5 ±0.2	0.5 ±0.4
#18	0.7 ±0.3	0.6 ±0.4

Figure 10. Results from energy balance calculations for three earlier thin-film experiments. All experiments used Li_2SO_4 in H_2O for the electrolyte and thin-film Ni coated cathodes.

provides added evidence that proton-metal reactions are responsible for the anomalous isotope and heat phenomena observed in LENR experiments. The situation where heavy water is used instead of light water, as reported in some other LENR studies (e.g., *44*), is less clear but again appears to involve proton-metal reactions. In that case, p-metal reactions could occur simultaneously with D-D reactions. More study is needed to resolve possible reactions involved in this important regime.

Another way of viewing these data is to calculate the energy released (the observed excess heat times the run time) and divide by the number of Ni atoms reacted (based again on the number of nucleons associated with the measured quantities of reaction products observed). Then, for the runs of Figure 10, an energy release on the order of 150 keV/Ni atom reacted is obtained. This large value is consistent with nuclear as opposed to chemical processes. It is several orders of magnitude less than the energy released in neutron-induced fission, but is roughly in the range of "soft" fission releases predicted for LENR conditions (*47*).

These results also bear on an issue that is often raised about the LENR experiments: how can a positive excess power occur since the base metal involved, such as Ni, has a binding energy per nucleon near the peak of the binding energy-mass curve? In the present analysis this can be explained by noting that the "fuel," i.e., the reactants, are a mixture of protons and metal. Then the average binding energy of the reactants (p + metal) is reduced below that of the metal alone. As a result, there is an expanded range of reaction product masses lying around the mass of the base metal that offer a positive energy release, i.e., a positive Q-value for the reaction. Still, the fact that some reaction products lie outside of this range might seem to imply that reactions occur despite a negative Q-value, but then a very large input energy would be needed to drive the reactions. This dilemma is overcome, however, if the

Downloaded by UNIV OF GUELPH LIBRARY on July 2, 2012 | http://pubs.acs.org
Publication Date: August 1, 2008 | doi: 10.1021/bk-2008-0998.ch009

reaction occurs through multi-step excitation and/or formation of a compound nucleus which can split up or fission into a variety of reaction products of different masses (*10, 47*). The energy balance requirement is that the formation energy of the compound nucleus must be supplied. Subsequently, the break-up energy is, in effect, shared among products.

Charged Particle Production During Thin-film Electrolysis

In order to obtain further proof for nuclear reactions (*37*) during thin-film cathode electrolysis, a search for emission of nuclear particles was undertaken. Earlier, using various Si surface barrier (SSB) detectors, including a dE-E telescope, Lipson et al. studied the emission of charged particles accompanying exothermic deuterium (hydrogen) desorption in Au/Pd/PdO:D(H) heterostructure (*48*). A new phenomenon, alpha particle generation in the energy range of $8.0 \leq E_\alpha \leq 14.0$ MeV after electrolytic loading of Au/Pd/PdO electrodes (either by deuterium or hydrogen) was discovered.

This range alpha emission was observed after the electrochemical loading of Pd with deuterium/hydrogen. Thus, it was of great interest to expand such to in-situ measurements during the electrolysis process. Unfortunately, it is hard to apply electronic SSB and X-ray detectors directly to the cathode during electrolysis experiments. Thus, a technique using non-electronic detectors (CR-39 and TLDs) was employed, as described next.

Experimental Technique – Charged Particles

The thin Pd-film cathodes and electrolysis procedure are described in (*49*). For charged particle detection the purified "Radtrack" CR-39 plastic track detectors (2.0×1.0 cm^2) by Landauer Inc. have been used. Special purification procedures utilized for detector manufacturing as well as hermetic saving condition allow the initial alpha track density of these CR-39 to be minimized to less than 10 cm^{-2}.

These detectors were calibrated with alpha-sources (in the range of 1.6-7.7 MeV) and by monoenergetic cyclotron alpha-beams (in the energy range of 10.0-30.0 MeV) as well as by proton beams with energy ranging from 2.0-3.0 MeV. (Figure 11). For energetic proton detection the detectors were also calibrated with Van de Graaff accelerator by monoenergetic proton beams (energy ranging from $0.75 \leq Ep \leq 3.0$ MeV) (Figure 12).

After the beam exposure, detectors were etched in 6N-NaOH at t = 70°C for 7 hours and investigated with an optic microscope. A picture of alpha-tracks is presented in Figure 13. Tracks from bombardment with a monoenergetic beam of alphas from a cyclotron exhibit an almost ideal circle-like shape. These nuclear tracks can be easily distinguished from the defects of CR-39 subsurface structures.

Downloaded by UNIV OF GUELPH LIBRARY on July 2, 2012 | http://pubs.acs.org
Publication Date: August 1, 2008 | doi: 10.1021/bk-2008-0998.ch009

Downloaded by UNIV OF GUELPH LIBRARY on July 2, 2012 | http://pubs.acs.org
Publication Date: August 1, 2008 | doi: 10.1021/bk-2008-0998.ch009

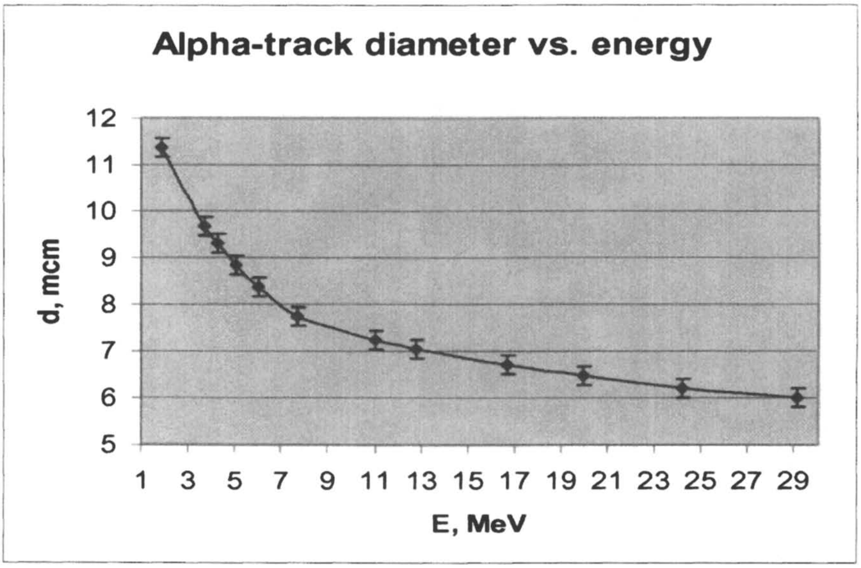

Figure 11. Energy range study for alpha-sources.

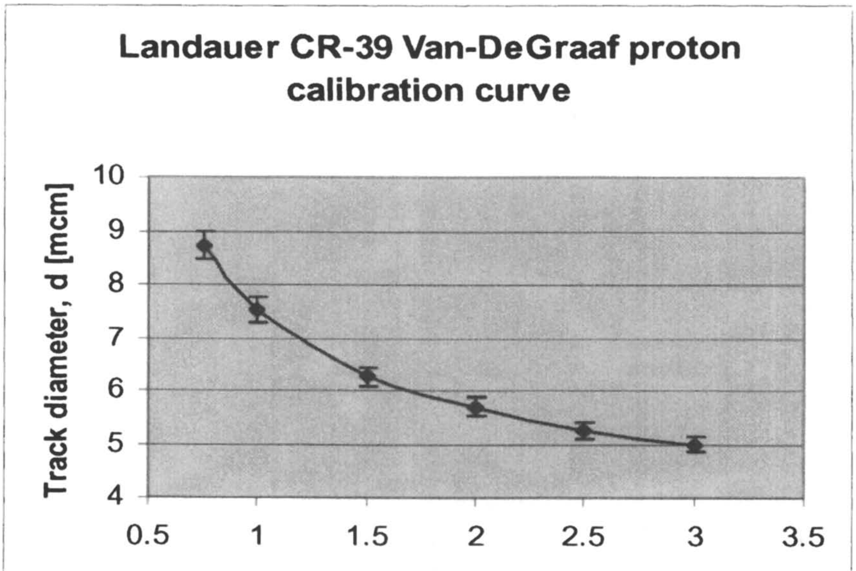

Figure 12. Landauer CR-39 Van de Graaff proton calibration curve.

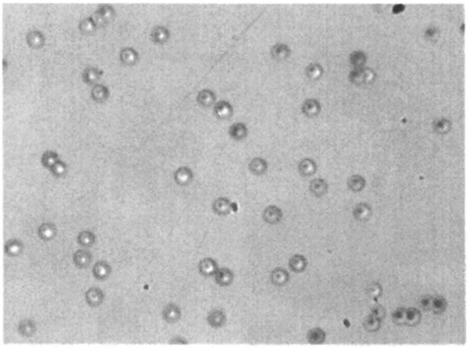

Figure 13. A typical alpha-track picture as seen under a microscope.

Downloaded by UNIV OF GUELPH LIBRARY on July 2, 2012 | http://pubs.acs.org
Publication Date: August 1, 2008 | doi: 10.1021/bk-2008-0998.ch009

The efficiencies of CR-39 detection with respect to different energy alphas and protons were estimated in accordance with their "critical angle" θ_c determined by the formula (*50*): $\theta_c = \sin^{-1}\{[1-(d_E/2h)^2]/[1+(d_E/2h)^2]\}$. Here d_E is the track diameter produced by a charged particle with energy E, and h = 9.1 μm is the depth of the etched layer in CR-39 under our etching conditions. Knowledge of the critical angles calculated from the above formula allow a determination of the efficiency ε of the charged particle detection by:

$$\varepsilon = \tfrac{1}{2}(1-\sin\theta_c) \qquad (3)$$

In electrolysis experiments the freshly opened CR-39 detector chips were attached either to the Pd thin-film cathode (foreground) or to the substrate side and/or immersed in electrolyte in the cell (background). Background experiments showed proportional growth of track density vs. time for CR-39 immersed in electrolyte (Figure 14). With a large background duration, two separate alpha-peaks with track diameters located at 8.0 and 9.0 μm, respectively, are observed in Figure 14. The energy positions of these peaks are in good agreement with conventional alpha-background and are normally corresponded to about 7.0 MeV radon (8.0 μm) and 5.0 MeV (9.0 μm) thoron series of natural alpha-nuclides.

In order to energy-analyze high-energy alpha and low-energy proton tracks, thin Cu foils (25 μm thick) were inserted between the cathode metallic coating and the CR-39 surface. A 25 μm Cu film completely absorbs all alpha particles and protons with energies below 9.0 and 2.3 MeV, respectively. Background measurements in experiments with Cu-covered CR-39 were performed similarly to that with uncovered detectors. As expected, these background experiments showed a significant reduction (~2 times) in the total track density (Figure 15).

Single-crystal TLD detectors (Landauer Inc.) covered with 50 μm polyethylene film were applied to the Pd surface of electrodes for in-situ detection of

Downloaded by UNIV OF GUELPH LIBRARY on July 2, 2012 | http://pubs.acs.org
Publication Date: August 1, 2008 | doi: 10.1021/bk-2008-0998.ch009

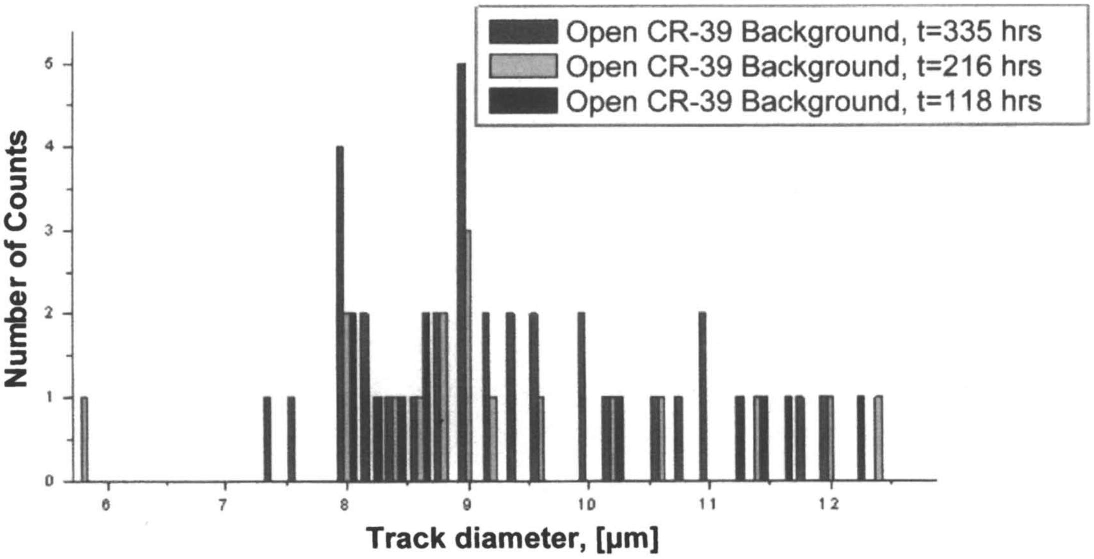

Figure 14. Alpha peak at large background duration for open CR-39.

Downloaded by UNIV OF GUELPH LIBRARY on July 2, 2012 | http://pubs.acs.org
Publication Date: August 1, 2008 | doi: 10.1021/bk-2008-0998.ch009

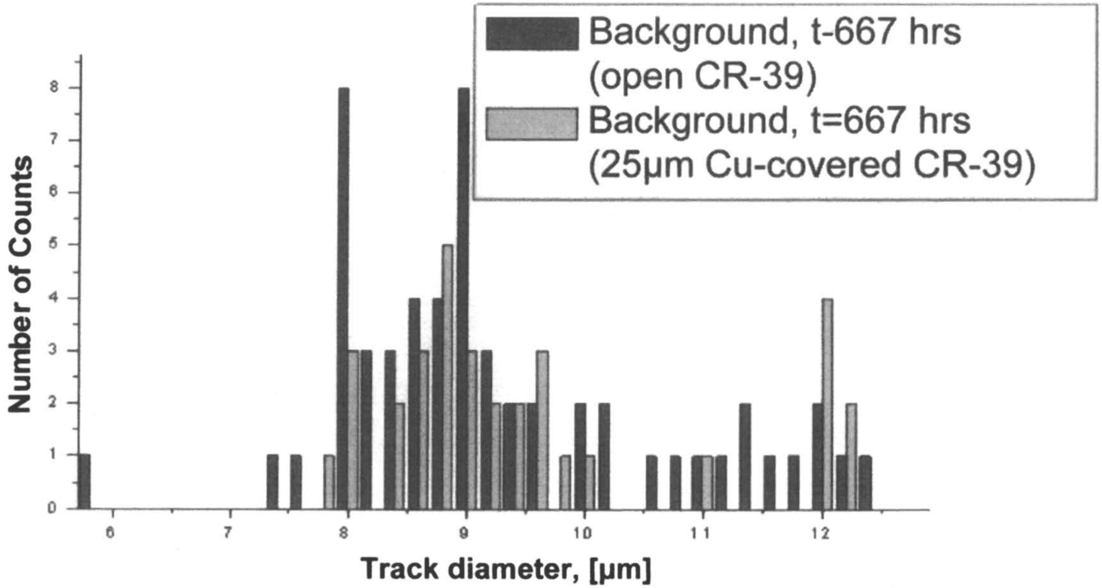

Figure 15. Background measurement with a Cu film covering the CR-39.

expected soft X-ray radiation during electrolysis. The background TLD was immersed at the bottom of the employed electrolytic cell. The TLD reading was carried out by Landauer Inc. The nominal sensitivities of TLD used (with a size of $S = 2.0 \times 2.0$ mm^2) with respect to absorbed dose of the soft X-ray photons (with energy $E_x \geq 2.0$ keV) was in the range of 0.1 (Al_2O_3:C) by the 1.0 (LiF) mrad. However, in fact, due to about 2 months' storage prior to use, initial background levels of the TLD detectors were about 10.0 mrad and 4.0 mrad for Al_2O_3:C and LiF, respectively. Thus, actual sensitivity of TLD in electrolysis experiments did not exceed 1-2 mrad.

Experiments on detection of nuclear products during electrolysis runs were carried out using both open and Cu-shielded CR-39 chips and foreground TLD detectors, all attached to the same thin-film cathode. Two background CR-39 (open and Cu-shielded) and background TLD were also fixed inside the electrolyte to measure the background.radiation. The charged particle and X-ray detection were carried out simultaneously with excess heat measurements in the open-type calorimeter described earlier. The electrolysis current and duration were normally in the range of 50-400 mA and 2-3 days, respectively.

Downloaded by UNIV OF GUELPH LIBRARY on July 2, 2012 | http://pubs.acs.org
Publication Date: August 1, 2008 | doi: 10.1021/bk-2008-0998.ch009

Results – Charged Particles

The runs with electrolysis of Pd thin-film cathode-exposed CR-39 detectors (t~2.0-30 days) showed the appearance of unusual diameter tracks that were not observed in background detectors exposed in the same electrolytic cell. Indeed, in the track diameters distribution N(d), two significant peaks located at 7.0 mm and 6.0 mm were observed in the runs (with electrolysis) with opened CR-39 detectors (Figure 16). At the same time, almost no tracks with d < 7.5 mm were found in the corresponding background runs for detectors exposed in the same electrolytic cells. The low-diameter tracks appeared to accompany electrolysis of the thin Pd-film and Pd-black cathodes. The intensity of charged-particle emissions and ratio between 6.0 and 7.0 μm peaks during electrolysis strongly depends on the cathode history and structure.

It should be stressed that generation of charged particle emissions during the electrolysis of thin Pd cathodes has a good reproducibility. In the control experiment with CR-39 detector attached to the thin-film NiO_x (obtained by annealing of an alumina/Ni (4000A) sample in air atmosphere) with a very low electrolysis current (I~1.0 mA), no tracks with d < 7.8 μm were detected (Table IV). This occurred despite applying a high (U~10.0 V) voltage.

In the foreground runs with the same cathode being carried out with 25-μm Cu film-shielded CR-39 chips, the 7.0 and 6.0 mm peaks disappeared. However, peaks ranging from 7.5-11.4 mm appeared that were not found in Cu-shielded background detectors (Figure 17).

The experiments with Cu-shielded detectors and a knowledge of CR-39 calibration curves (Figures 11, 12) allow an identification of the energy and type of particles emitted in the foreground runs. Taking into account stopping powers

Downloaded by UNIV OF GUELPH LIBRARY on July 2, 2012 | http://pubs.acs.org
Publication Date: August 1, 2008 | doi: 10.1021/bk-2008-0998.ch009

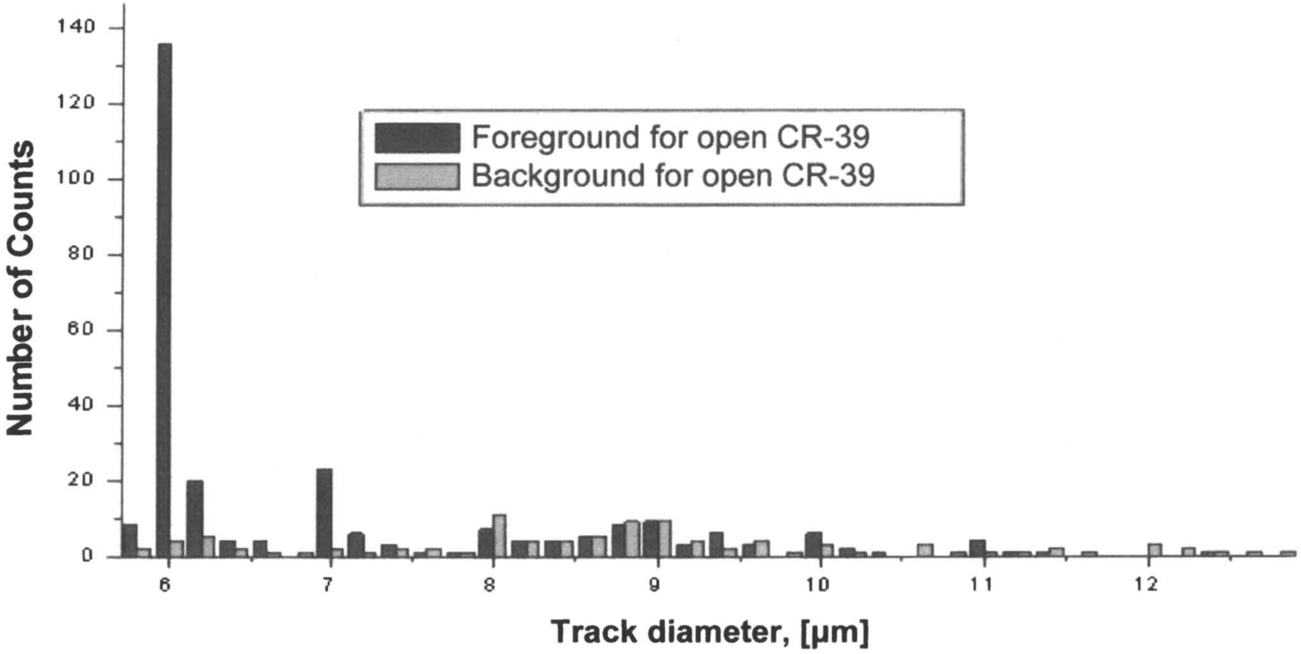

Figure 16. Foreground and background runs for CR-39 study.

Downloaded by UNIV OF GUELPH LIBRARY on July 2, 2012 | http://pubs.acs.org
Publication Date: August 1, 2008 | doi: 10.1021/bk-2008-0998.ch009

Table IV. Charged Particle Emissions (Alphas and Protons with Background Subtraction) During Electrolysis of Metal Thin-Film Cathodes, Measured Using CR-39 Detectors (X-ray doses were also measured using TLD detectors)

Sample	Glass/Pd(2000A)	Alumina/Pd (4000A)	Pt/Pd-black, Electroplated	Pd/Cu/Pd, electroplated	Alumina/NiOx
Time of exposure [hrs]	48	118	216	802	118
History of sample	Pd-coating fractured for 48 hrs. No excess heat	Survived, Excess heat, $E_{ex} \sim 20$ %	Pd-black partially detached, $E_{ex} \leq 8.0\%$	Survived. No excess heat	Survived. No electrolysis at the Ni-surface. No excess heat
$<N_\alpha>\times 10\text{-}4$, $[s^{-1}*cm^{-2}]$	4.8 ± 1.0	6.9 ± 1.2	0.80 ± 0.28	0.18 ± 0.08	0.0
$<N_p>\times 10^{-4}$, $[s^{-1}*cm^{-2}]$	28.6 ± 4.1	16.0 ± 0.2	5.8 ± 0.9	0.24 ±0.11	0.0
$<N_p>/<N_\alpha>$ *ratio*	6.0	2.3	7.2	1.5	-
X-ray, dose [mrad], TLD	2.0 ± 1.0 (LiF) 0.5± 0.5 (Al_2O_3:C)	0.2 ±1.0 (Al_2O_3:C)	No TLD measurement	No TLD measurement	0.1 ± 1.0 (Al_2O_3:C)

NOTE: The mean CR-39 detection efficiencies for 11.0-16.0 MeV alphas and 1.5-1.7 MeV protons are calculated as: $<\varepsilon_\alpha> = 0.13$ and $<\varepsilon_p> = 0.10$, respectively.

Downloaded by UNIV OF GUELPH LIBRARY on July 2, 2012 | http://pubs.acs.org
Publication Date: August 1, 2008 | doi: 10.1021/bk-2008-0998.ch009

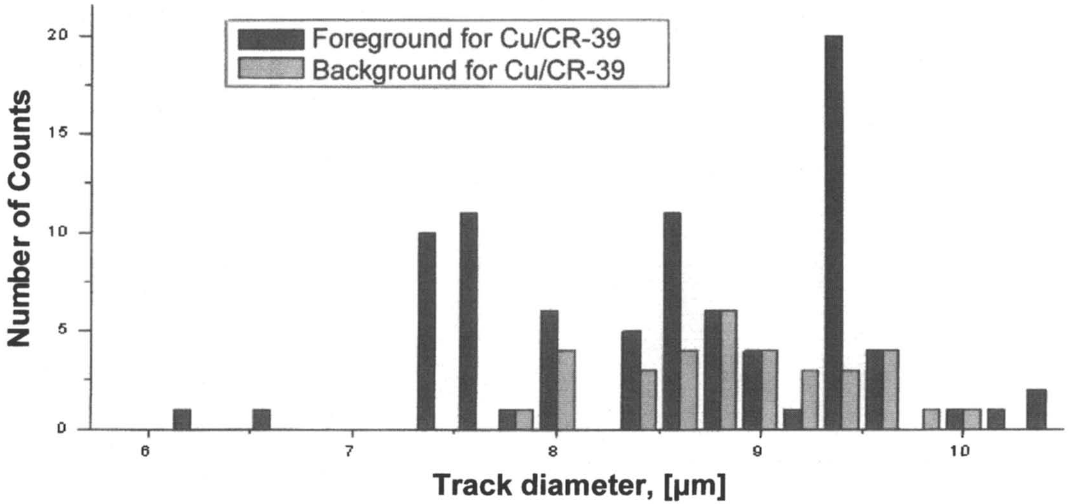

Figure 17. Foreground and background runs for Cu-covered CR-39 study.

and ranges of the 25 μm Cu film with respect to the alphas and protons with different energies, the initial energies of emitted particles were also calculated. Comparison of pictures obtained with open and shielded detectors shows that the 6 μm peak completely disappears while the broad peak near 7.0 μm in Figure 16 shifts to the larger-track diameters and is split at least by three narrow peaks (Figure 17). Disappearance of the 6.0 μm peak in a shielded detector suggests this peak is due to low MeV protons. Based on the cyclotron calibration data, the proton energy is estimated to be 1.5-1.7 MeV (Figure 18 a, b).

In contrast to the 6.0 μm peak, the 7.0 μm maximum can be ascribed to a broad 11-16 MeV alpha-peak. Indeed, the stopping range of alphas ranging from 11-16 MeV (for open CR-39) would be consistent with observed narrow bands with energies of 11.6, 12.5, and 14-16 MeV, respectively, for Cu-covered detectors (Figure 18a). Due to higher resolution of CR-39 alpha-tracks for the lower-energy particles (Figure 18b) the broad 11-16 MeV alpha band could be observed as single individual maximums after these particles pass through the Cu foil.

In conclusion, these results provide convincing evidence that thin-film Pd electrolysis produces a low-level flux of 1.5-1.7 MeV protons and 11-16 MeV alphas.

In contrast to charged particle results, the X-ray emission measurements were near background noise levels, making interpretation difficult. The best result was obtained for a Pd/glass electrode (that was completely destroyed during 2 days of electrolysis) with LiF TLD attached (the initial background level ~ 4.0 mrad). After background subtraction, the emitted X-ray influence was consistent with absorbed dose 2.0 ± 1.0 mrad. The experiments with the other cathodes and Al_2O_3:C TLD (Table II) do not show a statistically significant result, largely due to higher initial background levels (~10 mrad) for these TLDs. In accordance with the 2.0 mrad absorbed dose in LiF TLD, assuming the generation of 10.0 keV X-ray emission, the upper detection limit of X-ray emission yield in the cathodes employed is $Y_x = 5.0$ X-qunta/s×cm^2. Meanwhile, the expected level of X-ray Bremsstrahlung from emitted charged particles, including both protons and alphas (Figure 18a, b) is estimated as $N_x \sim 0.5\ s^{-1}\times cm^{-2}$. This level of X-ray emission is one order of magnitude below the detection limit of the TLD.

Thus, the X-ray measurement results suggest a weak emission of X-rays during the thin-film electrolysis. However, due to the low intensity levels involved, we cannot rule out the possibility that this X-ray emission is not due to some non-nuclear effect such as film stress fracture or detachment from the dielectric substrate.

Summary

This review shows that nuclear transmutations, excess heat, and charged particle emissions are frequently observed in LENR studies, and often

Downloaded by UNIV OF GUELPH LIBRARY on July 2, 2012 | http://pubs.acs.org
Publication Date: August 1, 2008 | doi: 10.1021/bk-2008-0998.ch009

Downloaded by UNIV OF GUELPH LIBRARY on July 2, 2012 | http://pubs.acs.org
Publication Date: August 1, 2008 | doi: 10.1021/bk-2008-0998.ch009

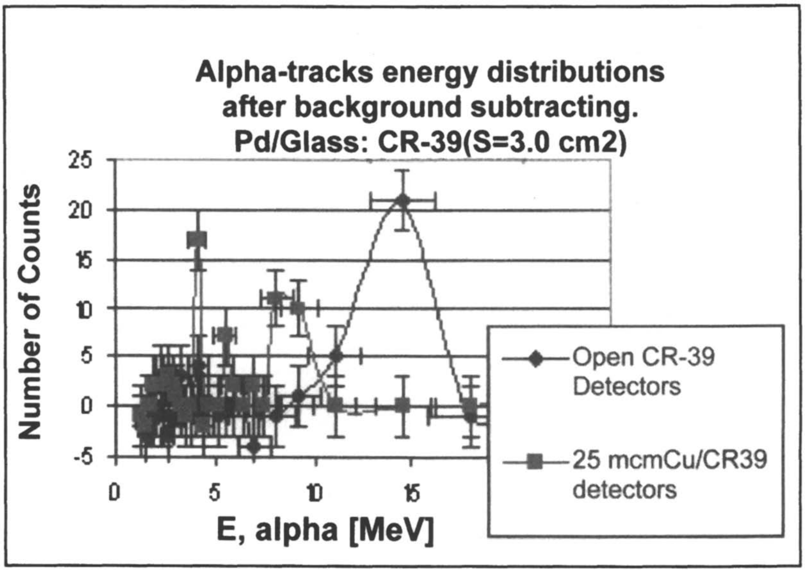

Figure 18a. Alpha-tracks energy distribution after background subtraction.

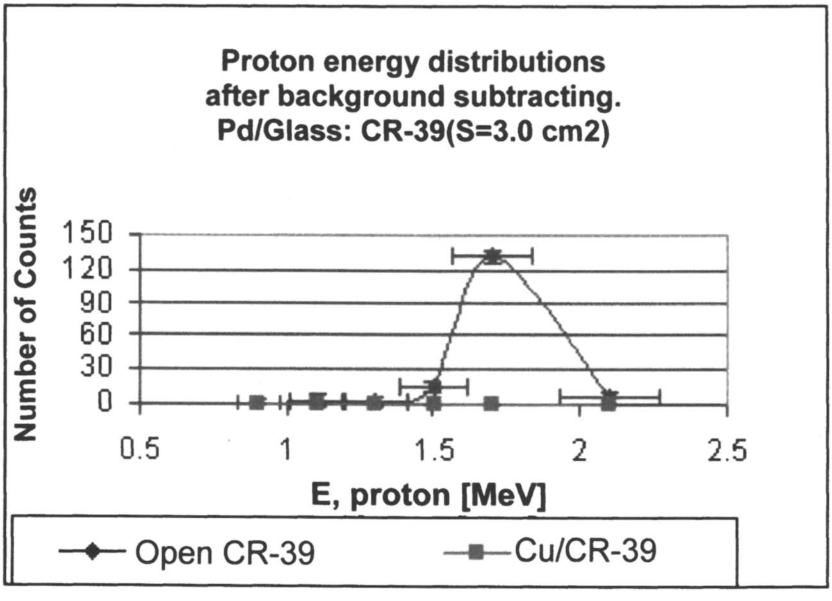

Figure 18b. Proton energy distribution after background subtraction.

simultaneously. The understanding of these reactions is gradually improving, both experimentally and theoretically, and this insight should accelerate the development of LENR for practical applications.

Transmutation reactions can be classified depending on the characteristic products. Some experiments yield a large array of products with mass numbers ranging across the periodic table. Other reactions give one or few distinct, isolated products. Studies carried out by Miley et al. (*10*) were of the former type and showed that higher-yield elements can occur in quantities well above maximum impurity limits in well-designed thin-film electrolysis experiments. Non-natural isotopic distributions were also found in these studies, further confirming a nuclear reaction source. The electrodes designed to study these effects at UIUC have shifted from using thin films on microspheres to thin films coated on a flat alumina substrate to allow a high current density and high proton flow rate. The uses of thin films remain a key ingredient in both geometries. Now, more recent electrode designs employing a Ni-fiber matt sandwiched between thin-film Pd layers have been developed to enhance desirable cluster reactions in the Ni felt nano-pore structure.

One of the best known experiments leading to single-species products, done by Iwamura et al., was also described. Their use of gas diffusion through a specially designed composite thin-film via gas diffusion, combined with in-situ XPS diagnostics, also provides strong protection against confusion with impurities.

It is noted that many laboratories worldwide are actively pursuing the study of transmutations in low energy nuclear reactions. Seventeen different laboratories were included in a brief review presented here (Table I). This emphasizes the strong evidence for the startling proposition that nuclear reactions can be created in solids using electrolytic D or H loading of metals such as Pd. The loading methodology and choice of electrode material varied in the studies surveyed, showing transmutations can be achieved in an amazing variety of experiments. Products with a mass lighter than the electrode material were most frequently found, but heavier elements were reported in a significant number of cases. Commonly reported elements are calcium, copper, zinc, and iron. Forty percent of the least frequently observed elements were from the lanthanide group, and it is widely accepted that these rare earth elements are less likely to be considered impurities. A number of studies also reported elements with a significant deviation from the natural abundance.

UIUC studies have also explored the possible production of excess heat associated with transmutations. Calorimetric measurements were carried out using the same electrodes and conditions employed for transmutation studies. Excess heat was consistently found for runs where the thin-film electrode remained in good condition throughout the run. No excess heat was measured if the metallic coating of the cathode sample was fractured and/or detached from the substrate, adding confidence in the calorimetric calibration. The best adhesion of Pd/Ni coating having a good film quality was achieved with alumina

Downloaded by UNIV OF GUELPH LIBRARY on July 2, 2012 | http://pubs.acs.org
Publication Date: August 1, 2008 | doi: 10.1021/bk-2008-0998.ch009

(with maximal roughness of about 10 kÅ) as a substrate. A special procedure involving high-vacuum annealing at t = 800°C was used to condition the electrodes prior to runs. Then the alumina/Pd-Ni electrode typically survived 2 weeks of electrolysis and produced an excess heat power reaching 20-25% of the input power, equivalent to 300 ± 30 mW.

Detailed energy and nucleon balance calculations were done for LENR experiments where reaction products were quantitatively measured to correlate yields with the excess heat measurements. A reasonable correlation is found, although the uncertainty limits the confidence level. The quantitative measurement of the many reaction products is complex and very time-consuming. Thus such data are only available for a few cases, so additional experiments are needed to fully verify this correlation.

Another important associated effect originally studied at UIUC is the simultaneous emission of energetic (multi-MeV) protons and alpha particles during thin-film electrolysis experiments. Alpha particles ranging from 11.0 16.0 MeV and protons near 1.7 MeV are reported. The mechanism behind the observed charged particle emission is thought to be the nuclear transmutation reaction, but there is no direct proof of this. It should be emphasized, however, that these emissions cannot be explained in terms of contamination of the electrode with radioactive species such as radon, or by cosmic ray interactions with the electrode. Thus these observations, combined with the transmutations and excess heat already described, provide extremely strong evidence for nuclear reactions occurring in the thin films during electrolysis.

A number of theories have been proposed to explain LENRs. Several that are reported to reproduce key features of the transmutation product distributions have been noted here. While there is not yet a general consensus on theoretical details, the concepts are slowly converging. The main challenge that must be faced is to provide a comprehensive explanation of the varied effects that appear to occur simultaneously. This suggests a common driving mechanism and the need for a comprehensive theory. If a comprehensive theory can be developed, that, combined with continued experimental progress, should lead LENR from the lab into various practical applications. There are numerous applications, ranging from energy production (excess heat) to driving nuclear transmutations for isotope production.

Acknowledgements

The willingness of many researchers cited here to provide data is gratefully acknowledged. Contributions by colleagues at UIUC including A. Lipson, M. Ragheb, and N. Luo, are also appreciated. Important discussions with H. Hora, W. Collis, D. Cravens, J. Patterson, L. Larsen, E. Storms, P. Hagelstein, and J. Kelly are also gratefully acknowledged.

Downloaded by UNIV OF GUELPH LIBRARY on July 2, 2012 | http://pubs.acs.org
Publication Date: August 1, 2008 | doi: 10.1021/bk-2008-0998.ch009

References

1. Miley, G.H.; Shrestha, P.J. On Transmutation Reactions and Associated LENR Effects in Solids. In *Condensed Matter Nuclear Science: Proceedings of the 10th International Conference on Cold Fusion*, Cambridge, MA, Aug. 24-29, 2003; Hagelstein, P. L.; Chubb, S. R., Eds.; World Scientific Publishing Co.: Singapore, 2006; 361-378.
2. Miley, G.H.; Narne, G.; Williams, M.J.; Patterson, J.; Cravens D.; Hora, H. Quantitative Observations of Transmutation Products Occuring in Thin-Film Coated Microspheres During Electrolysis. In *Proceedings of the Sixth International Conference on Cold Fusion: Progress in New Hydrogen Energy*, Hokkaido, Japan, Oct. 13-18, 1996; Okamoto, M., Ed.; New Energy and Industrial Technology Development Organization: Tokyo, 1996; 629-644.
3. Iwamura, Y.; Sakano M.; Itoh T. Elemental Analysis of Pd Complexes: Effects of D_2 Gas Permeation. *Japan Society of App. Physics*, **2002**, *41*, 4642-4650.
4. Iwamura, Y.; Itoh, T.; Sakano, M.; Sakai, S.; Kuribayashi, S. Low Energy Nuclear Transmutation in Condensed Matter Induced by D_2 Gas Permeation Through Pd Complexes: Correlation Between Deuterium Flux and Nuclear Products. In *Condensed Matter Nuclear Science: Proceedings of the 10th International Conference on Cold Fusion*, Cambridge, MA, Aug. 24-29, 2003; Hagelstein, P. L.; Chubb, S. R., Eds.; World Scientific Publishing Co.: Singapore, 2006; 435-446.
5. Karabut, A.B.; Kucherov, Y.R.; Savvatimova, I.B. Possible Nuclear Reactions Mechanisms at Glow Discharge in Deuterium. In *Frontiers of Cold Fusion: Proceedings of the Third International Conference on Cold Fusion*, Nagoya, Japan, October 21-25, 1992; Ikegami, H., Ed.; Universal Academic Press: Tokyo, 1993.
6. Bockris, J. O'M.; Minevski, Z. Two Zones Of "Impurities" Observed After Prolonged Electrolysis of Deuterium on Palladium. *Infinite Energy* **1995**, *5/6*, 67-73.
7. Mizuno, T.; Ohmori, T.; Akimoto, T.; Kurokawa, K.; Kitaichi, M.; Inoda, K.; Azumi, K.; Simokawa, S.; Enyo, M. Isotopic Distribution for the Elements Evolved in Palladium Cathode after Electrolysis in D_2O Solution. In *Proceedings of the Sixth International Conference on Cold Fusion: Progress in New Hydrogen Energy*, Hokkaido, Japan, Oct. 13-18, 1996; Okamoto, M., Ed.; New Energy and Industrial Technology Development Organization: Tokyo, 1996.
8. Mizuno, T.; Ohmori, T.; Enyo, M. Formation of 197Pt Radioisotopes in Solid State Electrolyte Treated by High Temperature Electrolysis in D_2 Gas. *Infinite Energy* **1996**, *2* (7), 10-13.
9. Mizuno, T.; Ohmori, T.; Enyo, M. Isotopic Changes of the Reaction Products Induced by Cathodic Electrolysis in Pd. *J. New Energy* **1996**, *1* (3), 31-45.

Downloaded by UNIV OF GUELPH LIBRARY on July 2, 2012 | http://pubs.acs.org
Publication Date: August 1, 2008 | doi: 10.1021/bk-2008-0998.ch009

10. Miley, G.H.; Patterson, J.A. Nuclear Transmutations in Thin-Film Nickel Coatings Undergoing Electrolysis. *J. New Energy* **1996**, *1*, 11-15.
11. Hora, H.; Kelly, J. C.; Patel, J. U.; Prelas, M. A.; Miley, G. H.; Tompkins, J. W. Screening in Cold Fusion Derived from D-D Reactions. *Physics Ltrs. A* **1993**, *175* (2), 138-143.
12. Miley, G. H.; Heinrich, H.; Lipson, A.; Kim, S. O.; Luo, N.; Castano, C. H.; Woo, T. Progress in Thin-Film LENR Research at the University of Illinois. In *Proceedings of the 9th International Conference on Cold Fusion: Condensed Matter Nuclear Science*, Beijing, China, May 19-24, 2002; Li, X. Z., Ed.; Tsinghua Univ. Press: Beijing, 2002; 255-260.
13. Di Giulio, M.; Filippo, E.; Manno, D.; Nassisi, V. Analysis of Nuclear Transmutations Observed in D- and H-Loaded Pd Films. *International Journal of Hydrogen Energy* **2002**, *27*, 527-531.
14. Di Giulio, M.; Castellano, C.; Dinescu, D.; Nassisi, V.; Conte, A.; Pompa, P. P. Nuclear Transmutation in Deuterated Pd Films Irradiated by an UV Laser. In *ICCF8: Proceedings of the Eighth International Conference on Cold Fusion*, Lerici (La Spezia), Italy, May 21-26, 2000; Scaramuzzi, F., Ed.; Italian Physical Society: Bologna, Italy, 2001; 287-292.
15. Ohmori T.; Mizuno, T. Observation of the Product Elements of Nuclear Transmutation Reaction on/in Several Metal Electrodes by the Cathodic Electrolysis in Light Water Solutions. In *Proceedings of the Seventh International Conference on Cold Fusion*, Vancouver, Canada, April 19-24, 1998; ENECO, Inc.: Salt Lake City, UT, 1988; 109.
16. Ohmori, T.; Mizuno, T.; Nodasaka Y.; Enyo, M. Transmutation in a Gold-Light Water Electrolysis System. *Fusion Technol.* **1998**, *33* (3), 367-382.
17. Chernov, I. P.; Nikitenkov, N. N.; Puchkareva, L. N.; Kolobov, Yu. R.; Krening, M.; Baumbach, B. Change of Isotopic Composition of Metals at Deuterium Charge. In *Proceedings of the Seventh International Conference on Cold Fusion*, Vancouver, Canada, April 19-24, 1998; ENECO, Inc.: Salt Lake City, UT, 1988; 42.
18. Ohmori, T.; Mizuno, T. Strong Excess Energy Evolution, New Elements Production, and Electromagnetic Wave and/or Neutron Emission in the Light Water Electrolysis with a Tungsten Cathode. In *Proceedings of the Seventh International Conference on Cold Fusion*, Vancouver, Canada, April 19-24, 1998; ENECO, Inc.: Salt Lake City, UT, 1988; 279-284.
19. Ohmori, T.; Yamada, H.; Narita, S.; Mizuno, T. Excess Energy and Anomalous Concentration of ^{41}K Isotopes in Potassium Formed on/in a Re Electrode during the Plasma Electrolysis in K_2CO_3/H_2O and K_2CO_3/D_2O Solutions. In *Proceedings of the 9th International Conference on Cold Fusion: Condensed Matter Nuclear Science*, Beijing, China, May 19-24, 2002; Li, X. Z., Ed.; Tsinghua Univ. Press: Beijing, 2002; 284-289.
20. Ohmori T.; Mizuno, T. Nuclear Transmutation Reaction Caused by the Light Water Electrolysis on Tungsten Cathode under an Incandescent Condition. *J. New Energy*, **2000**, *4* (4), 66-78.

Downloaded by UNIV OF GUELPH LIBRARY on July 2, 2012 | http://pubs.acs.org
Publication Date: August 1, 2008 | doi: 10.1021/bk-2008-0998.ch009

21. Nassisi V.; Longo, M.L. Experimental Results of Transmutation of Elements Observed in Etched Palladium Samples by an Excimer Laser. *Fusion Technol.* **2000**, *37* (3), 247-252.
22. Celani, F.; Spallone, A.; Righi, E.; Trenta, G.; Cappuccio, G.; Quercia, G.; Andreassi, V.; Marmigi, A.; Marini, P.; Stefano, V. D.; Nakamura, N.; Todarello, F.; Puchi, E.; Mancini, A.; Sona, P. G.; Fontana, F.; Gamberale, L.; Garbelli, D.; Celia, E.; Falcioni, F.; Marchesini, M.; Martini, U.; Biago, P. D.; Mastromatteo, U. Toward the Use of Nanoparticles for Stable Excess Heat in Pd-D System: Progress Report at INFN-LNF. Presented at the 7th International Workshop on Anomalies in Hydrogen/Deuterium Loaded Metals, Asti, Italy, Sept. 23-25, 2006.
23. Kozima, H. *The Science of the Cold Fusion Phenomenon in Search of the Physics and Chemistry behind Complex Experimental Data Sets*; Elsevier: 2006.
24. Storms, E. *The Science of Low Energy Nuclear Reaction*; World Scientific: Singapore, 2007.
25. Hora H.; Miley, G. H. Maruhn-Greiner-Maximum of Uranium Fission for Confirmation of Low Energy Nuclear Reactions (LENR) via a Compound Nucleus with Double Layer Magic Numbers. *J. Fusion Energy* **2007**, *26*, 349-353.
26. Miley, G. H.; Lipson, A.; Hora H.; Shrestha P. J. Cluster Reactions in LENRs. Presented at the 8th International Workshop on Anomalies in Hydrogen/Deuterium Loaded Metals, Catania, Sicily, Oct. 13-18, 2007.
27. Preparata, G. *QED Coherence in Matter.* World Scientific: Singapore, 1995.
28. Widom, A.; Larsen, L. Theoretical Standard Model Rates of Proton to Neutron Conversions Near Metallic Hydride Surfaces. 2006, arXiv: nucl-th/pdf/0608/0608059v1. arXiv.org e-Print archive. http://arxiv.org/PS_cache/nucl-th/pdf/0608/0608059v1.pdf (accessed August 2007).
29. Widom, A.; Larsen, L. Nuclear Abundances In Metallic Hydride. http://www.newenergytimes.com/Library/2006WidomA-NuclearAbundancesInMetallicHydride.pdf (accessed August 2007).
30. McKubre, M. C. H.; Crouch-Baker, S.; Rocha-Filho, R-C. Isothermal Flow Calorimetric Investigations of the D/Pd and H/Pd Systems. *J. Electroanal. Chem.* **1994**, *368*, 5.
31. Miles, M. H. Calorimetric Studies of Pd/D_2O+LiOD Electrolysis Cells. *J. Electroanal. Chem.* **2000**, *482*, 56.
32. Storms, E. How to Produce the Pons-Fleischmann Effect. *Fusion Technol.* **1996**, 29, 261.
33. Mills R. L.; Kneizys, S. P. Excess Heat Production by the Electrolysis of an Aqueous Potassium Carbonate Electrolyte and the Implications for Cold Fusion. *Fusion Technol.* **1991**, *20*, 65.
34. Notoya, R. Cold Fusion by Electrolysis in a Light Water-Potassium Carbonate Solution with a Nickel Electrode. *Fusion Technol.* **1993**, *24*, 202.

Downloaded by UNIV OF GUELPH LIBRARY on July 2, 2012 | http://pubs.acs.org
Publication Date: August 1, 2008 | doi: 10.1021/bk-2008-0998.ch009

35. Bauer, H. J.; Schmidbauer, E. Über den Einfluß elektrolytischer Wasserstoffbeladung auf die Magnetisierung von Nickel. *Z. Physik* **1961**, *164*, 367.
36. Jones, J.E.; Hansen, L.D.; Jones, S. E. Examination of Claims of Miles et al. in Pons-Fleischmann-Type Cold Fusion Experiments. *J. Phys. Chem.* **1995**, *99*, 6973.
37. Miley, G.H. Emerging Physics for a Breakthrough Thin-Film Electrolytic Power Unit. *Space Technol. Applic. Int. Forum* **1999**, *458*, 1227.
38. Castano, C. H.; Lipson, A. G.; Kim, S. O.; Miley, G. H. Caloremetric Measurements During Pd-Ni Thin Film–Cathodes Electrolysis in Li_2SO_4/H_2O Solution. In *Proceedings of the 9th International Conference on Cold Fusion: Condensed Matter Nuclear Science*, Beijing, China, May 19-24, 2002; Li, X. Z., Ed.; Tsinghua Univ. Press: Beijing, 2002; 24-28.
39. Glasstone, S. *An Introduction to Electrochemistry*; Wiley: New York, 1951, Chapter 13.
40. Miley, G. H.; Hora, H.; Batyrbekov, E. G.; Zich, R. L. Electrolytic Cell with Multilayer Thin-Film Electrodes. *Trans. Fusion Technol.* **1994**, *26*, 313.
41. McKubre, M.; Tanzella, F. The Correlation Between Heat and Helium in Experiments Performed at SRI. Presented at the 7th International Workshop on Anomalies in Hydrogen/Deuterium Loaded Metals, Asti, Italy, Sept. 23-25, 2006.
42. Miley, G. H. Possible Evidence of Anomalous Energy Effects in H/D-Loaded Solids-Low Energy Nuclear Reactions (LENRS). *Journal of New Energy* **1997**, *2* (3-4), 6-13.
43. Miley, G. H. Characteristics of Reaction Product Patterns in Thin Metallic Films Experiments. In *Proceedings of the Asti Workshop on Anomalies in Hydrogen/Deuterium Loaded Metals*. Asti, Italy, November 27-30, 1997; Collis, W. J. M. F., Ed.; Italian Physical Society: Bologna, Italy, 1999, 77-87.
44. Miley, G. H.; Selvaggi, G.; Tate, A.; Okuniewski, M.; Williams, M. J.; Chicea, D.; Hora, H.; Kelly, J. Advances in Thin-Film Electrode Experiments. In *ICCF8: Proceedings of the Eighth International Conference on Cold Fusion*, Lerici (La Spezia), Italy, May 21-26, 2000; Scaramuzzi, F., Ed.; Italian Physical Society: Bologna, Italy, 2001; 169-176.
45. Hora, H.; Miley, G. H. New Magic Numbers from Low Energy Nuclear Transmutations Predict Element^{306}X126 for Compound Reactions. *Czechoslovak Journal of Physics* **1998**, *48* (9), 1111-1116.
46. Hora, H.; Miley, G. H. Heavy Nuclide Synthesis by Neutrons in Astrophysics and by Screened Protons in Host Metals. *Czechoslovak Journal of Physics* **2000**, *50* (3), 433-439.
47. Takahashi, A.; Ohta, M.; Mizuno, T. A Model Analysis of Low-Energy Photo-Fission of Pd Isotopes Under Dynamic Condition of PdH(D). In *Proceedings of the 9th International Conference on Cold Fusion:*

Downloaded by UNIV OF GUELPH LIBRARY on July 2, 2012 | http://pubs.acs.org
Publication Date: August 1, 2008 | doi: 10.1021/bk-2008-0998.ch009

Condensed Matter Nuclear Science, Beijing, China, May 19-24, 2002; Li, X. Z., Ed.; Tsinghua Univ. Press: Beijing, 2002; 397-402.

48. Lipson, A. G.; Roussetski, A. S.; Miley, G. H.; Castano, C. H. In-Situ Charged Particles and X-ray Detection in Pd Thin Film-Cathodes During Electrolysis in Li_2SO_4/H_2O. In *Proceedings of the 9th International Conference on Cold Fusion: Condensed Matter Nuclear Science*, Beijing, China, May 19-24, 2002; Li, X. Z., Ed.; Tsinghua Univ. Press: Beijing, 2002; 218-223.
49. Lipson, A. G.; Lyakhov, B. F.; Roussetsky, A.S. Evidence for DD-Reaction and a Long-Range Alpha Emission in Au/Pd/PdO:D Heterstructure as a Result of Exothermic Deuterium Deposition. In *ICCF8: Proceedings of the Eighth International Conference on Cold Fusion*, Lerici (La Spezia), Italy, May 21-26, 2000; Scaramuzzi, F., Ed.; Italian Physical Society: Bologna, Italy, 2001; 231-239.
50. Oda, K.; Ito, M.; Miyake, H.; Michijima, M.; Yamamoto, J. Track Formation in CR-39 Detector Exposed to D-T Neutrons. *Nucl. Instr. Meth.* **1988**, *B35*, 50.

Additional references used for data tabulation for Figure 8 and Table I:

51. SPAWAR Systems Center, San Diego. Presentation at the Joint Services Environmental Management Conference, Columbus, OH, May 21-24, 2007.
52. Lipson, A. G.; Roussetski, A. S.; Castano, C. H.; Miley, G. H. In-Situ Long-Range Alpha Particles and X-ray Detection for Thin-film Pd Cathodes During Electrolysis in Li_2SO_4/H_2O. *Bulletin of the American Physical Society, APS Spring Meeting,* Indianapolis, IN, 2002, *47* (1, Pt. II), 1219.
53. Miley, G. H.; Hora, H. Nuclear Reactions in Solids. *American Physical Society 2002 Fall Nuclear Physics Meeting*, East Lansing, Michigan, October 7-10, 2002.
54. Miley, G. H.; Hora, H. Study of Compound Nuclei Produced in Low Energy Nuclear Reactions in Solids. *3rd Intl. Conf on Fission & Properties of Neutron-Rich Nuclei*, Sanibel Island, Florida, Nov. 3-9, 2002.
55. Miley, G. H.; Hora, H.; Lipson, A.; Kim, S. O.; Luo, N.; Castano, C. H.; Woo, T. Progress in Thin-Film LENR Research. In *Proceedings of the 9th International Conference on Cold Fusion: Condensed Matter Nuclear Science*, Beijing, China, May 19-24, 2002; Li, X. Z., Ed.; Tsinghua Univ. Press: Beijing, 2002; 255.
56. Luo, N.; Castano, C. H.; Kim, S. O.; Lipson, A. G.; Woo, T.; Miley, G. H. In-Situ Characterization of Sputtered Thin-Film Electrodes During Electrolysis. In *Proceedings of the 9th International Conference on Cold Fusion: Condensed Matter Nuclear Science*, Beijing, China, May 19-24, 2002; Li, X. Z., Ed.; Tsinghua Univ. Press: Beijing, 2002; 229-232.

Downloaded by UNIV OF GUELPH LIBRARY on July 2, 2012 | http://pubs.acs.org
Publication Date: August 1, 2008 | doi: 10.1021/bk-2008-0998.ch009

Downloaded by UNIV OF GUELPH LIBRARY on July 2, 2012 | http://pubs.acs.org
Publication Date: August 1, 2008 | doi: 10.1021/bk-2008-0998.ch009

57. Miley, G. H.; Shrestha, P. J.; Hora, H. Nuclear Reactions and X-Ray Emission Involving Solids Highly Loaded with D/H. In *Current Trends in International Fusion Research – Proceedings of the Fifth Symposium*; Panarella, E., Ed.; National Research Council of Canada Research Press: Ottawa, 2003.
58. Luo, N.; Miley, G. H. First-Principles Studies on the Ionic and Electronic Transport of Palladium Hydride/Deuteride. In *Condensed Matter Nuclear Science: Proceedings of the 10th International Conference on Cold Fusion*, Cambridge, MA, Aug. 24-29, 2003; Hagelstein, P. L.; Chubb, S. R., Eds.; World Scientific Publishing Co.: Singapore, 2006; 709-716.
59. Dufour, J. J.; Foos, J. H.; Dufour, X. J. C. Formation and Properties of Hydrex and Deutex. In *Proceedings of the Asti Workshop on Anomalies in Hydrogen/Deuterium Loaded Metals.* Asti, Italy, November 27-30, 1997; Collis, W. J. M. F., Ed.; Italian Physical Society: Bologna, Italy, 1999, 29-34.
60. Kozima, H. CF-Matter and Cold Fusion Phenomenon. In *Condensed Matter Nuclear Science: Proceedings of the 10th International Conference on Cold Fusion*, Cambridge, MA, Aug. 24-29, 2003; Hagelstein, P. L.; Chubb, S. R., Eds.; World Scientific Publishing Co.: Singapore, 2006; 919-928.
61. Takahashi, A.; Ohta, M.; Mizuno, T. Production of Stable Isotopes by Selective Channel Photofission of Pd. *J. Applied Physics* **2001**, *40*, 7031-7046.
62. Fisher, J. C. Liquid-Drop Model for Extremely Neutron Rich Nuclei. *Fusion Technol.* **1998**, *34* (1), 66-75.
63. Lipson, A. G.; Roussetski, A. S.; Miley, G. H.; Castano, C. H. In-Situ Charged Particles and X-ray Detection in Pd Thin-film Cathodes During Electrolysis in Li_2SO_4/H_2O. In *Proceedings of the 9th International Conference on Cold Fusion: Condensed Matter Nuclear Science*, Beijing, China, May 19-24, 2002; Li, X. Z., Ed.; Tsinghua Univ. Press: Beijing, 2002; 218-223.
64. Castano, C. H.; Lipson, A. G.; Kim S. O.; Miley, G. H. Calorimetric Measurements during Pd-Ni Thin Film–Cathodes Electrolysis in Li_2SO_4/H_2O Solution. In *Proceedings of the 9th International Conference on Cold Fusion: Condensed Matter Nuclear Science*, Beijing, China, May 19-24, 2002; Li, X. Z., Ed.; Tsinghua Univ. Press: Beijing, 2002; 24-28.
65. Miley G. H.; Hora, H. Nuclear Reactions in Solids. *American Physical Society 2002 Fall Nuclear Physics Meeting*, East Lansing, Michigan, October 7-10, 2002.
66. Lipson, A.; Miley, G. H.; Roussetski, A. Energetic Alpha and Proton Emissions on the Electrolysis of Thin-Pd Films. Presented at the American Nuclear Society Annual Meeting, San Diego, CA, June 1-5, 2003.
67. Miley G. H.; Shrestha, P. J. Evidence For Transmutation Reactions in Solids. Presented at the American Nuclear Society Annual Meeting, San Diego, CA, June 1-5, 2003.

68. Luo, N.; Miley, G. H.; Lipson, A. G. Modeling of Surface and Bulk Effects in Thin-Film Pd Cathodes with High Proton Loading. *Applied Surface Science* **2003**, *219* (1-2), 167-173.
69. Beaudette, C. G. *Excess Heat: Why Cold Fusion Research Prevailed*; Oak Grove Press: Concord, NH, 2000, 241-246.
70. Bush, R. T. Cold Fusion/Cold Fission Reactions to Explain Mizuno's Electrolytic Experiment Employing a Pd Cathode and Pt Anode. In *Proceedings of the Seventh International Conference on Cold Fusion*, Vancouver, Canada, April 19-24, 1998; ENECO, Inc.: Salt Lake City, UT, 1988; 34.
71. Claytor, T. N.; Schwab, M. J.; Tuggle, D. G. In-Situ Measurement of Tritium Concentration Variations During Plasma Excitation of Deuterium Loaded Palladium and Palladium Alloys. In *Proceedings of the Seventh International Conference on Cold Fusion*, Vancouver, Canada, April 19-24, 1998; ENECO, Inc.: Salt Lake City, UT, 1988; 48.
72. Dash, J.; Noble, G.; and Diman, D. Surface Morphology and Microcomposition of Palladium Cathodes After Electrolysis in Acified Light and Heavy Water: Correlation With Excess Heat. *Transactions of Fusion Technology* **1994**, *26*, 299-306.
73. Dash, J.; Kopecek, R.; Miguet, S. Excess Heat and Unexpected Elements from Aqueous Electrolysis with Titanium and Palladium Cathodes. In *Proc. 32nd Intersociety Energy Conversion Engineering Conference*, Honolulu, HI, , July 27-Aug. 1, 1997; 1350-1355.
74. Dash, J.; Savvatimova, I.; Frantz, S.; Weis, E.; Kozima, H. Effects of Glow Discharge with Hydrogen Isotope Plasmas on Radioactivity of Uranium. In *Proceedings of the 9th International Conference on Cold Fusion: Condensed Matter Nuclear Science*, Beijing, China, May 1924, 2002; Li, X. Z., Ed.; Tsinghua Univ. Press: Beijing, 2002; 77-81.
75. Dufour, J.; Murat, D.; Dufour, X.; Foos, J. Hydrex Catalyzed Transmutation of Uranium and Palladium. Experimental Part. In *ICCF8: Proceedings of the Eighth International Conference on Cold Fusion*, Lerici (La Spezia), Italy, May 21-26, 2000; Scaramuzzi, F., Ed.; Italian Physical Society: Bologna, Italy, 2001; 153-158.
76. Hanawa, T. X-ray Spectrometric Analysis of Carbon Arc Products in Water. In *ICCF8: Proceedings of the Eighth International Conference on Cold Fusion*, Lerici (La Spezia), Italy, May 21-26, 2000; Scaramuzzi, F., Ed.; Italian Physical Society: Bologna, Italy, 2001; 147-152.
77. Iwamura, Y.; Itoh, T.; Gotoh, N.; Sakano, M.; Toyoda I.; Sakata, S. Detection of Anomalous Elements, X-ray and Excess Heat Induced by Continuous Diffusion of Deuterium through Multi-Layer Cathode (Pd/CaO/Pd). In *Proceedings of the Seventh International Conference on Cold Fusion*, Vancouver, Canada, April 19-24, 1998; ENECO, Inc.: Salt Lake City, UT, 1988; 167-171.

Downloaded by UNIV OF GUELPH LIBRARY on July 2, 2012 | http://pubs.acs.org
Publication Date: August 1, 2008 | doi: 10.1021/bk-2008-0998.ch009

78. Iwamura, Y.; Itoh, T.; Sakano, M. Nuclear Products and Their Time Dependence Induced by Continuous Diffusion of Deuterium through Multi-Layer Palladium Containing Low Work Function Material. In *ICCF8: Proceedings of the Eighth International Conference on Cold Fusion*, Lerici (La Spezia), Italy, May 21-26, 2000; Scaramuzzi, F., Ed.; Italian Physical Society: Bologna, Italy, 2001; 141-146.
79. Jiang, X. L.; Chen, C. Y.; Fu, D. F. Tip Effect And Nuclear-Active Sites. In *Proceedings of the Seventh International Conference on Cold Fusion*, Vancouver, Canada, April 19-24, 1998; ENECO, Inc.: Salt Lake City, UT, 1988; 175-179.
80. Karabut, A. B. Analysis of Experimental Results on Excess Heat Power Production, Impurity Nuclides Yield in the Cathode Material and Penetrating Radiation in Experiments with High-Current Glow Discharge. In *ICCF8: Proceedings of the Eighth International Conference on Cold Fusion*, Lerici (La Spezia), Italy, May 21-26, 2000; Scaramuzzi, F., Ed.; Italian Physical Society: Bologna, Italy, 2001; 329-334.
81. Karabut, A.B. Excess Heat Power, Nuclear Products and X-ray Emission in Relation to the High Current Glow Discharge Experimental Parameters. In *Proceedings of the 9th International Conference on Cold Fusion: Condensed Matter Nuclear Science*, Beijing, China, May 19-24, 2002; Li, X. Z., Ed.; Tsinghua Univ. Press: Beijing, 2002; 151-154.
82. Kong, L. C.; Han, X. L.; Zheng, S. X.; Huang, H. F.; Yan, Y. J.; Wu, Q. L.; Deng, Y.; Lei, S. L.; Li, C. X.; Li, X. Z. Nuclear Products and Transmutation in a Gas-Loading D/PD and H/PD System. *Journal of Energy* **1998**, *3* (1), 20-23.
83. Kozima, H.; Hiroe, K.; Noruma, M.; Ohta, M. *On the Elemental Transmutation in Biological and Chemical Systems by Nuclear Fusion*; Shizuoka University Department of Physics: Shizuoka, Japan, 1996, pp 1-5.
84. Li, X. Z.; Yan, Y. J.; Jian, T.; Mei, M. Y.; Deng, Y.; Yu, W. Z.; Tang G. Y.; Cao, D. X. Nuclear Transmutation in Pd Deuteride. In *ICCF8: Proceedings of the Eighth International Conference on Cold Fusion*, Lerici (La Spezia), Italy, May 21-26, 2000; Scaramuzzi, F., Ed.; Italian Physical Society: Bologna, Italy, 2001; 123-128.
85. Li, X. Z.; Deng, Y.; Yan, Y. J.; Huang, H. F.; Yu, W. Z.; Li, C. X. Nuclear Transmutation Detection in the Pd/C Catalyst. *Journal of Energy* **2001**, *6* (1), 80-86.
86. Miguet, S.; Dash, J. Microanalysis of Pd Cathodes after Electrolysis in Aqueous Acids. *Journal of New Energy* **1996**, *1* (1), 23-27.
87. Miley, G. H. Product Characteristics and Energetics in Thin-Film Electrolysis Experiments. In *Proceedings of the Seventh International Conference on Cold Fusion*, Vancouver, Canada, April 19-24, 1998; ENECO, Inc.: Salt Lake City, UT, 1988; 241-246.
88. Mizuno, T., Ohmori, T.; Akimoto, T. Detection of Radiation Emission, Heat Generation and Elements from a Pt Electrode Induced by Electrolytic Discharge in Alkaline Solutions. In *Proceedings of the Seventh*

Downloaded by UNIV OF GUELPH LIBRARY on July 2, 2012 | http://pubs.acs.org
Publication Date: August 1, 2008 | doi: 10.1021/bk-2008-0998.ch009

International Conference on Cold Fusion, Vancouver, Canada, April 19-24, 1998; ENECO, Inc.: Salt Lake City, UT, 1988; 253-258.

89. Mizuno, T. Experimental Confirmation of the Nuclear Reaction at Low Energy Caused by Electrolysis in the Electrolyte. *Proceedings of the Symposium on Advanced Research in Energy Technology*, Hokkaido University: Hokkaido, Japan, 2000.
90. Mo, D. W.; Cai, Q. S.; Wang, L. M.; Li, X. Z. The Confirmation of Nuclear Transmutation Phenomenon in a Gas Loading H/Pd System Using NAA. In *Proceedings of the Seventh International Conference on Cold Fusion*, Vancouver, Canada, April 19-24, 1998; ENECO, Inc.: Salt Lake City, UT, 1988; 105.
91. Mo, D. W.; Cai, Q. S.; Wang, L. M.; Li, S. Z. The Evidence of Nuclear Transmutation Phenomenon in Pd-H System Using NAA Neutron Activation Analysis). In *Proceedings of the Seventh International Conference on Cold Fusion*, Vancouver, Canada, April 19-24, 1998; ENECO, Inc.: Salt Lake City, UT, 1988; 259-263.
92. Nassisi, V. Transmutation of Elements in Saturated Palladium Hydrides by An XeCl Excimer Laser. *Fusion Technol.* **1998**, *33* (4), 468-475.
93. Notoya, R. Nuclear Products of Cold Fusion Caused by Electrolysis in Alkali Metallic Ions Solutions. In *Proceedings of the Fifth International Conference on Cold Fusion*, Monte Carlo, Monaco, April 9-13, 1995; Pons, S., Ed.; IMRA Europe: Sophia Antipolis Cedex, France, 1995; 531-538.
94. Notoya, R.; Toshiyuki, O.; Yoichi, N. Products of Nuclear Processes Caused by Electrolysis on Nickel and Platinum Electrodes in Solutions of Alkali-Metallic Ions. In *Proceedings of the Seventh International Conference on Cold Fusion*, Vancouver, Canada, April 19-24, 1998; ENECO, Inc.: Salt Lake City, UT, 1988; 269-273.
95. Ohmori, T.; Mizuno, T.; Enyo, M. Isotopic Distributions of Heavy Metal Elements Produced During the Light Water Electrolysis on Gold Electrodes. *J. New Energy* **1996**, *1* (3), 90-99.
96. Ohmori, T.; Mizuno, T.; Minagawa, H.; Enyo, M. Low Temperature Nuclear Transmutation Forming Iron on/in Gold Electrode During Light Water Electrolysis. *Int. J. Hydrogen Energy* **1997**, *22* (5), 459-463.
97. Passell, T. O.; George, R. Trace Elements Added to Palladium by Exposure to Gaseous Deuterium. In *ICCF8: Proceedings of the Eighth International Conference on Cold Fusion*, Lerici (La Spezia), Italy, May 21-26, 2000; Scaramuzzi, F., Ed.; Italian Physical Society: Bologna, Italy, 2001; 129-134.
98. Savvatimova, I. B.; Kuchernov, Y. R.; Karabut, A. B. Cathode Material Change after Deuterium Glow Discharge Experiments. *Transactions of Fusion Technology* **1994**, *26*, 389-394.
99. Savvatimova, I. B.; Senchukov, A. B.; Chernov, I. P. Transmutation Phenomena in the Palladium Cathode after Ion Irradiation at Glow Discharge. In *Proceedings of the Sixth International Conference on Cold Fusion: Progress in New Hydrogen Energy*, Hokkaido, Japan, Oct. 13-18,

Downloaded by UNIV OF GUELPH LIBRARY on July 2, 2012 | http://pubs.acs.org
Publication Date: August 1, 2008 | doi: 10.1021/bk-2008-0998.ch009

1996; Okamoto, M., Ed.; New Energy and Industrial Technology Development Organization: Tokyo, 1996; 144.

100. Warner, H.; Dash, J. Electrolysis of D_2O with Titanium Cathodes: Enhancement of Excess Heat and Further Evidence of Possible Transmutation. In *Proceedings of the 9th International Conference on Cold Fusion: Condensed Matter Nuclear Science*, Beijing, China, May 19-24, 2002; Li, X. Z., Ed.; Tsinghua Univ. Press: Beijing, 2002; 118-119.
101. Yamada, H.; Uchiyama, K.; Kawata, N.; Kurisawa, Y.; Nakamura, M. Producing a Radioactive Source in a Deuterated Palladium Electrode under Direct-Current Glow Discharge. *Fusion Technol.* **2001**, *39*, 253-258.
102. Yamada, H.; Narita, S.; Fujii, Y.; Sato, T.; Sasaki, S.; Ohmori, T. Production of Ba and Several Anomalous Elements in Pd under Light Water Electrolysis. In *Proceedings of the 9th International Conference on Cold Fusion: Condensed Matter Nuclear Science*, Beijing, China, May 19-24, 2002; Li, X. Z., Ed.; Tsinghua Univ. Press: Beijing, 2002; 123.

Downloaded by UNIV OF GUELPH LIBRARY on July 2, 2012 | http://pubs.acs.org
Publication Date: August 1, 2008 | doi: 10.1021/bk-2008-0998.ch009

Downloaded by OHIO STATE UNIV LIBRARIES on July 1, 2012 | http://pubs.acs.org
Publication Date: August 1, 2008 | doi: 10.1021/bk-2008-0998.ch010

Chapter 10

Replication of Condensed Matter Heat Production

M. C. H. McKubre[1], F. L. Tanzella[1], I. Dardik[2], A. El Boher[3],
T. Zilov[3], E. Greenspan[4], C. Sibilia[5], and V. Violante[6]

[1]SRI International, 333 Ravenswood Avenue, Menlo Park, CA 94025–3493
[2]Energetics LLC, 7 Fieldview Lane, Califon, NJ 07830
[3]Energetics Technologies, P.O. Box 3026, Omer Industrial Park,
Omer, Israel
[4]Energetics Technologies and University of California at Berkeley, 4155
Etcheverry Hall, M.C. 1730, Berkeley, CA 94720
[5]University di Roma "La Sapienza", Via Scarpa 16, 00161 Rome, Italy
[6]ENEA, Centro Ricerche Frascati, C.P. 65-00044 Frascati, Roma, Italy

Two series of experiments have been performed independently at ENEA and SRI to replicate the results of excess heat experiments reported by Energetics. Successful replication was obtained at SRI in the original isoperibolic mode of calorimetry used by Energetics in Israel and using a sophisticated mass flow calorimeter at ENEA. Two factors were found to be critical in both replications: a high degree of microstructural metallurgical control achieved by ENEA allows electrodes to accept deuterium loading without damaging deformation; the complex superwave excitation function developed by Energetics produces a high level of deuterium loading and flux believed to be instrumental for the excess heat effect.

In Low-Energy Nuclear Reactions Sourcebook; Marwan, J., et al.;
ACS Symposium Series; American Chemical Society: Washington, DC, 2008.

Introduction

A series of experiments was undertaken to replicate isoperibolic calorimetry results obtained from heavy-water electrolysis using specially prepared Pd foil cathodes. The original experiments, reported by Energetics Technologies in Israel, were based on concepts developed by Dardik (*1-4*) in the United States. These experiments use complex, fractally nested, non-sinusoidal input currents rather than simple dc or pulse electrolysis, referred to as superwaves.

Experiments were performed in a 49 mm dia. by 185 mm tall cylindrical PTFE cup that comprises the electrochemical cell outer boundary. Two platinum anodes of dimension 20 mm × 80 mm × 100 μm sandwich a palladium cathode with anode-cathode separation 6 mm. This three-electrode structure is positioned at the center of the cell.

A tight-fitting cell top machined from PTFE and alumina insulation completes the cell boundary and acts to reduce vertical conductive heat transfer. The top is penetrated by:

1. two current wires to the anode and cathode (the cell voltage is measured just external to the cell),
2. four small wires used to make four terminal measurements of the cathode axial resistance, and
3. three stainless steel and PTFE sheathed 100Ω platinum resistance temperature device (RTD) sensors used to measure the cell electrolyte temperature at three positions in the cell, designated as T_1, T_2, and T_3.

Also penetrating the top is a 7 mm inside diameter PTFE tube connecting the vapor space of the cell to a tightly sealed chamber containing an Agua Gen® recombiner catalyst. Electrolytically generated O_2 and D_2 bubble from the electrolyte and rise to the recombiner to form D_2O and flow back down to the cell. The heat of recombination is thus largely communicated to the environment; the small fraction that is returned to the cell with the downcoming D_2O as well as influences of ambient temperature on the calorimetry are taken into account with the calibration.

The calorimeter is isoperibolic in the sense that two aluminum cups constitute the calorimetric boundary perimeters at constant temperature: the inner wall at temperature T_4, and the outer at temperature T_5. Separating the two boundaries is a barrier of alumina powder having a well-characterized (and constant) thermal conductivity. For the ideal case where the temperature of the inner and outer boundaries both can be represented by a single temperature measured as T_4 and T_5 respectively, then the steady state heat flow in or out of the calorimeter in the absence of ambient or recombinant effects is given by

$$H = K * [T_4 - T_5] \quad (1)$$

Downloaded by OHIO STATE UNIV LIBRARIES on July 1, 2012 | http://pubs.acs.org
Publication Date: August 1, 2008 | doi: 10.1021/bk-2008-0998.ch010

Downloaded by OHIO STATE UNIV LIBRARIES on July 1, 2012 | http://pubs.acs.org
Publication Date: August 1, 2008 | doi: 10.1021/bk-2008-0998.ch010

In practice the outer boundary T_5 is held constant by immersing the calorimeter in a water bath at a well–controlled, constant temperature. At both Energetics and SRI, a bath temperature of ~5°C was normally chosen to increase the extent of cathode deuterium absorption.

The working electrolyte volume of the cell is ~230 cm^3. Electrolytes were prepared by adding 5.25 ml of 9 wt. % LiOD/D_2O (Sigma – Aldrich CN 347450) to 225 ml of low tritium content D_2O (Sigma – Aldrich CN 151890) to yield an electrolyte concentration of 0.1 M LiOD.

The cathodes typically used by Energetics and SRI were foils 80 mm long, 7 mm wide, and ≤50 μm thick, prepared by successive rolling and annealing procedures, as described by Violante (*5*). Electrolysis current was supplied to the cathode by a 0.3 mm dia. Pt wire sheathed in PTFE. Four additional 0.3 mm dia. PTFE sheathed Pt wires were used to measure the axial resistance to determine the D/Pd (or H/Pd) loading.

The most pronounced excess heat results obtained by Energetics are reproduced as Figure 1. A maximum thermal output power of ~34 W was obtained twice at an input power of less than 1 W. The duration of this episode was approximately 14 h, terminating apparently spontaneously with an integrated energy of electrical input of 40 kJ, and integrated output heat energy of 1.14 MJ. The COPE referred to the right axis in Figure 1 is the ratio of the thermal output to electrical input power.

The SRI Energetics Replication Plan

Since 1989, SRI has attempted to replicate roughly ten experimental results reported in the field of cold fusion or condensed matter nuclear science (CMNS). A reproduction protocol has been developed to maximize the chances of success and useful learning in this process. The SRI reproduction protocol employed for the replication of Energetics' results described below involves three steps.

1. A "host hands off" rebuild by the original experimenter allowing simple technical support, but with conscientious effort not to improve the experiment at this point. This first phase is complete when the experiment is operating in the same manner as it was on the original site.
2. A complete transfer of procedures and performance characteristics from the guest to the host, complete when the experiment is running to the satisfaction of the originator and the host scientists believe they understand what is being done and what is required.
3. Host (SRI) operation of the experiment with added diagnostics as suggested or required from the results of Step 1. Only when the experiment is running in the same way and with the same results as for the originator is an attempt made to "improve." In the present program, such "improvement" was

Downloaded by OHIO STATE UNIV LIBRARIES on July 1, 2012 | http://pubs.acs.org
Publication Date: August 1, 2008 | doi: 10.1021/bk-2008-0998.ch010

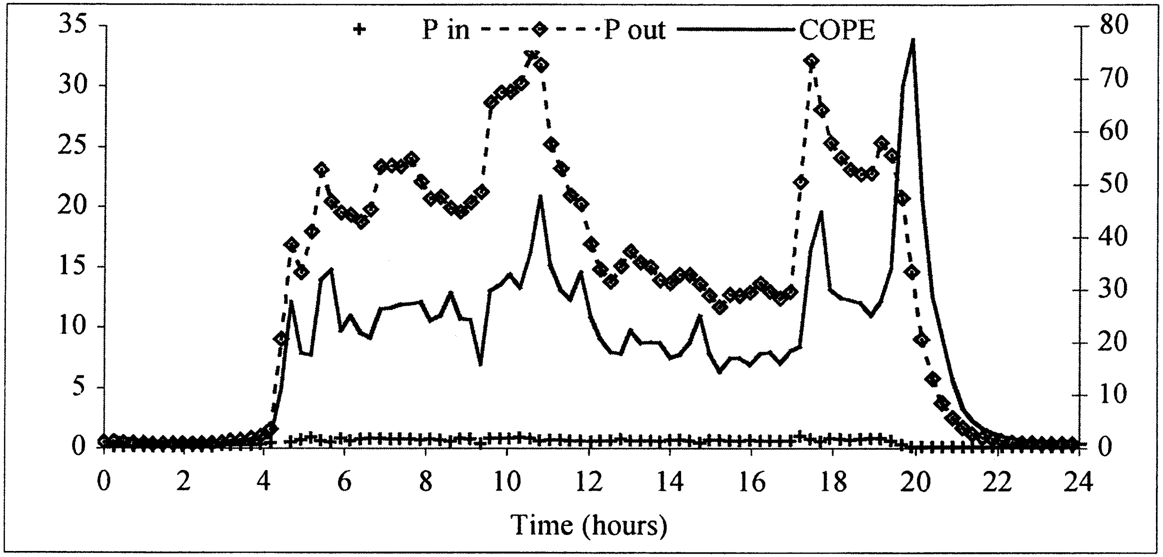

Figure 1. Energetics excess power results for cell ETE #64.

restricted to sophistication of the data analysis, as the underlying Energetics protocol was demonstrated to be sound.

SRI Replication

Calibrations and Power Measurement

A total of 6 calibrations with Joule heaters, 3 light-water experiments, and 23 heavy-water experiments were performed using two sets of instrumentation and control software corresponding to Steps 1 and 3 above. An initial set of calibrations and 8 experiments with 0.1 M LiOD electrolytes were performed at SRI using the data measurement protocol developed by Energetics (Step 1). Figure 2 shows the results of calibrating three different calorimeter bodies by substituting an electrical Joule heater for the electrode assembly in cells containing 230 ml of H_2O.

Output power can be calculated from equation 1. The constant K can be seen in Figure 2 to be not quite unity, and not quite constant for the three different cell bodies. Energetics data acquisition accommodates this temperature dependence of the heat flow coefficient by using a lookup table for K. Ar equivalent procedure was adopted at SRI by defining a parabolic function for K[1]

$$P_{Out} = \Delta T^{o} + a\,\Delta + b\,\Delta T^{2} \qquad (2)$$

The coefficients ΔT^{o}, a, and b are evaluated by linear regression fit of the calibration heater power versus Δas shown in Figure 2. The platinum RTDs used in this study[2] have a nominal 100Ω resistance (at T^{o} = 0 °C, R^{o}=100Ω with tolerance ±0.012%). In practice, the RTDs have R^{o}values different from 100Ω so that

$$\Delta T^{o} = \left(\frac{R_4}{R_4^{o}} - \frac{R_5}{R_5^{o}} \right) / \alpha \qquad (3)$$

where α is temperature linear coefficient of resistance of Pt (presumed to be known and identical for each RTD), and subscripts 4 and 5 refer to the calorimetric temperature sensors. This term is accommodated in the Energetic calibration procedure and contributes significantly to the curvature of K as ΔT tends to zero (Figure 2).

Excess power is defined as the difference between the output power determined calorimetrically from equation 1 or 2, and the measured electrical

---

[1] This function is so close to linear that orders higher than 2 were not needed.

[2] PTFC-100 manufactured by Sensotherm Temperatursensorik GmbH.

Downloaded by OHIO STATE UNIV LIBRARIES on July 1, 2012 | http://pubs.acs.org
Publication Date: August 1, 2008 | doi: 10.1021/bk-2008-0998.ch010

Downloaded by OHIO STATE UNIV LIBRARIES on July 1, 2012 | http://pubs.acs.org
Publication Date: August 1, 2008 | doi: 10.1021/bk-2008-0998.ch010

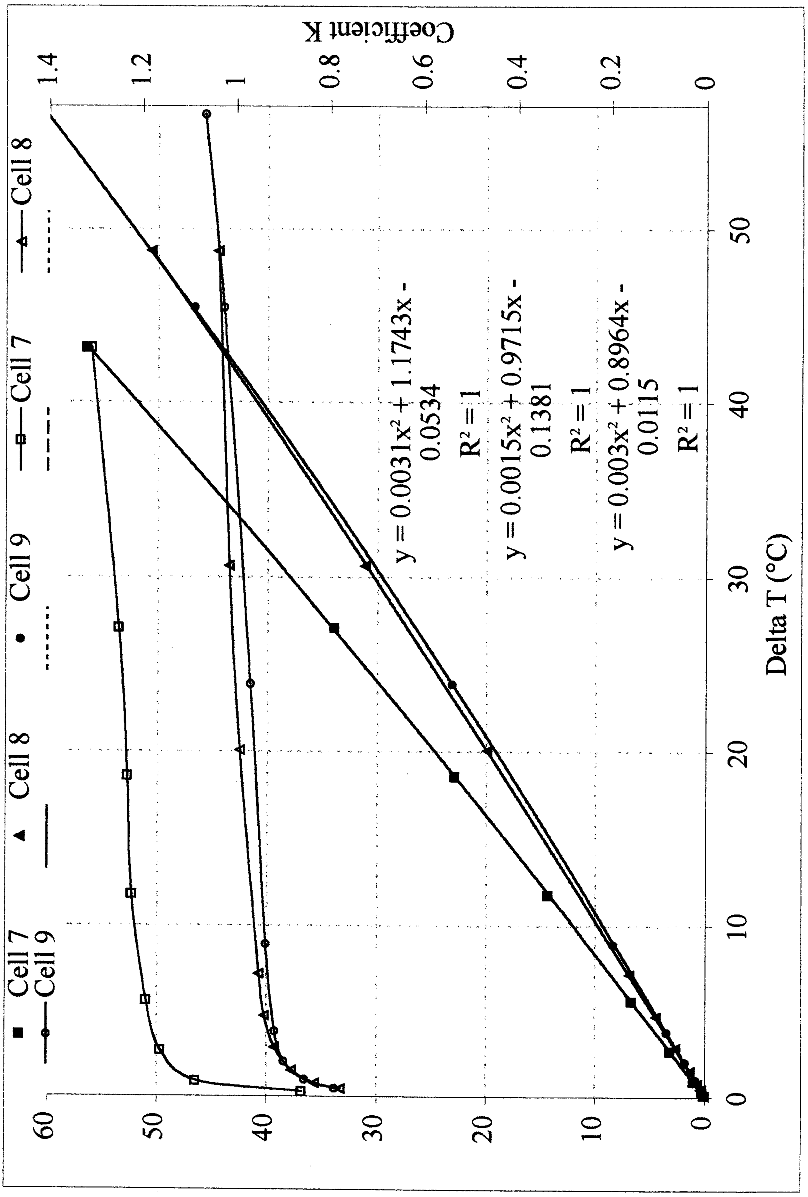

Figure 2. Calibration of calorimeters 7-9.

input to the cell. In thermodynamically open (although physically partially closed) cells such as those operated by Energetics, the chemical energy of the electrolyzed gases, D_2 or H_2 and O_2, are conveyed out of the cell. These gases may be vented or, as in the case of the Energetics cell design, externally recombined and the recombinant liquid returned to the cell. The rate of the return liquid flow is low at the currents used experimentally, and the return path is well coupled to the ambient so that the exothermic heat of recombination is deposited largely outside the calorimetric boundary. To account for this endothermic term, the electrolytic input power is modified as

$$P_{In} = I\,(V - V_{TN}) \qquad (4)$$

where V_{TN}, the thermo-neutral voltage, is 1.54V for the electrolysis of D_2O and 1.48V for H_2O; P_{In} , I, and V are all functions of time.

To increase calorimeter sensitivity between Steps 1 and 3 without affecting accuracy, the SRI data acquisition procedure incorporated a non-steady-state correction for the input power. The power that enters the calorimeter via equation 4 is presented and measured essentially immediately. In contrast, the resulting output heating is measured as a rise in T_4 that is converted to power using Equation 1 or 2. This rise in output power is substantially delayed by two factors:

i. the rate of heat transport from the electrodes to the cell walls and
ii. the time taken to establish a new dynamic balance between the heat flow in, and the heat flow out across the controlled heat leak path between the T_4 and T_5 boundaries.

We therefore expect the output power response of the calorimeter to a step function change in input power, ΔP_{In} at t°, to exhibit a double exponential delay, something of the form

$$P_{Out,New} = P_{Out,Old} + \Delta P_{In}\,(1-e^{-\Delta t/\tau_1})\,(1-e^{-\Delta t/\tau_2}) \qquad (5)$$

where $\Delta t = t - t°$ and τ_1 and τ_2 are time constants for heat transfer processes (i) and (ii) above. The three Energetics isoperibolic calorimeters delivered to SRI were observed to follow closely the form of equation 5, with $\tau_1 \leq 5$ and $\tau_2 \approx 53$ minutes.

Current Perturbation

Electrolysis conditions in the cells were controlled using a computer synthesized superwave signal delivered to the cells by four-quadrant Kepco BOP 50-M power supplies operated in controlled current mode. While not rigorously specified mathematically, the rules for generating a superwave

Downloaded by OHIO STATE UNIV LIBRARIES on July 1, 2012 | http://pubs.acs.org
Publication Date: August 1, 2008 | doi: 10.1021/bk-2008-0998.ch010

require a signal of self-similar character to a kernel function that increases in frequency and amplitude as the amplitude of the kernel increases.

In principle, the self-similar application of this rule up-scale and downscale to higher and lower frequencies occurs without limit in either direction. In practice we are constrained by our ability to deliver and measure signals. The low frequency limit is imposed by what is a practical or natural interval in the loading cycle of a PdD cathode. For most of the experiments described this interval, the cycle time was set at 15 or 20 minutes.[3]

A practical high-frequency limit is imposed by the ability of the power supply to deliver and the Faradaic electrochemical processes to accept high-frequency currents. The largely capacitive character of the electrode interfacial impedances demand higher and higher currents with increasing frequency. A second experimental limitation is imposed by our ability to measure accurately the average power input and thus to perform accurate calorimetry. The high-frequency limit was constrained by the Nyquist-Shannon sampling theorem[4] to 100 Hz, making the superwave effective frequency range ~1 mHz to ~100 Hz, a dynamic range of ~10^5.

Superwave perturbations were constructed within the constraints discussed above, using some additional rules relating to the maximum and minimum amplitudes discovered by Energetics to be effective in promoting loading and excess heat, and the imposed 1-minute (16.66 m Hz.) averaging and recording interval. Integral minute intervals were used to prevent aliasing in the measured data. One example of a superwave used in the experiments described below is shown in Figure 3. In this simple example the kernel is a sine squared function with a fundamental period of 15 minutes. Five levels of nesting are used, each 15 times higher in frequency than the preceding to yield a 1-minute periodicity consistent with the measurement input averaging interval, and higher terms.

Downloaded by OHIO STATE UNIV LIBRARIES on July 1, 2012 | http://pubs.acs.org
Publication Date: August 1, 2008 | doi: 10.1021/bk-2008-0998.ch010

Results

Table I provides a summary of the loading and excess heat results obtained in both Step 1 (Energetics) and Step 3 (SRI) phases of data acquisition. Three things should be noted:

1. Consistently high levels of loading were obtained
2. High reproducibility of the excess heat effect
3. High percentage excess heat relative to P_{In}.

---

[3] The diffusional time constant for 25 μm penetration with $D = 2\times10^{-7}\,cm^2\,s^{-1}$ is ~ 20 seconds.

[4] Exact reconstruction of a continuous-time baseband signal is possible if the signal is bandlimited and the sampling frequency is greater than twice the signal bandwidth.

Downloaded by OHIO STATE UNIV LIBRARIES on July 1, 2012 | http://pubs.acs.org
Publication Date: August 1, 2008 | doi: 10.1021/bk-2008-0998.ch010

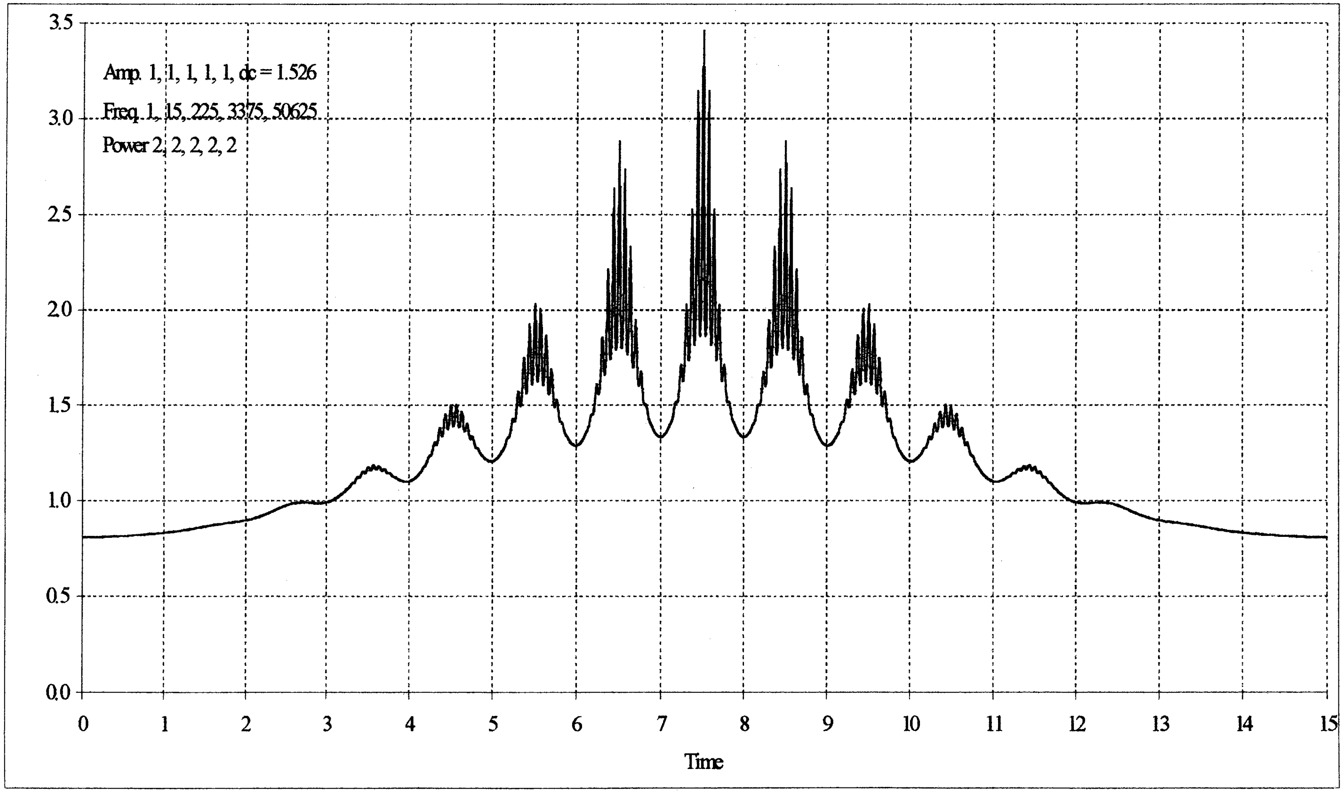

Figure 3. Fifth-order superwave.

In Low-Energy Nuclear Reactions Sourcebook; Marwan, J., et al.;
ACS Symposium Series; American Chemical Society: Washington, DC, 2008.

Downloaded by OHIO STATE UNIV LIBRARIES on July 1, 2012 | http://pubs.acs.org
Publication Date: August 1, 2008 | doi: 10.1021/bk-2008-0998.ch010

We attribute the highloadings to the metallurgical preparation of the palladium foils at ENEA, Frascati, including surface morphology screening conducted at the University of Rome, combined with the very high loading power of the superwave cathodic stimulus. High levels and reproducibility of excess power are a combined effect of the very high loading and the extraordinarily large deuterium interfacial fluxes created by the superwave currents.

Table I. Summary of the Loading and Excess Heat Results at SRI

Cell	*Site**	*Cathode*	*Min*	*Max.*	*Maximum Excess Power[6]*		*Total Excess*
Calorimeter			*R/R^o*	*D/Pd[5]*	*% of P_{In}*	*mW*	*Energy, kJ*
9-7	E	Lot A	1.77	0.895	<5%		
11-8	E	L5(2)	1.67	**0.915**	**60%**	**340**	**514**
12-9	E	Lot A	1.84	0.877	<5%		
15-7	E	L5(1)	1.77	0.895	<5%		
16-8	E	L5(4)	1.86	0.871	<5%		
17-9	E	L1(1)	1.55	**0.939**	**20%**	**460**	**407**
21-7	E	# 830	1.92	0.836	<5%		
22-8	E	L5(3)	1.8	**0.888**	**30%**	**200**	**188**
35-7	S	L17(1)	1.32	**0.985**	**12%**	**1800**	**553**
35-8	S	L17(2)	0.95	**1.059**	**13%**	**2066**	**313**
35-9	S	L17	1.39	0.971	1%		
43-7	S	L14-2	1.73	**0.903**	**80%**	**1250**	**245**
43-8	S	ETI	1.63	0.923	**5%**	**525**	**65**
43-9	S	L14-3	1.61	0.927	1%		
51-7	S	L25B-1	1.55	**0.939**	**12%**	**266**	**176**
51-8	S	L25A-2	1.52	**0.945**	**5%**	**133**	**14**
51-9	S	L19	1.54	**0.941**	**43%**	**79**	**28**
56-7	S	L24F	1.55	**0.939**	**15%**	**2095**	**536**
56-8	S	L24D	1.84	0.877	4%		
56-9	S	L25B-2	1.56	0.937	3%		
57-8	S	Pd-C	N.A.	N.A.	**300%**	**93**	**115**
58-9	S	L25A	1.69	**0.911**	**200%**	**540**	**485**
61-7	S	L25B-1	1.63	**0.923**	**50%**	**105**	**146**

*E = Energetics and S = SRI Data Acquisition.

---

[5] The loading was obtained from the measured resistance ratio using the method and calibration function described in Ref. (8).

[6] At any time in the experiment.

Figure 4 shows a null result obtained using the Energetics data acquisition method. The solid black line at the top of Figure 4 is the temperature-corrected resistance ratio referred to the right axis. Plotted on the left axis are the input, output, and excess power in watts, as these respond to the changing in cell current in amps. The sharp spikes in the input power correspond to the superwave current maxima shown in Figure 3.

The excess power, P_{XS}, calculated as the difference between the measured output and input powers without non-steady-state correction, shows considerable scatter (~10% of P_{In}). The average value of P_{XS} is, however, very close to zero and does not respond to the stepped increase in average current density. The total excess energy calculated as the integral of P_{XS} in the interval shown in Figure 4 was -0.1 ± 5 kJ.

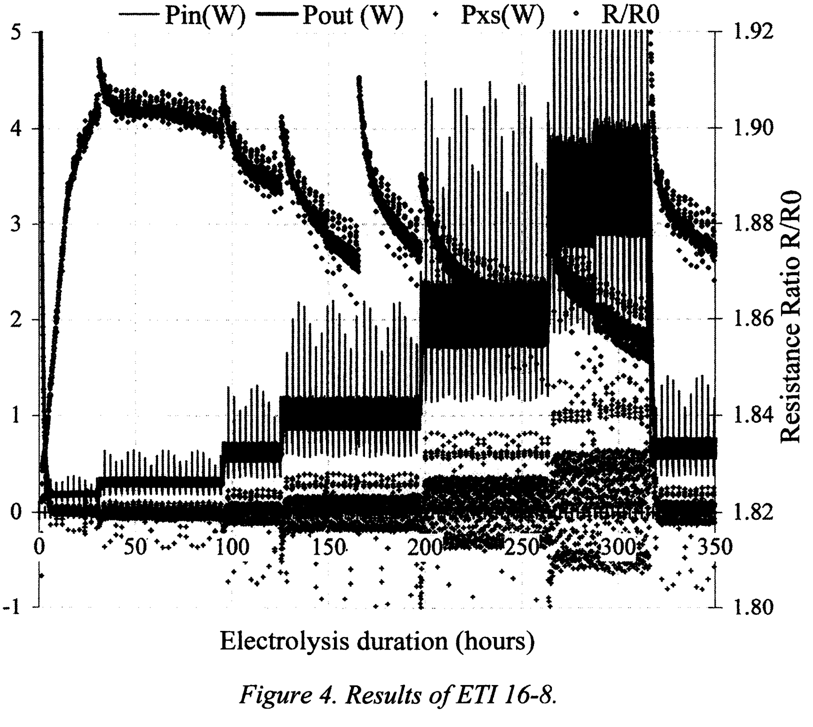

Figure 4. Results of ETI 16-8.

Results obtained using the Energetics data acquisition system were consistent with those using the SRI method. The implementation of a steady-state correction in the latter method, however, made the calorimetric results of small excess power easier to interpret in the presence of large superwave perturbation. Figure 5 shows a null result obtained using non-steady-state correction covering a wide dynamic range of power input. Three factors are significant in this result:

Downloaded by OHIO STATE UNIV LIBRARIES on July 1, 2012 | http://pubs.acs.org
Publication Date: August 1, 2008 | doi: 10.1021/bk-2008-0998.ch010

Downloaded by OHIO STATE UNIV LIBRARIES on July 1, 2012 | http://pubs.acs.org
Publication Date: August 1, 2008 | doi: 10.1021/bk-2008-0998.ch010

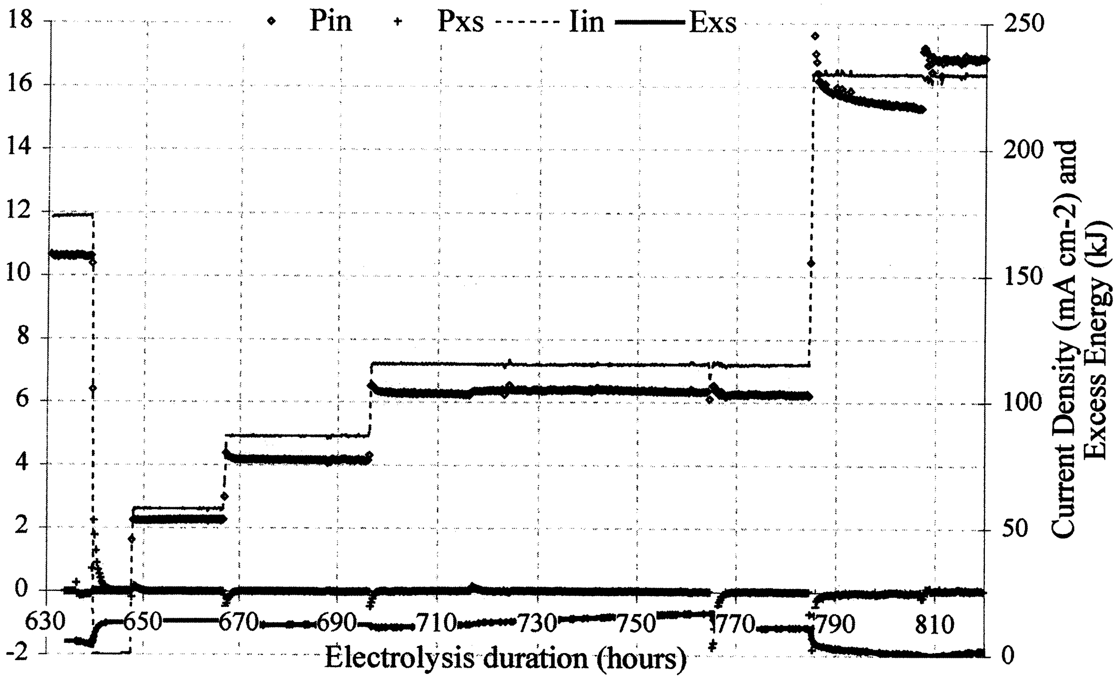

Figure 5. ETI 035-9 input and excess power, energy and current density.

1. Cell 35-9 obtained and maintained very high loading (D/Pd = 0.971) and high loading dynamics at high current density.
2. This calorimeter evidenced no excess heat at any time, although the electrolyte accumulated a significant amount of tritium.
3. This cathode was a commercial Johnson Matthey palladium foil.

Figure 6 shows a result of excess heat production from a cathode fabricated using ENEA and University of Rome protocols. The maximum loading obtained, D/Pd = 0.939, is significantly less than that in cell 35-9. Nevertheless a clear excess heat effect is observed, increasing in amplitude with current density above some non-zero current threshold value. At 232 h the calorimetric bath temperature was lowered from 23° to 3°C. This drop at a constant current of ~110 mA cm^{-2} resulted in an unexpected deloading of the cathode from D/Pd = 0.924 to 0.895. Despite this significant drop in loading with temperature, the excess power in Figure 6 makes a strong increase from ~0.6 to ~2.0 W (~15% of P_{In}) and then declines apparently spontaneously at constant current.

Figures 7 and 8 present calorimetric results for the first 500 hours of cell 58-9 on two different vertical scales. This cathode loaded very rapidly to a maximum D/Pd ratio of nearly 0.94 within 3 hours of operation. Accompanying this loading was significant excess heat from the beginning of effective calorimetry (~10 h into the experiment).

Although relatively small in absolute terms, the initial value of excess power (~330 mW) is already larger than the power input (~200 mW), resulting in a percentage excess of about 160%. Following a short anodic strip at ~47 h, the input power decreases, and the loading and excess power both increase, resulting in over 200% excess power.

Under constant conditions of superwave input current and bath temperature from ~170 to 420 hours, the excess power for cell ETI 56-7 decreases apparently spontaneously from ~0.55 to ~0.25 watts. This trend is not directly related to loading, however, which is on average essentially constant from the last current step at ~170 h to the current reversal at ~410 h that results in sharp deloading and the cessation of the excess heat effect. The two sharp transients of excess power seen in Figure 8 at ~316 and 347 h, which appear to arrest temporarily the decline of P_{XS} with time, do correlate with small stepped increases in the average loading at constant current.

ENEA Replication

Calorimeter

A parallel but independent set of experiments was performed at ENEA using a mass flow calorimeter and employing Energetic's superwave stimulus protocols and palladium foils fabricated at ENEA. The calorimetric cells have

Downloaded by OHIO STATE UNIV LIBRARIES on July 1, 2012 | http://pubs.acs.org
Publication Date: August 1, 2008 | doi: 10.1021/bk-2008-0998.ch010

Downloaded by OHIO STATE UNIV LIBRARIES on July 1, 2012 | http://pubs.acs.org
Publication Date: August 1, 2008 | doi: 10.1021/bk-2008-0998.ch010

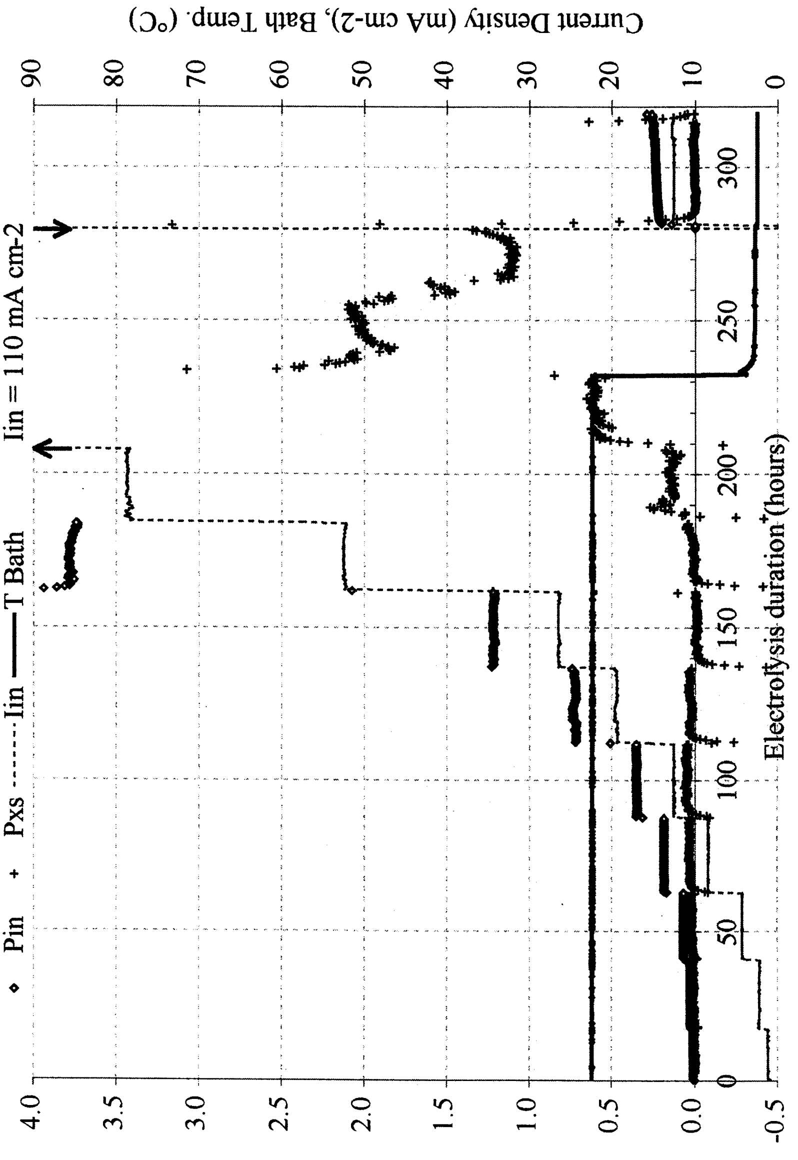

Figure 6. ETI 56-7 power, current density and bath temperature.

Downloaded by OHIO STATE UNIV LIBRARIES on July 1, 2012 | http://pubs.acs.org
Publication Date: August 1, 2008 | doi: 10.1021/bk-2008-0998.ch010

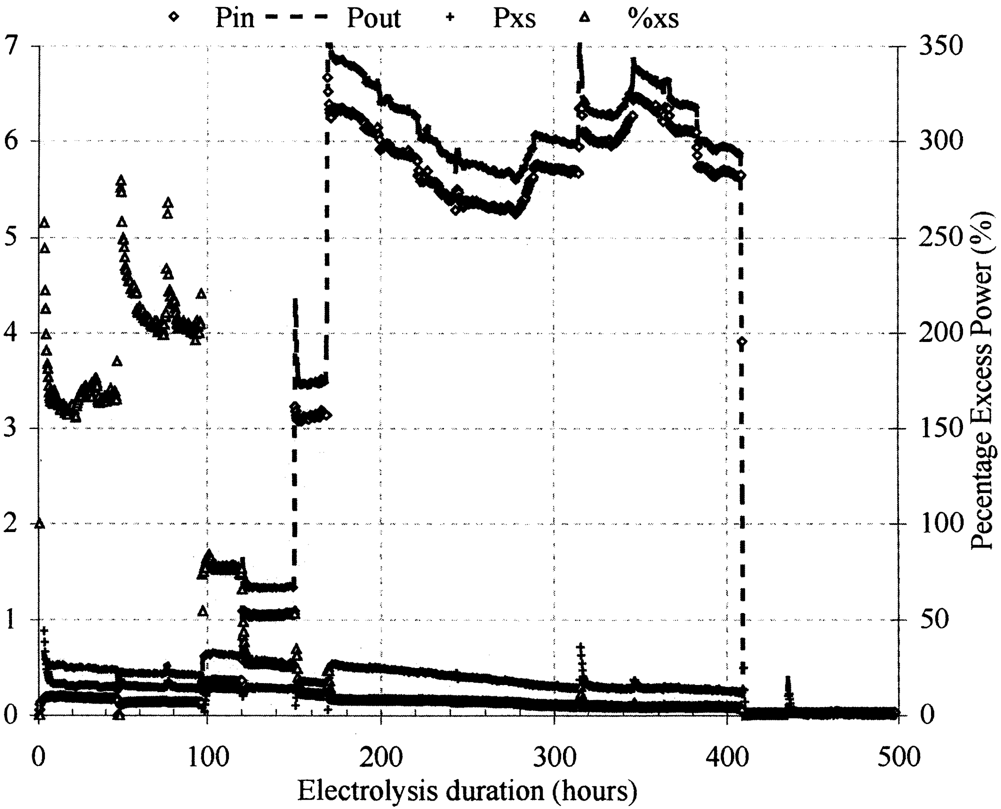

Figure 7. ETI 058-9 power and percentage excess power.

Downloaded by OHIO STATE UNIV LIBRARIES on July 1, 2012 | http://pubs.acs.org
Publication Date: August 1, 2008 | doi: 10.1021/bk-2008-0998.ch010

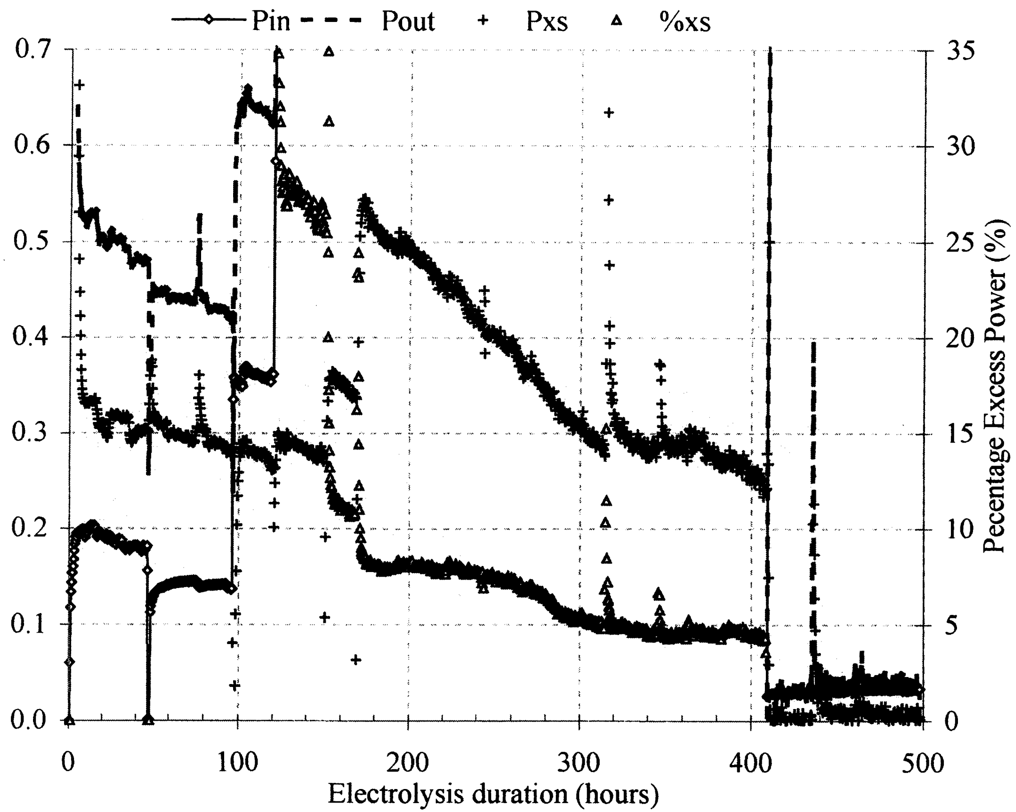

Figure 8. ETI 058-9 power and percentage excess power (expanded vertical scale).

Downloaded by OHIO STATE UNIV LIBRARIES on July 1, 2012 | http://pubs.acs.org
Publication Date: August 1, 2008 | doi: 10.1021/bk-2008-0998.ch010

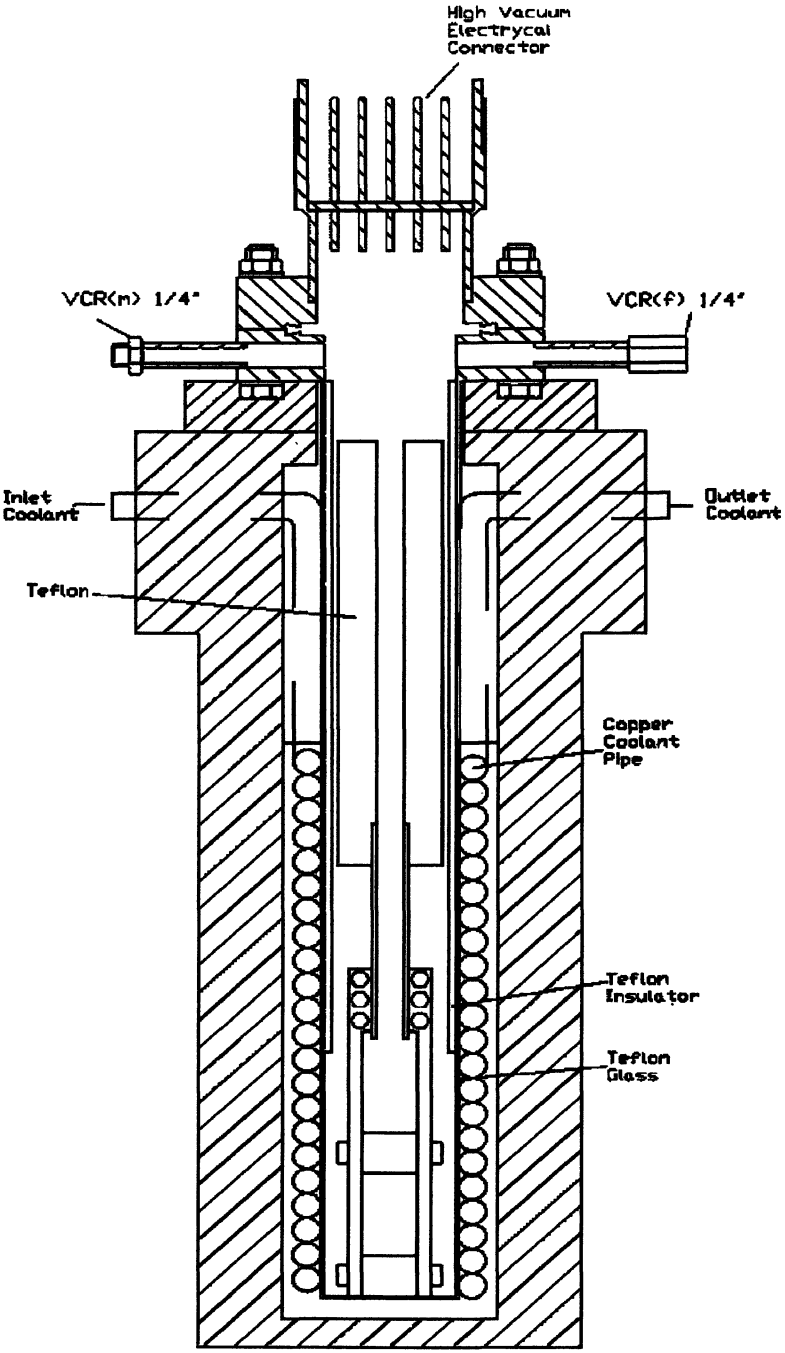
High Vacuum
Electrycal
Connector
VCR(m) 1/4"
VCR(f) 1/4"
Inlet
Coolant
Outlet
Coolant
Teflon
Copper
Coolant
Pipe
Teflon
Insulator
Teflon
Glass

Figure 9. Flow calorimeter electrochemical cell.

been modeled and designed to have the required sensitivity and measurement accuracy by using a three-dimensional, time-dependent, finite element approach. Figure 9 shows the cell with working electrolyte volume 30 ml. The calorimeter body is helium leak-tight. Calorimetry is performed by passing water at a constant rate through a copper cooling coil that is submerged into a water jacket containing the electrochemical cell.

Figure 10 shows an overview of the measurement apparatus. Output power is measured by means of the measured mass flow rate and coolant temperatures. The D/Pd loading is determined from the resistance ratio measured using a HP-4284 (four-wire measurement). Palladium foil cathodes were used (20 × 10 mm × 50 μm) sandwiched between two co-parallel platinum foils (symmetric 45 × 15 mm) with anode-cathode spacing of 6 mm. The sensitivity of the calorimeter was estimated to be 50 mW ± 20 mW.

Downloaded by OHIO STATE UNIV LIBRARIES on July 1, 2012 | http://pubs.acs.org
Publication Date: August 1, 2008 | doi: 10.1021/bk-2008-0998.ch010

Results

Several experiments were performed using light-water electrolytes to evaluate the thermal efficiency and check calorimeter function. No excess power production was observed by using H_2O although very high loadings (H/Pd = 0.97) were always achieved. Figure 11 shows the evolution of the input and output power and energy for one such experiment that may be considered as a reference or blank. No evidence of excess of power was observed and the output energy matches the calorimetric thermal efficiency of 97.5%. No attempt was made to correct the data for non-steady-state effects.

ENEA foil sample L14 showed a good loading up to D/Pd = 0.95 in 0.1 M LiOD electroyte with the maximum loading being achieved at very low current (<2 mA cm^{-2}) using superwave electrolysis current. Excess power occurred as shown in Figure 12 during the superwave current treatment. Both heat bursts are very well correlated with the electrolyte temperature plotted with respect to the right axis of Figure 12. The temperature of the electrolyte was monitored independently of the inlet and outlet coolant temperature. The maximum amplitude of excess achieved 80% of the electrolysis input power.

Large-ratio, although brief-duration power bursts were observed also with dc input current. Figure 13 shows the evolution of the input and output power for cathode L17. The second burst is long enough to allow the calorimeter to closely approach the steady state. During the excess power burst the input power reduces due to the strong heating of the cathode and electrolyte causing a reduction of the cathode interfacial impedance and the electrolyte resistivity (at constant dc current). The evolution of the temperature of the electrolyte is shown on the right axis of Figure 13. A maximum of 620 mW of output power was observed at an input of 125 mW so that the output power gain was 500%.

A more dramatic effect was observed with the specimen L30 where the excess power was so high that the temperature increase of the electrode caused a rapid deloading that apparently terminated the excess power. Figure 14 shows

Downloaded by OHIO STATE UNIV LIBRARIES on July 1, 2012 | http://pubs.acs.org
Publication Date: August 1, 2008 | doi: 10.1021/bk-2008-0998.ch010

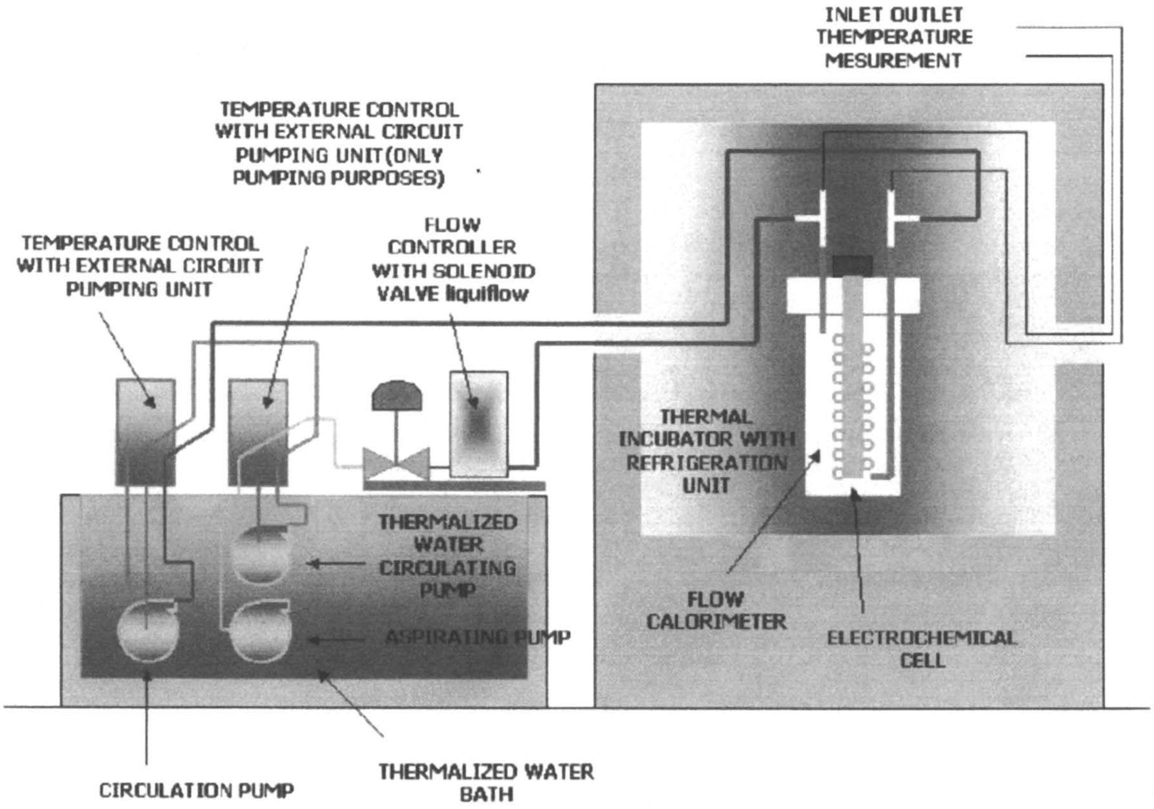
INLET OUTLET THEMPERATURE MESUREMENT
TEMPERATURE CONTROL WITH EXTERNAL CIRCUIT PUMPING UNIT(ONLY PUMPING PURPOSES)
TEMPERATURE CONTROL WITH EXTERNAL CIRCUIT PUMPING UNIT
FLOW CONTROLLER WITH SOLENOID VALVE liquiflow
THERMAL INCUBATOR WITH REFRIGERATION UNIT
THERMALIZED WATER CIRCULATING PUMP
ASPIRATING PUMP
FLOW CALORIMETER
ELECTROCHEMICAL CELL
CIRCULATION PUMP
THERMALIZED WATER BATH

Figure 10. System overview.

Downloaded by OHIO STATE UNIV LIBRARIES on July 1, 2012 | http://pubs.acs.org
Publication Date: August 1, 2008 | doi: 10.1021/bk-2008-0998.ch010

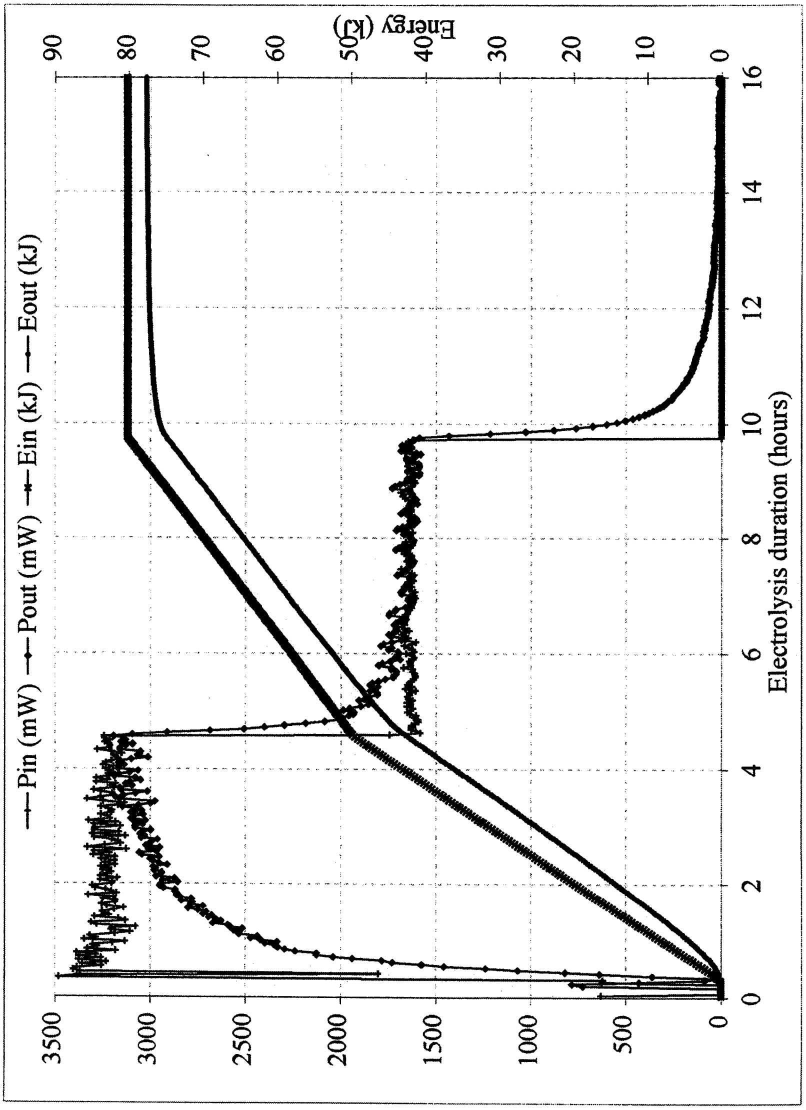

Figure 11. Input and output power and energy evolution with H_2O.

In Low-Energy Nuclear Reactions Sourcebook; Marwan, J., et al.;
ACS Symposium Series; American Chemical Society: Washington, DC, 2008.

Downloaded by OHIO STATE UNIV LIBRARIES on July 1, 2012 | http://pubs.acs.org
Publication Date: August 1, 2008 | doi: 10.1021/bk-2008-0998.ch010

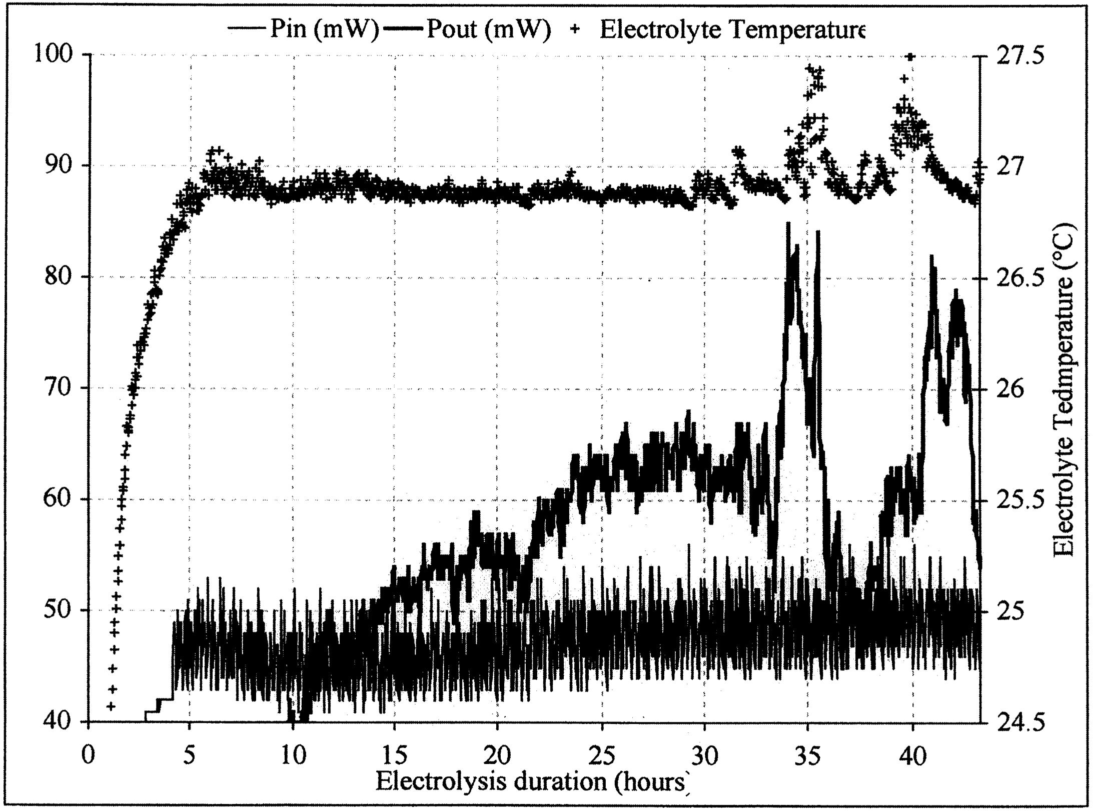

Figure 12. ENEA foil L14 power and electrolyte temperature.

Downloaded by OHIO STATE UNIV LIBRARIES on July 1, 2012 | http://pubs.acs.org
Publication Date: August 1, 2008 | doi: 10.1021/bk-2008-0998.ch010

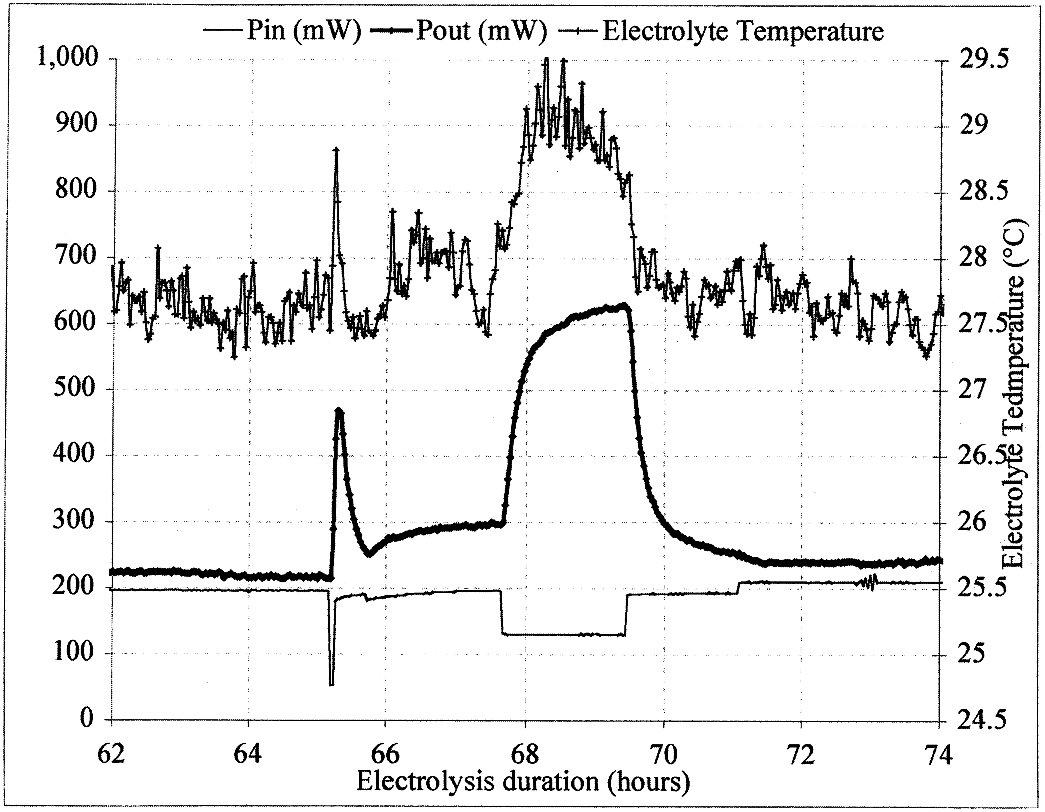

Figure 13. ENEA foil L17 power and electrolyte temperature.

Downloaded by OHIO STATE UNIV LIBRARIES on July 1, 2012 | http://pubs.acs.org
Publication Date: August 1, 2008 | doi: 10.1021/bk-2008-0998.ch010

this extraordinary excess power burst that survived only a few minutes. This power burst caused a rapid increase in the electrolyte temperature of more than 6 °C, as can be seen plotted on the right axis of Figure 14.

The lifetime of this excess power burst was short compared with the calorimeter thermal time constant (~10000s). After ~600 seconds P_{Out} was around 800 mW with an input of 100 mW. It is possible to reconstruct the peak height and duration of the excess power burst using the known thermal masses and transient response characteristics of the calorimeter. A satisfactory match with the output power response shown in Figure 14 can be achieved with a putative power pulse of 7 W occurring for 600 seconds. With an input power of 100 mW this would imply an excess power of 7000%, corresponding to a power density of 700 W cm^{-3}. This is the largest excess power observed at ENEA.

Table II summarizes results of six successful ENEA replication attempts, including the three discussed above. All results except L17 and L30 were obtained using Energetics superwave stimulus.

Table II. ENEA Excess Power Summary

Data Acquisition	Cathode	Min. R/R°	Max. D/Pd	P_{xs} % of P_{In}	Power Mode
ENEA	L14	1.54	0.941	80	B
ENEA	L17	1.40	0.969	500	B
ENEA	L19	1.70	0.909	100	A
ENEA	L23	1.69	0.911	37	B
ENEA	L25A	1.80	0.888	24	B
ENEA	L30	1.78	0.892	7000	B

Discussion and Conclusions

The Energetics calorimeters and cells were found to be well designed and calibrated, and capable of steady baseline operation in the absence of excess heat. The three-sigma (3σ) calorimetric uncertainty was estimated to be approximately 5% of the input power under normal input conditions. Of the fifteen experiments performed using SRI data acquisition and Energetics superwave current stimulation, eleven produced excess heat at or above the 3σ experimental uncertainty. As far as we are aware, this level of reproducibility is hitherto unprecedented in the fields of cold fusion or condensed matter nuclear science (CMNS). This high level of reproducibility is attributable to two conspicuous differences between Energetics experiments and all those that preceded them:

1. Very high deuterium atom loadings that result from superwave cathodization of appropriately prepared palladium foils.

Downloaded by OHIO STATE UNIV LIBRARIES on July 1, 2012 | http://pubs.acs.org
Publication Date: August 1, 2008 | doi: 10.1021/bk-2008-0998.ch010

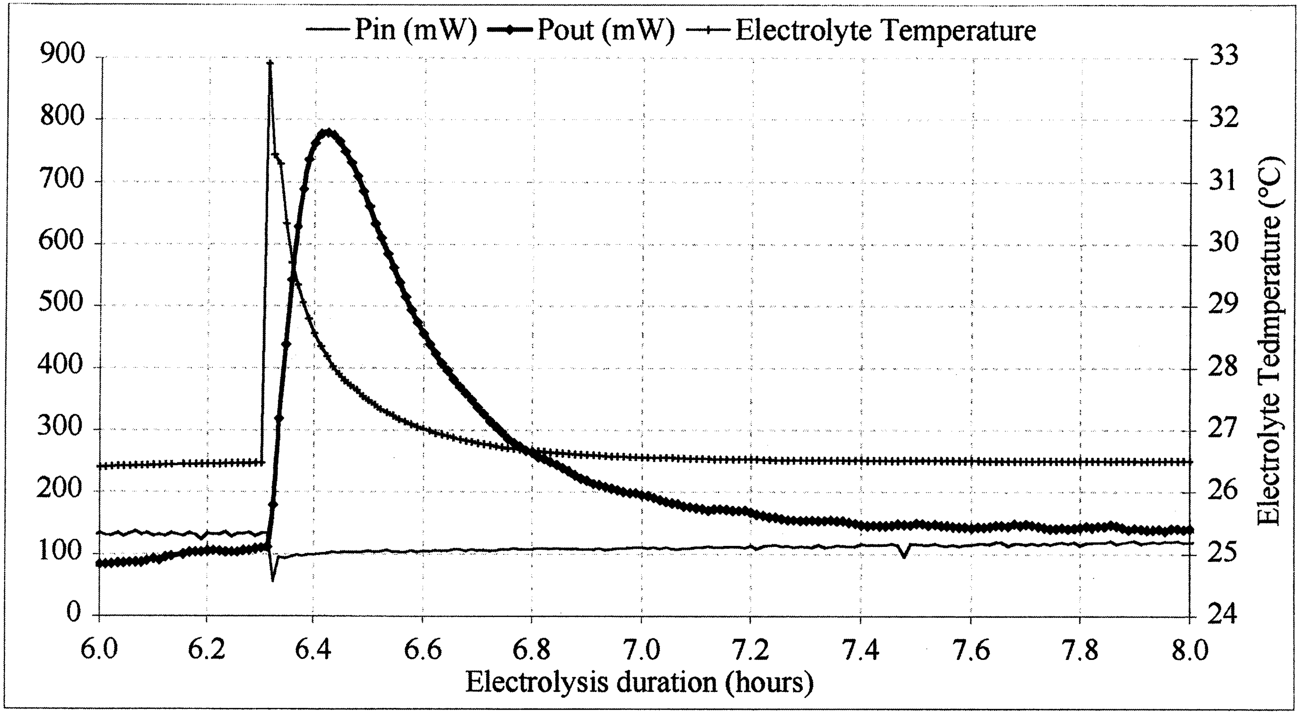

Figure 14. ENEA foil L30 power and electrolyte temperature.

2. The extraordinarily high interfacial flux of deuterium in and out through the palladium cathode surface that results from superwave stimulus.

Heat Effects

Excess power was observed to have two phenomenologically different forms that we tentatively identify as Modes A and B. The general features of these different modes are as follows.

Mode A. One example is shown in Figure 6. This behavior conforms closely to equation 6

$$P_{xs} = M(x - x^{\circ})^2 (i - i^{\circ})|i_D| \quad (6)$$

where M is a proportionality constant, i is the electrochemical current or current density and i° a critical threshold, x = D/Pd is the deuterium atom loading and x° the threshold loading below which no excess heat is observed – typically $x^{\circ} \approx 0.875$, and $|i_D|$ is the flux of D across the interface expressed as a current density.

The form of equation 6 was first recognized (6) in excess heat experiments conducted with 1 mm diameter palladium wire cathodes. The ~50 μm thick foils used in the experiments described in this report show similarities but also systematic differences with Pd wires in the constants of equation 6. The loading threshold observed in both cases is very similar with $x^{\circ} \approx 0.875$. For the foils examined in this study the current density thresholds, i°, were a factor of 5-10 lower than for 1 mm wires although this may partially result from the lesser degree of current uniformity for the foil geometry. For geometric reasons associated with anode-cathode areas and spacing, the accessible range of current density for foil electrolysis is very much less than for wires.

The interfacial flux can be calculated directly from the minimum and maximum loading values obtained from the resistance ratio measurements in the fundamental superwave interval (15 or 20 minutes). Probably more a result of the superwave dynamics than geometric effects the interfacial flux term, $|i_D|$, was up to an order of magnitude larger in the present study compared with previous dc electrolysis of palladium wires.

This combination of factors led to excess power effects of 5-50% of the input power, in Mode A, very consistent with previous excess heat results at SRI and elsewhere (7). Although the proportionality constant "M" of equation 6 is not well specified and probably reflects some properties of surface heterogeneity, this equation permits explanation of experiments that do not produce heat excess. The failure to meet and maintain the current, loading, and flux criteria simultaneously results in a failure to observe Mode A excess heat.

Mode B. A second mode of behavior was seen in three experiments at SRI and five at ENEA, and in all of those exhibiting excess power greater than 100%. This mode is more typical of that reported previously by Energetics (*1-4*).

Downloaded by OHIO STATE UNIV LIBRARIES on July 1, 2012 | http://pubs.acs.org
Publication Date: August 1, 2008 | doi: 10.1021/bk-2008-0998.ch010

In this mode the excess power is relatively insensitive to input power and current, and may be present early in the loading history of a cathode. One example is shown in Figures 7 and 8. This is also the characteristic of the protypical Energetics result shown in Figure 1. Observations were made of sustained excess power at very low input power levels. With the reduced denominator, measurements were made at SRI of P_{xs}/P_{In} = 50%, 80%, 200%, and over 300%. At very low input powers sustained observations were made of $P_{xs}/P_{In} = 28 \pm 1$ (i.e., 2800%) for 40 h or more. At ENEA even larger transient power gains were estimated.

The phenomenological differences between Mode A and Mode B behavior can be summarized as follows:

1. Mode B excess heat can initiate within 10 h of the application of cathodic current (or 4 h of maximum loading), whereas Mode A behavior requires a longer initiation time, typically several hundreds of hours.
2. Mode B responds sluggishly to input cathodic current density and, so far, exhibits no obvious current density threshold.
3. Mode B has not been observed at D/Pd loadings less than the threshold typical of Mode A behavior (D/Pd ≈ 0.875) but appears to respond only transiently to increased average loading.

Loading

Fifteen experiments were run with SRI hardware, software, and staffing, using the Energetics cells and cathodes prepared at ENEA, Energetics, and one other. Of these, eleven produced clear evidence of excess heat ranging to over 2 W or 25-75 W per cm^3 of cathode. A remarkable feature of this set of experiments was the consistency of loading and of excess heat. The loadings obtained were impressive. Only two had maximum loading D/Pd less than 0.9 (0.88 and 0.89). One cathode exhibited atomic loading ratios apparently greater than unity suggesting the possibility tetrahedral as well as octahedral site occupation. Such high loading values have not previously been reported for foils, and such loading consistency is unprecedented with any type of electrode in heavy-water electrolysis.

The extreme level of loading and high consistency of good loading are attributable to two features of this set of experiments:

1. A high degree of microstructural metallurgical control allows electrodes to accept loading without damaging deformation. This treatment process has been developed largely at ENEA and the University of Rome and involves not only control of the bulk crystallinity but extends to control of the surface roughness.
2. The superwave excitation function produces current driven fields which interact with the deuterium atom–ion dynamics in a number of ways.

Downloaded by OHIO STATE UNIV LIBRARIES on July 1, 2012 | http://pubs.acs.org
Publication Date: August 1, 2008 | doi: 10.1021/bk-2008-0998.ch010

Downloaded by OHIO STATE UNIV LIBRARIES on July 1, 2012 | http://pubs.acs.org
Publication Date: August 1, 2008 | doi: 10.1021/bk-2008-0998.ch010

Regions of interest are: the mass transport controlled boundary layer in the electrolyte, the charged electro-chemical double layer and the associated electrochemical kinetic process at the electrode/electrolyte interface, the dynamic diffusion region of absorbing D atoms just below the cathode surface, the possible role of surface roughness interacting with surface plasmons. The role or roles of superwaves in affecting these processes justifies further study both to understand excess heat results and as a potentially new and better means to load hydrogen into metals.

Although not exhaustively tested in the present study, it is apparent that superwave stimulus plays a vital second role in our excess heat results, at least in Mode A response. The superwave modulated currents result in a very large loading dynamic (interfacial deuterium atom flux) that is not present with dc or sinusoidal ac stimulation. Using superwaves, we have been able to achieve fluxes of up of 6×10^{16} particles per cm^2 per second through the interface, or 40 transitions per second for every atom absorption site on the cathode surface. We speculate that this huge flux provides a stimulus for the excess heat effect, but further work is needed to understand the detailed causes of this high flux and its possible nuclear consequences.

As a final exercise the results obtained in this phase of experimentation at SRI and ENEA were compared with those obtained during the previous 17 years of Pd/D_2O calorimetry. Figure 15 plots as a histogram experiments that produced excess heat and those that did not versus the maximum loading D/Pd of the cathode during the course of the experiment. A clear trend can be observed. Cathodes capable of achieving high average loading are also those capable of producing excess heat. This new experimental information allows us to further refine our knowledge of the heat/no-heat boundaries.

It should be noted, however, that the maximum loading criterion tells us something about whether (or not) a PdDx cathode is going to produce excess. In some experiments the maximum heat was produced at times other than maximum loading; the statistically important feature appears to be capacity to obtain high loading. To get more information about when and how much heat is produced[7] we need to have more information about conditions of surface stimulation (current, laser, etc.) and surface dynamics (deuterium flux).

One data point in Figure 15 remains anomalous. The inability of cathode 035-9 to evince excess heat cannot be accounted for by reference to the maximum loading criterion or by other obvious factors of equation 6. The cathode used in this experiment was a commercial Johnson Matthey foil rather than being fabricated at ENEA, Frascati. It is not yet known whether metallurgical or chemical impurity factors contribute to making cathode 035-9 a statistical anomaly. It is, however, very important to understand this case as it may provide insight into other successful and unsuccessful experiments and therefore into the fundamental question of the apparent irreproducibility of the excess heat effect.

---

[7] More accurately, heat rate or power.

Downloaded by OHIO STATE UNIV LIBRARIES on July 1, 2012 | http://pubs.acs.org
Publication Date: August 1, 2008 | doi: 10.1021/bk-2008-0998.ch010

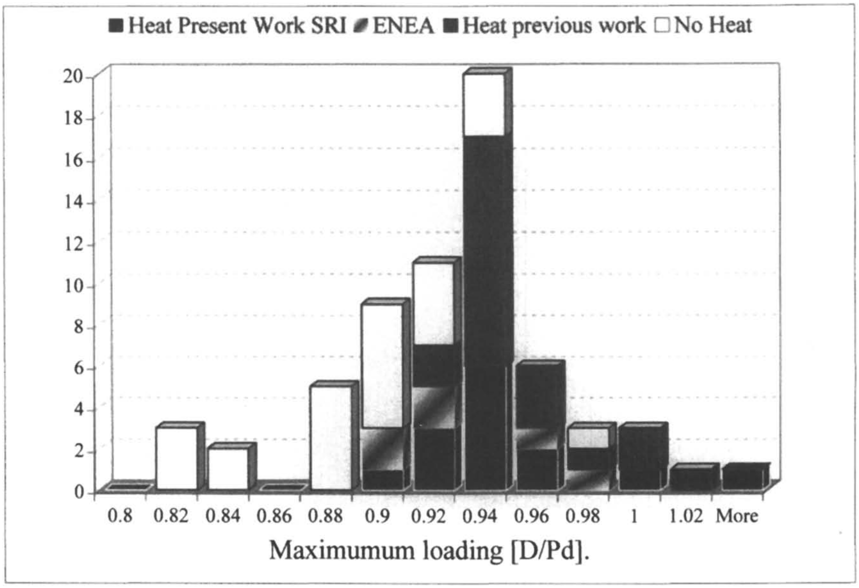

Figure 15. Incidence of excess heat versus Maximum D/Pd Loading.

Acknowledgements

The authors wish to acknowledge the significant financial support and vision of DARPA, the Italian Ministry of Economic Development and Mr. Sidney Kimmel, without which and whom this work could not have been undertaken.

References

1. Dardik, I.; Branover, H.; El-Boher, A.; Gazit, D.; Golbreich, E.; Greenspan, E.; Kapusta, A.; Khachatorov, B.; Krakov, V.; Lesin, S.; Michailovitch, B.; Shani, G.; Zilov, T. Intensification of Low Energy Nuclear Reactions Using Superwave Excitation. In *Condensed Matter Nuclear Science: Proceedings of the 10th International Conference on Cold Fusion*, Cambridge, MA, Aug. 24-29, 2003; Hagelstein, P. L.; Chubb, S. R., Eds.; World Scientific Publishing Co.: Singapore, 2006; 61.
2. Dardik, I.; Zilov, T.; Branover, H.; El-Boher, A.; Greenspan, E.; Khachatorov, B.; Krakov, V.; Lesin, S.; Tsirlin, M. Excess Heat in Electrolysis Experiments at Energetics Technologies. In *Condensed Matter Nuclear Science: Proceedings of the 11th International Conference on Cold Fusion*, Marseilles, France, Oct. 31 - Nov. 5, 2004; Biberian, J.-P., Ed.; World Scientific Publishing Co.: Singapore, 2006; 84.

3. Dardik, I.; Zilov, T.; Branover, H.; El-Boher, A.; Greenspan, E.; Khachaturov, B.; Krakov, V., S., L.; Tsirlin, M. Progress in Electrolysis Experiments at Energetics Technologies. In *Condensed Matter Nuclear Science: Proceedings of the 12th International Conference on Cold Fusion*, Yokohama, Japan, Nov. 27-Dec. 2, 2005; Takahashi, A.; Ota, K.-I.; Iwamura, Y., Eds.; World Scientific Publishing Co.: Singapore, 2006; 55.
4. Dardik, I.; Zilov, T.; Branover, H.; El-Boher, A.; Greenspan, E.; Khachaturov, B.; Krakov, V.; Lesin, S.; Tsirlin, M. Excess Heat in Electrolysis Experiments at Energetics Technologies. Presented at the Sixth International Workshop on Hydrogen/Deuterium Loaded Metals, Siena, Italy, May 13-15, 2005.
5. Violante, V.; Tripodi, P.; Di Gioacchino, D.; Borelli, R.; Pizzuto, A.; McKubre, M. C. H.; Tanzella, F.; Adrover, A.; Giona, M.; Capobianco, L. Metallurgical Effects on the Dynamic of Hydrogen Loading in Pd. In *Proceedings of the 9th International Conference on Cold Fusion: Condensed Matter Nuclear Science*, Beijing, China, May 19-24, 2002; Li, X. Z., Ed.; Tsinghua Univ. Press: Beijing, 2002; 383.
6. McKubre, M. C. H.; Crouch-Baker, S.; Hauser, A. K.; Smedley, S. I.; Tanzella, F. L.; Williams, M. S.; Wing, S. S., Concerning Reproducibility of Excess Power Production. In *Proceedings of the Fifth International Conference on Cold Fusion*, Monte Carlo, Monaco, April 9-13, 1995; Pons, S., Ed.; IMRA Europe: Sophia Antipolis Cedex, France, 1995; 17.
7. Storms, E. *The Science of Low Energy Nuclear Reactions*; World Scientific: Singapore, 2007.
8. McKubre, M. C. H.; Tanzella, F. L. Using Resistivity to Measure H/Pd and D/Pd Loading. In *Condensed Matter Nuclear Science: Proceedings of the 12th International Conference on Cold Fusion*, Yokohama, Japan, Nov. 27-Dec. 2, 2005; Takahashi, A.; Ota, K.-I.; Iwamura, Y., Eds.; World Scientific Publishing Co.: Singapore, 2006; 392.

Downloaded by OHIO STATE UNIV LIBRARIES on July 1, 2012 | http://pubs.acs.org
Publication Date: August 1, 2008 | doi: 10.1021/bk-2008-0998.ch010

Downloaded by CORNELL UNIV on July 2, 2012 | http://pubs.acs.org
Publication Date: August 1, 2008 | doi: 10.1021/bk-2008-0998.ch011

Chapter 11

Models Relevant to Excess Heat Production in Fleischmann–Pons Experiments

Peter L. Hagelstein* **and Irfan U. Chaudhary**

Research Laboratory of Electronics, Massachusetts Institute of Technology,
Cambridge, MA 02139
***Corresponding author: plh@mit.edu**

Observations of excess heat in the absence of commensurate energetic charged particles challenges local energy and momentum conservation, a foundation of nuclear physics. We have explored models based on excitation transfer, in which global energy is conserved but local energy conservation is violated. We present recent results on both excitation transfer and anomalous energy exchange within the context of lossless spin-boson models. We introduce a rotation that allows us to isolate terms in the rotated Hamiltonian responsible for both processes. Spin-boson type models augmented with loss appear to be sufficiently strong to account for the excess heat effect.

Claims of excess heat production in the Fleischmann-Pons experiment (*1-3*) were met with disbelief following the initial announcement of the effect in 1989 (*4*). In the controversy that followed, discussions centered on experimental questions of reproducibility, calorimetry, absence of energetic products correlated with the energy, and the initial lack of identification of an ash quantitatively correlated with the energy production. Discussions centered also on theoretical issues, such as the low associated reaction rates expected for conventional deuteron-deuteron fusion reactions due to the Coulomb barrier, competition with the primary n+^{3}He and p+t reaction channels, and on the seeming impossibility of coupling the MeV-scale nuclear reaction energy to low-energy atomic degrees of freedom associated with the solid state environment.

Research over the subsequent 18 years has clarified some of these issues. Several groups have reported good reproducibility in experiments with excess heat; similar positive results have been reported with very different calorimeters; and ^{4}He has been detected in amounts commensurate with the excess energy produced (see Ref. (*5*) and references therein). In the latter case, the reaction energy determined experimentally appears to be 24 MeV, suggesting an overall reaction mechanism consistent with

$$\mathrm{D+D} \rightarrow {}^4\mathrm{He} + 23.85\ \mathrm{MeV\ (heat)}$$

We recognize the existence of the conventional version of this reaction channel with ^{4}He and an energetic gamma in the exit channel; however, there is no evidence for energetic gammas being produced in amounts commensurate with the energy production in any Fleischmann-Pons experiment. In essence, excess heat in the Fleischmann-Pons experiment requires the existence of a new physical process, since no known nuclear reaction works this way.

The reaction energy from a conventional nuclear reaction, and in particular from a fusion reaction, is expressed through energetic particles as a consequence of local energy and momentum conservation. Local energy and momentum conservation has been a foundation of nuclear physics since the time of Rutherford (*6*), and one can find relevant expositions in modern nuclear physics texts (*7*). Excess heat production in the Fleischmann-Pons experiment challenges this foundation. Nuclear physicists since 1989 have been enthusiastic neither about the Fleischmann-Pons experiment nor about any discussion that includes a consideration of nuclear energy production in the absence of observations of energetic particles. No nuclear physics experiment within the entire nuclear physics literature dating back to before 1900 is thought to work this way, which leads to the tentative conclusion that this is because no nuclear reaction can produce energy without energetic particles.

Such a position was adopted in the 1989 ERAB report (*8*), and by Huizenga in his book (*4*). Until proven otherwise independent of the Fleischmann-Pons experiment, it is unlikely that the situation will change.

All of which provides motivation for the models discussed below. We have focused for several years on a class of models that seek to address violations of local energy and momentum conservation and also to address the problem of the conversion of a large energy quantum into a large number of smaller energy quanta (*9-11*). We view these two issues as separate problems, as will become clearer in the models themselves.

We take advantage of a quantum excitation transfer effect in order to violate local energy conservation, while preserving overall energy conservation. For example, if two deuterons react to form ^{4}He in such a model, the reaction energy is transferred elsewhere, so that there is no need for energetic particles from the initial four-nucleon system. Once this excitation transfer has occurred, we still need to convert the large MeV energy quantum into a very large number of atomic scale quanta. The basic mechanism under consideration for this is one in which the excitation is transferred one small energy quantum at a time in a very large number of interactions, including fast excitation transfer reactions to other nuclei, and self interactions.

Downloaded by CORNELL UNIV on July 2, 2012 | http://pubs.acs.org
Publication Date: August 1, 2008 | doi: 10.1021/bk-2008-0998.ch011

These notions already imply a set of models that can be studied, and we present below some results from our analysis of these systems. The results are interesting in the sense that we can establish an excitation transfer effect, as well as an energy exchange effect (in which a large quantum is split into a large number of small quanta), using very simple models composed of equivalent two-level systems and an oscillator. We would expect such models to fall short of describing the real system because they do not include loss effects. When we augment such models to include loss, we find that the excitation transfer and energy exchange effects become much stronger. Hence, models composed of two-level systems and an oscillator that are augmented with loss appear to be candidates to describe the excess heat effect in Fleischmann-Pons experiments.

Downloaded by CORNELL UNIV on July 2, 2012 | http://pubs.acs.org
Publication Date: August 1, 2008 | doi: 10.1021/bk-2008-0998.ch011

Anomalous Energy Exchange

We consider first the anomalous energy exchange effect. We consider a two-level system with a large transition energy ΔE coupled to a simple harmonic oscillator with a small characteristic energy $\hbar\omega_0$, with linear coupling. Our focus is on the rate at which energy is exchanged between the two systems. For this model, we adopt a spin-boson Hamiltonian given by

$$\hat{H} = \Delta E \frac{\hat{s}_z}{\hbar} + \hbar\omega_0\left(\hat{a}^\dagger\hat{a} + \frac{1}{2}\right) + V(\hat{a}^\dagger + \hat{a})\frac{2\hat{s}_x}{\hbar} \tag{1}$$

In writing this Hamiltonian, we use pseudospin operators $\hat{s}_z$ and $\hat{s}_x$ to describe the two-level system, and creation and annihilation operators for the simple harmonic oscillator. The coupling between the two systems has an interaction strength *V*. Models of this kind have been considered in the literature since the early work of Bloch and Siegert (*12*). Models for the energy shifts and resonance conditions for this problem have been discussed in the literature over the years (see (*13-17*)).

A direct computation of energy levels from this Hamiltonian leads to an empirical parameterization of the energy levels according to

$$E_{n,m} = \Delta E(g)m + \hbar\omega_0\left(n + \frac{1}{2}\right) \tag{2}$$

where the dressed two-level system energy ΔE (*g*) depends on the interaction strength and on the number of oscillator quanta through the dimensionless coupling strength g, which we define according to

$$g = \frac{V\sqrt{n}}{\Delta E} \tag{3}$$

The relation between ΔE (g) and g is roughly

$$\Delta E(g) = \sqrt{1+8g^2}\,\Delta E \tag{4}$$

as illustrated in Figure 1. One sees that this empirical parameterization is in reasonable agreement with the results from numerical calculations.

Level Anticrossing

We can study energy exchange between the two systems by focusing on the level splittings in the vicinity of an anticrossing. Consider a resonance between two states that differ by one unit of excitation in the two-level system quantum number m, and by an odd number of oscillator quanta n

$$\begin{aligned} E_{n,1/2} &= \frac{1}{2}\Delta E(g) + \hbar\omega_0\left(n+\frac{1}{2}\right) \\ E_{n+\Delta n,-1/2} &= -\frac{1}{2}\Delta E(g) + \hbar\omega_0\left(n+\Delta n+\frac{1}{2}\right) \end{aligned} \tag{5}$$

These two states anticross when their energies are equal, which occurs when

$$\Delta E(g) = \Delta n\hbar\omega_0 \tag{6}$$

In Figure 2 we illustrate the energy splitting that occurs at the level anticrossings as a function of the dimensionless coupling strength for calculations with $\Delta E \,/\, \hbar\omega_0 = 11$, 21, and 31. In the case of $\Delta E = 11\hbar\omega_0$ (the top curve in Figure 2) that resonances occur for Δn values of 13, 15, which are indicated by the solid circles on the curve starting from the left. For example, a resonance for the conversion of one unit of two-level system excitation for 13 oscillator quanta occurs near g=0.22, with an associated level splitting of about $10^{-5}\,\Delta E$.

Dynamics

In the vicinity of the anticrossing, the eigenfunctions are composed primarily of a mixture of the two states which anticross. On resonance, the mixing involves a 50-50 admixture of the two states, in which case the probability oscillates sinusoidally between the two states at a frequency related to the level splitting at the anticrossing. For example, if we initialize the system in state $\varphi_{n,1/2}$, then the subsequent occupation probabilities evolve according to

Downloaded by CORNELL UNIV on July 2, 2012 | http://pubs.acs.org
Publication Date: August 1, 2008 | doi: 10.1021/bk-2008-0998.ch011

Downloaded by CORNELL UNIV on July 2, 2012 | http://pubs.acs.org
Publication Date: August 1, 2008 | doi: 10.1021/bk-2008-0998.ch011

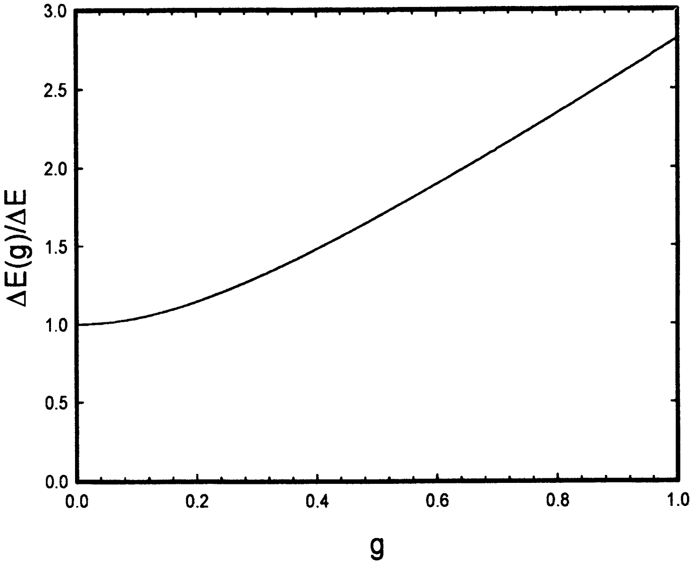

Figure 1. Plot of ΔE (g) as a function of g for ΔE = 11$\hbar\omega_0$. Result from numerical solutions – black line; empirical result $\sqrt{1+8g^2}$ – grey line.

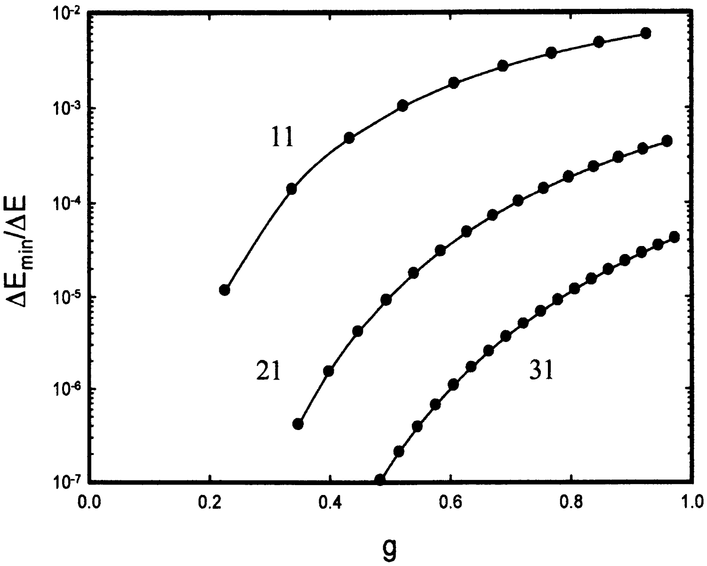

Figure 2. Level splitting at the level anticrossing as a function of the dimensionless coupling constant g. Calculations are presented for $\Delta E = 11\hbar\omega_0$, $21\hbar\omega_0$, and $31\hbar\omega_0$.

$$P_{n,1/2}(t) = \cos^2\left(\frac{\Delta E_{\min} t}{2\hbar}\right)$$
$$P_{n+\Delta n,-1/2}(t) = \sin^2\left(\frac{\Delta E_{\min} t}{2\hbar}\right) \tag{7}$$

In these oscillations, the system is exchanging energy between the two-level system, which has a large transition energy, and the oscillator, which has a small characteristic energy. In the results shown in Figure 2, the rightmost point on the $\Delta E = 31\hbar\omega_0$ curve is associated with an exchange of 85 oscillator quanta for a single dressed two-level system quantum.

Downloaded by CORNELL UNIV on July 2, 2012 | http://pubs.acs.org
Publication Date: August 1, 2008 | doi: 10.1021/bk-2008-0998.ch011

Discussion

This simple model illustrates that the simplest possible model of a single two-level system coupled to an oscillator exhibits an anomalous energy exchange effect, and that this can be demonstrated simply through a direct calculation. In order to see this effect in the spin-boson model, the dimensionless coupling constant g needs to be at least of intermediate strength. The models and solutions discussed here involved only a single two-level system coupled to an oscillator. Very similar results are obtained for a set of matched two-level systems, as long as *n* is large.

Rotation

It is possible to perform a rotation of the initial Hamiltonian that produces a dressed version of the problem in which the anomalous energy exchange effect can be studied more cleanly. We can rotate to eliminate the interaction term to first order to obtain (*10*)

$$\hat{H}' = \hat{U}\hat{H}\hat{U}^\dagger = \hat{H}_0 + \hat{V} + \hat{W} \tag{8}$$

Here, $\hat{H}'$ is the rotated Hamiltonian, $\hat{U}$ is a unitary operator, and the three operators on the right are terms that we interpret as an unperturbed part of the Hamiltonian ($\hat{H}_0$), and two perturbations. The unitary operator that accomplishes this rotation is

$$\hat{U} = \exp\left\{ i \ \arctan\left[\frac{2V\left(\hat{a}^\dagger + \hat{a}\right)}{\Delta E}\right]\frac{\hat{s}_y}{\hbar}\right\} \tag{9}$$

The unperturbed part of the rotated Hamiltonian can be written as

$$H_0 = \sqrt{\Delta E^2 + 8V^2y^2}\,\frac{\hat{s}_z}{\hbar} + \hbar\omega_0\left[-\frac{d^2}{dy^2} + y^2\right] \tag{10}$$

In writing this, we have used

$$y = \frac{\hat{a}^\dagger + \hat{a}}{\sqrt{2}} \tag{11}$$

The perturbation $\hat{V}$ is given by

$$\hat{V} = i\frac{\hbar\omega_0}{2}\frac{\sqrt{2}V}{\Delta E}\left\{\frac{1}{1+8V^2y^2/\Delta E^2}\frac{d}{dy} + \frac{d}{dy}\frac{1}{1+8V^2y^2/\Delta E^2}\right\}\frac{2\hat{s}_y}{\hbar} \tag{12}$$

We may write for $\hat{W}$

$$\hat{W} = \hbar\omega_0\frac{V^2}{\Delta E^2}\frac{1}{\left[1+8V^2y^2/\Delta E^2\right]^2}\left(\frac{2\hat{s}_y}{\hbar}\right)^2 \tag{13}$$

Energy Levels

The rotation is useful for a number of reasons. For example, we can solve the rotated $\hat{H}_0$ problem numerically with the result that the energy levels are given approximately by the parameterization of equation (*2*). In the event that the number of oscillator quanta is very large, then one can adopt a simple approximation for the eigenfunctions using SHO wavefunctions of the form

$$\phi_{n,m} = |n\rangle|s,m\rangle \tag{14}$$

This is an approximation since the exact eigenfunctions of $\hat{H}_0$ have a spread in *n*. A variational estimate for the energy eigenvalues can be obtained using

$$E_{n,m} = \langle\phi_{n,m}|H_0|\phi_{n,m}\rangle = \langle n|\sqrt{\Delta E^2 + 8V^2y^2/n}|n\rangle m + \hbar\omega_0\left(n+\frac{1}{2}\right) \tag{15}$$

This is consistent with

Downloaded by CORNELL UNIV on July 2, 2012 | http://pubs.acs.org
Publication Date: August 1, 2008 | doi: 10.1021/bk-2008-0998.ch011

$$\Delta E(g) = \Delta E \left\langle n \left| \sqrt{1 + 8g^2 y^2 / n} \right| n \right\rangle \tag{16}$$

which represents an improvement over our empirical dressed energy formula above. This result is sufficiently accurate that one could not distinguish it from the numerically exact result of Figure 1 if it were added to the plot. This result is consistent with the series expansion in the large n limit reported in (*15*), and with the expansion reported in (*17*). We have recently discussed this in (*18*).

Anomalous Energy Exchange in the Rotated Problem

The energy levels of the rotated $\hat{H}_0$ problem do not anticross, which is interesting because whatever is causing the level splitting at the anticrossing must be contained in the perturbations. We can develop a two-state approximation in the rotated frame to describe the level splitting (and hence the associated dynamics). The associated eigenvalue problem can be written as

$$E\begin{pmatrix} c_1 \\ c_2 \end{pmatrix} = \begin{pmatrix} \frac{\Delta E(g)}{2} + \hbar\omega_0\left(n + \frac{1}{2}\right) & \left\langle \phi_{n,1/2} \middle| \hat{V} \middle| \phi_{n+\Delta n,-1/2} \right\rangle \\ \left\langle \phi_{n+\Delta n,-1/2} \middle| \hat{V} \middle| \phi_{n,1/2} \right\rangle & -\frac{\Delta E(g)}{2} + \hbar\omega_0\left(n + \Delta n + \frac{1}{2}\right) \end{pmatrix}\begin{pmatrix} c_1 \\ c_2 \end{pmatrix} \tag{17}$$

The level splitting on resonance is given by

$$\Delta E_{\min} = 2\left|\left\langle \phi_{n,1/2} \middle| \hat{V} \middle| \phi_{n+\Delta n,-1/2} \right\rangle\right| \tag{18}$$

Results from this approximation are illustrated in Figure 3. One sees that the $\hat{V}$ perturbation combined with a simple two-state model leads to good agreement with numerical solutions of the initial Hamiltonian. We can understand anomalous energy exchange in this problem simply as arising from first-order transitions in the rotated frame (as discussed in (*19*)).

Discussion

We have found the rotated frame to be quite useful in understanding the systematics of the energy levels of the full problem, as presented here, and also in more extensive results that we do not have room to discuss. In addition, the level splittings can be understood simply in terms of matrix elements of one of the perturbations in the rotated version of the problem. The other perturbation gives a small energy shift that is not of interest in our discussion here.

Downloaded by CORNELL UNIV on July 2, 2012 | http://pubs.acs.org
Publication Date: August 1, 2008 | doi: 10.1021/bk-2008-0998.ch011

Downloaded by CORNELL UNIV on July 2, 2012 | http://pubs.acs.org
Publication Date: August 1, 2008 | doi: 10.1021/bk-2008-0998.ch011

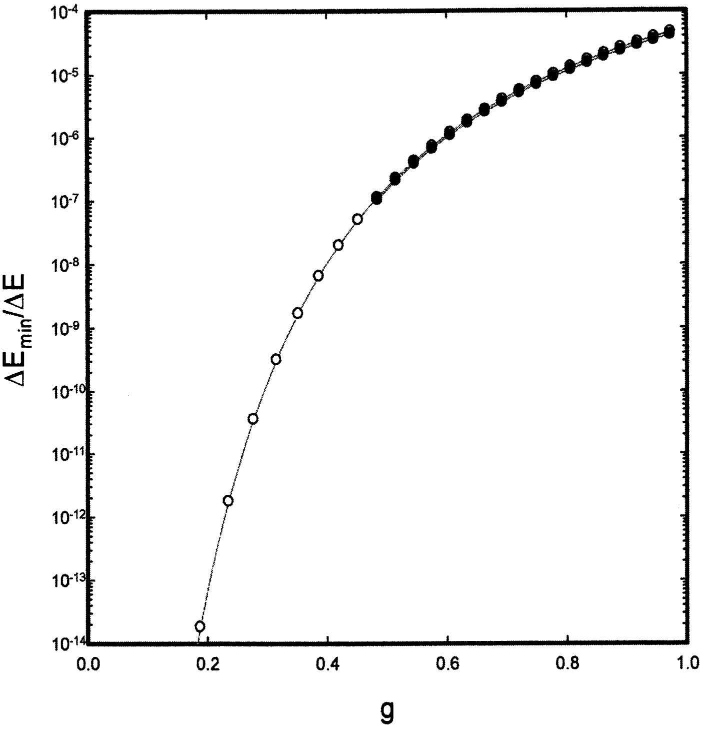

Figure 3. Level splittings computed from a direct numerical solution of some of the resonances from the original $\hat{H}$ problem – solid circles, and from a WKB approximation in the rotated $\hat{H}_0$ problem to the matrix element – open circles. The parameters used in this calculation were $\Delta E = 31\hbar\omega_0$ and $n = 10^8$.

Excitation Transfer

We can use a similar model to explore excitation transfer. In this case, we couple a pair of two-level systems to an oscillator, which is accomplished using the Hamiltonian

$$\hat{H} = \Delta E_1 \frac{\hat{s}_z^{(1)}}{\hbar} + \Delta E_2 \frac{\hat{s}_z^{(2)}}{\hbar} + \hbar\omega_0\left(\hat{a}^\dagger \hat{a} + \frac{1}{2}\right) + V_1\left(\hat{a}^\dagger + \hat{a}\right)\frac{2\hat{s}_x^{(1)}}{\hbar} + V_2\left(\hat{a}^\dagger + \hat{a}\right)\frac{2\hat{s}_x^{(2)}}{\hbar} \tag{19}$$

The energy levels in this case can be approximated by

$$E_{n,m_1m_2} = \Delta E_1(g_1)m_1 + \Delta E_2(g_2)m_2 + \hbar\omega_0\left(n+\frac{1}{2}\right) \qquad (20)$$

Where ΔE_1 (g_1) and ΔE_2 (g_2) are dressed excitation energies increased just as before. Here, there are two dimensionless coupling constants g_1 and g_2

$$g_1 = \frac{V_1\sqrt{n}}{\Delta E_1} \qquad g_2 = \frac{V2\sqrt{n}}{\Delta E_2} \qquad (21)$$

Excitation transfer can occur in this model when the dressed excitation energy of one two-level system matches the dressed excitation energy of the other, to within an even number of oscillator quanta

$$\Delta E_2(g_2) - \Delta E_1(g_1) = \Delta n \hbar\omega_0 \qquad (22)$$

In Figure 4 we show level splittings associated with excitation transfer in the case where $\Delta E_1 = 53\hbar\omega_0$ and $\Delta E_2 = 51\hbar\omega_0$, with $\Delta n = -2$. In this calculation, we scan g_1, and search to find a g_2 which gives a resonance. At the level anticrossing the two states mix, and can be described approximately using a two-state approximate as we did above. If the system is initialized at $t=0$ in a state $\phi_{n,-1/2,1/2}$, then the system evolves according to

$$p_{n,-1/2,1/2}(t) = \cos^2\left(\frac{\Delta E_{\min} t}{2\hbar}\right) \qquad p_{n+\Delta n,1/2,-1/2}(t) = \sin^2\left(\frac{\Delta E_{\min} t}{2\hbar}\right) \qquad (23)$$

These solutions illustrate the associated coherent dynamics, and oscillation frequency is determined by the level splittings.

Rotation

We can rotate to eliminate the coupling terms to first order as before, leading to a rotated Hamiltonian of the form (10)

$$\hat{H}' = \hat{U}\hat{H}\hat{U}^\dagger = \hat{H}_0 + \hat{V} + \hat{W} + \hat{V}_{12} \qquad (24)$$

Here, the unperturbed rotated Hamiltonian $\hat{H}_0$ is given by

$$H_0 = \sqrt{\Delta E_1^2 + 8V_1^2 y^2}\,\frac{\hat{S}_z^{(1)}}{\hbar} + \sqrt{\Delta E_2^2 + 8V_2^2 y^2}\,\frac{\hat{S}_z^{(2)}}{\hbar} + \hbar\omega_0\left[-\frac{d^2}{dy^2} + y^2\right] \qquad (25)$$

Downloaded by CORNELL UNIV on July 2, 2012 | http://pubs.acs.org
Publication Date: August 1, 2008 | doi: 10.1021/bk-2008-0998.ch011

Downloaded by CORNELL UNIV on July 2, 2012 | http://pubs.acs.org
Publication Date: August 1, 2008 | doi: 10.1021/bk-2008-0998.ch011

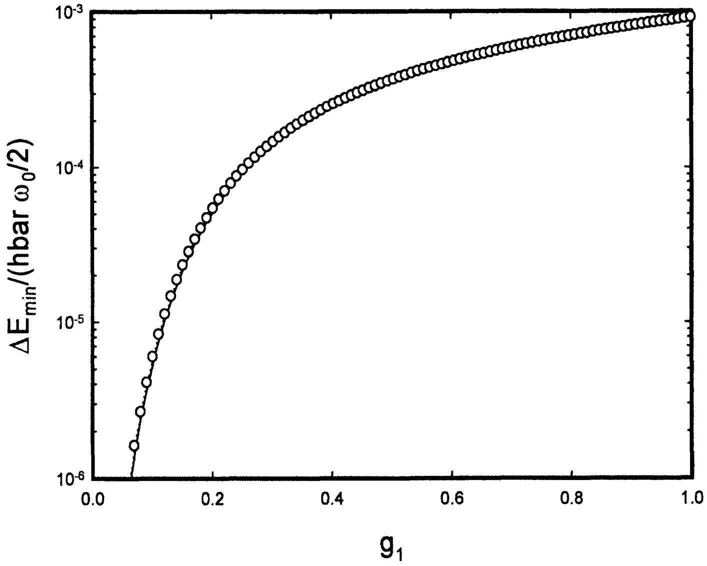

Figure 4. Level splittings at the anticrossings for excitation transfer for $\Delta E_1 = 53\hbar\omega_0$ and $\Delta E_2 = 51\hbar\omega_0$ with $\Delta n = -2$ and $n = 10^3$. Results are presented for direct calculations with $\hat{H}$ as given by Eq. (19) – open circles; and using perturbation theory from rotated frame solutions – solid line.

The perturbations $\hat{V}$ and $\hat{W}$ are simple generalizations of the ones we encountered previously. More interesting is the perturbation $\hat{V}_{12}$ that mediates excitation transfer processes, for which we may write

$$\hat{V}_{12} = 2\hbar\omega_0 \frac{V_1}{\Delta E_1}\frac{V_2}{\Delta E_2}\frac{1}{(1+8V_1^2y^2/\Delta E_1^2)(1+8V_2^2y^2/\Delta E_2^2)}\frac{2s_y^{(1)}}{\hbar}\frac{2s_y^{(2)}}{\hbar} \tag{26}$$

The level splittings in this case can be approximated using the eigenfunctions of the unperturbed rotated Hamiltonian $\hat{H}_0$ according to

$$\Delta E_{\min} = 2\left|\left\langle \phi_{n,-1/2,1/2}\right|\hat{V}_{12}\left|\phi_{n+\Delta n,1/2,-1/2}\right\rangle\right| \tag{27}$$

One can see good agreement between this expression and level splittings computed from the original problem in the results presented in Figure 4. We have found similar agreement as long as the anticrossings are not disrupted by energy exchange resonances, which is where a two-state approximation would no longer be valid.

Excitation Transfer and Energy Exchange

Models relevant to excess heat production in the Fleischmann-Pons experiment must implement both excitation transfer and anomalous energy exchange. We can develop very simple models that accomplish this to some degree by taking advantage of the simple Hamiltonian for a pair of two-level systems given above. In this case, we first isolate an energy exchange resonance for the second two-level system (through appropriate choices of ΔE_2 and g_2), and then select parameters for the first two-level system for which an excitation transfer resonance exists, but for which anomalous energy exchange is weak. In general, the coupling strength for one process will not match the coupling strength for the other. In most cases, they can be matched by varying the oscillator excitation n, since the anomalous energy exchange coupling remains approximately constant in n while the excitation transfer coupling varies approximately as inverse n. We are motivated to match the coupling strength so that we will be able to solve for the dynamics, and so that we will be able to see both effects present clearly in the solution.

Let us consider a specific example. Suppose that we first (arbitrarily) select $\Delta E_2 = 41\hbar\omega_0$, with $g_2 = 0.430287$ at which an energy exchange resonance occurs (in the rotated problem) in which $\Delta E_2\ (g_2) = 63\hbar\omega_0$ with a level splitting of $1.78\times10^{-10}\ \hbar\omega_0\ /\ 2$. We then (also arbitrarily) select $\Delta E_1 = 45\hbar\omega_0$ and $g_1 = 0.308606$, which causes the first two-level system to match the second with the exchange of four oscillator quanta: $\Delta E_1\ (g_1) = 67\hbar\omega_0$. It is possible to match the excitation transfer level splitting to the energy exchange level splitting (in a rotated frame calculation) using $n = 7.72\times10^6$, which will allow us to construct an easily solvable dynamics problem, as mentioned above. Energy exchange does not occur significantly with the first two-level system in this case, since with these parameters the energy splitting associated with energy exchange is lower by a factor of 6700 than the energy splitting associated with excitation transfer.

Under such conditions that the excitation transfer coupling is matched to the energy exchange coupling, with resonances occurring for both processes independently, then we can develop analytic dynamical solutions

$$p_{n-4,1/2,-1/2}(t) = \left[\frac{1+\cos(\Delta \mathrm{E}_{\mathrm{min}} t/2\hbar}{2}\right]^2$$

$$p_{n,-1/2,1/2}(t) = \left[\frac{\sin(\Delta E_{\mathrm{min}} t/2\hbar}{\sqrt{2}}\right]^2 \qquad (28)$$

$$p_{n+63,-1/2,-1/2}(t) = \left[\frac{1-\cos(\Delta \mathrm{E}_{\mathrm{min}} t/2\hbar}{2}\right]^2$$

Downloaded by CORNELL UNIV on July 2, 2012 | http://pubs.acs.org
Publication Date: August 1, 2008 | doi: 10.1021/bk-2008-0998.ch011

These dynamics are illustrated in Figure 5. In this example, we start with only the first two-level system excited (all states in this discussion are in the rotated frame). The system then transfers excitation (and four oscillator quanta) so that only the second two-level system is excited. Finally, the excitation of the second two-level system is transferred to the oscillator, so that neither two-level system is excited. The dynamics are coherent in this example, so that the system then proceeds to cycle back, and then repeat.

Discussion

The importance of this model is that it illustrates clearly within the context of a slightly generalized spin-boson model (now with a pair of two-level systems) that the basic dynamics needed for describing a new physical process are present. We have excitation transfer; we have anomalous energy exchange; and the resulting dynamics are coherent.

Downloaded by CORNELL UNIV on July 2, 2012 | http://pubs.acs.org
Publication Date: August 1, 2008 | doi: 10.1021/bk-2008-0998.ch011

Models Augmented with Loss

The nice feature of the spin-boson type models presented above is that the system is sufficiently simple that we can isolate the excitation transfer mechanism, the energy exchange mechanism, and develop idealized models illustrating the dynamics alone or in combination. It is also possible to extend these models to include collections of two-level systems in order to understand how the added coherence impacts the system.

However, these models seem to fall short of what is needed to account for excess heat production in the Fleischmann-Pons experiment, primarily since the associated rates are very small under conditions where $\Delta E / \hbar\omega_0$ is greater than 10^6. In essence, even though these models exhibit excitation transfer and energy exchange mechanisms, the effects are too weak in these models to do what is needed to be relevant to the excess heat problem. Something is missing.

Excitation Transfer Using Perturbation Theory

Consider first the situation in the case of excitation transfer. We can develop an approximate analytic expression for the energy splitting using perturbation theory. We consider a finite basis approximation with six basis states corresponding to

$$\begin{aligned} \phi_1 &= |n\rangle|s,1/2\rangle|s,-1/2\rangle & \phi_2 &= |n-1\rangle|s,-1/2\rangle|s,-1/2\rangle \\ \phi_3 &= |n+1\rangle|s,-1/2\rangle|s,-1/2\rangle & \phi_4 &= |n-1\rangle|s,1/2\rangle|s,1/2\rangle \\ \phi_5 &= |n+1\rangle|s,1/2\rangle|s,1/2\rangle & \phi_6 &= |n\rangle|s,-1/2\rangle|s,1/2\rangle \end{aligned} \qquad (29)$$

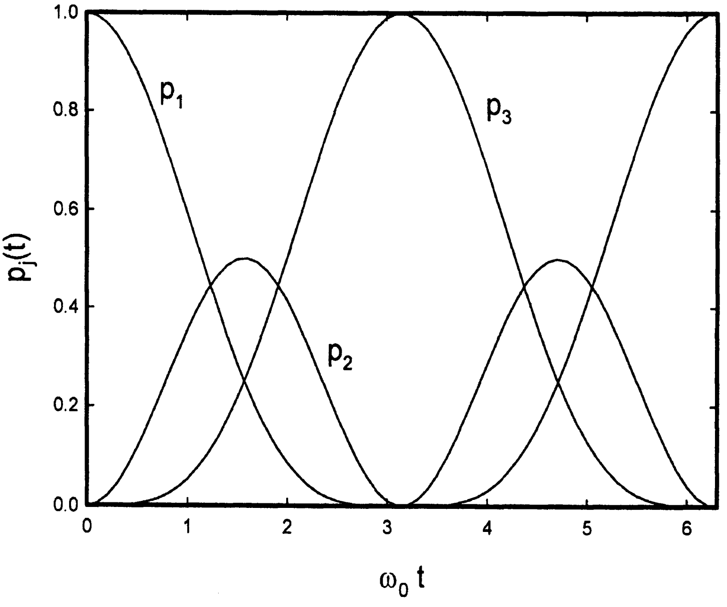

Figure 5. Probabilities for excitation transfer followed by energy exchange under conditions where all states are degenerate in the absence of coupling, and when the coupling strengths are matched. In the first state (with probability p_1), only the first two-level system is excited; in the second, only the second two-level system is excited; and in the third, neither two-level system is excited. The frequency ω_0 in this case is $\Delta E_{min}/2\hbar$.

Downloaded by CORNELL UNIV on July 2, 2012 | http://pubs.acs.org
Publication Date: August 1, 2008 | doi: 10.1021/bk-2008-0998.ch011

We assume that ϕ_1 and ϕ_6 are resonant in the absence of coupling $[\Delta E_1(g_1) = \Delta E_2(g_2)]$. The finite basis equations for the expansion coefficients $c_1 \ldots c_6$ can be written as

$$\begin{aligned}
Ec_1 &= H_1c_1 + V_1\sqrt{n}c_2 + V_1\sqrt{n+1}c_3 + V_2\sqrt{n}c_4 + V_2c_5 \\
Ec_2 &= H_2c_2 + V_1\sqrt{n}c_1 + V_2\sqrt{n}c_6 \\
Ec_3 &= H_3c_3 + V_1\sqrt{n+1}c_1 + V_2\sqrt{n+1}c_6 \\
Ec_4 &= H_4c_4 + V_2\sqrt{n}c_1 + V_1\sqrt{n}c_6 \qquad (30) \\
Ec_5 &= H_5c_5 + V_2\sqrt{n+1}c_1 + V_1\sqrt{n+1}c_6 \\
Ec_6 &= H_6c_6 + V_2\sqrt{n}c_2 + V_2\sqrt{n+1}c_3 + V_1\sqrt{n}c_4 + V_1\sqrt{n+1}c_5
\end{aligned}$$

We can eliminate the interior states ϕ_2 through ϕ_5 to obtain a reduced set of equations of the form

$$\begin{aligned} Ec_1 &= H_1 c_1 + \Sigma_1(E)c_1 + V_{16}(E)c_6 \\ Ec_6 &= H_6 c_6 + \Sigma_6(E)c_6 + V_{61}(E)c_1 \end{aligned} \tag{31}$$

The level splitting under resonant conditions in this model is

$$\Delta E_{\min} = 2\sqrt{|V_{16}(E)V_{61}(E)|} \tag{32}$$

An explicit calculation produces the result in this case that

$$\begin{aligned} V_{16}(E) = V_{61}(E) &= V_1 V_2 \left[\frac{n}{E-H_2} + \frac{n+1}{E-H_3} + \frac{n}{E-H_4} + \frac{n+1}{E-H_5} \right] \\ &\approx \frac{2\hbar\omega_0 V_1 V_2}{(\Delta E_1)^2 - (\hbar\omega_0)^2} \end{aligned} \tag{33}$$

This approximation gives good results for the level splitting associated with excitation transfer in the limit of small g_1 and g_2.

Inclusion of Loss Effects in the Model

In the intermediate states ϕ_2 and ϕ_3 above, both of the two-level systems are unexcited; hence, the coupled quantum system has available an energy E which is much greater than either of the basis state energies H_2 and H_3. In this case, if there exist loss channels for the oscillator at decay energies near the dressed two-level system energies, one would expect the system to undergo incoherent decay to these states. The existence of such decay modes has a dramatic impact on the model, which we need to include.

To do so, we augment the Hamiltonian to include loss

$$\begin{aligned} \hat{H} = {} & \Delta E_1 \frac{\hat{s}_z^{(1)}}{\hbar} + \Delta E_2 \frac{\hat{s}_z^{(2)}}{\hbar} + \hbar\omega_0 \left(\hat{a}^\dagger \hat{a} + \frac{1}{2} \right) - \frac{i\hbar}{2} \hat{\Gamma}(E) \\ & + V_1 (\hat{a}^\dagger + \hat{a}) \frac{2\hat{s}_x^{(1)}}{\hbar} + V_2 (\hat{a}^\dagger + \hat{a}) \frac{2\hat{s}_x^{(2)}}{\hbar} \end{aligned} \tag{34}$$

Here, the spin-boson model that we have been considering has been augmented with a loss term that implements the effect under discussion. For a more complete discussion of loss mechanisms and the development of relevant loss models, see Hagelstein and Chaudhary (*10*).

Downloaded by CORNELL UNIV on July 2, 2012 | http://pubs.acs.org
Publication Date: August 1, 2008 | doi: 10.1021/bk-2008-0998.ch011

Enhancement of Excitation Transfer

With the inclusion of loss terms in the model, the model undergoes qualitative changes. We can see this in the modification of the perturbation theory for excitation transfer discussed above. Let us now include loss for states ϕ_2 and ϕ_3, which we can do in a simple way by using a constant loss model. We write for these basis states

$$\begin{aligned} Ec_2 &= \left(H_2 - \frac{i\hbar\Gamma}{2}\right)c_2 + V_1\sqrt{n}c_1 + V_2\sqrt{n}c_6 \\ Ec_3 &= \left(H_3 + \frac{i\hbar\Gamma}{2}\right)c_3 + V_1\sqrt{n+1}c_1 + V_2\sqrt{n+1}c_6 \end{aligned} \tag{35}$$

When these states are eliminated, we still recover a reduced two-state model; however, the indirect coupling coefficients are now changed. We may write

$$V_{16}(E) = V_1V_2\left[\frac{n}{E-H_2+i\hbar\Gamma/2} + \frac{n+1}{E-H_3+i\hbar\Gamma/2} + \frac{n}{E-H_4} + \frac{n+1}{E-H_5}\right]$$

In the event that the loss term becomes very large ($\Gamma \to \infty$), then

$$V_{16}(E) \approx -\frac{2V_1V_2\Delta E_1(g_1)n}{(\Delta E_1)^2 - (\hbar\omega_0)^2} \tag{36}$$

This is orders of magnitude larger than what we found above in the lossless version of the model. We see that the inclusion of loss breaks the destructive interference that was initially present, and that is the reason.

Discussion and Conclusions

Our discussion has focused primarily on simple spin-boson type models that illustrate excitation transfer and anomalous energy exchange effects. These effects are of interest to us in general since they are required in the development of models for excess heat in the Fleischmann-Pons experiment.

We require the excitation transfer mechanism in order to violate local energy conservation (but retain global energy conservation) in the initial step of the reaction. Two deuterons interact to make ^{4}He, exchanging one or more phonons in the process, with the reaction energy transferred elsewhere. The coupling in this case is weak, since the transition is hindered by the presence of a Gamow factor due to coupling through the Coulomb barrier.

Downloaded by CORNELL UNIV on July 2, 2012 | http://pubs.acs.org
Publication Date: August 1, 2008 | doi: 10.1021/bk-2008-0998.ch011

Downloaded by CORNELL UNIV on July 2, 2012 | http://pubs.acs.org
Publication Date: August 1, 2008 | doi: 10.1021/bk-2008-0998.ch011

We require the anomalous energy exchange mechanism since there are no energetic particles observed commensurate with the energy produced. This energy exchange mechanism works through the exchange of a single oscillator quantum in association with every interaction (excitation transfer steps, or self-interaction steps, within the second set of equivalent two-level systems). It accomplishes the exchange of a large energy quantum associated with the two-level systems into a large number of low energy quanta associated with the oscillator. Both the excitation transfer effect and the anomalous energy exchange effect involve coherent dynamics within the models presented here, and within a larger set of models that we have investigated so far.

The lossless models are of interest as we have mentioned previously since we are able to set up simple models that exhibit each effect individually or both together. We are able to isolate the specific perturbation in the rotated Hamiltonian that mediates excitation transfer, and also the specific perturbation that mediates anomalous energy exchange. The effects can be studied in terms of direct solutions of the initial spin-boson type of Hamiltonian $\hat{H}$; from numerical and approximate solutions of the rotated unperturbed Hamiltonian $\hat{H}_0$; using the WKB approximation on the rotated problem; and through other methods as well. For example, in the text we discussed briefly an example in which we are able to develop an analytic solution for a problem in which excitation transfer is followed coherently by anomalous energy exchange where a total of 67 oscillator quanta make up the dressed transition energy of the first two-level system.

The lossless version of the problem results in simple toy models that we can analyze as we please, although it is probably clear from the specific examples that we considered that these models fall short of what is needed for modeling excess heat production. These toy problems also require very precise resonances to be present for any of the effects to occur, which seems not to be consistent qualitatively with excess heat observations.

Augmenting the models with loss changes things dramatically, as we have discussed briefly in the case of excitation transfer. The rate at which excitation transfer occurs in the lossy models is greatly enhanced, and also the rate at which anomalous energy exchange occurs is similarly enhanced. Lossy models can show both effects readily, even without resonant conditions being satisfied.

To connect these models to excess heat production experiments (in PdD), we identify a molecular D_2 state in the vicinity of a host atom vacancy as the upper state of the first two-level system(s), and ^{4}He with the lower state. The lower state of the second two-level system(s) we identify with ground state nuclei present in the host. Experiment so far does not make clear what excited nuclear states should be identified with the upper state of the second two-level system(s). Theoretical arguments point to excited states composed of a neutral particle and daughter; for example, a neutron plus ^{3}He in the case of a ^{4}He ground state; or ^{106}Pd plus a tetraneutron in the case of a ^{110}Pd ground state. Such excited states are favored due to the ability of the lattice to exchange phonons in transitions from the ground state. However, it remains to be established that such states can be stabilized sufficiently for the schemes under discussion to work properly.

References

1. Fleischmann, M.; Pons, S.; Hawkins, M. Electrochemically Induced Nuclear Fusion of Deuterium. *J. Electroanal Chem.* **1989**, *261*, 301; Errata, **1989**, *263*, 187. See also Fleischmann, M.; Pons, S.; Anderson, M. W.; Li, L. J.; Hawkins, M. Calorimetry of the Palladium-Deuterium-Heavy Water System. *J. Electroanal. Chem.* **1990**, *287*, 293.
2. Fleischmann, M.; Pons, S. Calorimetry of the Palladium-D-D_2O System. *Proceedings of the EPRI-NSF Workshop on Anomalous Effects in Deuterated Metals*, Washington, DC, October 16-18, 1989; EPRI: Palo Alto, CA, 1993.
3. Fleischmann, M.; Pons, S.; Anderson, M. W.; Li, L. J.; Hawkins, M. Calorimetry of the Palladium-Deuterium-Heavy Water System. *J. Electroanal. Chem.* **1990**, *287*, 293.
4. Huizenga, J. *Cold Fusion: The Scientific Fiasco of the Century*; University of Rochester Press: Rochester, NY, 1992.
5. Hagelstein, P. L.; McKubre, M. C. H.; Nagel, D. J.; Chubb, T. A.; Hekman, R. J. New Physical Effects in Metal Deuterides. In *Condensed Matter Nuclear Science: Proceedings of the 11th International Conference on Cold Fusion*, Marseilles, France, Oct. 31 - Nov. 5, 2004; Biberian, J.-P., Ed.; World Scientific Publishing Co.: Singapore, 2006; 23.
6. Darwin, C. G. Collision of α Particles with Light Atoms. *Phil. Mag.* **1914**, *27*, 499.
7. Marmier, P.; Sheldon, E. *Physics of Nuclei and Particles*; Academic Press: New York, NY, 1969.
8. Huizenga, J., et al. *Cold Fusion Research: A Report of the Energy Research Advisory Board to the Department of Energy*, Department of Energy document DOE/S-0073, November 1989.
9. Chaudhary, I. U.; Hagelstein, P. L. Inclusion of Phonon Exchange in a Nuclear Matrix Element. 2006, arXiv:cond-mat/0606585. arXiv.org e-Print archive. http://arxiv.org/abs/cond-mat/0606585.
10. Hagelstein, P. L.; Chaudhary, I. U. Two-Level Systems Coupled to an Oscillator: Excitation Transfer and Energy Exchange. 2006, arXiv:condmat/0612306. arXiv.org e-Print archive. http://arxiv.org/abs/cond-mat/0612306.
11. Hagelstein, P. L.; Chaudhary, I. U. Progress Toward a Theory for Excess Heat in Metal Deuterides. In *Current Trends in International Fusion Research – Proceedings of the Seventh Symposium*, Washington, DC, March 5-9, 2007; Panarella, E.; Raman, R., Eds.; National Research Council of Canada Research Press: Ottawa, 2007.

Downloaded by CORNELL UNIV on July 2, 2012 | http://pubs.acs.org
Publication Date: August 1, 2008 | doi: 10.1021/bk-2008-0998.ch011

12. Bloch, F.; Siegert, A. Magnetic Resonance for Nonrotating Fields. *Phys. Rev.* **1940**, *57*, 522.
13. Shirley, J. H. Solution to the Schrodinger Equation with a Hamiltonian Periodic in Time. *Phys. Rev.* **1965**, *138*, B979.
14. Cohen-Tannoudji, C.; Dupont-Roc, J.; Fabre, C. A Quantum Calculation of the Higher Order Terms in the Bloch-Siegert Shift. *J. Phys. B* **1973**, *6*, L214.
15. Ahmad, F.; Bullough, R. K. Theory of the Bloch-Siegert Shift. *J. Phys. B* **1974**, *7*, L275.
16. Fregenal, D.; Horsdal-Pedersen, E.; Hadsen, L. B.; Forre, M.; Hansen, J. P. ; Ostrovsky, V. N. Multiphoton Intrashell Resonances in Rydberg Atoms: Bloch-Siegert Shifts and Widths. *Phys. Rev. A* **2004**, *69*, 031401-1.
17. Ostrovsky, V. N.; Horsdal-Pedersen, E. Bloch-Siegert Shifts for Multiphoton Resonances: In Plane Configuration. *Phys. Rev. A* **2004**, *70*, 033413-1.
18. Hagelstein, P. L.; Chaudhary, I. U. Bloch-Siegert Shift for Multiphoton Resonances. 2007, arXiv:quant-ph/0709.1958v1. arXiv.org e-Print archive. http://arxiv.org/abs/0709.1958.
19. Hagelstein, P. L.; Chaudhary, I. U. Level Splitting in Association with the Multiphoton Bloch Siegert Shift. 2007, arXiv:quant-ph/0701.1961v1. arXiv.org e-Print archive. http://arxiv.org/abs/0701.1961.

Downloaded by CORNELL UNIV on July 2, 2012 | http://pubs.acs.org
Publication Date: August 1, 2008 | doi: 10.1021/bk-2008-0998.ch011

Downloaded by PENNSYLVANIA STATE UNIV on July 1, 2012 | http://pubs.acs.org
Publication Date: August 1, 2008 | doi: 10.1021/bk-2008-0998.ch012

Chapter 12

Transmutation Reactions in Condensed Matter

Tadahiko Mizuno

Laboratory of Nuclear and Environmental Materials, Graduate School of Engineering, Hokkaido University, Kita-ku, North 13, West 8, Sapporo 060–8628, Japan

The appearance of many elements on palladium electrodes after long-duration electrolysis in heavy water at high pressure, high temperature, and large current density was confirmed by several analytic methods. Mass numbers as high as 208 corresponding to elements ranging from hydrogen to lead were found, and the isotopic distributions of many of these elements were radically different from the naturally occurring ones. Changes in element distribution and in their isotopic abundances took place during electrolysis in both heavy and light water, whether or not excess energy was generated. If the transmutation mechanism can be understood, it may then be possible to control the reaction, and perhaps produce macroscopic quantities of rare elements by this method. In the distant future, industrial scale production of rare elements might become possible, and this would help alleviate material shortages worldwide.

Introduction

Many people have asserted that if nuclear reactions are induced by electrochemical reactions using solid electrodes there should also appear clear evidence of the generation of radioisotopes and of radiation. Moreover, the evolution rates of reaction products should be able to be quantitatively explained in terms of well-established nuclear reaction mechanisms, but this expectation would be valid only if the reaction mechanism is in accord with accepted nuclear theory. However, there is little reason to believe that a conventional mechanism applies to the nuclear reactions accompanying electrolysis. Hence,

In Low-Energy Nuclear Reactions Sourcebook; Marwan, J., et al.;
ACS Symposium Series; American Chemical Society: Washington, DC, 2008.

the expected emission of radiation and radioisotopes may not occur. This work presents evidence that a nuclear reaction takes place during electrolysis that produces isotopically changed elements on the cathode surface. These elements are generated by a mechanism that does not induce any detectable radiation. The anomalous isotopic abundances of these elements show that they do not come from contamination. We suggest that the operative nuclear mechanism is completely different from any known nuclear reaction.

Mizuno (*1*), Miley (*2*), Ohmori (*3*), Iwamura (*4*), and others have reported anomalous production of radiation-less foreign elements (Fe, Cr, Ti, Ca, Cu, Zn, Si, and so on) on cathode metals (mainly Pd) with heavy water or light water electrolysis experiments. These elements sometimes have drastically non-natural isotopic ratios.

Downloaded by PENNSYLVANIA STATE UNIV on July 1, 2012 | http://pubs.acs.org
Publication Date: August 1, 2008 | doi: 10.1021/bk-2008-0998.ch012

Experimental

Sample

The experimental details of the sample, cell, electrolysis, and the reaction conditions have been described elsewhere (*5*). After the Teflon coat of the sample electrodes was removed and the samples were washed in the Mill Q water, they were analyzed by means of energy dispersive X-ray spectroscopy (EDX), Auger electron spectroscopy (AES), secondary ion mass spectroscopy (SIMS), electron probe micro analyzer (EPMA), and inductively coupled plasma (ICP) spectrometry. Palladium rods used were of high purity (99.97% min.) supplied by Tanaka Noble Metals, Ltd. Impurities in the rods were as follows: B: 110, Si: 10, Ca: 9, Cr: 8, Cu: 6. Ti: 5, Ag: 41, Pt: 16, and Au: 23 ppm. Nothing more was detected by ICP measurement. The palladium rod was held in a vacuum of 5×10^{-5} Torr at 473 K for 6×10^{5} sec. Showa Denko, Ltd. supplied heavy water. It is 99.75% pure and includes 0.077 micro Ci/dm^3 of tritium. The heavy and light water were purified once in a quartz glass distiller. Reagent grade lithium hydroxide was obtained from Merck, Ltd. Impurities in the reagent were specified as follows: Li_2CO_3: 2% max, Cl: 0.05%, Pb: 16, Ca: 154, Fe: 13, K: 156, and Na: 135 ppm. Other impurities were under detectable limit by ICP analysis. The anode was a Pt plate and the recombiner catalyst was a Pt mesh, both high purity (99.99%). The Pt metal is specified to contain impurities as follows: Rh: 18 ppm, Si, Cr, and Pd: 2 ppm, Au, Ag, B, Ca, Cu, and Fe: less than one ppm. And other impurities were under detectable limits of ICP analysis.

Electrolysis

All electrolysis was performed in a closed cell made from a stainless steel cylinder. The cell has an inner Teflon cell made with a 1-mm thick wall and a 1-cm thick upper cap; the inner height and diameter are 20 cm and 7 cm, the volume is 770 cm^3 (Figure 1). Further details have been described elsewhere (*6, 7*). Before electrolysis, 400 cm^3 of electrolyte were pre-electrolyzed using another Pt mesh electrode at 1 A and 150°C for 7 days in the closed cell. After that the Pt electrode was removed and the palladium rod sample was connected to the electrical terminal. Electrolysis experiments were performed with the current density of 0.2 A/cm^2 or total current of 6.6 A ($33\ cm^2 \times 0.2\ A/cm^2$) for 32 days at 105°C.

Typical time variations of current, temperature, and D/Pd ratio during electrolysis in heavy water solution are shown in Figure 2. In the experiment shown here, some excess heat was generated after electrolysis, as indicated by the temperature rise of the electrolyte after the electrolysis was stopped at 766 hours. The phenomenon is very anomalous since the temperature would be expected to decrease after shutting off the input power. All electrolysis was carried out at 0.2 A/cm^2 or a total current of 6.6 A ($33\ cm^2 \times 0.2\ A/cm^2$) for 2.59×10^6 s (30 days) at around 100°C.

Downloaded by PENNSYLVANIA STATE UNIV on July 1, 2012 | http://pubs.acs.org
Publication Date: August 1, 2008 | doi: 10.1021/bk-2008-0998.ch012

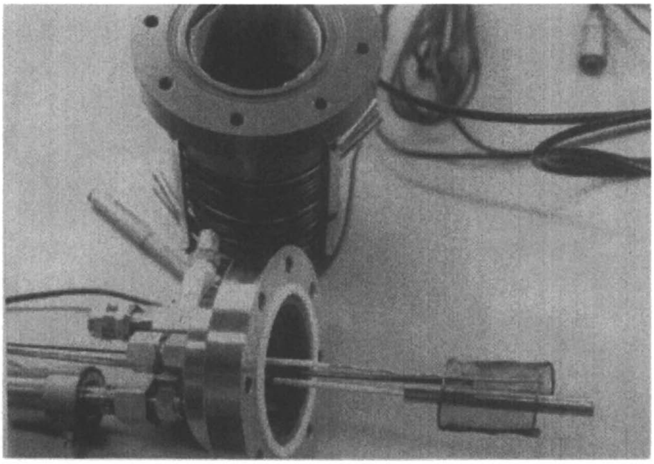

Figure 1. Photo of cell. The upper portion shows the cell cylinder and Pt recombiner. The lower portion shows the anode, cathode, pressure gauge, temperature sensor, and relief valve.

Element Analysis

After electrolysis the palladium rod was washed with Mill-Q water (Japan Millipore Ltd., model MillQ-lab) and covered by a Teflon tube. The analysis samples were prepared by cutting the rod into 1 cm segments with a diamond cutter, and then cutting the segments lengthwise into two semicircular-shaped masses. The sample electrode was removed from the Teflon coat, washed with

Downloaded by PENNSYLVANIA STATE UNIV on July 1, 2012 | http://pubs.acs.org
Publication Date: August 1, 2008 | doi: 10.1021/bk-2008-0998.ch012

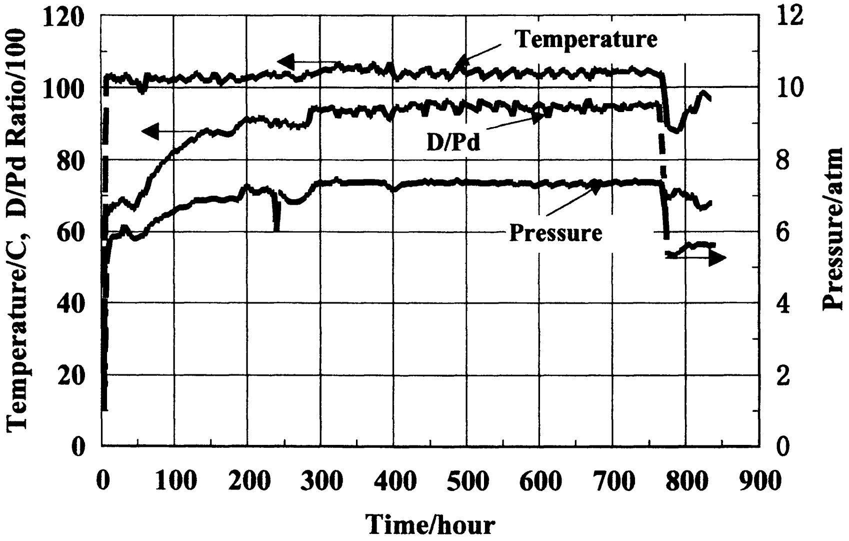

Figure 2. Changes of temperature, pressure, and D/Pd ratio during electrolysis.

Mill-Q water again, and analyzed with EDX, EPMA, AES, and ICP spectrometry, performed by the author. SIMS analysis was performed by Hitachi Measurement Engineering Co., Ltd., Ibaraki Laboratory (Hitachinaka City, Ibaraki prefecture), and Nissan Ark Co., Ltd. (Yokosuka City, Kanagawa prefecture).

EDX measurements were done with 20 keV electron irradiation, with variation of the scanning area. The energy spectra were measured with a silicon-lithium drift detector. The energy range of analysis was zero to 20 keV; the interesting range was divided into 1024 channels of energy width. The energy resolution was 150 eV at 5.9 keV, but for practical purposes it was 200 eV. Peaks were calibrated using high purity samples of C, Al, Si, Ti, Cr, Mn, Fe, Co, Zn, Sr, Nb, Mo, Pd, Ag, Sn, Ce, Hf, W, Pt, Au, and Pb. AES (ANELVA model AAS-200) analyses were performed to obtain the depth distribution of the elements; the ion irradiation energy and the current were 3 keV and 2.5 A, respectively.

An EPMA (Shimadzu Ltd. Model EPMA-8705) was used to obtain the elemental distribution on the samples. SIMS measurements (Hitachi Co. model IMA-3000) were made, with O_2^+ ions targeted onto the sample at a spot of 400 square micrometers, with primary energy of 10.5 keV and 100 nano Amperes ion current. Resolution for the mass measurement was m/e=10000. Mass numbers were calibrated with high-purity metals including Li, B, C, Al, Si, Ca, Ti, Cr, Mn, Fe, Co, Ni, Cu, Zn, Sr, Nb, Mo, Pd, Ag, Cd, Sn, Ce, Hf, W, Os, Pt, Au, and Pb. No isotopic changes over the natural deviations were noted in the calibration measurements. Careful estimations of the abundance of each element were required because many mass peaks due to molecules, oxides, hydrides, and other complex materials interfere. We used various analytic methods to obtain precise isotopic abundance. EPMA analysis was used first to estimate the element's distribution on the sample.

AES was employed to obtain the depth distribution of certain elements and EDX measurements determined the relative concentrations of various elements. These techniques were used complementarily because any one method could not necessarily be applicable to all of the elements. In later studies, the SIMS technique was adopted to determine the elemental abundances at various points on the sample surface. The entire palladium surface was dissolved in hydrofluoric acid and the solution was analyzed by ICP. The total atomic concentration was estimated.

Downloaded by PENNSYLVANIA STATE UNIV on July 1, 2012 | http://pubs.acs.org
Publication Date: August 1, 2008 | doi: 10.1021/bk-2008-0998.ch012

Results

Many elements were deposited on the electrode surface in an irregular distribution. The concentrations varied depending on the parameters of the electrolysis. The elements that have been detected on the samples were C, O, S, Cl, Si, Ca, Ti, Cr, Mn, Fe, Ni, Cu, Zn, Mo, Pd, Sn, Pt, Hg, and Pb. The amount of each element varied by the sample lots. This may mean that some factors such as surface conditions play an important role in the reaction. Several elements were also detected in the palladium sample by the EDX and ICP method; the measurements were taken to determine the rough level of concentration of the elements because mass peaks in the SIMS measurement can include signals from other molecular peaks.

Figure 3 shows a typical EDX spectrum for a sample that was electrolyzed in heavy water solution and evolved some excess heat (1.2×10^7 J) (*1*) after electrolysis. It shows data from before and after electrolysis. Several peaks of Pt, Cr, and Fe are clearly seen; these amounts were comparable to the Pd bulk peak. Smaller amounts of Sn, Ti, Cu, and Pb are also clearly observed.

The EDX analyses were repeated at various locations on the sample surface; the EDX counts sometimes varied by as much as a factor of ten depending on the location.

In the last stage of the analysis, the mass abundance for the elements was measured by SIMS. The EDX, AES, and EPMA methods were complimentarily used to attribute mass spectra to specific atoms and to determine isotopic distributions. The following procedure was used:

1. The mass numbers were established first for light to heavy mass number.
2. The mass numbers were confirmed by referring to the EDX and AES spectra.
3. The large count number of mass peaks was used to confirm the existence of their molecular ion and oxide ion peaks.

Downloaded by PENNSYLVANIA STATE UNIV on July 1, 2012 | http://pubs.acs.org
Publication Date: August 1, 2008 | doi: 10.1021/bk-2008-0998.ch012

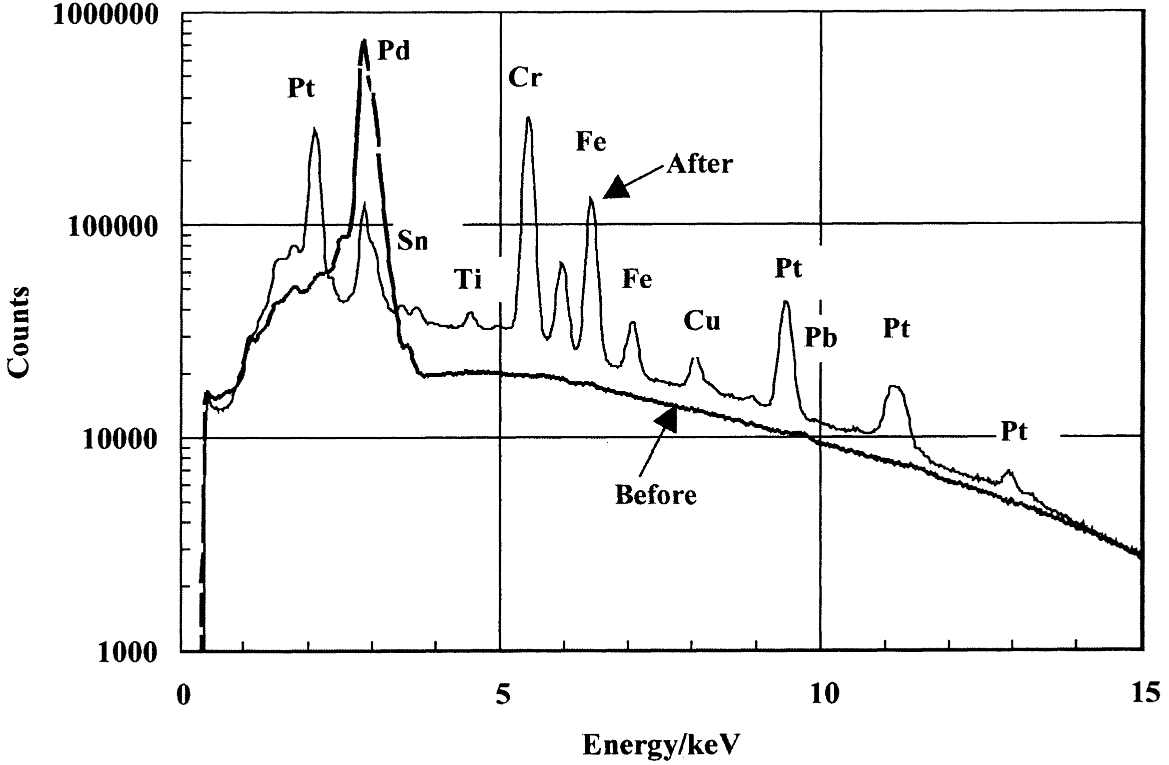

Figure 3. EDX spectrum of the Pd electrode surface electrolyzed in heavy water solution.

In Low-Energy Nuclear Reactions Sourcebook; Marwan, J., et al.;
ACS Symposium Series; American Chemical Society: Washington, DC, 2008.

4. The final mass spectra were estimated by applying the relative sensitivity factor (rsf) to the original count of mass depending on the element composition. This factor changes from high to low values for the inert gases and alkali metals when O_2^+ ion bombardment is used.

The atomic concentration on the palladium surface was estimated by the ICP method. Figure 4 shows the typical concentration in a 10 micrometer layer of the sample. Two values are shown, for before and after electrolysis that produced excess heat. Impurities before the experiment were as follows, where the Pd concentration is normalized at 100: B: 0.0012, Si: 0.001, Cr: 0.001, Fe: 0.0015, Pd: 100.0, Ag: 0.0040, Pt: 0.002, and Au: 0.0025. The total element concentration after electrolysis was: C: 100, O: 120, Si: 15, P: 7.5, S: 17, Ca: 3, Cr: 18, Fe: 7.5, Cu: 12, Zn: 37, Pd: 100.0, Xe: 1000, Pt: 0.9, Pb: 0.4. Based on this, it seems that the detected elements are distributed in atomic numbers close to those of the impurity elements that originally existed in the cell.

The total amount of the elements existing at a one-micrometer depth in the palladium surface were calculated as follows: C: 0.40, O: 8.84, Si: 0.15, S: 0.17, Cl: 0.06, Ca: 0.142, Ti: 0.76, Cr: 22.96, Fe: 10.06, Cu: 5.61, Zn: 3.35, Pd: 33.45, Pt: 9.65, Pb: 4.39, and others were less than 0.005 atomic percentage.

It should be stressed that the total amount of deposited elements on the palladium is much higher than the total impurity in the electrolyte and palladium

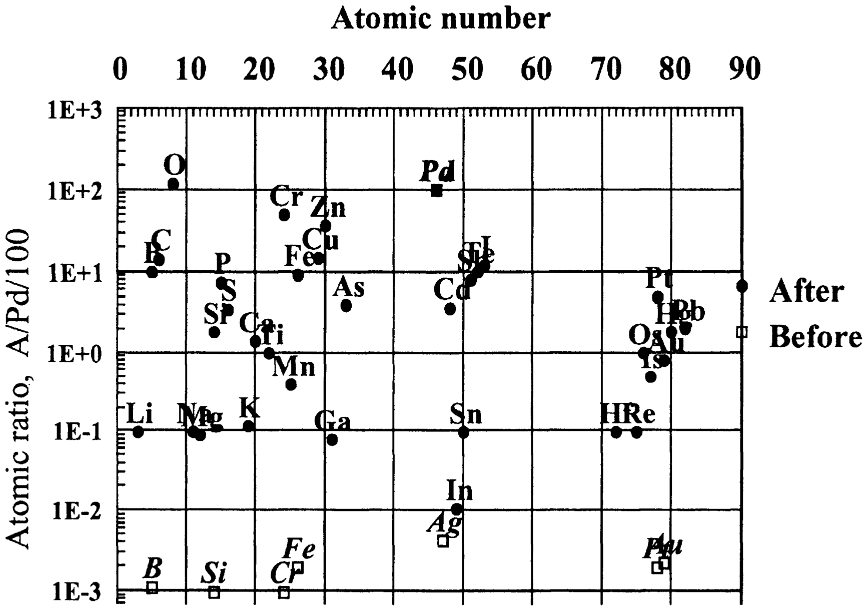

Figure 4. Atomic ratio for the palladium surface layer of 10 μm thickness: Before (□) and after (●) electrolysis.

Downloaded by PENNSYLVANIA STATE UNIV on July 1, 2012 | http://pubs.acs.org
Publication Date: August 1, 2008 | doi: 10.1021/bk-2008-0998.ch012

samples, except for Ca, Cl, Ti, and Hg. Note especially that measurable levels of Zn impurities did not exist in the cell before electrolysis.

Figure 5 shows weight abundance for the samples. Figure 5A shows the total material and impurities estimated by various methods in the electrolyte and electrodes. This includes anode material (Pt 24 g) and solute materials (Li 2.9 g, C 13.2 g, and O 10 g). Figure 5B indicates the total elements that existed in 1 micrometer thickness of a palladium cathode surface that generated excess heat after electrolysis. 5C indicates the total material that existed after electrolysis in heavy water that produced no excess heat. 5D shows the distribution of total materials that existed after electrolysis in light water solution that produced no excess heat Xenon and other rare gas atoms could not be measured by the ICP method, so these elements were not included in the graph. Major elements were Cr: 1.5, Fe: 0.7, Cu: 1.3, Zn: 3.9, Pt: 0.6, and Pb: 0.2 mg. On the other hand,

Downloaded by PENNSYLVANIA STATE UNIV on July 1, 2012 | http://pubs.acs.org
Publication Date: August 1, 2008 | doi: 10.1021/bk-2008-0998.ch012

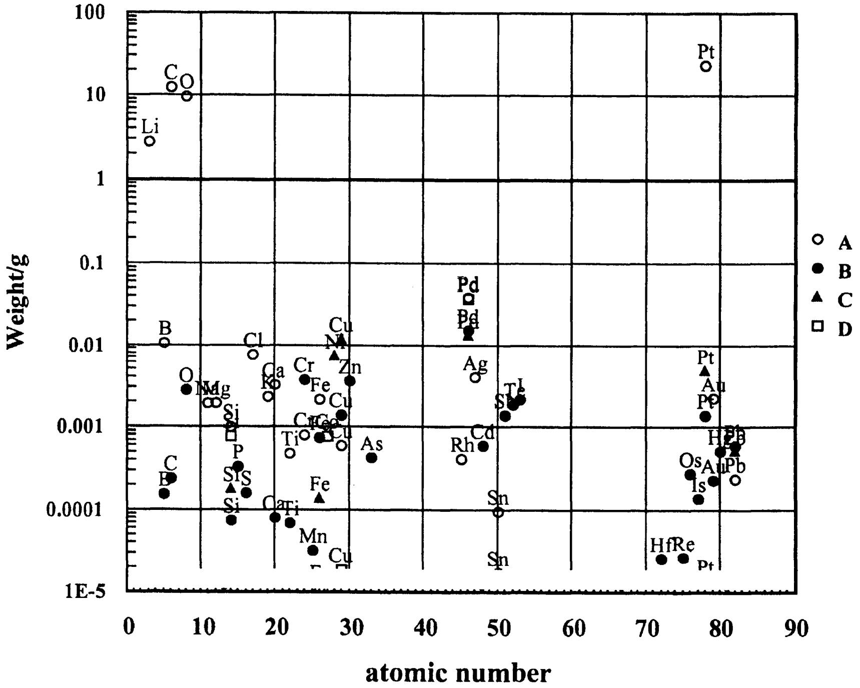

Figure 5. Atomic distributions of the major elements for samples detected by various methods. (A,○): Sample before electrolysis, this includes the solute, anode material, and total impurity in Pd, Pt, and electrolyte in the cell. (B,◆): Sample of the after-electrolysis Pd surface in heavy water solution that generated excess heat. (C,▲): Sample of the after-electrolysis Pd surface in heavy water solution that had no excess heat. (D,□): Sample of the after-electrolysis Pd surface in light water solution with no excess heat.

major elements for the case of no excess heat electrolyzed in heavy and light water solution are as follows:

- Heavy water producing no excess heat: Si: 0.2, Fe: 0.15, Ni: 7.6, Cu: 12.4, Pt: 5.1, and Pb: 0.5 mg
- H_2O, no excess heat: Si: 0.8 and Co: 0.8 mg.

Figure 6 shows the SIMS count spectra for palladium samples that were electrolyzed under various conditions: before electrolysis; after electrolysis in heavy water that generated excess heat; after electrolysis in heavy water that did not generate excess heat; and after electrolysis in light water that did not generate excess heat.

It is very interesting to note the change in the elements according to the electrolysis condition. The change in the element distribution before and after electrolysis is shown as a ratio of the mass spectra. The ratios of masses for the various atomic numbers were estimated by conventional procedures. The ratios are shown in Figure 7 after normalizing the total mass as one. Figure 7(A) shows pure Pd mass spectrum, other peaks can be considered that from low impurities such as Ag, Pt, Au, Fe, and irradiated species of O_2^+ ion.

We have observed no peaks by EDX except for Pd on the (A) sample. Pt and Pd concentrations in the electrolyte after the experiment were 10 and 15 ppm, respectively, by ICP measurement, and no other elements except for Li were observed.

Typical counts by EDX and SIMS ranged from 10^2 to 10^6 and were 10 to 100 times higher than the background counts for the sample of generated excess heat as shown in Figure 7B. Thus, the presence of Ca, Ti, Cr, Fe, Cu, Zn, Pt, and Pb was clearly confirmed. The spectra for these elements are distributed in four groups of mass number: the lightest elements under 50; light elements from 50 to 80; middle elements 100 to 140; and heavy elements from 180 to 208. The ratio of the mass number from 102 to 110, which corresponds to the Pd atom, was under 1% of the total even though it was the bulk substance; the large ratio found was for O and Xe. We assume that these are abundant because atoms of gas are released from the spot heated up by ion bombardment.

The SIMS analysis showed other elements: As, Ga, Sb, Te, I, Hf, Re, Ir, Br, and Xe. Other than Xe, these elements are difficult to detect with AES and EDX because the peaks are very close and sometimes overlap, and the amounts were lower than the detection limits of the measurements. Xe atoms are naturally difficult to detect with EDX because the gas atoms easily escape from the spot targeted by electron bombardment. The SIMS count numbers were observed in the range from 10^3 to 10^6 where the background counts were as low as ~10, so we are confident of these results.

In Figure 7, we show the atomic concentration profiles normalized with the total concentration value. The intensity of Xe was several tens of times larger than Pd; it may be that the gas was released by bombarding with O_2^+ ions, which caused a temperature rise at the sample.

Downloaded by PENNSYLVANIA STATE UNIV on July 1, 2012 | http://pubs.acs.org
Publication Date: August 1, 2008 | doi: 10.1021/bk-2008-0998.ch012

Downloaded by PENNSYLVANIA STATE UNIV on July 1, 2012 | http://pubs.acs.org
Publication Date: August 1, 2008 | doi: 10.1021/bk-2008-0998.ch012

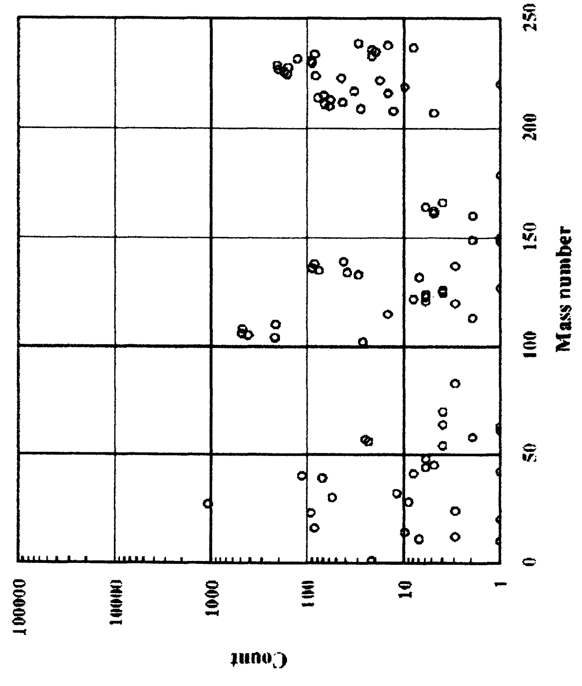

A

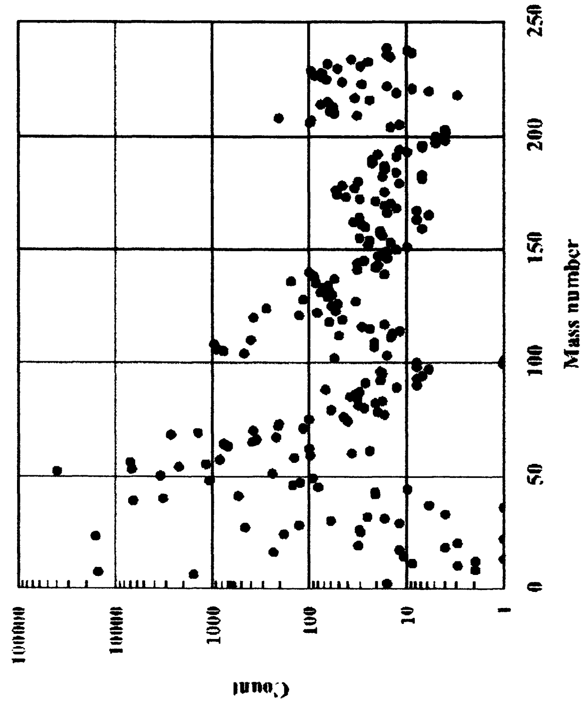

B

Downloaded by PENNSYLVANIA STATE UNIV on July 1, 2012 | http://pubs.acs.org
Publication Date: August 1, 2008 | doi: 10.1021/bk-2008-0998.ch012

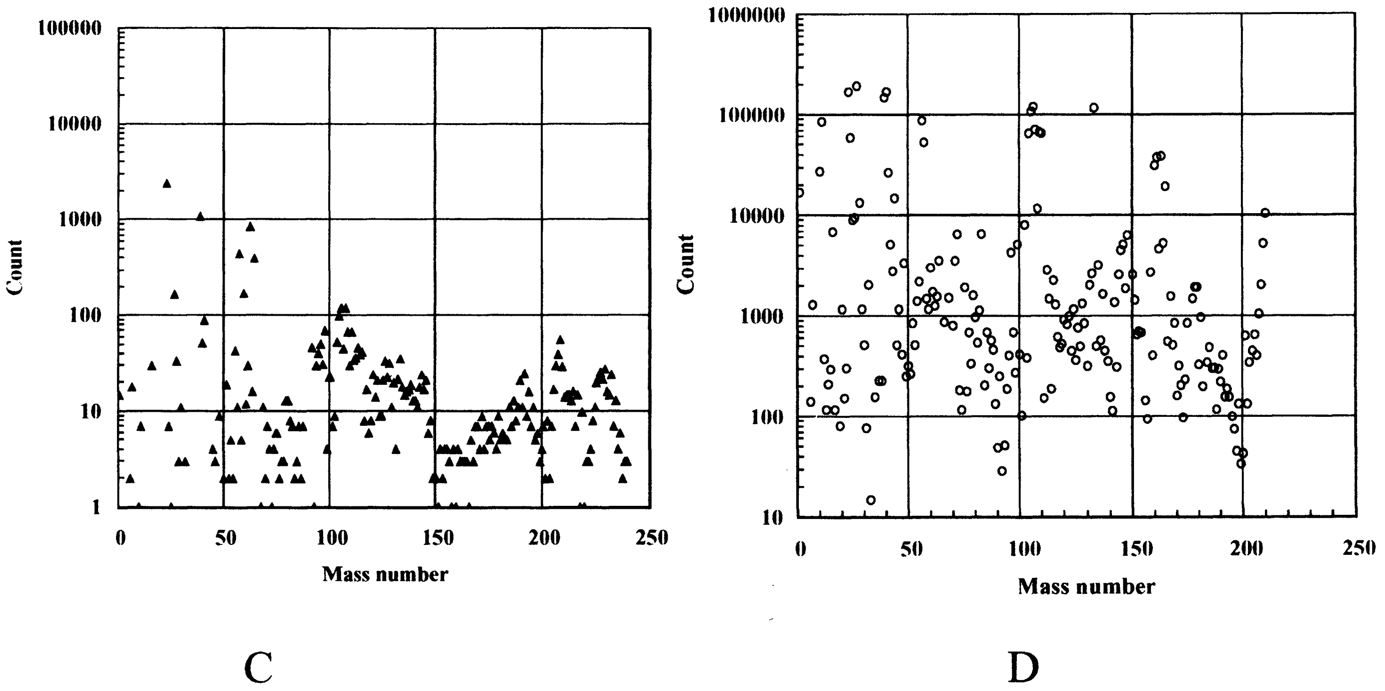

Figure. 6. SIMS counts for palladium cathodes. A: before electrolysis, B: after electrolysis in heavy water when excess heat was generated, C: after electrolysis in heavy water when no excess heat was generated, D: after electrolysis in light water with no excess heat.

Downloaded by PENNSYLVANIA STATE UNIV on July 1, 2012 | http://pubs.acs.org
Publication Date: August 1, 2008 | doi: 10.1021/bk-2008-0998.ch012

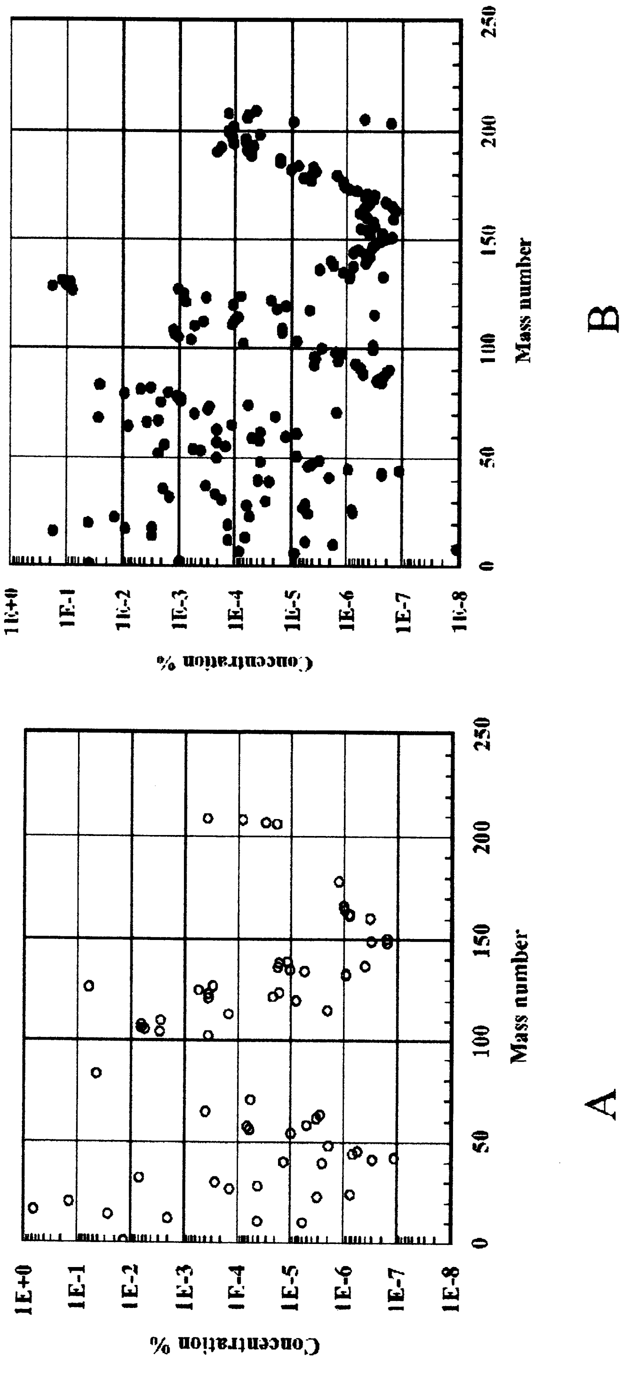

Downloaded by PENNSYLVANIA STATE UNIV on July 1, 2012 | http://pubs.acs.org
Publication Date: August 1, 2008 | doi: 10.1021/bk-2008-0998.ch012

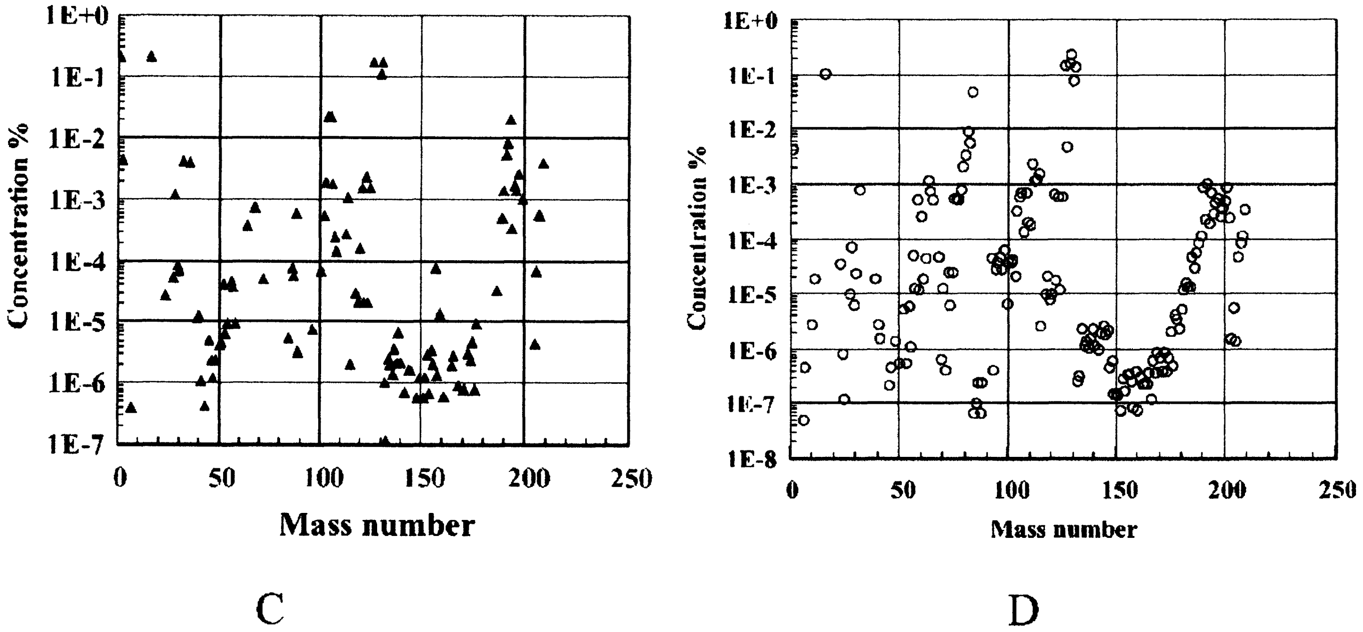

Figure 7. Intensity spectra corrected RSF to Figure 6. (A) before electrolysis; (B) after electrolysis in heavy water solution, excess heat generated; (C) after electrolysis in heavy water solution, no excess heat; (D) after electrolysis in light water, no excess heat.

Downloaded by PENNSYLVANIA STATE UNIV on July 1, 2012 | http://pubs.acs.org
Publication Date: August 1, 2008 | doi: 10.1021/bk-2008-0998.ch012

The palladium sample (Figure 7C) electrolyzed in heavy water solution which produced no excess heat showed several anomalous elements. Ni, Mo, and other heavier elements were found in larger amounts than the sample that did produce excess heat (Figure 7B).

Figure 8 shows the intensity ratio between the SIMS counts for several conditions of the palladium electrodes referred to palladium before electrolysis. We have to remember that the graphs show the ratios normalized by total atom number. Figures 8(B) and (C) are similar to but slightly different from Figure 8A. Light elements show higher intensity than do the heavy elements.

Figure 9A shows the intensity ratios for mass spectra for a sample that generated excess heat compared to the ratio of a sample that produced no excess heat, both with electrolysis in heavy water. All of the data points were averaged by the total SIMS count that was obtained from surface to one micrometer depth in the palladium.

Figure 9B shows intensity ratio for mass spectra between for a sample that generated heat in heavy water, and a sample electrolyzed in light water. There are large differences in the light elements in these two graphs. Apparently, many light elements are sometimes generated by an unknown nuclear reaction when excess heat is produced.

Abundant amounts of Cr detection can be seen in case of Pd that has excess heat generated as shown in Figure 5. For this reason, we consider the Cr isotope ratios in the surface. After electrolysis the amount of Cr exceeds the impurities included before the Pd electrolysis. Other elements that caused interference on the Cr isotopes when they were detected by the SIMS measurement have to be considered. All of the interference species that would affect the Cr isotopes are indicated as follows. Here, the presentation is described according to species, mass, and isotope abundance ratio.

For the case of Cr50 49.94605 (4.5%), there were Ti50: 49.94479 (5.4%), V50: 49.94716 (0.25%), Ru1002+: 49.95211 (12.6%) and Mo1002+: 49.95374 (9.63%). In this case, we have detected one order less abundance of Ti, no V, Mo and Ru atoms. There were no interference species on the abundance for Cr50 isotope.

In the case of Cr52, 51.94051 (83.79%), there were Pd104^{2+}: 51.95201 (9.3%) and Ru104^{2+}: 51.95271 (18.27%). Here, only Pd104^{2+} species may interfere, because the mass difference is only 0.022%. However, the amount of the Pd^{2+} species is usually far less than the Pd^{+}. In fact, the Cr52 ratio approaches the normal one toward the inside of Pd sample, where Pd abundance is higher than the surface.

The Cr53 isotope (atomic mass 52.94065, 9.5% natural abundance) is affected by species of Pd105^{2+} (mass 52.45254, 22.6%), Pd106^{2+} (mass 52.95174, 27.1%) and Cd106^{2+} (mass 52.95323, 1.22%). Here, only Pd106^{2+} can be expected to affect the apparent abundance, and as stated above, the double charged ion is extremely rare and there is not enough to cause measurable interference.

Cr54 (atomic mass 53.93888, 2.37% natural abundance) may be affected by Ag107^{2+} (mass 53.45255, 51.35%) and Fe54 (mass 53.93961, 5.8%). Here, Fe is the only species to affect the abundance. But the Fe abundance is almost one order less than the Cr.

Large differences in isotopic distributions compared with the natural distributions were observed by the SIMS method for Cr, Cu, Zn, Xe, Pd, and Pt. Typical concentrations and their ratios for chromium isotopes are shown in Figure 10A and 10B. For example, the concentrations except for Cr52 decreased exponentially with depth. But Cr52 first increases, reaching a peak at 0.5 micrometers, then decreases. These elements show a large shift in isotopic ratios from the natural ones, as indicated at 30,000A in Fig.10B. That means that the isotope ratio of Cr52 is less than natural value, especially at the surface region.

These isotopic distribution changes occurred mainly within most outer surface layer of one micrometer and their ratios approached normal values toward the inner bulk layer. Here, Cr is one of the most accurate cases, because the concentration was very high, more than 10 percent by weight of the palladium surface layer.

In Figure 11, the palladium also shows large shifts in isotopic abundances. In the case of palladium isotope, there were no interference species other than Pb^{2+} ions in the palladium surface. However, these Pb species are two orders less abundant than Pd, so their effect on the isotopic ratio of Pd is very small. All other elements, other than Cr and Zn, were also present in extremely small quantities compared to the weight of the palladium. Their concentrations are represented as the ratio to Pd106, which was selected because it is the most abundant natural isotope. Moreover, species such as Ar-Zn, Zr-O, Sr-O, and Cd that may interfere with the measurement of Pd isotopic abundances were not detected at all.

Palladium atomic concentration increased with depth. This means that the relative concentration of other deposits decreased. Especially, amounts of Pd102, 104, and 110 are more than the natural ones. These values approach the normal values toward the inside of palladium as indicated as in the figure. The phenomenon has never been seen in palladium before electrolysis.

Figures 12 and 13 show the results from a palladium sample that was electrolyzed in heavy water but did not produce excess heat. The process did produce some isotope changes in the deposited elements on the sample. There existed large amounts of Ni and Mo, which was not seen with palladium samples that generated excess heat, which had elements such as Cr and Fe instead. Nickel has 5 stable isotopes. In this sample we found mainly four isotopes: Ni58, Ni60, Ni61, and Ni62. We did not find Ni64, which has a natural abundance of 0.91%. All of the interference species that may affect SIMS detection of Ni isotopes are shown in Table I.

Because the mass difference between Fe58 and Ni58 is 0.0035%, it is very difficult to distinguish between them with the SIMS method. However, in this sample, Ni was 7.6 wt % and Fe was only 0.15 wt %, so Ni was 50 times more abundant than Fe, and the effect of the Fe58 on the apparent isotopic ratio of Ni58 was negligible.

Downloaded by PENNSYLVANIA STATE UNIV on July 1, 2012 | http://pubs.acs.org
Publication Date: August 1, 2008 | doi: 10.1021/bk-2008-0998.ch012

Downloaded by PENNSYLVANIA STATE UNIV on July 1, 2012 | http://pubs.acs.org
Publication Date: August 1, 2008 | doi: 10.1021/bk-2008-0998.ch012

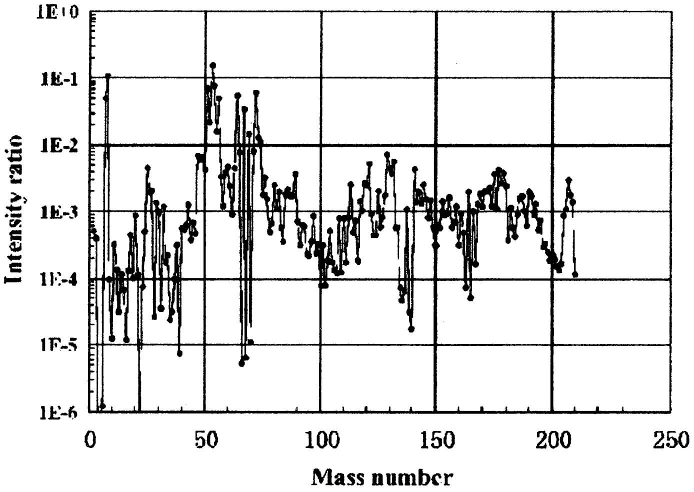

(A)

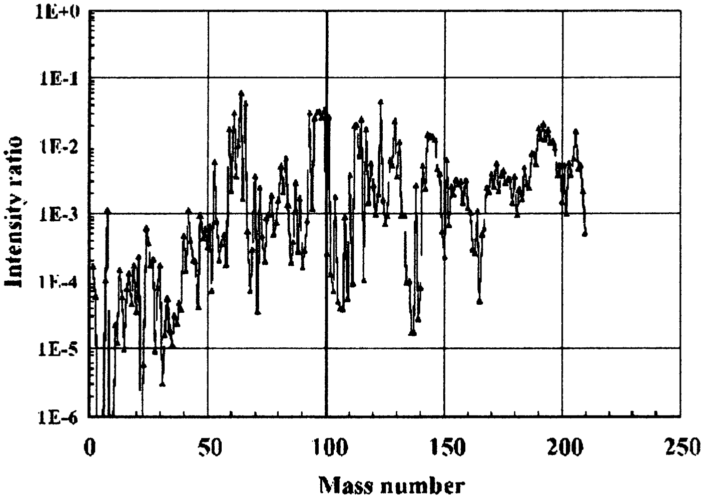

(B)

Downloaded by PENNSYLVANIA STATE UNIV on July 1, 2012 | http://pubs.acs.org
Publication Date: August 1, 2008 | doi: 10.1021/bk-2008-0998.ch012

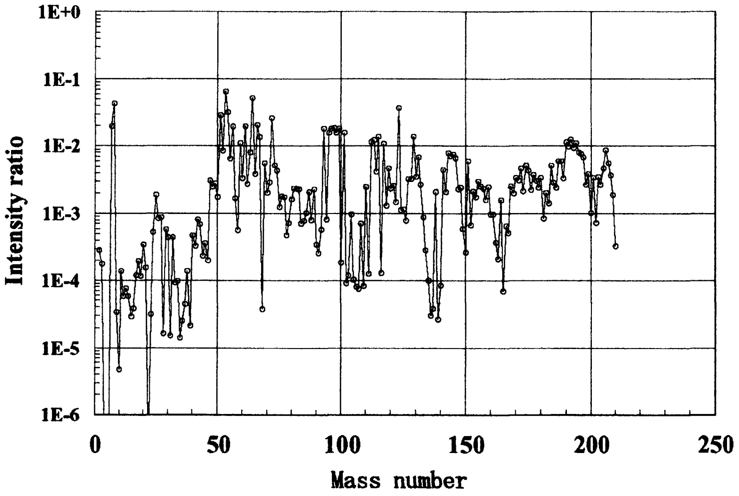

(C)

Figure 8. Intensity ratios based on the counts before electrolysis, obtained from Fig. 5. A: after electrolysis in heavy water solution when excess heat was generated. B: after electrolysis in heavy water solution with no excess heat. C: after electrolysis in light water with no excess heat.

Downloaded by PENNSYLVANIA STATE UNIV on July 1, 2012 | http://pubs.acs.org
Publication Date: August 1, 2008 | doi: 10.1021/bk-2008-0998.ch012

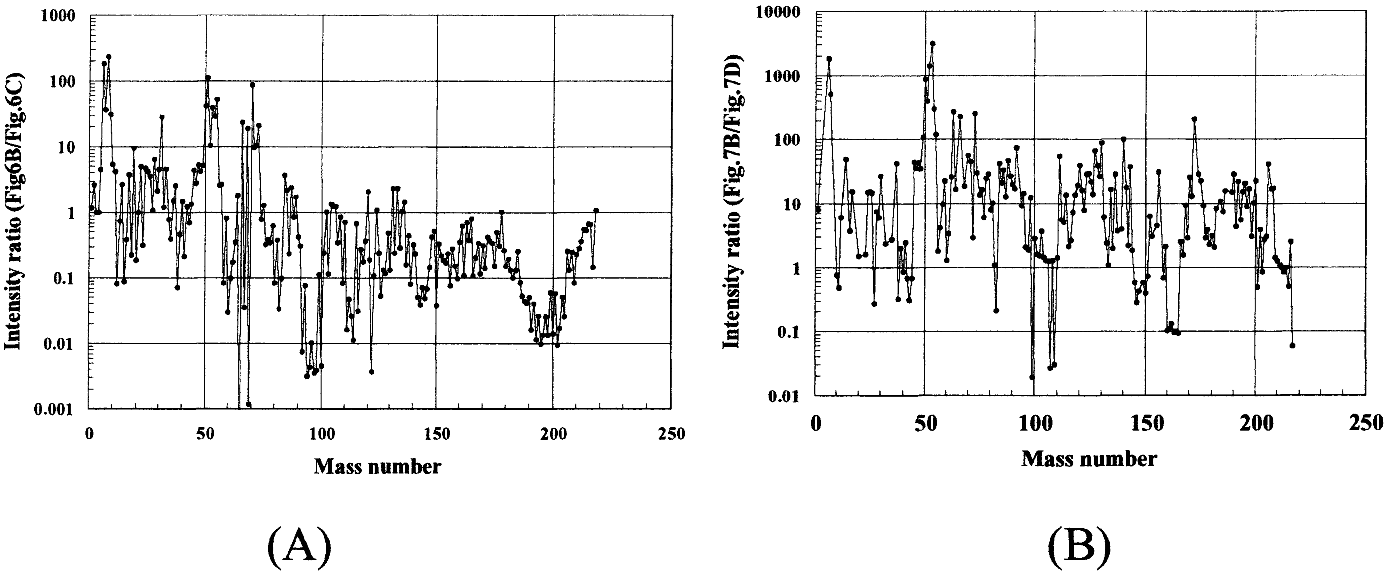

Figure 9. A: Intensity ratios for mass spectra for electrolysis in heavy water with excess heat compared to results with no excess heat. All data points were averaged by the total SIMS count obtained from surface and 3 μm depth of the palladium sample. B: Intensity ratio of mass spectra between palladium in heavy water that produced excess heat and in light water that produced no excess heat.

Downloaded by PENNSYLVANIA STATE UNIV on July 1, 2012 | http://pubs.acs.org
Publication Date: August 1, 2008 | doi: 10.1021/bk-2008-0998.ch012

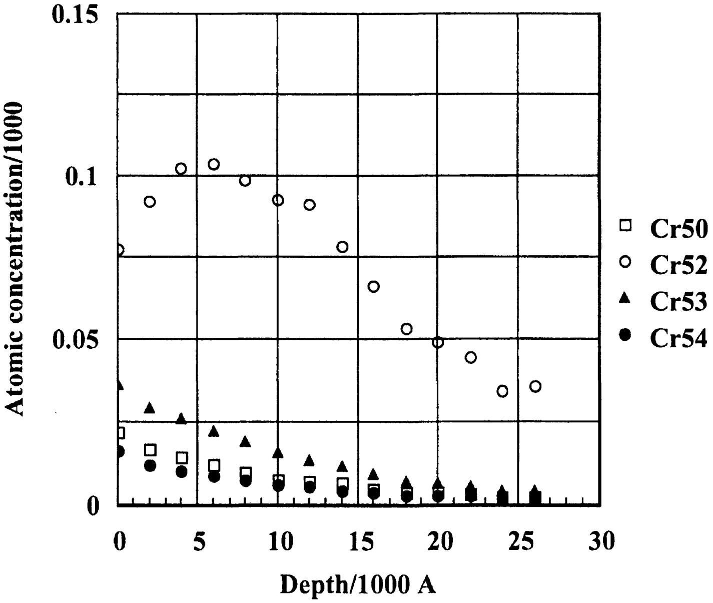

Figure 10A. Concentration profiles for Cr isotopes.

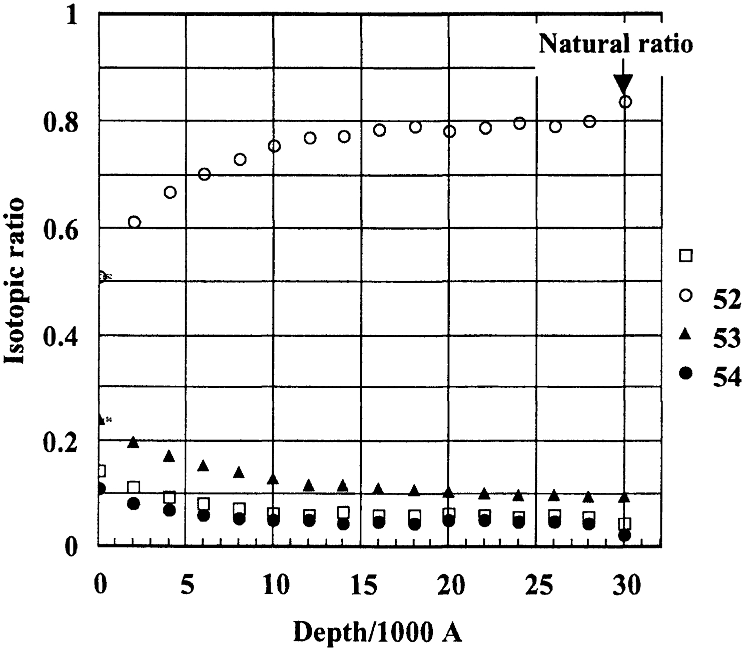

Figure 10 B. Profiles of Cr isotope ratio in Pd.

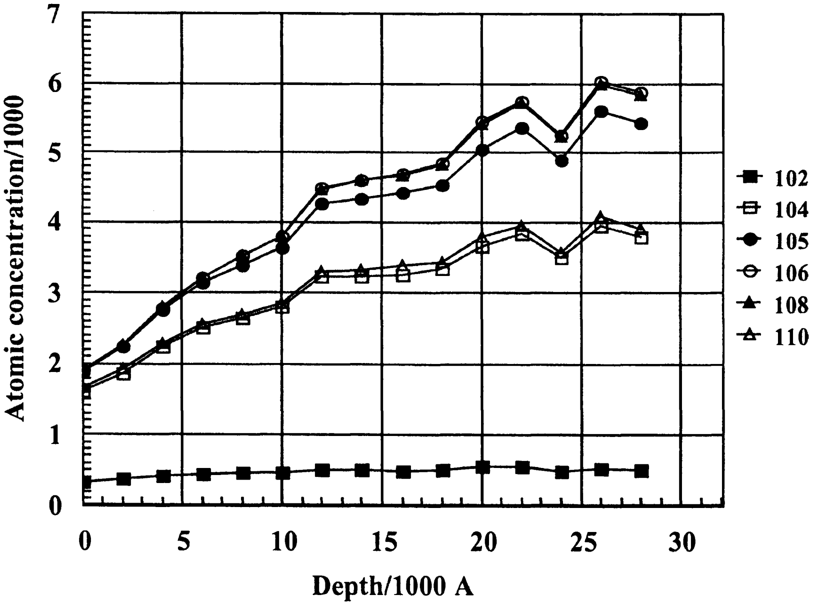

Figure 11A. Concentration profiles for Pd isotopes.

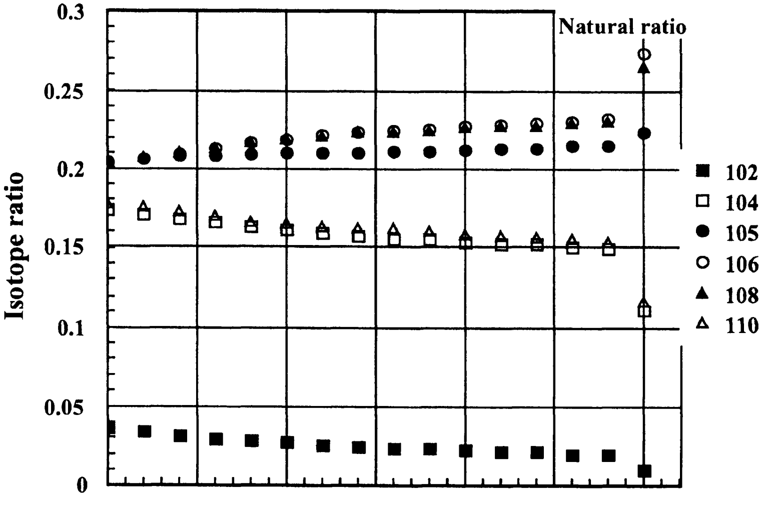

Figure 11B. Profiles of Pd isotope ratio in Pd rod.

Downloaded by PENNSYLVANIA STATE UNIV on July 1, 2012 | http://pubs.acs.org
Publication Date: August 1, 2008 | doi: 10.1021/bk-2008-0998.ch012

Downloaded by PENNSYLVANIA STATE UNIV on July 1, 2012 | http://pubs.acs.org
Publication Date: August 1, 2008 | doi: 10.1021/bk-2008-0998.ch012

Table I. Interference Species for Ni Isotopes

Ni isotope	*Mass number*	*Natural abundance*	*Interference species*	*Mass number*	*Natural abundance*
Ni58	57.93535	68.27%	Fe58	57.93328	0.28%
			Sn116^{2+}	57.95087	14.53%
			Cd116^{2+}	57.95238	7.49%
Ni60	59.93079	26.1%	Sn120^{2+}	59.95110	32.59%
Ni61	59.93106	1.13%	Sn122^{2+}	60.95172	4.63%
Ni62	61.92835	3.59	Sn124^{2+}	61.95264	5.79%
			Xe124^{2+}	61.95329	0.10%
Ni64	63.92797	0.91%	Zn64^{+}	63.92915	48.60%
			Xe128^{2+}	63.95177	1.91%

For other Ni isotopes as well, the interference species were present in only negligible amounts, except for Zn64^{+} in a cathode that did not generate excess heat. Depth profiles for the concentration of Ni isotopes in the Pd cathode are shown in Figure 12A. Since there was a significant amount of Zn in the deposited elements, and Zn interferes with Ni64, the depth profile for Ni64 is not shown in this figure. Figure 12B shows the ratio of Ni isotopes 60, 61, and 62 to mass number 58, because Ni58 is the most common Ni isotope (at 68.27%). The depth profile of the concentration of Ni isotopes in the Pd peaked near the surface and gradually decreased toward the inside of the Pd bulk. The abundances for Ni isotopes were quite different from the natural abundances on the surface region of the cathode, but they approach the natural ratio toward the inside.

Palladium also shows a large change in the isotopic abundance at the surface and then rapidly approaches natural abundance below the surface. These abundances are represented in Figure 13 by the ratio with the Pd106 isotope. The atomic concentration increased with depth as shown in Figure 13A. Here, Pd108 and Pd110 show large difference from natural isotopic abundance at the surface. On the other hand Pd102, 104, 105, 106, and 110 are close to the natural abundance throughout the sample. The isotopic change for Pd corresponds to the change in Ni.

When Pd was electrolyzed in heavy water, changes in isotopic abundance occurred at the surface of the electrode. If the changes were induced by hydrogen penetration, the transmutation reaction would occur not only at the Pd surface but also in inner layers. However, only the surface layer was changed. Iwamura's transmutation products also occurred near the surface (*4*), which is another indication that the reaction occurs at the surface, and in Iwamura's cell the transmutations were induced by deuterium gas permeation, which clearly indicates the key role that deuterium plays in the reaction.

We have not observed isotopic change with light water electrolysis. We conclude that the phenomenon is characteristic of heavy water electrolysis.

Downloaded by PENNSYLVANIA STATE UNIV on July 1, 2012 | http://pubs.acs.org
Publication Date: August 1, 2008 | doi: 10.1021/bk-2008-0998.ch012

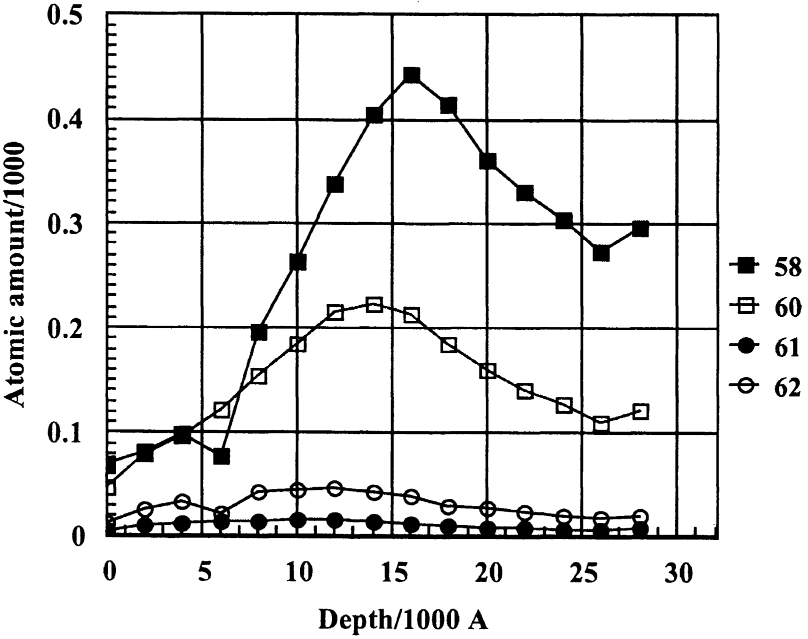

Figure 12A. Concentration profiles for Ni isotopes.

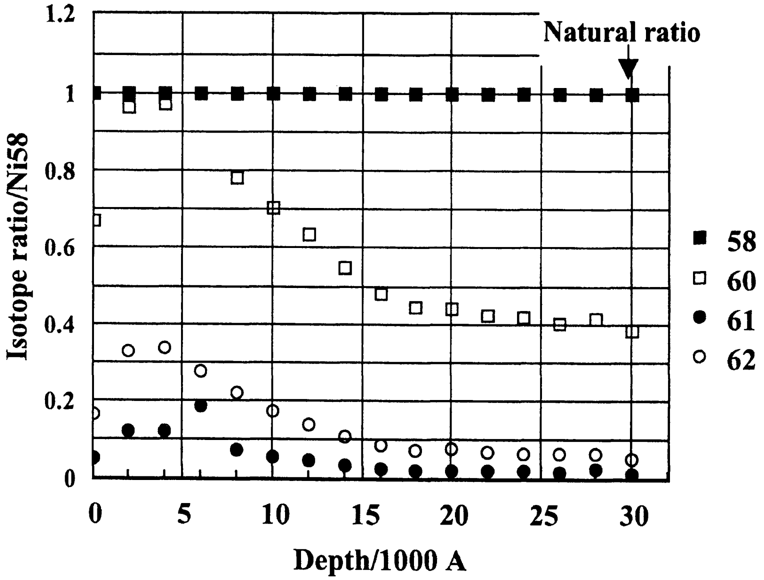

Figure 12B. Profiles of Ni isotope ratio in Pd.

Downloaded by PENNSYLVANIA STATE UNIV on July 1, 2012 | http://pubs.acs.org
Publication Date: August 1, 2008 | doi: 10.1021/bk-2008-0998.ch012

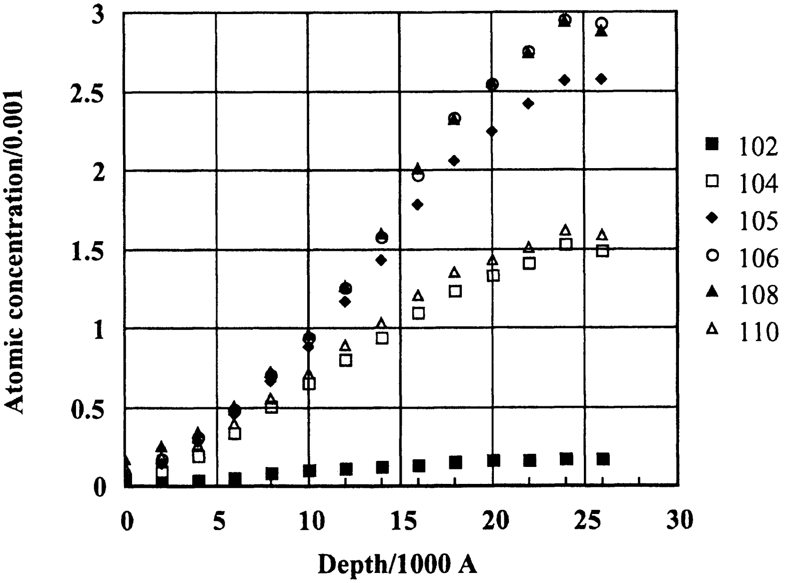

Figure 13A. Concentration profiles for Pd isotopes.

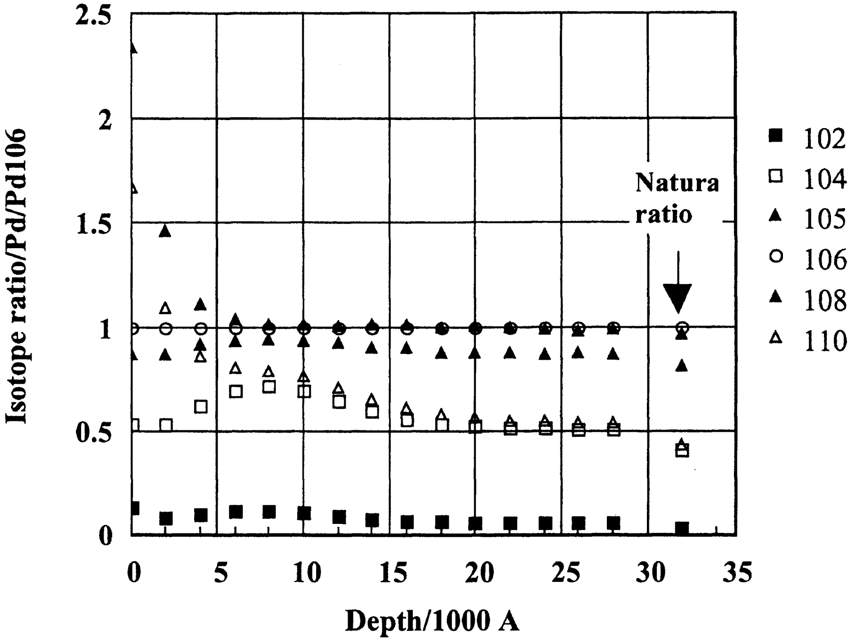

Figure 13B. Profiles of Pd isotope ratio in Pd rod.

Conclusions

Our conclusions are summarized as follows:

1. Various elements were found to be abundant in the electrolyte and in the electrode material after electrolysis. The same phenomenon was confirmed with high reproducibility at high cathodic current density ranging from 0.2 to 0.8 A/cm^2.
2. We may suppose that impurities such as Cr, Fe, Cu, and Zn in the system accumulated in the cathode. Moreover, the amount of all the impurities is several times smaller than the total amount of the deposit detected.
3. Different isotopic distributions were obtained depending on the solvent of the electrolyte and on whether or not there was excess energy generation.
4. It is impossible to explain the generation and shifts in the isotopic distribution of the elements by chemical reaction. Hence it must be concluded that some novel nuclear reactions have occurred.
5. We assume that palladium was the starting material for these nuclear reactions, but it is also possible that impurities and other cell components such as Li, D_2O, Pd, and Pt may have provided the starting material.

Downloaded by PENNSYLVANIA STATE UNIV on July 1, 2012 | http://pubs.acs.org
Publication Date: August 1, 2008 | doi: 10.1021/bk-2008-0998.ch012

Acknowledgements

The author is grateful to Professor Richard Oriani and Mr. Jed Rothwell for important discussions and assistance editing the paper.

References

1. Mizuno, T.; Ohmori, T.; Kurokawa, K.; Akimoto, T.; Kitaichi, M.; Inoda, K.; Azumi, K.; Shimokawa, S.; Enyo, M. Anomalous Isotopic Distribution of Elements Deposited on Palladium Induced by Cathodic Electrolysis. *Denki Kagaku* **1996**, *64*, 1160-1165.
2. Miley, G. H.; Patterson, J. A. Nuclear Transmutations in Thin-Film Nickel Coatings Undergoing Electrolysis. *J. New Energy* **1996**, *1*, 5-39.
3. Ohmori, T.; Mizuno, T.; Nodasaka, Y.; Enyo, M. Transmutation in a Gold-Light Water Electrolysis System. *Fusion Technol.* **1988**, *33*, 367-382.
4. Iwamura, Y.; Sakano, M.; Itoh, T. Elemental Analysis of Pd Complexes: Effects of D2 Gas Permeation. *Jpn. J. Appl. Phys.* **2002**, *41*, 4642-4648.
5. Mizuno, T.; Akimoto, T.; Azumi, K.; Enyo, M. Diffusion Rate of Deuterium In Pd During Cathodic Charging. *Denki Kagaku* **1992**, *60*, 405-411.
6. Mizuno, T.; Akimoto, T.; Sato, N. Neutron Evolution from Annealed Palladium Cathode in Liod-D2O Solution. *Denki Kagaku* **1989**, *57*, 742-743.
7. Mizuno, T.; Akimoto, T.; Azumi, K.; Sato, N. Tritium Evolution During Cathode Polarization of Palladium Electrode in D2O Solution. *Denki Kagaku* **1991**, *59*, 789-790.

Downloaded by PENNSYLVANIA STATE UNIV on July 2, 2012 | http://pubs.acs.org
Publication Date: August 1, 2008 | doi: 10.1021/bk-2008-0998.ch013

Chapter 13

Experimental Observation and Modeling of Cs-137 Isotope Deactivation and Stable Isotopes Transmutation in Biological Cells

Vladimir I. Vysotskii[1], Alexandr B. Tashyrev[2], and Alla A. Kornilova[3]

[1]Kiev Shevchenko University, Vladimirskaya Str. 64, 01033, Kiev, Ukraine
[2]Kiev Institute of Microbiology, Zabolotnogo Str. 154, 03680, Kiev, Ukraine
[3]Moscow State University, 119899, Moscow, Russia

The report presents the results of combined (Mössbauer and mass-spectroscopy) qualifying examinations of stable isotope transmutation processes in growing microbiological cultures, in the iron-region of atomic masses. It is shown that isotope transmutation during the process of growth of microbiological cultures, at optimal conditions, is 10-20 times more effective than the same transmutation process in the form of "one-line" (clean) microbiological cultures that we have studied previously. In the work, the process of direct, controlled decontamination of highly active long-lived isotopes through the process of growing microbiological systems has been studied. For the first time, an accelerated de-activation rate is observed that is 35 times greater than the controlled deactivation of the Cs^{137} isotope.

In Low-Energy Nuclear Reactions Sourcebook; Marwan, J., et al.;
ACS Symposium Series; American Chemical Society: Washington, DC, 2008.

Introduction and Foundation of the Effect of Isotope Transmutation in Biological Systems

The problem of transmutation of stable and active isotopes in biological systems is one of most mysterious in modern nuclear physics.

The hypothesis about the possibility of nuclear transmutation of chemical elements and their isotopes in physical, biological, and geological systems with low energy of relative movement of interacting nuclei has been frequently discussed during the last decades. Interest in this issue grew after the beginning of systematic study of the phenomenon of cold nuclear fusion (CNF) based on dd-reactions in solid bodies.

In our opinion, there is no reason to consider the process of transformation of isotopes and elements in biological transmutation to be separate and different from the general physical forms of transmutation that can occur from comparable forms of transformation of isotopes through transmutation that can occur through alternative processes, governed by the laws of physics. We believe that all the observed isotopic effects (assuming they are real and supported by adequate and reliable measurements) can be characterized as the "regular" process of transmutation of isotopes and elements, which occurs in biological systems, and the efficacy of which is determined precisely by the specific characteristics and behavior of such systems.

Many additional specific questions arise when analyzing the problem of transmutation of isotopes in growing biological cultures (especially the case of transmutation with generation of isotopes of chemical elements that are not required by a growing culture under normal conditions). The most important of these questions are: why does a growing culture need this kind of process, how is this process accomplished, and can this process be controlled?

In the distant future, more refined studies will provide more complete, and potentially full and final answers to these questions. The authors recognize all the complexity of this problem. Our thesis, which is outlined below, can be interpreted only as one possible solution, based on our understanding of the problem. To be consistent with our position of the objective regularity of such a process, we must note that an explanation ought to be sought among the known laws of physics, chemistry, and biology.

In our opinion, the process of transmutation is evolution's answer to the global dilemma: how is it possible to combine development and adaptation of biological objects, each one of which contains a genetically predetermined set of elements, with a random character and dissimilar distribution of elements in the outer environment, as well as constant environmental changes?

This process occurs in places where there is competition based on the stereochemical analogy (at least in transporting and fermentation systems). The area where this competition takes place determines the area where transmutation itself is performed. Can we point to a specific spot, or set of conditions, where this ingenious nuclear reaction process takes place? It is possible that there are

Downloaded by PENNSYLVANIA STATE UNIV on July 2, 2012 | http://pubs.acs.org
Publication Date: August 1, 2008 | doi: 10.1021/bk-2008-0998.ch013

Downloaded by PENNSYLVANIA STATE UNIV on July 2, 2012 | http://pubs.acs.org
Publication Date: August 1, 2008 | doi: 10.1021/bk-2008-0998.ch013

many such places or sets of conditions (otherwise, reactions would be such rare events that they would be impossible to detect). Also note that transmutation occurs with a higher probability in structural parts of biological objects that are subjected to dynamic influences (zone of growth, non-stationary transport systems, dynamic response systems to any kind of agitation, and so on).

The physical aspects of transmutation processes are related to general problems of low-energy nuclear reactions. To date, over 400 works have been published which — with various degrees of agreement and disagreement — present different physical models that are capable, according to their authors, of explaining the phenomenon of "cold nuclear synthesis," or at least of providing a framework for finding ways to possibly explain these kinds of effects. Our point of view with respect to explaining this problem has been presented in our book (*1*). We think that, in the case of dynamic biological systems, the most effective mechanism, as we suggested earlier in 1994-1996, is capable of removing — for a brief time — the influence of the Coulomb barrier of a nuclear reaction occurring in a nonstationary potential well with a structure that is close to being parabolic.

Experimental Investigation of Fusion of Iron-Region Stable Isotopes in Optimal Growing Microbiological Associations

Several years ago we studied and reported on the process of transmutation of stable isotopes in growing "one-line" (one type, "clean") microbiological cultures like *Escherichia coli* or *Deinicocus radiodurans* in two kinds of nuclear reactions (*1*), based on the following reactions:

$$Mn^{55}+d^{2}=Fe^{57},$$
$$Na^{23}+P^{31}=Fe^{54}.$$

It was shown that the transmutation process during the growth of such microbiological cultures had taken place, but its effectiveness had been low. Expressed in relative units (defined by the ratio between accumulated number of $N(Fe^{57})$ of Fe^{57} nuclei to the number $N(Mn^{55})$ of Mn^{55} nuclei) the rate (λ) of Fe^{57} production had been low and had equaled

$$\lambda = N(Fe^{57})/N(Mn^{55})\Delta t \approx 10^{-8}$$

(synthesized Fe^{57} nuclei per s and per single Mn^{55} nucleus) in the case of the reaction with light isotope $Mn^{55}+d^{2}=Fe^{57}$, and

$$\lambda \approx 10^{-10}\ s^{-1}$$

in the reaction for the middle range mass isotopes $Na^{23}+P^{31}=Fe^{54}$.

The typical Mössbauer spectrum of one-line culture *Saccharomyces cerevisiae T-8*, grown in D_2O with the presence of Mn^{55} isotope (*2*), is presented in Figure 1.

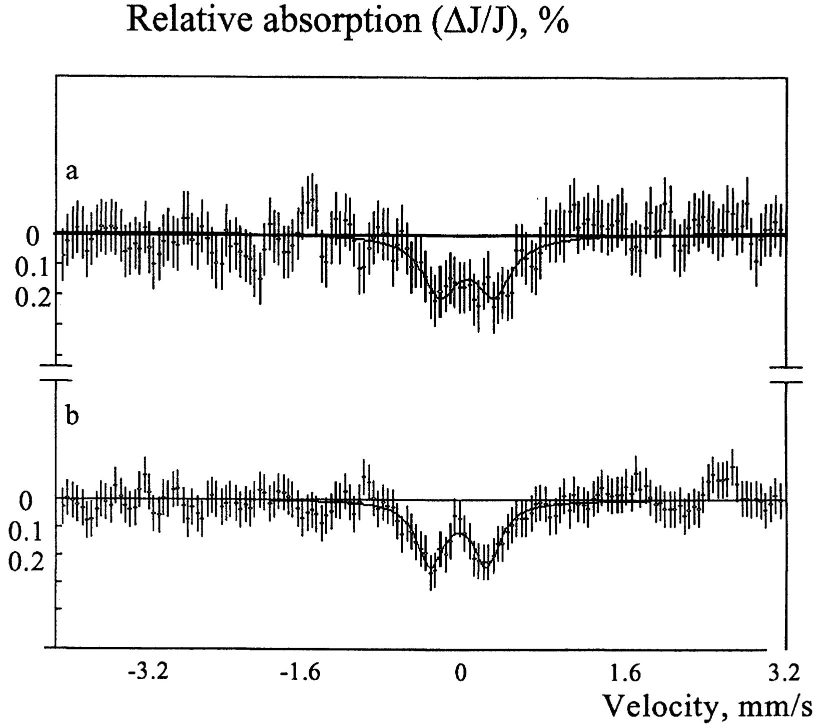

Figure 1. Mössbauer spectra of grown cultures in different identical flasks. Culture Saccharomyces cerevisiae T-8 *grown in D_2O with presence of Mn^{55} isotope.*

Downloaded by PENNSYLVANIA STATE UNIV on July 2, 2012 | http://pubs.acs.org
Publication Date: August 1, 2008 | doi: 10.1021/bk-2008-0998.ch013

The low relative amplitude of Mössbauer resonance ($\Delta J/J \approx 0.2\%$) in these experiments was the result of low absolute and relative concentration of created Fe^{57} isotope in the culture.

There are two main reasons for the low effectiveness of nuclear transmutation in one-line microbiological cultures:

- The relatively low efficiency for creating these reactions is the result of the narrow interval of optimal functional individual characteristics for initiating nuclear activity in any one-line type of culture. Each of the one-line cultures individually requires a set of specific conditions (temperature, hydrogen ion exponent pH, balanced contents of nutrient medium, etc.) for achieving optimal metabolic conditions during the complete period of growth. Such conditions are often absent in real experiments.

- During the growth of a one-line culture, we hypothesize that processes involving forms of auto-intoxication of nutrient media by metabolic products take place. This hypothesis is consistent with forms of growth impairment.

Downloaded by PENNSYLVANIA STATE UNIV on July 2, 2012 | http://pubs.acs.org
Publication Date: August 1, 2008 | doi: 10.1021/bk-2008-0998.ch013

In contrast to these one-line cultures, we have investigated microbiological associates that include great numbers of types of different cultures.

The base of the MCT ("microbial catalyst-transmutator") compound that was used is the microbe syntrophin associations of thousands of different microorganism kinds that are in the state of complete symbiosis (*3*). These microorganisms pertain to different physiological groups that represent practically the whole variety of the microbe metabolism and are relevant to all kinds of microbe accumulation mechanisms. We postulate that the state of complete symbiosis of the syntrophin associations results from the possibility of maximal adaptation of the microorganisms' association in response to changes in any external conditions.

These cultures are in a state of natural complete symbiosis and grow as a total correlated multisystem. There are a lot of different types of intraspecific and interspecific stimulated and symbiotic connections between different cultures in the volume of syntrophin associations. This correlated microbiological multisystem adequately reacts to modifications of exterior requirements, to composition of nutrient medium, and to biochemical properties of a system because of metabolic, growth, and transmutation processes.

The spectrum of their functional characteristics is very wide. We believe that it should be expected that this would lead to high efficiency/effectiveness for stimulating transmutation processes. This model is presented in symbolic form in Figure 2.

The MCT compound involves special granules that include:

- concentrated biomass of metabolically active microorganisms (microbe syntrophin association);
- organic sources of carbon and energy, phosphorus, nitrogen, etc.; and
- gluing substances that keep all components, in the form of granules, stable in water solutions for a long period of time, even when they are subjected to many, and possibly external conditions.

The general aim of that investigation was to find biotechnology-based methods of effective isotope transmutation. The possibility of a potential reaction, $Mn^{55}+d^2=Fe^{57}$, with heavy water in growing MCT was investigated in

Downloaded by PENNSYLVANIA STATE UNIV on July 2, 2012 | http://pubs.acs.org
Publication Date: August 1, 2008 | doi: 10.1021/bk-2008-0998.ch013

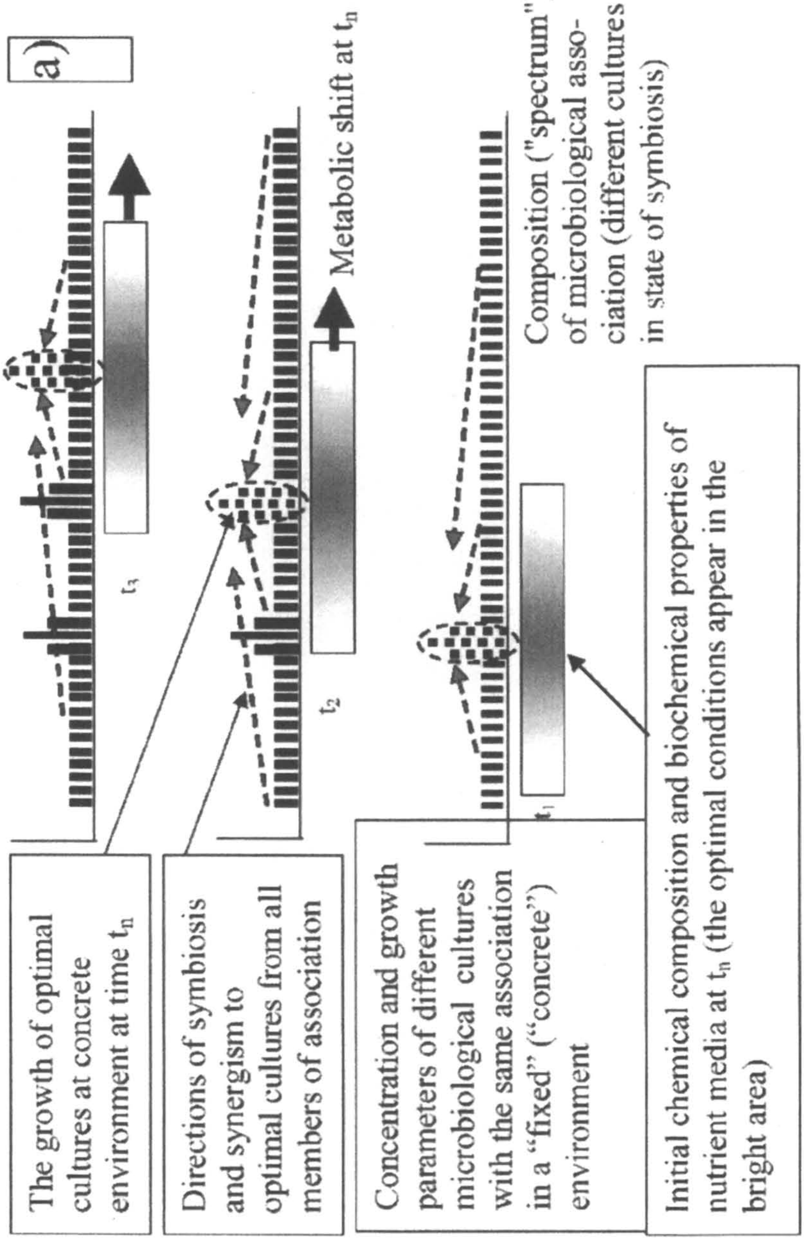
a)
Metabolic shift at t_n
Composition ("spectrum") of microbiological association (different cultures in state of symbiosis)
t3
t2
t1
The growth of optimal cultures at concrete environment at time t_n
Directions of symbiosis and synergism to optimal cultures from all members of association
Concentration and growth parameters of different microbiological cultures with the same association in a "fixed" ("concrete") environment
Initial chemical composition and biochemical properties of nutrient media at t_n (the optimal conditions appear in the bright area)

Downloaded by PENNSYLVANIA STATE UNIV on July 2, 2012 | http://pubs.acs.org
Publication Date: August 1, 2008 | doi: 10.1021/bk-2008-0998.ch013

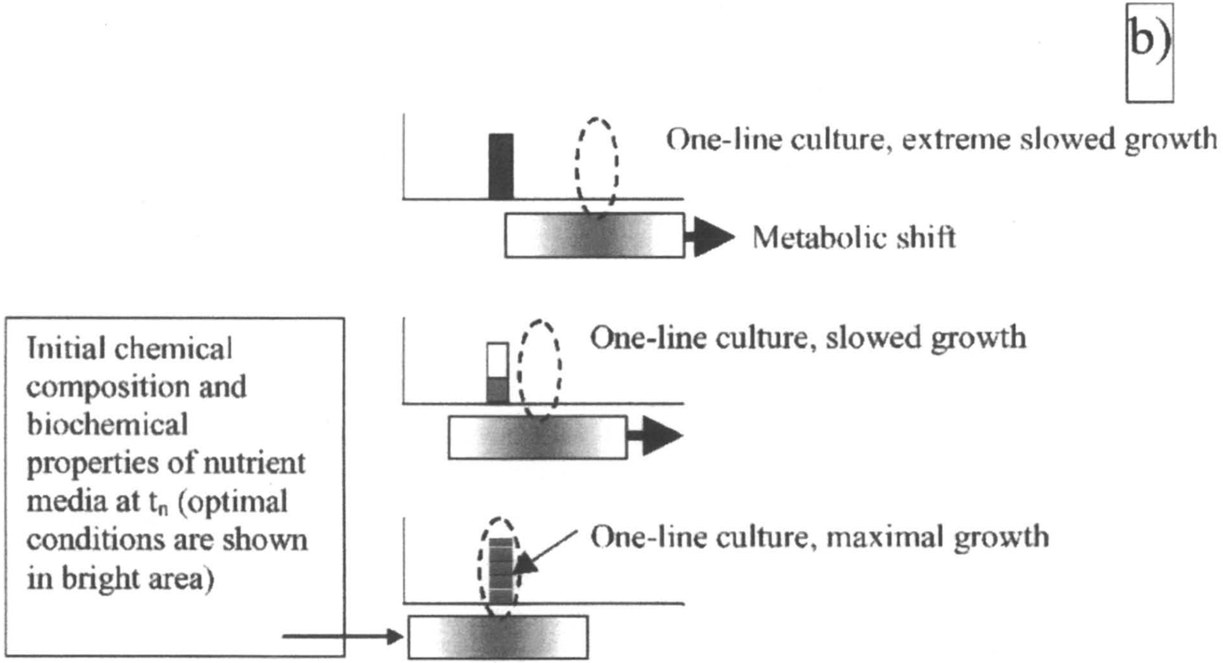
b)
One-line culture, extreme slowed growth
Metabolic shift
One-line culture, slowed growth
One-line culture, maximal growth
Initial chemical composition and biochemical properties of nutrient media at t_n (optimal conditions are shown in bright area)

Figure 2. Changes in the directions of symbiosis and synergism in microbiological association (case a) to optimal growing cultures involving changes in types of chemical composition and biochemical properties of nutrient media and environment. Changes in types of optimal cultures are the result of metabolic shifts of chemical composition and biochemical properties of nutrient media. The case b) presents the process of growth impairment in one-line culture with metabolic shifts.

the system. This was initiated starting from a more general form of reaction of the form: $D_2O + Mn^{55} + MCT$ + additional isotope components.

The control experiments were conducted in another system: $H_2O + Mn^{55} + MCT$ + the same additional isotope components.

A typical series of experiments involving potential forms of nuclear transmutation of Mn^{55} elements consisted of growing certain microbiological cultures in 3 disks simultaneously.

The first disk contained fully-compounded heavy-hydrous (D_2O) nutrient medium with $MnSO_4$, the second one contained heavy-hydrous (D_2O) nutrient medium without $MnSO_4$, and the third one contained light-hydrous (H_2O) fully-compounded with 0.05% of $MnSO_4$ nutrient medium. Such series of experiments were conducted for MCT over a period of 20 days at a temperature of 25° C.

After completing each series, the biological substance that was obtained was collected, cleaned in distilled water, and dried. The dried substance in the form of unstructured granules (like peat) were separated using a non-iron containing instrument, ground to a powder, and placed in the same amounts in the Mössbauer spectrometer. The mass of the dried biological substance that was investigated was about 0.3 g.

The results of the Mössbauer measurements of the optimally dried biological substances are presented in Figure 3.

In this experiment the large amplitude of the Mössbauer resonance $(\Delta J_{max}/J)_{\text{transmut}} \approx 3.1$ %) at the same mass of investigated dried biological substance was observed and measured.

The total, relative number of Fe^{57} nuclei that was created is about 10^{17} nuclei per 1 g of grown and dried biological substances, which is between 10 and 20 times more than the comparable, relative, maximal number of Fe^{57} nuclei that is created in one-line grown and dried cultures (*1*). The total mass of Fe^{57} isotopes that is created is about 10^{-5} g per each g of dried biological substance. The efficiency has increased, in particular, because the association has been allowed to grow during a 20-day period.

One-line cultures cannot be grown for such a long period of time in heavy water because of "self-intoxication" of the medium by the metabolic products (in our former experiments (*1*) the one-line *Escherichia coli* culture was grown during a 72-hour period).

The relative efficiency rate λ of such forms of transmutation (the coefficient of transmutation) is the following:

$$\lambda \approx (0.5...1).10^{-6} \text{ (synthesized } Fe^{57} \text{ nuclei per } s \text{ and per single } Mn^{55} \text{ nucleus).}$$

For verification of these results, additional examinations of the isotopic ratio of the same dried biological substances (both control and transmutated)

Downloaded by PENNSYLVANIA STATE UNIV on July 2, 2012 | http://pubs.acs.org
Publication Date: August 1, 2008 | doi: 10.1021/bk-2008-0998.ch013

Downloaded by PENNSYLVANIA STATE UNIV on July 2, 2012 | http://pubs.acs.org
Publication Date: August 1, 2008 | doi: 10.1021/bk-2008-0998.ch013

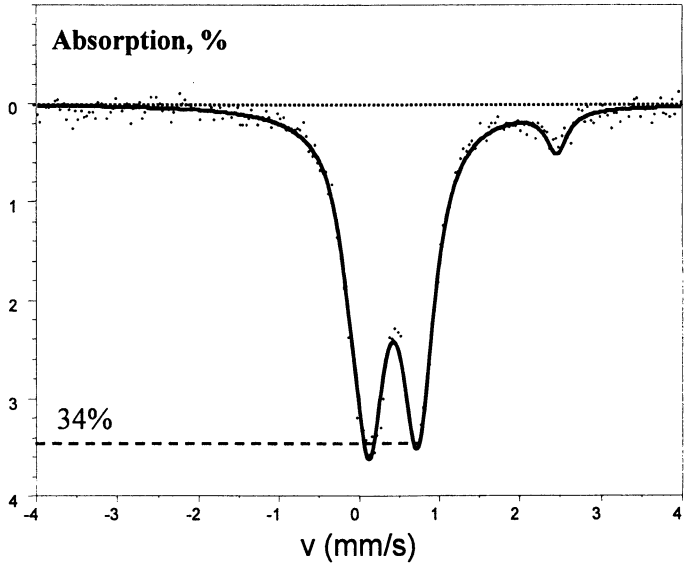

Figure 3. Mössbauer spectra of microbiological MCT grown in the volume with presence of D_2O and Mn^{55} isotope (experiments on transmutation): $\Delta J_{max}/J \approx 3.4$ % is the magnitude of the Mössbauer resonance.

were conducted by TIMS (Thermal Ion Mass Spectroscopy, «Finnigan» MAT-262).

The results of TIMS measurements are presented in Figure 4 and Table I.

The amounts of Fe^{57} isotopes that are created are approximately the same in the case of Mössbauer resonant gamma-spectroscopy and *TIMS* measurements (concentrations of Fe^{57} isotopes that are created increase by factors of 2...3).

The effectiveness of isotope transmutation during the process of growth of microbiological associations at optimal conditions increases by factors of 10-20 times more than the effectiveness of the same transmutation in one-line (clean) microbiological cultures.

The structure and half-width of Mössbauer spectra of control and transmutated microbiological associations are identical. So, the process of transmutation does not appear to change the spatial structure of the growing biological culture. Created and natural Fe are identical in the biochemical sense.

Decreases in the amounts of the additional Mn^{55} isotope in the transmutation flask are synchronized with the creation of Fe^{57} isotopes in the same flask. This appears to provide proof (a "form of acknowledgement" or a "footprint") of nuclear synthesis in processes associated with a "growing" biological system.

Downloaded by PENNSYLVANIA STATE UNIV on July 2, 2012 | http://pubs.acs.org
Publication Date: August 1, 2008 | doi: 10.1021/bk-2008-0998.ch013

Experiments on Controlled Decontamination of Long-Lived Active Isotopes in Biological Cells

The process of decontamination (deactivation) of radioactive waste through the action of growth in microbiological systems is connected with transmutation of long-lived active nuclei to different non-radioactive isotopes during growth and metabolic processes involving MCT granules.

The research was carried out using the identical distilled water but with a process that involves Cs^{137} with an activity of 2.10^4 bq. In the experiments, 8 identical closed glass flasks with very thin walls and with 10 ml of the same active water in each were used (see Figure 5). The MCT compound was placed in 7 glass flasks.

In six different flasks, different pure K, Ca, Na, Fe, Mg and P salts as single admixture were added to the active water. These chemical elements are vitally necessary for any cultures.

Each of these specific replacements completely blocks all possible transmutation channels, in which any of biochemical analogs of the specific chemical element can be used.

Table I. Parameters of Mass-Spectroscopy Investigation of Control and Transmutated Cultures

Isotope (natural concentration)	*Natural isotopic ratio (in relation to Fe^{56})*	*Concentration in dried biological substance in control experiment: H_2O + $MnSO_4$ + nutrient medium*	*Isotopic ratio in control biological substance*	*Concentration in dried biological substance in experiment on transmutation: D_2O + $MnSO_4$ + nutrient medium, (normalized)*	*Isotopic ratio in the experiment on transmutation*
Mn^{55}, 100%	–	0.15 ± 0.012	Mn^{55}/Fe^{57} = 6.6	0.13 ± 0.012	Mn^{55}/Fe^{57} = 7.7
Fe^{56}, 91.7%	1	1	1	1	1
Fe^{57}, 2.2 %	Fe^{56}/Fe^{57} = 41.7	0.024 ± 0.002	Fe^{56}/Fe^{57} = 42.5	0.051 ± 0.003	Fe^{56}/Fe^{57} = 19.5

Downloaded by PENNSYLVANIA STATE UNIV on July 2, 2012 | http://pubs.acs.org
Publication Date: August 1, 2008 | doi: 10.1021/bk-2008-0998.ch013

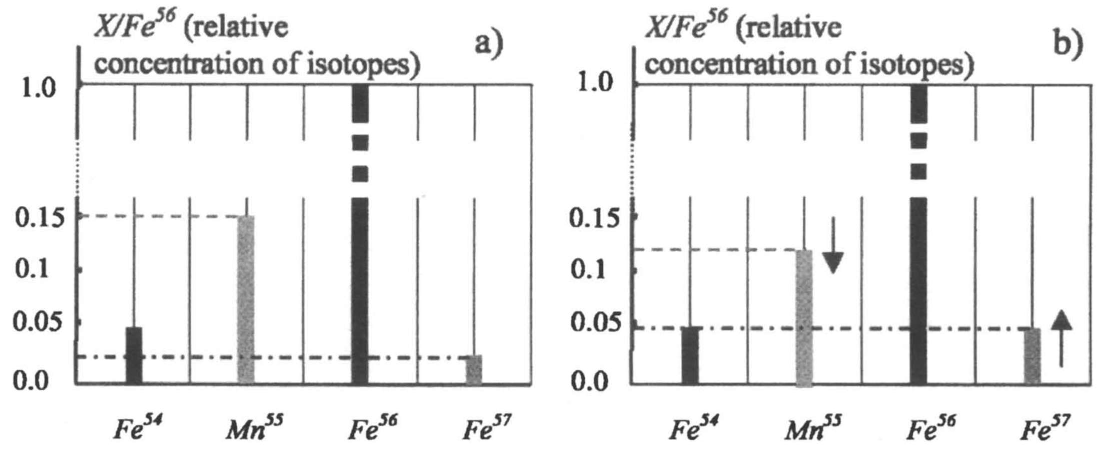

Figure 4. Mass-spectrum of iron-region of microbiological associations (dried biological substances) that were grown in the control nutrient medium with H_2O and Mn^{55} (case a) and in the experimental nutrient medium with D_2O and the same quantity of Mn^{55} isotope (case b). Here $X = Fe^{54}$; Mn^{55}; Fe^{57}. The process of increasing (↑) of concentration of Fe^{57} isotope is accompanied by decreasing (↓) of concentration of Mn^{55} isotope.

Downloaded by PENNSYLVANIA STATE UNIV on July 2, 2012 | http://pubs.acs.org
Publication Date: August 1, 2008 | doi: 10.1021/bk-2008-0998.ch013

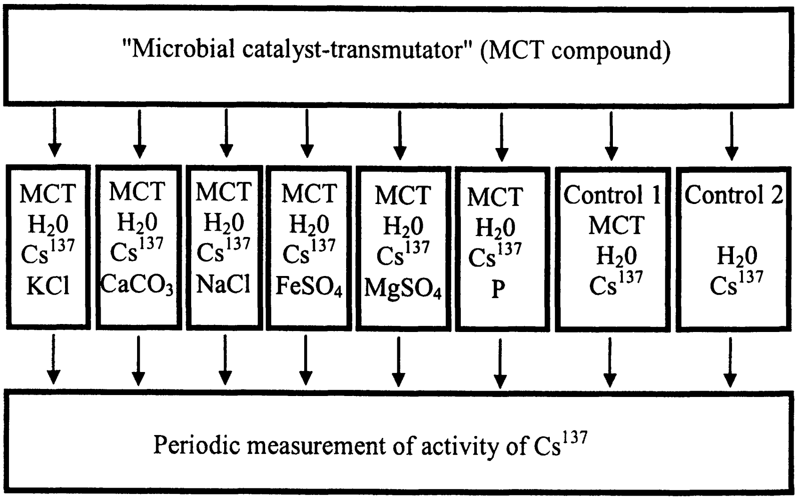
"Microbial catalyst-transmutator" (MCT compound)
MCT H2O Cs137 KCl
MCT H2O Cs137 CaCO3
MCT H2O Cs137 NaCl
MCT H2O Cs137 FeSO4
MCT H2O Cs137 MgSO4
MCT H2O Cs137 P
Control 1 MCT H2O Cs137
Control 2 H2O Cs137
Periodic measurement of activity of Cs137

Figure 5. Study of utilization of active isotopes in different conditions.

We hypothesize that the reason these reactions can be blocked when these replacements are used is related to the formation of an optimal balance of microelements. The results obtained appear to confirm this hypothesis and, by implication, the importance of these kinds of replacements, as potentially blocking potential transmutations.

Two additional flasks were used for control experiments: one flask contained the active water and MCT (but without additional salts) and in another one was only active water (without salts and MCT).

The cultures were grown at a temperature of 20° C. Activity of all closed flasks was measured every 7 days by precise, large amplitudes, using a Ge detector.

The results of the investigation of the change in relative activity Q(t)/Q(0) of isotopes are presented in Figure 6 and Table II.

We observed increased rates of decay of Cs^{137} isotope in all experiments with MCT and with the presence of different additional salts over more than 100 days.

In the control experiment (flask with active water but without MCT), the "usual" law of nuclear decay applies, and the lifetime was about 30 years.

The most rapidly increasing decay rate, which occurred with a lifetime $\tau^* \approx$ 310 days (involving an increase in rate, and decrease in lifetime by a factor of 35 times) was observed in the presence of Ca salt. In the presence of an abnormal (redundant) quantity of potassium in the nutritious media, the process of cesium transmutation becomes very weak and the lifetime of the decay was about 10 years.

A possible reaction of Cs^{137} isotope utilization is:

$$Cs^{137} + p^1 = Ba^{138} + \Delta E.$$

Downloaded by PENNSYLVANIA STATE UNIV on July 2, 2012 | http://pubs.acs.org
Publication Date: August 1, 2008 | doi: 10.1021/bk-2008-0998.ch013

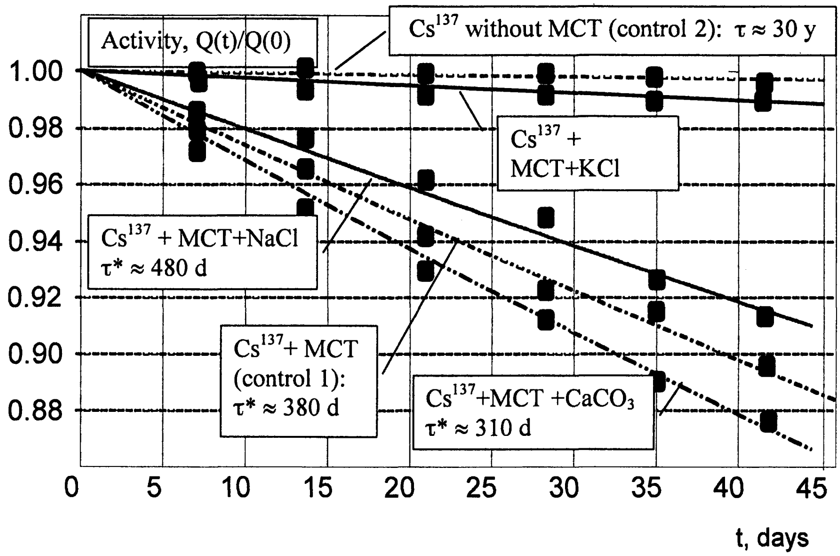

Figure 6. Accelerated deactivation (accelerated decay) of Cs ^{137} isotope in "biological cells" in presence of different chemical elements.

Table II. Deactivation of Different Active Isotopes in Optimal Experiment (MCT + active water with presence of Cs^{137}+ $CaCO_3$ salt)

	Start	*Finish of experiments (in 100 days)*			
Isotope, energy keV	*N_1, registered events per 10^3 s*	*N_2, registered events per 10^3 s*	*Error (absolute/ relative)*	*Natural decay per 100 d*	*Change $(N_2-N_1)/N_2$*
Cs^{137} 661.7	266900	216800	±478(±0.2%)	-0.6 %	-24 %

The result of this reaction is the creation of a stable Ba^{138} isotope. This reaction is energetically favorable ($\Delta E = 5.58$ MeV is positive).

The Ba^{2+} and K^+ ions are chemically alike and have approximately the same ionic radii of the associated ionic state ($R_{Ba} \approx 1.4$ A, $R_K \approx 1.33$ A). We speculate that substitution of the element K can result in one, of among several, vitally necessary elements. In principle, Ba^{2+} ions can be created (as in the last reaction) by substituting elements involving K^+ ions in metabolic process while microbiological cultures are growing.

This substitution is potentially more effective than the "direct" replacement of cesium with potassium because the ionic radius of cesium is $R_{Cs} \approx 1.65\text{-}1.69$ A, which is larger than the ionic radius of $R_K \approx 1.33$ A of potassium.

We observed earlier in experiments with microculture *Blastocladiella emersonii* (*4*) that the substitution of K^+ ions for Rb^+ and Ba^{2+} ions have taken place. These ions can replace each other in transporting ions through a membrane to a cell.

Why is the efficiency of transmutation increased when the concentration of calcium is increased?

These phenomena are probably connected with general problems of metabolic processes involving microbiological cultures: optimal growth of microcultures takes place when a balanced relation of microelements occurs. The phenomenon of low energy transmutation of chemical elements and isotopes in biological systems, and the creation of conditions for sustaining it, are based upon the heuristic proposition that if some of the required elements or microelements are not present in the living environment (or nutrient media), then, assuming certain pre-requisites are met, they will be synthesized as a result of the transmutation. In fact such an approach unambiguously suggests that the ratio of all the necessary elements in each type of living organism is fixed.

These results reveal a non-trivial nature of interactions of different microelements.

By changing the makeup of the nutrient medium, it is possible to control the speed of a culture's growth. Lacking at least one of the microelements in the nutrient medium hinders the development of the entire biological object.

References

1. Vysotskii, V. I.; Kornilova, A. A. *Nuclear Fusion and Transmutation of Isotopes in Biological Systems*; "MIR" Publishing House: Moscow, 2003.
2. Vysotskii, V. I.; Kornilova, A. A.; Samoylenko, I. I. Experimental Discovery and Investigation of the Phenomenon of Nuclear Transmutation of Isotopes in Growing Biological Cultures. *Infinite Energy* **1996**, *2*, 63-66.
3. Vysotskii, V. I.; Odintsov, A.; Pavlovich, V. N.; Tashirev, A. B.; Kornilova, A. A. Experiments on Controlled Decontamination of Water Mixture of Long-Lived Active Isotopes in Biological Cells. In *Condensed Matter*

Downloaded by PENNSYLVANIA STATE UNIV on July 2, 2012 | http://pubs.acs.org
Publication Date: August 1, 2008 | doi: 10.1021/bk-2008-0998.ch013

Nuclear Science: Proceedings of the 11th International Conference on Cold Fusion, Marseilles, France, Oct. 31 - Nov. 5, 2004; Biberian, J.-P., Ed.; World Scientific Publishing Co.: Singapore, 2006; 530-536.

4. Van Brunt, J.; Caldwell, J. H.; Harold, F. M. Circulation of Potassium Across the Plasma Membrane of Blastocladiella emersonii: K+ Channel. *J. Bacteriol.* **1982**, *150*, 1449-1561.

Downloaded by PENNSYLVANIA STATE UNIV on July 2, 2012 | http://pubs.acs.org
Publication Date: August 1, 2008 | doi: 10.1021/bk-2008-0998.ch013

Downloaded by CORNELL UNIV on July 1, 2012 | http://pubs.acs.org
Publication Date: August 1, 2008 | doi: 10.1021/bk-2008-0998.ch014

Chapter 14

Detection of Energetic Particles and Neutrons Emitted During Pd/D Co-Deposition

Pamela A. Mosier-Boss[1], Stanislaw Szpak[1], Frank E. Gordon[1], and Lawrence P. G. Forsley[2]

[1]SPAWAR Systems Center San Diego, Code 230, San Diego, CA 92152
[2]JWK International Corporation, 7617 Little River Turnpike, Suite 1000, Annandale, VA 22003

In this communication, results obtained using CR-39, a solid state nuclear track detector, in Pd/D co-deposition experiments are described. These results show that pits occur on the surface of the CR-39 detectors where the Pd/D cathode was in contact with it. Control experiments indicate that the pits are not due to radioactive contamination of the cell components nor do they have a chemical origin. The presence of triple and double tracks on the surface of the CR-39, as well as the presence of tracks on the backside of the CR-39, are suggestive of neutrons.

Introduction

Columbia Resin 39 (CR-39) is an allyl glycol carbonate plastic that is widely used as a solid state nuclear track detector. When energetic, charged particles travel into or through a CR-39 detector, they create along their ionization track a region that is more sensitive to chemical etching than the rest of the bulk. After treatment with an etching agent, tracks remain as holes or pits. The size and shape of these pits provide information about the mass, charge, energy, and direction of motion of the particles. CR-39 detectors, in conjunction with magnets and/or special ranging filters, have been used to detect and identify fusion products resulting from inertial-confinement-fusion (ICF) experiments (*1*). Primary fusion products detected using CR-39 are (p, D, T, ^{3}He, α); secondary fusion products (p); "knock-on" particles (p, D, T), elastically scattered by primary neutrons; and ions from the shell used to house the D_2, D^3He, DT, or DTH fuel. Advantages of CR-39 for ICF experiments

In Low-Energy Nuclear Reactions Sourcebook; Marwan, J., et al.;
ACS Symposium Series; American Chemical Society: Washington, DC, 2008.

include its insensitivity to electromagnetic noise, its ability to distinguish the types and energies of individual particles, and its resistance to mechanical damage. These same attributes make CR-39 detectors attractive for use to detect energetic particles in Pd/D electrolysis experiments. In addition, CR-39 detectors, like photographic film, are examples of constantly integrating detectors meaning that events are permanently stamped on the surface of the detector. Earlier, using CR-39 detectors immersed in the electrolyte, Oriani and Fisher (*2*) detected charged particles. The detectors were placed both above and below the Pd cathode. Using 50 μm thick Pd foils in contact with the CR-39, Lipson et al. (*3, 4*) demonstrated that 11-16 MeV α particles and 1.7 MeV p were emitted from the cathode during electrolysis. In this communication, the use of CR-39 to detect nuclear products emitted during Pd/D co-deposition experiments is described.

Downloaded by CORNELL UNIV on July 1, 2012 | http://pubs.acs.org
Publication Date: August 1, 2008 | doi: 10.1021/bk-2008-0998.ch014

Experimental Procedure

Cell assembly and experimental procedures have been described elsewhere (*5, 6*). In these experiments, Pd is plated out, from a $PdCl_2$-LiCl-D_2O solution, onto a cathode substrate that is in contact with the CR-39 detector (Fukuvi). Placing the cathode in close proximity to the detector optimizes the geometry to detect any energetic particles emitted during the Pd/D co-deposition. Cathode materials used include Ni screen and Ag/Au/Pt wires. After the Pd is completely plated out onto the cathode, the external electric or magnetic field is applied and the current is ramped up in a step-wise fashion, to a final applied current of -100 mA. A regulated high voltage source (EMCO model 4330) is used to apply 6000 V DC (and has a ~6% AC component) across two Cu plates taped to the sides of the cell. Two NdFeB magnets are used to apply the magnetic field. The strength of the magnetic field is 2500 Gauss. At the completion of the experiment, the cell is disassembled and the CR-39 detector is etched in a 6.5 N NaOH solution for 6 hr at 66 °C. After etching, the CR-39 detector is subjected to microscopic examination and is scanned using an automated track analysis system. The automated scanning system measures the track length and diameter, optical density (average image contrast), and image symmetry.

Results and Discussion

Effect of External Electric and Magnetic Fields on the Pd/D System

The use of external electric fields (*7*) and magnetic fields (*8*) to stimulate heat generation and the production of nuclear ash has been explored by earlier researchers. The external electric field experiments were performed on a thin sheet of Pd in a D_2 gas atmosphere (*7*). In these experiments, the electric field was applied across the length of the Pd sheet. Application of an electric field shortened the loading time and resulted in both an increase in temperature of the cathode and in the production of ^{4}He. Bockris et al. (*8*) showed that placing a Pd/D electrochemical cell in a magnetic field resulted in an increase in the temperature of the electrolyte. The larger the magnetic field, the greater the observed change in temperature. Upon removal of the magnets, the temperature of the electrolyte decreased and returned to normal.

The effect of external electric and magnetic fields on the Pd/D co-deposition process was examined using SEM (*5*) and EDX (*6*) analysis as well as CR-39 (*9*). In the absence of an external electric/magnetic field, SEM analysis showed that the Pd deposit has a uniform cauliflower-like structure and consists of aggregates of spherical micro-globules (*5*). In the presence of an external electric field, the following structural features were observed: branches (fractals), dendritic growths, craters, rods, wires, and folded thin films. The development of these features requires high energy expenditure. Analysis of these features using EDX shows the presence of "new elements" (Al, Ca, Mg, and Si) that could not be attributed to contamination (*6*). The arguments against contamination are (i) Al, Ca, and Mg cannot be co-deposited onto the cathode from an aqueous solution and (ii) if these elements could be co-deposited, they would be uniformly distributed throughout the electrode volume and not localized. When the Pd deposit is exposed to a magnetic field, SEM analysis shows that the Lorenz forces of the magnetic field cause the Pd micro-globules to form star-like features. EDX analysis of these features shows the presence of Al, Cr, Fe, Ni, and Zn. It should be noted that the new elements that have been observed in the Pd/D co-deposition-external electric/magnetic field experiments are the same as those that have been reported by others in their electrolysis experiments using conventional Pd electrodes (*10*).

The Pd/D co-deposition experiments were then conducted in the presence of CR-39 detectors. In these experiments, the Pd/D co-deposition reaction was performed with the cathode in contact with the CR-39 detector. Because there is close proximity between the cathode and the detector, this geometry is most favorable for the detection of any particles that could potentially be emitted by the cathode. Experiments were first conducted using Ni screen as the substrate material onto which the Pd was plated out. Initial experiments were done in the absence of either an external electric or magnetic field. After etching, hollows were observed where the Pd had deposited inside the eyelet of the Ni screen, Figure 1a. No pits were observed, even at higher magnifications. Similar results were obtained when a CR-39 detector, in direct contact with Cu screen, was exposed to a ^{137}Cs γ-ray source. This suggests that the damage observed for the Pd/D co-deposition reaction on Ni screen in the absence of an external field is due to X-rays. There have been previous reports of soft X-ray emission by Pd/D substrates as measured using photographic film (*11, 12*), HPGe γ-ray and Li doped Si X-ray detectors (*13, 14*), and CaF_2 thermoluminescence dosimeters (*15*). When the Pd/D co-deposition reaction is conducted in the presence of either an external electric or magnetic field, pits are observed in the CR-39 detector in the areas where the Pd plated out inside the eyelets of the Ni screen,

Downloaded by CORNELL UNIV on July 1, 2012 | http://pubs.acs.org
Publication Date: August 1, 2008 | doi: 10.1021/bk-2008-0998.ch014

Figure 1b. These results indicate that, in the case of Ni screen substrates, an external electric/magnetic field is needed to generate pits in the CR-39 detector. For higher Z cathodic substrates such as Au, Ag, and Pt, an external field was not required to generate pits in the CR-39 detector. The difference in behavior observed for Ni vs. Ag/Au/Pt could be attributed to either the electrode substrate or to the current density (the individual wires will exhibit a higher current density than the screen). Additional research is needed to determine how cathode composition and size influences the generation of pits and how external electric/magnetic fields influence the generation of these pits.

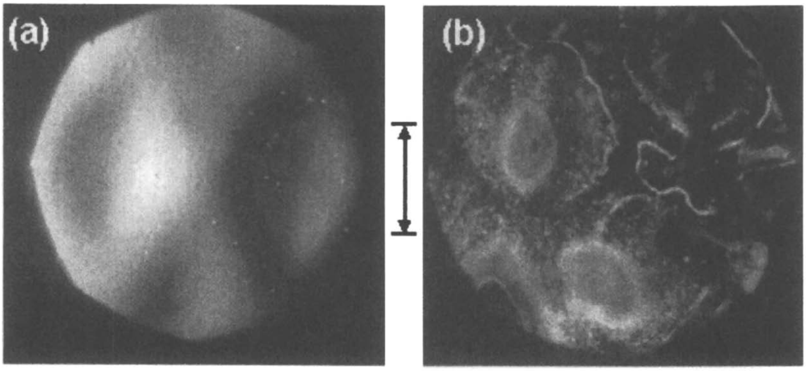

Figure 1. (a) 20X microscopic image of a CR-39 detector that was in contact with a Pd film deposited on a Ni screen in the absence of an external field. (b) 20X microscopic image of a CR-39 detector that was in contact with a Pd film deposited on a Ni screen subjected to an external magnetic field. Scale represents 1 mm.

Nuclear vs. Chemical

A Pd/D co-deposition experiment was conducted in the presence of an external magnetic field. All microphotographs shown in this communication were obtained for CR-39 that had been etched in accordance with the previously discussed experimental protocol. Figure 2a shows an image of the CR-39 detector, at 20X magnification. Damage to the detector is observed where the cathode was in contact with the surface of the detector. This indicates that the source of the damage is the palladium that had been plated on the Au wire. Figure 2b shows an image obtained at higher magnification that was taken near the edge of the cathode where the damage to the CR-39 detector is less. The image shows the presence of both small and large, dark pits as well as what look like double and triple pits. These pits are very similar to those that have been reported by Lipson et al. (*3*, *4*).

Downloaded by CORNELL UNIV on July 1, 2012 | http://pubs.acs.org
Publication Date: August 1, 2008 | doi: 10.1021/bk-2008-0998.ch014

Downloaded by CORNELL UNIV on July 1, 2012 | http://pubs.acs.org
Publication Date: August 1, 2008 | doi: 10.1021/bk-2008-0998.ch014

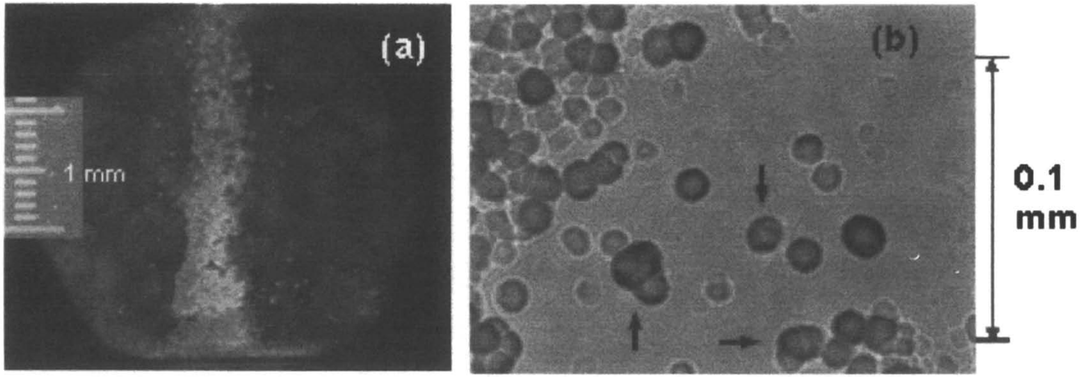

Figure 2. (a) 20X magnification of a cloudy area observed where the Au/Pd cathode was in contact with the CR-39 detector during an external magnetic field experiment. (b) 500X magnification taken near the edge of the Au/Pd cathode where less damage to the CR-39 detector is observed. Arrows indicate what appear to be double and triple pits.

Are the pits observed in Figure 2b due to energetic particles impinging upon the surface of the CR-39 detector or are they the result of chemical damage? When an energetic charged particle collides with the CR-39 detector, it forms an etch pit that is conical in shape (16). Figure 3 shows images of pits obtained for CR-39 that was exposed to an ^{241}Am source that emits 5.5 MeV α particles. When viewed through a microscope, these nuclear generated pits are symmetrical and dark in color, Figure 3. The pits can be circular or oval in shape, Figure 3a. Such pits result from particles that have entered the surface at normal incidence.

The pits can also exhibit elliptical shapes, Figure 3b. These pits result from particles entering the surface at an angle. The nuclear generated pits also exhibit high optical contrast. By focusing deeper into the CR-39, a bright spot, due to the bottom tip of the track, is seen in the image, Figure 3b. Features resulting from chemical damage and other false events, such as voids present inside the plastic, are irregularly shaped, bright, and shallow (*1, 17*). Examples of features consistent with chemical damage are shown in Figure 4, which shows the results obtained when a Pd/D co-deposition experiment was conducted using a TASL brand CR-39 detector in place of the Fukuvi brand CR-39 detector usually used in these experiments. The detector is clear where the cathode had been in close contact with the CR-39 but is otherwise cloudy in appearance. An image of the "interface," Figure 4a, is shown indicating the transition from the cloudy area that has been damaged by the electrolyte during electrolysis to the clear area under the cathode. The clear area under the cathode shows dark, circular pits while the area away from the cathode shows irregularly shaped features that are distinctly different from the circular shapes observed under the cathode. Figure 4b shows another image that was taken in an area that had not been in contact with the cathode. The irregularly shaped features are shallow and show no contrast. These features are the result of chemical damage due to electrolysis. These results show (i) that CR-39 from some suppliers are more susceptible to chemical damage than others and is probably related to the amount of cross-linking in the polymer and (ii) that it is possible to differentiate features due to the interaction with nuclear particles from those resulting from chemical damage.

Figure 5 shows images of two representative pits obtained on a CR-39 detector as a result of a Pd/D co-deposition experiment. The pits are dark in color, circular or oval in shape, and show bright spots inside when focusing deeper inside the pits. These features are consistent with those that are expected from authentic tracks caused by energetic charged particles. The pit shown in Figure 5a is perfectly circular in shape and is 14.6 μm in diameter. In contrast, the pit shown in Figure 5b is elliptical in shape and is 12.5 μm in diameter on the long axis.

Co-deposition experiments were conducted in which $CuCl_2$ was used in place of $PdCl_2$. In both the $CuCl_2$ and $PdCl_2$ systems, metal plates out in the presence of evolving D_2 gases at the cathode and O_2 and Cl_2 gas evolution occurs at the anode. In both systems, OD^- ions form on the cathode during the reduction of D_2O and the resultant metal deposits exhibit dendritic morphologies.

Downloaded by CORNELL UNIV on July 1, 2012 | http://pubs.acs.org
Publication Date: August 1, 2008 | doi: 10.1021/bk-2008-0998.ch014

Downloaded by CORNELL UNIV on July 1, 2012 | http://pubs.acs.org
Publication Date: August 1, 2008 | doi: 10.1021/bk-2008-0998.ch014

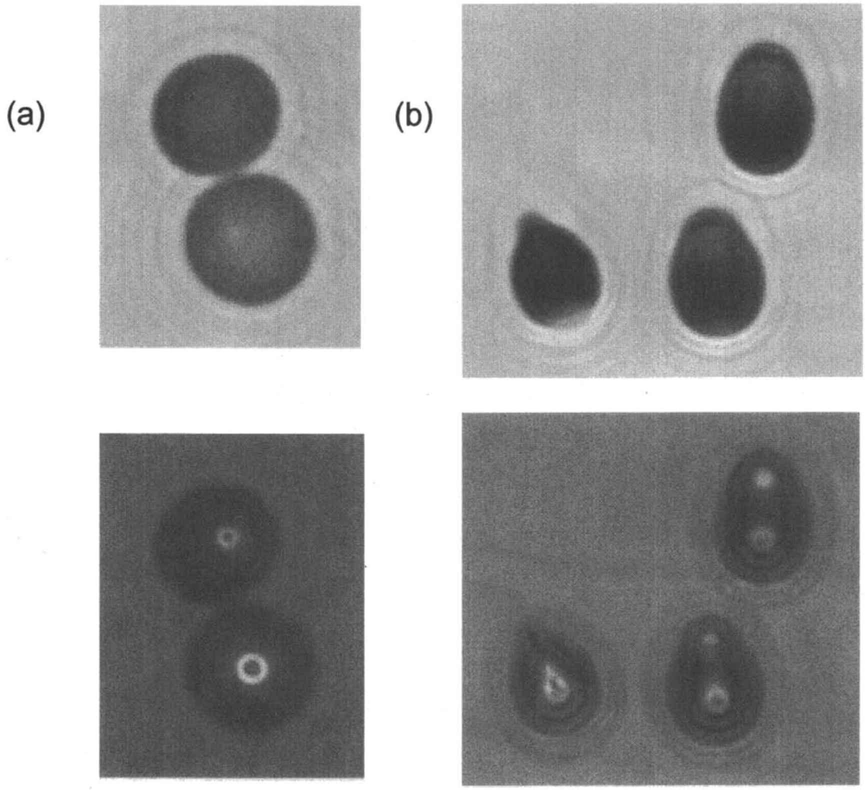

Figure 3. Images of representative pits due to 5.5 MeV α particles emitted by an ^{241}Am source. (a) bottom 9.6 μm diameter circular pit and top 11.5 μm diameter, long axis, oval pit. (b) 11.5-14.4 μm diameter, long axis, elliptical pits. In the top images, the focus is on the surface of the CR-39 detector. Bottom images are an overlay of two images taken at two different focal lengths (top and bottom of pit).

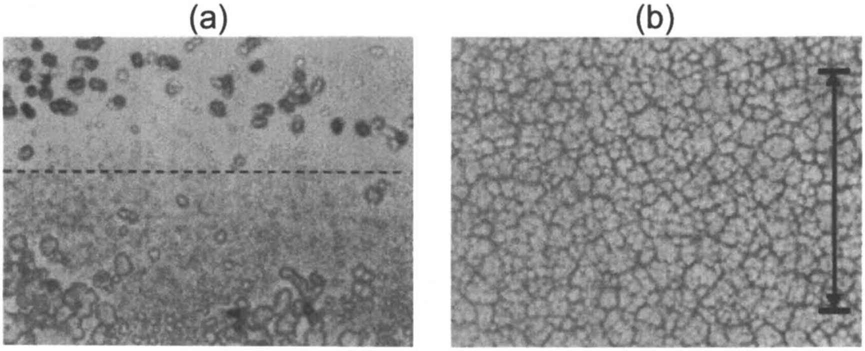

Figure 4. Microscopic images obtained for a Ag/Pd/D co-deposition reaction done in a magnetic field using a TASL CR-39 detector. 500× magnification, scale represents 100 μm. (a) Image taken at the interface. The area above the dotted line was directly underneath the cathode. The area below the dotted line is outside the cathode. (b) Image taken of a cloudy area that was not in contact with the cathode.

Downloaded by CORNELL UNIV on July 1, 2012 | http://pubs.acs.org
Publication Date: August 1, 2008 | doi: 10.1021/bk-2008-0998.ch014

The only significant difference is that Pd absorbs deuterium and Cu does not. While pits are obtained in the Pd/D co-deposition, no pits are observed for the Cu/D co-deposition. These results indicate that (i) the pits are not due to metal dendrites piercing into the CR-39 detector, (ii) the pits are not due to localized production of OD^- ions that etch into the CR-39 detector, and (iii) the pits are not due to dendrite enhanced fusion. According to the dendrite enhanced fusion model (*18*), the dendrite tips exhibit a high surface potential where local dielectric breakdown occurs to form D^+ ions which are accelerated along field lines into adsorbed deuterons to create fusion products. Such a mechanism does not require a hydrogen absorbing material such as Pd.

As shown by the image in Figure 2a, a Pd/D co-deposition experiment conducted using $PdCl_2$, LiCl, and D_2O in an external field yields a large number of pits. A series of control experiments were conducted (i) to determine if there was a chemical explanation for the formation of the pits and (ii) to determine the necessary experimental conditions to generate pits. These experiments and their results are summarized in Table I. These results indicate that the pits shown in Figures 1, 2, and 5 are not due to radioactive contamination of either the cathode materials used, the $PdCl_2$, LiCl, or D_2O. The results also show that LiCl is not required to generate pits. Pits are obtained when H_2O is used in place of D_2O, however, the density of pits are approximately a thousand times less than results obtained in the D_2O experiments. The H_2O experiments were conducted in both external electric and magnetic fields. The production of pits in H_2O experiments was not unexpected as the earlier CR-39 work done by Lipson et al. (3) had been conducted in H_2O. What was surprising was that the number of pits created in H_2O was several orders of magnitude less than those obtained when D_2O was used.

Downloaded by CORNELL UNIV on July 1, 2012 | http://pubs.acs.org
Publication Date: August 1, 2008 | doi: 10.1021/bk-2008-0998.ch014

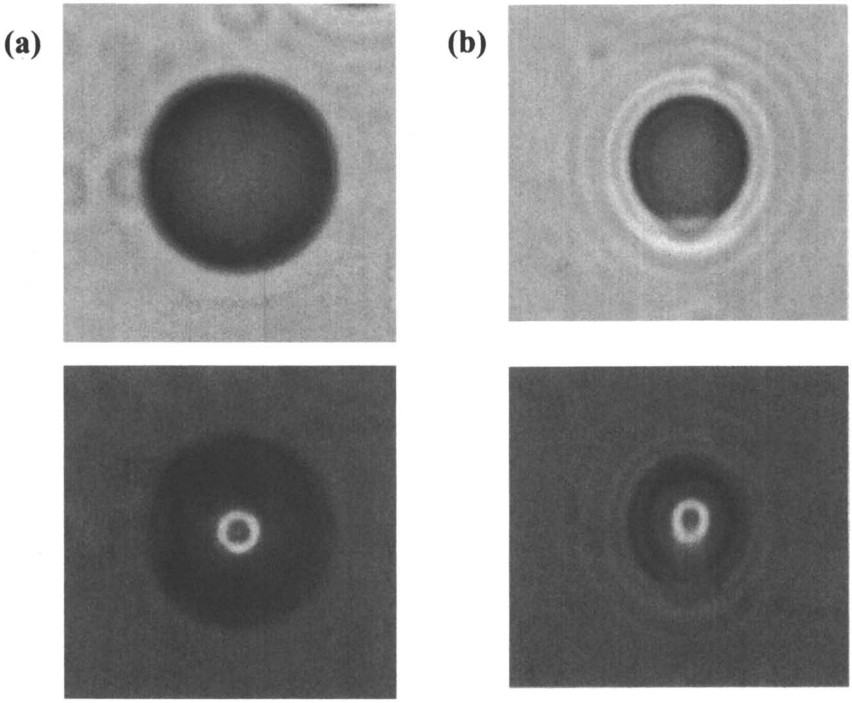

Figure 5. Images of representative pits obtained from a Pd/D co-deposition experiment conducted on a Au cathode in the presence of a magnetic field. (a) 14.6 μm diameter circular pit. (b) 12.5 μm diameter, long axis, elliptical pit. In the top images, the focus is on the surface of the CR-39 detector. Bottom images are an overlay of two images taken at two different focal lengths (top and bottom of pit).

The natural abundances of H and D are 99.985% and 0.0115%, respectively. It is possible that the pits observed in the light water experiments are actually due to the D_2O that is present in the light water. This could explain the dramatic reduction in the number of pits observed in the H_2O experiments. When a Pd wire is used in place of the Pd/D co-deposition, a few bursts of pits are observed where the wire was in contact with the CR-39 detector. Furthermore, the density of pits is far less than observed in a Pd/D co-deposition experiment.

The images shown in Figure 2 show the presence of numerous tracks. Each track represents a nuclear event. At this time it cannot be determined whether these tracks are due to α, p, ^{3}He, or T particles. Additional work, using spacer materials and LET curves, needs to be done to determine what kind(s) of particles are being generated as well as their energies. While the number of tracks in Figure 2 are impressive, it needs to be reiterated that these measurements were done over a two-week period (one week to plate the Pd out of solution and another to ramp the cathodic current up to 100 mA). That two-week period translates into an average flux rate of less than one event per second. What makes it possible to detect this low flux rate is (i) CR-39 is a constantly integrating detector and (ii) the inherently low background. Because CR-39 is a constant integration detector, events are permanently stamped on the surface of the detector. The disadvantage is that it is not known when the events have occurred. The advantage is that, during periods of non-activity, the signals due to nuclear events do not get averaged away as had been observed in previous radiation measurements (*13*).

Downloaded by CORNELL UNIV on July 1, 2012 | http://pubs.acs.org
Publication Date: August 1, 2008 | doi: 10.1021/bk-2008-0998.ch014

Double and Triple Tracks: Evidence of Neutrons

Microscopic examination of the CR-39 detectors after a Pd/D co-deposition experiment shows the presence of what appear to be triple, Figures 6a and 6b, and double, Figure 6c, tracks. Possible explanations of these tracks are (i) that they are due to overlapping single tracks or (ii) they are the result of reactions that emit two or three particles of similar mass and energy. Focusing inside the tracks to examine the bottom of the pit, it appears that the individual lobes of the double and triple tracks are splitting apart from a central point. This favors explanation (ii) as the source of these double and triple tracks. The main constituent of CR-39 is ^{12}C (32% by weight). A neutron can be captured by a carbon atom to form the metastable $^{13}C^*$. This metastable carbon atom can then shatter into three α particles and the residuals of the reaction can be viewed in the CR-39 detector as a three-prong star similar to those shown in Figures 6a and 6b (*19*). The breakup of $^{13}C^*$ into a four-body final state can occur through one or more of the following channels summarized in Table II (*19*).

The double-α events, such as those shown in Figure 6c, are probably due to unresolved triple-α tracks and may be due to a reaction of the type $^{12}C(n,\alpha)^9Be$. To form triple tracks in CR-39, the neutron energy has to be on the order of 14.3±1.6 MeV (*19*).

Table I. Summary of Control Experiments

Experiment	*Results/Conclusion*
1. Cathode materials and $PdCl_2$ in contact with CR-39	1. No pits. No radioactive contaminant in cathode materials or $PdCl_2$.
2. CR-39 immersed in plating solution	2. No pits. No radioactive contaminant in $PdCl_2$, LiCl, or D_2O.
3. Cathode in contact with CR-39. Electrolysis in LiCl- D_2O , no $PdCl_2$	3. No pits. Impingement of D_2 gases on surface of CR-39 not responsible for pits.
4. Pd/D co-deposition using KCl in place of LiCl	4. High density of pits. LiCl is not necessary.
5. Pd/D co-deposition using H_2O in place of D_2O	5. Pits, but several orders of magnitude less than that observed for D_2O.
6. Replace Pd/D co-deposition with a Pd wire 6.	6. Observe bursts of pits where wire was in contact with CR-39. Number of pits orders of magnitude less than observed in a Pd/D co-deposition experiment.
7. Replace $PdCl_2$ with $CuCl_2$	7. No pits. Electrochemically generated D_2, O_2, Cl_2, and $OD^-$are not responsible for pit formation.

Knock-ons: Further Evidence of Neutrons

Depending on its energy, the interaction a neutron will have with an atom is generally scattering or capture. Neutron capture can also cause the atom to shatter as shown by the double and triple tracks in Figure 6. Additional experiments were conducted in which spacers were placed between the cathode and the CR-39 detector. The spacers used were 62 μm polyethylene film and a 150 μm thick borosilicate glass cover slip. Results are summarized in Figure 7. In both sets of experiments, the spacer material prevented direct contact between the CR-39 detector and the Pd/D co-deposited film.

Figure 7a and 7b show microscopic images obtained for a CR-39 detector in which the spacer material used is polyethylene. As can be seen in the images, there are numerous pits on the surface of the CR-39. Although the polyethylene film separates the cathode from the CR-39 detector, the density of pits on CR-39

Downloaded by CORNELL UNIV on July 1, 2012 | http://pubs.acs.org
Publication Date: August 1, 2008 | doi: 10.1021/bk-2008-0998.ch014

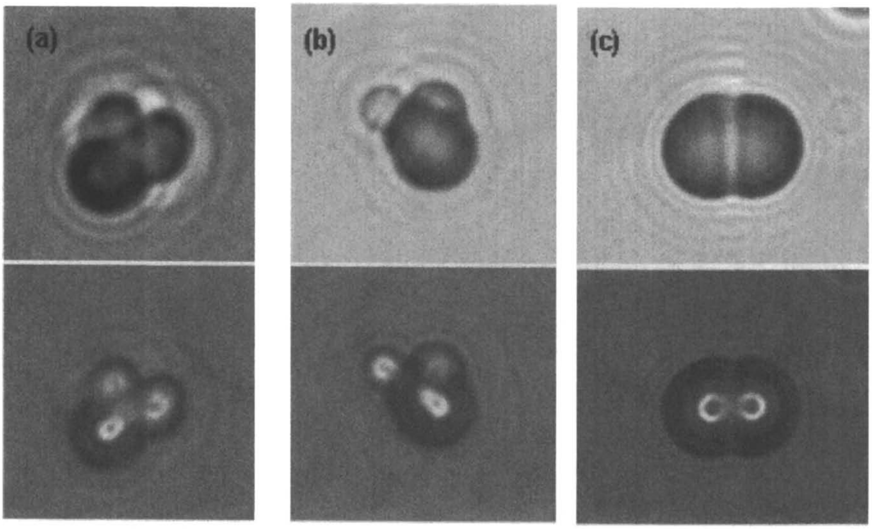

Figure 6. Images of triple (a and b) and double (c) tracks, 1000X magnification. In the top images, the focus is on the surface of the CR-39 detector. Bottom images are an overlay of two images taken at two different focal lengths (top and bottom of pit).

Table II. The Channels Summarizing the Breakup of $^{13}C^*$ into a Four-Body Final State

	Nomenclature Describing Channel		*Channel Reactions*
1.	$n + {}^{12}C(\alpha)\ {}^{8}Be^*\ (2\alpha)$	1.	${}^{13}C^* \rightarrow n + {}^{12}C^*$ ${}^{12}C^* \rightarrow \alpha + {}^{8}Be^*$ ${}^{8}Be^* \rightarrow 2\alpha$
2.	$\alpha + {}^{9}Be^*(n)\ {}^{8}Be^*\ (2\alpha)$	2.	${}^{13}C^* \rightarrow \alpha + {}^{9}Be^*$ ${}^{9}Be^* \rightarrow n + {}^{8}Be^*$ ${}^{8}Be^* \rightarrow 2\alpha$
3.	$n + {}^{12}C \rightarrow \alpha + {}^{9}Be^*(\alpha)\ {}^{5}He^*\ (n,\alpha)$	3.	$n + {}^{12}C \rightarrow \alpha + {}^{9}Be^*$ ${}^{9}Be^* \rightarrow \alpha + {}^{5}He^*$ ${}^{5}He^* \rightarrow n + \alpha$
4.	${}^{8}Be^*\ (2\alpha) + {}^{5}He^*\ (n,\alpha)$	4.	${}^{13}C^* \rightarrow {}^{8}Be^* + {}^{5}He^*$ ${}^{8}Be^* \rightarrow 2\alpha$ ${}^{5}He^* \rightarrow n + \alpha$
5.	$n + \alpha + \alpha + \alpha$	5.	${}^{13}C^* \rightarrow n + 3\alpha$

Downloaded by CORNELL UNIV on July 1, 2012 | http://pubs.acs.org
Publication Date: August 1, 2008 | doi: 10.1021/bk-2008-0998.ch014

is greatest directly below the cathode, indicating that the source of the pits is the cathode. Polyethylene that is 62 μm thick will only allow ≥ 1.83 MeV p and ≥ 7.2 MeV α through. It is unlikely that these particles are being produced as the size of the pits observed in Figures 7a and 7b are comparable to the size of the pits obtained in the absence of the polyethylene spacer, Figure 2b. If ≥ 1.83 MeV p and/or ≥ 7.2 MeV α particles had traversed the 62 μm thick polyethylene, they would lose energy and would create larger tracks on the surface of the CR-39 (*3, 4*). This is not observed. Another explanation for the tracks on the CR-39 detector is that they are due to knock-ons. Polyethylene has a high hydrogen content and is considered to be a neutron "radiator" meaning that it scatters neutrons efficiently. When neutrons are incident upon a hydrocarbon material, they collide with the atomic nuclei resulting in recoil nuclei, which migrate in the plastic network causing further damage (*20*). Depending upon the energy of the neutrons and the angle of incidence, these recoils can occur throughout the 62 μm thick polyethylene film. On the backside of the polyethylene film, the recoil protons, or "knock-ons," will hit the surface of the CR-39 detector creating the tracks that are observed in Figures 7a and 7b.

These suppositions are supported by the results of the borosilicate glass cover slip experiment. In this experiment, a piece of 150 μm thick borosilicate glass covered half the CR-39 detector. Using this experimental configuration, half the CR-39 detector was in direct contact with the cathode and the other half was not. Figure 7c shows a 20X magnification of the CR-39 detector at the glass cover-slip/CR-39 interface. To the right of the interface, numerous pits are observed where the cathode had been in direct contact with the CR-39 detector. Very few pits are observed to the left of the interface where the glass cover slip was in contact with the CR-39 detector. Higher magnification analysis of the borosilicate glass-covered side of the CR-39 detector, Figure 7d, shows the presence of some dark, circular pits (with bright spots in the middle) along with shallow, bright features. These shallow, bright features are attributed to background. The dark, circular pits in Figure 7d are due to alpha particles. Glass has no protons present to thermalize neutrons. Consequently it is a poor neutron radiator and will not create knock-ons. However borosilicate glass is 10% boric oxide. One isotope of boron, ^{10}B which has a 19.9 % natural abundance, has a high neutron capture cross section. After neutron capture, ^{10}B* decays into an α and ^{7}Li. The pits on the CR-39 below the glass cover slip are attributed to neutron capture by the boron present in the glass.

If neutrons are generated during the Pd/D co-deposition, knock-ons would also occur inside the CR-39 detector. Further etching of the CR-39 detector would reveal tracks due to these knock-ons inside the CR-39. Figure 8 shows images obtained for a CR-39 detector that had been used in a Pd/D co-deposition experiment after additional etchings. As the CR-39 detector is etched longer, the pits on the surface get larger in size and shallower. In Figure 8a, a large dark circular pit is observed on the upper part of the image. This pit was first observed on the surface. After longer etching, the pit is now 20 μm in

Downloaded by CORNELL UNIV on July 1, 2012 | http://pubs.acs.org
Publication Date: August 1, 2008 | doi: 10.1021/bk-2008-0998.ch014

Downloaded by CORNELL UNIV on July 1, 2012 | http://pubs.acs.org
Publication Date: August 1, 2008 | doi: 10.1021/bk-2008-0998.ch014

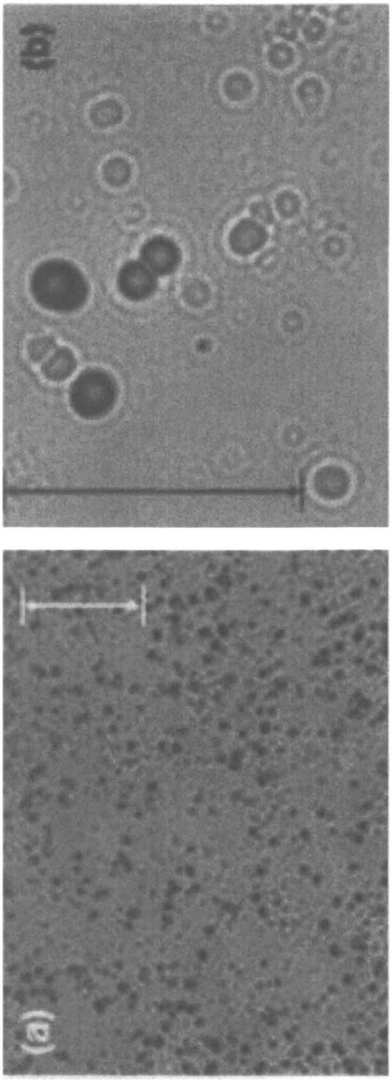

Downloaded by CORNELL UNIV on July 1, 2012 | http://pubs.acs.org
Publication Date: August 1, 2008 | doi: 10.1021/bk-2008-0998.ch014

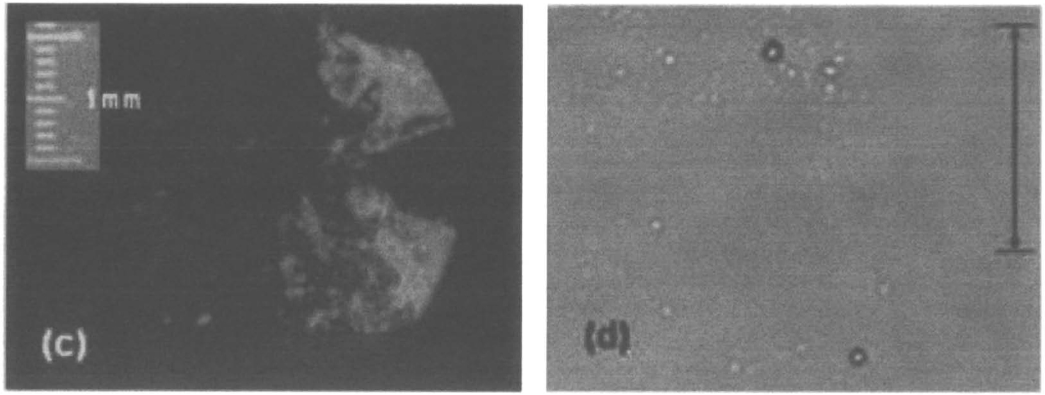

Figure 7. Microscopic images obtained for CR-39 in which 62 μm thick polyethylene was placed between the cathode and detector. Images obtained at magnifications of (a) 200X and (b) 500X. Unless otherwise indicated, scales represent 0.1 mm. Microscopic images obtained for CR-39 in which 150 μm thick borosilicate glass cover slip was used as the spacer. (c) 20X magnification of the cover slip/CR-39 interface. (d) 380X magnification of an area of the CR39 detector beneath the borosilicate glass cover slip.

diameter. Longer etching also reveals a track below the 20 μm pit and another one to the right of the 20 μm pit. Both new pits are elliptical in shape. Figure 8b shows another image obtained after further etching of the CR-39 detector. The surface pit is now 50 μm in diameter. On the left hand side of the pit, a new elliptical track attributed to a knock-on is observed.

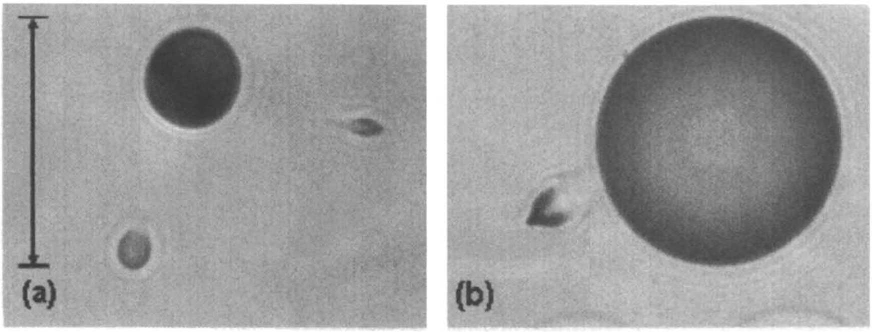

Figure 8. Images of CR-39 detectors taken after longer etching times. Magnification is 1000X. Scale represents 0.05 mm.

Downloaded by CORNELL UNIV on July 1, 2012 | http://pubs.acs.org
Publication Date: August 1, 2008 | doi: 10.1021/bk-2008-0998.ch014

Quantitative Analysis of CR-39 Detectors

Analysis of the tracks on the CR-39 detectors was done using an automated scanning system which is comprised of a high quality optical microscope and a motorized stage to accurately control the x,y position of the detector. The images obtained by the microscope are analyzed by the proprietary software that makes 15 characteristic measurements of each feature in the image. These measurements, which include track length and diameter, optical density (average image contrast) and image symmetry, are used to discriminate between actual tracks and background features present in the plastic detector. Figure 9 summarizes the quantitative analysis obtained for a CR-39 detector that had been exposed to depleted uranium, DU. Depleted uranium alphas derive from the decay of each of the uranium isotopes, and their respective contributions, ordered by a function of their half life and abundance, are ^{234}U, 4.8 MeV; ^{238}U, 4.2 MeV; and ^{235}U, 4.4 MeV. The average alpha energy, not taking into account self-shielding of the depleted uranium source will be nearly 4.8 MeV. Figure 9a shows the size distribution of the tracks obtained for DU. The parameter X_t is the sum of the major axis, M_j, and the tail of the track. In Figure 9a, the DU α's fall between 6 and 14 μm in length. This distribution in size results from scattering of the α's and from the angle of incidence at which the particles hit the surface of the detector. Figure 9b shows a plot of the minor axis, m_j, and X_t, which is a measure of the ellipticity of the tracks. An α particle that hits normal to the plane of the CR-39 will leave a circular pit whose minor axis

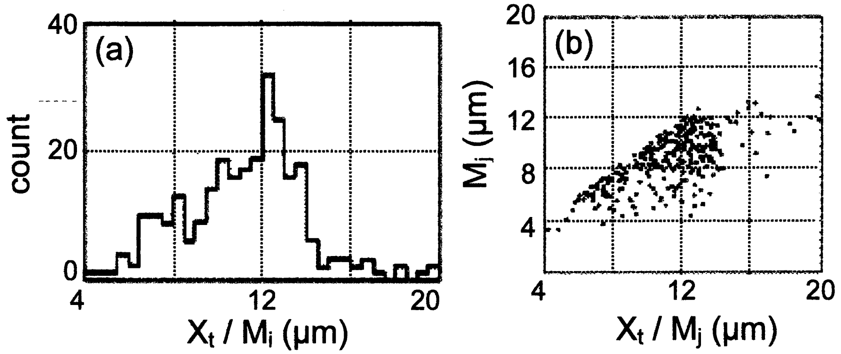

Figure 9. Quantitative analysis of tracks on CR-39 obtained upon exposure to depleted uranium. (a) Size distribution. (b) Plot of minor axis, m_j, and major axis, X_t / M_j.

approximately equals the major axis. Conversely, an α particle that doesn't hit normal to the plane of the CR-39 will leave an elliptical pit whose major axis will be longer than the minor axis.

A CR-39 detector from a Pd/D co-deposition experiment was then subjected to analysis using the automated scanning system. The detector that was analyzed was from an external electric field experiment (voltage applied across the cell was 6000 V). In this experiment, the Pd was plated onto Pt, Ag, and Au wires that were connected in series. Prior to the experiment, the backside of the CR-39 detector had been exposed to a DU source to provide internal calibration. At the completion of the experiment, etching revealed the presence of numerous tracks on the front surface of the CR-39 detector. The tracks coincided with the placement of the wires. Scans of a 1 mm × 20 mm area of the CR-39 detector, both front and back surfaces, were done. The spatial distribution of tracks on the front and back surfaces are shown in Figure 10. The criteria used by the software to distinguish between actual tracks and background features ignore overlapping tracks, clusters of tracks, and low contrast areas. As a result the number of tracks on the front surface, Figure 10a, are underestimated by at least an order of magnitude. Despite this, the software identified tracks that spatially align with the placement of the Pt, Ag, and Au wires. On the back surface of the CR-39, it was expected that a homogeneous distribution of tracks due to the DU α particles would be observed. However, as shown in Figure 10b, a high density of tracks were observed behind the Pt and Au wires. This suggests that there are two contributions of tracks on the back surface of the CR-39 detector – the tracks due to the DU calibration source (which had no prior knowledge as to where the wires were going to be placed on the front surface of the detector) and tracks due to the nuclear reactions occurring in the Pt/Pd and Au/Pd cathodes. Furthermore, the particles generated at the Pt/Pd and Au/Pd cathodes have passed through the 1 mm thick CR-39.

Downloaded by CORNELL UNIV on July 1, 2012 | http://pubs.acs.org
Publication Date: August 1, 2008 | doi: 10.1021/bk-2008-0998.ch014

The only particles that can go through 1 mm thick CR-39 are > 40 MeV α, > 10 MeV p, or neutrons.

Figure 11 shows the size distributions and plots of minor vs major axis for the front and back surfaces. On the front surface, the tracks predominantly range in size from 6 to 16 μm (with the peak occurring at 9.5 μm), Figure 11a, and show elliptical behavior, Figure 11b. These track properties are consistent with what has been reported for α particles. On the back surface, the tracks are larger than those observed on the front surface, Figure 11c, and show elliptical behavior, Figure 11d. The tracks are larger in size than those obtained using a DU source, Figure 9a. This indicates that the tracks are not due to DU nor are they due to alphas or protons as these would leave small diameter tracks on the back of the CR-39. However, neutron knock-ons can be responsible for these large diameter tracks. It has been demonstrated that neutron elastic interactions with CR-39 leave latent recoil charged particle tracks and that these tracks range in size from 5 to 40 μm (*21*). Figure 12a shows an image of tracks in CR-39 caused by knock-on neutrons from a ^{238}PuO source. Besides large circular and elliptical tracks, very small tracks are observed that are attributed to latent tracks that are deeper in the plastic. As neutrons pass through the CR-39 detector, they will cause knock-ons throughout the plastic. Additional etching will expose the tracks that are inside the plastic, as was shown in Figure 8. Figure 12b shows tracks on the CR-39 detector that were generated from the Pd/D co-deposition, external electric field experiment that was done on the Au electrode. These tracks are on the back surface of the CR-39 detector and show the same features as observed in Figure 12a – large circular and elliptical tracks as well as smaller tracks that appear to be deeper in the plastic. Additional work needs to be done to determine why Au and Pt electrodes generate tracks on the back surface of the CR-39 detector while Ag does not and to determine the energies of the particles causing the tracks observed in the CR-39 detectors.

Downloaded by CORNELL UNIV on July 1, 2012 | http://pubs.acs.org
Publication Date: August 1, 2008 | doi: 10.1021/bk-2008-0998.ch014

Conclusions

It has been shown that pits are formed on the surface of CR-39 detectors during the Pd/D co-deposition process. The Pd cathode is the source of these pits. Control experiments show that the pits are not due to radioactive contamination of the cell components nor are they due to impingement of D_2 gas on the surface of the CR-39 or to chemical reactions between CR-39 and electrochemically generated D_2, O_2, Cl_2, or OD^-. The pits on the CR-39 resulting from Pd/D co-deposition are dark and either circular, oval, or elliptical in shape. When focusing deeper inside the pit, a bright center is observed. These features are consistent with those observed for nuclear generated tracks. Microscopic examination of the CR-39 detectors shows the presence of triple and double pits, which are suggestive of neutrons shattering carbon atoms. Pits are observed on the CR-39 when either a polyethylene or borosilicate spacer is placed between the Pd cathode and the detector. These pits are attributed to

Downloaded by CORNELL UNIV on July 1, 2012 | http://pubs.acs.org
Publication Date: August 1, 2008 | doi: 10.1021/bk-2008-0998.ch014

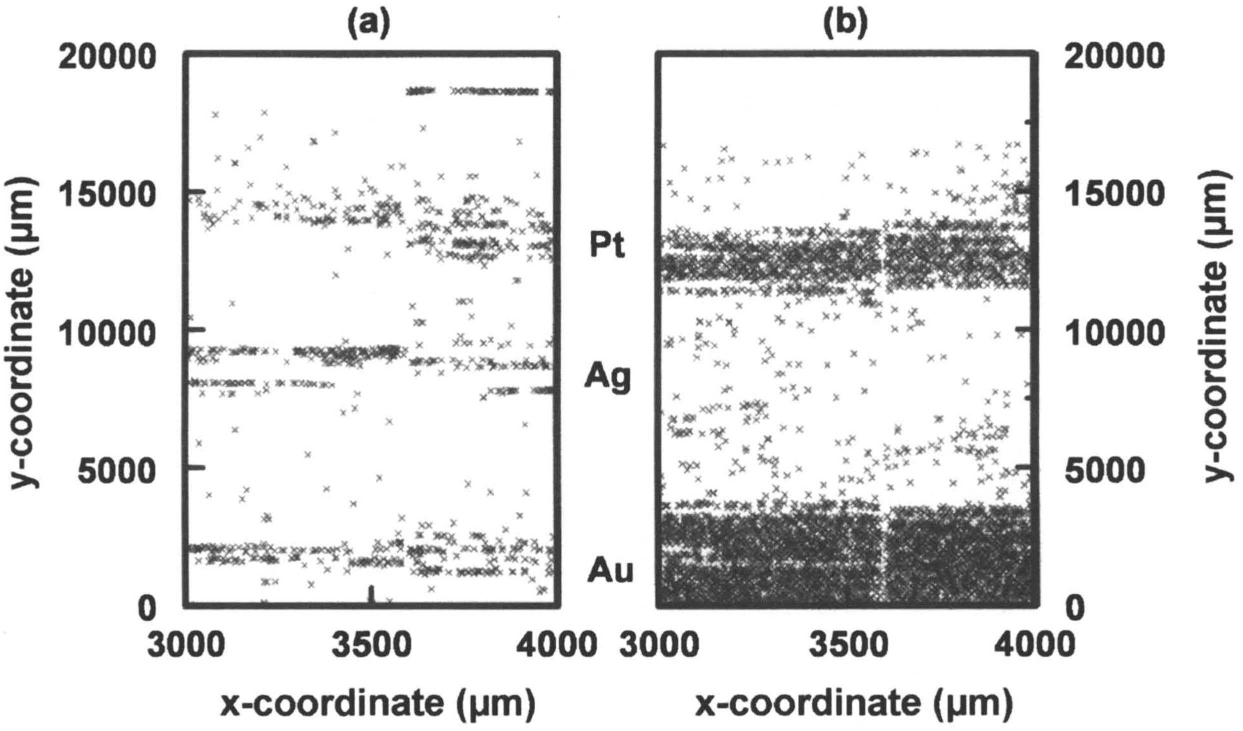

Figure 10. Spatial distribution of tracks on the (a) front and (b) back surfaces of a 1 mm × 20 mm area on the CR-39 detector that was used in a Pd/D co-deposition experiment. Placement of the Pt, Ag, and Au wires is indicated.

Downloaded by CORNELL UNIV on July 1, 2012 | http://pubs.acs.org
Publication Date: August 1, 2008 | doi: 10.1021/bk-2008-0998.ch014

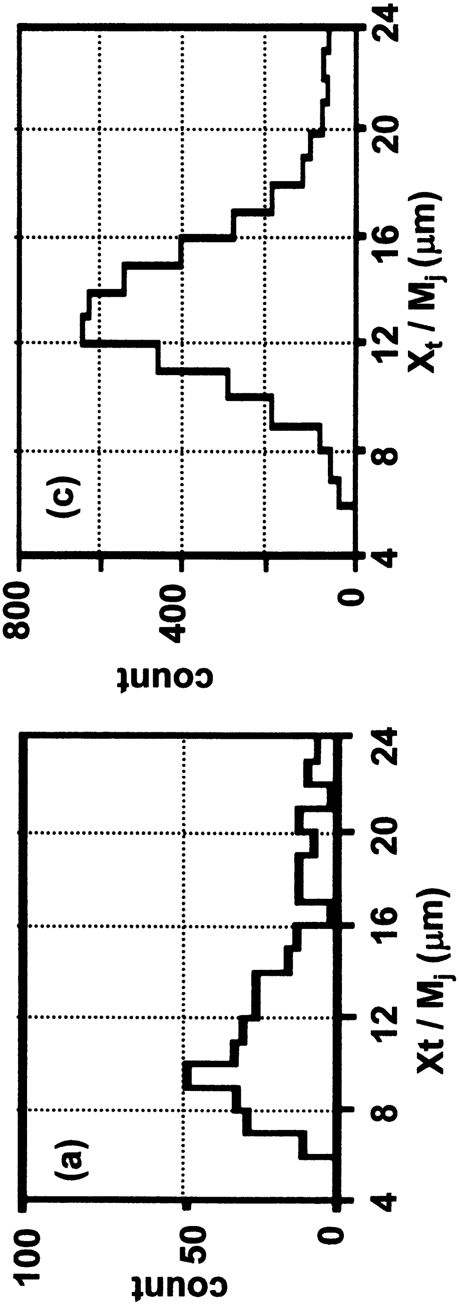

Downloaded by CORNELL UNIV on July 1, 2012 | http://pubs.acs.org
Publication Date: August 1, 2008 | doi: 10.1021/bk-2008-0998.ch014

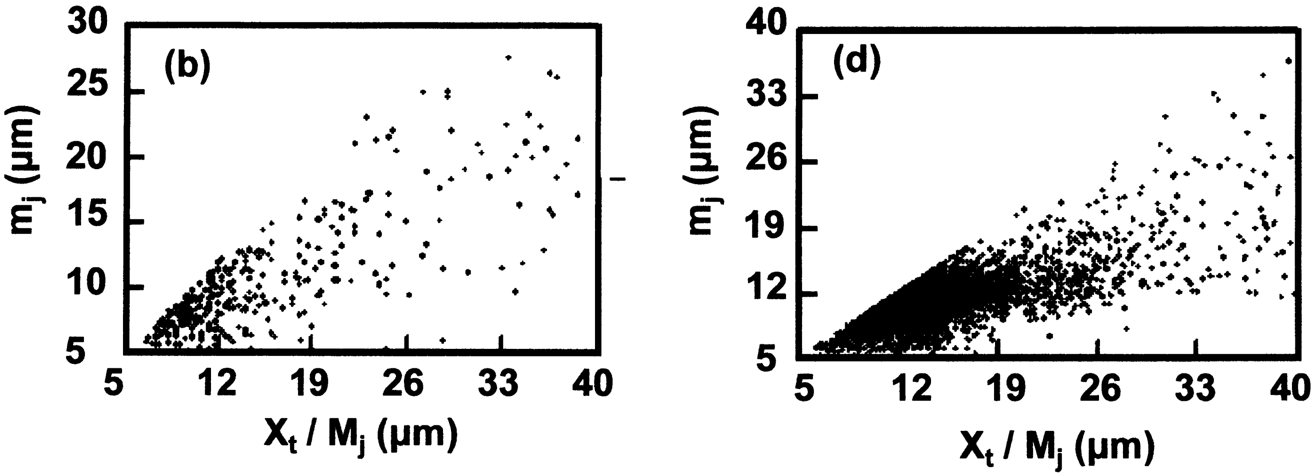

Figure 11. Quantitative analysis of the tracks on the 1 mm × 20 mm area on the CR-39 used in a Pd/D co-deposition experiment. Front surface: (a) Size distribution and (b) Plot of minor axis, m_j, and major axis, X_t/M_j. Back surface: (c) Size distribution and (d) Plot of minor axis, m_j, and major axis, X_t/M_j. The spatial orientation of the tracks on the detector is shown in Figure 10.

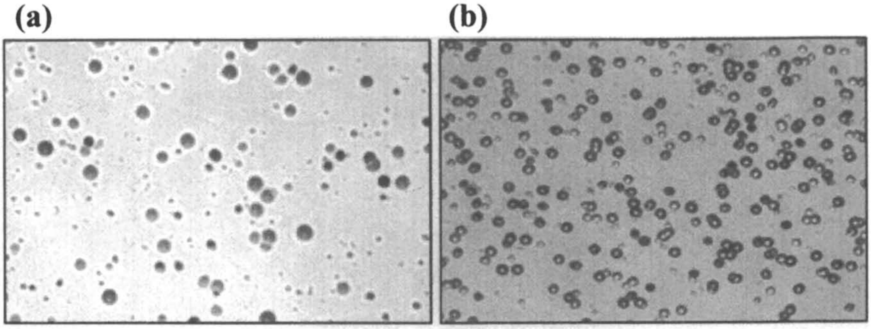

Figure 12. Tracks in CR-39. Magnification 200X. (a) Tracks generated by knock-on neutrons from a ^{238}PuO source (21). (b) Tracks on the back surface of the detector used in a Pd/D co-deposition experiment. This image was obtained beneath the Au electrode of the external electric filed experiment.

Downloaded by CORNELL UNIV on July 1, 2012 | http://pubs.acs.org
Publication Date: August 1, 2008 | doi: 10.1021/bk-2008-0998.ch014

knock-ons due to neutrons. Further etching of the CR-39 detector reveals additional tracks due to knock-ons inside the CR-39 detector. A CR-39 detector from a Pd/D co-deposition experiment was analyzed using an automated scanning system. Tracks on the front surface were observed that coincided with the placement of the Pt, Ag, and Au wires that were used as cathodic substrates. The size distribution and ellipticity of the tracks were consistent with those obtained for α particles. On the back surface, tracks were observed behind the Pt and Au electrodes. The size distribution and ellipticity of the tracks suggest that the tracks were caused by knock-on neutrons.

Acknowledgements

The effort at SSC-SD was funded by the ILIR program. The authors would like to thank Dr. Gary Phillips, nuclear physicist, retired Naval Research Laboratory, US Navy, Radiation Effects Branch, for valuable discussions in interpreting the data. We wish to thank Mr. Josh Perelman, owner of Trophy Mart, Inc. in Annandale, VA for his expert laser machining of nuclear diagnostic bezels. We also wish to thank Dr. Jay W. Khim, CEO of JWK Corporation, for funding Project GeNiE at JWK International, and for his valuable discussions with regards to experiments and data analysis.

References

1. Séguin, F. H.; Frenje, J. A.; Li, C. K.; Hicks, D. G.; Kurebayashi, S.; Rygg, J. R.; Schwartz, B.-E.; Petrasso, R. D.; Roberts, S.; Soures, J. M.;

Meyerhofer, D. D.; Sangster, T. C.; Knauer, J. P.; Sorce, C.; Glebov, V. Y.; Stoeckl, C.; Phillips, T. W.; Leeper, R. J.; Fletcher, K.; Padalino, S. Spectrometry of Charged Particles from Inertial-Confinement-Fusion Plasmas. *Rev. Sci. Instrum.* **2003**, *74*, 975-995.

2. Oriani, R. A.; Fisher, F. C. Generation of Nuclear Tracks during Electrolysis. Jpn. *J. Appl. Phys.* **2002**, *41*, 6180-6183.
3. Lipson, A. G.; Roussetski, A. S.; Miley, G. H.; Castano, C. H. In-Situ Charged Particles and X-ray Detection in Pd Thin Film-Cathodes during Electrolysis in Li_2SO_4 /H_2O. In *Condensed Matter Nuclear Science: Proceedings of the 9th International Conference on Cold Fusion*, Beijing, China, May 19-24, 2002; Li, X. Z., Ed.; Tsinghua Univ. Press: Beijing, 2002; 218-223.
4. Lipson, A. G.; Roussetski, A. S.; Miley, G. H.; Saunin, E. I. Phenomenon of an Energetic Charged Particle Emission from Hydrogen/Deuterium Loaded Metals. In *Condensed Matter Nuclear Science: Proceedings of the 10th International Conference on Cold Fusion*, Cambridge, MA, Aug. 24-29, 2003; Hagelstein, P. L.; Chubb, S. R., Eds.; World Scientific Publishing Co.: Singapore, 2006; 539-558.
5. Szpak, S.; Mosier-Boss, P. A.; Young, C.; Gordon, F. E. The Effect of an External Electric Field on Surface Morphology of Co-Deposited Pd/D Films. *J. Electroanal. Chem.* **2005**, *580*, 284-290.
6. Szpak, S.; Mosier-Boss, P. A.; Young, C.; Gordon, F. E. Evidence of Nuclear Reactions in the Pd Lattice. *Naturwissenschaften* **2005**, *92*, 394-397.
7. Iazzi, F.; Botta, E.; Bressani, T.; Fanara, C.; Tesio, A. Correlated Measurements of D_2 Loading and ^{4}He Production in Pd Lattice. In *Proceedings of the Seventh International Conference on Cold Fusion*, Vancouver, Canada, April 19-24, 1998; ENECO, Inc.: Salt Lake City, UT, 1988.
8. Bockris, J. O'M.; Sundaresan, R.; Minevski, Z.; Letts, D. Triggering of Heat and Sub-Surface Changes in Pd-D Systems. In *Proceedings of the Fourth International Conference on Cold Fusion*, Lahaina, Maui, Dec. 6-9, 1993; Passell, T. O., Ed.; Electric Power Research Institute: Palo Alto, CA, 1994.
9. Szpak, S.; Mosier-Boss, P. A.; Gordon, F. E. Further Evidence of Nuclear Reactions in the Pd Lattice: Emission of Charged Particles. *Naturwissenschaften* **2007**, *94*, 511-514.
10. Miley, G. H.; Shrestha, P. J. Overview of Light Water/Hydrogen-based Low Energy Nuclear Reactions. In *Condensed Matter Nuclear Science: Proceedings of the 12th International Conference on Cold Fusion*, Yokohama, Japan, Nov. 27-Dec. 2, 2005; Takahashi, A.; Ota, K.-I.; Iwamura, Y., Eds.; World Scientific Publishing Co.: Singapore, 2006; 34-43.
11. Miles, M.; Bush, B. F.; Lagowski, J. J. Anomalous Effects Involving Excess Power, Radiation, and Helium Production during D_2O Electrolysis Using Palladium Cathodes. *Fusion Technol.* **1994**, *25*, 478-486.

Downloaded by CORNELL UNIV on July 1, 2012 | http://pubs.acs.org
Publication Date: August 1, 2008 | doi: 10.1021/bk-2008-0998.ch014

12. Szpak, S.; Mosier-Boss, P. A.; Smith, J. J. On the Behavior of Pd Deposited in the Presence of Evolving Deuterium. *J. Electroanal. Chem.* **1990**, *30*, 255-260.
13. Szpak, S.; Mosier-Boss, P. A.; Smith, J. J. On the Behavior of the Cathodically Polarized Pd/D System: Search for Emanating Radiation. *Phys. Lett. A* **1995**, *210*, 382-390.
14. Violante, V.; Tripodi, P.; Di Gioacchino, D.; Borelli, R.; Bettinali, L.; Santoro, E.; Rosada, A.; Sarto, F.; Pizzuto, A.; McKubre, M. C. H.; Tanzella, F. X-Ray Emission during Electrolysis of Light Water on Palladium and Nickel Thin Films. In *Condensed Matter Nuclear Science: Proceedings of the 9th International Conference on Cold Fusion*, Beijing, China, May 19-24, 2002; Li, X. Z., Ed.; Tsinghua Univ. Press: Beijing, 2002.
15. Li, X. Z. The Precursor of Cold Fusion Phenomenon in Deuterium/Solid Systems. In *Anomalous Nuclear Effects in Deuterium/Solid Systems*, American Institute of Physics Conference Proceedings 228, Provo, UT, Oct. 1990; American Institute of Physics: New York, 1991.
16. Yoshioka, T.; Tsuruta, T.; Iwano, H.; Danhara, T. Spontaneous Fission Decay Constant of ^{238}U Determined by SSNTD Method using CR-39 and DAP Plates. *Nucl. Instr. and Meth. in Phys. Res. A* **2005**, *555*, 386-395.
17. Ho, J. P. Y.; Yip, C. W. Y.; Nikezie, D.; Yu, K. N. Differentiation Between Tracks and Damages in SSNTD under the Atomic Force Microscope. *Radiat. Meas.* **2003**, *36*, 155-159.
18. Bockris, J. O'M.; Lin, G. H.; Kainthla, R. C.; Packham, N. J. C.; Velev, O. Does Tritium Form at Electrodes by Nuclear Reactions? In *Proceedings of the First International Conference on Cold Fusion*, Salt Lake City, UT, Mar. 28-31, 1990; National Cold Fusion Institute: Salt Lake City, 1990.
19. Abdel-Moneim, A. M.; Abdel-Naby, A. A Study of Fast Neutron Beam Geometry and Energy Distribution using Triple-α Reactions. *Radiat. Meas.* **2003**, *37*, 15-19.
20. El-Sersy, A. R.; Eman, S. A., Khaled, N. E. Fast Neutron Spectroscopy using CR-39 Track Detectors. *Nucl. Instr. and Meth. in Phys. Res.* **2004**, *226*, 345-350.
21. Phillips, G. W.; Spann, J. E,; Bogard, J. S.; VoDinh, T.; Emfietzoglou, D.; Devine, R. T.; Moscovitch, M. Neutron Spectrometry using CR-39 Track Etch Detectors. *Radiat. Prot Dosim.* **2006**, *120*, 457-460.

Downloaded by CORNELL UNIV on July 1, 2012 | http://pubs.acs.org
Publication Date: August 1, 2008 | doi: 10.1021/bk-2008-0998.ch014

Chapter 15

Thermal Changes in Palladium Deuteride Induced by Laser Beat Frequencies

Dennis Letts[1], Dennis Cravens[2], and Peter L. Hagelstein[3]

[1]12015 Ladrido Lane, Austin, TX 78727 (lettslab@sbcglobal.net)
[2]P.O. Box 1317, Cloudcroft, NM 88317 (physics@tularosa.net)
[3]Research Laboratory of Electronics, Massachusetts Institute of Technology, Cambridge, MA 02139 (plh@mit.edu)

Downloaded by YORK UNIV on July 2, 2012 | http://pubs.acs.org
Publication Date: August 1, 2008 | doi: 10.1021/bk-2008-0998.ch015

We present preliminary experimental evidence that two lasers irradiating a deuterated Pd cathode at a single spot can induce significant thermal changes larger than that expected from laser heating alone. We also report that this effect is observed only when the lasers are tuned to a beat frequency around 8 THz, 15 THz, and 20 THz. These experiments support the notion that optical phonon modes may be involved in the excess heat process.

Introduction

In the Fall of 2000, Letts and Cravens observed that the stimulation of a deuterated palladium cathode with twin red laser pointers, each with a radiant power output of 1 mW, could trigger a 4 C cell temperature increase in 100 mL of LIOD electrolyte (*1-3*). As discussed in reference (*2*), the cathode was prepared following a 17-step fabrication procedure that involved cold-rolling followed by annealing of the palladium used to make the cathode.

It was also found experimentally that plating gold onto the cathode after loading with deuterium was required to see a cell temperature response to laser stimulation. Storms has shown that all of our 17 steps are not necessary to make the cathode responsive to laser stimulation (*4*) but the presence of gold plating on the cathode continues to be required. The role of gold plating is not yet understood.

This result stimulated a number of efforts seeking to replicate the effect. Excess heat bursts were observed in association with laser stimulation in references (*4-7*), confirming the existence of the effect. Bazhutov and coworkers reported observing neutron emission correlated with laser stimulation (*8*). That the excess heat effect was sensitive to polarization was noted in the initial experiments of Letts and Cravens (see reference (*2*)). Experiments at ENEA Frascati pursued the issue of polarization dependence (*7*). It was found that excess power occurs with p polarization (TM polarization) in which the electric field has a component normal to the surface, and not with s polarization (TE polarization) in which the electric field is transverse. The coupling of the laser light to surface plasmons in connection with these experiments has been studied theoretically in reference (*9*).

In 2002 the experimental results of Letts and Cravens came to the attention of the third author, who had been working on the theoretical aspects of heat producing mechanisms in PdD for more than a decade. A number of ideas and suggestions were offered concerning laser stimulation of deuterated metals. One of those ideas was the use of two lasers to intentionally create a beat frequency in the terahertz range (10^{12} Hz). The band edges of the acoustic and optical phonon modes of deuterated palladium are observed by neutron spectroscopy to be in the terahertz range (*10*). Under the assumption that phonons are involved in the process that produces excess heat, a demonstration that this is the case would require stimulation of the phonon modes and the observation of a corresponding response in the excess heat signal. It was suspected that our first twin laser experiment might have provided such a stimulation. Five years later (in March 2007) Letts and Cravens returned to Hagelstein's beat frequency stimulation idea with positive results. The details of this single experiment and possible theoretical implications form the basis of this paper.

Downloaded by YORK UNIV on July 2, 2012 | http://pubs.acs.org
Publication Date: August 1, 2008 | doi: 10.1021/bk-2008-0998.ch015

Experimental

Experiment No. 662 was conducted at the personal laboratory of Dennis Letts in Austin, TX with daily collaboration provided by Dennis Cravens from his personal laboratory in Cloudcroft, NM. The experiment was configured in a manner similar to that reported in reference (*2*).

Figure 1 shows our electrolytic cell used for experiment 662. The cell was kept in a controlled environment where airflow was constant and ambient temperature was maintained at 25 +/- 0.03 C. Cell power was also kept constant with a variation of approximately +/-0.01 W. Typical cell power was in the 7-10 watt range.

Two Beta Therm thermistors were used to measure cell temperature. We relied upon the manufacturer for the calibration constants. One thermistor was positioned low in the cell and the other was positioned slightly above the cathode. The cell was not mechanically stirred. The mixing efficiency is reflected by the temperature gradient between the two probes, which was

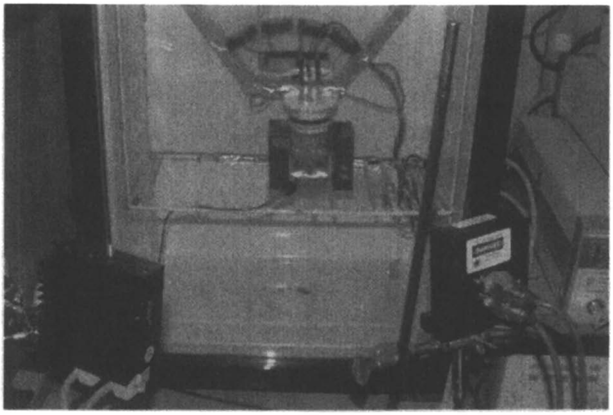

Figure 1. Cell 662 undergoing dual laser stimulation.

Downloaded by YORK UNIV on July 2, 2012 | http://pubs.acs.org
Publication Date: August 1, 2008 | doi: 10.1021/bk-2008-0998.ch015

typically 0.1 C or less. Labview was used to collect data from the cell. The temperature difference ΔT is taken to be the average of temperatures measured internal to the cell minus the enclosure ambient (two thermistor average) temperature; we found that ΔT was typically 30 °C-35 °C.

The thermal output power P_{th} was estimated using Fick's law, assuming that

$$P_{th} = K\,\Delta T$$

The calibration constant K was determined by assuming the thermal output power was matched to the input cell power P_{cell} (the product of current and voltage minus the thermoneutral potential) before the lasers were switched on. The calibration constant determined before laser stimulation was found to be in good agreement with the value determined well afterward. The excess power during the live part of the experiment is then

$$P_{xs} = P_{th} - P_{cell}$$

This method worked fairly well to establish a long zero run before the lasers were switched on. With ambient temperature and cell power controlled tightly, it was obvious when the heat producing reaction began because cell temperature would increase very quickly. The variation in the thermal output of the calorimeter was approximately 10 mW while the increase in thermal output was typically 100-300 mW. The signal to noise ratio from our calorimeter seemed high enough to eliminate mundane measurement error as an explanation for our results.

Dual tunable lasers (seen in the foreground of Figure 1) were used to provide beat frequencies in the 3 to 24 THz range. Lasers were controlled to a precision of about 0.25 nm. The laser diodes were typically off-the-shelf red lasers. The diodes typically had an optical power output of 20-30 mW with a linewidth of approximately 1 nm. The laser diode power output was measured using an Ophir power meter. The linewidth of the laser diodes was measured using a Stellarnet optical spectrometer with a resolution of approximately .25 nm. The two beams were mixed in air and typically irradiated a single spot on the cathode approximately 1 mm in diameter. Beam polarization was controlled using a half-wave filter in a holder marked in degrees. Using this method, the polarization angle of laser 1 can be rotated until it is in alignment with the polarization angle of laser 2. It appears to be necessary that the two laser beams match with respect to polarization angles. In this experiment, the cell seemed to respond only to the beat frequency and not to the wavelength of either laser.

Figure 2 shows the electrolytic cell of experiment No. 662 inside the temperature controlled enclosure being stimulated by dual lasers. Laser 1 wavelength was centered near 685 nm, and laser 2 wavelength was centered near 658 nm. Each laser could be tuned over a range of 4-6 nm. These two lasers could provide the 15 THz and 20 THz beat frequencies. To reach the 8 THz beat frequency, a third laser centered at 664 nm was used. Two permanent magnets surrounded the cell, providing approximately 700 Gauss at the cathode. The direction of the magnetic field does not seem to matter; however, the relationship of the laser beam polarization and the magnetic field direction appeared to be important. Cravens observed that when the laser beam polarization was parallel with the magnetic field lines, the cell did not respond to laser stimulation. When the beam polarization was perpendicular to the magnetic field lines, the cell response was maximized. Cell No. 662 was loaded for 120 hours at 0.05 Amps without magnets; then magnets were applied and current was increased to 1 Amp for 24 hours. The loading ratio was not measured during the experiment but our experience has shown that loading in this manner usually results in a cathode that will respond to single or dual laser stimulation. McKubre et al have reported that a maximum bulk D/Pd loading ratio near 0.93 is required to observe exothermic reactions in deuterated palladium (*11*).

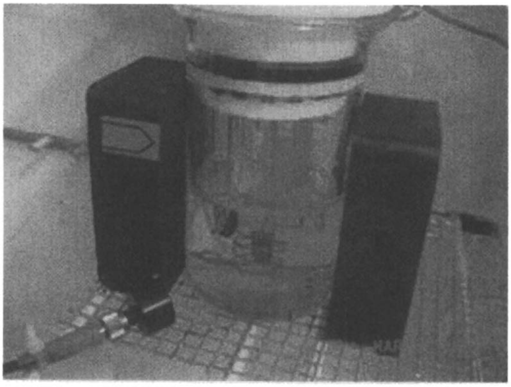

Figure 2. Cell 662 positioned in a magnetic field of 700 Gauss.

Downloaded by YORK UNIV on July 2, 2012 | http://pubs.acs.org
Publication Date: August 1, 2008 | doi: 10.1021/bk-2008-0998.ch015

The electrolyte used was 100 mL of LiOD at a concentration of 0.5 M. Heavy water was obtained from Sigma Aldrich, 99.9 atom % D, stock # 151882-500g, batch 05512EE. Lithium was obtained from Sigma Aldrich, 99.9%+, stock # 499811-25g, batch 02313TC. The cathode was a billet of palladium 5 mm x 12mm x 0.20mm, 0.999 purity obtained from Scott Little of Austin, Texas. The anode was 0.999 pure Pt wire from Alfa Aesar, with an anode diameter of 10 mm, and four turns over the cathode. The cell was closed, with recombination of the electrolysis gases provided by the small pellets visible below the O-ring seal. These pellets were obtained from Alfa Aesar, 0.5% Pt on 1/8 in Alumina, stock # 89106, lot B17Q15. The cell lid was Teflon with glass electrode holders. The tops of the glass pass-thrus were epoxied.

To the upper left of the cathode is a small piece of 0.999 gold. In previous work (in 2000) we found that plating gold onto the cathode was necessary before laser stimulation would trigger exothermic reactions on the cathode surface. Gold was plated onto the cathode "in situ" by connecting the gold electrode to the positive side of the power supply providing electrolysis DC power. Gold ions went into solution and subsequently plated onto the cathode. We do not at present have a quantitative method for determining exactly how much gold is required. When the surface has turned dark, that is generally sufficient for the laser to trigger exothermic reactions on the cathode. We kept the lasers at the far left and far right of the cell so the angle of incidence would be 45 degrees or greater with respect to normal incidence in order to couple with TM polarization.

In Figure 3 we show results from a control run made with no laser stimulation. Without laser stimulation, the input power was equal to the output power to within approximately +/-0.01 watts at 9 watts of DC input power.

In Figure 4 we present results from a second control run using dual lasers with a beat frequency in the 3-7 THz range (where the system does not respond). As long as the beat frequency remained below 8 THz, exothermic reactions were not observed and the cell remained in power balance. We note that the optical phonon branch in PdD does not extend below 8 THz.

Downloaded by YORK UNIV on July 2, 2012 | http://pubs.acs.org
Publication Date: August 1, 2008 | doi: 10.1021/bk-2008-0998.ch015

Experimental Results

After the cathode had loaded for 120 hours at 0.05 Amps without magnets, magnets were placed around the cell as described above. Current to the cell was increased to 1.25 Amps and held for 24 hours. Gold was then plated into solution for about 20 minutes. After another 24 hours, the cathode became dark and dual laser stimulation began. The cell temperature was kept above 55 °C.

We scanned the beat frequency over the frequency range associated with optical phonons (between 8 THz and 20 THz), as well as outside this region. We observed that cell temperature tended to increase noticeably only when the dual laser beat frequency was near 8, 15, or 20 THz. At other beat frequencies, the change in cell temperature was very small or zero within the same irradiation

Downloaded by YORK UNIV on July 2, 2012 | http://pubs.acs.org
Publication Date: August 1, 2008 | doi: 10.1021/bk-2008-0998.ch015

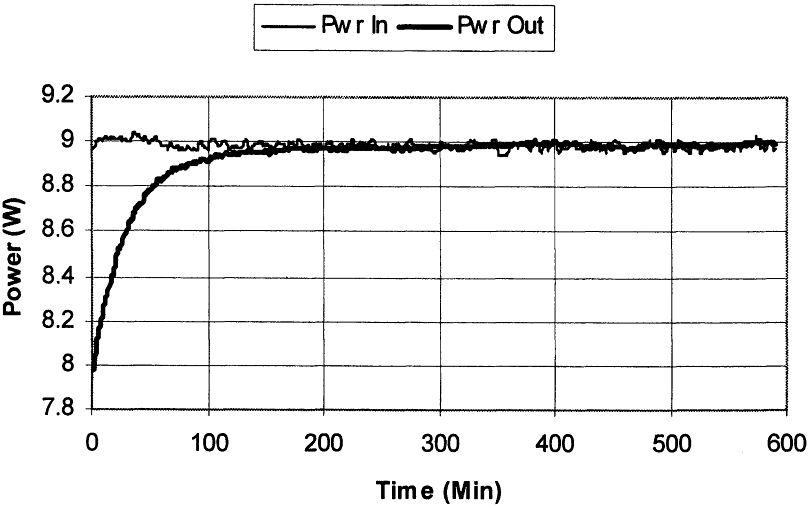

Figure 3. Input electrical power and output thermal power (W) as a function of time (minutes) with no laser stimulation.

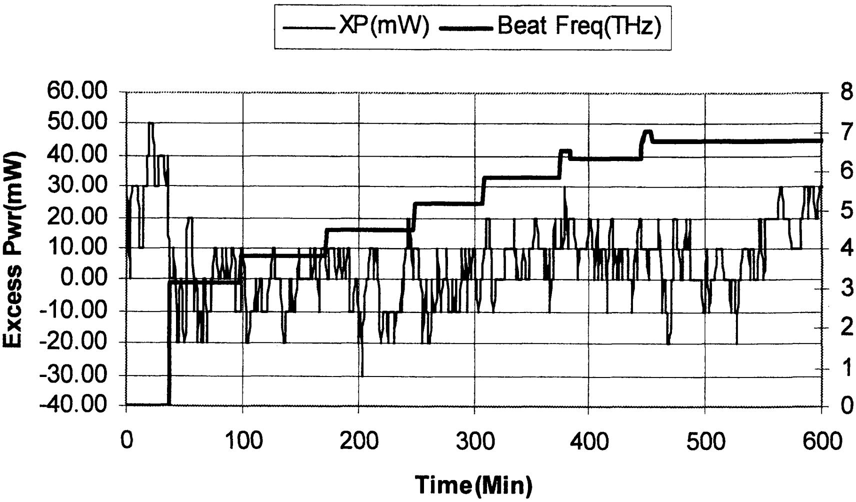

Figure 4. Excess power (thermal power out minus electrical power in) in mW as a function of time (minutes) – thin black line; beat laser frequency (THz) as a function of time – thick black line. The data points in this plot and in others appear to be discrete due to inadvertently recording too few digits in the results being plotted, a defect that will be addressed in future work.

time interval (see Figures 4, 7, 9, 10, 11, 12, and 13). Our largest and clearest cell response to beat frequency stimulation was observed during two runs, 662o and 662o2 as shown in Figure 5 and Figure 6 below. The beat frequency was near 20 THz in both runs.

The cell's response in Figure 6 was very similar to that shown in Figure 5. Stimulation at approximately 20 THz resulted in a gain of about 250 mW from two 25 mW lasers. A few minutes after the lasers were turned on at a beat frequency of 19.4 THz, cell temperature began to increase as if 150 to 200 mW had been dissipated in the electrolyte. The effect continued until the lasers were turned off, even though the beat frequency had advanced to 22 THz. It seemed that once triggered, the exothermic reaction was hard to extinguish. Our seven years of experience with laser stimulation has shown that most of the time the excess power signal continues for 24 to 120 hours after the laser stimulation is removed. In a few cases (perhaps only ~ 10%) the excess power signal declines when the laser stimulation is switched off.

We also observed cell temperature increases in response to beat frequency stimulation around 15 THz. The thermal responses at 15 THz were in general not as robust as 20 THz stimulation. Figure 7 shows a sharp thermal response to beat frequency stimulation at 14.5 THz. The initial excess power was about 200 mW but the excess power declined to zero as the beat frequency advanced during scanning. As the scan advanced past 15 THz, the thermal response declined to zero. The time constant for the isoperibolic calorimeter is 10 minutes. Typically if cell temperature is elevated by 2 degrees by addition of a resistive heat pulse, the cell temperature will return to baseline in about 60 minutes. The increase in thermal output suddenly stopped at minute 310 and returned to zero around minute 377. The observed thermal decline is consistent with the time constant of the calorimeter. Why the reaction stopped suddenly is a mystery, since the thermal effect normally continues for many hours, even after the lasers are switched off.

Figures 8 and 9 tell two stories. At first, the cell failed to respond to 20 THz stimulation, so the beat frequency was lowered to 14.5 THz. There was still no thermal cell response. Magnets were in place around the cell, with the magnetic field of 700 gauss across the face of the cathode. We rotated the polarization of laser 2 by 90 degrees so it matched the polarization angle of laser 1 (with both lasers now TM polarized). The cell gave an immediate thermal response, as shown in Figure 8. This run told us that a beat frequency near 15 THz could trigger a thermal response from the cell but that the polarization angle of the lasers with respect to each other and the cathode is important. It is important to note the results from rotating the relative polarization of the two lasers severely limits simple chemical explanations of triggered heat release. In Figure 9 is shown the excess power as a function of time and also the beat frequency.

We also observed that the cell was responsive to beat frequency stimulation near 8 THz. Due to equipment limitations we did not run many tests at 8 THz. Results from run # 662G are shown in Figure 10. As this figure shows, when the lasers were turned off, the cell cooled slowly and then came to equilibrium above the baseline before the lasers were turned on.

Downloaded by YORK UNIV on July 2, 2012 | http://pubs.acs.org
Publication Date: August 1, 2008 | doi: 10.1021/bk-2008-0998.ch015

Downloaded by YORK UNIV on July 2, 2012 | http://pubs.acs.org
Publication Date: August 1, 2008 | doi: 10.1021/bk-2008-0998.ch015

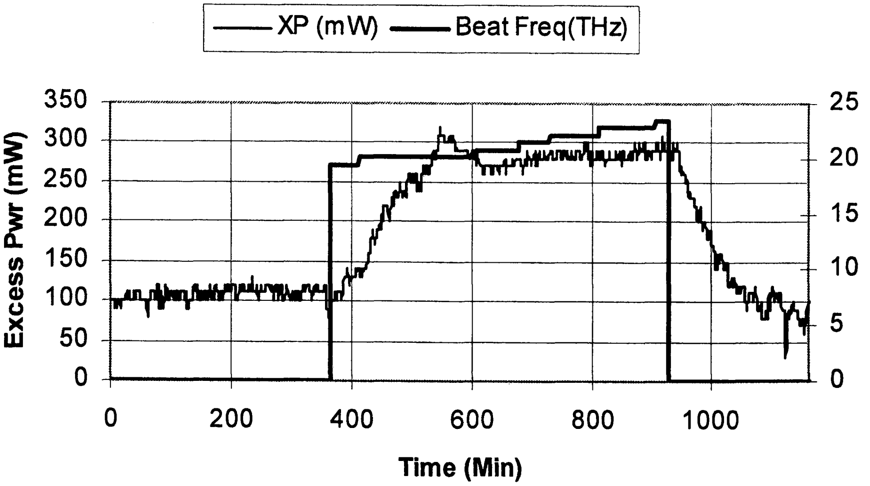

Figure 5. Excess power (mW) as a function of time – thin black line; beat frequency (THz) as a function of time (minutes) – thick black line. There appears to be a thermal response to an initial beat frequency of 19.4 THz.

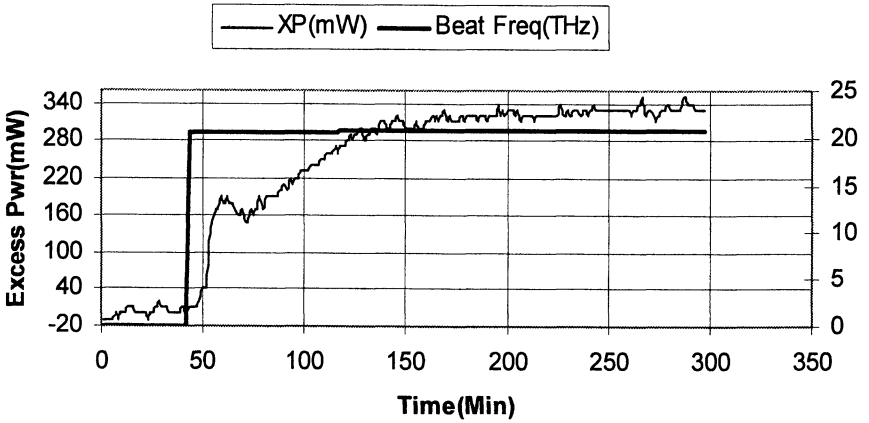

Figure 6. Excess power as a function of time – thin black line; beat frequency (THz) as a function of time (minutes) –thick black line. This run was an effort to repeat the cell response depicted in Figure 5.

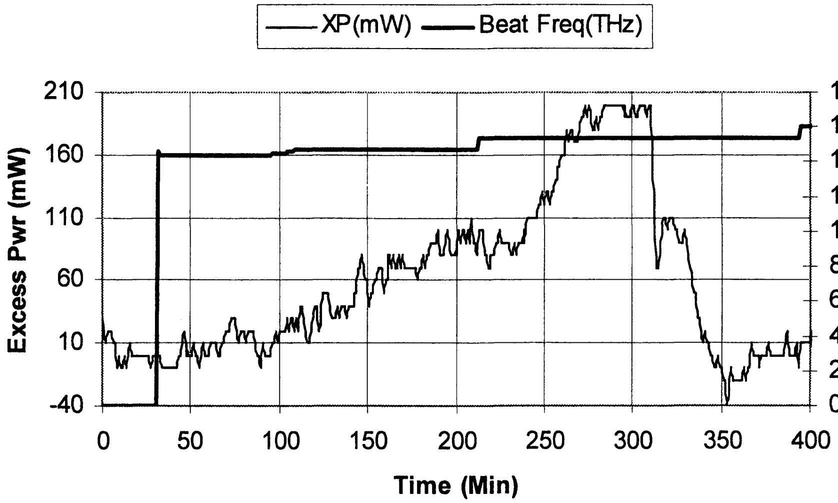

Figure 7. Excess power (mW) as a function of time (minutes) – thin black line; beat frequency (THz) as a function of time – thick black line. One observes an initial thermal response to a beat frequency stimulation of 14.5 THz.

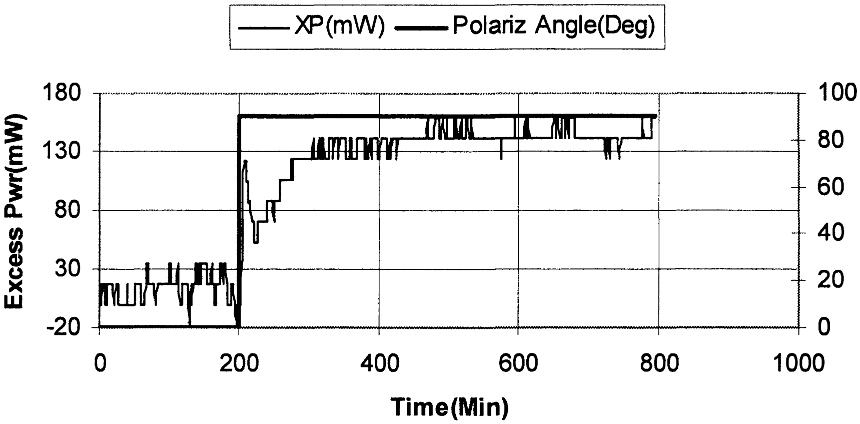

Figure 8. Excess power (mW) as a function of time (minutes) – thin black line; laser polarization angle as a function of time – thick black line. The polarization of laser #2 was rotated 90 degrees using a half-wave filter at 203 minutes, which resulted in the onset of excess power.

Downloaded by YORK UNIV on July 2, 2012 | http://pubs.acs.org
Publication Date: August 1, 2008 | doi: 10.1021/bk-2008-0998.ch015

Downloaded by YORK UNIV on July 2, 2012 | http://pubs.acs.org
Publication Date: August 1, 2008 | doi: 10.1021/bk-2008-0998.ch015

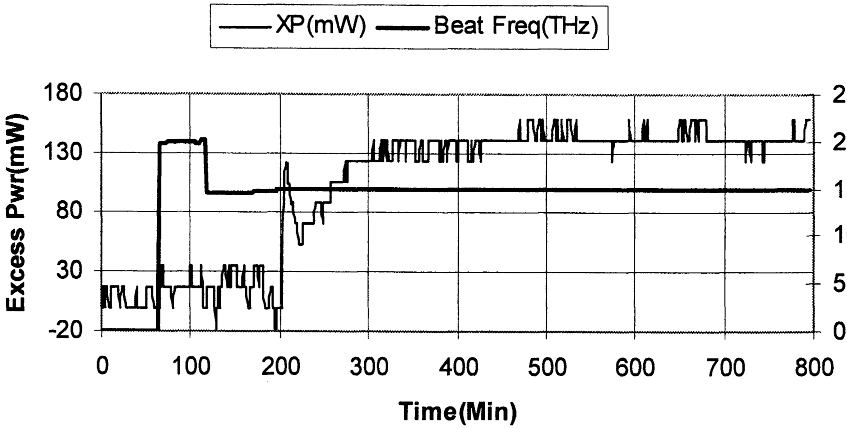

Figure 9. Excess power (mW) as a function of time (minutes) – thin black line; Beat frequency (THz) as a function of time – thick black line. The beat frequency stimulation at 14.8 THz did not trigger a temperature increase in the cell until the beam of laser #2 was rotated 90 degrees to the right to match the polarization angle of laser #1.

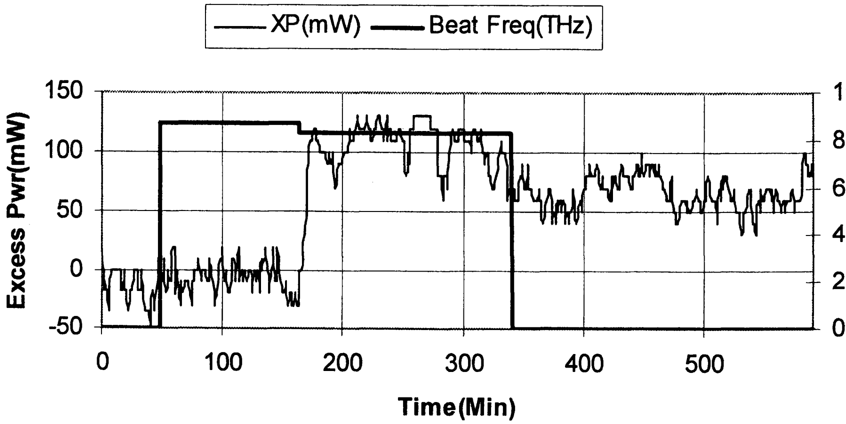

Figure 10. Excess power (mW) as a function of time (minutes) – thin black line; beat frequency (THz) as a function of time – thick black line. Excess power initiated at a beat frequency at 8.3 THz.

As was typical for experiments in this campaign, the laser beating was effective in stimulating an excess power event, but once initiated the excess power often remained (even if the beat frequency was altered, or if the lasers were turned off).

As shown in Figure 11, we could not keep laser 2 tuned at a low enough temperature to produce the 8.3 THz beat. The laser tuner lost control of the diode temperature and tuning drifted up slowly. When tuning was lost, cell temp declined slightly, suggesting some sensitivity to the 8 THz "sweet spot."

This sensitivity to specific beat frequencies was also observed in experiment 662t1, shown in Figure 12. The cell ran for 6 hours with thermal power out in balance with electrical power in with both lasers on providing a beat frequency of 18.3 to 18.7 THz. Cell temperature did not increase significantly until the beat frequency reached 18.9 THz.

Another example of beat frequency sensitivity was also observed in experiment 662i2, shown in Figure 13. This experiment ran for approximately 13 hours with thermal power out in balance with electrical power in. During this time both lasers were on providing a beat frequency ranging from 18.2 THz to 18.9 THz, just below the left edge of the trigger frequency identified previously. Suddenly, when the beat frequency reached 19.2 THz, cell temperature began to increase, producing a slight excess power of about 60 mW. The beat frequency continued to advance and excess power doubled to 120 mW. The sharpest increase in excess power occurred when the beat frequency was at 21.4 THz.

Discussion

The experiments presented in the paper show that two lasers tuned to specific beat frequencies appear to be able to trigger excess power events when incident on the surface of a deuterated cathode. Excess power was observed correlated with specific frequencies near 8, 15, and 20 THz. Laser beating at other frequencies was not observed to initiate excess power events (see Figures 4, 7, 9, 10, 11, 12, and 13 for examples). For example, no response was seen at beat frequencies of 3-7 THz and 16-18 THz. However, laser stimulation at beat frequencies of 8, 14.8 and 19.4 THz triggered excess power increases in the range of 150 to 250 mW. This is 15 to 25 times larger than our calorimeter's power variation.

In the basic Fleischmann-Pons experiment, if an excess power event was observed, one could obtain evidence to support the contention that some new and unexpected physical effect was present. In the event that the total energy associated with the event was sufficiently great such that it could not be accounted for by either experimental artifact or by chemistry, then the observation could be interpreted as supporting the hypothesis that the origin of the effect was nuclear. The absence of energetic particles commensurate with the energy produced could be used to support the contention that the new effect was not due to conventional nuclear reactions, and provide positive support for the existence of a new kind of nuclear process. Observations of ^{4}He

Downloaded by YORK UNIV on July 2, 2012 | http://pubs.acs.org
Publication Date: August 1, 2008 | doi: 10.1021/bk-2008-0998.ch015

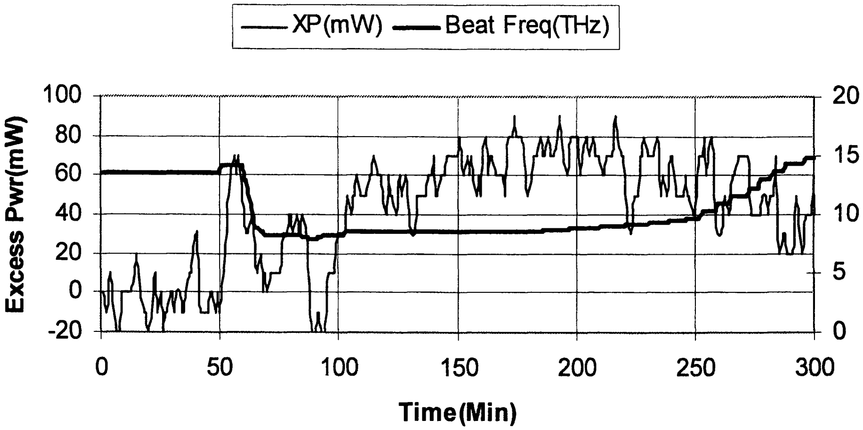

Figure 11. A small response can be seen to stimulation at 8.3 THz.

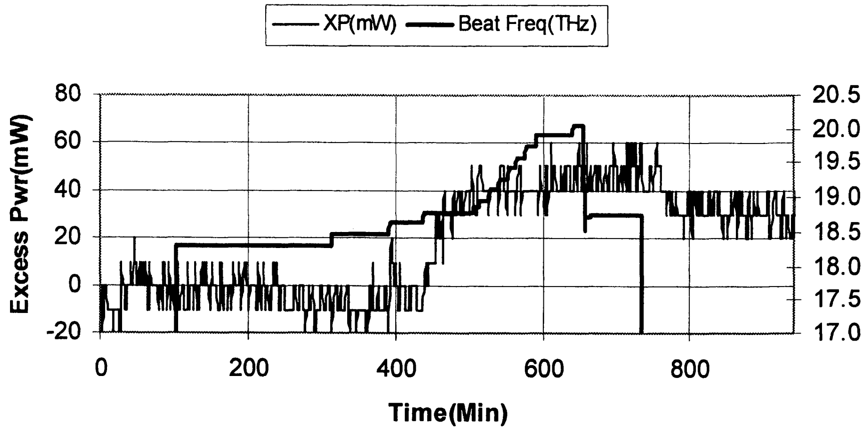

Figure 12. This plot shows that beat frequencies of 18.3 to 18.7 THz did not trigger a thermal response but 18.9 THz did trigger a response.

Downloaded by YORK UNIV on July 2, 2012 | http://pubs.acs.org
Publication Date: August 1, 2008 | doi: 10.1021/bk-2008-0998.ch015

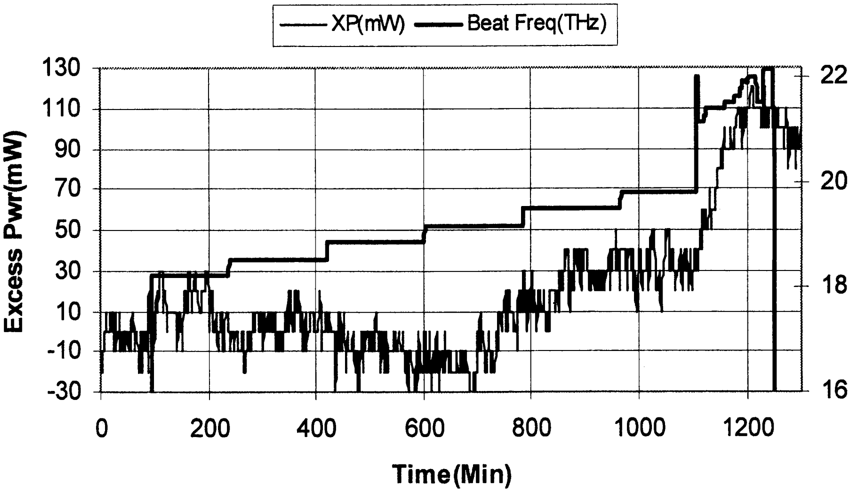

Figure 13. This plot also shows a beat frequency sensitivity that starts near 19 THz and extends to 21.4 THz. Note that at minute marker 700 the thermal output of the cell increased when the beat frequency was near 19 THz. At minute marker 1100, cell thermal output increased again when the beat frequency reached 21.4 THz.

quantitatively correlated with the energy produced at 24 MeV/^{4}He atom provide support for a new kind of reaction process in which deuterons somehow react to form ^{4}He without energetic particle emission.

However, in none of these experiments can one gain much information as to precisely what the new physical process is which causes the reactions and leads to the excess heat. The Fleischmann-Pons experiment has been frustrating over the years in that it tells us that something new is happening, but in general is silent as to the reaction mechanism.

In the initial laser stimulation experiments (*1-3*) it was demonstrated that a weak surface stimulation could initiate an excess heat event. Given that the laser frequency is so high, the only condensed matter response that could reasonably be invoked would involve plasmons, or perhaps more specifically, surface plasmons (for example, see (*9*)). If one adopts a theoretical picture in which deuterons participate to form ^{4}He in line with experimental observations, then it is not obvious how a weak excitation provided to surface electrons impacts the deuterons in a significant way.

The new experiments described in this paper are qualitatively different in this regard. In this case the system appears to be responding to the beat frequency of two lasers at specific frequencies in the vicinity of the optical phonon modes. This suggests that optical phonon modes may be involved in the new physical process, which is significant since in PdD the optical phonon modes involve to within an excellent approximation only vibrations of the

Downloaded by YORK UNIV on July 2, 2012 | http://pubs.acs.org
Publication Date: August 1, 2008 | doi: 10.1021/bk-2008-0998.ch015

Downloaded by YORK UNIV on July 2, 2012 | http://pubs.acs.org
Publication Date: August 1, 2008 | doi: 10.1021/bk-2008-0998.ch015

deuterons. The acoustical mode frequencies are lower, with the band edge occurring near 5 THz. At 5 THz and below, it is the Pd nuclei that vibrate, with little contribution from the deuterons. No significant response was seen below 8 THz in these experiments, consistent with the participation of optical phonon modes which occur in the 8-20 THz range. These experiments are the first that appear to implicate deuteron vibrational modes in particular. That is why they are important. We know from the Frascati work (*7*) that the system responds to TM polarization, and it is a reasonable assumption in the present experiments that both polarizations must be TM to observe the beat frequency excess heat effect. Hence, not only are optical phonon modes implicated, but also most likely these experiments implicate compressional optical phonon modes.

It remains to be explained precisely how the system is responding to the beat frequency. Although frequency mixing is known, there are not many examples of frequency mixing at such low laser intensities. The two beams must have the same linear polarization for beats to develop by superposition (the E fields of the two beams must be aligned). Notice that the anomalous heat was triggered only during such conditions, and was not triggered when the beam polarizations were not in alignment with each other or when they were lacking components perpendicular to the cathode surface (Figure 8). The alignment of polarization is a strong indication that the heat generation was not chemical in nature but involves the generation of phonons within the lattice at the beat frequency. The triggering of the effect by rotation of the polarization of one beam, and by moving the beat frequency, is consistent with the effect being due to D/Pd compressional optical phonon interactions within the lattice. These results, showing that TM polarization is required to produce apparent excess power, support the results of the Frascati work as reported in reference (*7*).

These new experimental results also appear to support aspects of recent modeling of the new physical process responsible for excess heat (*12*). In this model, two deuterons interact via the strong force to produce a ^{4}He nucleus, exchanging one or more phonons in association with the interaction. The excitation energy associated with the transition is transferred to other nuclei in a highly off-resonant excitation transfer process. Rapid excitation transfer reactions within these receiver nuclei in the model leads to energy exchange with lattice vibrational modes, and loss of excitation. Of interest here is that the matrix element for the D_2 to ^{4}He transition requires a compressional mode (compressional optical phonon modes are candidates). Also, calculations of the strong force matrix element suggest that S=2 nuclear spin states of D_2 interact more strongly, which may at some point provide a theoretical connection between the observations of reaction sensitivity to an external magnetic field.

References

1. Letts, D. *Bulletin of the American Physical Society*, March Meeting 2003, paper Z33.005.

2. Letts, D.; Cravens, D. Laser Stimulation of Deuterated Palladium: Past and Present. In *Condensed Matter Nuclear Science: Proceedings of the 10th International Conference on Cold Fusion*, Cambridge, MA, Aug. 24-29, 2003; Hagelstein, P. L.; Chubb, S. R., Eds.; World Scientific Publishing Co.: Singapore, 2006; 159.
3. Cravens, D.J.; Letts, D.G. Practical Techniques in CF Research: Triggering Methods. In *Condensed Matter Nuclear Science: Proceedings of the 10th International Conference on Cold Fusion*, Cambridge, MA, Aug. 24-29, 2003; Hagelstein, P. L.; Chubb, S. R., Eds.; World Scientific Publishing Co.: Singapore, 2006; 171.
4. Storms, E. Use of a Very Sensitive Seebeck Calorimeter to Study the Pons-Fleischmann and Letts Effects. In *Condensed Matter Nuclear Science: Proceedings of the 10th International Conference on Cold Fusion*, Cambridge, MA, Aug. 24-29, 2003; Hagelstein, P. L.; Chubb, S. R., Eds.; World Scientific Publishing Co.: Singapore, 2006; 183.
5. McKubre, M.; Tanzella, F.; Hagelstein, P. L.; Mullican, K.; Trevithick, M. The Need for Triggering in Cold Fusion Reactions. In *Condensed Matter Nuclear Science: Proceedings of the 10th International Conference on Cold Fusion*, Cambridge, MA, Aug. 24-29, 2003; Hagelstein, P. L.; Chubb, S. R., Eds.; World Scientific Publishing Co.: Singapore, 2006; 199.
6. Swartz, M. R. Photo-induced Excess Heat from Laser-Irradiated Electrically-Polarized Palladium Cathodes in D_2O. In *Condensed Matter Nuclear Science: Proceedings of the 10th International Conference on Cold Fusion*, Cambridge, MA, Aug. 24-29, 2003; Hagelstein, P. L.; Chubb, S. R., Eds.; World Scientific Publishing Co.: Singapore, 2006; 213.
7. Apicella, M.; Castagna, E.; Capobianco, L.; D'Aulerio, L.; Mazzitelli, G.; Sarto, F.; Rosada, A.; Santoro, E.; Violante, V.; McKubre, M.; Tanzella, F.; Sibilia, C. Some Recent Results at ENEA. In *Condensed Matter Nuclear Science: Proceedings of the 12th International Conference on Cold Fusion*, Yokohama, Japan, Nov. 27-Dec. 2, 2005; Takahashi, A.; Ota, K.-I.; Iwamura, Y., Eds.; World Scientific Publishing Co.: Singapore, 2006; 117.
8. Bazhutov, Y. N.; Bazhutova, S. Y.; Nekrasov, V. V.; Dyad'kin, A. P.; Sharkov, V. F. Calorimetric And Neutron Diagnostics of Liquids During Laser Irradiation. In *Condensed Matter Nuclear Science: Proceedings of the 11th International Conference on Cold Fusion*, Marseilles, France, Oct. 31 - Nov. 5, 2004; Biberian, J.-P., Ed.; World Scientific Publishing Co.: Singapore, 2006; 374.
9. Castagna, E.; Sibilia, C.; Paoloni, S.; Violante, V.; Sarto, F. Surface Plasmons and Low-Energy Nuclear Reactions Triggering. In *Condensed Matter Nuclear Science: Proceedings of the 12th International Conference on Cold Fusion*, Yokohama, Japan, Nov. 27-Dec. 2, 2005; Takahashi, A.; Ota, K.-I.; Iwamura, Y., Eds.; World Scientific Publishing Co.: Singapore, 2006; 156.
10. Rowe, J. M.; Rush, J. J.; Smith, H. G.; Mostoller, M.; Flotow, H. E. Lattice Dynamics of a Single Crystal of $PdD_{0.63}$. *Phys. Rev. Lett.*, **1974**, *33*, 1297.

Downloaded by YORK UNIV on July 2, 2012 | http://pubs.acs.org
Publication Date: August 1, 2008 | doi: 10.1021/bk-2008-0998.ch015

11. McKubre, M.; Bush, B.; Crouch-Baker, S.; Hauser, A.; Jevtic, N.; Smedley, S.; Srinivasan, M.; Tanzella, F.; Williams, M.; Wing, S. Loading, Calorimetric and Nuclear Investigation of the D/Pd System. In *Proceedings of the Fourth International Conference on Cold Fusion*, Lahaina, Maui, Dec. 6-9, 1993; Passell, T. O., Ed.; Electric Power Research Institute: Palo Alto, CA, 1994; 5-1.

12. Hagelstein, P. L.; Chaudhary, I. U. Progress Toward a Theory for Excess Heat in Metal Deuterides. In *Current Trends in International Fusion Research – Proceedings of the Seventh Symposium*, Washington, DC, March 5-9, 2007; Panarella, E.; Raman, R., Eds.; National Research Council of Canada Research Press: Ottawa, 2007.

Downloaded by YORK UNIV on July 2, 2012 | http://pubs.acs.org
Publication Date: August 1, 2008 | doi: 10.1021/bk-2008-0998.ch015

Chapter 16

Study of the Nanostructured Palladium Hydride System

Jan Marwan

Dr. Marwan Chemie, Rudower Chaussee 29, 12489 Berlin, Germany

Downloaded by UNIV OF GUELPH LIBRARY on July 1, 2012 | http://pubs.acs.org
Publication Date: August 1, 2008 | doi: 10.1021/bk-2008-0998.ch016

Electrochemical deposition of metals from hexagonal lyotropic liquid crystalline phases produces metal films with a unique ordered nanostructure in which the cylindrical pores of 1.7 to 3.5 nm running through the film are arranged in hexagonal arrays. Nanostructured Pd films were deposited electrochemically from the template mixture of either $C_{16}EO_8$ or Brij®56. Electrochemical studies showed that both metal films have a high electroactive surface area with the specific surface area on the order of 91 m^2/g. These values together with the TEM and X-ray data are consistent with the expected H_1 nanostructure. The hydrogen region of nanostructured Pd in the cyclic voltammetry in 1 M H_2SO_4 was more resolved than that of plain Pd because of the thin walls of the nanostructure and the high surface area. We could distinguish the hydrogen adsorption and absorption processes. The permeation of hydrogen into the Pd metal lattice occurs with fast kinetics when the Pd surface is blocked by either crystal violet or Pt. We believe that the hydrogen absorption process takes place without passing through the adsorbed state so that hydrogen diffuses directly into the Pd bulk. This process speeds up when the formation of adsorbed hydrogen is suppressed by the coverage of poisons.

In Low-Energy Nuclear Reactions Sourcebook; Marwan, J., et al.;
ACS Symposium Series; American Chemical Society: Washington, DC, 2008.

Introduction

In this review we mainly focus our attention on the palladium electrochemistry, in particular to characterize the hydride adsorption/absorption process and the kinetic behavior of the hydride permeation into the metal bulk. This review can be seen as contributing to this book on "Low Energy Nuclear Reactions" by providing a fundamental background of the palladium hydride system which might be of significant interest for further research on cold fusion.

Outlining the electrochemistry of the nanostructured hydride system, we found it necessary to first illustrate the fabrication process of the nanostructure so that the reader may have an idea what kind of materials we have been using in our research to come up with the results shown here. We report the fabrication of nanostructured palladium exploiting the physical properties of non-ionic liquid crystalline media for use as a template. Liquid crystalline media mainly consists of surfactant and water, and the surfactant itself consists of an alkyl chain with the non-polar hydrocarbon entity and the ethylene group as the polar entity. Depending on the surfactant-to-water ratio and the temperature chosen, the liquid crystals exhibit different phases, such as micellar, hexagonal, cubic, and lamellar, ranging from a low to a high surfactant-to-water ratio. At room temperature the hexagonal phase, used as a template from which the metal fabrication in a nanostructure occurs, covers a wide range of surfactant concentration.

The idea of using lyotropic liquid crystalline phases of non-ionic surfactants to template the deposition of inorganic materials was first introduced by G. Attard and his research group in Southampton, who demonstrated the formation of nanostructured silica by hydrolysis of tetramethyl orthosilicate (*1*) and the formation of nanostructured platinum by chemical reduction of hexachloroplatinic acid (*2, 3*). In this approach a high concentration of the non-ionic surfactant, typically 40 to 60 weight percent, is employed and the nanostructure is a direct cast of the structure of the lyotropic phase used to template the deposition in a process which can be described as "true liquid crystal templating." This method has several significant advantages, to be outlined below.

The deposition process is not restricted to the formation of silica; the method can be used to form a wide range of different nanostructured materials. The nanostructure of the final material is determined by the structure of the lyotropic liquid crystalline phase. Consequently, the dimensions and topology of the structure can be varied in a predictable fashion by the choice of surfactant and by the addition of co-solvents, based upon the knowledge of the phase behavior of the system. A wide range of different lyotropic phases exists with varying topologies which can be exploited in this fashion. The method can be used to produce nanostructured materials, both by chemical and by electrochemical means. The latter approach has the additional advantage that it can be used to form nanostructured films at electrode surface. The thickness of the films can be directly controlled through the amount of charge passed to carry out the deposition.

Downloaded by UNIV OF GUELPH LIBRARY on July 1, 2012 | http://pubs.acs.org
Publication Date: August 1, 2008 | doi: 10.1021/bk-2008-0998.ch016

Downloaded by UNIV OF GUELPH LIBRARY on July 1, 2012 | http://pubs.acs.org
Publication Date: August 1, 2008 | doi: 10.1021/bk-2008-0998.ch016

Although different lyotropic phases can be used as templates, including the cubic and the lamellar phases, the hexagonal phase is the most widely reported. In the hexagonal phase the surfactant molecules assemble into long cylindrical micelles and these micelles then pack into a hexagonal array in which the separation between the micelles is comparable to their diameter (*4*). When these phases are used to template the electrochemical deposition of metal films the metal salt and electrolyte are dissolved into the aqueous component of the mixture and metal deposition occurs, out from the electrode surface, around the surfactant micelles (Figure 1). Once the deposition is complete the surfactant is removed by washing to leave a metal film punctured by a regular hexagonal array of uniform pores (Figure 2 shows a schematic representation of the porous structure). The thickness of the film is directly controlled by the total charge passed. The resulting nanostructured films are denoted as H_I-e films to indicate their regular nanoarchitecture and the topology of the pores within the structure.

The use of this template deposition technique allows considerable control over the structure of the mesoporous film. For example, by changing the surfactant used for platinum deposition from octaethyleneglycol monohexadecyl ether ($C_{16}EO_8$) to octaethyleneglycol monododecyl ether ($C1_2EO_8$) it is possible to change both the diameter of the pores and the thickness of the metal walls between them from 2.5 nm to 1.7 nm (*2, 3*). On the other hand, by adding an organic co-solvent, such as heptane, to the $C_{16}EO_8$ plating mixture, it is possible

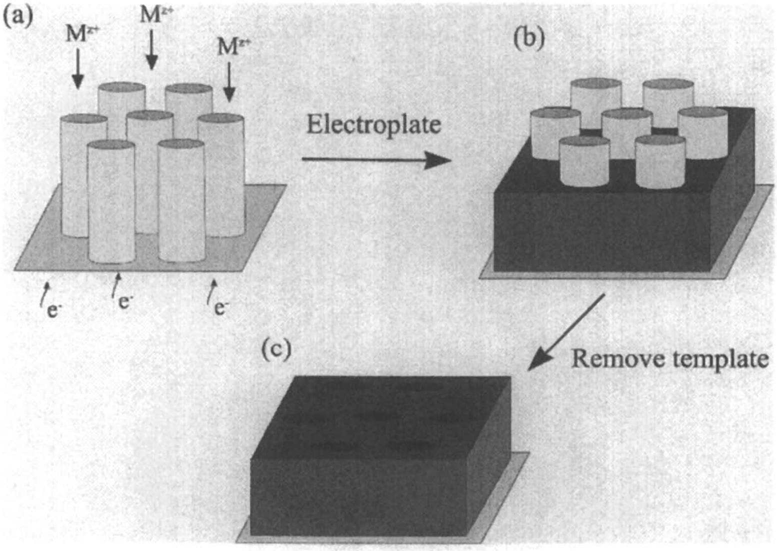

Figure 1. Schematic representation of the templating process used to deposit the nanostructured metal films. The cylinders represent the micellar rods in the lyotropic liquid crystalline phase. Within the aqueous domains of this phase the metal is dissolved and, after electrochemical deposition of the metal and removal of surfactant, the nanostructured metal is produced with hexagonally arranged pores continuously running through the film.

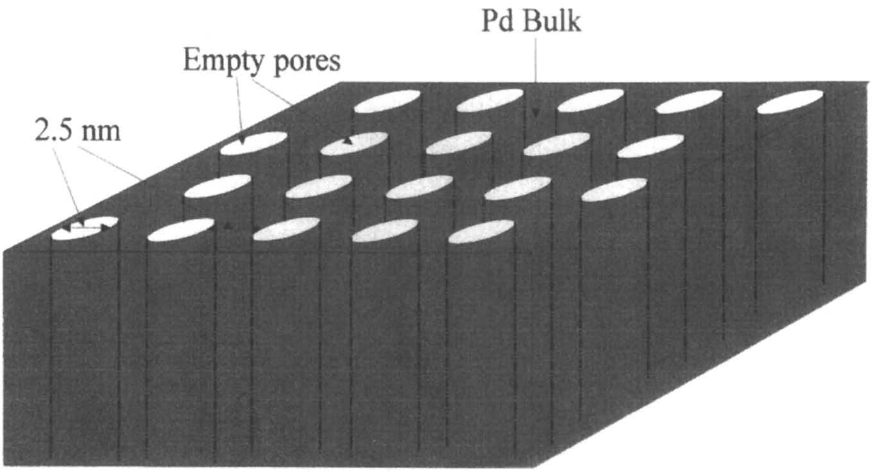

Figure 2. Schematic representation of a nanostructured metal film punctured hexagonally by pores running continuously through the film.

Downloaded by UNIV OF GUELPH LIBRARY on July 1, 2012 | http://pubs.acs.org
Publication Date: August 1, 2008 | doi: 10.1021/bk-2008-0998.ch016

to swell the surfactant micelles without changing their separation and thus to increase the diameter of the pores in the mesoporous metal film to 3.5 nm while leaving the thickness of the walls the same.

The first part of this article describes the phase behavior of the plating system and focuses on the characterization of the deposited nanostructured Pd film. Here we describe the surface morphology using Scanning Electron Microscopy and prove the existence for the hexagonal arrangement and regular pore distribution by Transmission Electron Microscopy and X-Ray Diffraction.

In the second part we describe the electrochemical properties of the H_I–e Pd film. The H_I-e Pd electrodes were studied over the full range of potentials including the adsorption and desorption of hydrogen and oxygen.

On the one hand our attention was drawn to potential regions where the surface oxide was formed. From the charge passed for the surface stripping reaction in the cyclic voltammetry we can calculate the electrochemical active surface area. To our knowledge, different surface oxide states can be produced on the Pd metal surface following through the cyclic voltammetry when applying periodic potential cycling to Pd electrodes.

On the other hand we focused our attention to more negative potentials in the voltammetry where the hydrogen adsorption/absorption on the Pd surface and into the bulk-Pd takes place. The palladium-hydrogen system has been the subject of several studies in the past (*5-8*). The electrochemistry of palladium differs significantly from that of platinum. The Pd process has the special ability for hydrogen to enter and permeate rapidly through the lattice in large quantities. It is well known that thin layers of Pd limit the amount of hydrogen absorbed into the bulk-Pd (*9*). We are therefore interested to see the effect of the thin walls (2.5 nm) of our nanostructured Pd films on this process. As outlined in the literature the use of thin films of Pd as electrodes enhances the distinction between the adsorption and absorption of hydrogen (*9-11*). We focus on the separation between these two features and describe in detail the permeation of hydrogen through the metal lattice and the transition from the α- to the β-hydride phase.

To our mind, this study of the nanostructured palladium hydride system presented here is an essential contribution to this book, although it does not contain experimental results evidencing low energy nuclear reactions. This article provides the reader with a fundamental background of the palladium electrochemistry, outlining the hydrogen absorption/adsorption characteristics, necessarily of interest when focusing on nuclear reactions on metal hydride electrodes, such as palladium.

Downloaded by UNIV OF GUELPH LIBRARY on July 1, 2012 | http://pubs.acs.org
Publication Date: August 1, 2008 | doi: 10.1021/bk-2008-0998.ch016

Experimental

Hydrochloric acid (AnalaR BDH), sulfuric acid (AnalaR BDH), ammonium tetrachloropalladate (premion-99.998% Alfa Aesar), hydrogen hexachloroplatinate (IV) hydrate (99.9% Aldrich), Brij56® (Aldrich), crystal violet (Aldrich), octaethyleneglycol monohexadecyl ether ($C_{16}EO_8$, Fluka), and heptane (99%, Lancaster) were all used as received. All aqueous solutions were freshly prepared using reagent-grade water (18 MΩ cm) from a Whatman "Stillplus" system coupled to a Whatman RO 50. All glassware were soaked overnight in a 3% Decon/deionized water solution and washed thoroughly at least three times with deionized water prior to use.

All electrochemical experiments were carried out using an EG&G Model 263A potentiostat/galvanostat with a large area platinum gauze counter electrode and either a homemade saturated mercury sulfate (SMSE) or saturated calomel electrode (SCE) reference electrode. The counter electrode was a large area platinum gauze. The SMSE was used to avoid chloride contamination of the sulfuric acid electrolyte solution used in the studies of the nanostructured metal electrodes and all potentials are reported with respect to this reference electrode (potentials with respect to SMSE are shifted 0.45 V negatively of the corresponding potential vs. SCE). The reference electrode was used in conjunction with a luggin capillary and stored in a saturated potassium sulfate solution when not in use.

The phase of the lyotropic liquid crystalline plating mixtures was confirmed by polarized light microscopy using an Olympus BH-2 polarized light microscope equipped with a Linkam TMS90 heating stage and temperature control unit. Phases were assigned on the basis of their characteristic optical textures.

The H_I-e Pd films were freshly prepared before each electrochemical experiment by electrochemical deposition onto gold disc electrodes (area 0.0079 m^2) formed by sealing 1 ± 0.1 mm diameter gold wire in glass. Immediately before use, the gold disc electrodes were freshly polished using silicon carbide paper (Cc 1200, English Abrasives) and then alumina/water slurries (Buehler) starting with a particle size of 25 µm and ending with a particle size of 0.3 µm. H_I-e Pd films were deposited from a solution containing 12 wt% $(NH_4)PdCl_4$, 47 wt% $C_{16}EO_8$ or Brij56®, 39 wt% water and 2 wt% heptane at 25 °C. These conditions correspond to the hexagonal (H_I) lyotropic phase for both mixtures as determined by studies of the phase diagram for the system. These deposition mixtures are highly viscous and must be prepared with care to ensure a uniform composition. After all of the components were mixed, the mixture was heated and stirred to ensure homogeneity and then cooled before use. Pd was deposited from the liquid crystalline plating mixture at 0.1 V. After deposition the H_I-e metal films were rinsed in purified water to remove the adherent surfactant mixture.

Electrochemical measurements on the H_I-e Pd films were carried out at room temperature (18-23°C) in 1 M H_2SO_4. Before each experiment the solution was sparged for 10-15 min with a stream of highly purified argon gas to displace dissolved oxygen. The electrochemical active surface areas of the H_I-e Pd films were estimated by integrating the charge passed in the surface oxide stripping reaction recorded in 1 M sulfuric acid following the procedure suggested by Rand and Woods. Small amounts of Pt were deposited onto the H_I-e Pd surface from an aqueous solution containing 25 mM H_2PtCl_6 and 1 M HCl. The surface coverages were calculated from the charge passed to deposit the Pt and the surface areas of the H_I-e Pd films determined from the voltammetry.

SEM images were obtained using a JOEL 300 scanning electron microscope. Samples for SEM analysis were prepared by electroplating Pd from the template mixture onto evaporated gold electrodes (area 1 cm^2) prepared by evaporation of a 10nm thick layer of chromium (to ensure good adhesion) followed by 200 nm of gold on 1 mm thick glass microscope slides. These evaporated gold electrodes were cleaned in an ultrasonic bath of 2-propanol for 10 min immediately before use. For transmission electron microscopy studies a JOEL 2000 TEM was used. The nanostructured Pd samples were strongly adherent on the gold electrode surface and samples for TEM analysis were prepared by scrapping small samples of palladium off the evaporated gold electrode surface and onto the TEM grid using a scalpel.

Downloaded by UNIV OF GUELPH LIBRARY on July 1, 2012 | http://pubs.acs.org
Publication Date: August 1, 2008 | doi: 10.1021/bk-2008-0998.ch016

Results and Discussion

Phase Behavior

The nanostructure of the metals deposited from the lyotropic liquid crystalline phases of non-ionic surfactant mixtures are directly determined by the structures of the lyotropic phases used. We therefore found it necessary to characterize the phase behavior of mixtures of non-ionic surfactant, water, and palladium salt.

Two non-ionic surfactants were used in this work: octaethyleneglycol monohexadecyl ether ($C_{16}EO_8$) and Brij®56. $C_{16}EO_8$ is available as highly purified, monodisperse material whereas Brij®56 is a polydisperse commercial cheaply available surfactant which is predominantly polyoxyethylene(10) cetyl ether (decaethyleneglycol monohexadecyl ether ($C_{16}EO_{10}$)) but also contains a range of other surfactants.

Figure 3 shows the phase diagram obtained using mixtures of $C_{16}EO_8$ and ammonium tetrachloropalladate solution. The most common lyotropic liquid crystalline phases were observed: hexagonal, cubic, and lamellar. The hexagonal phase, H_1, exists from 30 to 40 wt% $C_{16}EO_8$ up to 80 to 90 wt% and is stable up to 55 °C for compositions around 55 wt% $C_{16}EO_8$. The cubic phase, V1, occupies a smaller region of existence between 55 to 60 wt% and 80-90 wt% of $C_{16}EO_8$ in water at higher temperatures than the hexagonal phase with the maximum temperature point (61 °C) around 60 wt%. At higher concentrations of surfactant in water the lamellar phase, L_α, predominates. The domain of existence of the lamellar phase starts between 55 and 60 wt% of surfactant in water and continues above 90 wt%.

Figure 4 shows the phase diagram of Brij®56 from which the similar phase behavior is observed. The large region of the phase diagram is occupied by the hexagonal phase which domain of existence starts between 30-40 wt% of surfactant in water and continues to 80-90 wt%. In this case the hexagonal phase is stable to a similar value of temperature compared to the phase diagram of $C_{16}EO_8$ with the maximum point of 53 °C at 55 wt% surfactant. The cubic phase, V_1, has a slightly reduced range of stability. Although it exists in the same range of surfactant concentration as in the phase diagram for $C_{16}EO_8$ the maximum point occurs at 59 °C at 60 wt% of surfactant in water.

The domain of existence of the cubic phase shown in both phase diagrams does not cover a large range of temperature and no evidence has been found for the existence of this phase at room temperature. However, the electrodeposition of mesoporous Pd from this phase can lead to a relatively high surface area which is of interest for the use of mesoporous Pd films as high surface area metal catalyst deposited on low-power micropellistors.

Brij®56 is a bulk commercial surfactant and slight variations in compositions occur between the different batches. Measurements using two different batches of material showed essentially the same phase behavior when mixed with water and ammonium tetrachloropalladate solutions except there was a variation of ±1.5 °C in the positions of the hexagonal/cubic and cubic/lamellar boundaries.

Characterization of the H_I-e Pd Films

The H_I-e Pd films electrochemically deposited at 0.1 V vs SCE from the hexagonal phase are adhered well to the evaporated gold electrodes used for the deposition. Figure 5 shows a scanning electron micrograph of an H_I-e Pd film. Scanning Electron Microscopy (SEM) was used to examine the surface morphology of the deposited mesoporous Pd film. This figure shows the edge of view of the mesoporous Pd film at a tilt angle of 70 ° deposited on gold/glass.

Downloaded by UNIV OF GUELPH LIBRARY on July 1, 2012 | http://pubs.acs.org
Publication Date: August 1, 2008 | doi: 10.1021/bk-2008-0998.ch016

Downloaded by UNIV OF GUELPH LIBRARY on July 1, 2012 | http://pubs.acs.org
Publication Date: August 1, 2008 | doi: 10.1021/bk-2008-0998.ch016

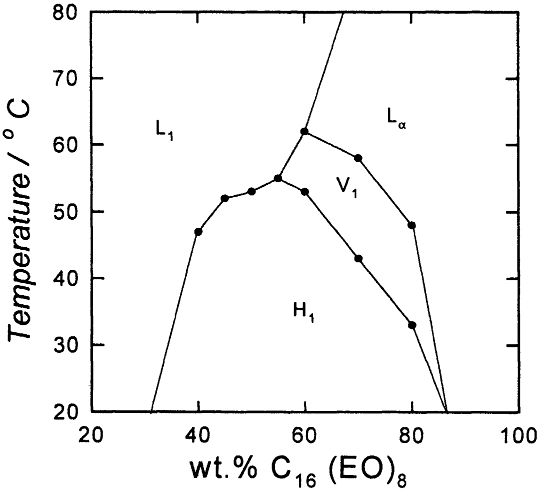

Figure 3. Phase diagram for mixtures of a 1.40 mol/l solution of $(NH_4)_2PdCl_4$ in water and $C_{16}EO_8$. The concentration (by weight) of surfactant was increased from 20 to 80%. H_1 is the hexagonal phase, V_1 the cubic phase, L_α the lamellar phase, and L_1 the micellar solution. The weight ratio between $(NH_4)_2PdCl_4$ and water was kept fixed at 0.4 and the weight ratio of surfactant to heptane was kept constant at 22.

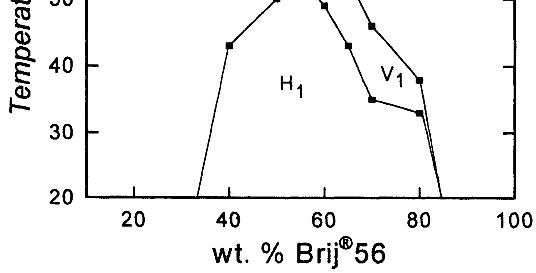

Figure 4. Phase diagram for mixtures of a 1.40 mol/l solution of $(NH_4)_2PdCl_4$ in water, Brij®56, and heptane. The ratio between $(NH_4)_2PdCl_4$ / water (0.4) and surfactant / heptane (22) was kept constant. The composition (by weight) of surfactant in the aqueous solution was increased from 20 to 80%. H_1 is the hexagonal phase, V_1 the cubic phase, L_α the lamellar phase, and L_1 the micellar solution.

Downloaded by UNIV OF GUELPH LIBRARY on July 1, 2012 | http://pubs.acs.org
Publication Date: August 1, 2008 | doi: 10.1021/bk-2008-0998.ch016

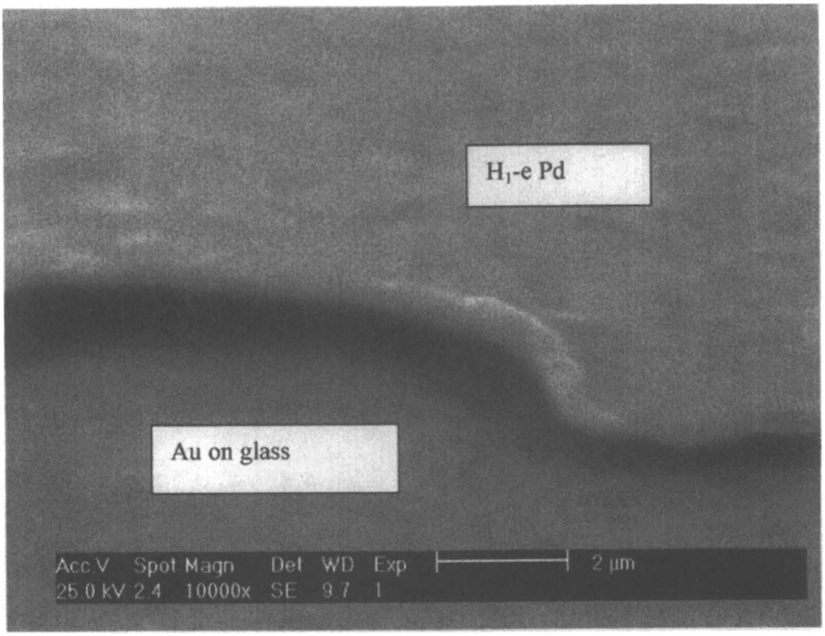

Figure 5. Scanning electron micrograph of an H_I-e Pd film deposited on an evaporated gold electrode. The film was deposited from a mixture of 12 wt% $(NH_4)_2PdCl_4$, 47 wt% $C_{16}EO_8$, 39 wt% water, 2 wt% heptane. The total charge passed for deposition was 0.55 C/ cm^2.

The H_1–e Pd film is starting to lift away from the substrate. The film is dense, uniform and continuous over the whole range with no evidence of nanostructure on the SEM scale.

To examine the nanostructure of the electrochemically deposited Pd films it is necessary to use Transmission Electron Microscopy (TEM). To provide clear evidence for the hexagonal arrangement of Pd films in nanometer-sized dimensions is subject to the orientation of the TEM image. The evidence for the hexagonal array of the pores running through the Pd film can be given if the image shows a "pores end on" view. However, the experiments carried out at the Southampton microscopy center revealed that the pores end on image is rather unlikely to be obtained. This is certainly the case for Pd films prepared from the Brij®56 template mixture. The experimental findings often revealed an orientation of the TEM image from which the hexagonal array of the pores cannot be seen, but we observe the porous channels running through the film. Inspection of these pores shows that they are continuous and approximately straight over their whole length.

Figure 6 shows the TEM image of H_1–e Pd scraped from the electrode surface. This image shows an orientation of the sample which approaches the "pores end on" view. From the results obtained we can conclude that clear evidence for hexagonal arranged pores cannot be given. We note slight indication of a porous structure consisting of cylindrical pores with pore size diameter of (25 ± 2) Å and wall thickness of (25 ± 2 Å). The measurements were taken using the software program Scanimage.

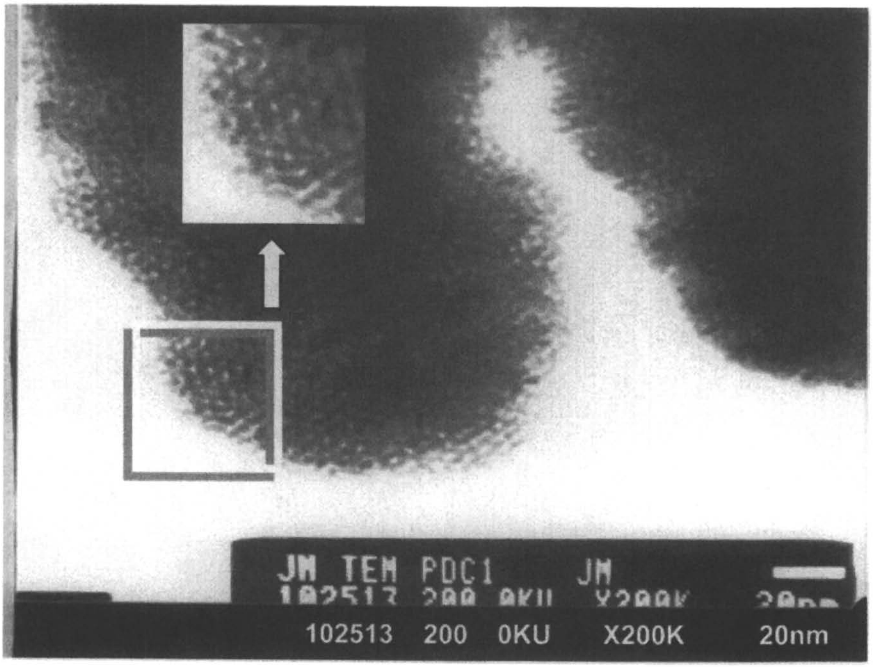

Figure 6. Transmission electron micrograph of a sample scraped from an H_I-e Pd film deposited from the template solution of 12 wt% $(NH_4)_2PdCl_4$, 47 wt% $C_{16}EO_8$, 39 wt% water, 2 wt% heptane on an evaporated gold electrode. The charge passed for deposition was 0.55 C/cm^2.

From all our experiments we conclude that the porous structure only appears at the edge of the TEM image of the Pd-film scraped from the electrode surface. Most of the image appears to be dark since the sample is too thick and therefore the electron beam cannot travel through.

Better evidence for a regular pore distribution in H_I-e Pd films may be given by X-ray diffraction. The Pd films formed by electrochemical deposition from the template mixture were studied by low-angle XRD. Figure 7 shows the low-angle XRD patterns obtained for the hexagonal phase of the Pd template mixture. The low-angle x-ray reflection of the Pd film shows a diffraction peak corresponding to the (100) diffraction plane of the hexagonal structure with a d-spacing of

Downloaded by UNIV OF GUELPH LIBRARY on July 1, 2012 | http://pubs.acs.org
Publication Date: August 1, 2008 | doi: 10.1021/bk-2008-0998.ch016

Downloaded by UNIV OF GUELPH LIBRARY on July 1, 2012 | http://pubs.acs.org
Publication Date: August 1, 2008 | doi: 10.1021/bk-2008-0998.ch016

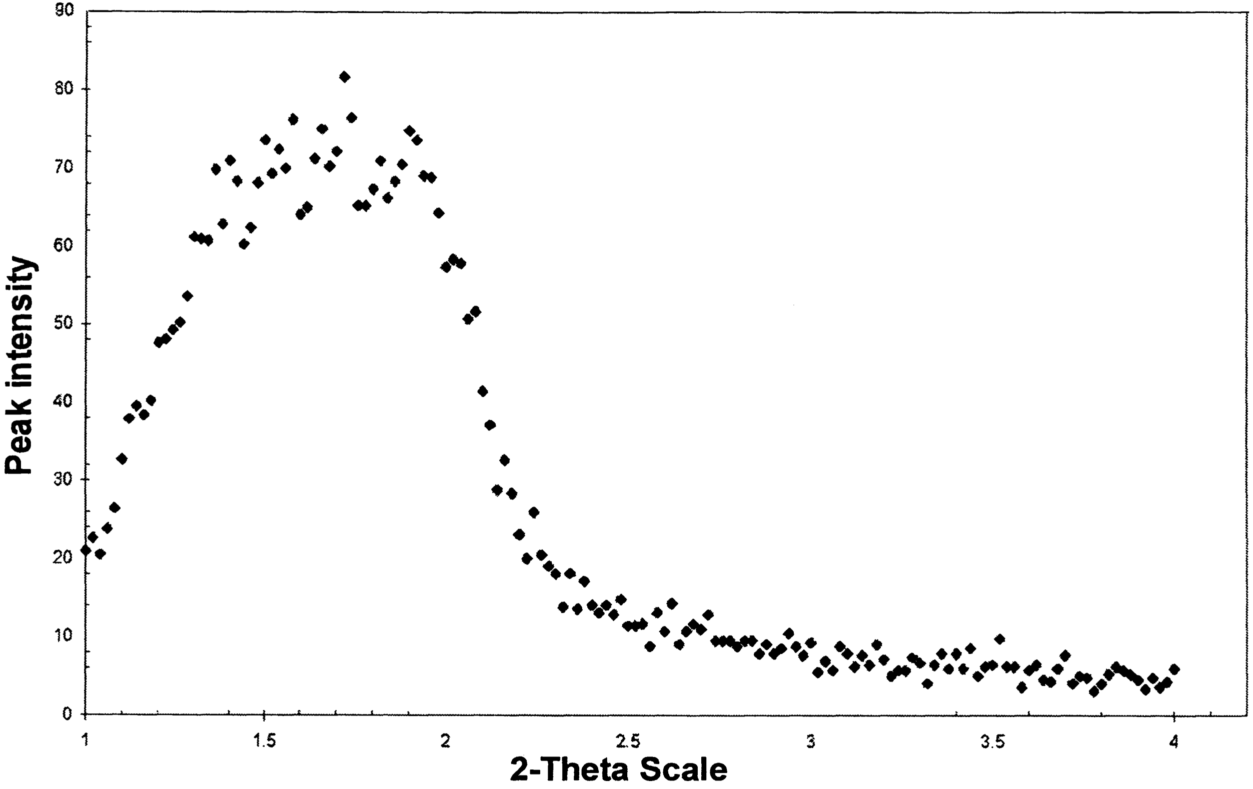

Figure 7. Low-angle x-ray reflection of an H_I-e Pd film deposited on an evaporated gold electrode from the template solution 12 wt% $(NH_4)_2PdCl_4$, 47 wt% $C_{16}EO_8$, 39 wt% water, 2 wt% heptane.

55 Å. This value was estimated using the Bragg equation. Although the peak maximum in Figure 7 appears to be broad, the value calculated for the d-spacing is consistent with the deposition of Pd films with a nanostructure of regular pore distribution derived from the structure of the template solution. The pore-to-pore distance for this hexagonal array, given by d_{100} / cos30 °, was found to be 63.5 Å.

Electrochemical Characterization of the Electroactive Surface Area

Cyclic voltammetric measurements were used to characterize the electrochemically active surface area of H_I-e Pd films estimated from the charge passed for the oxide stripping peak. To estimate the total surface area from the oxide stripping peak, Rand and Woods (*12-13*) used the conversion factor of 424 $\mu C/cm^2$. They investigated the voltammetry of polycrystalline Pd in 1 M sulfuric acid. We transferred this conversion factor to our studies (Figure 8), assuming that the surface oxide layer formed on our nanostructured Pd electrodes is the same as that formed on bulk Pd electrodes. We obtained a specific surface area of $91 m^2/g$ and an area per unit volume of $1.1 \times 10^7 cm^2/cm^3$, a value which is consistent with the nanostructure found by TEM and XRD and implies that the pores running throughout the nanostructured film are completely accessed by the electrolyte solution. Taking all prepared samples into account we found on average a variation in the estimated surface area of 20%.

Cyclic voltammetric measurements revealed the existence of high surface area Pd metal films electrochemically deposited on nanoscale. To access electrochemically the high surface area given by the nanostructure with the first cyclic voltammetric cycle it was necessary to soak the freshly prepared Pd films in acid media to replace the surfactant left in the pores of the nanostructure by the electrolyte solution. The longer the pores become due to the increase in thickness of the metal film the more time it takes to wash out the surfactant. Proceeding from the fact that we can obtain nanostructured Pd metal films by direct-templating from the liquid crystalline phases with access to the high electroactive surface area, we can now focus on the hydrogen region given in the cyclic voltammogram of these H_I–e Pd films.

Hydrogen Electrode Reaction

The hydrogen electrode reaction at transition metal electrodes can take place in alkaline as well as in acid media by the multistep sequence which can be described as the Volmer-Heyrovsky-Tafel-mechanism (*6, 14, 15*). The hydrogen electrode reaction on the metal surface is determined in detail by three well-known steps.

The first step in this process is the formation of adsorbed hydrogen on the metal surface originated from H atoms discharged from H_2O or H_3O^+ ions (Volmer reaction).

Downloaded by UNIV OF GUELPH LIBRARY on July 1, 2012 | http://pubs.acs.org
Publication Date: August 1, 2008 | doi: 10.1021/bk-2008-0998.ch016

$$H_3O^+ + e^- \rightarrow H^\bullet{}_{ads} + H_2O \tag{1}$$

$H^\bullet{}_{ads}$ represents the adsorbed hydrogen on the metal surface.

This is followed by either the electrochemical process (Heyrovsky reaction)

$$H^\bullet{}_{ads} + H_3O^+ + e^- \rightarrow H_2 + H_2O \tag{2}$$

or the chemical catalytic recombination-type desorption process (Tafel reaction).

$$H^\bullet{}_{ads} + H^\bullet{}_{ads} \rightarrow H_2 \tag{3}$$

The relative importance of the Tafel or Heyrovsky reactions depends on the electrode potential.

The hydrogen electrode reaction at palladium electrodes is further complicated by extensive permeation of atomic hydrogen into the metal lattice to form α- and β-hydride. In the literature no clear consensus has been found about the mechanism by which hydrogen enters the metal and in which way the adsorbed hydrogen is an intermediate between the adsorbed and absorbed hydrogen process. It has been suggested that the transition from the adsorbed to the absorbed state occurs via an intermediate subsurface state as dissolved hydrogen (*6, 14, 16*). The chemisorbed hydrogen then undergoes the diffusion from the metal surface into the bulk-metal in competition with the Tafel- and Heyrovsky reaction. According to this the relationship between the adsorption and absorption process can be represented as follows:

$$H^+ + e^- + M \Rightarrow MH_{ads} \Rightarrow MH_{diss} \Rightarrow MH_{abs} \tag{4}$$

This sequence indicates the formation of the subsurface layer where H occupies interstitial sites in the host lattice below the surface.

Electrochemical Measurements

Figure 8 shows the comparison between the H_I–e Pd film and the plain Pd film deposited from the aqueous solution. The total amount of charge used to deposit Pd for both films was the same. Outlining the differences between both voltammograms we can see that the charge estimated from the surface oxide stripping peak is much larger for the H_I–e Pd film than for the corresponding plain Pd film. This difference results from the greater surface area of H_I–e Pd due to the dense array of the cylindrical pores puncturing the film. However, it is notable that the oxidation and reduction processes occur at the same potential for both films.

The second striking difference which is apparent from the voltammograms is the fact that the two voltammograms differ significantly at more negative potentials. The H_I–e Pd film exhibits a very sharp pair of peaks (denoted by H_I

Downloaded by UNIV OF GUELPH LIBRARY on July 1, 2012 | http://pubs.acs.org
Publication Date: August 1, 2008 | doi: 10.1021/bk-2008-0998.ch016

and H_6) around -0.45 V vs SMSE with a smaller, broader pair of peaks (H_2 and H_5) at -0.52 V vs SMSE and then a rapidly increasing reduction current at the cathodic scan which is associated with the peak in the oxidation current at -0.625 V vs SMSE (H_3 and H_4) on the return scan. We can clearly see that this voltammogram at negative potentials is very different from the voltammetry of plain Pd. For plain Pd a rather featureless and unresolved peak can be seen. Similar results were obtained for a polycrystalline Pd wire (not shown). This difference in the voltammetry between the H_I–e Pd film and the plain Pd film is due to the presence of the nanostructure. The well-resolved pair of peaks of the H_I–e Pd film (H_1 and H_6) corresponds to the formation and removal of adsorbed hydrogen atoms at the Pd surface. This corresponds to the Volmer-reaction (Eq. (1)). The evidence for the attribution of the peaks H_1 and H_6 to the hydrogen adsorption is given in an experiment shown later in which crystal violet, known as inhibitor for the H-adsorption, suppresses H_1 and H_6.

Similar results have been obtained by Baldauf and Kolb (*17*) in studies of 1-10 monolayers Pd films deposited on gold single crystal. Tateishi et al. (*10-11*) also focused on cyclic voltammetric studies of small Pd particles supported on carbon electrode surfaces. In both cases well-resolved (not as well-resolved as in our studies) peaks of adsorbed hydrogen can be obtained caused by the fact that the current for the formation of absorbed hydrogen into bulk Pd does not dominate in the voltammetry as it does for bulk Pd electrodes.

For our H_I–e Pd films it was not possible to carry out voltammetric studies below 0.1 M without encountering significant distortion in the voltammetry. This was caused by the fact that significant concentration changes can be expected to occur within narrow pores in the structure during the voltammetry. If we refer, for example, to the charge passed in the peaks H_1 and H_6 59 and 88 μC in Figure 8 and convert this to the corresponding change in the proton concentration within the pores of the nanostructure, we find a change in the proton concentration on the order of several molar. In addition, at low electrolyte concentration or at high sweep rates, the voltammetry can be distorted by the IR drop occurring along the pores.

The existence of the hydrogen adsorption peak in the cyclic voltammetry was proved by Baldauf and Kolb (*17*) in showing that the mid-peak potential for the adsorbed H-couple varied with the proton concentration. In their studies the authors measured the dependence of the current peaks on the proton and sulfate concentration and noticed that the potential of one pair of the current peaks in the hydrogen region shifts linearly with proton concentration in a solution of constant sulfate concentration (0.1 M Na_2SO_4). The slope was estimated to be 60 mV $decade^{-1}$. On the other hand their data did not reveal any potential shift at constant pH when the sulfate concentration was altered. This shows evidently that this pair of current peaks is caused by the hydrogen adsorption reaction.

The second possibility to confirm the assignment of hydrogen adsorption peaks was also provided by Baldauf and Kolb (*17*) showing the influence of an appropriate surface modification on the hydrogen adsorption peaks. The addition of crystal violet to the solution completely blocks the H-adsorption but leaves the amount of hydrogen absorbed into the bulk Pd unaltered.

Downloaded by UNIV OF GUELPH LIBRARY on July 1, 2012 | http://pubs.acs.org
Publication Date: August 1, 2008 | doi: 10.1021/bk-2008-0998.ch016

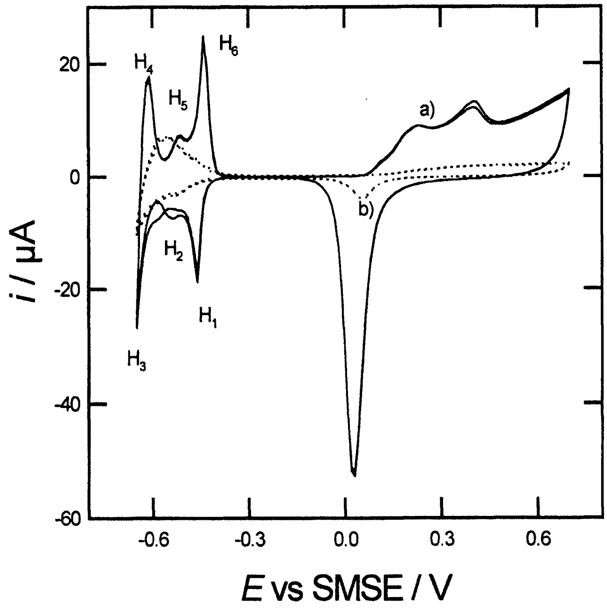

Figure 8. Cyclic voltammogram at 20 mV/s in 1 M sulfuric acid of H_I*-e Pd (0.53* cm^2*), a) deposited from the template mixture of 12 wt%* $(NH_4)_2PdCl_4$*, 47 wt% Brij® 56, 39 wt% water, 2 wt% heptane and Pd (0.052* cm^2*) b) deposited from the aqueous solution containing 50 mM* $(NH_4)_2PdCl_4$*, 1 M HCl and 1 M* NH_4Cl *on the gold electrode (1 mm electrode). The charge passed for deposition for both films was 3.5 mC.*

We also investigated the effect of crystal violet on the voltammetry. Figure 9 shows very similar results to those reported by Baldauf and Kolb (17). In the presence of 1 mM crystal violet the peaks H_1 and H_6 were totally suppressed confirming that they arise from the formation of the adsorbed hydrogen at the electrode surface. Based on the total charge passed for the formation of adsorbed hydrogen and comparing this to the charge of the corresponding oxide stripping peak, the H to the surface Pd ratio was found to be 0.20. In further experiments on hydrogen absorption, crystal violet plays an important role in influencing the rate of hydrogen sorption into the Pd metal lattice (shown later).

In our next experiment shown here we focused on the electrochemical adsorption/absorption features when loading hydrogen into Pd. It was of interest to first find out how much time the system requires until the hydrogen loading into bulk Pd is saturated. By comparing the peaks on the anodic sweep corresponding to the oxidation of absorbed hydrogen atoms in bulk Pd we realized that the area underneath the peak increases until the length of time of 120 s is reached. We did not find any significant increase in the area underneath the peak when hydrogen was loaded into the bulk Pd for more than 120 s. This was also

Downloaded by UNIV OF GUELPH LIBRARY on July 1, 2012 | http://pubs.acs.org
Publication Date: August 1, 2008 | doi: 10.1021/bk-2008-0998.ch016

Downloaded by UNIV OF GUELPH LIBRARY on July 1, 2012 | http://pubs.acs.org
Publication Date: August 1, 2008 | doi: 10.1021/bk-2008-0998.ch016

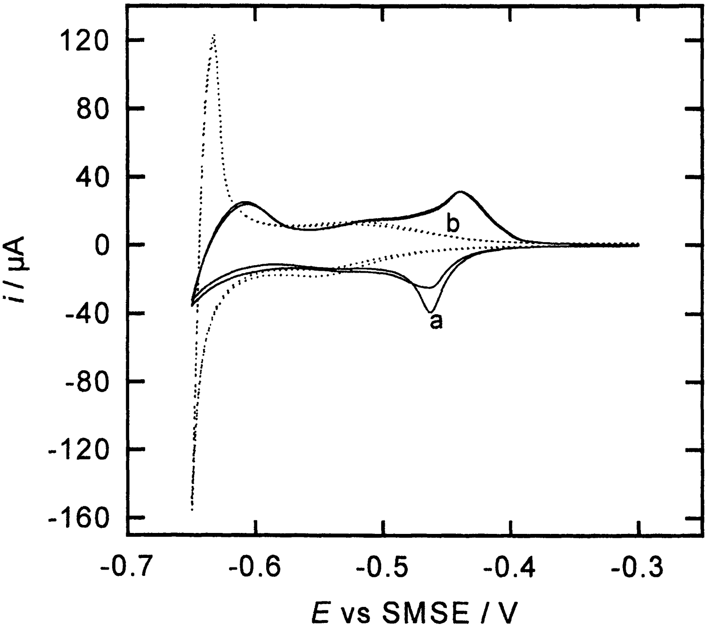

Figure 9. Cyclic voltammograms for a 200 nm thick H_I-e Pd film deposited onto a 1 mm diameter gold electrode recorded at 20 mV/s in 1 M H_2SO_4 without (curve a) and with (curve b) 1 mM crystal violet present.

found to be the case when the electrode was stepped to far negative potentials (-0.76 V vs SMSE). We therefore found the length of time of 120 s to absorb hydrogen into Pd bulk of our H_I–e Pd films sufficient to equilibrate at each potential.

Figure 10 shows the reverse scan of a typical cyclic voltammogram of H_I–e Pd at 10 mV/s in 1 M sulfuric acid after stepping the potential of the electrode from -0.56 V to -0.72 V vs SMSE and held at this potential for 120 s. The corresponding potential step experiment is shown as an inset in the same figure. On the reverse voltammetric sweep there are two well-resolved peaks. The peak at -0.6 V vs SMSE corresponds to the reduction of β-hydride, while the peak at -0.453 V vs SMSE corresponds to the reduction of the adsorbed hydrogen on the Pd surface. The oxidation occurs at the same potential as shown in Figure 8 for the pair of peaks H_1 and H_6. It is also of interest to note that the peaks in the voltammetry are better resolved than the corresponding peaks reported from similar experiments on thin Pd films (300 to 500 monolayer equivalents) by Czerwinski et al. (9). This indicates that the permeation of hydrogen into bulk-Pd and the H-adsorption on the Pd surface occurs for the H_I–e Pd films more rapidly than for thin Pd films studied by Czerwinski et al. (*9*). By decreasing the potential of the electrode below -0.65 V vs SMSE we obtain the resulting anodic

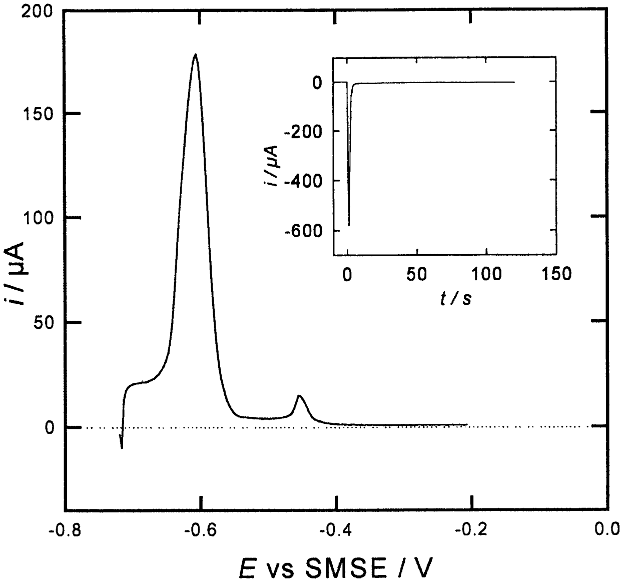

Figure 10. Example of a voltammgram for the oxidation of hydrogen absorbed and adsorbed on an H_I-e Pd film in 1 M H_2SO_4 recorded at 10 mV/s. The electrode was stepped from -0.2 to -0.72 V vs SMSE and held there for 120 s to load the electrode with hydrogen immediately before the anodic scan. The inset shows the corresponding current transient for loading the electrode with hydrogen at -0.72 V. The H_I-e Pd film was deposited (3.5 mC) from the Brij®56 plating bath onto a 1 mm diameter gold disc electrode.

voltammetric sweep from which the α- and the β-hydride phase can be clearly distinguished.

By carrying out a series of experiments in which the potential of the electrode was stepped to different cathodic values we integrate the charge passed in the reverse anodic sweep corresponding to the reduction of absorbed hydrogen and build up a plot of the charge as a function of the potential. We then converted the charge to the hydrogen/palladium ratio at each potential using the faradaic law and the total charge passed in the deposition of the Pd film. We considered the faradaic efficiency of 95% for the deposition of H_I–e Pd calculated from EQCM-measurements (*18*). The resulting plot for 3.5 mC (curve a) and 7 mC (curve b) as charge passed for deposition of H_I–e Pd films is shown in Figure 11. Below -0.55 V vs SMSE the H/Pd ratio increases slowly as the potential becomes more cathodic. This corresponds to the formation of α-hydride which is stable up to H/Pd less than about 0.05 (*19*). The sharp rise in the H/Pd ratio at -0.653 V (equivalent to 0.046 V vs SHE) corresponds to the formation of the β-hydride phase. Within the experimental error this is consistent with Czerwinski et al. (*9*) who carried out similar experiments on thin

Downloaded by UNIV OF GUELPH LIBRARY on July 1, 2012 | http://pubs.acs.org
Publication Date: August 1, 2008 | doi: 10.1021/bk-2008-0998.ch016

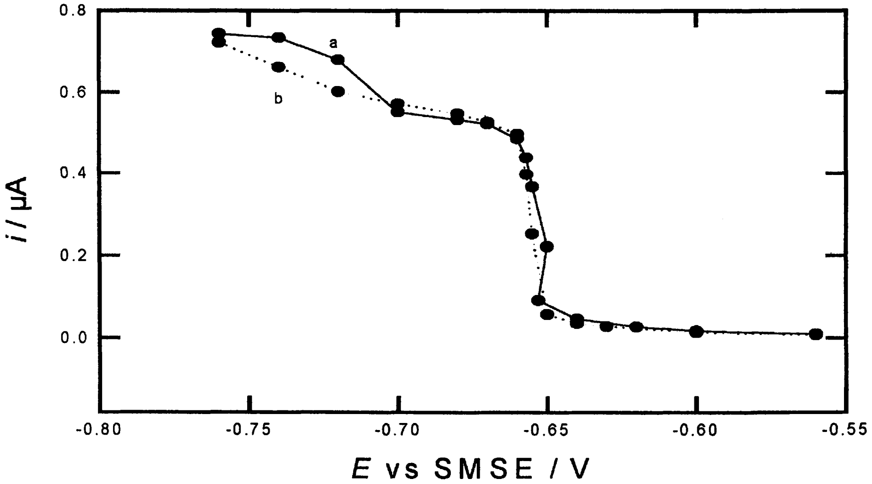

Figure 11. Plot of the H/Pd ratio as a function of potential for an H_I-e Pd film. The hydrogen loading of the electrode was determined from anodic voltammetric sweeps of the type shown in Figure 10 after stepping the electrode to different cathodic potentials. The total palladium loading was calculated from the charge passed to deposit the H_I-e Pd film – 3.5 mC (curve a) and 7 mC (curve b) for 1 mm diameter electrode – and the measured faradaic efficiency of 95% for the deposition.

Pd films (300 to 500 monolayers equivalent). The transition from the α- to the β-phase was reported to be -0.23 V vs SCE in 0.5 M H_2SO_4. It is of interest to note that the transition between both phases for an H_I–e Pd film occurs over a significantly smaller range (~20 mV as compared to ~50mV) in comparison to Czerwinski et al. (*9*).

Furthermore we can see from Figure 11 that at more cathodic potentials the H/Pd ratio curve tends towards a plateau at around -0.70 V before increasing again at potentials more negative than -0.70 V vs SMSE. This significant increase in the H/Pd ratio at negative potentials more than -0.70 V is unexpected and was not reported elsewhere in the literature. From the literature (*9*) we would normally expect the β-hydride phase to reach a plateau. If we return to the voltammetric anodic sweep of the H_I–e Pd film in Figure 10 we can see at potentials between -0.65 V to -0.72 V an additional current as contribution to the stripping charge. This additional current appears to be capacitative and can only be explained as a result of a nanostructured Pd film used in our studies where the surface area of the Pd film is large compared to the volume of the metal. It has also to be stressed that the physical properties of our H_I–e Pd film are not to be compared with those of a plain Pd film used by Czerwinski et al. (*9*). The surface area is essentially less. However, it is not clear why the double layer capacitance should be so much greater than that of the Pd metal.

Downloaded by UNIV OF GUELPH LIBRARY on July 1, 2012 | http://pubs.acs.org
Publication Date: August 1, 2008 | doi: 10.1021/bk-2008-0998.ch016

Effect of Surface Species

It is the focus of this section to investigate the effect of poisons on the process of hydrogen absorption into bulk palladium. We compare the peaks associated with the formation and oxidation of the β-hydride phase of palladium in a convenient range of potential with and without the addition of crystal violet to the sulfuric acid solution and with and without the submonolaver coverage of Pt on top of Pd.

The voltammetric features corresponding to the hydrogen absorption process seen for H_I-e Pd in the presence of crystal violet and for the Pt-Pd bilayer system are very similar (*20*), and therefore it is likely that they can be accounted for by a single mechanism. However, in all the experiments shown so far we have not provided the reader with the evidence that H-adsorption on the Pd surface disappears completely in the presence of Pt deposited on top of H_I-e Pd. In case the H-adsorption on the Pd surface is suppressed when Pt is deposited onto H_I-e Pd, it would extend the range of poisons from crystal violet (from which we know that it functions as an inhibitor blocking the H-adsorption) to Pt promoting the H-sorption into the metal lattice in a way that hydrogen diffuses directly into the bulk Pd without passing through the adsorbed state. In the next section we can demonstrate the absence of the hydrogen adsorption peak on H_I-e Pd when Pt was deposited on top of H_I-e Pd.

Figure 12 shows a set of cyclic voltammograms at 10 mV/s in 1 M sulfuric acid of H_I-e Pt deposited from the aqueous solution containing 25 mM H_2PtCl_6 and 1 M HCl onto H_I-e Pd with increasing number of Pt atoms covering the Pd surface. H_I-e Pd a) was initially deposited onto the gold disc electrode (0.0079 cm^2 area; 3.5 mC total deposition charge). We note that with increasing number of Pt atoms deposited onto H_I-e Pd a continuous shift in peak potential of the hydrogen absorption peak on the anodic sweep from a) -0.58 V to b) -0.595 V to c) -0.615 V appears. In addition, the H-absorption peak becomes increasingly sharper from a) 70 mV to b) 40 mV to c) 20 mV as values for the width at half height. The H-adsorption peak, seen in voltammogram a) and enlarged in the inset in Figure 12, disappears completely with subsequent Pt coverage in curve b) and c).

To conclude, increasing the thickness of H_I-e Pt deposited onto H_I-e Pd results in the disappearance of the H-adsorption peak. The H-absorption peak shifts in potential and becomes increasingly sharper. Hence the deposition of a dissimilar metal onto H_I-e Pd causes the inhibition of the H-adsorption onto the Pd surface enhancing the direct diffusion of H into the Pd metal. These features are similar to those seen for the voltammetry of H_I-e Pd where crystal violet was added to the acid solution to block the surface sites. These results are also consistent with those shown for the H_I-e Pt-Pd bilayer system (*20*) with the total deposition charge of 3.5 mC for each metal, where small amounts of Pt get onto the Pd surface in the pores. This causes the same effect as shown in the experiment described in Figure 12.

However, to accomplish this study as conclusively and properly as we can, we thought about an experiment in which the amount of crystal violet added to

Downloaded by UNIV OF GUELPH LIBRARY on July 1, 2012 | http://pubs.acs.org
Publication Date: August 1, 2008 | doi: 10.1021/bk-2008-0998.ch016

the acid solution varies significantly from 0.5 to 1 mM. This is necessary to show the reader the general effect of poisons on the hydrogen absorption process.

Figure 13 shows the same sort of experiment as in Figure 12, but for crystal violet surface coverage. We can see a set of cyclic voltammograms at 10 mV/s in 1 M sulfuric acid of H_l-e Pd deposited on a gold disc electrode. Figure 13 a) shows the cyclic voltammogram of an H_l-e Pd film electrode without crystal violet whereas b) and c) present the cyclic voltammograms of H_l-e Pd in the presence of crystal violet with increasing concentration of 0.5 mM b) and 1 mM c) corresponding to increasing surface coverage.

We observe similar behavior to that seen for the Pt-Pd bilayer system. With increasing concentration of crystal violet added to the acid solution, we note a continuous shift in peak potential of the hydrogen absorption on the anodic sweep from a) -0.58 V to b) -0.60 V to c) -0.61 V. Again, as already seen in the previous figure, the hydrogen absorption peak becomes increasingly sharper from a) 70 mV to b) 40 mV to c) 25 mV as values for the width at half height. The H-adsorption peak, present in voltammogram a), disappears completely with the addition of crystal violet.

Downloaded by UNIV OF GUELPH LIBRARY on July 1, 2012 | http://pubs.acs.org
Publication Date: August 1, 2008 | doi: 10.1021/bk-2008-0998.ch016

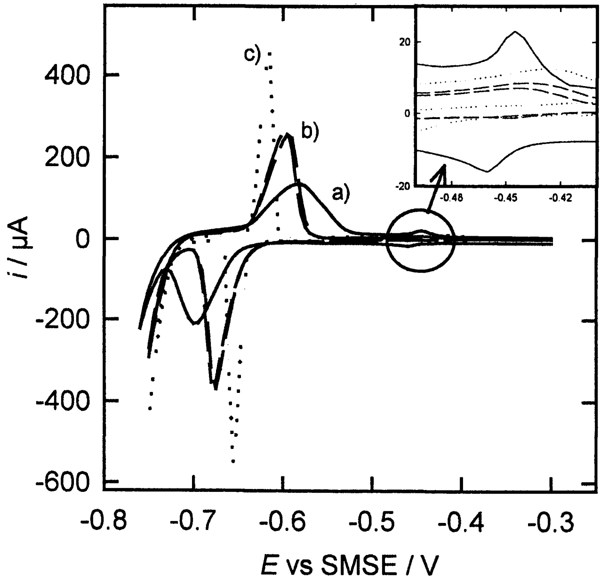

Figure 12. Set of cyclic voltammograms at 10 mV/s in 1 M sulfuric acid of Pt deposited from the aqueous solution containing 25 mM H_2PtCl_6 and 1 M HCl onto H_l-e Pd with increasing number of Pt atoms covering the Pd surface. H_l-e Pd a) was initially deposited onto a (0.0079 cm^2) gold disc electrode (3.5 mC total deposition charge). In curve b) 1 Pt atom and in curve c) 3 Pt atoms are deposited for every 10 Pd atoms. This corresponds to a Pt coverage on the Pd surface of 0.1 and 0.3 monolayers.

In showing the cyclic voltammetry of H_I-e Pd electrodes, we demonstrated convincingly the effect of blocking the Pd surface sites on promoting the hydrogen sorption into the metal lattice with increasing the amount of crystal violet and Pt covering the Pd surface. Since no difference has been found in the electrochemical properties between the Pt-Pd bilayer system and crystal violet added to the acid solution, we postulate that the same mechanism of H entry into the bulk Pd occurs in both cases and suggest that this occurs without passing through the adsorbed state.

Downloaded by UNIV OF GUELPH LIBRARY on July 1, 2012 | http://pubs.acs.org
Publication Date: August 1, 2008 | doi: 10.1021/bk-2008-0998.ch016

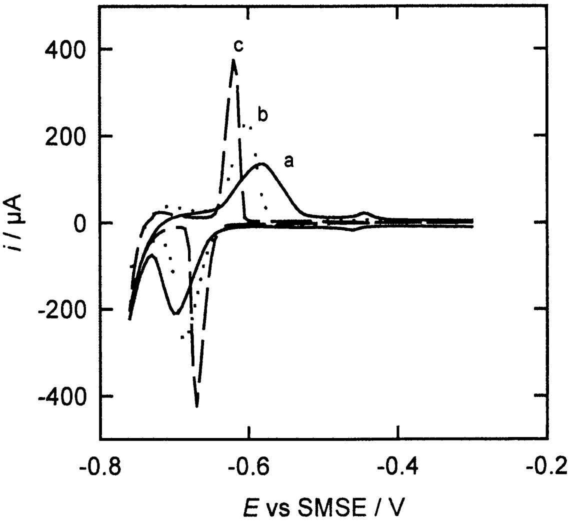

Figure 13. Set of cyclic voltammograms of H_I-e Pd (200nm thick, deposition charge 3.5 mC, deposited from the Brij®56 plating bath) deposited on a gold disc electrode (area 0.0079 cm^2) recorded at 10 mV/s in 1 M H_2SO_4 a) without crystal violet and in the presence of b) 0.5 mM and c) 1 mM crystal violet.

With the coverage of poisons onto the Pd surface and the inhibition of H-adsorption the H-absorption process speeds up so that faster kinetics could be seen in the voltammetries. To prove this as a general and consistent mechanism, we provided the reader with the evidence that the H-adsorption on the Pd surface disappears and the kinetics of the H-absorption become faster with increasing the coverage of platinum. This was also shown on H_I-e Pd electrodes in acid solutions to which an increasing amount of crystal violet was added.

References

1. Attard, G. S.; Bartlett, P. N.; Coleman, R. B.; Elliott, J. M.; Owen, J. R. Lyotropic Liquid Crystalline Properties of Nonionic Surfactant/Water/ Hexachloroplatinic Acid Ternary Mixtures Used for the Production of Nanostructured Platinum. *Langmuir* **1998**, *14*, 7340.
2. Attard, G. S.; Bartlett, P. N.; Coleman, N. R. B.; Elliott, J. M.; Owen, J. R.; Wang, J. H. Mesoporous Platinum Films from Lyotropic Liquid Crystalline Phases. *Science* **1997**, *278*, 838.
3. Attard, G. S.; Goeltner, C. G.; Corker, J. M.; Henke, S.; Templer, R. H. Liquid-Crystal Templates for Nanostructured Metals. *Angew. Chem. Int. Ed.* **1997**, *36*, 1315.
4. Mitchell, D. J.; Tiddy, G. J. T.; Waring, L.; Bostock, T.; Donald, M. P. M. Phase Behaviour of Polyoxyethylene Surfactants with Water. *J. Chem. Soc. Faraday Trans. I* **1983**, *79*, 975.
5. Chevillot, J.-P.; Farcy, J.; Hinnen, C.; Rousseau, A. Electrochemical Study of Hydrogen Interaction with Palladium and Platinum *J. Electroanal. Chem.* **1975**, *64*, 39.
6. Conway, B. E.; Jerkiewicz, G. Thermodynamic and Electrode Kinetic Factors in Cathodic Hydrogen Sorption into Metals and its Relationship to Hydrogen Adsorption and Poisoning. *J. Electroanal. Chem.* **1993**, *357*, 47.
7. Czerwinski, A.; Marassi, R.; Zamponi, S. The Absorption of Hydrogen and Deuterium in Thin Palladium Electrodes. Part I: Acidic Solutions. *J. Electroanal. Chem.* **1991**, *316*, 211.
8. Lewis, F. *The Palladium-Hydrogen System*; Academic Press: London, 1967.
9. Czerwinski, A.; Marassi, R. The Adsorption of Hydrogen and Deuterium in Thin Palladium Electrodes. Part II: Basic Solutions *J. Electroanal. Chem.* **1992**, *322*, 373.
10. Tateishi, N.; Yahikozawa, K.; Nishimura, K.; Takasu, Y. Hydrogen Electrode Reaction on Electrodes of Glassy Carbon-Supported Ultrafine Pd Particles in Alkaline Media. *Electrochimica Acta* **1992**, *37*, 2427.
11. Tateishi, N.; Yahikozawa, K.; Nishimura, K.; Suzuki, M.; Iwanaga, Y.; Watanabe, M.; Enami, E.; Matsuda, Y.; Takasu, Y. Electrochemical Properties of Ultrafine Palladium Particles for Adsorption and Absorption of Hydrogen in an Aqueous $HClO_4$ Solution. *Electrochimica Acta* **1990**, *36*, 1235.
12. Rand, D. A. J.; Woods, R. A Study of the Dissolution of Platinum, Palladium, Rhodium and Gold Electrodes in 1M Sulfuric Acid by Cyclic Voltammetry. *J. Electroanal. Chem.* **1972**, *35*, 209.
13. Rand, D. A. J.; Woods, R. The Nature of Adsorption Oxygen on Rhodium, Palladium and Gold Electrodes. *J. Electroanal. Chem.* **1970**, *31*, 29.
14. Mengoli, G.; Bernardini, M.; Fabrizio, M.; Manduchi, C.; Zannoni, G. The Insertion/Extraction of Deuterium (Hydrogen) at Pd Sheet Electrodes in D_2O (H_2O) + LiOD (LiOH) Electrolyte. *J. Electroanal. Chem.* **1996**, *403*, 143.

Downloaded by UNIV OF GUELPH LIBRARY on July 1, 2012 | http://pubs.acs.org
Publication Date: August 1, 2008 | doi: 10.1021/bk-2008-0998.ch016

15. Zhang, W. S.; Zhang, X. W.; Li, H. Q. The Maximum Hydrogen (Deuterium) Loading Ratio in the Pd/H_2O (D_2O) Electrochemical System. *J. Electroanal. Chem.* **1997**, *434*, 31.
16. Czerwinski, A.; Kiersztyn, I.; Grden, M.; Czapla, J. The Study of Hydrogen Sorption in Palladium Limited Volume Electrodes (Pd-LVE). I. Acidic Solutions. *J. Electroanal. Chem.* **1999**, *471*, 190.
17. Baldauf, M.; Kolb, D. M. A Hydrogen Adsorption and Absorption Study with Pd Overlayers on Au(111) and Au(100). *Electrochimica Acta* **1993**, *38*, 2145.
18. Guerin, S. Planar Pellistors: An Application of Electrodeposited Mesoporous Palladium Films for the Detection of Combustible Gases. Ph.D. thesis, Southampton University, Department of Chemistry, Southampton, U.K., 1999.
19. Rafizadeh, H. A. Lattice Dynamics of Metal Hydride. *Phys. Rev. B* **1981**, *23*, 1628.
20. Bartlett, P. N.; Marwan, J. Electrochemical Deposition of Nanostructured (H_{I}-E) Layers of Two Metals in Which Pores within the Two Layers Interconnect. *Chem. Mater.* **2003**, *15*, 2962.

Downloaded by UNIV OF GUELPH LIBRARY on July 1, 2012 | http://pubs.acs.org
Publication Date: August 1, 2008 | doi: 10.1021/bk-2008-0998.ch016

Author Index

Chaudhary, Irfan U., 249
Chubb, Scott R., 99
Cravens, Dennis, 337
Dardik, I., 219
De Ninno, A., 127
Del Giudice, E., 127
El Boher, A., 219
Fleischmann, Martin, 19, 153
Forsley, Lawrence P. G., 311
Frattolillo, A., 127
Gordon, Frank E., 311
Greenspan, E., 219
Hagelstein, Peter L., 249, 337
Kornilova, Alla A., 295
Krivit, Steven B., 3
Letts, Dennis, 337
Li, X. Z., 39
Liu, B., 39
Marwan, Jan, 353
McKubre, M. C. H., 219
Miles, Melvin H., 153
Miley, George H., 173
Mizuno, Tadahiko, 271
Mosier-Boss, Pamela A., 311
Shrestha, Prajakti J., 173
Sibilia, C., 219
Storms, Edmund, 85
Szpak, Stanislaw, 311
Takahashi, Akito, 57
Tanzella, F. L., 219
Tashyrev, Alexandr B., 295
Violante, V., 219
Vysotskii, Vladimir I., 295
Wei, Q. M., 39
Yabuuchi, Norio, 57
Zilov, T., 219

Downloaded by 89.163.34.136 on July 1, 2012 | http://pubs.acs.org
Publication Date: August 1, 2008 | doi: 10.1021/bk-2008-0998.ix001

Subject Index

A

Accelerators, reactions, 40
Accuracy
  precision and, of calorimetric systems, 153–154, 168
  sources of error in calorimetry measurements, 192*t*
  See also Isoperibolic calorimetry
Active isotopes, controlled decontamination of, in biological cells, 304, 306–308
After-effect, phenomenon, 32
Ag/Pd/D co-deposition
  images for, in magnetic field, 316, 318*f*
  See also Pd/D co-deposition
Alpha emission, testing theory, 90–91
Alpha particles
  energy distribution, 205, 206*f*
  energy range study for, 196, 197*f*
  picture under microscope, 198*f*
  simultaneous emission of protons and, 208
  See also Charged particles
Alumina/Pd-Ni cathodes, heat generation, 190
Americium-241 source, images of pits for CR-39 detector exposed to, 316, 317*f*
Anomalous energy exchange
  dimensionless coupling strength g, 251–252
  dynamics, 252, 254
  interaction strength V, 251
  level anticrossing, 252
  level splitting at level anticrossing vs. g, 253*f*
  lossless model, 265
  model, 251–254
  perturbation, 255
  plot of $\Delta E(g)$ vs. g, 253*f*
  rotated Hamiltonian, 254
  rotation, 254–256
  rotation energy levels, 255–256
  spin-boson Hamiltonian, 251
  unitary operator $\hat{U}$, 254
  unperturbed part of rotated Hamiltonian, 255
Assumptions, mathematical logic and, 86
Asymptotic Freedom (AF), objection against cold fusion, 128
Atomic distributions, elements for samples before and after electrolysis, 278*f*
Atomic ratio, palladium surface before and after electrolysis, 277*f*
Au cathode, pits from Pd/D co-deposition in magnetic field, 316, 319*f*

B

Barium, discovery, 39
Barrier factor
  calculated, for 2d-pair and 4d-cluster, 78*t*
  equation, 75
Beam-target experiment, 3-deuteron fusion reaction, 48*f*
Beat frequency
  cell response at, 14.5 THz, 343, 345*f*
  cell response at, 18.3 to 18.7 THz, 347, 348*f*

Downloaded by 89.163.34.136 on July 1, 2012 | http://pubs.acs.org
Publication Date: August 1, 2008 | doi: 10.1021/bk-2008-0998.ix002

  - cell response at, 19.4 THz, 341, 343, 344*f*
  - cell response at, 19 to 21.4 THz, 347, 349*f*
  - cell response at, 8.3 THz, 343, 346*f*, 348*f*
  - cell response to, stimulation, 341, 343
  - optical phonon modes, 349–350
  - sensitivity of system to, 347, 348*f*, 349*f*
  - *See also* Palladium deuteride and laser stimulation

Beating phenomenon, momentum transfer to quasi-particles, 118–119

Beta emission, testing theory, 91

Biological systems
  - accelerated deactivation of Cs^{137} isotope in "biological cells", 307*f*
  - controlled decontamination of long-lived active isotopes in, 304, 306–308
  - isotope transmutation, 296–297
  - transmutation of isotopes, 296
  - *See also* Microbiological associations

Blastocladiella emersonii, substitution of K^+ for Rb^+ and Ba^{2+} ions, 308

Bloch oscillations, 118

Bloch's theorem
  - generalized form, 117
  - multiple scattering theory, 113, 115
  - Zener tunneling, 118–119

Bloch symmetry, 105

Boil-offs, excess heat after, 9–10

Born-von Karman boundary conditions
  - not requiring, 115
  - requiring, 109

Borosilicate glass cover slip, spacer between cathode and detector, 323, 325*f*

Boundaries, solids, 103

Bragg resonant scattering, trapping photons, 101

Bragg scattering of light, coupling to electrons and deuterons, 116

Bravais lattice vectors, defining spatial displacements, 109

Brij® 56, phase diagram of surfactant, 358–359, 360*f*

C

Calibrations
  - calorimeters, 224*f*
  - SRI replication, 223, 225

Calorimetry
  - cell designs, 154, 155*f*
  - correlation between excess heat and abnormal deuterium flux, 49–50, 51*f*
  - electrode reactions, 26
  - ENEA replication, 231, 235*f*, 236
  - equations, 154, 157–162
  - excess heat, 6, 8*f*
  - isoperibolic, 220–221
  - Pd-D system, 26
  - precision and accuracy, 153–154, 168
  - replicating isoperibolic calorimetry, 220
  - self-sustaining reactor and neutrino emission, 50
  - sources of error of measurements, 191*t*
  - *See also* Isoperibolic calorimetry

Cesium, X-ray photoelectron spectroscopy (XPS), 184*f*

Cesium-137 isotope
  - accelerated deactivation in "biological cells", 307*f*
  - possible reaction for utilization, 306
  - transmutation, 306, 308
  - *See also* Microbiological associations

Downloaded by 89.163.34.136 on July 1, 2012 | http://pubs.acs.org
Publication Date: August 1, 2008 | doi: 10.1021/bk-2008-0998.ix002

Charge
  propagation through quasi-particle wave-packets, 114
  relationship to mass, velocity and momentum, 103–104
Charged particle collisions, Bloch oscillations, 118
Charged particles
  alpha peak at large background during for open CR-39, 199*f*
  alpha-track picture under microscope, 198*f*
  alpha-tracks energy distribution after background subtraction, 206*f*
  background measurement with Cu film covering CR-39, 200*f*
  comparing open and shielded detectors, 201
  CR-39 detection efficiency, 196
  CR-39 plastic track detectors, 196
  emission during electrolysis of metal thin-film cathodes, 203*t*
  energy range study for alpha-sources, 197*f*
  experimental technique, 196, 198, 201
  foreground and background runs for Cu-covered CR-39 study, 204*f*
  foreground and background runs for open CR-39, 202*f*
  Landauer CR-39 Van de Graaff proton calibration curve, 197*f*
  production during thin-film electrolysis, 195–205
  proton energy distribution after background subtraction, 206*f*
  study results, 201, 205
  See also Transmutation studies
Chemical potential, d in palladium, 135, 136*f*
Chemistry, nuclear processes, 19, 20*f*
Chemists, scientific discovery, 39–40
Chromium
  abundant amounts of Cr detection, 284
  comparing isotopic and natural distributions, 285, 289*f*
  concentration profiles for Cr isotopes, 289*f*
  Cr isotopes, 284–285
  element analysis techniques, 273–275
  profiles of Cr isotope ratio in Pd, 289*f*
  See also Electrolysis
Co-deposition experiments
  low energy nuclear reactions in PdD, 120
  See also Pd/D co-deposition
Coherence domains
  cold fusion, 130–131
  electromagnetic field, 132
  fusion, 145, 148
Coherent dynamics, cold fusion, 130–131
Cold explosions, energy release, 129
Cold fusion
  alpha emission, 90–91
  beta emission, 91
  calibrations of Icarus cell for Pd-D system, 27*f*, 28*f*
  coherent dynamics in, 130–131
  Coulomb barrier, 87
  division of solid phases into coherent and incoherent, 25
  electrolytic charge of palladium cathodes with deuterons, 25
  energy output of, 131, 132*f*
  excess enthalpy generation, 29, 31
  excess heat, 5, 131
  gamma emission, 92
  inherent irreproducibility, 26
  mathematics and assumptions, 86
  measurement of thermal balances, 25
  media labeling field, 3
  neutron emission, 88–90

Downloaded by 89.163.34.136 on July 1, 2012 | http://pubs.acs.org
Publication Date: August 1, 2008 | doi: 10.1021/bk-2008-0998.ix002

objections, 128
panel for review, 4, 13
phenomenon, 85, 128
proton layer oscillations on Pd surface, 129
public confusion, 5
research milestones, 30*t*
scheme of research leading to, 20*f*
selectivity towards surface diffraction, 22, 24*f*
surface x-ray diffraction, 22, 23*f*
terminology of Q.E.D., 21–22
testing theory, 87–92
thin-film palladium cathode after, experiment, 132*f*
true believers and true unbelievers, 128
variety of "cold fusion"-like nuclear reactions, 174, 175*f*
See also Isoperibolic calorimetry

Cold fusion experiment
black diagram of cell and helium sampling circuit, 141*f*
chemical potential μ of d in Pd, 135, 136*f*
content of ^{4}He in heavy-water experiments, 140
electrolytic loading of extended deposition and loading of strip, 135, 137*f*
experimental design, 137–142
features of palladium hydrides (Pd-H), 134
giant dipole resonance (GDR), 145, 148
^{4}He production from electrolytic cell, 145*t*
mass spectroscopy techniques, 139
measurements, 144
nuclear microfurnaces, 144
Nuclear Shell Model, 145
nuclear transmutations at low energies, 145, 148
objections by scientific community, 133
overall outcome, 142, 146*f*, 147*f*
palladium cathode geometry for, 138, 139*f*
QED (quantum electrodynamics) coherence, 145, 148
QED description of Pd-H system, 133–135
Quadrupole Mass Analyzer (QMA), 139, 140*f*
resistance, 135
theoretical framework, 138
theoretic prediction of QED, 133
unpredictability of start and stop time of excess heat, 137–138
values of ionic current by QMA, 140*f*

Cold nuclear fusion (CNF), phenomenon, 296

Cole nuclear synthesis, phenomenon, 297

Collisions, degeneracies, 102

Columbia resin 39 (CR-39)
solid state nuclear track detector, 311–312
See also Pd/D co-deposition

Condensed matter heat production
cathodes by Energetics and SRI, 221
comparing SRI and ENEA experimentation, 245
ENEA replication, 231, 236–241
Energetics excess power results for cell ETE 64, 221, 222*f*
heat effects, 243–244
incidence of excess heat vs. maximum D/PdD loading, 245, 246*f*
isoperibolic calorimetry results, 220–221
loading, 244–245
SRI energetics replication plan, 221, 223
SRI replication, 223–231
superwave stimulus, 245

Downloaded by 89.163.34.136 on July 1, 2012 | http://pubs.acs.org
Publication Date: August 1, 2008 | doi: 10.1021/bk-2008-0998.ix002

  See also ENEA replication; SRI Energetics replication
Condensed matter nuclear science (CMNS)
  field, 3–4
  See also Low energy nuclear reactions (LENR)
Conservation, momentum and energy, 101–102, 250
Constructive interference, occurrence, 102
Controlled decontamination
  active isotopes in biological cells, 304, 306–308
  See also Biological systems
Copper(II) chloride, co-deposition experiments, 316, 318
Coulomb barrier
  quantum electro-dynamic (QED) barrier vs., 104
  resonance or tunneling, 87
Coupling, larger metal crystals, 100
Crystal violet, voltammetry, 366–367, 368*f*, 373*f*
Current perturbation, SRI replication, 225–226
Cyclic voltammetry
  effect of crystal violet, 366–367, 368*f*, 373*f*
  electroactive surface area, 364
  reverse scan, 368, 369*f*
  See also Nanostructured palladium hydride system

D

Dalton's Law of Partial Pressures, gas pressure within cell, 158
Decontamination of active isotopes
  controlled, in biological cells, 304, 306–308
  See also Biological systems
Degeneracy
  associated coupling, 102
  collisions, 102
  simplest forms of, 113–114
  symmetry, 111
Deinicocus radiodurans, nuclear reactions, 297
Delocalization, quantum field theory, 128–129
Deposition experiments
  nanostructured materials, 354
  See also Nanostructured palladium hydride system; Pd/D co-deposition
Detectors. *See* Pd/D co-deposition
Deuterium
  byproducts of palladium-D experiments, 7
  gas permeation through palladium complex, 184*f*, 185*f*
  low energy nuclear reaction (LENR), 6
  Pd/D system investigation, 25–26
  See also Pd/D co-deposition
Deuterium flux, correlation between excess heat and abnormal, 49–50, 51*f*
3-Deuteron fusion reaction
  beam-target experiment, 48*f*
  resonant tunneling, 48–49
Deuterons
  coupling by Bragg scattering of light, 116
  electrolytic charge of palladium cathodes with, 25
  nuclear potential well, 40
  See also 4D/tetrahedral symmetric condensate (4D/TSC)
Deuteron-triton, hot fusion data, 42
Direct thermal imaging, hot spots on surfaces of electrodes, 31–32
4D/tetrahedral symmetric condensate (4D/TSC)
  4D fusion rates, 73, 75–80
  acryonyms, 59
  barrier factor, 75

Downloaded by 89.163.34.136 on July 1, 2012 | http://pubs.acs.org
Publication Date: August 1, 2008 | doi: 10.1021/bk-2008-0998.ix002

Downloaded by 89.163.34.136 on July 1, 2012 | http://pubs.acs.org
Publication Date: August 1, 2008 | doi: 10.1021/bk-2008-0998.ix002

  barrier factors for 2d-pair and 4d-cluster, 78*t*
  d-d trapping potential of, 72, 76*f*
  distortion of double platonic arrangement, 71*f*
  distortion of system Coulomb energy by d-d distance fluctuation, 64–68
  empirical treatment for multi-body interaction, 58
  expectation position and Platonic symmetry, 80
  friction term of Langevin equation, 71, 75*f*
  fusion rate equations, 76, 77
  fusion rates by Fermi's golden rule, 76, 79*t*
  fusion yield, 79
  Gamow integral, 73, 75
  Gaussian squared wave function for d-d pair, 63*f*
  Gaussian wave function and shielded trapping Coulomb potential for Cooper-pair dd molecule, 70*f*
  Gaussian wave function and shielded trapping Coulomb potential for D_2 molecule, 69*f*
  Gaussian wave function and shielded trapping Coulomb potential for ddμ molecule, 67*f*
  Gaussian wave functions, 61–64
  heavy mass electronic quasi-particle expansion theory (HMEQPET) method, 71–73
  illustration of, condensation motion to TSC-min state, 61*f*
  Langevin calculation results for 4D/TSC motion, 72*f*
  mean particle kinetic energies of "dede" system of TSC, 72, 77*f*
  microscopic fusion yield, 77–78
  model of 4D/TSC formation in PdDx lattice, 60*f*
  models, 58–59
  molecular dynamics motion of, 58
  non-linear Langevin equation for TSC motion, 59–61
  numerical solution by Verlet method, 68–71
  optical potential <W> values, 76–77, 79*t*
  parameters for HMEQPET potentials, 74*t*
  potential for balancing force term, 70, 74*f*
  quantum mechanical electron cloud for, 62*f*
  quantum mechanical fluctuation of deuteron positions, 61–73
  screened tapping Coulomb potential of EQPET dde* molecule, 63*f*
  search for ground state d-d distance and d-d pair energy values, 66*f*
  selection of Gaussian wave function for dd-muon, 65*f*
  system Hamiltonian with reduced mass, 63
  wave function and trapping Coulomb potential for muonic-dt molecule, 68*f*
Dynamics, energy exchange, 252, 254
Dynamic trigger, parameter for excess heat, 9

E

Efficiency, charged particle detection, 196
Electric fields
  effect on palladium/deuterium system, 312–314
  See also Pd/D co-deposition
Electrochemical deposition
  nanostructured hydride system, 354
  See also Nanostructured palladium hydride system

Electrochemistry, electroactive surface area, 364
Electrochemists, generating nuclear energy as heat, 3–4
Electrode design
  Massive Cluster Electrode (MCE), 183
  thin-film plate-type, at University of Illinois, 176, 179*f*
  transmutation reactions, 176
Electrode reactions, calorimetry, 26
Electrodiffusion
  deuterium in palladium, 31
  hydrogen in Pd lattice, 129
Electrodynamical considerations, stressing metal, 104
Electrolysis
  abundant amounts of Cr detection, 284–285
  atomic concentration profiles normalized with total concentration value, 279, 282*f*, 283*f*
  atomic distributions of elements before and after, 278*f*
  atomic ratio for Pd surface layer before and after, 277*f*
  Auger electron spectroscopy (AES) method, 274–275
  changes of temperature, pressure and D/Pd ratio during, 274*f*
  charged particle emissions during thin-film, 203*t*
  charged particle production during thin-film, 196–205
  comparing isotopic distributions with natural distributions, 285, 289*f*
  concentration profiles for Cr isotopes, 289*f*
  concentration profiles for Ni isotopes, 291, 292*f*
  concentration profiles for Pd isotopes, 285, 290*f*, 291, 293*f*
  Cr50 isotope, 284
  Cr52 isotope, 284
  Cr53 isotope, 284
  Cr54 isotope, 285
  distribution of deposited elements on electrode surface, 275
  EDX (energy dispersive X-ray spectroscopy) measurements, 274
  EDX spectrum of Pd electrode surface electrolyzed in heavy water, 276*f*
  electrochemical reactions inducing nuclear reactions, 271–272
  electron probe micro analyzer (EPMA) method, 274
  element analysis, 273–275
  excess heat production during thin-film, with transmutations, 186–192
  experimental, 272–275
  intensity ratios based on counts before and after, 284, 286*f*, 287*f*
  intensity ratios for mass spectra for, in heavy and in light water, 284, 288*f*
  intensity ratios for mass spectra for, in heavy water with and without excess heat, 284, 288*f*
  interference species for Ni isotopes, 285, 291*t*
  palladium atomic concentration vs. depth, 285
  photo of cell, 273*f*
  procedure, 272–273
  procedure for determining mass numbers, 275, 277
  profiles of Cr isotope ratio in Pd, 289*f*
  profiles of Ni isotope ratio in Pd, 285, 291, 292*f*
  profiles of Pd isotope ratio in Pd rod, 285, 290*f*, 291, 293*f*
  sample and cell details, 272–273
  secondary ion mass spectroscopy (SIMS) method, 274

Downloaded by 89.163.34.136 on July 1, 2012 | http://pubs.acs.org
Publication Date: August 1, 2008 | doi: 10.1021/bk-2008-0998.ix002

  - SIMS count spectra for Pd before and after, 279, 280*f*, 281*f*
  - typical counts by EDX and SIMS, 279

Electrolysis of heavy water, low energy nuclear reactions, 12

Electromagnetic fields
  - coherence domain, 132
  - trapped photons, 121

Electromagnetic interaction (EMI). *See* Resonant electromagnetic interaction (EMI)

Electrons
  - coupling by Bragg scattering of light, 116
  - propagation in regions where wave equations apply, 115–116

Elements
  - atomic distributions of, for samples before and after electrolysis, 278*f*
  - atomic ratio for palladium surface before and after electrolysis, 277*f*
  - frequency of observations for transmutations, 179, 180*f*
  - intensity ratio between SIMS counts before and after electrolysis, 284, 286*f*, 287*f*
  - intensity spectra normalized with total concentration, 279, 282*f*, 283*f*
  - secondary ion mass spectrometry (SIMS) counts for Pd cathodes, 279, 280*f*, 281*f*
  - *See also* Electrolysis

Emissions, metallic-hydride or metallic-deuteride compounds, 100

ENEA replication
  - calorimeter, 231, 236
  - comparison to SRI replication, 245, 246*f*
  - evolution of input and output power and energy, 236, 238*f*
  - evolution of input and output power for cathode L17, 236, 240*f*
  - excess power during superwave current treatment, 236, 239*f*
  - flow calorimeter electrochemical cell, 235*f*
  - lifetime of excess power burst, 241
  - power burst and electrolyte temperature, 236, 240*f*
  - successful attempts, 241*t*
  - system overview, 237*f*
  - *See also* Condensed matter heat production; SRI Energetics replication

Energetics
  - calorimeters and cells, 241, 243
  - SRI replication plan, 221, 223
  - *See also* SRI Energetics replication

Energy
  - conservation, 112
  - conservation of momentum and, 101–102, 250
  - excitation transfer mechanism violating local, conservation, 264
  - growth with increasing time, 103
  - nuclear reaction, 87
  - quantum excitation transfer effect, 250

Energy balance
  - calculations for thin-film experiments, 195*f*
  - He-4 production, 107
  - low energy nuclear reactions, 207–208

Energy band theory, generalization of semi-classical model, 104

Energy distribution
  - alpha-tracks, 205, 206*f*
  - proton, 205, 206*f*

Energy exchange
  - excitation transfer and, 260–261
  - *See also* Anomalous energy exchange

Downloaded by 89.163.34.136 on July 1, 2012 | http://pubs.acs.org
Publication Date: August 1, 2008 | doi: 10.1021/bk-2008-0998.ix002

Downloaded by 89.163.34.136 on July 1, 2012 | http://pubs.acs.org
Publication Date: August 1, 2008 | doi: 10.1021/bk-2008-0998.ix002

Energy/nucleon balances, transmutations and excess heat, 193–196
Energy output, cold fusion, 131
Energy range
  alpha-sources, 196, 197*f*
  See also Charged particles
Energy release, low energy nuclear reactions, 9
Enthalpy
  excess, generation, 29, 31
  extreme, generation, 32
  nature of nuclear reaction
    generating excess, 132
  rate of, removal by gas stream,
    158–159
Enthalpy of vaporization of D_2O, L
  equation, 158
  values at several temperatures,
    159*t*
Environmental issues, low energy nuclear reactions, 12
Error analysis, excess heat, 190, 192
Escherichia coli, nuclear reactions, 297
Excess energy, coherence dynamics, 131
Excess enthalpy
  generation, 29, 31, 167
  nature of nuclear reaction
    generating, 132
Excess heat
  accuracy and error of calorimetry measurements, 191*t*
  after boil-offs, 9–10
  alumina/Pd-Ni cathodes, 190
  binding energies to compute theoretical excess power, 193
  burst with laser stimulation, 338
  byproducts of palladium-deuterium experiments, 7
  calorimeter "heat recovery" value R, 188, 189*t*
  cold fusion, 5, 131
  computation of excess power, 193*f*
  correlation between, and abnormal deuterium flux, 49–50, 51*f*
  correlation between transmutation products and, 192–196
  electrolysis results, 188–190
  Energetics reproducing, 221, 222*f*
  energy balance calculations for three thin-film experiments, 195*f*
  energy/nucleon balances, 193–196
  error analysis, 190, 192
  experimental technique, 187–188
  Fleischmann–Pons experiment, 249, 250
  metal-hydrogen electrochemical systems, 187
  nuclear energy without strong nuclear radiation, 50, 52
  parameters of electrolysis and R values for Pt-Pt runs, 189*t*
  production during thin-film electrolysis with transmutations, 186–192
  production rate vs. mass number, 191*f*
  Pt-Pt electrodes, 189
  reaction pathways and reaction product-heat relationship, 192–193
  required threshold parameters for, 7, 9
  thin-film electrolysis with transmutations, 186–192
  unpredictability of start and stop time, 137–138
  See also Fleischmann–Pons experiment modeling; Transmutation studies
Excess power
  binding energies computing theoretical, 193
  calculation, 229
  calorimetry for first 500 hours of cell, 231, 233*f*, 234*f*
  definition, 223, 225

  ENEA summary, 241*t*
  Energetics reproducing, 221, 222*f*
  equation, 339
  generation, 162, 165, 166*f*
  heat effects, 243–244
  lifetime of, burst, 241
  superwave current treatment, 236, 239*f*
  See also Condensed matter heat production; Palladium deuteride and laser stimulation; Power
Excitation transfer
  and energy exchange, 260–261
  enhancement of, 264
  model, 257–259
  rotation, 258–259
  using perturbation theory, 261–263
Experimental design, cold fusion experiment, 137–142

F

Fermi's golden rule, fusion rates, 76, 79*t*
Fick's law, thermal output power, 339
Films. *See* Nanostructured palladium hydride system
First law of thermodynamics, power equation, 157
Fleischmann, Martin
  condensed matter nuclear science (CMNS), 3–4
  corroboration by Oriani, 5
  discovery of conditions for nuclear-active-environment (NAE), 85
  objections from physicists, 39
  See also Fleischmann–Pons experiment modeling; Pons–Fleischmann (P-F) reaction
Fleischmann–Pons experiment modeling
  anomalous energy exchange, 251–254
  anomalous energy exchange in rotated problem, 256
  claims of excess heat production, 249
  connecting models to excess heat production experiments, 265–266
  dimensionless coupling strength g, 251–252
  dynamics, 252, 254
  energy eigenvalues, 255
  energy levels, 255–256
  energy levels from Hamiltonian, 251
  enhancement of excitation transfer, 264
  excitation transfer, 257–259
  excitation transfer and energy exchange, 260–261
  excitation transfer mechanism violating local energy conservation, 264
  excitation transfer using perturbation theory, 261–263
  generalized spin-boson model, 261
  inclusion of loss effects in model, 263
  interaction strength V, 251
  level anticrossing, 252
  level splitting at level anticrossing vs. g, 253*f*
  level splitting on resonance, 256, 257*f*
  level splittings at anticrossings for excitation transfer, 258, 259*f*
  local energy and momentum conservation, 250
  lossless models, 265
  models augmented with loss, 261–264
  overall reaction mechanism, 250
  perturbation, 255
  plot of $\Delta E(g)$ as function of g, 253*f*

Downloaded by 89.163.34.136 on July 1, 2012 | http://pubs.acs.org
Publication Date: August 1, 2008 | doi: 10.1021/bk-2008-0998.ix002

Downloaded by 89.163.34.136 on July 1, 2012 | http://pubs.acs.org
Publication Date: August 1, 2008 | doi: 10.1021/bk-2008-0998.ix002

  probabilities for excitation transfer and energy exchange, 260–261, 262*f*
  quantum excitation transfer effect, 250
  reaction energy, 250
  requiring anomalous energy exchange mechanism, 265
  rotated frame for understanding systematics of energy levels, 256
  rotated Hamiltonian, 254
  rotation, 254–256, 258–259
  simplest single two-level system model, 254
  spin-boson Hamiltonian, 251
  unitary operator Û, 254
  unperturbed part of rotated Hamiltonian, 255
Fusion
  coherence domains, 145, 148
  Wilson cloud chamber, 129
Fusion rates
  barrier factor equation, 75
  barrier factors, 78*t*
  coherence dynamics, 130
  4D, 73, 75–80
  expectation position and Platonic symmetry, 80
  Fermi's golden rule, 76, 79*t*
  fusion yield, 77, 79
  Gamow integral, 73, 75
  optical potential <W>, 76–77, 79*t*
Fusion yield, definition, 77–79

G

Gamma emission
  single gamma ray, 107
  testing theory, 92
Gamma rays
  conversion, 100–101
  spectrum identifying and quantifying emitting element, 176, 177*f*
Gamow integral
  fusion rates, 73, 75
Giant Dipole Resonance (GDR), phenomenon, 145, 148

H

Hahn, Otto, barium discovery, 39
Hamiltonian
  excitation transfer, 257
  including loss, 263
  rotated, 254
  spin-boson, 251
Heat
  effects by different modes, 243–244
  excess, 5
  excess production in Fleischmann–Pons experiment, 250
  generation by nuclear energy, 3–4
  See also Condensed matter heat production; Excess heat
Heat-after-death
  nuclear energy without strong nuclear radiation, 50, 52
  phenomenon, 32
Heat-after-life, phenomenon, 32
Heat capacities (Cp)
  assumptions by temperature, 158
  values at several temperatures, 159*t*
Heat transfer coefficients
  determination using backward integration, 162, 163*f*
  determination using forward integration, 162, 164*f*
  mean values of, and heat capacities, 165*t*
  obtaining integral, 162
  pseudoradiative, 159–162
  various types, 161
  See also Isoperibolic calorimetry

Heavy mass electronic quasi-particle
  expansion theory (HMEQPET)
  method, 71–73
  model, 58
  parameters of HMEQPET
    potentials, 73, 74*t*
Heavy water
  low energy nuclear reactions, 12
  See also Electrolysis
Helium-4 production
  cold fusion, 106
  cold fusion experiment, 142, 146*f*, 147*f*
  diagram of cell and helium
    sampling circuit, 141*f*
  electrolytic cell, 145*t*
  energy balance, 107
  importance of quantum electrodynamic (QED) barrier, 105–108
  See also Cold fusion experiment
Hexagonal phase, templates, 355
Heyrovsky reaction, hydrogen
  electrode, 365
Hidden agendas, research projects,
  21*f*, 23
High current density, parameter for
  excess heat, 9
Hot fusion
  data justifying selectivity of
    resonant tunneling, 41–42
  investigation of, 29, 31
Hot spots on electrode surface, direct
  thermal imaging, 31–32
Huizenga, John, leading cold fusion
  panel, 4
Hydrides
  adsorption/absorption process,
    354
  See also Nanostructured palladium
    hydride system
Hydrogen absorption, voltammetry
  features, 371
Hydrogen adsorption, cyclic
  voltammetry, 366
Hydrogen electrode reaction, Volmer–Heyrovsky–Tafel mechanism, 364–365

I

Inorganic materials, deposition, 354
Insulator model, fully-loaded PdD,
  119
Ionic charge, entering and leaving
  solid, 102–103
Iron-region stable isotopes
  Fe^{57} nuclei production rate, 297
  mass spectrum of iron-region of
    microbiological associations,
    303, 305*f*
  relative number of Fe^{57} nuclei
    created, 302
  See also Microbiological
    associations
Irreproducibility, inherent, of system,
  26
Isoperibolic calorimetry
  ability to measure excess power,
    167
  accuracy using integration
    methods, 167
  actual radiative power, 168
  calculated value for power from
    gas stream exiting cell (P_{gas}),
    157, 159*t*
  calorimetric equations, 154, 157–162
  cell components, 155*f*
  CpM (heat capacity of system) and
    error, 161–162
  enthalpy of vaporization of D_2O
    (L), 158
  evaluation of heat transfer
    coefficient $(k_R')_{262}$ and CpM for
    days 9 and 10, 162, 163*f*
  evaluation of $(k_R')_{362}$ and CpM for
    days 9 and 10, 162, 164*f*
  excess power, 162, 165

Downloaded by 89.163.34.136 on July 1, 2012 | http://pubs.acs.org
Publication Date: August 1, 2008 | doi: 10.1021/bk-2008-0998.ix002

  experiments, 154
  experiments replicating, 220
  heat transfer coefficients, 161, 167–168
  mean values for k_R' and CpM, 165*t*
  palladium-boron alloy producing excess power effect, 167
  plot of raw data of measurement cycles, 154, 156*f*
  power equations, 157, 168
  precision and accuracy, 153–154, 168
  pseudoradiative heat transfer coefficients, 159–162, 167–168
  rate of enthalpy removal by gas stream, 158–159
  rates of excess enthalpy generation using integral values of k_R', 162, 165, 166*f*
  thermoneutral potential, E_H, 158, 159*t*
  values for L, E_H, and heat capacities for several temperatures, 159*t*
Isotope transmutation
  biological systems, 296–297
  See also Biological systems; Microbiological associations
Isotopic distribution, transmutation elements, 181*f*

K

K-capture, process, 88
Kirchhoff's law, calculating heat of vaporization of D_2O (L), 158
Knock-ons, evidence of neutrons, 321, 323, 326

L

Laser stimulation
  control runs with and without, 341, 342*f*
  dual tunable lasers, 339–340
  excess heat bursts, 338
  rotating polarization of lasers, 343, 345*f*, 346*f*
  See also Palladium deuteride and laser stimulation
Level anticrossing, anomalous energy exchange, 252, 253*f*
Level splittings, excitation transfer, 258, 259*f*
Light water. *See* Electrolysis
Loading, comparison of SRI and ENEA replications, 244–245
Loading ratios, parameter for excess heat, 7
Lossless models, anomalous energy exchange, 265
Low energy nuclear reactions (LENR)
  calorimetry, 6, 8*f*
  "cold fusion" label by media, 3
  comments about theory, 183, 186, 208
  comparing Pons–Fleischmann (P–F) cold fusion, LENR, and hot fusion reactions, 175*f*
  dynamic trigger, 9
  environmental issues, 12
  excess heat, 5
  excess heat after boil-offs, 9–10
  facts known, 7
  Fleischmann and Pons, 3–4
  high current density, 9
  history, 4
  loading ratios, 7
  many photons and many charged particles in LENR in PdD, 115–121
  mass-flow calorimetry, 6, 8*f*
  materials, 6
  methods, 12
  normal water reactions, 11
  nuclear evidence, 11–12
  power and energy release, 9
  proposed theories, 12–13
  public confusion, 5

Downloaded by 89.163.34.136 on July 1, 2012 | http://pubs.acs.org
Publication Date: August 1, 2008 | doi: 10.1021/bk-2008-0998.ix002

Downloaded by 89.163.34.136 on July 1, 2012 | http://pubs.acs.org
Publication Date: August 1, 2008 | doi: 10.1021/bk-2008-0998.ix002

  research at University of Illinois (UIUC), 174–176
  sensitivity to solid environment, 86
  spectrum of products in University of Illinois research, 175–176
  term, 3, 85, 174
  testing theory, 87–92
  threshold parameters for excess heat, 7, 9
  transmutation of heavy elements, 10–11
  worldwide transmutation studies, 176, 179–180
  See also Resonant electromagnetic interaction (EMI)
Lyotropic phases, templates, 355

M

Magnetic fields
  effect on palladium/deuterium system, 312–314
  See also Pd/D co-deposition
Manganese-55 isotope
  mass spectrum of iron-region of microbiological associations, 303, 305*f*
  Mössbauer spectra of optically dried biological substances, 302, 303*f*
  Mössbauer spectrum of one-line culture *Saccharomyces cerevisiae*, 298*f*
  nuclear transmutation of, 302
  relative to Fe^{57} isotope, 297
  See also Microbiological associations
Mass, relationship to charge, velocity and momentum, 103–104
Mass-flow calorimetry, excess heat, 6, 8*f*
Massive Cluster Electrode (MCE), new class of electrode, 183
Mathematical expressions, power, 157
Mathematical logic, assumptions and, 86
Mechanism
  excitation transfer, violating local energy conservation, 264
  neutron emission, 89
  overall reaction, in Fleischmann–Pons experiment, 250
Media, "cold fusion" label, 3
Metal crystals, coupling, 100
Metal-hydrogen electrochemical systems, heat generation, 187
Metallic-deuteride, protocols for experiments, 100
Metallic-hydride, protocols for experiments, 100
Microbial catalyst transmutator (MCT) compound
  microbe syntrophin associations, 299
  special granules, 299
  utilization of active isotopes, 306*f*
Microbiological associations
  accelerated deactivation of Cs^{137} isotope in "biological cells", 307*f*
  biotechnology-based methods of isotope transmutation, 299, 302
  control experiments, 306
  deactivation of different active isotopes, 307*t*
  experiments involving potential nuclear transmutation of Mn^{55} elements, 302
  Fe^{57} nuclei, 302
  mass-spectrum of iron region of, 305*f*
  microbial catalyst transmutator (MCT) compound, 299, 306*f*
  Mössbauer measurements of optically dried biological substances, 302, 303*f*
  Mössbauer spectra of grown cultures, 298*f*
  natural complete symbiosis, 299

Downloaded by 89.163.34.136 on July 1, 2012 | http://pubs.acs.org
Publication Date: August 1, 2008 | doi: 10.1021/bk-2008-0998.ix002

  - nuclear transmutation in one-line, 298–299
  - one-line cultures, 302
  - optimal growth of microcultures, 308
  - parameters of mass spectroscopy investigation of control and transmuted cultures, 304*t*
  - rate of Fe^{57} production, 297
  - relative efficiency rate, 302
  - study of utilization of active isotopes, 306*f*
  - symbiosis and synergism in, 300*f*, 301*f*
  - thermal ion mass spectroscopy (TIMS), 303, 305*f*
  - transmutation process during growth of cultures, 297
  - *See also* Biological systems
- Models
  - alpha emission, 90–91
  - anomalous energy exchange effect, 254
  - augmented with loss, 261–264
  - beta emission, 91
  - excitation transfer, 257–259
  - gamma emission, 92
  - inclusion of loss effects in, 263
  - insulator, for fully loaded PdD, 119
  - lossless, 265
  - neutron emission, 88–90
  - symbiosis and synergism in microbiological association, 300*f*, 301*f*
  - testing theory, 87–92
  - tetrahedral symmetric condensate (TSC) formation, 58–59
  - Trapped Neutron Catalyzed Fusion, 88
  - *See also* Fleischmann–Pons experiment modeling
- Molecular dynamics, 4D/tetrahedral symmetric condensate (4D/TSC), 58
- Momentum
  - conservation, 112
  - conservation of, and energy, 101–102, 250
  - finite crystal of PdD, 102
  - growth with increasing time, 103
  - relationship to mass, velocity and charge, 103–104
- Mössbauer effect, phenomenon, 128
- Multiple-scattering theory, Bloch's theorem, 113, 115

N

- Nanostructured palladium hydride system
  - characterization of H_I-e Pd films, 359, 361–364
  - comparing H_I-e Pd and plain Pd films, 365–366, 367*f*
  - crystal violet surface coverage, 372, 373*f*
  - deposition of inorganic materials, 354
  - deposition process, 354
  - effect of blocking Pd surface sites, 373
  - effect of crystal violet on voltammetry, 366–367, 368*f*
  - effect of surface species, 371–373
  - electrochemical adsorption/absorption features when loading H into Pd, 367–368
  - electrochemical characterization of electroactive surface area, 364
  - electrochemical experiments, 357
  - electrochemical measurements, 365–370
  - electrochemical measurements on H_I-e Pd films, 358
  - experimental, 357–358
  - hexagonal phase, 355

  hydrogen adsorption in cyclic voltammetry, 366
  hydrogen electrode reaction, 364–365
  lyotrophic phases, 355
  nanostructure of electrochemically deposited Pd film by transmission electron microscopy (TEM), 361, 362*f*
  non-ionic surfactants, 358–359, 360*f*
  palladium electrochemistry, 354
  phase behavior, 358–359
  phase diagram for mixtures of $(NH_4)_2PdCl_4$ in Brij® 56 (surfactant), heptane, and water, 358–359, 360*f*
  phase diagram for mixtures of $(NH_4)_2PdCl_4$ in $C_{16}EO_8$ (octaethyleneglycol monohexadecyl ether) and water, 358–359, 360*f*
  plot of H/Pd ratio as function of potential for H_I-e Pd film, 369, 370*f*
  pore distribution in H_I-e Pd films by X-ray diffraction, 362, 363*f*
  potential regions for surface oxide formation, 356
  preparation of H_I-e Pd films, 357–358
  Pt coverage on Pd surface, 371, 372*f*
  reverse scan of typical cyclic voltammogram of H_I-e Pd, 368, 369*f*
  scanning electron microscopy (SEM) method, 358
  schematic of nanostructured metal film punctured hexagonally by pores, 356*f*
  schematic of templating process, 355*f*
  SEM of H_I-e Pd film deposited on evaporated gold electrode, 359, 361*f*
  template deposition technique, 355–356
  thickness of H_I-e Pt deposited onto H_I-e Pd and H-adsorption, 371
  Volmer–Heyrovsky–Tafel mechanism, 364–365
  voltammetric features corresponding to H absorption process, 371
  voltammetry and hydrogen adsorption/absorption, 356–357
National Nuclear Data Center (NNDC), comparing theory and experiment, 42, 43*f*
Neutrino emission, self-sustaining reactor and, 50
Neutron activation analysis (NAA), gamma ray spectrum, 176, 177*f*
Neutron emission
  k-capture, 88
  mechanism, 89
  neutron production, 89–90
  resonance, 41
  testing theory, 88–90
  Trapped Neutron Catalyzed Fusion model, 88
Neutrons
  double and triple tracks, 320, 322*f*
  knock-ons as evidence of, 321, 323, 326
  nuclear reactions, 40
  See also Pd/D co-deposition
Nickel
  concentration profiles for Ni isotopes, 292*f*
  element analysis techniques, 273–275
  image of detector in contact with Pd film on Ni screen, 314*f*
  interference species for Ni isotopes, 285, 291*t*

Downloaded by 89.163.34.136 on July 1, 2012 | http://pubs.acs.org
Publication Date: August 1, 2008 | doi: 10.1021/bk-2008-0998.ix002

- profiles of Ni isotope ratio in Pd, 291, 292*f*
- *See also* Electrolysis

Nickel-hydrogen system, heat production, 186

Nickel nuclei, nuclear transmutations of Pd, 148

Non-linear Langevin equation
- tetrahedral symmetric condensate (TSC) motion, 59–61, 62*f*
- *See also* 4D/tetrahedral symmetric condensate (4D/TSC)

Normal water
- reactions, 11
- *See also* Electrolysis; Heavy water

Nuclear-active-environment (NAE), conditions, 85

Nuclear energy
- Ernst Rutherford, 39
- without strong nuclear radiation, 50, 52
- *See also* Resonant tunneling

Nuclear fission, discovery, 50

Nuclear fusion, possible forms in PdD, 103

Nuclear physics
- division of solid phases into coherent and incoherent structures, 25
- local energy and momentum conservation, 250
- strange reports, 130

Nuclear potential well, wave of penetrating deuterons, 40

Nuclear processes, quantum mechanics (QM), 19, 20*f*

Nuclear radiation
- low energy nuclear reactions, 11–12
- nuclear energy without strong, 50, 52
- *See also* Resonant tunneling

Nuclear reactions
- conditions, 85–86
- energy, 87
- generation of excess enthalpy, 132
- neutrons, 40

Nuclear Shell Model, giant dipole resonance, 145, 148

Nuclear transmutations
- one-line microbiological cultures, 298–299
- quantum electrodynamic (QED) coherence, 145, 148

O

Octaethyleneglycol monohexadecyl ether, phase diagram of surfactant, 358–359, 360*f*

One-line cultures, nuclear transmutations, 298–299

Optical phonon modes
- system responding to beat frequency, 349–350
- *See also* Palladium deuteride and laser stimulation

Optical potential <W>, fusion, 76–77, 79*t*

Oriani, Richard, corroboration paper, 5

P

Palladium
- atomic concentration vs. depth, 285
- atomic ratio for, surface layer before and after electrolysis, 277*f*
- byproducts of Pd-deuterium experiments, 7
- calibrations of Icarus cell for Pd-D system, 27*f*, 28*f*
- calorimetry of Pd-D system, 26
- cathode geometry for cold fusion experiment, 138, 139*f*
- co-deposition experiments, 120

Downloaded by 89.163.34.136 on July 1, 2012 | http://pubs.acs.org
Publication Date: August 1, 2008 | doi: 10.1021/bk-2008-0998.ix002

Downloaded by 89.163.34.136 on July 1, 2012 | http://pubs.acs.org
Publication Date: August 1, 2008 | doi: 10.1021/bk-2008-0998.ix002

- concentration profiles for Pd isotopes, 285, 290*f*, 291, 293*f*
- D_2 gas permeation through Pd complex, 184*f*, 185*f*
- electrolytic charge of, cathodes with deuterons, 25
- element analysis techniques, 273–275
- excess heat generation with Pd cathode, 186
- intervention of positive feedback in Pd-D system, 26, 29
- low energy nuclear reaction (LENR), 6
- many photons and many charged particles in LENR in PdD, 115–121
- nuclear transmutations, 148
- Pd/D system investigation, 25–26
- profiles of Pd isotope ratio in Pd rod, 285, 290*f*, 291, 293*f*
- secondary ion mass spectrometry (SIMS) counts for Pd cathodes, 279, 280*f*, 281*f*
- thin-film Pd cathode after cold fusion experiment, 132*f*
- trapped photons, 121
- X-ray photoelectron spectroscopy (XPS), 185*f*
- *See also* Electrolysis; Nanostructured palladium hydride system; Pd/D co-deposition

Palladium-boron alloy, producing excess power effect, 167

Palladium deuteride and laser stimulation
- beat frequency at 8.3 THz, 343, 346*f*
- cell positioned in magnetic field, 340*f*
- cell response at beat frequencies of 18.3 to 18.7 THz, 347, 348*f*
- cell response at beat frequencies of 19 to 21.4 THz, 347, 349*f*
- cell response to beat frequency of 19.4 THz, 341, 343, 344*f*
- cell temperature by Beta Therm thermistors, 338–339
- cell undergoing dual laser stimulation, 339*f*
- control run using dual lasers, 341, 342*f*
- control run without laser stimulation, 341, 342*f*
- dual tunable lasers, 339–340
- excess heat bursts, 338
- excess power, 339
- excess power events, 347, 349–350
- experimental, 338–341
- laser beating at various frequencies, 347
- losing laser control, 347
- optical phonon modes, 341, 349–350
- plating gold onto cathode, 337
- polarization rotation, 349–350
- rotating polarization of second laser, 343, 345*f*
- sensitivity to beat frequencies, 347, 348*f*, 349*f*
- thermal output power, 339
- thermal response to beat frequency of 14.5 THz, 343, 345*f*
- thermal response with and without polarization rotation, 343, 345*f*, 346*f*
- twin red laser pointers, 337

Palladium hydride system. *See* Nanostructured palladium hydride system

Palladium-hydrogen system, quantum electrodynamics (QED) of, 133–135

Palladium/nickel cathodes, heat generation experiments, 190

Parametric down-conversion (PDC) processes, 100–101
- single gamma ray, 107–108

Pd/D co-deposition

borosilicate glass cover slip as spacer, 323, 325*f*
channels summarizing breakup of ^{13}C into four-body final state, 322*t*
chemical damage by electrolysis, 316
Columbia Resin 39 (CR-39) detectors, 311–312
control experiments, 321*t*
double and triple tracks as evidence of neutrons, 320, 322*f*
effect of external electric and magnetic fields on, 312–314
etching of CR-39 detector, 323, 326
experimental procedure, 312
experiments replacing $PdCl_2$ with $CuCl_2$, 316, 318
experiment using $PdCl_2$, LiCl, and D_2O in external field, 318, 320
image of damaged CR-39 in contact with Au/Pd cathode, 314, 315*f*
images for Ag/Pd/D reaction in magnetic field, 316, 318*f*
images of pits for CR-39 exposed to ^{241}Am source, 316, 317*f*
images of triple and double tracks, 322*f*
knock-ons as evidence of neutrons, 321, 323, 326
microscopic image of CR-39 detector contacting Pd film on Ni screen with and without external magnetic field, 314*f*
nuclear vs. chemical, 314, 316, 318, 320
pits from, on Au cathode in magnetic field, 316, 319*f*
polyethylene film as spacers, 321, 323, 324*f*
quantitative analysis of CR-39 detectors, 326–328
size distributions and plots of minor vs. major axis for front and back surfaces, 328, 330*f*, 331*f*
spatial distribution of tracks on front and back surfaces of CR-39 detector, 329*f*
track representing nuclear event, 320
tracks in CR-39 by knock-on neutrons from ^{238}PuO source, 328, 332*f*
tracks on back surface of CR-39 used in, experiment, 328, 332*f*
tracks on CR-39 upon exposure to depleted uranium, 327*f*

Peebles' assumption, strong damping, 42
Peebles' calculation, resonance, 41
Perturbations
  current, in SRI replication, 225–226
  superwave, 226, 227*f*
Perturbation theory, excitation transfer using, 261–263
Phase diagrams, $(NH_4)_2PdCl_4$ in water and surfactants, 358–359, 360*f*
Photons, propagation in regions where wave equations apply, 115–116
Physics problems, self-sustaining reactor, 52
Pits in detectors. *See* Pd/D co-deposition
Plasmas, picture involving, in solids, 118
Platinum (Pt)
  hydrogen absorption/adsorption and, coverage on Pd surface, 371, 372*f*
  Pd surface sites, 373
  reference experiments with Pt-Pt electrodes, 189
Polarization of lasers
  cell response, 343, 345*f*, 346*f*

Downloaded by 89.163.34.136 on July 1, 2012 | http://pubs.acs.org
Publication Date: August 1, 2008 | doi: 10.1021/bk-2008-0998.ix002

  See also Palladium deuteride and laser stimulation
Polyethylene film, spacer between cathode and detector, 321, 323, 324*f*
Pons, Stanley
  condensed matter nuclear science (CMNS), 3–4
  corroboration by Oriani, 5
  discovery of conditions for nuclear-active-environment (NAE), 85
  objections from physicists, 39
  See also Fleischmann–Pons experiment modeling
Pons–Fleischmann (P–F) reaction
  original DD fusion, 174, 175*f*
  See also Cold fusion
Pore distribution, palladium hydride films, 362, 363*f*
Potential energy density, low energy nuclear reactions, 9
Power
  binding energies computing theoretical excess, 193
  bursts, 236, 240*f*, 241, 242*f*
  electrolytic input, 225
  excess, generation, 162, 165, 166*f*
  first law of thermodynamics, 157
  input and output, and energy evolution, 236, 238*f*
  isoperibolic calorimetry measuring excess, 167
  low energy nuclear reactions, 9
  measurement in SRI replication, 223, 225
  output, response, 225
  palladium-boron alloy measuring excess, effect, 167
  thermal output, 339
  transferring to charge in rest from of ordered solid, 119–120
  See also Palladium deuteride and laser stimulation
Praseodymium (Pr), X-ray photoelectron spectroscopy (XPS), 185*f*
Precision
  accuracy and, of calorimetric systems, 153–154, 168
  See also Isoperibolic calorimetry
Proposed theories, low energy nuclear reactions, 12–13
Protons
  energy distribution, 205, 206*f*
  simultaneous emission with alpha particles, 208
  See also Charged particles
Pseudoradiative heat transfer coefficients
  calorimetric equations, 159–162
  isoperibolic calorimetry, 167–168
  See also Isoperibolic calorimetry
Public confusion, cold fusion, 5
^{238}PuO source, tracks by knock-on neutrons from, 328, 332*f*

Q

Quadrupole mass analyzer (QMA)
  ionic current, 139, 140*f*
  mass spectroscopy, 139
Quantum electro-dynamic (QED) barrier
  Coulomb barrier vs., 104
  importance, 105–108
  role of time-dependent effects, 107
  single gamma ray, 107
Quantum electrodynamics (QED)
  coherence domains, 130–131
  hidden agendas of research projects, 21*f*
  importance of, 21
  investigation of role of, 29
  nuclear transformations of deuterons compressed into Pd, 129

Downloaded by 89.163.34.136 on July 1, 2012 | http://pubs.acs.org
Publication Date: August 1, 2008 | doi: 10.1021/bk-2008-0998.ix002

  nuclear transmutations at low energies, 145, 148
  palladium-hydrogen system, 133–135
  paradigm, 20
  scheme of research leading to "cold fusion", 20*f*
  terminology, 21–22
  See also Cold fusion; Cold fusion experiment
Quantum excitation transfer effect, energy conservation, 250
Quantum Field Theory (QFT)
  delocalization possibility, 128–129
  many-body problem within context of, 23, 25
  quantum mechanics, 19
Quantum mechanical electron cloud, 4D/tetrahedral symmetric condensate (4D/TSC), 59, 62*f*
Quantum mechanical fluctuation of deuteron positions
  adiabatic potential for molecule dde* and ground state squared wave function, 63*f*
  concept of heavy mass Cooper pair, 73
  d-d trapping potential of 4D/TSC, 72, 76*f*
  distortion of double platonic arrangement, 64–65, 71*f*
  distortion of system Coulomb energy by d-d distance fluctuation, 64–68
  friction term of Langevin equation, 71, 75*f*
  Gaussian wave function and shielded trapping Coulomb potential for Cooper-pair dd molecule, 64, 70*f*
  Gaussian wave function and shielded trapping Coulomb potential for D_2, 64, 69*f*
  Gaussian wave function and shielded trapping Coulomb potential for ddμ molecule, 64, 67*f*
  Gaussian wave functions, 61–64
  ground state d-d distance and d-d pair energy values with Gaussian wave function of ddμ molecule, 64, 66*f*
  heavy mass electronic quasi-particle expansion theory (HMEQPET) method, 71–73
  kinetic energy of electron in "d-e-d-e" system of TSC, 72, 77*f*
  numerical solution by Verlet method, 68–71
  parameters of HMEQPET potentials, 74*t*
  potential for balancing force term, 70, 74*f*
  squared wave function of Gaussian form, 61–62
  survey for σ-formula, 64, 65*f*
  system Hamiltonian with reduced mass, 63
  wave function and trapping Coulomb potential for muonic-dt molecule, 64, 68*f*
Quantum mechanics (QM)
  expression of fusion cross-section of S-wave, 41
  nuclear processes, 19, 20*f*
Quasi-particles, beating phenomenon, 118–119
Quasi-particle wave-packets, propagation of charge, 114

R

Ramsey, Norman, cold fusion review, 13
Reaction energy, Fleischmann–Pons experiment, 250

Downloaded by 89.163.34.136 on July 1, 2012 | http://pubs.acs.org
Publication Date: August 1, 2008 | doi: 10.1021/bk-2008-0998.ix002

Reactions
  accelerators, 40
  conditions for nuclear-active-environment (NAE), 85
Reciprocal lattice vector, definition, 111–112
Replication
  isoperibolic calorimetry, 220
  See also ENEA replication; SRI Energetics replication
Replication experiments. *See* Condensed matter heat production
Research
  hidden agendas, 21*f*
  leading to cold fusion project, 20*f*
Research laboratories, worldwide transmutation studies, 182*t*
Research milestones, cold fusion, 30*t*
Resistance
  equation, 135
  Pd-H system, 134
Resonance
  boundary conditions, 42, 44
  Coulomb barrier, 87
  hot fusion data justifying selectivity of tunneling, 41–42
  importance of, on tunneling, 40–41
  neutron emission, 41
  selectivity of, tunneling, 41
  tunneling current, 44, 45
Resonant electromagnetic interaction (EMI)
  approximately ordered crystals, 101
  conservation of momentum and energy, 101–102
  degeneracy, 102
  finite crystal of PdD, 102
  gamma ray conversion, 100–101
  generalization of semi-classical model of energy band theory, 104
  importance of EMIs, 104–105
  importance of quantum electrodynamic (QED) barrier in $d + d \rightarrow \alpha + \gamma$ and $d + d \rightarrow$ He-4 + 23.8 MeV, 105–108
  ionic charge entering and leaving solids, 102–103
  larger metal crystals, 100
  many photons and many charged particles in low energy nuclear reactions (LENR) in PdD, 115–121
  metallic-hydride or metallic-deuteride compounds, 100
  momentum and energy growing with increasing time, 103
  parametric down-conversion (PDC) processes, 100–101
  particles and photons sharing common phase, 101–102
  possible forms of nuclear fusion in PdD, 103
  potential new effects, 104
  presence of collisions, 102
  relationship between mass, velocity, charge and momentum, 103–104
  role of time-dependent effects in QED phenomena, 107
  selection rules, 99–100
  single gamma ray, 107
  single-particle resonant processes in solids, 108–115
  symmetry-related effects, 104–105
Resonant tunneling
  boundary conditions for beam-target configuration, 44*f*
  boundary condition for pair of confined deuterons in lattice potential well, 46*f*
  correlation between excess heat and abnormal deuterium flux, 49–50, 51*f*
  3-deuteron fusion reaction, 48–49
  flight-time of deuteron, 45
  Gamow penetration factor, 45
  life-time of deuteron, 47

Downloaded by 89.163.34.136 on July 1, 2012 | http://pubs.acs.org
Publication Date: August 1, 2008 | doi: 10.1021/bk-2008-0998.ix002

  selectivity of, for pair of confined deuterons, 42, 44–45, 47
  sharp selectivity, 47*f*
Riflex model, low energy nuclear reaction (LENR), 183, 186
Rotation
  anomalous energy exchange effect, 254–256
  cell response with polarization of lasers, 343, 345*f*, 346*f*
  energy levels, 255–256
  Hamiltonian, 254
  perturbation, 255
  unitary operator, 254
  unperturbed part of rotated Hamiltonian, 255
Rutherford, Ernst, nuclear energy, 39

S

Saccharomyces cerevisiae, Mössbauer spectrum of one-line culture, 298*f*
Scanning electron microscopy (SEM)
  method, 358
  palladium hydride film on Au electrode, 359, 361*f*
Scattering, well-defined form, 112
Schröedinger equation, single-particle, 109
Scientific discovery, 39–40
Seaborg, Glenn T., cold fusion review, 4
Selectivity
  resonant tunneling, 41
  resonant tunneling for pair of confined deuterons, 42, 44–45. 47
Self-sustaining reactor
  neutrino emission, 50
  physics problems, 52
Sensitivity
  cell response to specific beat frequencies, 347, 348*f*, 349*f*
  nuclear reactions and solid environment, 86
Single-particle resonant processes
  Bravais lattice vectors, 109
  charge propagation through quasi-particle wave-packets, 114
  conserving energy and momentum, 112
  degeneracy, 113–114
  energy band eigenvalue, 108–109
  finite crystal lattice, 110
  many-body, physical picture, 113
  minimizing overlap with ground state (GS), 111
  multiple-scattering situation, 113
  perfect or nearly perfect forms of resonance, 114–115
  reciprocal lattice vector, 111–112
  Schröedinger equation, 109
  semi-classical picture, 114
  solids, 108–115
  symmetry and implicit degeneracy, 111–112
  translation operator, 109–110
  wave-packet propagation, 114
  wave-vectors and reciprocal lattice vectors, 112
Single-product transmutation, direct-type, 182–183
Solids, boundaries, 103
SPAWAR protocol, emissions of radioactivity, 100–101
Spin-boson Hamiltonian, anomalous energy exchange, 251
Spin-boson models
  excitation transfer and energy exchange, 260–261, 262*f*
  models augmented with loss, 261–264
SRI Energetics replication
  calibration of calorimeters, 224*f*
  calibrations and power measurement, 223, 225
  calorimeters and cells, 241, 243

Downloaded by 89.163.34.136 on July 1, 2012 | http://pubs.acs.org
Publication Date: August 1, 2008 | doi: 10.1021/bk-2008-0998.ix002

Downloaded by 89.163.34.136 on July 1, 2012 | http://pubs.acs.org
Publication Date: August 1, 2008 | doi: 10.1021/bk-2008-0998.ix002

  calorimetry for first 500 h of cell, 231, 233*f*, 234*f*
  comparison to ENEA replication, 245, 246*f*
  condensed matter nuclear science (CMNS), 221, 223
  current perturbation, 225–226
  electrolytic input power, 225
  excess heat production from cathode using ENEA and University of Rome protocols, 231, 232*f*
  excess power calculation, 229
  excess power definition, 223, 225
  loading and excess heat results, 226, 228*t*
  null result using Energetics data acquisition method, 229*f*
  output power response, 225
  power and percentage excess power, 231, 233*f*, 234*f*
  result using non-steady-state correction, 229, 230*f*
  superwave perturbations, 226, 227*f*
  See also ENEA replication
Stimulation. *See* Palladium deuteride and laser stimulation
Superwave perturbations, SRI replication, 226, 227*f*
Surface x-ray diffraction
  experiment, 22, 23*f*
  See also X-ray diffraction (XRD)
Surfactants
  non-ionic, 358–359
  phase diagrams, 360*f*
  templating process, 355
  See also Nanostructured palladium hydride system
Swimming electron layer (SEL), theory, 176
Symbiosis
  changes in directions of, and synergism in microbiological associations, 300*f*, 301*f*
  cultures, 299
  See also Microbiological associations
Symmetry
  implicit degeneracy, 111
  resonant electromagnetic interactions (EMI), 104–105
Synergism
  changes in directions of symbiosis and, in microbiological associations, 300*f*, 301*f*
  See also Microbiological associations

T

Tafel reaction, hydrogen electrode, 365
Templating process, nanostructured metal films, 355*f*
Tetrahedral symmetric condensate (TSC)
  concept, 58
  See also 4D/tetrahedral symmetric condensate (4D/TSC)
Theories
  alpha emission, 90–91
  beta emission, 91
  gamma emission, 92
  neutron emission, 88–90
  proposed, for low energy nuclear reactions, 12–13
  testing, 87–92
Thermal balances, measurement, 25
Thermal ion mass spectroscopy (TIMS), microbiological associations, 303, 305*f*
Thermal output power, equation, 339
Thermodynamic principles, power equation, 157
Thermoneutral potential E_H
  compensating for enthalpy, 158
  values at several temperatures, 159*t*
Thin-film electrolysis
  charged particle emissions, 203*t*

Downloaded by 89.163.34.136 on July 1, 2012 | http://pubs.acs.org
Publication Date: August 1, 2008 | doi: 10.1021/bk-2008-0998.ix002

- charged particle production, 196–205
- excess heat production during, with transmutations, 186–192

Thin-metal film cathodes, heat generation of metal-hydrogen systems, 187

Threshold parameters, required, for excess heat, 7, 9

Tracks
- double and triple, evidence of neutrons, 320, 322*f*
- representing nuclear event, 320
- *See also* Pd/D co-deposition

Translation operator, equation, 109–110

Transmission electron microscopy (TEM), palladium hydride films, 361, 362*f*

Transmutation elements
- frequency of observation, 179, 180*f*
- isotopic distribution, 181*f*

Transmutation reactions
- biological, 296
- classification, 175, 205, 207
- isotope, in biological cells, 306–308
- low energy nuclear, 10–11, 29
- microbiological cultures, 297
- *See also* Electrolysis; Microbiological associations

Transmutation studies
- classifications of reactions, 175, 205, 207
- comments about low energy nuclear reaction (LENR) theory, 183, 186, 208
- correlation between, products and excess heat, 192–195
- D_2 gas permeation through Pd (Pd/CaO/Pd) deposited with Cs, 184*f*, 185*f*
- electrode design, 176, 179*f*
- energy/nucleon balances, 193–196
- excess heat production during thin-film electrolysis with, 186–192
- gamma ray spectrum from neutron activation analysis (NAA), 176, 177*f*
- isotopic distribution of, elements by various labs, 179, 181*f*
- most commonly reported elements for, 179, 180*f*
- production rate vs. mass number, 191*f*
- reaction pathways, 192–193
- reaction product-heat relationship, 192–193
- reaction rate for product production vs. mass number, 178*f*
- reactions and products, 174, 175*f*
- research at University of Illinois (UIUC), 174–176, 207, 208
- single-product "direct"-type, 182–183
- spectrum of products, 175–176
- swimming electron layer (SEL) theory, 176
- thin-film plate-type electrode at UIUC, 179*f*
- time variation in number of Cs and Pr atoms, 184*f*
- worldwide LENR studies, 176, 179–183, 186
- worldwide research laboratories conducting, 182*t*
- XPS spectrum for Cs, 184*f*
- XPS spectrum for Pd, 185*f*
- XPS spectrum for Pr, 185*f*
- *See also* Charged particles; Excess heat

Trapped Neutron Catalyzed Fusion model, neutron emission, 88

Trapped photons
- Bragg resonant scattering, 101
- localization of electromagnetic fields, 121
- phenomena, 108

Triggers, parameter for excess heat, 9
Triple coincidence experiment
  cold fusion, 138, 142, 143*f*
  See also Cold fusion experiment
Tunneling
  beating phenomenon, 118–119
  collisions by charged particles, 118–119
  concept of tunneling current, 44
  Coulomb barrier, 87
  current, 44, 45
  3-deuteron fusion reaction, 48–49
  hot fusion data justifying selectivity of resonant, 41–42
  importance of resonance, 40–41
  rapid for nuclear reaction, 119
  selectivity of resonant, 41
  selectivity of resonant, for pair of confined deuterons, 42, 44–45, 47
  single-particle resonant processes, 108–115
  two independent steps, 41
  See also Resonant tunneling

U

University of Illinois (UIUC)
  emission of energetic protons and alpha particles during thin-film electrolysis, 208
  low energy nuclear reactions (LENR) research, 174
  transmutation product studies, 174–176, 207
Uranium, tracks on detector CR-39 on exposure to depleted, 326, 327*f*

V

Velocity, relationship to mass, momentum and charge, 103–104
Volmer reaction, hydrogen electrode, 364

W

Water. *See* Electrolysis
Water reactions
  low energy nuclear reactions, 12
  normal, 11
  See also Electrolysis
Wave-packets, propagation of charge, 114
Wilson cloud chamber, fusion, 129
Worldwide research laboratories
  low energy nuclear reactions (LENR), 176, 179–180
  transmutation studies, 182*t*

X

X-ray diffraction (XRD)
  experiment on surface, 22, 23*f*
  selectivity towards surface diffraction, 22, 24*f*
X-ray photoelectron spectroscopy (XPS), spectra of Cs, Pr, and Pd, 184*f*, 185*f*

Downloaded by 89.163.34.136 on July 1, 2012 | http://pubs.acs.org
Publication Date: August 1, 2008 | doi: 10.1021/bk-2008-0998.ix002